

Javad Mohammadpour
Carsten W. Scherer *Editors*

Control of Linear Parameter Varying Systems with Applications

 Springer

Control of Linear Parameter Varying Systems with Applications

Javad Mohammadpour • Carsten W. Scherer
Editors

Control of Linear Parameter Varying Systems with Applications

 Springer

Editors

Javad Mohammadpour
Department of Mechanical Engineering
University of Houston
Calhoun Road 4800
77204-4006 Houston Texas
N204, Engineering Bldg. 1
USA

Carsten W. Scherer
Department of Mathematics
University of Stuttgart
Allmandring 5B, Room 1.12
Pfaffenwaldring
70569 Stuttgart
Germany

ISBN 978-1-4614-1832-0 e-ISBN 978-1-4614-1833-7
DOI 10.1007/978-1-4614-1833-7
Springer New York Dordrecht Heidelberg London

Library of Congress Control Number: 2012932216

© Springer Science+Business Media, LLC 2012

All rights reserved. This work may not be translated or copied in whole or in part without the written permission of the publisher (Springer Science+Business Media, LLC, 233 Spring Street, New York, NY 10013, USA), except for brief excerpts in connection with reviews or scholarly analysis. Use in connection with any form of information storage and retrieval, electronic adaptation, computer software, or by similar or dissimilar methodology now known or hereafter developed is forbidden.

The use in this publication of trade names, trademarks, service marks, and similar terms, even if they are not identified as such, is not to be taken as an expression of opinion as to whether or not they are subject to proprietary rights.

Printed on acid-free paper

Springer is part of Springer Science+Business Media (www.springer.com)

Foreword

When Carsten and Javad asked me to write a foreword for a book dedicated to LPV techniques, I had to think 20 years back and recall the ambient work of this period. LPV techniques are certainly the most beautiful by-product of our compulsive insistence to write huge (linear) symmetric matrix expressions with an inequality symbol on the right-hand side of the page. Some used a * character to avoid replicating symmetric terms to save space for conference papers, which also proved useful for short journal papers. One could also save a row and a column by using Schur complements. These were my secret tricks to save money for extra pages!

More seriously, the LMI period has continued to be a fertile field yielding sound solutions to new problem classes. Some may be deemed arguable in my opinion, either because more plausible proxies preexisted or since lack of practical significance was evident. LPV techniques indisputably form a core contribution and deserve special attention. The why and how can be sketched as follows.

The need for gain-scheduling or gain interpolation is a recurring design step which arises in most if not all real-world applications, ranging from aerospace, automotive, to process plants to cite a few. The rationale being that when plant variations become prevalent, some form of adjustment of control or filter mechanisms to the actual system dynamics is insuperable. Viewed differently, gain-scheduling techniques offer a cheap and fairly transparent way of carrying out nonlinear control design.

The conventional approach to gain-scheduling is a repetitive design procedure in which classical linear design methods are the elementary building tools. Such implementations frequently enjoy success and are deployed in many realistic control systems. Beyond being extremely laborious, the conventional approach is critically mistake prone for the following reasons:

- Engineering insight and ad hoc rules are required to bypass combinatorial explosion when dealing with systems evolving in large operating domains. In addition, exhaustive and costly validations remain mandatory.

- Since they rely on discretization of the operating domain, such approaches incur a serious risk to miss critical system configurations.
- It is a challenging task to guarantee stability and performance when switching or interpolating over a finite family of separately designed (local) controllers.
- More importantly, these techniques tacitly assume that parameters are frozen in time and ignore the nonstationary nature of parameter variations. These phenomena represent a major source of failure and may well floor the overall control scheme.

Nearly 20 years ago, LPV techniques emerged as neat and beautiful means in response to these troubles. In essence, they offer capabilities to handle the whole operating domain without recourse to discretization. They provide stability and performance certificates against parameter variations. And as a key ingredient, they offer an indisputable degree of operational simplicity. In many practical problems, approximating nonlinear dynamics with LPV dynamics makes sense. LPV models in open or closed loop with LPV controllers or filters possess a unique feature which one often refers to as low computational complexity. More concretely, LPV problems are convex and amenable to LMI computations, the latter being supported by efficient and reliable software tools. Altogether, this makes these techniques practical and good candidates for designers' toolkit.

A comprehensive account of the current state-of-the-art, as well as of the most recent advances on LPV techniques was becoming pressing. And this is the goal of this book entitled *Control of Linear Parameter Varying Systems with Applications*, edited by Profs. Carsten Scherer and Javad Mohammadpour. Their efforts should be acknowledged as the realm of LPV techniques has ramified in many directions along with multiple variants and extensions. This volume is not merely a collection of chapters. Through these pages, one will find background knowledge for nonexperts and explorations of most recent frontiers of LPV techniques, all useful to both theoreticians and practitioners. LPV control and estimation, LPV modeling and identification are discussed by leading researchers. This is complemented by a rich set of exciting applications which help conveying concepts, giving insights, and motivating unfamiliar people. There is no doubt that it will rest as a major reference for all those loving elegant theory or those willing to go beyond classical techniques.

ONERA & Mathematics Institute
Université Paul Sabatier
Toulouse, France

Prof. Pierre Apkarian

Preface

Linear parameter varying (LPV) systems are described by linear differential equations whose describing data depend—possibly in a nonlinear fashion—on time-varying parameters. The goal of the LPV synthesis problem is to design a controller of the very same structure such that the overall controlled system satisfies certain desired specifications on stability and performance over the entire set of permissible parameter trajectories. Hence, the implementation of LPV controllers takes online measurements of the time-varying parameters into account in order to improve the performance over robust controllers, which are compensators without any adaptation capabilities. Since the time-varying parameters often admit the interpretation of describing the location of the system’s operating point, LPV control methods are viewed as a viable alternative to classical gain-scheduling designs for controlling nonlinear systems. In particular, LPV control theory offers advantages over classical gain-scheduled control in that the resulting LPV controllers are automatically gain-scheduled, and no ad hoc methods of interpolation of gains are needed. In addition, it guarantees stability, performance, and robustness properties, which are generally difficult to achieve with traditional design methodologies. Last but not least, LPV synthesis exploits the power of available computational tools from convex optimization.

Since the introduction of the gain-scheduling paradigm about two decades ago (by Jeff Shamma—then at MIT—and his PhD advisor Michael Athans), the LPV framework has drawn the attention of many researchers all over the world and a significant body of related work has emerged. Unfortunately, the history of the theoretical developments and the applications of LPV theory have not yet been collectively addressed in a monograph. This volume seeks to bridge this gap by examining past, recent, and novel state-of-the-art methods and providing an outlook on modeling, identification, complexity reduction, performance analysis, and control design of time-varying and nonlinear systems described in the LPV framework. The book has an interdisciplinary character by emphasizing techniques that can be commonly applied in various engineering fields. It also includes a rich

collection of illustrative applications in diverse domains which substantiates the effectiveness of the design methodology and provides pointers to open research directions.

The book is divided into three parts. Part I collects two chapters of a more tutorial character on the background of LPV systems. The chapter by Jeff Shamma introduces the role of LPV systems and the technical delicacies involved in analyzing stability properties of LPV systems. This contribution describes the essential ideas on how to handle LPV systems using techniques from convex optimization (linear matrix inequalities) and set-invariance methods, and it provides a nice compilation of references to the LPV literature. The chapter by Roland Tóth et al. gives a theoretical overview of prediction-error-based identification techniques for modeling LPV systems. It provides useful guidelines in order to choose suitable methods for the construction of LPV models that can be used for the application of the techniques in the remainder of the book.

In Part II, we gathered chapters that are devoted to the theoretical advancement of LPV analysis and synthesis methods. In Chap. 3 by Franco Blanchini et al. the problem of interpolating parametric controllers is considered, irrespective of the underlying design philosophy. By using the Youla–Kucera parameterization, it is revealed how to interpolate controllers for frozen parameters such that stability of the overall closed-loop system is preserved when the parameters vary arbitrarily fast. Maurício de Oliveira considers the construction of controllers whose structure matches the affine parameter dependence of the system for established LPV synthesis frameworks in Chap. 4. Controller design for systems linearized around trajectories leads to time-varying LPV systems for which a design approach is proposed in Chap. 5 by Mazen Farhood. To deal with multiple performance objectives including classical regulation constraints, Hakan Köroğlu develops a suitable design methodology for LPV systems in Chap. 6. A nonconservative state-feedback synthesis technique for switched LPV systems based on path-dependent Lyapunov functions is proposed by Ji-Woong Lee and Geir Dullerud in Chap. 7. Robustification of LPV controllers against disturbance inputs in the parameter measurements is the topic of Chap. 8 contributed by Masayuki Sato and Dimitri Peaucelle. In Chap. 9, Tri Tran et al. consider time-varying splitting systems in the context of model-predictive control, in which dissipation-based techniques similar to those appearing in LPV theory play a central role. Joost Veenman et al. propose an algorithm for designing gain-scheduled estimators that are robust against structured uncertainties described by general integral quadratic constraints (IQCs) in Chap. 10. The more theoretically oriented part is concluded by Chap. 11 on the design of delay-dependent output-feedback controllers for LPV systems that are affected by time delays, contributed by Rohit Zope et al.

Part III of the volume showcases concrete applications of LPV modeling and control techniques in a wide range of technological areas. To comply with industry standards, the authors Fabiano Daher Adegas et al. of Chap. 12 propose a structured controller synthesis algorithm for an LPV model of a wind turbine which includes features of fault tolerance and robustness. Small-satellite attitude regulation with magnetic actuators is improved by incorporating measurements of the magnetic

field in the controller through LPV modeling and state-feedback synthesis, as demonstrated in Chap. 13 by Andrea Corti and Marco Lovera. Jan de Caigny et al. propose to model LPV systems by interpolation and apply it together with a variety of LPV synthesis approaches to a vibroacoustic application with high temperature sensitivity in Chap. 14. Anh-Lam Do et al. investigate how to control semi-active dampers in a quarter-car model in Chap. 15. Highly nonlinear flexible hypersonic air-breathing vehicles are controlled on the basis of the so-called gridding approach to LPV synthesis in Chap. 16 by Hunter Hughes and Fen Wu. Andreas Kominek et al. suggest tools for generating reduced order LPV models through system identification and provide an illustration for controlling a turbocharged combustion engine in Chap. 17. Freeway traffic control is the subject of Chap. 18, in which Tamas Luspay et al. use scheduling techniques for handling hard constraints and suppressing undesired phenomena on the network through disturbance attenuation. Elasticity generates resonance modes that might create performance limitations for controlling flexible systems; in Chap. 19, Peter Seiler et al. use LPV analysis to certify conventional controllers for NASA Dryden's X-53 active aeroelastic wing testbed and provide a comparison with their own synthesized LPV controller. The book is concluded with Chap. 20 addressing integrated vehicle chassis control in which Zoltan Szabo et al. provide an illustration of how to use the LPV technology for designing hierarchical control architectures.

It is our sincere hope that the readers will enjoy the breadth and depth of this collection of chapters on LPV theory and applications. Our special thanks go to Steven Elliot, the former Senior Editor—Engineering and Merry Stuber at Springer for their assistance throughout this project. Most importantly, we would like to thank all the contributors for their outstanding effort in composing their contributions to this book.

Houston, TX, USA
Stuttgart, Germany

Javad Mohammadpour
Carsten W. Scherer

Contents

Part I Introduction to Modeling and Control of LPV Systems

- 1 **An Overview of LPV Systems** 3
Jeff S. Shamma
- 2 **Prediction-Error Identification of LPV Systems: Present and Beyond** 27
Roland Tóth, Peter S.C. Heuberger, and Paul M.J. Van den Hof

Part II Theoretical Advances in LPV Control and Estimation

- 3 **Parametric Gain-scheduling Control via LPV-stable Realization** 61
Franco Blanchini, Daniele Casagrande, Stefano Miani, and Umberto Viaro
- 4 **Explicit Controller Parametrizations for Linear Parameter-Varying Affine Systems Using Linear Matrix Inequalities** 91
Maurício C. de Oliveira
- 5 **A Parameter-Dependent Lyapunov Approach for the Control of Nonstationary LPV Systems** 105
Mazen Farhood
- 6 **Generalized Asymptotic Regulation for LPV Systems with Additional Performance Objectives** 127
Hakan Koroğlu
- 7 **Robust Stabilization and Disturbance Attenuation of Switched Linear Parameter-Varying Systems in Discrete Time**..... 157
Ji-Woong Lee and Geir E. Dullerud

8	Gain-Scheduled Output-Feedback Controllers with Good Implementability and Robustness	181
	Masayuki Sato and Dimitri Peaucelle	
9	Decentralised Model Predictive Control of Time-Varying Splitting Parallel Systems	217
	Tri Tran, H.D. Tuan, Q.P. Ha, and Hung T. Nguyen	
10	Robust Estimation with Partial Gain-Scheduling Through Convex Optimization	253
	Joost Veenman, Carsten W. Scherer, and I. Emre Köse	
11	Delay-Dependent Output Feedback Control of Time-Delay LPV Systems	279
	Rohit Zope, Javad Mohammadpour, Karolos Grigoriadis, and Matthew Franchek	
Part III Recent Applications of LPV Methods in the Control of Complex Systems		
12	Structured Linear Parameter Varying Control of Wind Turbines	303
	Fabiano Daher Adegas, Christoffer Sloth, and Jakob Stoustrup	
13	Attitude Regulation for Spacecraft with Magnetic Actuators: An LPV Approach	339
	Andrea Corti and Marco Lovera	
14	Modeling and Control of LPV Systems: A Vibroacoustic Application	357
	Jan De Caigny, Juan F. Camino, Ricardo C.L.F. Oliveira, Pedro L.D. Peres, and Jan Swevers	
15	LPV Modeling and Control of Semi-active Dampers in Automotive Systems	381
	Anh-Lam Do, Olivier Sename, and Luc Dugard	
16	LPV H_∞ Control for Flexible Hypersonic Vehicle	413
	Hunter D. Hughes and Fen Wu	
17	Identification of Low-Complexity LPV Input–Output Models for Control of a Turbocharged Combustion Engine	445
	Andreas Kominek, Herbert Werner, Maiko Garwon, and Matthias Schultalbers	
18	Constrained Freeway Traffic Control via Linear Parameter Varying Paradigms	461
	T. Luspay, T. Péni, and B. Kulcsár	

19 Linear Parameter-Varying Control for the X-53 Active Aeroelastic Wing 483
Peter Seiler, Gary J. Balas, and Andrew Packard

20 Design of Integrated Vehicle Chassis Control Based on LPV Methods 513
Zoltán Szabó, Péter Gáspár, and József Bokor

Index 535

Contributors

Fabiano Daher Adegas Department of Electronic Systems, Aalborg Universitet, Fredrik Bajers, Aalborg, Denmark

Pierre Apkarian Institut de Mathematiques, Université Paul Sabatier, Toulouse, France

Gary J. Balas MUSYN, Inc., Minneapolis, MN, USA

Franco Blanchini Department of Mathematics and Computer Science, University of Udine, Udine, Italy

József Bokor Systems and Control Laboratory, Computer and Automation Research Institute, Hungarian Academy of Sciences, Budapest, Hungary

Jan De Caigny Department of Mechanical Engineering, Katholieke Universiteit Leuven, Celestijnenlaan, Heverlee, Belgium

Juan F. Camino School of Mechanical Engineering, University of Campinas – UNICAMP, Campinas, SP, Brazil

Daniele Casagrande Department of Electrical, Managerial and Mechanical Engineering, University of Udine, Udine, Italy

Andrea Corti Dipartimento di Elettronica e Informazione, Politecnico di Milano, Milano, Italy

Anh-Lam Do GIPSA-Lab, Control Systems Department, CNRS-Grenoble INP, St Martin d'Hères cedex, France

Luc Dugard GIPSA-Lab, Control Systems Department, CNRS-Grenoble INP, St Martin d'Hères cedex, France

Geir E. Dullerud Department of Mechanical Science and Engineering, The University of Illinois at Urbana-Champaign, Urbana, IL, USA

Mazen Farhood Aerospace and Ocean Engineering Department, Virginia Tech, Blacksburg, USA

Matthew A. Franchek Department of Mechanical Engineering, University of Houston, Houston, TX, USA

Maiko Garwon IAV GmbH Ingenieurgesellschaft Auto und Verkehr, Berlin, Germany

Péter Gáspár Systems and Control Laboratory, Computer and Automation Research Institute, Hungarian Academy of Sciences, Budapest, Hungary

Karolos Grigoriadis Department of Mechanical Engineering, University of Houston, Houston, TX, USA

Quang P. Ha Faculty of Engineering and Information Technology, University of Technology, Sydney, Ultimo, NSW, Australia

Peter S.C. Heuberger Delft Center for Systems and Control, Delft University of Technology, Delft, The Netherlands

Hunter D. Hughes Georgia Tech Research Institute, Smyrna, GA, USA

Andreas Kominek Hamburg University of Technology, Hamburg, Germany

Hakan Koroğlu Electrical Engineering Department, King Fahd University of Petroleum and Minerals, Dhahran, Saudi Arabia

I. Emre Köse Department of Mechanical Engineering, Boğazici University, Istanbul, Turkey

Balázs Kulcsár Department of Signals and Systems, Chalmers University of Technology, Gothenburg, Sweden

Ji-Woong Lee Department of Electrical Engineering, The Pennsylvania State University, University Park, PA, USA

Marco Lovera Dipartimento di Eletttronica e Informazione, Politecnico di Milano, Milano, Italy

Tamás Luspáy Systems and Control Laboratory, Computer and Automation Research Institute, Hungarian Academy of Sciences, Kende u, Budapest, Hungary

Stefano Miani Department of Electrical, Managerial and Mechanical Engineering, University of Udine, Udine, Italy

Javad Mohammadpour Department of Mechanical Engineering, University of Houston, Houston, TX, USA

Hung T. Nguyen Faculty of Engineering and Information Technology, University of Technology, Sydney, Ultimo, NSW, Australia

Maurício C. de Oliveira Department of Mechanical and Aerospace Engineering, University of California, San Diego, CA, USA

Ricardo C.L.F. Oliveira School of Electrical and Computer Engineering, University of Campinas – UNICAMP, Campinas, SP, Brazil

Andrew Packard MUSYN, Inc., Berkeley, CA, USA

Dimitri Peaucelle CNRS; LAAS; 7, avenue du Colonel Roche, Toulouse, France.
Universite de Toulouse; UPS, INSA, INP, ISAE, UTM, UT1; LAAS; Toulouse,
France.

Tamás Péni Systems and Control Laboratory, Computer and Automation Research
Institute, Hungarian Academy of Sciences, Kende u, Budapest, Hungary

Pedro L.D. Peres School of Electrical and Computer Engineering, University of
Campinas – UNICAMP, Campinas, SP, Brazil

Masayuki Sato Japan Aerospace Exploration Agency, Tokyo , Japan

Carsten W. Scherer Department of Mathematics, University of Stuttgart,
Stuttgart, Germany

Matthias Schultalbers IAV GmbH Ingenieurgesellschaft Auto und Verkehr,
Berlin, Germany

Peter Seiler MUSYN, Inc., Minneapolis, MN, USA

Olivier Sename GIPSA-Lab, Control Systems Department, CNRS-Grenoble INP,
St Martin d'Hères cedex, France

Jeff S. Shamma School of Electrical and Computer Engineering, Georgia
Institute of Technology, Atlanta, GA, USA

Christoffer Sloth Department of Computer Science, Aalborg Universitet, Aalborg,
Denmark

Jakob Stoustrup Department of Electronic Systems, Aalborg Universitet, Fredrik
Bajers, Aalborg, Denmark

Jan Swevers Department of Mechanical Engineering, Katholieke Universiteit
Leuven, Celestijnenlaan, Heverlee, Belgium

Zoltán Szabó Systems and Control Laboratory, Computer and Automation
Research Institute, Hungarian Academy of Sciences, Budapest, Hungary

Roland Tóth Delft Center for Systems and Control, Delft University of
Technology, Delft, The Netherlands

Tri Tran Faculty of Engineering and Information Technology, University of
Technology, Sydney, Ultimo, NSW, Australia

Hoang D. Tuan Faculty of Engineering and Information Technology, University
of Technology, Sydney, Ultimo, NSW, Australia

Paul M.J. Van den Hof Delft Center for Systems and Control, Delft University of
Technology, Delft, The Netherlands

Joost Veenman Department of Mathematics, University of Stuttgart, Stuttgart, Germany

Umberto Viaro Department of Electrical, Managerial and Mechanical Engineering, University of Udine, Udine, Italy

Herbert Werner Hamburg University of Technology, Hamburg, Germany

Fen Wu North Carolina State University, Mechanical and Aerospace Engineering, NC, USA

Rohit Zope Department of Mechanical Engineering, University of Houston, Houston, TX, USA

Part I
Introduction to Modeling and Control
of LPV Systems

Chapter 1

An Overview of LPV Systems

Jeff S. Shamma

Abstract The framework of Linear Parameter Varying (LPV) systems concerns linear dynamical systems whose state-space representations depend on exogenous nonstationary parameters. Since its introduction by Shamma and Athans in 1988 to model gain-scheduling, the LPV paradigm has become a standard formalism in systems and controls, with many papers devoted to analysis, controller synthesis, and system identification of LPV models. This chapter reviews basic concepts and presents a representative selection of analytical approaches for LPV systems.

1.1 Introducing LPV Systems

1.1.1 Origins

The framework of Linear Parameter Varying (LPV) systems concerns linear dynamical systems whose state-space representations depend on exogenous non-stationary parameters, as in

$$\begin{aligned}\dot{x} &= A(\theta)x + B(\theta)u, \\ y &= C(\theta)x,\end{aligned}\tag{1.1}$$

where u is an input, y is an output, and θ is an exogenous parameter that can be time dependent.

The LPV paradigm was introduced in the Ph.D. thesis of Shamma [74] for the analysis of the control design practice of “gain-scheduling” [4, Chap. 9]. In brief,

J.S. Shamma (✉)
School of Electrical and Computer Engineering, Georgia Institute of Technology,
Atlanta, GA, USA
e-mail: shamma@gatech.edu

gain-scheduling is a control design approach that constructs a nonlinear controller for a nonlinear plant by patching together a collection of linear controllers. These linear controllers are blended in real time (e.g., via switching or interpolation) according to available online measurements. See [44, 65, 74, 76, 78, 79, 81] for early analytical work in gain-scheduling and [46, 66] for survey articles.

The architecture induced by gain-scheduling suggests the LPV framework as a “middle ground” between linear and nonlinear dynamics. The relationship is as follows. An analysis of gain-scheduling produces an indexed collection of linear systems. Likewise, an LPV model consists of an indexed collection of linear systems, in which the indexing parameter is *exogenous*, i.e., independent of the state. In gain-scheduling, this “parameter” is actually a function of the state, and hence *endogenous*, as in

$$\begin{aligned}\dot{x} &= A(z)x + B(z)u. \\ y &= C(z)x. \\ z &= h(x).\end{aligned}\tag{1.2}$$

The LPV framework abstracts away this nonlinear dependency, resulting in linear, but nonstationary, dynamics.

1.1.2 LPV vs LTI vs LTV

The terminology “linear parameter varying” was introduced¹ in [74] to distinguish LPV systems from both LTI (linear time-invariant) and LTV (linear time varying) systems. The distinction from LTI systems is clear in that LPV systems are nonstationary. The distinction from LTV systems is less apparent, because for any trajectory of the parameter $\theta(\cdot)$, the dynamics of (1.1) constitute a linear time-varying system. Rather, LPV systems are distinguished from LTV systems in the *perspective taken* on both analysis and synthesis.

First consider analysis questions such as stability. Typical assumptions on the exogenous parameters are bounds on magnitudes and rate of variations, e.g., for all $t \geq 0$,

$$-\mu \leq \theta(t) \leq \mu, \tag{1.3}$$

$$-\rho \leq \dot{\theta}(t) \leq \rho. \tag{1.4}$$

¹The now standard LPV acronym appears in [81] in 1992 and gained popularity with the works of [2, 3, 8, 11, 12, 61, 82], among others.

This characterization defines a *family* of admissible parameter trajectories. Accordingly, LPV analysis concerns assessing properties (such as stability, disturbance rejection, tracking, etc.) that hold for a *family* of LTV systems, rather than a single LTV system. To highlight this issue going forward, let \mathcal{Q} denote some specified family of parameter trajectories (so that $\theta(\cdot) \in \mathcal{Q}$).

The distinction between LPV and LTV systems is more pronounced in control design or synthesis. One typically assumes that the exogenous parameter can be measured in real time. For example, a state feedback controller may take the form

$$u(t) = F(\theta(t))x(t),$$

where the feedback gain is a function of the current parameter value. More generally, a state feedback controller may depend on the entire past history of parameter measurements, as represented by

$$u(t) = F(\theta|_{[0,t]})x(t). \quad (1.5)$$

In either case, the control is constrained to be a *causal* function of the parameter—*current control values cannot depend on future parameter values*. Contrast this constraint with the classical treatment of LTV systems, e.g., for linear quadratic optimal control (a standard reference is [42]). For LTV systems, the optimal controller is again a time-varying linear state feedback law, similar to (1.5). Unlike (1.5), the optimal state feedback matrix depends exclusively on *future* parameter trajectories, e.g.,

$$u(t) = K(\theta|_{[t,\infty)})x(t),$$

thereby violating the causality constraint on the control.

1.1.3 Connections

There are two other modeling formalisms worth highlighting in the context of LPV systems. The first is *hybrid dynamical systems* (e.g., [69]). Hybrid dynamical systems possess both continuous and discrete state variables. Accordingly, in the special case of discrete valued parameters, e.g.,

$$\theta(t) \in \{\theta_1, \dots, \theta_n\}. \quad (1.6)$$

LPV systems constitute a specific case of hybrid dynamical systems (namely, where the underlying continuous dynamics are linear and the discrete switching dynamics are exogenous). Not surprisingly, many similar discussion and approaches have been considered separately in both contexts (cf., stability analysis issues in [48]).

The second formalism is *jump linear systems* (e.g., [28]). Jump linear systems can be viewed as a case of LPV systems in which parameter trajectories evolve

according to a probabilistic rule. The treatment of both LPV and jump linear systems shares the aforementioned perspectives on control, namely, that control laws must have causal dependencies on parameter trajectories. In the jump linear system case, the design of control laws typically exploits the known transition probabilities of the parameter's stochastic evolution.

1.1.4 Applications

The LPV paradigm has been used for modeling and control in a variety of applications. Traditionally, gain-scheduling was a prevalent design approach for flight control, and not surprisingly, many of the first papers exploiting the LPV framework concerned flight control. These have been followed by several papers using the LPV framework in a variety of settings. A representative (and incomplete!) selection of LPV application areas includes:

- Flight control² and missile autopilots [9, 27, 34, 51, 62, 82, 86]
- Aeroelasticity [10, 40, 43, 93]
- Turbofan engines [6, 26, 36, 85]
- Magnetic bearings [52, 94, 95]
- Automotive systems [7, 35, 38, 64, 91, 99]
- Energy [15, 47, 55, 68]

as well as microgravity [54], IC manufacturing [90], anesthesia delivery [49], and diabetes control [63].

1.1.5 Outline

The remainder of this overview chapter presents various results on both analysis and control design for LPV systems. The chapter begins with stability and robustness of LPV systems. As previously discussed, a main concern is understanding what properties hold for *families* of parameter variations. The chapter continues with a discussion of control design for LPV systems, focusing on three complementary approaches: linear matrix inequality (LMI) methods, stable realizations, and set-invariance methods. Again, the issue of *causal dependency* on parameter variations is an important concern. Finally, the chapter presents some concluding remarks regarding other aspects of LPV systems not discussed herein.

Regarding the forthcoming presentation, *the analysis and theorems stated herein are presented in an informal manner*. Technical details may (and should) be found in the associated references. Finally, standard notation is used throughout, with clarifications provided as needed.

²Boeing 747, F-14, F-16, and VAAC Harrier.

1.2 LPV Stability Analysis

As stated in section, analysis questions for LPV systems ask what properties hold for *families* of parameter trajectories. A baseline assumption is that any control design produces an LPV system that is stable for constant parameter trajectories. This assumption stems from the relationship to gain-scheduling, where both stability and performance are guaranteed *by design* under constant parameter values. An important issue is then determining what properties are preserved under parameter time variations. The following sections discuss the basic stability question and presents various theoretical results for two limiting cases: (1) slow time variations and (2) arbitrary time variations. The section concludes with a broader discussion of robust stability, which also sets the stage for a forthcoming section on controller design.

1.2.1 Instability and Time Variations

1.2.1.1 Induced Instability

A well-known phenomenon from linear systems analysis is that time variations can induce instability. There are examples (e.g., [53]) of LTV systems

$$\dot{x} = A(t)x$$

such that the eigenvalues of $A(t)$ are in the left half plane for all $t \geq 0$, but for which solutions, $x(t)$, grow exponentially.

The usual intuition behind this phenomenon is illustrated in Fig. 1.1. This figure depicts state trajectories of the LPV system

$$\dot{x} = \begin{pmatrix} 0 & 1 \\ -\theta^2 & 0 \end{pmatrix} x$$

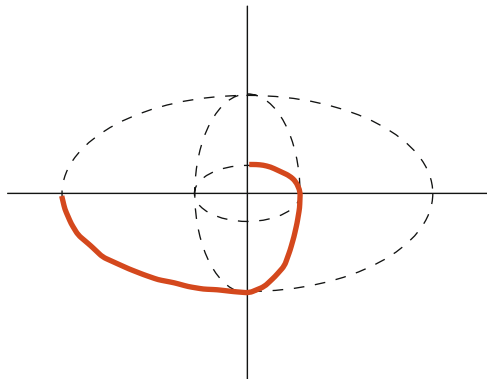


Fig. 1.1 Instability induced by switching dynamics

with θ periodically switching between two values, e.g., $\theta(t) \in \{\omega_a, \omega_b\}$. Although for each fixed value of θ the LTI system is (marginally) stable, the state undergoes phases of increasing and decreasing magnitude. Instability occurs by an alignment of phases of increasing magnitude.

1.2.1.2 Induced Non-Minimum Phasedness

Related to induced instability is induced “non-minimum phasedness.” Right-half-plane zeros in the transfer function of an LTI system impose fundamental limitations in achievable performance (cf., [21, 33]). While time-varying systems do not have right-half-plane zeros per se, there are similar notions and similar resulting limits of performance. Shamma [75] defines a non-minimum phased property for nonlinear time-varying systems where an unbounded input produces a bounded output. Shamma [75] goes on to show that this property imposes fundamental limitations on closed-loop disturbance rejection (see also [73]). Just as parameter time variations can induce instability, they can also induce such non-minimum phased behaviors. That is, an LPV system can be minimum phase for constant parameter values, but non-minimum phase under time variations, and thereby have fundamental limits of achievable performance that are not apparent from the constant parameter analysis. Shamma and Athans [81] present such an example as a “potential hazard” of gain-scheduling.

1.2.2 Stability: Slow Time Variations

This section presents a collection of results that formalize the following statement: *Stability for constant parameter trajectories implies stability for slowly time-varying parameter trajectories.*

1.2.2.1 Stability vs Peaking

While the forthcoming conditions for stability have different specific setups and proofs, they all share a similar intuition.

First, let Θ denote the set of admissible parameter values.³ When convenient, we may distinguish between a continuum or discrete set. Accordingly, let Θ_c denote the continuous set defined in (1.3), and let Θ_d denote the discrete set defined in (1.6). Now assume that for any $\theta_0 \in \Theta$, the LTI system

$$\dot{x} = A(\theta_0)x \tag{1.7}$$

³Whereas \mathcal{Q} denotes admissible trajectories for $\theta(\cdot)$, the related Θ denotes admissible values of $\theta(t)$.

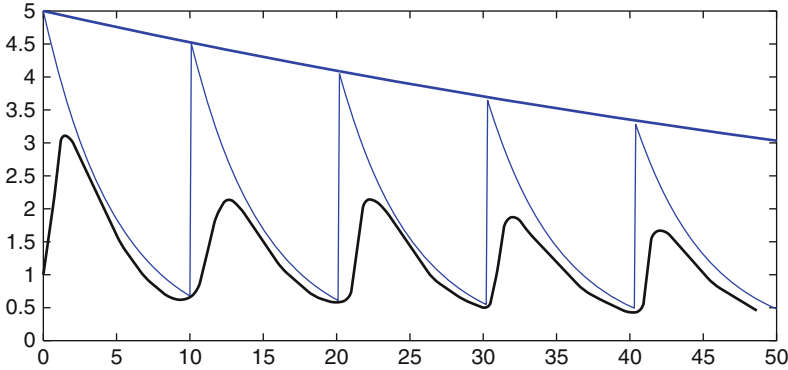


Fig. 1.2 Stability vs peaking. The bottom line indicates the actual state magnitude. The thin middle line indicates a succession of upper bounds implied by $me^{-\lambda t}$. Finally the top line top line is an exponentially decaying overall upper bound

is exponentially stable. In particular, let $m \geq 1$ and $\lambda > 0$ be such that for any $\theta_0 \in \Theta$, solutions of (1.7) satisfy⁴

$$|x(t)| \leq me^{-\lambda t} |x(0)|.$$

The parameter m is referred to as the “peaking constant” [32]. In terms of the previous discussion on induced instability, the peaking constant reflects that the state may increase in magnitude before decaying exponentially.

Figure 1.2 illustrates the main intuition behind stability under slow time variations. Assuming the discrete case Θ_d , after each switched parameter value, there may be a period of peaking before exponential decay sets in. As long as switching does not occur too rapidly, then there cannot be an alignment of phases of peaking (as in Fig. 1.1).

1.2.2.2 Characterizing Slow Variations

The following are various specifications of “slowly time-varying.”

- *Continuous case*, Θ_c : Assume Lipschitz continuity of $A(\cdot)$, i.e., for some $L_A > 0$,⁵

$$\|A(\theta) - A(\theta')\| \leq L_A |\theta - \theta'|$$

for all $\theta, \theta' \in \theta_c$.

- Persistently slow:

$$|\dot{\theta}| < \varepsilon.$$

⁴ $|x|$ denotes the Euclidean norm of $x \in \mathbf{R}^n$.

⁵ $\|A\|$ denotes the induced matrix norm, $\sup_{x \neq 0} |Ax| / |x|$.

- Slow on average:

$$\inf_{T>0} \sup_{t_0 \geq 0} \frac{1}{T} \int_{t_0}^{t_0+T} |\dot{\theta}| dt < \varepsilon$$

over any interval $[t_0, t_0 + T]$ is small.

- *Discrete case, Θ_d* : Let t_0, t_1, t_2, \dots denote switching times such that $\theta(t)$ is constant over intervals $[t_n, t_{n+1})$. Define “dwell times,” $T_n = t_n - t_{n-1}$.
 - Large average dwell time:

$$\sup_{n^* \geq 1} \inf_{n \geq 1} \frac{T_{n+1} + \dots + T_{n+n^*}}{n^*} > \frac{1}{\varepsilon} \quad (1.8)$$

for any n .

Theorem 1.1. *In any of the above settings, the LPV system (1.1) is exponentially stable for sufficiently small $\varepsilon > 0$.*

Stability results for sufficiently slow time variations, particularly the persistently slow case, trace back to classical results in ordinary differential equations (cf., [31, p. 125]). Nonetheless, a suitable analysis can derive revealing explicit bounds in each of the above cases:

- Persistently slow [74] and slow on average [41]:

$$\varepsilon < \frac{\lambda^2}{4L_A m \log(m)}.$$

- Average dwell time [48]: There exists an n^* such that (1.8) is satisfied with

$$\varepsilon < \frac{\lambda}{\log(m)}.$$

An interesting implication from the above bounds is that time variations can be arbitrarily fast when $m = 1$. In terms of the previous discussion, $m = 1$ implies that trajectories in the constant parameter case have no peaking, and therefore cannot align to produce instability.

1.2.3 Stability: Arbitrary Time Variations

1.2.3.1 Stability: Arbitrary Time Variations

As opposed to the case of sufficiently slow variations, this section discusses the stability question from the other extreme, namely, arbitrary time variations. It turns out that answering such questions is subject to computational complexity limitations.

For this discussion, consider the discrete-time LPV system:

$$x(t+1) = A(\theta(t))x(t), \quad (1.9)$$

where Θ_d is a finite set.

Theorem 1.2 ([20, 87, 88]).

- *Determining whether solutions of (1.9) are bounded is undecidable (even for binary Θ_d).*
- *Determining whether (1.9) is asymptotically stable is NP-hard.*

Consequently, deriving efficient algorithms for assessing stability will remain to be elusive.

1.2.3.2 Quadratic vs Non-Quadratic

A consequence of the complexity result is that one must settle for non-definitive methods or inefficient algorithms to assess stability. The following sufficient condition is known as quadratic stability (e.g., [60]):

Proposition 1.1. *Let $X \in \mathbf{R}^{n \times n}$ be symmetric, positive definite, and satisfy*

$$XA(\theta) + A^T(\theta)X < 0$$

for all $\theta \in \Theta$. Then the LPV system (1.1) is exponentially stable for all (Θ -valued) trajectory families \mathcal{Q} .

An immediate proof is that $x^T X x$ is a Lyapunov function for the LPV system. In fact, the hypothesis of Proposition 1.1 is that $x^T X x$ is a Lyapunov function for all associated constant parameter LTI systems. There is an interesting connection to the previous discussion on slowly varying systems. Namely, the change of variables $z = X^{1/2}x$ produces an LPV system with $m = 1$ for all constant parameter values, which recovers the conclusions of Proposition 1.1 for arbitrary variations.

Of course, Proposition 1.1 is only a sufficient condition. The following counterexample is due to [30]. The setup is a second-order system whose dynamics matrix can switch between two matrices:

$$\dot{x} \in \{A_1 x, A_2 x\}.$$

This can be viewed as an LPV system with $\Theta_d = \{1, 2\}$. [30] show that for

$$A_1 = \begin{pmatrix} -1 & -1 \\ 1 & -1 \end{pmatrix} \quad \text{and} \quad A_2 = \begin{pmatrix} -1 & -a \\ 1/a & -1 \end{pmatrix},$$

and $3 + \sqrt{8} < a < 10$: (1) the above system is stable for arbitrary switching and (2) there does *not* exist an X satisfying the conditions of Proposition 1.1.

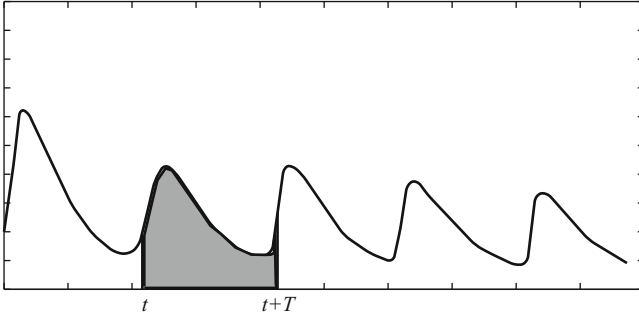


Fig. 1.3 Illustration of integral for Lyapunov function construction

1.2.3.3 Lyapunov Structure

While quadratic Lyapunov functions need not characterize stability under arbitrary parameter variations, one can derive certain special structures of suitable Lyapunov functions. The following discussion is motivated by the results of [45, 58].

First, some notation. Let

$$\Phi(t, \tau; \theta([\tau, t]))$$

denote the state transition matrix for an LPV system where the dependence on the parameter trajectory (over the interval $[\tau, t]$) is explicit. Accordingly,

$$x(t) = \Phi(t, \tau; \theta([\tau, t]))x(\tau).$$

Assuming that an LPV system is exponentially stable for all parameter trajectories, there exist m and $\lambda > 0$ such that

$$\|\Phi(t, \tau; \theta([\tau, t]))\| \leq me^{-\lambda(t-\tau)}.$$

Let T be such that $me^{-\lambda T} < 1$, and define the following Lyapunov function candidate (based on converse Lyapunov function methods, e.g., [92]):

$$V(x, t) = \int_t^{t+T} |\Phi(\tau, t; \theta([t, \tau]))x|^2 d\tau.$$

Figure 1.3 illustrates the construction of this function. In words, this function is the energy of the solution over the interval $[t, t+T]$. One can show that $V(x(t), t)$ is decreasing along solutions of the LPV system. In particular,

$$V(x(t+h), t+h) - V(x(t), t) \approx -h|x(t)|^2 + h|x(t+T)|^2 < -(1 - me^{-\lambda T})|x|^2.$$

Neglecting issues of differentiability, the above construction suggests that

$$\frac{d}{dt}V(x(t),t) < -c|x|^2.$$

Inspecting the structure of this Lyapunov function, one sees that it can be written as a quadratic function in x , where the defining matrix is a function of the future parameter trajectory, i.e.,

$$V(x(t),t) = x^T(t)X\left(\theta([t,t+T])\right)x(t).$$

In fact, one can reparameterize the function to be a function of past parameter trajectories, as in

$$V(x(t),t) = x^T(t)\tilde{X}\left(\theta([t-T,t])\right)x(t).$$

Lee and Dullerud [45] used a similar construction to derive the following:

Theorem 1.3 ([45]). *An LPV system is exponentially stable for arbitrary time variations if and only if there exists a trajectory dependent quadratic Lyapunov function of the form*

$$V(x,t) = x^T X\left(\theta([t-T,t])\right)x.$$

In discrete time, Lee and Dullerud [45] uses this result to derive a numerical search for Lyapunov functions. Regarding the previous discussion on complexity, this search may need to admit progressively longer intervals of trajectory dependence.

It turns out that one can eliminate the dependence on the parameter trajectory altogether. The intuition is as follows. From the Lyapunov function in Theorem 1.3, define

$$\bar{V}(x) = \inf_{\theta([t-T,t])} x^T X\left(\theta([t-T,t])\right)x.$$

In words, the new Lyapunov function is the former Lyapunov function evaluated at a “worst case trajectory” that is x -dependent. Again, an informal analysis illustrates that this parameter-independent Lyapunov function decreases along the solution of the LPV system for all parameter trajectories. This motivates the existence in general of a pseudo-quadratic Lyapunov function.

Molchanov and Pyatnitskiy [58] establish the following:

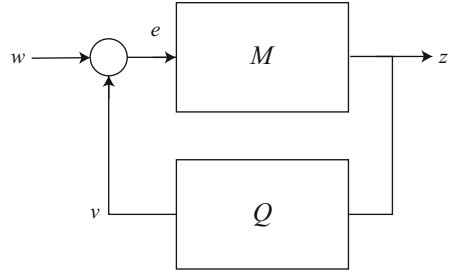
Theorem 1.4 ([58]). *An LPV system is exponentially stable for arbitrary time variations if and only if there exists a Lyapunov function of the form*

$$V(x) = x^T X(x)x$$

for some family of matrices $X(\cdot)$, with the property that $X(\alpha x) = X(x)$ for $\alpha \geq 0$.

For further discussion, see [56, 57] which go on to characterize alternative piecewise linear structures for exponentially stable LPV systems. See also the survey [17], monograph [18], and references therein.

Fig. 1.4 Block diagram for robust stability analysis



1.2.4 Robust Stability

Beyond basic stability in feedback control systems is the broader issue of robust stability. Robust stability concerns maintaining stability in the presence of possible modeling errors. Many questions of robust stability can be represented in the form of Fig. 1.4 (see [100]). The idea is that the stable system M is perturbed by feedback with an “error” dynamical system, Q . Nominally, $Q = 0$. Robust stability asks whether feedback with Q leads to a closed-loop stable configuration for all $Q \in \mathbf{Q}$, where \mathbf{Q} defines a class of admissible perturbations. The following discussion presents two approaches to this issue: slowly varying operators and small-gain conditions.

1.2.4.1 Slowly Varying Operators

One could anticipate that the previous discussion on slowly varying systems could be applicable to robust stability analysis as well. One issue is that the analysis was restricted to ordinary differential equations, and particularly, finite dimensional systems, whereas a model perturbation, Q , may be infinite dimensional (e.g., time-delay).

Daleh et al. [29, 80, 98] develop slowly varying approach for classes of infinite dimensional systems. Shamma and Athans [80] assumes an LPV system in the forward loop and a convolution operator in the feedback loop, resulting in a so-called Volterra integrodifferential equation:

$$\dot{x}(t) = A(\theta(t))x(t) + \int_0^t B(\theta(t))q(t - \tau)C(\theta(\tau))x(\tau) d\tau.$$

Daleh et al. [29, 98] do not make explicit connection to LPV systems, and so the presentation here is an adaptation. Let M denote the parameter dependent input/output operator (cf., [31]),

$$z(t) = \sum_{\tau=0}^t m(t - \tau, \theta(t))e(\tau).$$

This can be viewed as a collection of convolution kernels, indexed by θ . Likewise, D is defined by

$$v(t) = \sum_{\tau=0}^t q(t-\tau, \theta(t))z(\tau).$$

One can show that if θ is slowly varying, then these input/output operators are also slowly varying according to a notion defined in [29].

These works make an additional assumption, namely, that the feedback configuration with constant θ has some added margin of stability (compare to $\lambda > 0$ in the finite dimensional case). The main result in both [80] and [29] is that, assuming the added margin of stability in the constant parameter case, stability is preserved under sufficiently slow parameter variations.

1.2.4.2 Small-Gain Condition

A well-known result for robust stability analysis is the small-gain theorem [31]. While small-gain theorems are applicable to a broad class of dynamical systems, the presentation here focuses on the linear, and in particular, LPV case.

First, define the induced norm of an LPV system as follows. Let M denote the operator relationship between u and y characterized by the LPV system (1.1) under zero initial conditions (also denoted by $M \sim \{A(\theta), B(\theta), C(\theta)\}$). Now define⁶

$$\|M\|_{i,2} = \sup_{\theta(\cdot) \in \mathcal{Q}} \sup_u \frac{\|y\|_2}{\|u\|_2}.$$

The following is an LPV generalization of the bounded real lemma (e.g., [23]).

Proposition 1.2. *Let $X : \mathbf{R}^p \rightarrow \mathbf{R}^{n \times n}$ be symmetric positive definite, differentiable, and satisfy*

$$\sum_{i=1}^p \dot{\theta}_i \frac{\partial X}{\partial \theta_i}(\theta) + X(\theta)A(\theta) + A^T(\theta)X(\theta) + X(\theta)B(\theta)B^T(\theta)X(\theta) + C^T(\theta)C(\theta) < 0$$

or equivalently

$$\begin{pmatrix} \left(\sum_{i=1}^p \dot{\theta}_i \frac{\partial X}{\partial \theta_i}(\theta) + X(\theta)A(\theta) + A^T(\theta)X(\theta) \right) & X(\theta)B(\theta) & C^T(\theta) \\ B^T(\theta)X(\theta) & -I & 0 \\ C(\theta) & 0 & -I \end{pmatrix} < 0$$

for all $\theta(\cdot) \in \mathcal{Q}$ and $\theta \in \Theta_c \subset \mathbf{R}^p$. Then $M \sim \{A(\theta), B(\theta), C(\theta)\}$ satisfies

$$\|M\|_{i,2} < 1.$$

⁶For $f : \mathbf{R} \rightarrow \mathbf{R}^n$, $\|f\|_2 = \left(\int_0^\infty f^T(t)f(t) dt \right)^{1/2}$.

A simple proof of the first statement is to use the above matrix equation and positive definiteness of $X(\cdot)$ to verify that

$$\frac{d}{dt} \left(x^T(t) X(\theta(t)) x(t) \right) < u^T(t) u(t) - y^T(t) y(t).$$

Integrating this inequality gives the desired result. The equivalent second statement stems from an application of Schur complement arguments.

Proposition 1.2 coupled with the standard small-gain theorem provides a numerical approach to robust stability analysis for LPV systems.

Theorem 1.5. *Let $M \sim \{A(\theta), B(\theta), C(\theta)\}$ satisfy the hypotheses of Proposition 1.2. Then the feedback configuration of Fig. 1.4 is stable for all Q satisfying $\|Q\|_{i,2} \leq 1$.*

The appeal of this approach is the opportunity to incorporate algorithms for linear matrix inequalities [22, 23] to verify numerically the conditions of Proposition 1.2 (cf., forthcoming section on control design).

1.3 LPV Control Design

The following sections review selected approaches to LPV control design, namely, (1) LMI methods, (2) stable realizations, and (3) set-invariance methods.

1.3.1 Linear Matrix Inequality Methods

There have been several developments contributing to LMI methods for LPV control design. First is the development of LMI-based analysis (and synthesis) methods for LTI systems (e.g., [21]). Second is the generalization of these results to LPV systems (e.g., the previous discussion on robust stability and induced norms). Third is the broad availability of advanced convex optimization software (e.g., `cvx`⁷).

The following steps summarize the general idea in LMI methods for LPV systems:

- *Step 1:* Derive a (in general, sufficient) analysis condition for a desired closed-loop property.
- *Step 2:* Evaluate this condition on the closed-loop LPV system (plant and controller in feedback).
- *Step 3:* Transform the search for control parameters into a convex search.
- *Step 4:* If the convex search is successful, extract controller parameters.

⁷<http://cvxr.com/cvx/>.

The following presentation illustrates these steps for the basic problem of stabilization.

Step 1: The following is a slight generalization of Proposition 1.1.

Proposition 1.3. *Let $X : \mathbf{R}^p \rightarrow \mathbf{R}^{n \times n}$ be symmetric positive definite, differentiable, and satisfy*

$$\sum_{i=1}^p \dot{\theta}_i \frac{\partial X}{\partial \theta_i}(\theta) + X(\theta)A(\theta) + A^T(\theta)X(\theta) < 0 \quad (1.10)$$

for all $\theta(\cdot) \in \mathcal{Q}$ and $\theta \in \theta_c \subset \mathbf{R}^p$. Then the LPV system

$$\dot{x} = A(\theta)x$$

is stable.

Step 2: Now consider designing a state feedback $u = F(\theta)x$. Applying Proposition 1.3 to the closed-loop dynamics results in

$$\sum_{i=1}^p \dot{\theta}_i \frac{\partial X}{\partial \theta_i}(\theta) + X(\theta)(A(\theta) + B(\theta)F(\theta)) + (A(\theta) + B(\theta)F(\theta))^T X(\theta) < 0, \quad (1.11)$$

where $X(\theta) = X^T(\theta) > 0$ and $F(\theta)$ are to be determined.

Step 3: The condition (1.11) in Proposition 1.3 involves a search for $X(\cdot)$ and feedback matrix $F(\cdot)$. Because of the product term, the set of $X(\cdot)$ and $F(\cdot)$ satisfying (1.11) is not convex. To remedy this issue, let

$$Y(\theta) = X^{-1}(\theta) \quad \text{and} \quad G(\theta) = F(\theta)X^{-1}(\theta),$$

and multiply (1.11) on the left and right by the symmetric $Y(\theta)$ (which does not change the definiteness). This leads to

$$\sum_{i=1}^p \dot{\theta}_i \frac{\partial Y}{\partial \theta_i}(\theta) + A(\theta)Y(\theta) + B(\theta)G(\theta) + Y(\theta)A^T(\theta) + G^T(\theta)B^T(\theta) < 0. \quad (1.12)$$

Note that (1.12) imposes a convex constraint on $Y(\cdot)$ and $G(\cdot)$. Accordingly, one can use convex optimization to assess the feasibility of (1.12) and construct a suitable solution if possible. Note that an actual implementation would require a discretization of the space of parameter values, Θ_c .

Step 4: Reconstruct the controller feedback matrix as

$$F(\theta) = G(\theta)Y^{-1}(\theta).$$

There have been considerable advances beyond stabilization, particularly for LPV disturbance rejection and induced norm minimization. The starting point (for *Step 1*) is the induced norm condition for LPV systems, as in Proposition 1.2. A representative sampling of this area includes [1, 2, 8, 11, 59, 61, 70, 96, 97]. See also the review in [66].

1.3.2 Stable Realization

Initial research in LPV control design focused on constant parameter stability and performance, and issues of parameter variations and the impact on stability were analyzed after the fact. In research that followed, the possibility of parameter variations was recognized in the control design process and sufficient conditions for stability were included as part of the controller construction. As a consequence, the prospect of time variations limited the constant parameter designs. A middle ground is the following challenge: design for constant parameter performance with guaranteed varying parameter stability. Recent work [19] exploits a thus far neglected degree of freedom to meet this challenge. This degree of freedom is in the *realization* of the controller. The following proposition illustrates this concept:

Proposition 1.4 ([19]). *Let $M \sim \{A(\theta), B(\theta), C(\theta)\}$ where $A(\theta)$ is Hurwitz for all $\theta \in \Theta_c$. There exists an $M' \sim \{A'(\theta), B'(\theta), C'(\theta)\}$ that is stable for arbitrary parameter variations and satisfies*

$$C(\theta)(sI - A(\theta))^{-1}B(\theta) = C'(\theta)(sI - A'(\theta))^{-1}B'(\theta)$$

for all (constant) $\theta \in \Theta_c$.

It is important to note that M and M' are *not* the same LPV system. Rather, they are two equivalent realizations for constant values of θ , but they have different dynamic behaviors for varying trajectories.

A derivation is as follows. The stability condition on $A(\theta)$ implies the existence of a symmetric positive definite parameter dependent $X(\theta)$ such that

$$X(\theta)A(\theta) + A(\theta)^T X(\theta) < 0.$$

Let $X(\theta) = R^T(\theta)R(\theta)$ and define

$$A'(\theta) = R(\theta)A(\theta)R^{-1}(\theta), \quad B'(\theta) = R(\theta)B(\theta), \quad \text{and} \quad C'(\theta) = C(\theta)R^{-1}(\theta).$$

By construction, the resulting realization of M' satisfies the quadratic stability condition of Proposition 1.1.

Of course, this degree of freedom only can be applied to the controller. Blanchini et al. [19] combine this idea with stable parametrization methods from [39] to derive

the following result. First, define an LPV system $P \sim \{A(\theta), B(\theta), C(\theta)\}$ to be *LPV-stabilizable* if there exists an LPV controller $K \sim \{A_K(\theta), B_K(\theta), C_K(\theta), D_K(\theta)\}$ such that the (closed-loop) LPV system

$$\begin{aligned}\dot{x} &= A(\theta)x + B(\theta)(C_K(\theta)z + D_K(\theta)C(\theta)x) \\ \dot{z} &= A_K(\theta)z + B_K(\theta)C(\theta)x\end{aligned}$$

is stable for arbitrary parameter variations. Blanchini et al. [19] provide conditions for stabilizability, but the verification of these conditions (and, accordingly, controller construction) is subject to the aforementioned complexity concerns.

Theorem 1.6 ([19]). *Assume*

- $P \sim \{A(\theta), B(\theta), C(\theta)\}$ is LPV-stabilizable.
- $K \sim \{F(\theta), G(\theta), H(\theta)\}$ stabilizes P for all constant parameter values.

Then there exists a $K' \sim \{F'(\theta), G'(\theta), H'(\theta)\}$ that stabilizes P for arbitrary parameter variations and furthermore satisfies

$$H(\theta)(sI - F(\theta))^{-1}G(\theta) = H'(\theta)(sI - F'(\theta))^{-1}G'(\theta)$$

for all $\theta \in \Theta_c$.

Thus, K' realizes the same controller as K for constant parameter values, but assures closed-loop stability for arbitrary parameter variations. Note that K and K' need not have the same order (the derivation is more involved than applying Proposition 1.4).

1.3.3 Set-Invariance Methods

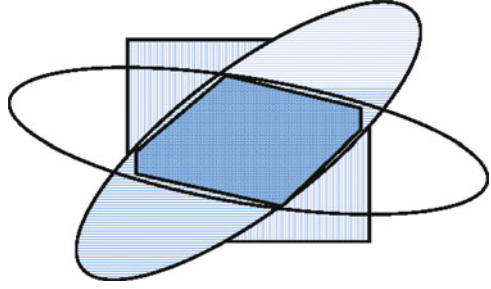
As previously discussed, LPV stability need not be characterized by quadratic Lyapunov functions, but rather convex functions, which can be approximated as piecewise linear or piecewise quadratic. This recognition recalls prior work on constructive approaches to stability analysis and control design for classes of uncertain system [14, 24, 25, 72]. See also the survey [17], monograph [18], and references therein. This section reviews such set-invariance methods specialized to constructing nonlinear controllers for LPV systems. The presentation here follows [84] as well as [77, 83].

The framework for this section is discrete-time LPV systems as follows:

$$x(t+1) = A(\theta(t))x(t) + B(\theta(t))u(t) + Ld(t). \quad (1.13)$$

A few comments regarding this setup are: (1) The discussion herein concerns state feedback, and so there is no output equation. (2) The dynamics have an explicit disturbance term. (3) The set of parameter values, Θ_d , is finite and discrete.

Fig. 1.5 Illustration of controlled invariance algorithm (1.14)



(4) Arbitrary time variations are admissible. Regarding this final comment, Shamma and Xiong [84] also discuss the more general setup of constrained parameter variations (e.g., bounded rates).

1.3.3.1 Disturbance Rejection

The performance objective, termed “constrained regulation,” is as follows. Given a penalized output

$$z(t) = \begin{pmatrix} E x(t) \\ D u(t) \end{pmatrix}$$

maintain⁸

$$|z(t)|_{\infty} \leq 1, \quad t = 0, 1, 2, \dots$$

in the presence of all disturbance trajectories satisfying

$$|d(t)|_{\infty} \leq 1, \quad t = 0, 1, 2, \dots$$

The constrained regulation objective is to limit the effect of disturbances, d , on the penalized output, z , which includes weighted states and controls.

The set-invariance approach is to execute the following recursive algorithm:

$$S_0 = \{x \in \mathbf{R}^n : |E x|_{\infty} \leq 1\}, \quad (1.14a)$$

$$S_{j+1} = S_j \quad (1.14b)$$

$$\cap \{x : \exists u \text{ s.t. (1) } A(\theta)x + B(\theta)u + Ld \in S_j, \forall |d|_{\infty} \leq 1 \text{ and (2) } |Du|_{\infty} \leq 1\}. \quad (1.14c)$$

Note that variants of the algorithm described by (1.14) have emerged in a variety of settings, ranging from safety verification [37] to viability theory [5].

The above algorithm progressively prunes states for which a suitable disturbance could eventually violate the constrained regulation objective (illustrated in Fig. 1.5)

⁸For $|x|_{\infty} = \max_{1 \leq i \leq n} |x_i|$ for $x \in \mathbf{R}^n$.

regardless of the control law. The set S_0^c are all states that immediately violate the constrained regulation. The set S_1^c are all states that, for any selection of admissible controls, violate constrained regulation in one stage for a suitable disturbance/parameter trajectory combination. Likewise, S_j^c has similar interpretations for constrained violation after j stages.

Versions of the following theorem may be found in [16, 84].

Theorem 1.7. *Constrained regulation is achievable if and only if*

$$S_\infty = \bigcap_{j=0}^{\infty} S_j$$

is nonempty.

While the algorithm described by (1.14) conceptually decides the issue of constrained regulation, there remain lingering issues for implementing computations. Blanchini [16, 84] go on to discuss:

- Set representations and linear programming implementations
- Finite termination conditions for “almost” constrained regulation
- Controller computation and construction

A product of this construction—if constrained regulation is indeed achievable—is a piecewise linear function of the state that assures constrained regulation. In the case of constrained parameter evolution, the feedback law is also a function of the current parameter value [84].

1.3.3.2 NonQuadratic Cost Minimization

The set representation and linear programming implementations derived for constrained regulation are also applicable to nonquadratic cost minimization problems of the form:

$$\inf_{u(\cdot)} \sum_{t=0}^{\infty} |z(t)|_\infty$$

for the LPV system (1.13) without disturbances (i.e., $d \equiv 0$).

The setup is suitable for the application of dynamic programming, and in particular, value iteration [13] as described by the following recursive algorithm:

$$J_0(x) = |Ex|_\infty \tag{1.15a}$$

$$J_{k+1}(x) = \min_u \max_{\theta \in \Theta_d} \left(\left| \begin{pmatrix} Ex \\ Du \end{pmatrix} \right|_\infty + J_k(A(\theta)x + B(\theta)u) \right). \tag{1.15b}$$

Because of the underlying structure of LPV dynamics, these value functions are homogeneous (i.e., $J_k(\alpha x) = \alpha J_k(x)$), and can be represented in terms of level sets, e.g., $\{x : J_k(x) \leq 1\}$.

The remaining issues for executing value iteration (1.15b) parallel those for controlled invariance: representation, implementation, termination, and control computation. Shamma and Xiong [84] discuss these issues for LPV systems with either arbitrary or constrained trajectories.

Set theoretic methods have an appealing generality, and their ability to address constraints increases the appeal for application to nonlinear systems (e.g., [89]). Nonetheless, it should be noted that despite this appeal, the resulting (off-line) computations can be intensive for higher dimensional systems.

1.4 Final Remarks

This chapter has presented a brief overview of LPV systems, from their origins to a sampling of various approaches for analysis and control design. The presentation has not attempted to be comprehensive, and among the serious omissions is a discussion on system identification for LPV system (cf., the forthcoming collection [67]).

To conclude, it is very exciting⁹ to see the widespread adoption of the LPV paradigm since its introduction in 1988, as well as the continued interest reflected by short courses [71], special journal issues [50], and this (and future) monographs.

References

1. Apkarian P, Adams R (1998) Advanced gain-scheduling techniques for uncertain systems. *IEEE Trans Contr Syst Technol* 6(1):21–32
2. Apkarian P, Gahinet P (1995) A convex characterization of gain-scheduled \mathcal{H}_∞ controllers. *IEEE Trans Autom Contr* AC-40(5):853–864
3. Apkarian P, Gahinet P, Biannic JM (1995) Self-scheduled \mathcal{H}_∞ control of a missile via linear matrix inequalities. *AIAA J Guid Contr Dynam* 18(3):532–538
4. Astrom K, Wittenmark B (1995) *Adaptive control*. Addison-Wesley, Reading, MA
5. Aubin J (1991) *Viability theory*. Birkhäuser, Boston
6. Balas G (2002) Linear parameter-varying control and its application to a turbofan engine. *Int J Robust Nonlin Contr* 12(9):763–796
7. Balas G, Fialho I (2002) Road adaptive active suspension design using linear parameter-varying gain scheduling. *IEEE Trans Contr Syst Technol* 10(1):43–54
8. Balas G, Fialho I, Lee L, Nalbantoglu V, Packard A, Tan W, Wemhoff E, Wolodkin G, Wu F (1997a) Theory and application of linear parameter varying control techniques, Workshop Notes: American Control Conference
9. Balas G, Fialho I, Packard A, Renfrow J, Mullaney C (1997b) On the design of LPV controllers for the F-14 aircraft lateral-directional axis during powered approach. In: *Proceedings of the American Control Conference*, pp 123–127
10. Barker J, Balas G (2000) Comparing linear parameter-varying gain-scheduled control techniques for active flutter suppression. *J Guid Navigation Contr* 23(5):948–955

⁹and personally gratifying.

11. Becker G, Packard A (1994) Robust performance of linear parametrically varying systems using parametrically-dependent linear feedback. *Syst Contr Lett* 23:205–215
12. Becker G, Packard A, Philbrick D, Balas G (1993) Control of parametrically-dependent linear systems: a single quadratic Lyapunov approach. In: *Proceedings of the American Control Conference*, pp 2795–2799
13. Bertsekas D (1995) *Dynamic programming and optimal control*. Athena Scientific, Belmont, MA
14. Bertsekas D, Rhodes I (1971) On the minimax reachability of target sets and target tubes. *Automatica* 7:233–247
15. Bianchi F, Mantz R, Christiansen C (2005) Gain scheduling control of variable-speed wind energy conversion systems using quasi-LPV models. *Contr Eng Practice* 13(2):247–255
16. Blanchini F (1995) Nonquadratic Lyapunov functions for robust control. *Automatica* 31(3):451–462
17. Blanchini F (1999) Set invariance in control—a survey. *Automatica* 35(11):1747–1767
18. Blanchini F, Miani S (2008) *Set-theoretic methods in control*. Birkhäuser Boston, Boston, MA, USA
19. Blanchini F, Casagrande D, Miani S, Viaro U (2010) Stable LPV realization of parametric transfer functions and its application to gain-scheduling control design. *IEEE Trans Autom Contr* 55(10):2271–2281
20. Blondel V, Tsitsiklis J (2000) The boundedness of all products of a pair of matrices is undecidable. *Syst Contr Lett* 41:135–140
21. Boyd S, Barratt C (1991) *Linear controller design—Limits of performance*. Prentice-Hall, Englewood Cliffs, NJ, USA
22. Boyd S, Vandenberghe L (2004) *Convex optimization*. Cambridge University Press, Cambridge, United Kingdom
23. Boyd S, Ghaoui LE, Feron E, Balakrishnan V (1994) *Linear matrix inequalities in system and control theory*. SIAM, Philadelphia
24. Brayton R, Tong C (1979) Stability of dynamical systems: a constructive approach. *IEEE Trans Circ Syst CAS-26*(4):224–234
25. Brayton R, Tong C (1980) Constructive stability and asymptotic stability of dynamical systems. *IEEE Trans Circ Syst CAS-27*(11):1121–1130
26. Bruzelius F, Breitholtz C, Pettersson S (2002) LPV-based gain scheduling technique applied to a turbo fan engine model. In: *Proceedings of the 2002 International Conference on Control Applications*, pp 713–718
27. Carter L, Shamma J (1996) Gain-scheduled bank-to-turn autopilot design using linear parameter varying transformations. *AIAA J Guid Contr Dynam* 19(5):1056–1063
28. Costa O, Fragoso M, Marques R (2005) *Discrete-time Markov jump linear systems*. London
29. Dahleh M, Dahleh M (1991) On slowly time-varying systems. *Automatica* 27(1):201–205
30. Dayawansa W, Martin C (1999) A converse Lyapunov theorem for a class of dynamical systems which undergo switching. *IEEE Trans Autom Contr* 44(4):751–760
31. Desoer C, Vidyasagar M (1975) *Feedback systems: input–output properties*. Academic Press, New York
32. Francis B, Glover K (1978) Bounded peaking in the optimal linear regulator with cheap control. *IEEE Trans Autom Contr* 23(4):608–617
33. Freudenberg J, Looze D (1985) Right half plane poles and zeros and design tradeoffs in feedback systems. *IEEE Trans Autom Contr* 30(6):555–565
34. Ganguli S, Marcos A, Balas G (2002) Reconfigurable LPV control design for Boeing 747-100/200 longitudinal axis. In: *Proceedings of the American Control Conference*, pp 3612–3617
35. Gaspar P, Szasi I, Bokor J (2004) The design of a combined control structure to prevent the rollover of heavy vehicles. *Euro J Contr* 10(2):148–162
36. Gilbert W, Henrion D, Bernussou J, Boyer D (2010) Polynomial LPV synthesis applied to turbofan engines. *Contr Eng Pract* 18(9):1077–1083

37. Guéguen H, Lefebvre MA, Zaytoon J, Nasri O (2009) Safety verification and reachability analysis for hybrid systems. *Annu Rev Contr* 33(1):25–36
38. He B, Yang M (2006) Robust LPV control of diesel auxiliary power unit for series hybrid electric vehicles. *IEEE Trans Power Electr* 21(3):791–798
39. Hespanha JP, Morse AS (2002) Switching between stabilizing controllers. *Automatica* 38(11):1905–1917
40. Jadbabaie A, Hauser J (2002) Control of a thrust-vectoring flying wing: a receding horizon—LPV approach. *Int J Robust Nonlin Contr* 12:869–896
41. Krause J, Kumar K (1986) An alternative stability analysis framework for adaptive control. *Syst Contr Lett* 7(1):19–24
42. Kwakernaak H, Sivan R (1972) *Linear optimal control systems*. Wiley-Interscience, New York
43. Lau E, Krener A (1999) Lpv control of two dimensional wing flutter. In: *Proceedings of the 38th IEEE Conference on Decision and Control*, pp 3005–3010
44. Lawrence D, Rugh W (1995) Gain scheduling dynamic linear controllers for a nonlinear plant. *Automatica* 31(3):381–390
45. Lee JW, Dullerud G (2006) Uniform stabilization of discrete-time switched and Markovian jump linear systems. *Automatica* 42:205–218
46. Leith D, Leithead W (2000) Survey of gain-scheduling analysis and design. *Int J Contr* 73(11):1001–1025
47. Lescher F, Zhao J, Borne P (2006) Switching LPV controllers for a variable speed pitch regulated wind turbine. In: *IMACS Multiconference on Computational Engineering in Systems Applications*, pp 1334–1340
48. Liberzon D, Morse A (1999) Basic problems in stability and design of switched systems. *IEEE Contr Syst Mag* 19(5):59–70
49. Lin H, Beck C, Bloom M (2008) Multivariable LPV control of anesthesia delivery during surgery. In: *Proceedings of the 2008 American Control Conference*, pp 825–831
50. Lovera M, Novara C, dos Santos P, Rivera D (2011) Guest editorial special issue on applied LPV modeling and identification. *IEEE Trans Contr Syst Technol* 19(1):1–4
51. Lu B, Wu F, Kim SW (2006) Switching LPV control of an F-16 aircraft via controller state reset. *IEEE Trans Contr Syst Technol* 14(2):267–277
52. Lu B, Choi H, Buckner G, Tammi K (2008) Linear parameter-varying techniques for control of a magnetic bearing system. *Contr Eng Practice* 16(10):1161–1173
53. Marcus L, Yamabe H (1960) Global stability criteria for differential systems. *Osaka Math J* 12:305–317
54. Mehendale C, Fialho I, Grigoriadis K (2009) A linear parameter-varying framework for adaptive active microgravity isolation. *J Vib Contr* 15:773–800
55. Mercère G, Palsson H, Poinot T (2011) Continuous-time linear parameter-varying identification of a cross flow heat exchanger: a local approach. *IEEE Trans Contr Syst Technol* 19(1):64–76
56. Molchanov A, Pyatnitskii E (1986a) Lyapunov functions that specify necessary and sufficient conditions of absolute stability of nonlinear nonstationary control systems I. *Automat Rem Contr* 47:344–354
57. Molchanov A, Pyatnitskii E (1986b) Lyapunov functions that specify necessary and sufficient conditions of absolute stability of nonlinear nonstationary control systems II. *Automat Rem Contr* 47:443–451
58. Molchanov A, Pyatnitskiy Y (1989) Criteria of asymptotic stability of differential and difference inclusions encountered in control theory. *Syst Contr Lett* 13:59–64
59. Packard A (1994) Gain-scheduling via linear fractional transformations. *Syst Contr Lett* 22:79–92
60. Packard A, Becker G (1992) Quadratic stabilization of parametrically-dependent linear systems using parametrically-dependent linear, dynamic feedback. In: *Advances in Robust and Nonlinear Control Systems*, vol DCS-Vol. 43, ASME Winter Annual Meeting, pp 29–36

61. Packard A, Kantner M (1996) Gain scheduling the LPV way. In: Proceedings of the 35th IEEE Conference on Decision and Control, pp 3938–3941
62. Papageorgiou G, Glover K, D’Mello G, Patel Y (2000) Taking robust LPV control into flight on the VAAC harrier. In: Proceedings of the 39th IEEE Conference on Decision and Control, pp 4558–4564
63. Peña R, Ghersin A (2010) LPV control of glucose for diabetes type I. In: 2010 Annual International Conference of the IEEE Engineering in Medicine and Biology Society, pp 680–683
64. Poussot-Vassal C, Sename O, Dugard L, PGáspar, Szabó Z, Bokor J (2008) A new semi-active suspension control strategy through LPV technique. *Contr Eng Pract* 6(12):1519–1534
65. Rugh W (1991) Analytical framework for gain-scheduling. *IEEE Contr Syst Mag* 11(1):79–84
66. Rugh W, Shamma J (2000) A survey of research on gain scheduling. *Automatica* 36:1401–1425
67. dos Santos P, Perdicoulis T, Novara C (eds) (2011) *Linear Parameter-Varying System Identification: New Developments and Trends*. World Scientific Publishing Company. Hackensack, NJ, USA
68. dos Santos P, et al (2011b) An LPV modeling and identification approach to leakage detection in high pressure natural gas transportation networks. *IEEE Trans Contr Syst Technol* 19(1):77–92
69. van der Schaft A, Schumacher JM (1999) *An introduction to hybrid dynamical systems*. Springer, London
70. Scherer C, Gahinet P, Chilali M (1997) Multiobjective output-feedback control via LMI optimization. *IEEE Trans Automat Contr* AC-42(7):896–911
71. Scherer C, Heuberger P, (organizers) (2006) *Dutch institute of systems and control summer school on identification and control of LPV systems*. Veldhoven, The Netherlands
72. Schweppe F (1973) *Uncertain dynamic systems*. Prentice-Hall, Englewood Cliffs, NJ
73. Seron M, Braslavsky J, Goodwin G (1997) *Fundamental limitations in filtering and control*. Springer-Verlag, London
74. Shamma J (1988) *Analysis and design of gain scheduled control systems*. PhD thesis, Massachusetts Institute of Technology, Department of Mechanical Engineering, advised by M. Athans
75. Shamma J (1991) Performance limitations in sensitivity reduction for nonlinear plants. *Syst Contr Lett* 17:43–47
76. Shamma J (1996a) Linearization and gain-scheduling. In: Levine W (ed) *The Control Handbook*, CRC Press, Inc., Boca Raton, FL, pp 388–398
77. Shamma J (1996b) Optimization of the l_∞ -induced norm under full state feedback. *IEEE Trans Autom Contr* AC-41(4):533–544
78. Shamma J (1999) Gain-scheduling. In: Webster J (ed) *Encyclopedia of electrical and electronics engineering*, John Wiley & Sons, New York
79. Shamma J, Athans M (1990) Analysis of nonlinear gain scheduled control systems. *IEEE Trans Autom Contr* AC-35(8):898–907
80. Shamma J, Athans M (1991) Guaranteed properties of gain scheduled control of linear parameter-varying plants. *Automatica* 27(3):898–907
81. Shamma J, Athans M (1992) Gain scheduling: potential hazards and possible remedies. *IEEE Contr Syst Mag* 12(3):101–107
82. Shamma J, Cloutier J (1993) Gain-scheduled missile autopilot design using linear parameter varying transformations. *AIAA J Guid Contr Dynam* 16(2):256–264
83. Shamma J, Xiong D (1997) Linear non-quadratic optimal control. *IEEE Trans Automat Contr* AC-42(6):875–879
84. Shamma J, Xiong D (1999) Set-valued methods for linear parameter varying systems. *Automatica* 35:1081–1089

85. Shu-qing L, Sheng-xiu Z (2010) A modified LPV modeling technique for turbofan engine control system. In: 2010 International Conference on Computer Applications and System Modeling (ICCSM), pp V5-99–V5-102
86. Tan W, Packard A, Balas G (2000) Quasi-LPV modeling and LPV control of a generic missile. In: Proceedings of the 2000 American Control Conference, pp 3892–2696
87. Toker O (1997) On the complexity of the robust stability problem for linear parameter varying systems. *Automatica* 33(11):2015–2017
88. Tsitsiklis J, Blondel V (1997) The Lyapunov exponent and joint spectral radius of pairs of matrices are hard—when not impossible—to compute and to approximate. *Math Contr Signals Syst* 10:31–40
89. Tu KH, Shamma J (1998) Nonlinear gain-scheduled control design using set-valued methods. In: Proceedings of the 1998 American Control Conference, pp 1195–1199
90. Wassink M, van de Wal M, Scherer C, Bosgra O (2005) LPV control for a wafer stage: beyond the theoretical solution. *Contr Eng Pract* 13(2):231–245
91. Wei X, del Re L (2007) Gain scheduled h_∞ control for air path systems of engines using LPV techniques. *IEEE Trans Contr Syst Tech* 15(3):406–415
92. Willems J (1971) *The Analysis of Feedback Systems*. MIT Press, Cambridge, MA
93. van Wingerden JW, Gebraad P, Verhaegen M (2010) LPV identification of an aeroelastic flutter model. In: Proceedings of the 49th IEEE Conference on Decision and Control, pp 6839–6844
94. Witte J, Balini H, Scherer C (2010) Robust and LPV control of an amb system. In: Proceedings of the American Control Conference, pp 2194–2199
95. Wu F (2001) Switching LPV control design for magnetic bearing systems. In: Proceedings of the 2001 IEEE International Conference on Control Applications (CCA '01), pp 41–46
96. Wu F, Yang X, Packard A, Becker G (1996) Induced \mathcal{L}_2 -norm control for LPV systems with bounded parameter variation rates. *Int J Contr* 6(9/10):983–998
97. Yu J, Sideris A (1997) \mathcal{H}_∞ control with parametric Lyapunov functions. *Syst Contr Lett* 30:57–69
98. Zames G, Wang L (1991) Local global algebras for slow \mathcal{H}_∞ adaptation: part I inversion and stability. *IEEE Trans Autom Contr* 36(2):130–142
99. Zhang F, Grigoriadis K, Franchek M (2007) Linear parameter-varying lean burn air-fuel ratio control for a spark ignition engine. *J Dyn Syst Meas Contr* 129(4):404–414
100. Zhou K, Doyle J, Glover K (1996) *Robust and optimal control*. Prentice-Hall, Inc., Upper Saddle River, NJ

Chapter 2

Prediction-Error Identification of LPV Systems: Present and Beyond

Roland Tóth, Peter S.C. Heuberger, and Paul M.J. Van den Hof

Abstract The proposed chapter aims at presenting a unified framework of prediction-error based identification of LPV systems using freshly developed theoretical results. Recently, these methods have got a considerable attention as they have certain advantages in terms of computational complexity, optimality in the stochastic sense and available theoretical tools to analyze estimation errors like bias, variance, etc., and the understanding of consistency and convergence. Beside the introduction of the theoretical tools and the prediction-error framework itself, the scope of the chapter includes a detailed investigation of the LPV extension of the classical model structures like ARX, ARMAX, Box–Jenkins, OE, FIR, and series expansion models, like orthonormal basis functions based structures, together with their available estimation approaches including linear regression, nonlinear optimization, and iterative IV methods. Questions of model structure selection and experimental design are also investigated. In this way, the chapter provides a detailed overview about the state-of-the-art of LPV prediction-error identification giving the reader an easy guide to find the right tools of his LPV identification problems.

2.1 Introduction

To design efficient *linear parameter-varying* (LPV) controllers, it is has a paramount importance to have an accurate but at the same time low-complexity LPV model of the underlying behavior of the system at hand. In engineering, it is common to use *first-principle laws* of physics, chemistry, biology, etc., to construct dynamic

R. Tóth (✉) • P.S.C. Heuberger • P.M.J. Van den Hof
Delft Center for Systems and Control, Delft University of Technology, Mekelweg 2,
2628 CD, Delft, The Netherlands
e-mail: r.toth@tudelft.nl; p.s.c.heuberger@tudelft.nl; p.m.j.vandenhof@tudelft.nl

models. However, such a procedure requires a detailed process knowledge from specialists. To assemble the existing knowledge into a coherent and compact mathematical description is not only a challenging task but it usually results in a too complex model as it is hard to distinguish relevant effects from negligible terms. The selection of the *scheduling variable* itself is also often restricted by the way of model construction and likely different choices follow from linearization-based or direct conversion based methods, see [15, 19, 23]. Therefore, modeling is often found to be very laborious and expensive. If the specialist's knowledge is lacking, like in case of poorly understood systems, the derivation of a model from first principles is even impossible. Moreover, certain quantities, like coefficients, rates, etc., required for the model, are likely unknown and have to be estimated by performing dedicated experiments.

Descriptions of systems can alternatively be derived by *system identification* (ID), where the estimation of a dynamical model is accomplished directly from measured input–output data. The *expert's knowledge* still has a major role, as it gives the basic source of information in decisions on parametrization, model-structure selection, experiment design, and the actual way of deriving the estimate. This knowledge also helps in judging the quality and applicability of the obtained models. Even if system identification requires human intervention and expert's knowledge to arrive at appropriate models, it also gives a general framework in which most of the steps can be automated, providing a less laborious and cost intensive modeling process.

In the current literature, many LPV identification approaches have been developed using model structures that are formulated in terms of *state-space* (SS) and *linear-fractional representations* (LFR), e.g., [7, 18, 22, 33, 34], *input–output* (IO) representations, e.g., [1, 3, 11, 36], or *series-expansion* forms, e.g., [23, 27, 28]. Most of the existing approaches use a discrete-time setting and commonly assume *static* dependence on the scheduling variable $p : \mathbb{Z} \rightarrow \mathbb{P}$, with $\mathbb{P} \subseteq \mathbb{R}^m$. Here, static dependence means dependence of the model coefficients only on the instantaneous value of p . For a recent overview of the available methods, see [4, 23].

Recently, LPV–IO model structures based methods have got a considerable attention as they appear to have certain advantages w.r.t. other identification approaches of the field. One of the major benefits is that identification of this representation-based model structures can be addressed via the extension of the LTI *prediction-error* (PE) framework [23, 25]. In opposition with other approaches, this enables the stochastic analysis of the estimates, treatment of general noise models [13, 25], experimental design [6, 12, 36], model structure selection, and direct identification of the involved dependencies [11, 30, 31] often in a computationally attractive manner and also in continuous time [14]. Moreover, in this setting it is also relatively easy to identify models with *dynamic dependence* (dependence of the coefficients on time shifted instances of p), which is often required for high accuracy identification of nonlinear systems (see [23]). However, the main stream LPV control-synthesis approaches are based on models defined in an SS or an LFR form, hence the delivered IO model needs to be converted to such representation forms. Due to the fact that multiplication with any time operator is not commutative over

the p -dependent coefficients, the existing realization theory is more complicated than in the LTI case and often introduces rational dynamic dependence on p in the resulting state-minimal SS forms [26, 32]. It is possible to avoid this phenomenon by aiming at minimal realization in terms of the involved dependency as well, which often requires either auxiliary state variables or special parametrization of the polynomial forms [24]. Improving SS realization of IO models in terms of finding the state basis that provide the simplest scheduling dependence and minimal state dimension is in the focus of current research activities in this area.

In this chapter, we give an overview about the state-of-the-art of LPV prediction-error identification. In particular, we focus on what is feasible by the available approaches, what the practical advantages are, and what developments are still needed. Due to the broad scope of the topic, we will address here only the discrete-time case.

The chapter is organized as follows: First in Sect. 2.2, the concept of LPV series expansion representations is introduced which makes it possible to formulate predictors and model manipulations later on. Next in Sect. 2.3, the basic setting of the LPV prediction-error framework is defined with the concept of the data-generating system, noise models, and one-step-ahead predictors. A general structure of parameterized models and the perspective of estimation in the ℓ_2 -optimal prediction-error sense, identifiability of model structures and informativity of datasets are also studied. Then in Sect. 2.4, the LPV extension of the classical model structures is introduced and their properties are analyzed. This is followed in Sect. 2.5 by a detailed investigation of the available estimation approaches w.r.t. these models in terms of linear regression, nonlinear optimization and iterative instrumental variable methods and their stochastic properties.

2.2 LPV Series-Expansion Representations

In the LTI case, many key concepts and model manipulations in the PE framework are based on a transfer function representation of the dynamic behavior (see [16]). One of the major problems which has so far prevented the analysis of the PE methods in the LPV case has been the lack of a transfer function representation of LPV systems which expresses signal relations in the frequency domain. To illustrate the problem, consider the classical LPV filter form of discrete-time IO representations, often defined in the *single-input single-output* (SISO)¹ case as:

$$\sum_{i=0}^{n_a} a_i(p(k))q^{-i}y(k) = \sum_{j=0}^{n_b} b_j(p(k))q^{-j}u(k), \quad (2.1)$$

¹LPV-IO representations can also be defined for *multiple-input multiple-output* (MIMO) systems in a similar form as (2.1), see [23].

where $u : \mathbb{Z} \rightarrow \mathbb{R}$ is the input, $y : \mathbb{Z} \rightarrow \mathbb{R}$ is the output, and $p : \mathbb{Z} \rightarrow \mathbb{P}$ is the scheduling variable of the LPV system \mathcal{S} represented by (2.1); q is the (forward) time-shift operator, i.e., $q^{-1}u(k) = u(k-1)$, $n_a, n_b \geq 0$ and $a_i : \mathbb{P} \rightarrow \mathbb{R}$ and $b_j : \mathbb{P} \rightarrow \mathbb{R}$ are functions of $p(k)$ (instantaneous value of p) which is called *static dependence*. The functions a_i and b_j can have arbitrary complexity ranging from simple linear to rational or real *meromorphic*² dependence. To guarantee well-posedness of (2.1), it is often assumed that all a_i and b_j are bounded on \mathbb{P} .

In identification, we aim to estimate a dynamical model of the system based on measured data, which corresponds to the estimation of each a_i and b_j in (2.1). To formulate estimation of these functions, it is attractive to introduce

$$A(q^{-1}, p(k)) = \sum_{i=0}^{n_a} a_i(p(k))q^{-i} \quad \text{and} \quad B(q^{-1}, p(k)) = \sum_{j=0}^{n_b} b_j(p(k))q^{-j}$$

as polynomials in q^{-1} with varying coefficients $a_i(p(k))$ and $b_j(p(k))$ and, inspired by the LTI system theory, to write

$$y(k) = F(q^{-1}, p(k))u(k) \quad \text{with} \quad F(q^{-1}, p(k)) = \frac{B(q^{-1}, p(k))}{A(q^{-1}, p(k))}. \quad (2.2)$$

However, $F(q^{-1}, p(k))$ in (2.2) relates to a transfer function if and only if $p(k)$ is a constant signal, i.e., $p(k) = p$ for all k , where $p \in \mathbb{P}$. This is justified by the fact that if q is substituted with the complex z variable, then $F(z^{-1}, p(k))$ is a mixed frequency–time relationship. If $Y(z)$ and $U(z)$ denote the Z -transform of the signals u and y on an appropriate region of convergence, then $Y(z) = F(z^{-1}, p(k))U(z)$ has a meaning if and only if p , associated with (u, y) , is a constant (not-varying with time). Furthermore, $F(q^{-1}, p(k))$ is ill-defined also as an operator because multiplication with q^{-1} is not commutative over time-dependent coefficients such as $b_j(p(k))$, i.e., $q^{-1}b_j(p(k)) = b_j(p(k-1))q^{-1}$. Therefore, multiplication from the left or right has different meaning. In (2.2), it is ambiguous whether left or right multiplication is intended to derive this rational operator form. Currently no theoretical framework is available (to the author’s knowledge) to handle rational time-operator forms with time-dependent coefficients (such a framework does exist in case of constant coefficients, i.e., in the LTI case, see [37]).

To overcome this “representation” problem, it has been shown in [23] that the dynamic mapping between u and y can be characterized as a convolution involving p and u . This so-called *impulse response representation* (IRR) is given as

$$y(k) = \sum_{i=0}^{\infty} (g_i \diamond p)(k)u(k-i) = \left(\sum_{i=0}^{\infty} (g_i \diamond p)q^{-i}u \right)(k) = ((G(q) \diamond p)u)(k), \quad (2.3)$$

² $h : \mathbb{R}^n \rightarrow \mathbb{R}$ is a real meromorphic function if $h = f/g$ with f, g analytic and $g \neq 0$.

where the so-called *impulse response coefficients* g_i are functions of $p(k)$ and of multiple, but finite many, time-shifted instances of p , like $g_i(p(k + \tau_1), \dots, p(k - \tau_2))$ with $\tau_1, \tau_2 \geq 0$. This is called *dynamic dependence*. To express such a broad range of dependencies conveniently, we apply the operator $\diamond: (\mathcal{R}, \mathbb{P}^{\mathbb{Z}}) \rightarrow \mathbb{R}_{\infty}^{\mathbb{Z}}$, where \mathcal{R} is the set of all real meromorphic functions with finite dimensional domain, such that $(g_i \diamond p)(k) = g_i(p(k + \tau_1), \dots, p(k - \tau_2))$. Note that in the sequel, we will use \diamond to express dynamic or general dependence like $(g_i \diamond p)(k)$ whenever it is needed and we will use $g_i(p(k))$ to express if a coefficient has only static dependence. For an illustration, consider the following example.

Example 2.1. Given an asymptotically stable discrete-time LPV–IO representation:

$$y = -0.1 p q^{-1} y - 0.2 q^{-2} y + \sin(p) q^{-1} u, \quad (2.4)$$

with $\mathbb{P} = [0, 1]$. By recursive substitution for $q^{-1}y, q^{-2}y, \dots$, the following IRR, equivalent with (2.4), results

$$\begin{aligned} y = & \underbrace{\sin(p)}_{g_1 \diamond p} q^{-1} u + \underbrace{(-0.1 p \sin(q^{-1} p))}_{g_2 \diamond p} q^{-2} u \\ & + \underbrace{(0.01 p (q^{-1} p) - 0.2) \sin(q^{-2} p)}_{g_3 \diamond p} q^{-3} u + \dots, \end{aligned}$$

where the sequence of functions $g_i \diamond p$ converges to zero as $i \rightarrow \infty$.

Equation (2.3) can be considered as a series expansion of \mathcal{S} in terms of q^{-i} which is convergent if \mathcal{S} is asymptotically stable. Furthermore, (2.3) can be seen as the generalization of LPV–SS and LPV–IO representations with appropriate equivalence transformations available (see [23]).

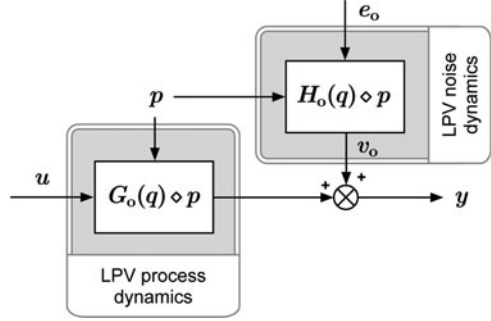
2.3 An LPV Prediction-Error Framework

By using the LPV impulse response representation, established in the previous section, it becomes possible to extend the classical PE framework to the LPV case allowing sophisticated analysis of the estimation of LPV–IO models. To do so, we will first define the concept of an LPV data-generating system. This will be followed by deriving a one-step-ahead predictor for the observed output sequence that we will use to formulate the estimation of parametrized models under a mean-squared prediction-error criterion.

2.3.1 Data-Generating System

According to the classical PE setting, the *data-generating system* is considered as a discrete-time deterministic filter G_o whose output is influenced by a stochastic

Fig. 2.1 LPV concept of the data-generating system



noise process v_o in an additive manner (see Fig. 2.1). It is assumed that v_o is a *quasi-stationary* noise process with a bounded *power spectral density* $\Phi_{v_o}(\omega)$. In case G_o is linear, it is possible to lump many different sources of disturbances in v_o , such as noise-corrupted actuation, uncontrollable inputs, process noise, etc., because, under minor restrictions, all these effects can be propagated through G_o . In the LTI case, this suggests that for many systems it is valid to assume that $\Phi_{v_o}(\omega)$ is a rational function, i.e., that v_o can be represented as a filtered zero-mean white noise process.

Using this concept, a data-generating LPV system \mathcal{S}_o can be analogously formulated as

$$y(k) = (G_o(q) \diamond p)(k) u(k) + v_o(k), \quad (2.5)$$

where the process part is represented by an LPV impulse response form

$$G_o(q) \diamond p = \sum_{i=0}^{\infty} (g_i^o \diamond p) q^{-i}, \quad (2.6)$$

with g_i being bounded w.r.t. every $p \in \mathcal{P}$, where $\mathcal{P} \subseteq \mathbb{P}^{\mathbb{Z}}$ denotes all possible trajectories of p that are allowed during the operation of the system. In order to guarantee that (2.6) is convergent, it is a necessary assumption that G_o under \mathcal{P} represents an asymptotically stable LPV system. Additionally, it is assumed that the disturbance v_o can be described as

$$v_o(k) = (H_o(q) \diamond p)(k) e_o(k), \quad (2.7)$$

where H_o is a convergent LPV-IRR, i.e., it corresponds to an asymptotically stable LPV filter, it is monic, i.e., $H_o(\infty) = 1$, and $e_o(k)$ is a zero-mean white noise process. Similar to the LTI case, asymptotic stability of H_o in the deterministic sense is a necessary assumption of the PE setting (see [16]), otherwise $\Phi_{v_o}(\omega)$ would not be bounded yielding that ID of $G_o(q)$ is an ill-posed problem. Furthermore, it is important to point out that in terms of (2.7), $\mathbb{E}\{v_o(k)\} = 0$ for each k , where \mathbb{E} denotes the expectation operator, but the autocorrelation of v_o , i.e., $R_{v_o, v_o}(k, \tau) = \mathbb{E}\{v_o(k)v_o(k - \tau)\}$, is time-dependent. However in the asymptotic

sense, $\lim_{N \rightarrow \infty} \frac{1}{N} \sum_{k=1}^N R_{v_o, v_o}(k, \tau)$ exists for a given p and for all $\tau \in \mathbb{Z}$ due to the convergence properties of $H_o(q)$ and the independence of p from e_o . Hence v_o qualifies as a quasi-stationary signal (see [25] for the detailed proof).

2.3.2 One-Step-Ahead Prediction of v_o

In order to formulate the estimation of parametrized LPV models of (2.5) in a prediction-error setting, it is necessary to derive a predictor of y . The simplest case is to characterize a *one-step-ahead predictor* of y , for which it is essential to clarify how we can predict $v_o(k)$ at a given time-step k if we have observed $v_o(\tau)$ for $\tau \leq k-1$. In terms of (2.7):

$$v_o(k) = (h_0^o \diamond p)(k) e_o(k) + \sum_{i=1}^{\infty} (h_i^o \diamond p)(k) e_o(k-i), \quad (2.8)$$

meaning that $\{v_o(\tau)\}_{\tau \leq k-1}$ and a given trajectory of p defines $\{e_o(\tau)\}_{\tau \leq k-1}$. Note that if each h_i^o depends only on the current and the backward-time-shifted values of p , e.g., $p(k), p(k-1), p(k-2)$, etc., which is called *causal dynamic dependence*, then only the knowledge of $\{p(\tau)\}_{\tau \leq k}$ and $\{v_o(\tau)\}_{\tau \leq k-1}$ is sufficient to characterize $\{e_o(\tau)\}_{\tau \leq k-1}$. In case the noise process has an LPV-IO representation in terms of (2.7) with only static p -dependence, then the equivalent IRR form (2.8) is guaranteed to have only causal dependence [23]. In most practical applications, causal dynamic dependence on p is quite realistic.

To follow the classical concept of defining the prediction of $v_o(k)$, assume that observations of $e_o^{(k-1)} = \{e_o(\tau)\}_{\tau \leq k-1}$ and $p^{(k)} = \{p(\tau)\}_{\tau \leq k}$ are given. Under this information set, our objective is to compute the one-step-ahead prediction of $v_o(k)$ w.r.t. the ℓ_2 -loss:

$$\hat{v}_o(k|k-1) = \arg \min_{\delta \in \mathbb{R}} \mathbb{E} \left\{ \|v_o(k) - \delta\|_{\ell_2}^2 \mid e_o^{(k-1)}, p^{(k)} \right\}. \quad (2.9)$$

In [23, 25] it is shown that if $p^{(k)}$ is fully known, then (2.9) is equal to

$$\hat{v}_o(k|k-1) = \sum_{i=1}^{\infty} (h_i^o \diamond p)(k) e_o(k-i). \quad (2.10)$$

It easily follows that (2.9) also minimizes the mean-squared error of the prediction. Of course it is not practical to assume that $e_o^{(k-1)}$ is known. To formulate prediction of $v_o(k)$ in terms of observation of $v_o^{(k-1)} = \{v_o(\tau)\}_{\tau \leq k-1}$, it is required that H_o has a stable inverse, i.e., there exists a monic convergent LPV-IRR denoted as H_o^\dagger such that $(H_o^\dagger(q)H_o(q)) \diamond p = 1$. Note that if such a H_o^\dagger exists, then it is a bi-lateral inverse

of H , i.e., $H_0^\dagger(q)H_0(q) = H_0(q)H_0^\dagger(q) = 1$, which can be shown based on telescopic sums, see [25]. This implies that

$$e_o(k) = (H_0^\dagger(q) \diamond p)(k) v_o(k). \quad (2.11)$$

Then using (2.11), we can write (2.10) as

$$\hat{v}_o(k|k-1) = ((H_0(q) - 1) \diamond p)(k) e_o(k) = (1 - H_0^\dagger(q) \diamond p)(k) v_o(k), \quad (2.12)$$

which is the LPV form of the classical one-step-ahead predictor result [16].

2.3.3 One-Step-Ahead Prediction of v_o with Noisy p

In the previous derivation, it was essential that full, i.e., noise-free observation of the sequence $p^{(k)}$ is available, which we will call the “ p -true case”. In the LPV literature, such an assumption is generally taken as a technical necessity regardless of the used identification setting (see [6, 7, 12, 18, 22, 33, 34, 36], exceptions: [3, 5]) and the resulting methods based on it are almost exclusively applied in practical situations where measurements of p are polluted by noise with various stochastic properties. The reason for this theoretical gap lies in the difficulty to establish a conditional expectation of $v_o(k)$ in the situation when instead of $p(k)$ only observations of

$$p_*(k) = p(k) + w_o(k), \quad (2.13)$$

with $w_o(k)$ is an iid noise process, are available as each h_i^o can be a nonlinear function with dynamic dependence on p . For systems with simple dependencies, formulation of $\hat{v}_o(k|k-1)$ is possible but no general formula can be given based on the current results (see [3] for an analysis of consistency for LPV *autoregressive with exogenous input* (ARX) models under stochastic p). It has been only recently shown that a general approach to formulate the one-step-ahead predictor in case of noisy observations of $p(k)$ can be derived from moment-generating functions of the underlying distribution of $w_o(k)$ [25]. Furthermore, a parametrized noise model to capturing nonwhite noise on p can also be applied. However, currently the stochastic properties of the estimated models are not well understood in that case. For the sake of simplicity and coherence of our overview, we will restrict our attention to the p -true case and investigate estimation under such an assumption.

2.3.4 One-Step-Ahead Prediction of y

As a next step, we need to formulate the one-step-ahead predictor of $y(k)$ to address identification of a parametrized model in terms of minimizing the prediction error,

i.e., the difference between $y(k)$ and the predicted model output, which is the primary goal in the PE setting. Consider the p -true case with $y^{(k-1)} = \{y(\tau)\}_{\tau \leq k-1}$, $u^{(k)} = \{u(\tau)\}_{\tau \leq k}$, and $p^{(k)} = \{p(\tau)\}_{\tau \leq k}$ (in case of causal dependence). Since (2.5) implies that

$$v_o(k) = y(k) - \sum_{i=0}^{\infty} (g_i^o \diamond p)(k) u(k-i), \quad (2.14)$$

$v_o(\tau)$ is characterized for $\tau \leq k-1$ w.r.t. the information set $(u^{(k)}, p^{(k)}, y^{(k-1)})$. Based on (2.12), it is not complicated to show that under the given information set, the one-step-ahead prediction of $y(k)$ w.r.t. the ℓ_2 loss is

$$\hat{y}(k|k-1) = ((H_o^\dagger(q)G_o(q)) \diamond p)(k) u(k) + (1 - H_o^\dagger(q) \diamond p)(k) y(k). \quad (2.15)$$

This corresponds to the LPV form of the classical result of the LTI case (see [16]). Note that in a similar manner, k -step-ahead predictors can also be formulated in this setting. For a detailed proof, see [23, 25].

2.3.5 Parametrized Models and Estimation

Now, introduce an LPV parametrized model in the form of

$$(G(q, \theta_g), H(q, \theta_h)), \quad (2.16)$$

where $G(q, \theta_g)$ and $H(q, \theta_h)$ are the IRRs of the process part, denoted as \mathcal{G}_{θ_g} , and the noise part, denoted as \mathcal{H}_{θ_h} , of the model structure, respectively, and $\theta_g \in \Theta_g \subseteq \mathbb{R}^{n_g}$ with $\theta_h \in \Theta_h \subseteq \mathbb{R}^{n_h}$ are the parameters to be estimated. Note that these parameters are not necessarily associated with the parametrization of impulse response coefficients directly, but can correspond to the parametrization of the coefficients of the process and noise models given in an SS or IO form. Then these parametrized structures are represented by the IRRs: G and H . Also introduce $\theta = \text{col}(\theta_g, \theta_h) \in \Theta \subseteq \mathbb{R}^{n_\theta}$, the vector of independent parameters in θ_g and θ_h .

Denote $\mathcal{G} = \{\mathcal{G}_{\theta_g} \mid \theta_g \in \Theta_g\}$ and $\mathcal{H} = \{\mathcal{H}_{\theta_h} \mid \theta_h \in \Theta_h\}$ the collection of all process and noise models with the considered parametrization and similarly denote the overall parametrized model (2.16) as \mathcal{M}_θ . Then, based on the model structure \mathcal{M}_θ , the model set, denoted as \mathcal{M} , takes the form

$$\mathcal{M} = \{ (\mathcal{G}_{\theta_g}, \mathcal{H}_{\theta_h}) \mid \theta = \text{col}(\theta_g, \theta_h) \in \Theta \}. \quad (2.17)$$

This set corresponds to the set of candidate models in which we seek the model that explains data gathered from \mathcal{S}_o the best, under a given criterion. We denote by $\mathcal{S}_o \in \mathcal{M}$, when the data-generating system is in the model set, i.e., $\exists \theta_o = \text{col}(\theta_{o,g}, \theta_{o,h}) \in \Theta$ such that $G_o(q) \diamond p = G(q, \theta_{o,g}) \diamond p$ and $H_o(q) \diamond p = H(q, \theta_{o,h}) \diamond p$.

With respect to (2.16), we can define the *one-step-ahead prediction error* as

$$e_\theta(k) = y(k) - \hat{y}(k | \theta, k-1), \quad (2.18)$$

where

$$\hat{y}(k | \theta, k-1) = (W_u(q, \theta) \diamond p)(k) u(k) + (W_y(q, \theta) \diamond p)(k) y(k). \quad (2.19)$$

is the one step-ahead predictor of the model output with *subpredictors*

$$W_u(q, \theta) = H^\dagger(q, \theta_g)G(q, \theta_h) \quad \text{and} \quad W_y(q, \theta) = 1 - H^\dagger(q, \theta_h) \quad (2.20)$$

according to (2.15). Denote a data sequence of \mathcal{S}_o by $\mathcal{D}_N = \{y(k), u(k), p(k)\}_{k=1}^N$. Then the basic philosophy of PE-based identification is to find θ w.r.t. a given parametrized model \mathcal{M}_θ with parameter space $\Theta \subseteq \mathbb{R}^{n_\theta}$ and a dataset \mathcal{D}_N such that the one-step-ahead predictor (2.19) associated with θ provides a prediction error e_θ which resembles a zero-mean white noise “as much as possible”.

Based on the predictor form (2.19), many different classical *identification criteria* can be applied to achieve this objective in terms of “minimization” of e_θ subject to θ . A particularly interesting choice is the *mean-squared prediction error* or more often called as the *least-squares* (LS) criterion:

$$V(\mathcal{D}_N, \theta) = \frac{1}{N} \sum_{k=1}^N e_\theta^2(k) = \frac{1}{N} \|e_\theta\|_{\ell_2}^2, \quad (2.21)$$

such that the parameter estimate is

$$\hat{\theta} = \underset{\theta \in \Theta}{\operatorname{argmin}} V(\mathcal{D}_N, \theta). \quad (2.22)$$

Other criteria can also be used to characterize estimation of θ in (2.16) as a minimization of (2.18) w.r.t. a chosen measure (see [16]) or to introduce other objectives, e.g., minimization of the support of θ , or weights, like forgetting factors. However for sake of simplicity, we restrict the main stream of discussion to the classical LS case.

2.3.6 Identifiability and Informativity

To guarantee uniqueness of (2.22), one condition is that \mathcal{M}_θ is *globally identifiable*.

Definition 2.1 (Identifiability, based on [8]). The model structure \mathcal{M}_θ , defined by (2.16) with a parameter domain $\Theta \subseteq \mathbb{R}^{n_\theta}$, is called locally identifiable at a $\theta_1 \in \Theta$, if $\exists \delta > 0$ such that for all $\theta_2 \in \Theta$ in $\|\theta_1 - \theta_2\| \leq \delta$:

$$W_y(q, \theta_1) = W_y(q, \theta_2) \quad \text{and} \quad W_u(q, \theta_1) = W_u(q, \theta_2) \quad \Rightarrow \quad \theta_1 = \theta_2. \quad (2.23)$$

The model structure is said globally identifiable at θ_1 if the same holds for arbitrary large δ . It is called globally identifiable if it is globally identifiable at all $\theta_1 \in \Theta$.

Another condition for uniqueness (2.22) is the *informativity* of the data set \mathcal{D}_N .

Definition 2.2 (Informative data, based on [8]). For a model structure \mathcal{M}_θ , defined by (2.16) with a parameter domain $\Theta \subseteq \mathbb{R}^{n_\theta}$, a quasi-stationary data set $\mathcal{D}_N = \{u(k), y(k), p(k)\}_{k=1}^N$ is called informative, if for any $\theta_1, \theta_2 \in \Theta$

$$\begin{aligned} & \bar{\mathbb{E}}\{(W_y(q, \theta_1) \diamond p)y - (W_y(q, \theta_2) \diamond p)y + (W_u(q, \theta_1) \diamond p)u \\ & \quad - (W_u(q, \theta_2) \diamond p)u\}^2 = 0, \end{aligned} \quad (2.24)$$

with $\bar{\mathbb{E}}$ being the generalized expectation operator,³ implies that

$$W_y(q, \theta_1) = W_y(q, \theta_2) \quad \text{and} \quad W_u(q, \theta_1) = W_u(q, \theta_2). \quad (2.25)$$

In terms of these definitions, if the model set is globally identifiable (no two different parameters θ_1 and θ_2 give rise to the same predictor) and the data set \mathcal{D}_N is informative, then $V(\theta, \mathcal{D}_N)$ has a global optimum in the statistical sense.

2.3.7 Consistency and Convergence

When applying the quadratic ID criterion (2.21), the asymptotic properties of the resulting parameter estimate can be analyzed in the situation when $N \rightarrow \infty$, similarly as in the LTI case. Consider the following definitions of consistency and convergence.

Definition 2.3 (Convergence). For an informative data set \mathcal{D}_N and model structure \mathcal{M}_θ , the parameter estimate $\hat{\theta}$ is called convergent if $N \rightarrow \infty$ implies that $\hat{\theta} \rightarrow \theta^*$ with probability one, i.e., $P(\hat{\theta} = \theta^*) = 1$, where $\theta^* = \arg \min_\theta \bar{\mathbb{E}}\{e_\theta^2\}$.

Note that convergence implies that the asymptotic parameter estimate is independent of the particular noise realization in the data sequence and \mathcal{M}_θ is locally identifiable at θ^* .

Definition 2.4 (Consistency). For model structure \mathcal{M}_θ with model set \mathcal{M} and a data set \mathcal{D}_N which is informative w.r.t. \mathcal{M}_θ , a convergent parameter estimate $\hat{\theta} \rightarrow \theta^*$ is called consistent if either of the following conditions holds:

- If $\mathcal{S}_o \in \mathcal{M}$, then $G_o(q) = G(q, \theta_g^*)$ and $H_o(q) = H(q, \theta_h^*)$.
- If $\mathcal{S}_o \notin \mathcal{M}$ but $\mathcal{S}_o \in \mathcal{G}$, then $G_o(q) = G(q, \theta_g^*)$.

We will investigate these properties w.r.t. the particular identification approaches we consider in Sect. 2.5.

³The notation $\bar{\mathbb{E}}\{x\} = \lim_{N \rightarrow \infty} \frac{1}{N} \sum_{k=1}^N \mathbb{E}\{x(k)\}$ is adopted from the prediction-error framework of [16].

2.4 Classical Model Structures

Next we can investigate how the classical model structures can be formulated in the introduced LPV–PE setting. To follow the classical formulations, we will construct both the process and the noise components using an LPV–IO representation form. For the sake of simplicity, we treat these model structures such that their coefficients have only static dependence on p . Extension of these definitions using coefficients with dynamic dependence follows naturally.

2.4.1 Process Model

Consider the parametrized model \mathcal{M}_θ , where the process part \mathcal{G}_{θ_g} , whose IRR is given by $G(q, \theta_g)$, is defined by

$$A(q^{-1}, p(k), \theta_g) \check{y}(k) = B(q^{-1}, p(k), \theta_g) q^{-\tau_d} u(k). \quad (2.26)$$

Here \check{y} is the noise-free output of the process part, $\tau_d \geq 0$ is the input delay and the p -dependent polynomials

$$\begin{aligned} A(q^{-1}, p(k), \theta_g) &= 1 + \sum_{i=1}^{n_a} a_i(p(k), \theta_g) q^{-i}, \\ B(q^{-1}, p(k), \theta_g) &= \sum_{j=0}^{n_b} b_j(p(k), \theta_g) q^{-j}, \end{aligned}$$

with $n_a, n_b, \tau_d \geq 0$, are parametrized as:

$$a_i(p(k), \theta_g) = \sum_{l=0}^{n_\alpha} a_{i,l} \alpha_{i,l}(p(k)), \quad b_j(p(k), \theta_g) = \sum_{l=0}^{n_\beta} b_{j,l} \beta_{j,l}(p(k)), \quad (2.27)$$

with $\alpha_{i,0}(\cdot) = \beta_{j,0}(\cdot) = 1$. In this particular parametrization, which is called *linear parametrization*, $\{\alpha_{i,l}\}_{i=1, l=1}^{n_a, n_\alpha}$ and $\{\beta_{j,l}\}_{j=0, l=1}^{n_b, n_\beta}$ are priori given functions (chosen by the user) which are bounded on \mathbb{P} and

$$\theta_g = [a_{1,0} \cdots a_{n_a, n_\alpha} \ b_{0,0} \cdots b_{n_b, n_\beta}]^\top \in \Theta_g \subseteq \mathbb{R}^{n_g},$$

with $n_g = n_a(n_\alpha + 1) + (n_b + 1)(n_\beta + 1)$, represents the unknown parameters to be estimated for the process part. Note that parametrizations other than (2.27) are possible; however, the advantage of (2.27) is that a large number of functional depen-

dencies can be represented, based on the choice of $\{\alpha_{i,l}\}_{i=1,l=1}^{n_a,n_\alpha}$ and $\{\beta_{j,l}\}_{j=0,l=1}^{n_b,n_\beta}$, and it is linear in θ_g . Additionally for the structure (2.26) with static coefficient dependence, the impulse response coefficients $(g_i \diamond p)(k)$ have only causal dynamic dependence on p [23]. A particular advantage of linear parametrization is that it not only reduces the complexity of the associated estimation problem but at the same time it also makes the adequate selection of the structural dependencies well posed [23]. In terms of (2.27), this selection problem translates to a search for a set of functions $\{\alpha_{i,l}\}_{i=1,l=1}^{n_a,n_\alpha}$ and $\{\beta_{j,l}\}_{j=0,l=1}^{n_b,n_\beta}$ such that the true p -dependent coefficients a_i^o and b_j^o , associated with the IO representation of the underlying system, satisfy $a_i^o \in \text{Span}(\{\alpha_{i,l}\}_{l=0}^{n_\alpha})$ and $b_j^o \in \text{Span}(\{\beta_{j,l}\}_{l=0}^{n_\beta})$. In case of a black-box scenario, the choice of these functions can be arbitrary. One can consider all $\alpha_{i,l}$ and $\beta_{j,l}$ to be rational functions or polynomials with a fixed degree and a fixed order of dynamic dependence. However, the number of possible choices is enormous. Including a too large set of functions can easily lead to over-parametrization, while restriction of $\alpha_{i,l}$ and $\beta_{j,l}$ to only a few basic functions can lead to serious structural bias. In order to assist the selection of an efficient set of functional dependencies in the parametrization of linear regression models, recently practically applicable approaches have been proposed in [11, 30, 31]. In [11] a *dispersion functions* based method while in [30] a *support vector machine* approach, both originating from the *machine learning* field, have been developed. These approaches aim to learning the underlying static or dynamic nonlinear dependence of the coefficients with great efficiency. In [31], a coefficient shrinkage method, the so-called *nonnegative garrote* (NNG) approach originating from statistics, has been introduced for this purpose. The NNG uses regularization in terms of weights to penalize individual elements of the parameter vector θ . In this way, the approach starts with a relatively large set of possible functional dependencies from which those functions that do not contribute significantly to the validity of the estimated model are eliminated by decreasing their weights.

2.4.2 Noise Model

The noise model \mathcal{H}_{θ_h} , whose IRR is given by $H(q, \theta_h)$, is defined as

$$C(q^{-1}, p(k), \theta_h) v(k) = D(q^{-1}, p(k), \theta_h) e(k), \quad (2.28)$$

where $e(k)$ is a zero-mean white noise process and the p -dependent polynomials C and D are defined similarly as A and B with order $n_c, n_d \geq 0$. These polynomials are also considered to be monic in the sense that $c_0(\bullet) = d_0(\bullet) = 1$ and to have linear parameterization in terms of the functions $\{\gamma_{i,l}\}_{i=1,l=1}^{n_c,n_\gamma}$, $\{\delta_{j,l}\}_{j=1,l=1}^{n_d,n_\delta}$ bounded on \mathbb{P} and parameters

$$\theta_h = [c_{1,0} \cdots c_{n_c, n_\gamma} \ d_{1,0} \cdots d_{n_d, n_\delta}] \in \Theta_h \subseteq \mathbb{R}^{n_h},$$

with $n_h = n_c(n_\gamma + 1) + n_d(n_\delta + 1)$, respectively. Furthermore, it is assumed that the IRR $H(q, \theta_h)$ of (2.28) has a stable inverse denoted as $H^\dagger(q, \theta_h)$ for all values of $\theta_h \in \Theta_h$. Note that (2.28) is able to express a large variety of different noise processes. It also includes LTI noise models which admit a polynomial description since for $n_\gamma = 0$ and $n_\delta = 0$, C and D correspond to polynomials with constant coefficients and hence $H(q, \theta_h)$ can also be expressed as a transfer function. Similar to the process part, static coefficient dependence of (2.28) implies that $H(q, \theta_h)$ has causal dynamic dependence.

2.4.3 Overall Model Structure

Finally, we can define the overall model structure in terms of (2.26) and (2.28). Let $\theta = \text{col}(\theta_g, \theta_h) \in \Theta_g \times \Theta_h \subseteq \mathbb{R}^{n_\theta}$ with $n_\theta = n_g + n_h$ in case the parametrizations of \mathcal{G}_{θ_g} and \mathcal{H}_{θ_h} are independent. Otherwise θ is constructed from θ_g and θ_h such that it contains only independent parameters. Then the signal relations of the overall parametrized model \mathcal{M}_θ are given as

$$A(q^{-1}, p(k), \theta_g) \check{y}(k) = B(q^{-1}, p(k), \theta_g) q^{-\tau_d} u(k), \quad (2.29a)$$

$$C(q^{-1}, p(k), \theta_h) v(k) = D(q^{-1}, p(k), \theta_h) e(k), \quad (2.29b)$$

$$y(k) = \check{y}(k) + v(k). \quad (2.29c)$$

Note that in this general model structure, we can distinguish specific cases which correspond to the classical model structures used in the LTI setting.

2.4.3.1 LPV-ARX and ARMAX structures

By considering $C(q^{-1}, p(k), \theta_h) \triangleq A(q^{-1}, p(k), \theta_g)$ and $D(q^{-1}, p(k), \theta_h) \triangleq 1$ in (2.29a–c), the LPV version of the so-called *autoregressive with exogenous input* (ARX) model structure results:

$$A(q^{-1}, p(k), \theta_g) y(k) = B(q^{-1}, p(k), \theta_g) q^{-\tau_d} u(k) + e(k), \quad (2.30)$$

with $\theta = \theta_g$. It is important to acknowledge here that w.r.t. (2.19):

$$\hat{y}(k | \theta, k-1) = \underbrace{B(q^{-1}, p(k), \theta_g) q^{-\tau_d} u(k)}_{(W_u(q, \theta) \diamond p)(k)} + \underbrace{1 - A(q^{-1}, p(k), \theta_g)}_{(W_y(q, \theta) \diamond p)(k)} y(k). \quad (2.31)$$

This means that if A and B are linearly parametrized then the predictor (2.19) (and hence (2.18)) is linear in θ , giving that the solution of (2.22) can be analytically computed (see Sect. 2.5.1.1). A particularly interesting feature of this structure in

the LPV case is that it explicitly assumes that v is correlated with p through the same nonlinearities as the noise-free output signal. Hence, it generally applies a more restrictive assumption on the noise than in the LTI case. This type of model structure is most commonly applied in LPV-ID approaches that are based on least-squares estimates (e.g., [1, 9, 35]).

An extension of this model structure can be achieved by introducing a *moving average* part on e , i.e., when $D(q^{-1}, p(k), \theta_h) \neq 1$. This significantly reduces the restrictiveness of the modeling assumption on the noise, but the price to be paid is that the predictor (2.19) is not linear in θ any more as

$$(W_u(q, \theta) \diamond p)(k) = \sum_{i=0}^{\infty} (1 - D(q^{-1}, p(k), \theta_h))^i B(q^{-1}, p(k), \theta_g) q^{-\tau_d}, \quad (2.32a)$$

$$(W_y(q, \theta) \diamond p)(k) = 1 - \sum_{i=0}^{\infty} (1 - D(q^{-1}, p(k), \theta_h))^i A(q^{-1}, p(k), \theta_g). \quad (2.32b)$$

Note that here the infinite sum term results due to the inversion of the scheduling dependent noise model. This term is convergent as H^\dagger is defined to be stable. Furthermore, due to noncommutativity of q in this setting, the polynomial terms do not commute, e.g., (2.32a) is not equal to $B(q^{-1}, p(k), \theta_g) q^{-\tau_d} \sum_{i=0}^{\infty} (1 - D(q^{-1}, p(k), \theta_h))^i$.

2.4.3.2 LPV-FIR and Series Expansion Structures

Considering the IRR form (2.6) of the process part of \mathcal{S}_o , a particularly interesting idea is to truncate this series expansion to get an approximation of the original system (2.5) in the following form:

$$y(k) \approx \sum_{i=0}^{n_f} (g_i^\circ \diamond p)(k) u(k-i) + v_o(k). \quad (2.33)$$

Note that if n_f is large enough, the approximation error is negligible in (2.33). This gives that by introducing a polynomial model structure⁴:

$$y(k) = \sum_{i=0}^{n_f} g_i(p(k), \theta_g) u(k-i) + v(k) = F(q^{-1}, p(k), \theta_g) u(k) + v(k), \quad (2.34)$$

where each coefficient g_i of the polynomial F is linearly parameterized in terms of the functions $\{\alpha_{i,l}\}_{i=0, l=1}^{n_f, n_\alpha}$ and parameters θ_g , a rather simple but effective approximation of the original system can be achieved. This model structure is

⁴It is more natural to use dynamic dependence in the parametrization of the coefficients in (2.34), but for the sake of simplicity we use only static dependence here.

the LPV form of the well-known LTI *finite impulse response* (FIR) models and has the attractive property of being *linear-in-the-coefficients* if $v(k)$ is a white noise, as in this case, its associated one-step-ahead predictor is $\hat{y}(k | \theta, k-1) = F(q^{-1}, p(k), \theta_g)u(k)$. Note that in the latter case, which corresponds to an *output-error* (OE) noise model, this model structure can also be derived from (2.29a–c) by setting A, B, C to 1 and $B(q^{-1}, p(k), \theta_g) \triangleq F(q^{-1}, p(k), \theta_g)$.

FIR models have many advantages in identification due to their simple structure. However, their well-known disadvantage, both in the LTI and the LPV cases, is that the expansion may have a slow convergence rate, meaning that it requires a relatively large number of parameters for an adequate approximation of the system. In order to benefit from the same properties, but achieve faster convergence rate of the expansion, it is attractive to use basis functions which, opposite to q^{-i} , have infinite impulse responses. A particular choice of such a basis follows through the use of *orthonormal basis functions* (OBFs), which are specific basis functions in \mathcal{H}_2 (*Hardy space* of square integrable complex functions) and have already proven their usefulness in LTI identification (see [10]). Based on this idea, it is possible to show that any asymptotically stable LPV system has a series expansion in terms of an OBF basis set $\{\phi_i(z)\}_{i=1}^{\infty} \subset \mathcal{H}_2$ (see [23]), via the expansion of each q^{-i} in (2.3) in terms of $\{\phi_i(q)\}_{i=1}^{\infty}$. Thus, (2.5) can be written as

$$y(k) = (w_0^0 \diamond p)(k)u(k) + \sum_{i=1}^{\infty} (w_i^0 \diamond p)(k)\phi_i(q)u + v_o(k), \quad (2.35)$$

where w_i^0 are functions with dynamic dependence on p . An obvious choice of model structure is to use a truncated expansion, i.e., truncating (2.35) to a finite sum in terms of $\{\phi_i\}_{i=1}^{n_w}$, and introducing a parametrization of the expansion coefficients:

$$y(k) = w_0(p(k), \theta_g)u(k) + \sum_{i=1}^{n_w} w_i(p(k), \theta_g)\phi_i(q)u + v(k), \quad (2.36)$$

where each w_i is parametrized as in the FIR case using functions with static dependence on p . Similar to the FIR, this structure is linear in the coefficients $\{w_i\}_{i=1}^{n_w}$ if $v(k)$ is assumed to be white, but with $n_w \ll n_f$ for the same approximation capability. Furthermore, it is proven that structures like (2.36), i.e., a OBF filter bank followed by a static nonlinearity are general approximators of nonlinear systems with fading memory, i.e., nonlinear dynamic systems with convolution representation [2]. Additionally, OBF and FIR models have a direct and simple SS and LFR realization, a somewhat unique property among polynomial IO structures [23]. An important question that arises is whether the basis functions ϕ_i can be chosen such that a fast convergence rate can be achieved for all possible trajectories of p , i.e., how $\{\phi_i(q)\}_{i=1}^{n_w}$ with minimal n_w should be chosen such that the approximation error is adequate for the problem at hand. For this purpose the Kolmogorov n -width theory gives an effective way to characterize optimal

convergence rate as an optimization problem in terms of the poles of the basis functions $\{\phi_i\}_{i=1}^{N_w}$ [28]. Using this concept, data-driven basis selection methods can be introduced to optimize the basis set w.r.t. to the dynamical behavior of the system at hand, see [23, 28] for further details.

2.4.3.3 LPV–BJ and OE Structures

Independent parametrization of \mathcal{G}_{θ_g} and \mathcal{H}_{θ_h} with the complete structure of (2.29a–c) corresponds to an LPV *Box–Jenkins* (BJ) model structure, which allows to describe a wide range of noise dynamics in a general sense. Of course this generality have a heavy price in terms of a complicated one-step-ahead predictor characterized by

$$\begin{aligned} (W_u(q, \theta) \diamond p)(k) &= \sum_{j=0}^{\infty} (1 - D(q^{-1}, p(k), \theta_h))^j C(q^{-1}, p(k), \theta_h) \\ &\quad \times \sum_{i=0}^{\infty} (1 - A(q^{-1}, p(k), \theta_g))^i B(q^{-1}, p(k), \theta_g) q^{-\tau_d}, \end{aligned} \quad (2.37a)$$

$$(W_y(q, \theta) \diamond p)(k) = 1 - \sum_{j=0}^{\infty} (1 - D(q^{-1}, p(k), \theta_h))^j C(q^{-1}, p(k), \theta_h). \quad (2.37b)$$

A simplification of this structure in terms of $C(q^{-1}, p(k), \theta_h) \triangleq D(q^{-1}, p(k), \theta_h) \triangleq 1$ leads to the so-called *output-error* (OE) type of model structure with

$$(W_u(q, \theta) \diamond p)(k) = \sum_{i=0}^{\infty} (1 - A(q^{-1}, p(k), \theta_g))^i B(q^{-1}, p(k), \theta_g) q^{-\tau_d}, \quad (2.38a)$$

$$(W_y(q, \theta) \diamond p)(k) = 1. \quad (2.38b)$$

Regarding LPV–BJ models an extra distinction can be introduced w.r.t. p -independent noise models. For instance, assuming $H(q, \theta_h)$ to be a rational LTI transfer function leads to a simplified LPV–BJ model for which a refined instrumental variable estimation approach has been developed recently (see [13]).

2.4.4 Informativity and Identifiability

Regarding the introduced model structures, we can investigate conditions under which informativity of a given data set and identifiability of a particular model structure itself can be assured. As these are the basic ingredients for a successful identification of the system, it is important to review the available results even if they are rather sparse.

For the case of LPV–ARX models with polynomial dependence of the coefficients on the parameters, conditions for identifiability and informativity have been studied in [6, 9, 36]. Based on these results, the following theorem holds true.

Theorem 2.1 (Identifiability, LPV–ARX case). *The LPV–ARX model structure (2.30) with linear parametrization (2.27) is globally identifiable, if and only if each set of functions $\{\alpha_{i,l}(\cdot)\}_{l=1}^{n_\alpha}$ and $\{\beta_{j,l}(\cdot)\}_{l=1}^{n_\beta}$ for all $i \in \{1, \dots, n_a\}$ and $j \in \{0, \dots, n_b\}$, used in the parametrization (2.27), are linearly independent on \mathbb{P} .*

For a detailed proof see [6]. Identifiability conditions for other model structures require linear independence (necessary condition) of the functions used in the parametrization of each p -dependent coefficient and also co-primeness of certain pairs of polynomials just like in the LTI case, see [8]. However, the sufficient conditions to guarantee identifiability in these cases have not been established yet.

To establish a condition on informativity in the ARX case, define

$$\Delta W_y(q) = W_y(q, \theta_1) - W_y(q, \theta_2), \quad \Delta W_u(q) = W_u(q, \theta_1) - W_u(q, \theta_2).$$

Then it follows that (2.24) equals to

$$\bar{\mathbb{E}} \left\{ \left([\Delta W_u(q) - \Delta W_y(q)G_o(q)] \diamond p \right) u + \left([\Delta W_y(q)H_o(q)] \diamond p \right) e \right\}^2 = 0. \quad (2.39)$$

Straightforward application of \mathbb{E} in $\bar{\mathbb{E}}$ gives that (2.39) is equivalent with

$$\bar{\mathbb{E}} \left\{ \left([\Delta W_u(q) - \Delta W_y(q)G_o(q)] \diamond p \right) u \right\}^2 = 0, \quad (2.40a)$$

$$\bar{\mathbb{E}} \left\{ \left([\Delta W_y(q)H_o(q)] \diamond p \right) e \right\}^2 = 0. \quad (2.40b)$$

Now we can seek for conditions on u and p for which the above conditions imply that $\Delta W_u(q) = \Delta W_y(q) = 0$. As p is independent of e , (2.40b) holds if and only if $\bar{\mathbb{E}}\{\Delta W_y(q) \diamond p\} = 0$ whenever $e \neq 0$. However, $\bar{\mathbb{E}}\{\Delta W_y(q) \diamond p\} = 0$ does not necessarily imply $\Delta W_y(q) = A(q^{-1}, p(k), \theta_1) - A(q^{-1}, p(k), \theta_2) = 0$. In case of global identifiability of \mathcal{M}_θ , the necessary and sufficient condition to guarantee this is that the data matrix $\Phi_y = [\varphi_y(1) \cdots \varphi_y(N)]^\top$ satisfies that $\bar{\mathbb{E}}\{\Phi_y^\top \Phi_y\} \succ 0$ where

$$\varphi_y(k) = [\alpha_{1,1}(p(k)) \cdots \alpha_{n_a, n_\alpha}(p(k))]^\top.$$

Next we need to find necessary and sufficient conditions on u and p such that

$$\bar{\mathbb{E}}\{(\Delta W_u(q) \diamond p)u\}^2 = 0 \quad \Rightarrow \quad \Delta W_u(q) = 0. \quad (2.41)$$

In case of an LPV–ARX model:

$$\Delta W_u(q) = B(q^{-1}, p(k), \theta_1) q^{-\tau_d} - B(q^{-1}, p(k), \theta_2) q^{-\tau_d}. \quad (2.42)$$

Assume that the LPV-ARX model is globally identifiable. Now in order to guarantee that (2.41) holds with (2.42), a necessary and sufficient condition is that $\Phi_u = [\varphi_u(1) \cdots \varphi_u(N)]^\top$ satisfies $\mathbb{E}\{\Phi_u^\top \Phi_u\} \succ 0$ where

$$\varphi_u(k) = \left[u(k - \tau_d) \quad \beta_{0,1}(p(k))u(k - \tau_d) \quad \cdots \quad \beta_{n_b, n_\beta}(p(k))u(k - \tau_d - n_b) \right]^\top.$$

Theorem 2.2 (Informative dataset, LPV-ARX case). *Given a globally identifiable LPV-ARX model structure (2.30), denoted by \mathcal{M}_θ , with linear parametrization (2.27), then a quasi-stationary data set \mathcal{D}_N generated by $\mathcal{S}_0 \in \mathcal{M}$ is informative w.r.t. \mathcal{M}_θ , if for $\Phi_u = [\varphi_u(1) \cdots \varphi_u(N)]^\top$ and $\Phi_y = [\varphi(1) \cdots \varphi(N)]^\top$ it holds that $\mathbb{E}\{\Phi_u^\top \Phi_u\} \succ 0$ and $\mathbb{E}\{\Phi_y^\top \Phi_y\} \succ 0$.*

Note that in case of a given data set \mathcal{D}_N with finite N , the above conditions translate to the existence of a set of time instances $\mathcal{K}_y, \mathcal{K}_u \subseteq \{1, \dots, N\}$ with $\text{Card}(\mathcal{K}_y) = n_a n_\alpha = n_y$ and $\text{Card}(\mathcal{K}_u) = (n_b + 1)(n_\beta + 1) = n_u$ such that $\Phi_y = [\varphi_y(k_1) \cdots \varphi_y(k_{n_y})]^\top$ with $\{k_1, \dots, k_{n_y}\} = \mathcal{K}_y$ and $\Phi_u = [\varphi_u(k_1) \cdots \varphi_u(k_{n_u})]^\top$ with $\{k_1, \dots, k_{n_u}\} = \mathcal{K}_u$ satisfy that $\Phi_u^\top \Phi_u \succ 0$ and $\Phi_y^\top \Phi_y \succ 0$. Note that these conditions are the minimal conditions which are required to be satisfied by the data set \mathcal{D}_N to guarantee informativity. It is also possible to formulate these conditions w.r.t. typical scheduling trajectories to derive easily understandable design rules. This has been investigated in [6] where the above conditions are interpreted in case of piecewise and periodic scheduling trajectories. Informativity conditions for other type of model structures are in the focus of current research.

2.5 Identification with the LS Criterion

Using the LS criterion (2.21), in this section we will investigate the estimation of the LPV model structures introduced in Sect. 2.4 with linear parametrization. According to the available approaches in the literature, identification of (2.29a-c) can be investigated from two perspectives: *local* setting (identification for constant p and interpolation) and the *global* setting (identification with varying p). Here we will concentrate on global approaches as only this setting allows to address the minimization of the prediction error e_θ which is our aim with the introduced PE framework. We will see that in the considered global PE setting, the predictor (2.19), w.r.t. each of the introduced model structures, can be rewritten as a linear or a pseudolinear regression. This yields that estimation of these structures is available via a (iterative) least-squares estimate. Alternatively, other nonlinear optimization schemes can also be applied in the absence of the linear-in-the-coefficients property of (2.19). Furthermore, we will explore identification with *instrumental variables* (IV) in this context as well, showing why such approaches can be rather advantageous in the LPV case. In addition, consistency and variance properties of the estimated parameters will be also investigated.

2.5.1 Prediction-Error Based Identification in the ARX Case

In terms of the considered global setting, we aim at the direct minimization of (2.21) in terms of the parametrized model structure (2.29a–c) using a dataset \mathcal{D}_N where p is varying. This data set is assumed to be informative w.r.t. (2.29a–c) to have a well-posed problem for identification. To fulfill our estimation objective, several approaches can be introduced for the various model structures given in Sect. 2.4. For the sake of clarity, we will study these estimation approaches step-by-step, starting from the most simplest case of ARX models where the estimation can be addressed via simple linear regression.

2.5.1.1 Linear Regression

Consider the LPV–ARX model structure (2.30). A particular property of this structure with the linear parametrization (2.27) of A and B is that the predictor (2.19) is linear in the parameters $\theta = \theta_g$, see (2.31), and hence can be written as

$$\hat{y}(k | \theta, k-1) = \varphi^\top(k) \theta, \quad (2.43)$$

where

$$\begin{aligned} \varphi(k) = & \left[-y(k-1) - \alpha_{1,1}(p(k))y(k-1) \quad \cdots \quad -\alpha_{n_a, n_a}(p(k))y(k-n_a) \right. \\ & \left. u(k-\tau_d) \quad \beta_{0,1}(p(k))u(k-\tau_d) \quad \cdots \quad \beta_{n_b, n_b}(p(k))u(k-\tau_d-n_b) \right]^\top. \end{aligned} \quad (2.44)$$

As (2.43) is a linear regression equation, thus by defining $\Phi = [\varphi(1) \cdots \varphi(N)]^\top$ and $Y = [y(0) \cdots y(N)]^\top$, the minimum of (2.21) is unique and equal to

$$\hat{\theta}_{LS} = \Phi^+ Y, \quad (2.45)$$

if $\text{rank}(\Phi) = n_\theta$, where $\Phi^+ = \left(\frac{1}{N} \Phi^\top \Phi\right)^{-1} \frac{1}{N} \Phi^\top$ is the regularized *Moore–Penrose pseudoinverse*. This approach is summarized in terms of Algorithm 1. Equation (2.45) has been used in many works, e.g., [1], to estimate LPV–IO models, however, in the introduced PE framework it is justified that (2.45) is the minimizer of (2.21) in case of an LPV–ARX model structure. It is also important to mention that (2.43) can be also considered as an LTI *multiple-output multiple-input* (MIMO) ARX model with “virtual” input and output signals $\{\beta_{j,l}(p)u\}$ and $\{\alpha_{i,l}(p)y\}$.

To get an insight of the stochastic behavior of the LS estimator (2.45), assume that $\mathcal{S}_0 \in \mathcal{G}$ and consider the “optimal” residual error e_{θ_0} , which based on (2.43) is

$$e_{\theta_0}(k) = y(k) - \hat{y}(k | \theta_0, k-1) = y(k) - \varphi^\top(k) \theta_0. \quad (2.46)$$

Algorithm 1: LPV-ARX identification, LS global method

-
- Require:** a data record $\mathcal{D}_N = \{u(k), y(k), p(k)\}_{k=1}^N$ of \mathcal{S}_0 , the LS identification criterion V , and the LPV-ARX model structure (2.30) with linear parametrization (2.27) and parameters $\theta = [a_{1,0} \cdots a_{n_a, n_a} \ b_{0,0} \cdots b_{n_b, n_b}] \in \mathbb{R}^{n_\theta}$. Assume that \mathcal{D}_N is informative w.r.t. (2.30) and (2.30) is globally identifiable.
- 1: calculate the signals $x_{i,l} = -\alpha_{i,l}(p)q^{-i}y$ and $x_{j+n_a+1,l} = \beta_{j,l}(p)q^{-j-\tau_d}u$ and let $\varphi = [x_{0,0} \cdots x_{n_a+n_b+1, n_b}]^\top$ giving that $y(k) = \varphi^\top(k)\theta + e_\theta(k)$.
 - 2: estimate θ in terms of $\hat{\theta} = \arg \min_{\theta} V(\theta, \mathcal{D}_N)$. In case of (2.21), $\hat{\theta} = \Phi^+ Y$ with $Y = [y^\top(1) \cdots y^\top(N)]^\top$ and $\Phi = [\varphi(1) \cdots \varphi(N)]^\top$.
 - 3: **return** estimated model (2.30).
-

As a consequence, (2.45) satisfies that

$$\hat{\theta}_{\text{LS}} = \theta_0 + \left(\sum_{k=1}^N \varphi(k) \varphi^\top(k) \right)^{-1} \cdot \sum_{k=1}^N \varphi(k) e_{\theta_0}(k). \quad (2.47)$$

Equation (2.47) yields that $\hat{\theta}_{\text{LS}}$ is a consistent estimate of θ_0 (unbiased for finite data) if the following conditions are respected:

$$\bar{\mathbb{E}} \left\{ \varphi(k) \varphi^\top(k) \right\} \succ 0 \quad \text{and} \quad \bar{\mathbb{E}} \left\{ \varphi(k) e_{\theta_0}(k) \right\} = 0. \quad (2.48)$$

While the first condition is satisfied in case \mathcal{D}_N is informative w.r.t. (2.30), the second condition only holds if e_{θ_0} is a white noise. Unfortunately, this is only true when the data-generating system \mathcal{S}_0 itself has an ARX noise structure. In that case, based on the classical proofs, it is possible to show that if the model set \mathcal{M} is uniformly asymptotically stable w.r.t. a compact Θ and it is globally identifiable, then under the assumption that the data set \mathcal{D}_N is informative and quasi-stationary, the estimates $\hat{\theta} \rightarrow \hat{\theta}_* = \arg \min_{\theta \in \Theta} \bar{\mathbb{E}} \{ \|e_\theta\|_{\ell_2}^2 \}$ with probability 1 where θ_* is unique [25]. Furthermore, if $\theta_0 = \theta_{0,g}$ associated with G_0 satisfies that $\theta_0 \in \Theta$, then $\theta_* = \theta_0$. This proves consistency and convergence of the estimation. In case of noisy observation of p , convergence of the LS estimates can be shown, but in general, consistency does not hold (see [3] for a motivation). It has been recently shown that this problem can be circumvented by using a regressor with estimated moment functions associated with p_* , see [25] for further details.

In practice, the ARX modeling assumption often appears to be rather restrictive. Even though it might be a fair assumption to consider that the process is well parametrized by (2.29a), the noise model $A(q^{-1}, p(k), \theta_g)v(k) = e(k)$ is often not rich enough to capture v_0 . Indeed, in most cases, there is no reasonable explanation to justify why the noise v_0 and the process part of \mathcal{S}_0 should contain the same dynamics and nonlinearities. In terms of estimation, this means that using the LS method in practice will most often lead to biased estimates. Consequently, some methods have been developed in order to cope with the error induced by this invalid assumption on the noise. A method proposed in [3] and relying on an instrumental variable approach is described in the next section.

2.5.1.2 Instrumental Variable Approach

The original aim of instrumental variable methods is to cope with the fact that in most cases, e_{θ_0} is a colored process. The idea is to introduce an instrument $\zeta : \mathbb{Z} \rightarrow \mathbb{R}^{n_\theta}$ which is used to produce a consistent estimate independently on the noise model taken. The IV estimate is given as

$$\hat{\theta}_{\text{IV}} = \left(\sum_{k=1}^N \zeta(k) \varphi^\top(k) \right)^{-1} \cdot \sum_{k=1}^N \zeta(k) y(k), \quad (2.49)$$

which implies that

$$\hat{\theta}_{\text{IV}} = \theta_0 + \left(\sum_{k=1}^N \zeta(k) \varphi^\top(k) \right)^{-1} \cdot \sum_{k=1}^N \zeta(k) e_{\theta_0}(k). \quad (2.50)$$

Therefore, and similarly to the LS solution, $\hat{\theta}_{\text{IV}}$ is a consistent estimate of θ_0 if

$$\mathbb{E} \left\{ \zeta(k) \varphi^\top(k) \right\} \succ 0 \quad \text{and} \quad \mathbb{E} \left\{ \zeta(k) e_{\theta_0}(k) \right\} = 0. \quad (2.51)$$

There is a considerable amount of freedom in the choice of an instrument respecting these conditions. In the LTI context, the choice of the instrument has been widely studied and most of the advanced IV methods offer similar performance as extended LS methods or other PE minimization methods (see [17, 20]). A particularly interesting fact is that, under the ARX model assumption, the variance of the IV estimate is minimal if the instrument is chosen as the noise-free version of the regressor [21]. In other words, when directly applying the IV theory to the LPV-ARX model (2.30) (the LPV-ARX model can be seen as an LTI model), the optimal IV estimate is given by

$$\hat{\theta}_{\text{IV}}^{\text{opt}} = \left(\sum_{k=1}^N \zeta_{\text{opt}}(k) \varphi^\top(k) \right)^{-1} \cdot \sum_{k=1}^N \zeta_{\text{opt}}(k) y(k), \quad (2.52)$$

where the optimal instrument is defined as:

$$\zeta_{\text{opt}}(k) = \left[-\check{y}_o(k-1) \quad -\alpha_{1,1}(p(k))\check{y}_o(k-1) \quad \cdots \quad -\alpha_{n_a, n_a}(p(k))\check{y}_o(k-n_a) \right. \\ \left. u(k-\tau_d) \quad \beta_{0,1}(p(k))u(k-\tau_d) \quad \cdots \quad \beta_{n_b, n_b}(p(k))u(k-\tau_d-n_b) \right]. \quad (2.53)$$

Here \check{y}_o denotes the noise-free output of the data-generating system \mathcal{S}_o which is a priori unknown in practice. Consequently, often an estimate of \check{y}_o is applied as an instrument, like the simulated output of a previously obtained model estimate which in turn can be refined iteratively. Note that if $\mathcal{S}_o \in \mathcal{M}$, then both the IV solution

(2.52) and the LS solution (2.47) are consistent and statistically optimal (minimum variance and unbiased). Furthermore, consistency of (2.52) also holds in the p -noisy case, see [3].

To construct the optimal instrument ζ_{opt} , a particular approach is the IV4 method [16], proposed in the LPV case in [3]. In this approach, the instrument is built using the simulated data generated from an estimated auxiliary ARX model. This method is given in detail by Algorithm 2. In [3], it was shown that in case

Algorithm 2: LPV–ARX identification, IV4 global method

Require: a data record $\mathcal{D}_N = \{u(k), y(k), p(k)\}_{k=1}^N$ of \mathcal{S}_o , the LS identification criterion V , and the LPV–ARX model structure (2.30) with linear parametrization (2.27) and parameters $\theta = [a_{1,0} \cdots a_{n_a, n_a} \ b_{0,0} \cdots b_{n_b, n_b}] \in \mathbb{R}^{n_\theta}$. Assume that \mathcal{D}_N is informative w.r.t. (2.30) and (2.30) is globally identifiable on Θ .

- 1: estimate an LPV–ARX model by Algorithm 1.
 - 2: generate an estimate $\hat{y}_o(k)$ of $\check{y}_o(k)$ based on the resulting ARX model of the previous step.
 - 3: build an instrument based on $\hat{y}_o(k)$ and then estimate θ via (2.49).
 - 4: **return** estimated model (2.30).
-

\mathcal{S}_o corresponds to an LPV–OE model ($v_o = e_o$), Algorithm 2 leads to an unbiased estimate. Moreover, like in the LTI case, any structural modeling error of the noise results in a bias for the LS estimate while, using this IV method, only the variance of $\hat{\theta}_{\text{IV}}$ is increased. Nevertheless, the bigger the difference between the true noise process and the noise model assumed is, the higher the resulting variance in the IV estimate is. Depending on the size N of the dataset, the variance increase of the IV estimate can lead to worse results than by the LS estimator (for which the variance is known to remain low). Consequently, it is highly important to assume a noise model as realistic as possible in the first place. In the LTI case, many IV methods are dedicated to more general noise models such as OE or BJ [39]. In Sect. 2.5.2.3, we consider some available methods for LPV–OE and LPV–BJ model structures which were introduced in [13].

2.5.1.3 Estimation of FIR and OBF Models

Even if LPV–FIR and OBF models have different representation capabilities than ARX models, if the noise v_o is assumed to be zero mean and white, the one-step-ahead predictor can be written as a liner regression similar to (2.43) where

$$\varphi(k) = [u(k) \ \alpha_{0,1}(p(k))u(k) \ \cdots \ \alpha_{n_f, n_\alpha}(p(k))u(k - n_f)]^\top. \quad (2.54)$$

Due to this fact, the LS approach can be used to estimate such models and as the regressor does not contain any output terms, the LS estimate is consistent even if

the noise v_0 is not white or p is polluted by noise, till these noise effects are not correlated with u . However, in case of OBF models, the selection of the basis set $\{\phi_i(q)\}_{i=1}^{n_w}$ has a paramount importance as it governs the size of parametrization and the approximation error directly. To provide a computationally attractive data-driven selection of efficient sets of basis functions, a *Fuzzy clustering* based approach has been proposed in [28]. For more on LPV–OBF models and issues of basis selection and identification, see [23, 28].

2.5.2 Prediction-Error Based Identification with General Noise Models

Next we consider the global identification of model structures which utilize extended noise models to increase the validity of the noise modeling. Unfortunately, due to the more complicated noise models, the linear-in-the-coefficient property is lost in these cases, causing (2.22) to be a nonlinear optimization problem whose solution is more complicated than in the previous case. First a particular idea of rewriting the one-step-ahead predictor as a pseudolinear regression is extended from the LTI framework to the LPV case, allowing to derive a computationally attractive solution. Then we also consider general nonlinear optimization to solve the estimation problem. Finally, it is shown how the IV approach can offer a simple solution for the estimation of θ in case of a more general noise model than in Sect. 2.5.1.2.

2.5.2.1 Pseudolinear Regression

Consider first the LPV–ARMAX case, where A, B, D are (linearly) parametrized as in (2.27). By multiplying (2.19) with $D(q^{-1}, p(k), \theta_h)$ on the left, it follows that $D(q^{-1}, p(k), \theta_h) \sum_{j=0}^{\infty} (1 - D(q^{-1}, p(k), \theta_h))^j = 1$ and hence

$$\begin{aligned} D(q^{-1}, p(k), \theta_h) \hat{y}(k | \theta, k-1) &= B(q^{-1}, p(k), \theta_g) u(k - \tau_d) \\ &\quad + (D(q^{-1}, p(k), \theta_h) - A(q^{-1}, p(k), \theta_g)) y(k) \end{aligned} \quad (2.55)$$

in terms of the subpredictors (2.32a–b). By adding $(1 - D(q^{-1}, p(k), \theta_h)) \hat{y}(k | \theta)$ to both sides of (2.55) and using (2.18), (2.19) is equivalent with

$$\begin{aligned} \hat{y}(k | \theta, k-1) &= B(q^{-1}, p(k), \theta_g) u(k - \tau_d) + (1 - A(q^{-1}, p(k), \theta_g)) y(k) \\ &\quad + (D(q^{-1}, p(k), \theta_h) - 1) e_{\theta}(k). \end{aligned} \quad (2.56)$$

Then by considering a regressor $\varphi^\top(k|\theta)$ defined as before (see (2.44)), but extended with $\delta_{1,1}(p(k))e_\theta(k-1), \dots, \delta_{n_d, n_\delta}(p(k))e_\theta(k-n_d)$, the predictor (2.56) can be rewritten as

$$\hat{y}(k|\theta, k-1) = \varphi^\top(k|\theta)\theta. \quad (2.57)$$

This equation corresponds to a *pseudolinear regression*, hence minimization of (2.21) follows by an iterative LS approach where an estimate of $e_\theta(k)$ is generated by a model obtained in a previous iteration, see Algorithm 3.

Algorithm 3: LPV-ARMAX identification, iterative LS global method

Require: a data record $\mathcal{D}_N = \{u(k), y(k), p(k)\}_{k=1}^N$ of \mathcal{S}_0 , the LS identification criterion V , and the LPV-ARMAX model structure (2.29a-c) with $C(q^{-1}, p(k), \theta_h) \triangleq A(q^{-1}, p(k), \theta_g)$ and linear parametrization (2.27) with parameters $\theta = [a_{1,0} \cdots b_{n_b, n_\beta} \ d_{1,0} \cdots d_{n_d, n_\delta}] \in \mathbb{R}^{n_\theta}$. Assume that \mathcal{D}_N is informative w.r.t. (2.29a-c) and (2.29a-c) is globally identifiable on Θ .

1: estimate an ARX model by Algorithm 1 resulting in $\hat{\theta}_g^{(0)}$. Set $D(q^{-1}, p(k), \theta_h^{(0)}) = 1$,

$$\hat{\theta}^{(0)} = \left[\left(\hat{\theta}_g^{(0)} \right)^\top \left(\hat{\theta}_h^{(0)} \right)^\top \right]^\top \text{ and } \tau = 0.$$

2: **repeat**

3: generate an estimate $\hat{e}_\theta^{(\tau)}(k)$ based on the resulting model of the previous step, i.e., $\hat{\theta}^{(\tau)}$.

4: calculate the signals $x_{i,l} = -\alpha_{i,l}(p)q^{-i}y$, $x_{j+n_a+1,l} = \beta_{j,l}(p)q^{-j-\tau_d}u$ and

$$x_{i+n_a+n_b+1,l} = -\delta_{i,l}(p)q^{-i}\hat{e}_\theta^{(\tau)} \text{ and let } \varphi_\tau = [x_{0,0} \cdots x_{n_a+n_b+n_d+1, n_\delta}]^\top.$$

5: estimate θ in terms of $\hat{\theta}^{(\tau+1)} = \Phi_\tau^\dagger Y$ with $Y = [y^\top(1) \cdots y^\top(N)]^\top$ and

$$\Phi_\tau = [\varphi_\tau(1) \cdots \varphi_\tau(N)]^\top. \text{ Increase } \tau \text{ by } 1.$$

6: **until** $\hat{\theta}_\tau$ has converged or the maximum number of iterations is reached.

7: **return** estimated model (2.29a-c).

Now consider the LPV-OE case. In this case, $\theta_h = \emptyset$ and (2.19) read as

$$\hat{y}(k|\theta, k-1) = \sum_{i=0}^{\infty} (1 - A(q^{-1}, p(k), \theta_g))^i B(q^{-1}, p(k), \theta_g) q^{-\tau_d} u(k). \quad (2.58)$$

Define $\check{y} = (G(q, \theta_g) \diamond p)u$ as the noise-free output of the LPV-OE model. Then, (2.58) can be rewritten as

$$\hat{y}(k|\theta, k-1) = (1 - A(q^{-1}, p(k), \theta_g))\check{y}(k) + B(q^{-1}, p(k), \theta_g) q^{-\tau_d} u(k). \quad (2.59)$$

This gives the idea again to introduce the regressor

$$\varphi^\top(k|\theta) = [-\check{y}(k-1) \quad -\alpha_{1,1}(p(k))\check{y}(k-1) \quad \cdots \quad -\alpha_{n_a, n_\alpha}(p(k))\check{y}(k-n_a) \\ u(k-\tau_d) \quad \beta_{0,1}(p(k))u(k-\tau_d) \quad \cdots \quad \beta_{n_b, n_\beta}(p(k))u(k-\tau_d-n_b)], \quad (2.60)$$

to write (2.59) in the form of (2.57). Again an iterative LS algorithm, similar to Algorithm (3), can be introduced to obtain an estimate.

A pseudolinear regression form can be obtained for the LPV–BJ case by combining the approaches of the ARMAX and OE cases. In the LPV–BJ case

$$\hat{y}(k | \theta, k-1) = (W_u(q, \theta) \diamond p)(k)u(k) + (W_y(q, \theta) \diamond p)(k)y(k), \quad (2.61)$$

where the subpredictors are defined by (2.37a–b). Again introduce $\check{y} = (G(q, \theta_g) \diamond p)u$ as the noise-free model output and multiply (2.61) with $D(q^{-1}, p(k), \theta_h)$ on the left giving:

$$\begin{aligned} D(q^{-1}, p(k), \theta_h) \hat{y}(k | \theta, k-1) &= C(q^{-1}, p(k), \theta_h) \check{y}(k) + D(q^{-1}, p(k), \theta_h) y(k) \\ &\quad - C(q^{-1}, p(k), \theta_h) y(k). \end{aligned} \quad (2.62)$$

As $e_\theta(k) = y(k) - \hat{y}(k | \theta, k-1)$, we can write

$$e_\theta(k) = (1 - D(q^{-1}, p(k), \theta_h))e_\theta(k) + C(q^{-1}, p(k), \theta_h) (y(k) - \check{y}(k)). \quad (2.63)$$

Note that C is monic. We also know that

$$\check{y} = (1 - A(q^{-1}, p(k), \theta_g))\check{y}(k) + B(q^{-1}, p(k), \theta_g)u(k). \quad (2.64)$$

Let $\xi = y - \check{y}$, then (2.63) reads as

$$e_\theta(k) = y(k) - \varphi^\top(k | \theta)\theta, \quad (2.65)$$

where

$$\begin{aligned} \varphi^\top(k) &= [-\check{y}(k-1) \quad -\alpha_{1,1}(p(k))\check{y}(k-1) \quad \cdots \quad -\alpha_{n_a, n_a}(p(k))\check{y}(k-n_a) \\ &\quad u(k-\tau_d) \quad \beta_{0,1}(p(k))u(k-\tau_d) \quad \cdots \quad \beta_{n_b, n_b}(p(k))u(k-\tau_d-n_b) \\ &\quad -\xi(k-1) \quad -\gamma_{1,1}(p(k))\xi(k-1) \quad \cdots \quad -\gamma_{n_c, n_c}(p(k))\xi(k-n_c) \\ &\quad e_\theta(k-1) \quad \delta_{1,1}(p(k))e_\theta(k-1) \quad \cdots \quad \delta_{n_d, n_d}(p(k))e_\theta(k-n_d)]. \end{aligned} \quad (2.66)$$

As $e_\theta(k) = y(k) - \hat{y}(k | \theta, k-1)$, (2.65), can be written as (2.57). Again an iterative LS algorithm, similar to Algorithm (3) can be introduced to obtain an estimate.

As we could see, despite noncommutativity of the time operator q , the rather complicated LPV model structures in the considered PE setting could have been relatively easily transformed to a pseudo linear regression form, hence their estimation is available by different iterative schemes. However, there is a particular difficulty to establish consistency and convergence results w.r.t. these schemes. Namely, the optimal regressor is required by the linear regression form to achieve such properties. However, as these items are approximated, we can analyze the estimation properties only in the case if the corresponding iterative approximations have converged. Such convergence properties, just like in the LTI case, are not fully

understood in general. In terms of application of these approaches, it has a prime importance that convergence is quite sensitive on the modeling assumption and the largeness of parametrization which are typically ill-chosen in most applications. Nevertheless, the introduced schemes, if they converge, provide computationally efficient estimation approaches in the considered context.

2.5.2.2 Nonlinear Optimization

Alternatively, minimization of (2.21) is available by general nonlinear optimization methods, like gradient-based minimization which can be applied directly computing the partial derivatives of the predictor (2.19) w.r.t. θ . Even the advanced LSQNONLIN approach of MATLAB can be directly used to obtain an estimate. As the application of these nonlinear optimization schemes only extends to the solution of the underlying optimization problem, these approaches are not presented in detail. However, there are two particular difficulties that can hinder the application of nonlinear optimization schemes:

1. In case of over-parametrization of the scheduling dependencies, the number of possible saddle points of (2.21) can seriously increase which can slow down or even prevent the convergence to the global optimum.
2. In case of large-scale systems, the computational time can be substantial compared to other approaches.

2.5.2.3 Instrumental Variable Approach

As the alternative of the previous estimation method, we can also introduce an instrumental variable approach that makes possible the direct identification of LPV–BJ models with p -independent noise part. Hence it improves considerably the achievable variance of the IV4 method in case of more complicated noise processes. To derive such an improved IV scheme, we first start with rewriting the process equation (2.29a) as

$$F(q^{-1}, \theta_g) \check{y}(k) + \sum_{i=1}^{n_a} \sum_{l=1}^{n_\alpha} a_{i,l} \tilde{y}_{i,l}(k) = \sum_{j=0}^{n_b} \sum_{l=0}^{n_\beta} b_{j,l} \tilde{u}_{j,l}(k), \quad (2.67)$$

where $F(q^{-1}, \theta_g) = 1 + \sum_{i=1}^{n_a} a_{i,0} q^{-i}$ is an LTI filter, $\tilde{y}_{i,l}(k) = \alpha_{i,l}(p(k)) \check{y}(k-i)$ and $\tilde{u}_{j,l}(k) = \beta_{j,l}(p(k)) u(k-j-\tau_d)$. Note that in this way the process part is rewritten as a MISO LTI model with $n_a n_\alpha + (n_b + 1)(n_\beta + 1)$ input signals $\{\tilde{y}_{i,l}\}_{i=1, l=1}^{n_a, n_\alpha}$ and $\{\tilde{u}_{j,l}\}_{j=0, l=0}^{n_b, n_\beta}$. However, this is not a representation of the original LPV behavior of (2.29a) as it contains lumped output terms. As a second step, assume that the noise part is not dependent on p , hence it is modeled as a stable LTI filter $H(q, \theta_h) = D(q^{-1}, \theta_h) / C(q^{-1}, \theta_h)$, which is a technical assumption we need to take to derive the intended approach. Given the fact that the polynomial operator F commutes in

(2.67) over the constant coefficients, thus (2.67) can be rewritten as

$$y(k) = - \sum_{i=1}^{n_a} \sum_{l=1}^{n_\beta} \frac{a_{i,l}}{F(q^{-1}, \theta_g)} \tilde{y}_{i,l}(k) + \sum_{j=0}^{n_b} \sum_{l=0}^{n_\beta} \frac{b_{j,l}}{F(q^{-1}, \theta_g)} \tilde{u}_{j,l}(k) + H(q, \theta_h) e(k), \quad (2.68)$$

which can be considered again as a “pseudolinear” form. This reformulation makes possible to introduce IV estimation of the considered LPV–BJ models. An approach that has been successfully applied in this context is an extended version of the *refined instrumental variable* (RIV) approach of the LTI identification framework [13].

As a refinement of the IV scheme presented in Sect. 2.5.1.2, IV methods have been developed to cope with more general noise structures such as the BJ case, where the data equation, under the assumption of $\mathcal{S}_o \in \mathcal{M}$, can be written as

$$y(k) = \varphi^\top(k) \theta_{o,g} + Q(q, \theta_o) e_{\theta_o}(k), \quad (2.69)$$

with $Q(q, \theta_o)$ being an LTI transfer function, $Q^{-1}(q, \theta_o)$ being stable, and $e_{\theta_o}(k)$ is a white noise. In the LPV–BJ case with p -independent noise part, this can be achieved by taking

$$\varphi(k) = \left[-y(k-1) \cdots -y(k-n_a) \quad -\tilde{y}_{1,1}(k) \cdots -\tilde{y}_{n_a, n_\alpha}(k) \quad \tilde{u}_{0,0}(k) \cdots \tilde{u}_{n_b, n_\beta}(k) \right]^\top$$

and

$$Q(q, \theta_o) = F(q^{-1}, \theta_{o,g}) \frac{D(q^{-1}, \theta_{o,h})}{C(q^{-1}, \theta_{o,h})}.$$

Based on this form, the extended-IV estimate in the ℓ_2 sense can be given as [21]:

$$\hat{\theta}_{g, \text{XIV}} = \arg \min_{\theta_g \in \mathbb{R}^{n_g}} \left\| \frac{1}{N} \sum_{k=1}^N L(q) \zeta(k) L(q) \varphi^\top(k) \theta_g - \frac{1}{N} \sum_{k=1}^N L(q) \zeta(k) L(q) y(k) \right\|_{\ell_2}^2, \quad (2.70)$$

where $\zeta(k)$ is the instrument and $L(q)$ is a stable prefilter. The conditions for consistency in this case read as:

$$\mathbb{E} \left\{ L(q) \zeta(k) L(q) \varphi^\top(k) \right\} \succ 0 \quad \text{and} \quad \mathbb{E} \{ L(q) \zeta(k) L(q) e_{\theta_o}(k) \} = 0. \quad (2.71)$$

Again, there is a considerable amount of freedom in the choice of the instruments. In [21, 38] it has been shown that the minimum variance estimator can be achieved in the BJ case if ζ is chosen as the noise-free version of the extended regressor φ and $L(q) = Q^{-1}(q, \theta_o)$. Furthermore, it holds true that in case of noise modeling error, the extended IV method is consistent and the variance of the estimates should

be significantly decreased with respect to the IV4 method: even if the noise process is not in the noise model set defined, it is more likely to be better described by an BJ model than by an ARX model.

In terms of the estimation, it is important to notice that φ contains the noise-free output terms $\{\tilde{y}_{i,l}\}$. Therefore, by momentarily assuming that $\{\tilde{y}_{i,l}(k)\}_{i=1,l=0}^{n_a,n_\alpha}$ are known a priori and that the data-generating system \mathcal{S}_o is in the model set, then the previously discussed conditions for optimal estimates lead to the choice of optimal instrument [13]:

$$\zeta_{\text{opt}}(k) = \begin{bmatrix} -\check{y}_o(k-1) & \cdots & -\check{y}_o(k-n_a) & -\tilde{y}_{1,1}^o(k) & \cdots & -\tilde{y}_{n_a,n_\alpha}^o(k) \\ \tilde{u}_{0,0}(k) & \cdots & \tilde{u}_{n_b,n_\beta}(k) \end{bmatrix}^\top \quad (2.72)$$

while the optimal filter is given as

$$L_{\text{opt}}(q) = Q^{-1}(q, \theta_o) = \frac{C(q^{-1}, \theta_{o,h})}{D(q^{-1}, \theta_{o,h})F(q^{-1}, \theta_{o,g})}. \quad (2.73)$$

In a practical situation, the optimal instrument (2.72) and filter (2.73) are unknown a priori. Therefore, the RIV estimation normally involves an iterative (or relaxation) algorithm in which, at each iteration, an “auxiliary model” is used to generate an estimate of (2.72) and (2.73). This auxiliary model is based on the parameter estimates obtained at the previous iteration. Consequently, if convergence occurs, the optimal instrument and filter are obtained. Based on the previous considerations, the RIV algorithm dedicated to the LPV case is summarized in Algorithm 4.

Using a similar concept, the so-called *simplified* RIV (SRIV) method can also be developed for the estimation of LPV–OE models. As in this case $C(q^{-1}, \theta_h) = D(q^{-1}, \theta_h) = 1$, Step 7 of Algorithm 4 can be skipped. In practical cases, it is a fair assumption to consider that the noise model assumed is incorrect for both LPV–OE and LPV–BJ models. In this case, the LPV–SRIV algorithm might perform as well as the LPV–RIV algorithm: the BJ assumption might be more realistic, but this is compensated by the reduced number of parameters to be estimated under the OE assumption. Additionally, both the RIV and SRIV algorithms can be also extended to be applicable in a closed-loop setting [29].

2.6 Conclusion

By using an impulse response representation of LPV systems, it has been shown in this chapter that a unified prediction-error framework for the identification of LPV polynomial models can be established. We have seen that this framework allows to understand the role of general noise models in the LPV setting, making possible to formulate the LPV extensions of classical model structures of the LTI case, like ARX, ARMAX, Box–Jenkins, OE, FIR, and series expansion models. Furthermore estimation of these models is computationally rather attractive and allows

Algorithm 4: LPV–BJ identification, RIV global method

Require: a data record $\mathcal{D}_N = \{u(k), y(k), p(k)\}_{k=1}^N$ of \mathcal{S}_0 , the LS identification criterion V , and the LPV–BJ model structure (2.29a–c) with linear parametrization (2.27), an LTI noise model characterized by $C(q^{-1}, \theta_h)$ and $D(q^{-1}, \theta_h)$ and with parameters $\theta_g = [a_{1,0} \cdots b_{n_b, n_\beta}]^\top \in \mathbb{R}^{n_g}$ and $\theta_h = [c_1 \cdots d_{n_d}]^\top \in \mathbb{R}^{n_h}$. Assume that \mathcal{D}_N is informative w.r.t. (2.29a–c) and (2.29a–c) is globally identifiable on Θ .

1: estimate an ARX model by Algorithm 1 resulting in $\hat{\theta}_g^{(0)}$. Set

$$C(q^{-1}, \hat{\theta}_h^{(0)}) = D(q^{-1}, \hat{\theta}_h^{(0)}) = 1, \hat{\theta}^{(0)} = \left[\left(\hat{\theta}_g^{(0)} \right)^\top \left(\hat{\theta}_h^{(0)} \right)^\top \right]^\top \text{ and } \tau = 0.$$

2: **repeat**

- 3: compute an estimate of $\check{y}(k)$ via $A(p_k, q^{-1}, \hat{\theta}_g^{(\tau)})\check{y}(k) = B(p_k, q^{-1}, \hat{\theta}_g^{(\tau)})u(k)$ and generate the auxiliary signals $\{\check{y}_{i,l}\}_{i=1, l=1}^{n_a, n_\alpha}$ and $\{\check{u}_{j,l}\}_{j=0, l=0}^{n_b, n_\beta}$ according to (2.67).
 4: compute the filter:

$$L(q^{-1}, \hat{\theta}^{(\tau)}) = \frac{C(q^{-1}, \hat{\theta}_h^{(\tau)})}{D(q^{-1}, \hat{\theta}_h^{(\tau)})F(q^{-1}, \hat{\theta}_g^{(\tau)})}$$

and the associated filtered signals $\{\check{u}_{j,l}^f(k)\}_{j=0, l=0}^{n_b, n_\beta}$, $y_f(k)$ and $\{\check{y}_{i,l}^f(k)\}_{i=1, l=0}^{n_a, n_\alpha}$.

5: build the filtered estimated regressor $\hat{\phi}_f^{(\tau)}(k)$ and the filtered instrument $\hat{\zeta}_f^{(\tau)}(k)$ as:

$$\hat{\phi}_f^{(\tau)}(k) = \left[-y_f(k-1) \cdots -y_f(k-n_a) \quad -\check{y}_{1,1}^f(k) \cdots -\check{y}_{n_a, n_\alpha}^f(k) \quad \check{u}_{0,0}^f(k) \cdots \check{u}_{n_b, n_\beta}^f(k) \right]^\top$$

$$\hat{\zeta}_f^{(\tau)}(k) = \left[-\check{y}_f(k-1) \cdots -\check{y}_f(k-n_a) \quad -\check{y}_{1,1}^f(k) \cdots -\check{y}_{n_a, n_\alpha}^f(k) \quad \check{u}_{0,0}^f(k) \cdots \check{u}_{n_b, n_\beta}^f(k) \right]^\top$$

6: calculate $\hat{\theta}_g^{(\tau+1)} = \left(\frac{1}{N} \Gamma_\tau^\top \Phi_\tau \right)^{-1} \left(\frac{1}{N} \Gamma_\tau^\top Y \right)$ with $Y = [y(1) \cdots y(N)]^\top$,

$$\Phi_\tau = \left[\hat{\phi}_f^{(\tau)}(1) \cdots \hat{\phi}_f^{(\tau)}(N) \right]^\top \text{ and } \Gamma_\tau = \left[\hat{\zeta}_f^{(\tau)}(1) \cdots \hat{\zeta}_f^{(\tau)}(N) \right]^\top.$$

7: estimate the noise signal v_o as $\hat{v}(k) = y(k) - \check{y}(k)$. Based on \hat{v} , the estimation of $\hat{\theta}_h^{(\tau+1)}$ follows using the ARMA estimation algorithm of the MATLAB identification toolbox (an IV approach can also be used for this purpose, see [39]). Increase τ by 1.

8: **until** $\theta^{(\tau)}$ has converged or the maximum number of iterations is reached.

9: **return** estimated model (2.29a–c).

to derive stochastic properties of the model estimates which is a unique property among the available approaches of the LPV identification literature. We could see that the present research focus in this framework not only lies in further developing results on these stochastic properties or understanding the rather challenging case of the p -noisy case but also establishing model structure selection tools and experiment design methods which allow better application of data-driven LPV modeling by the engineering community.

References

1. Bamieh B, Giarré L (2002) Identification of linear parameter varying models. *Int Journal of Robust Nonlin Contr* 12:841–853
2. Boyd S, Chua LO (1985) Fading memory and the problem of approximating nonlinear operators with Volterra series. *IEEE Trans Circ Syst* 32(11):1150–1161
3. Butcher M, Karimi A, Longchamp R (2008) On the consistency of certain identification methods for linear parameter varying systems. In: *Proceedings of the 17th IFAC world congress, Seoul, Korea*, pp 4018–4023
4. Casella F, Lovera M (2008) LPV/LFT modelling and identification: overview, synergies and a case study. In: *Proceedings of IEEE international symposium on computer-aided control system design, San Antonio, TX, USA*, pp 852–857
5. Cerone V, Regruto D (2008) Set-membership identification of LPV models with uncertain measurements of the time-varying parameter. In: *Proceedings of the 47th IEEE conference on decision and control, Cancun, Mexico*, pp 4491–4496
6. Dankers AG, Tóth R, Heuberger PSC, Bombois X, Van den Hof PMJ (2011) Identifiability and the informativity of data sets for LPV–ARX identification. *Proceedings of the 50th IEEE conference on decision and control, Orlando, FL, USA*, pp 799–804
7. dos Santos PL, Ramos JA, de Carvalho JLM (2007) Identification of linear parameter varying systems using an iterative deterministic-stochastic subspace approach. In: *Proceedings of the European Control Conf, Kos, Greece*, pp 4867–4873
8. Gevers M, Bazanella AS, Bombois X, Mišković L (2009) Identification and the information matrix: how to get just sufficiently rich? *IEEE Trans Automat Contr* 54(12):2828–2840
9. Giarré L, Bauso D, Falugi P, Bamieh B (2006) LPV model identification for gain scheduling control: an application to rotating stall and surge control problem. *Contr Eng Prac* 14(4):351–361
10. Heuberger PSC, Van den Hof PMJ, Bo Wahlberg (2005) *Modeling and Identification with Rational Orthonormal Basis Functions*. Springer-Verlag, London
11. Hsu K, Vincent TL, Poolla K (2008) Nonparametric methods for the identification of linear parameter varying systems. In: *Proceedings of the international symposium on computer-aided control system design, San Antonio, TX, USA*, pp 846–851
12. Khalate AA, Bombois X, Tóth R, Babuška R (2009) Optimal experimental design for LPV identification using a local approach. In: *Proceedings of the 15th IFAC symposium on system identification, Saint-Malo, France*, pp 162–167
13. Laurain V, Gilson M, Tóth R, Garnier H (2010) Refined instrumental variable methods for identification of LPV Box–Jenkins models. *Automatica* 46(6):959–967
14. Laurain V, Tóth R, Gilson M, Garnier H (2011) Direct identification of continuous-time LPV input/output models. *Special issue, IET Contr Theor Appl* 4(10):2082–2096
15. Leith DJ, Leithhead WE (1998) Gain-scheduled controller design: an analytic framework directly incorporating non-equilibrium plant dynamics. *Int J Contr* 70:249–269
16. Ljung L (1999) *System Identification, theory for the user*. Prentice Hall, London
17. Ljung L (2009) Experiments with identification of continuous time models. In: *Proceedings of the 15th IFAC symposium on system identification, Saint-Malo, France*
18. Lovera M, Mercère G (2007) Identification for gain-scheduling: a balanced subspace approach. In: *Proceedings of the American Control Conf, New York City, USA*, pp 858–863
19. Murray-Smith R, Johansen TA (1997) *Multiple model approaches to modeling and control*. Taylor and Francis, London
20. Rao GP, Unbehauen H (2004) Identification of continuous-time systems: direct or indirect? *Syst Sci* 30(3):25–50
21. Söderström T, Stoica P (1983) *Instrumental variable methods for system identification*. Springer-Verlag, New York
22. Sznaier M, Mazzaro C, Inanc T (2000) An LMI approach to control oriented identification of LPV systems. In: *Proceedings of the American Control Conf, Chicago, IL, USA*, pp 3682–3686

23. Tóth R (2010) Modeling and Identification of Linear Parameter-Varying Systems. Lecture notes in control and information sciences, Vol. 403, Springer, Germany
24. Tóth R, Abbas H, Werner W (2011a) On the state-space realization of LPV input–output model: practical approaches. *IEEE Trans Contr Syst Technol* 20(1):139–153
25. Tóth R, Bitar E, Heuberger PSC, Van den Hof PMJ, Poolla K (2011b) A prediction-error identification framework for linear parameter-varying systems. In prep.
26. Tóth R, Felici F, Heuberger PSC, Van den Hof PMJ (2007) Discrete time LPV I/O and state space representations, differences of behavior and pitfalls of interpolation. In: Proceedings of the European Control Conf, Kos, Greece, pp 5418–5425
27. Tóth R, Heuberger PSC, Van den Hof PMJ (2008) Flexible model structures for LPV identification with static scheduling dependency. In: Proceedings of the 47th IEEE conference on decision and control, Cancun, Mexico, pp 4522–4527
28. Tóth R, Heuberger PSC, Van den Hof PMJ (2009a) Asymptotically optimal orthonormal basis functions for LPV system identification. *Automatica* 45(6):1359–1370
29. Tóth R, Laurain V, Gilson M, Garnier H (2011c) On the closed loop identification of LPV models using instrumental variables. In: Proceedings of the 18th IFAC World Congress, Milano, Italy
30. Tóth R, Laurain V, Zheng W, Poolla K (2011d) A support vector machine approach for LPV linear-regression models. Proceedings of the 50th IEEE Conf. on Decision and Control, Orlando, FL, USA, pp 3192–3197
31. Tóth R, Lyzell C, Enqvist M, Heuberger PSC, Van den Hof PMJ (2009b) Order and structural dependence selection of LPV–ARX models using a nonnegative garrote approach. In: Proceedings of the 48th IEEE conference on decision and control, Shanghai, China, pp 7406–7411
32. Tóth R, Willems JC, Heuberger PSC, Van den Hof PMJ (2011e) The behavioral approach to linear parameter-varying systems. *IEEE Trans Autom Contr* 56(11):2499–2514
33. van Wingerden JW, Verhaegen M (2009) Subspace identification of bilinear and LPV systems for open- and closed-loop data. *Automatica* 45(2):372–381
34. Verdult V, Verhaegen M (2005) Kernel methods for subspace identification of multivariable LPV and bilinear systems. *Automatica* 41(9):1557–1565
35. Wei X (2006) Advanced LPV techniques for diesel engines. PhD thesis, Johannes Kepler University, Linz
36. Wei X, Del Re L (2006) On persistent excitation for parameter estimation of quasi-LPV systems and its application in modeling of diesel engine torque. In: Proceedings of the 14th IFAC symposium on system identification, Newcastle, Australia, pp 517–522
37. Willems JC, Yamamoto Y (2007) Behaviors defined by rational functions. *Linear algebra and its applications* 425:226–241
38. Young PC (1984) Recursive estimation and time-series analysis. Springer-Verlag, Berlin
39. Young PC (2008) The refined instrumental variable method: unified estimation of discrete and continuous-time transfer function models. *J Euro Syst Autom* 42:149–179

Part II
Theoretical Advances in LPV Control
and Estimation

Chapter 3

Parametric Gain-scheduling Control via LPV-stable Realization

Franco Blanchini, Daniele Casagrande, Stefano Miani, and Umberto Viaro

Abstract It has been recently shown that, given a plant described by a parametric transfer function, any compensator that internally stabilizes the plant for each constant value of the parameter can be realized in such a way that the closed-loop stability is guaranteed under arbitrary variations of the parameter (LPV stability), provided that certain necessary and sufficient stabilizability conditions are satisfied. The realization of such an LPV stabilizing compensator is based on the Youla–Kucera parametrization of all stabilizing compensators; precisely, closed-loop LPV-stability can be ensured by taking an LPV-stable realization of the Youla–Kucera parameter. In this chapter, the technique is further explored, and several issues concerning the practical implementation of the control are considered. The applications include pointwise optimality with guaranteed LPV stability, online parameter tuning, and parametric pole assignment. Some design examples are worked out to show the features of the proposed approach.

3.1 Introduction

Linear parameter-varying (LPV) systems are a useful generalization of linear time-invariant (LTI) systems not only because they provide the natural setting for the adaptive (gain-scheduling) control of linear plants whose parameters vary in time, but also because many nonlinear plants can conveniently be embedded into a linear differential inclusion and, therefore, treated as LPV systems (see, for

F. Blanchini (✉)
Department of Mathematics and Computer Science, University of Udine, 33100 Udine, Italy
e-mail: blanchini@uniud.it

D. Casagrande • S. Miani • U. Viaro
Department of Electrical, Managerial and Mechanical Engineering, University of Udine,
33100 Udine, Italy
e-mail: daniele.casagrande@uniud.it; miani.stefano@uniud.it; viaro@uniud.it

instance, Sect. 4.3 in [14] and [28, 38]). In fact, recent surveys have pointed out the importance given to the LPV framework in the modern control system literature [33, 37].

Nevertheless, the stability analysis of LPV systems is still a challenging subject since most of the classic tools used in the LTI case are no longer valid. Lyapunov theory is a notable exception. In particular, it has been shown that the stability, or stabilizability, of an LPV system is equivalent to the existence of a Lyapunov norm [8, 15, 16, 30–32]. Extensive research is being carried out in this area [6, 20].

It is common practice, in the control of LPV systems, to determine a family of compensators, each of which is suitable for particular parameter values. However, the systematic stability analysis of this type of design solution is rather recent [39]. Since the early 1990s, many papers have dealt with gain-scheduling stabilization and performance of LPV systems [1, 5, 23, 35]. Most of them exploit quadratic Lyapunov functions, with some exceptions that consider parameter-dependent and polyhedral Lyapunov functions [10, 22]. A technique based on pole assignment via state feedback has been considered in [36].

It has recently been shown [9] that the stabilizability of an LPV plant by means of a linear gain-scheduled compensator may be related to the existence of a polyhedral Lyapunov function. This result exploits a duality property and the separation principle presented in [10, 12]. Here, these issues are further developed and extended to discrete-time systems. The theoretical results are then applied to various problems of practical interest.

An intriguing question in LPV control is whether the (parametric) transfer function of a controller that ensures internal stability for fixed values of the parameter can be realized so as to ensure stability when this parameter varies in time [33]. Recently, by adapting results from [12] and [24], it has been proved [9] that an LPV stabilizing realization of any stabilizing parametric compensator transfer function does exist.

In many cases, the parameters of the plant are constant most of the time, so that standard LTI techniques seem to be appropriate. However, the occasional parameter changes may endanger the stability of the LPV system. It is, therefore, reasonable to seek pointwise optimality together with LPV stability, which can indeed be achieved by realizing the compensator properly.

This chapter is organized as follows. First, necessary and sufficient conditions for the stabilizability of an LPV plant with a separation principle are revised from [9]. Then, the LPV-stable transfer function realization problem is described. Precisely, any transfer function, stable for fixed values of the parameter, admits a realization that is stable under arbitrary parameter variations. By resorting to the Youla–Kucera parametrization in its observer-based version, a procedure is subsequently considered to realize the (parametric) compensator transfer function for a parametric plant in such a way that closed-loop LPV stability is guaranteed. Several applications of the suggested technique are finally outlined with particular reference to pointwise optimality with LPV stability, pole placement, and online tuning.

3.2 Problem Statement

Given a parametric proper¹ rational matrix transfer function

$$W(s, w) = \frac{N(s, w)}{d(s, w)}, \quad w \in \mathcal{W}, \quad (3.1)$$

where w is a parameter and $\mathcal{W} \subset \mathbb{R}^\ell$ a compact set, the state-space representation

$$\begin{aligned} \dot{z}(t) &= F(w)z(t) + G(w)\omega(t), \\ \xi(t) &= H(w)z(t) + K(w)\omega(t), \end{aligned} \quad (3.2)$$

or, more concisely,

$$\Sigma(w) = \left[\begin{array}{c|c} F(w) & G(w) \\ \hline H(w) & K(w) \end{array} \right], \quad (3.3)$$

is a realization of $W(s, w)$ if

$$W(s, w) = H(w)[sI - F(w)]^{-1}G(w) + K(w), \quad \forall w \in \mathcal{W}. \quad (3.4)$$

As long as $w \in \mathcal{W}$ is constant and (3.3) is minimal, the following two properties are equivalent: (1) $d(s, w)$ is a Hurwitz polynomial; (2) the realization (3.3) is asymptotically stable. Instead, if w varies in time, the condition that $d(s, w)$ is a Hurwitz polynomial for any fixed value of w is only necessary for (3.3) to be asymptotically stable. Therefore, the following definition is opportune.

Definition 3.1 (LPV-stable realization). Assuming that $d(s, w)$ is a Hurwitz polynomial for all fixed w , the realization (3.3) of (3.1) is *LPV-stable* if the system

$$\dot{z}(t) = F(w(t))z(t) \quad (3.5)$$

is asymptotically stable for any function $w(t)$ taking values in \mathcal{W} .

As shown below, finding an LPV-stable realization, if any, of a transfer function with Hurwitz denominator is very useful in parametric control design.

Consider now a strictly proper LPV plant described by

$$\begin{aligned} \dot{x}(t) &= A(w)x(t) + B(w)u(t), \\ y(t) &= C(w)x(t), \end{aligned} \quad (3.6)$$

¹A parametric transfer function of the form (3.1) is called *proper* if the degree of $d(s, w)$ as a polynomial function of s is strictly greater than the degree of every entry of $N(s, w)$ as a polynomial function of s .

where $x(t) \in \mathbb{R}^n$, $u(t) \in \mathbb{R}^m$, $y(t) \in \mathbb{R}^p$, and $w \in \mathscr{W}$, with $A(\cdot), B(\cdot), C(\cdot)$ continuous functions of w . Let (3.1) be the transfer function of a parametric compensator ensuring that the closed-loop control system for the plant (3.6) is internally stable for any constant value of w .

In the sequel, reference will be made to the following definition.

Definition 3.2 (LPV stabilizing controller realization). The realization (3.3) is an *LPV stabilizing realization* of the parametric compensator transfer function (3.1) if the closed-loop control system with the controller realized as in (3.3) is asymptotically stable when the parameter w varies with time according to any arbitrary function $w(t)$ taking values in the compact set \mathscr{W} .

Taking Definition 3.2 into account, the main problem to be solved can be stated as follows.

Problem 3.1 (LPV synthesis). Given a plant (3.6) and a parametric compensator transfer function (3.1) ensuring internal closed-loop stability for all constant values of $w \in \mathscr{W}$, find an LPV stabilizing controller realization (3.3).

As already said, Problem 3.1 is motivated by the fact that the closed-loop LPV system may be unstable if the parametric compensator transfer function is not realized properly.

Example 3.1 (Motivating example). Consider the plant described by the first-order parametric differential equation

$$\dot{y}(t) = -\alpha y(t) + w(t)u(t), \quad \alpha > 0, \quad (3.7)$$

with $0 < w^- \leq w(t) \leq w^+$, for all t , and assume that the transfer function of the feedback controller is

$$-\frac{\kappa(w)}{s + \beta}, \quad \beta > 0, \quad (3.8)$$

with $\kappa(w) = \kappa_0/w$, $\kappa_0 > 0$. When w is constant, the feedback control system is internally stable with characteristic polynomial:

$$d(s) = s^2 + (\beta + \alpha)s + \alpha\beta + \kappa_0. \quad (3.9)$$

The controller (3.8) admits the two realizations:

$$\Sigma_1(w) = \left[\begin{array}{c|c} -\beta & 1 \\ \hline -\kappa_0/w & 0 \end{array} \right], \quad \Sigma_2(w) = \left[\begin{array}{c|c} -\beta & -\kappa_0/w \\ \hline 1 & 0 \end{array} \right],$$

yielding, respectively, the closed-loop system matrices:

$$A_1(w) = \begin{bmatrix} -\alpha - \kappa_0 & \\ 1 & -\beta \end{bmatrix}, \quad A_2(w) = \begin{bmatrix} -\alpha & w \\ -\kappa_0/w & -\beta \end{bmatrix}.$$

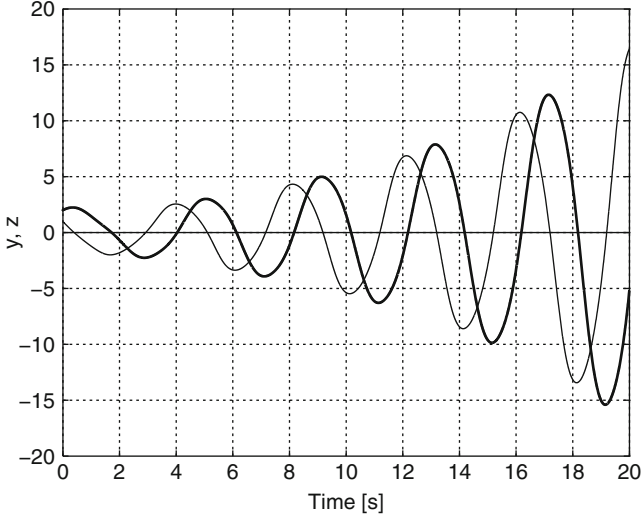


Fig. 3.1 Plant output $y(t)$ (solid line) and controller state $z(t)$ (thin line) starting from $y(0) = 2$ and $z(0) = 1$, respectively, when the controller is realized according to $\Sigma_2(w)$ with $\beta = \alpha = 0.1$ and $w(t) = 3/2 + \sin(t)/2$

$\Sigma_1(w)$ leads to an asymptotically stable feedback system independently of how w varies in time, whereas $\Sigma_2(w)$ may not [29]. For instance, if $\alpha = \beta = 0.1$ and $w(t) = 3/2 + \sin(t)/2$, the system is unstable (see Fig. 3.1). In [28], instability has been attributed to the existence of “hidden coupling terms.” Conditions ensuring that hidden coupling terms do not exist have been derived for the case in which the LPV system arises from the linearization of a nonlinear plant (see [33, Theorem 10]). It will be shown next that framing the design problem as an LPV gain-scheduling problem avoids this issue.

3.3 Preliminary Results

The results described in this section rely on either quadratic or absolute stabilizability conditions which are stated in Assumption 3.1 and Assumption 3.2, respectively.

Assumption 3.1. *There exist two positive-definite constant matrices P and Q , and two matrices $U(w)$ and $Y(w)$, dependent on the parameter w , such that*

$$PA(w)^T + A(w)P + B(w)U(w) + U(w)^T B(w)^T < 0, \quad (3.10)$$

$$A(w)^T Q + QA(w) + Y(w)C(w) + C^T(w)Y(w)^T < 0, \quad (3.11)$$

where $A(w)$, $B(w)$, and $C(w)$ are defined in (3.6).

Assumption 3.1 is standard in quadratic stabilizability studies (see, e.g., [5]).

Definition 3.3. A matrix $M(w)$ that is a continuous function of $w \in \mathcal{W}$, \mathcal{W} compact, is of class \mathcal{H}_1 if there exists $\tau > 0$ such that $\|I + \tau M(w)\|_1 < 1$ for all $w \in \mathcal{W}$. Similarly, $M(w)$ is of class \mathcal{H}_∞ if there exists $\tau > 0$ such that $\|I + \tau M(w)\|_\infty < 1$ for all $w \in \mathcal{W}$.

Definition 3.4. Given a full-column rank matrix R (a full-row rank X), the positive-definite function $\Psi(x) = \|Rx\|_\infty$ (the positive-definite function $\Psi(x) = \min\{\|z\|_1 : Xz = x\}$, respectively) is a *polyhedral Lyapunov function* for the system $\dot{x}(t) = A(w(t))x(t)$ if

$$(D^+ \Psi)(x, A(w)x) \doteq \lim_{h \rightarrow 0^+} \frac{\Psi(x + hA(w)x) - \Psi(x)}{h} \leq -\beta \Psi(x)$$

for some $\beta > 0$.

It is known that the existence of a polyhedral Lyapunov function is necessary and sufficient for the stability of an LPV system [8, 15, 16, 30–32] (see [11] for further details).

Proposition 3.1. *The following assertions are equivalent:*

- The LPV system (3.6) is stable.
- The LPV system admits a polyhedral Lyapunov function.
- The following equation holds for some full-column rank R and $Q(w) \in \mathcal{H}_\infty$

$$RA(w) = Q(w)R.$$

- The following equation holds for some full-row rank X and $P(w) \in \mathcal{H}_1$

$$A(w)X = XP(w).$$

Assumption 3.2. *There exist a full-row rank $n \times \mu$ matrix X , a full-column rank $\nu \times n$ matrix R , as well as an $m \times \mu$ matrix $U(w)$, a $\nu \times p$ matrix $L(w)$ and matrices $P(w) \in \mathcal{H}_1$ and $Q(w) \in \mathcal{H}_\infty$ dependent on w such that*

$$A(w)X + B(w)U(w) = XP(w), \quad (3.12)$$

$$RA(w) + L(w)C(w) = Q(w)R. \quad (3.13)$$

The importance of Assumptions 3.1 and 3.2 is pointed out by the following theorems.

Theorem 3.1. *The following two conditions are equivalent:*

- (1) *The inequalities (3.10) and (3.11) of Assumption 3.1 are satisfied.*
- (2) *The LPV plant (3.6) is quadratically stabilizable by means of a compensator of the form (3.3).*

The proof of Theorem 3.1 can be found in [5]. Note only that the observer-based controller described by

$$\frac{d}{dt}\hat{x}(t) = [A(w) + L(w)C(w) + B(w)J(w)]\hat{x}(t) - L(w)y(t), \quad (3.14)$$

$$u(t) = J(w)\hat{x}(t) + v(t), \quad (3.15)$$

$$v(t) = 0, \quad (3.16)$$

with $J(w) = U(w)P^{-1}$ and $L(w) = Q^{-1}Y(w)$, is a quadratically stabilizing compensator.²

Theorem 3.2. *The following two conditions are equivalent:*

- (1) *Equations (3.12) and (3.13) of Assumption 3.2 are satisfied.*
- (2) *The LPV plant (3.6) is stabilizable by means of a compensator of the form (3.3) and the closed-loop system admits a polyhedral Lyapunov function.*

Proof. See [9]. □

The conditions of Theorems 3.1 and 3.2 are numerically hard, in general. However, if $A(w)$ has the polytopic structure:

$$A(w) = \sum_{i=1}^{\rho} A_i w_i, \quad w_i \geq 0, \quad \sum_{i=1}^{\rho} w_i = 1,$$

for some integer ρ , and B and C are constant matrices, the algorithms suggested in [11, 13] can profitably be used to compute X and R .

The results obtained in [12, 24] for linear switching systems will presently be extended to LPV systems. In particular, the following result, taken from [12], is used later.

Proposition 3.2. *Assume that either pair of stabilizability conditions of Theorems 3.1 or 3.2 is satisfied and let $W(s, w)$ be the transfer function of a compensator ensuring that the closed loop is internally stable for a fixed value of w . Then, $W(s, w)$ can be realized in the form³*

$$\dot{r}(t) = Q(w)r(t) - L(w)y(t) + RB(w)u(t), \quad (3.17)$$

$$\hat{x}(t) = Mr(t), \quad (3.18)$$

$$\dot{z}(t) = F_{\text{SF}}(w)z(t) + G_{\text{SF}}(w)\hat{x}(t), \quad (3.19)$$

$$u(t) = H_{\text{SF}}(w)z(t) + K_{\text{SF}}(w)\hat{x}(t) + v(t), \quad (3.20)$$

$$v(t) = \mathcal{L}^{-1}\{T(s, w)\mathcal{L}\{C(w)\hat{x}(t) - y(t)\}\} = \mathcal{L}^{-1}\{T(s, w)\mathcal{L}\{o(t)\}\}, \quad (3.21)$$

²The reason for introducing the dummy signal $v(t) = 0$ will become clear later.

³With \mathcal{L} we denote the Laplace operator.

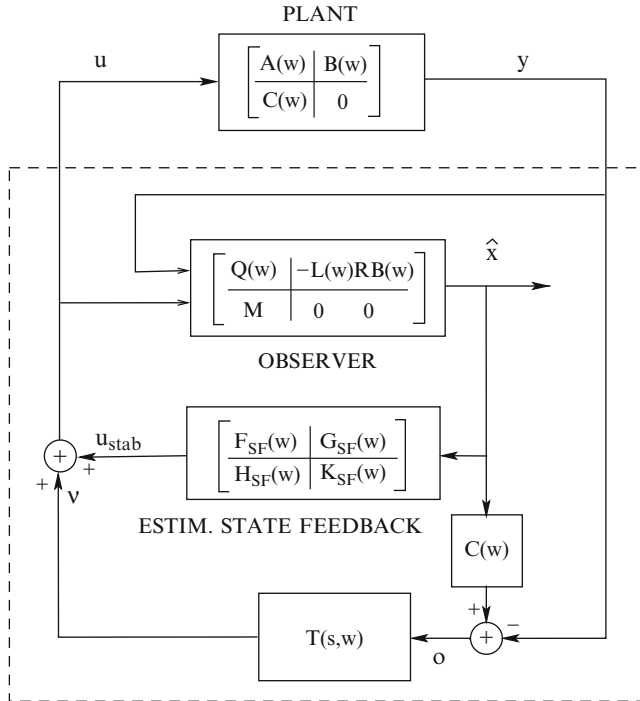


Fig. 3.2 Plant and observer-based controller parametrization © IEEE 2010 [9]

or in the form (3.14)–(3.16) with (3.16) replaced by (3.21), where $T(s,w)$ is a stable transfer function (the Youla–Kucera parameter [27,40]) and $o(t) = C(w)\hat{x}(t) - y(t)$.

The structure of the resulting compensator is shown in Fig. 3.2.

3.4 LPV-stable Realization of a Parametric Transfer Function

This section shows how to derive an LPV-stable realization from a transfer function with a Hurwitz denominator. To this aim the following definition is useful.

Definition 3.5 (Stable regular parametric (SRP) transfer function). A proper rational transfer function $N(s,w)/d(s,w)$, where N is a $p \times m$ polynomial matrix in s and $d(s,w)$ is a monic polynomial of degree ν in s , with N and d continuous functions of $w \in \mathcal{W} \subset \mathbb{R}^\ell$ and \mathcal{W} compact, is called a *stable regular parametric (SRP) transfer function* if $d(s,w)$ is Hurwitz for all $w \in \mathcal{W}$.

The following result is proved in [9].

Theorem 3.3. *Any SRP transfer function admits an LPV-stable realization.*

In fact one such realization can be obtained as follows.

Procedure 3.4.1 1. *Take any realization $\{\tilde{F}(w), \tilde{G}(w), \tilde{H}(w), \tilde{K}(w)\}$ of the SRP transfer function $N(s, w)/d(s, w)$, so that*

$$N(s, w)/d(s, w) = \tilde{H}(w)(sI - \tilde{F}(w))^{-1} \tilde{G}(w) + \tilde{K}(w), \quad (3.22)$$

where $\tilde{F}(w)$ is a Hurwitz matrix continuous in w for all $w \in \mathcal{W}$.

2. *Compute the positive-definite solution $P(w)$ of the Lyapunov equation*

$$\tilde{F}^T(w)P(w) + P(w)\tilde{F}(w) = -I. \quad (3.23)$$

3. *Factorize $P(w)$ as*

$$P(w) = R^T(w)R(w), \quad (3.24)$$

where $R(w)$ is an upper-triangular matrix (Cholesky's decomposition).

4. *Realize the given SRP function according to*

$$\begin{aligned} \dot{z}(t) &= F(w)z(t) + G(w)\omega(t), \\ \xi(t) &= H(w)z(t) + K(w)\omega(t), \end{aligned}$$

where $F(w) = R(w)\tilde{F}(w)R^{-1}(w)$, $G(w) = R(w)\tilde{G}(w)$, $H(w) = \tilde{H}(w)R^{-1}(w)$, and $K(w) = \tilde{K}(w)$.

3.4.1 Transfer Functions with Factorized Denominator

Simple solutions are possible when the Hurwitz denominator $d(s, w)$ is expressed in the factorized form

$$d(s, w) = \prod_i [s + \lambda_i(w)] \prod_j [s^2 + 2\sigma_j(w)s + \sigma_j^2(w) + \omega_j^2(w)],$$

where $\lambda_i(w)$ and $\sigma_j(w)$ are positive. In this case, the transfer function can be expanded into partial fractions as

$$\frac{N(s, w)}{d(s, w)} = D + \sum_i \frac{\hat{\alpha}_i}{s + \lambda_i(w)} + \sum_j \frac{\hat{\beta}_j s + \hat{\gamma}_j}{s^2 + 2\sigma_j(w)s + \sigma_j^2(w) + \omega_j^2(w)},$$

whose numerator coefficients $\hat{\alpha}_i, \hat{\beta}_j, \hat{\gamma}_j$ can be computed by solving linear equations. In this case, an LPV-stable realization is provided by

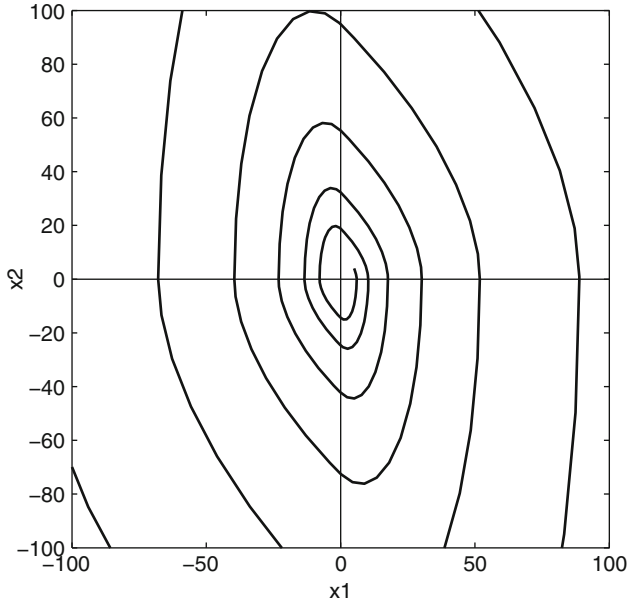


Fig. 3.3 Diverging state-space trajectory of system (3.25) originating from $x_1(0) = 5$, $x_2(0) = 4$ with $w(t) = \text{sgn}(x_1 x_2)$

$$\begin{aligned}
 F(w) &= \text{block-diag} \left\{ -\lambda_i(w), \begin{bmatrix} -\sigma_j(w) & \omega_j(w) \\ -\omega_j(w) & -\sigma_j(w) \end{bmatrix} \right\}, \\
 G(w) &= [1 \ 1 \ \cdots \ [0 \ 1] \ [0 \ 1] \ \cdots]^\top, \\
 H(w) &= [\alpha_1 \ \alpha_2 \ \cdots \ [\beta_1 \ \gamma_1] \ [\beta_2 \ \gamma_2] \ \cdots], \\
 K(w) &= D,
 \end{aligned}$$

where α_i , β_j , and γ_j are simply related to $\hat{\alpha}_i$, $\hat{\beta}_j$, and $\hat{\gamma}_j$.

Example 3.2. The system described by

$$\tilde{F}(w) = \begin{bmatrix} 0 & 1 \\ -(2+w) & -1 \end{bmatrix}, \quad \tilde{G} = \tilde{H} = I, \quad \tilde{K} = 0 \quad (3.25)$$

is stable for any fixed value of w in the interval $0 \leq w \leq 10$, but it is not always LPV-stable [29]. For instance, if the parameter w varies according to $w(t) = \text{sgn}(x_1 x_2)$, the system turns out to be unstable. Figure 3.3 depicts the diverging state-space trajectory starting from $x_1(0) = 5$, $x_2(0) = 4$.

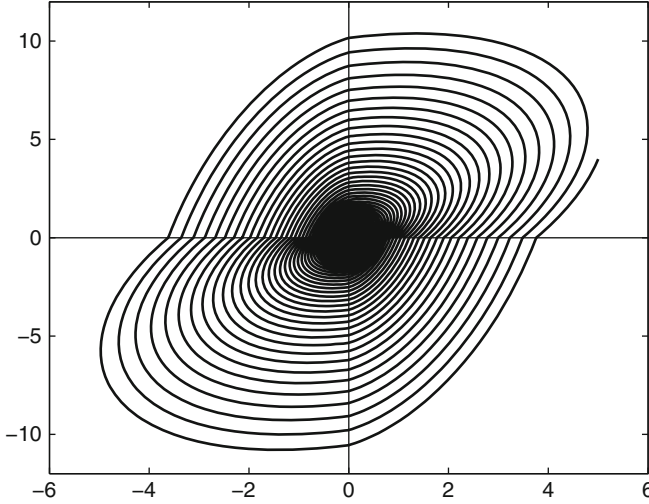


Fig. 3.4 The state-space trajectories of system (3.26) converge to the origin for the same variation of w that leads to the instability of system (3.25)

Remembering that $P = R^T R$, the solution of the Lyapunov equation $\tilde{F}(w)^T P + P \tilde{F}(w) = -I$ is

$$P = \begin{bmatrix} \beta^2 & \gamma\beta \\ \gamma\beta & \delta^2 + \gamma^2 \end{bmatrix} = \begin{bmatrix} \beta & 0 \\ \gamma & \delta \end{bmatrix} \begin{bmatrix} \beta & \gamma \\ 0 & \delta \end{bmatrix},$$

where

$$\begin{aligned} \beta^2 &= (\alpha^2 + \alpha + 1)/(2\alpha), \\ \gamma &= 1/(2\alpha\beta), \\ \delta^2 &= (1 + \alpha)/(2\alpha) - \gamma^2, \end{aligned}$$

with $\alpha = 2 + w$. Then

$$G = R = \begin{bmatrix} \beta & \gamma \\ 0 & \delta \end{bmatrix}, \quad H = R^{-1} = \begin{bmatrix} 1/\beta & -\gamma/(\beta\delta) \\ 0 & 1/\delta \end{bmatrix},$$

and

$$F = R\tilde{F}R^{-1} = \begin{bmatrix} -\gamma\alpha/\beta & \gamma^2\alpha/(\beta\delta) + (\beta - \gamma)/\delta \\ -\delta\alpha/\beta & -1 + \gamma\alpha/\beta \end{bmatrix}, \quad (3.26)$$

which is similar to \tilde{F} since it has the same characteristic polynomial. However, F ensures LPV stability while \tilde{F} does not. Figure 3.4 shows the state trajectory of system (3.26) for the same variation of the parameter considered in Fig. 3.3.

3.5 Parametrization of all LPV Stabilizing Compensator Realizations

If the plant to be controlled is LPV-stable (as in the example illustrated at the end of Sect. 3.2), the required controller realization can be structured as in Fig. 3.5, where $T(s, w)$ is a stable transfer function (Youla–Kucera parameter). Recall, in this regard, that if the parameter has a constant value, then any stabilizing compensator W for a stable plant $P = C(sI - A)^{-1}B$ can be written as $W = -(I - TP)^{-1}T$ (see, e.g., [34,42]) which corresponds to the subdiagram enclosed by a dashed line in Fig. 3.5.

As Fig. 3.5 suggests, LPV stability, too, is ensured if and only if the block $T(s, w)$ is LPV-stable [12,24]. Indeed, by realizing $T(s, w)$ according to (3.2), the state-space representation of the closed-loop system becomes, assuming the external inputs equal to zero, i.e., $d = 0$ and $r = 0$:

$$\frac{d}{dt}x(t) = A(w)x(t) + B(w)u(t), \tag{3.27}$$

$$\frac{d}{dt}\hat{x}(t) = A(w)\hat{x}(t) + B(w)u(t), \tag{3.28}$$

$$\hat{y}(t) = C(w)\hat{x}(t), \tag{3.29}$$

$$\frac{d}{dt}z(t) = F(w)z(t) + G(w)(\hat{y}(t) - y(t)), \tag{3.30}$$

$$u(t) = H(w)z(t) + K(w)(\hat{y}(t) - y(t)). \tag{3.31}$$

Note that (3.28) and (3.29) represent a copy of the plant. Letting $e(t) \doteq \hat{x}(t) - x(t)$ and choosing $[x^T(t) \ z^T(t) \ e^T(t)]^T$ as the state vector, the state matrix of the closed-loop system takes the block-triangular form:

$$\begin{bmatrix} A(w) & B(w)H(w) & B(w)K(w)C(w) \\ 0 & F(w) & G(w)C(w) \\ 0 & 0 & A(w) \end{bmatrix}.$$

Therefore, the closed loop is LPV-stable as long as $F(w(t))$ is so.

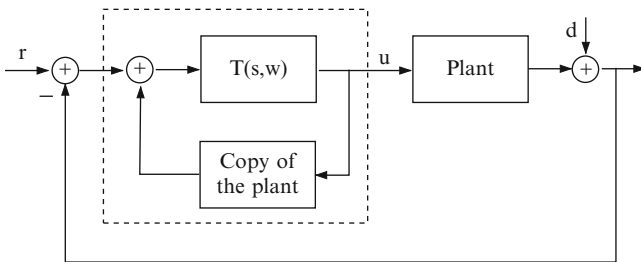


Fig. 3.5 LPV-stable plant and stabilizing controller parametrization

Since the subdiagram inside the dashed line in Fig. 3.5 parametrizes all stabilizing compensator transfer functions (see [34, p. 67]), in the case of LPV-stable plants Problem 3.1 admits a solution for any assigned transfer function $W(s, w)$. Precisely, this solution is obtained by forming the Youla–Kucera parameter according to

$$T(s, w) = W(s, w)[C(w)(sI - A(w))^{-1}B(w)W(s, w) - I]^{-1} \quad (3.32)$$

and realizing it so as to ensure LPV stability.

Problem 3.1 can be solved in the case of an LPV unstable plant, too, provided the plant satisfies the stabilizability conditions of Sect. 3.3. The interested reader is referred to [9, 12] for the relevant theorems and realization procedures.

Remark 3.1. Often the plant parameters are constant most of the time and are subject to variations only occasionally. In these cases, it is reasonable to design the controller in such a way that it is optimal for the prevailing parameter values while ensuring LPV stability. Optimality can be achieved, e.g., by determining the Youla–Kucera parameter according to the Wiener–Hopf design [40]. For slow processes, it is possible to compute online (within the sampling interval) the optimal compensator as a function of the current w . The only additional requirement is that the Youla–Kucera parameter be properly realized.

3.6 The Discrete-time Case

The results presented in the previous sections are based on the solution of a continuous-time Lyapunov equation. Therefore, in the case of discrete-time systems, some of them, e.g., Procedure 3.4.1, need to be reformulated. To this purpose, let the parametric transfer function of a discrete-time regulator be

$$W(z, w) = \frac{N(z, w)}{d(z, w)}$$

that can be realized as

$$\begin{aligned} z(k+1) &= F(w)z(k) + G(w)\omega(k), \\ \xi(k) &= H(w)z(k) + K(w)\omega(k), \end{aligned} \quad (3.33)$$

with

$$W(z, w) = H(w)[zI - F(w)]^{-1}G(w) + K(w).$$

Also, assume that the plant is described by the usual discrete-time equations

$$\begin{aligned} x(k+1) &= A(w)x(k) + B(w)u(k), \\ y(k) &= C(w)x(k). \end{aligned} \quad (3.34)$$

Assumption 3.3. *There exist two positive-definite constant matrices P and Q , and two matrices $U(w)$ and $Y(w)$, dependent on the parameter w , such that*

$$\begin{aligned} & A(w)PA(w)^T + B(w)U(w)A(w)^T + A(w)U(w)^T B(w)^T \\ & + B(w)U(w)P^{-1}U(w)^T B(w)^T - P < 0, \end{aligned} \quad (3.35)$$

$$\begin{aligned} & A(w)^T QA(w) + C(w)^T Y(w)^T A(w) + A(w)^T Y(w)C(w) \\ & + C(w)^T Y(w)^T Q^{-1}Y(w)C(w) - Q < 0. \end{aligned} \quad (3.36)$$

where $A(w)$, $B(w)$, and $C(w)$ are defined by (3.34).

Theorem 3.4. *The following two conditions are equivalent:*

- (1) *The inequalities (3.35) and (3.36) of Assumption 3.3 are satisfied.*
- (2) *The LPV plant (3.34) is quadratically stabilizable by a compensator of the form (3.33).*

Proof. The proof parallels closely the one of Theorem 3.1 [9]. □

To generalize the stability concept to LPV stability (not necessarily quadratic), we need to resort to nonquadratic Lyapunov functions.

Definition 3.6. Given a full-column rank matrix R (a full-row rank X) the positive-definite function $\Psi(x) = \|Rx\|_\infty$ (the positive-definite function $\Psi(x) = \min\{\|z\|_1 : Xz = x\}$, respectively) is a *polyhedral Lyapunov function* for the system $x(k+1) = A(w(k))x(k)$ if

$$\Delta\Psi(x) \doteq \Psi(A(w)x) \leq \lambda\Psi(x),$$

for some positive $\lambda < 1$.

Again, the existence of a polyhedral Lyapunov function is necessary and sufficient for LPV stability [2–4, 15, 16] (see also [11] for further details).

Proposition 3.3. *The following assertions are equivalent:*

- *The LPV system*

$$x(k+1) = A(w(k))x(k)$$

is stable.

- *The LPV system admits a polyhedral Lyapunov function.*
- *The following equation holds for some full-column rank R and $\|Q(w)\|_\infty \leq \lambda < 1$*

$$RA(w) = Q(w)R.$$

- *The following equation holds for some full-row rank X and $\|P(w)\|_1 \leq \lambda < 1$*

$$A(w)X = XP(w).$$

The following theorem holds for the discrete-time case.

Theorem 3.5. *The following two conditions are equivalent:*

- (1) *There exist a full-row rank $n \times \mu$ matrix X , a full-column rank $\nu \times n$ matrix R , as well as an $m \times \mu$ matrix $U(w)$, a $\nu \times p$ matrix $L(w)$, and square matrices, $P(w)$ and $Q(w)$ with norms $\|P(w)\|_1 \leq \lambda < 1$ and $\|Q(w)\|_\infty \leq \lambda < 1$ such that*

$$A(w)X + B(w)U(w) = XP(w), \quad (3.37)$$

$$RA(w) + L(w)C(w) = Q(w)R. \quad (3.38)$$

- (2) *The LPV plant (3.34) is stabilizable by means of a compensator of the form (3.33) and the closed-loop system admits a polyhedral Lyapunov function.*

Proof. (1) \Rightarrow (2) Assume that a stabilizing compensator of the form (3.3) exists. The related (stable) closed-loop system matrix is

$$\begin{bmatrix} A(w) + B(w)K(w)C(w) & B(w)H(w) \\ G(w)C(w) & F(w) \end{bmatrix}.$$

In view of Proposition 3.3, there exists $\|P(w)\|_1 \leq \lambda < 1$ such that

$$\begin{bmatrix} A(w) + B(w)K(w)C(w) & B(w)H(w) \\ G(w)C(w) & F(w) \end{bmatrix} \begin{bmatrix} X \\ Z \end{bmatrix} = \begin{bmatrix} X \\ Z \end{bmatrix} P(w). \quad (3.39)$$

The upper block row of (3.39) yields

$$A(w)X + B(w)K(w)C(w)X + B(w)H(w)Z = XP(w),$$

and, by setting $U(w) = K(w)C(w)X + H(w)Z$, (3.37) follows. The necessity of (3.38) can be proved by duality [10].

(2) \Rightarrow (1) Assume that (3.37) and (3.38) are satisfied, and consider the compensator of order $\nu + \mu - n$ described by

$$r(k+1) = Q(w)r(k) - L(w)y(k) + RB(w)u(k), \quad (3.40)$$

$$\hat{x}(k) = Mr(k), \quad (3.41)$$

$$z(k+1) = F_{\text{SF}}(w)z(k) + G_{\text{SF}}(w)\hat{x}(k), \quad (3.42)$$

$$u(k) = H_{\text{SF}}(w)z(k) + K_{\text{SF}}(w)\hat{x}(k) + v(k), \quad (3.43)$$

$$v(k) = 0, \quad (3.44)$$

where M is any left inverse of R , i.e., a matrix such that $MR = I$, and $F_{\text{SF}}(w)$, $G_{\text{SF}}(w)$, $H_{\text{SF}}(w)$, and $K_{\text{SF}}(w)$ can be computed from

$$\begin{bmatrix} K_{\text{SF}}(w) & H_{\text{SF}}(w) \\ G_{\text{SF}}(w) & F_{\text{SF}}(w) \end{bmatrix} = \begin{bmatrix} U(w) \\ V(w) \end{bmatrix} \begin{bmatrix} X \\ Z \end{bmatrix}^{-1}, \quad (3.45)$$

where Z is any complement of X that makes the square matrix $\begin{bmatrix} X \\ Z \end{bmatrix}$ invertible and

$$V(w) \doteq ZP(w).$$

Letting

$$s(k) \doteq R x(k) - r(k)$$

and choosing $[x^T z^T s^T]^T$ as the state vector, after simple manipulations the following closed-loop matrix is obtained:

$$\left[\begin{array}{cc|c} A(w) + B(w)K_{\text{SF}}(w) & B(w)H_{\text{SF}}(w) & -B(w)K_{\text{SF}}(w)M \\ \hline G_{\text{SF}}(w) & F_{\text{SF}}(w) & -G_{\text{SF}}(w)M \\ \hline 0 & 0 & Q(w) \end{array} \right]. \quad (3.46)$$

The LPV system is stable if and only if the diagonal blocks of the block-triangular state matrix (3.46) are LPV-stable. Now, the upper left diagonal block is LPV-stable because it satisfies (3.39), while the lower right block $Q(w)$, $\|Q(w(t))\|_{\infty} < \lambda < 1$, is the state matrix of an LPV-stable system. \square

The synthesis of parametric compensators which are LPV-stable, can be performed by means of the techniques described in the continuous-time case, provided that an LPV-stable realization of the Youla–Kucera parameter is considered. This can be found as follows.

Procedure 3.6.1 1. Take any realization $\{\tilde{F}(w), \tilde{G}(w), \tilde{H}(w), \tilde{K}(w)\}$ of the SRP transfer function $N(z, w)/d(z, w)$, so that

$$N(z, w)/d(z, w) = \tilde{H}(w)(zI - \tilde{F}(w))^{-1}\tilde{G}(w) + \tilde{K}(w), \quad (3.47)$$

where $\tilde{F}(w)$ is a matrix continuous in w for all $w \in \mathscr{W}$ and having the eigenvalues within the unit circle.

2. Compute the positive-definite solution $P(w)$ of the Lyapunov equation:

$$\tilde{F}^T(w)P(w)\tilde{F}(w) - P(w) = -I. \quad (3.48)$$

3. Factorize $P(w)$ as

$$P(w) = R^T(w)R(w), \quad (3.49)$$

where $R(w)$ is an upper-triangular matrix (Cholesky's decomposition).

4. Realize the given SRP function according to

$$\begin{aligned} z(k+1) &= F(w)z(k) + G(w)\omega(k), \\ \xi(k) &= H(w)z(k) + K(w)\omega(k), \end{aligned} \quad (3.50)$$

where $F(w) = R(w)\tilde{F}(w)R^{-1}(w)$, $G(w) = R(w)\tilde{G}(w)$, $H(w) = \tilde{H}(w)R^{-1}(w)$, and $K(w) = \tilde{K}(w)$.

Therefore, the following theorem can be stated.

Theorem 3.6. *Any SRP transfer function admits an LPV-stable realization computable by means of Procedure 3.6.1.*

Proof. Consider a realization obtained by Procedure 3.6.1. Equation (3.48) can be rewritten as

$$R^T(w)F^T(w)R^{-T}(w)P(w)R^{-1}(w)F(w)R(w) - R^T(w)R(w) = -I$$

which, by premultiplying by $R^{-T}(w)$ and postmultiplying by $R^{-1}(w)$, becomes

$$F^T(w)IF(w) - I = -R^{-T}(w)R^{-1}(w) = -P^{-T}(w).$$

By continuity, $P^{-T}(w)$ is positive-definite and lower bounded, which means that the system $z(k+1) = F(w)z(k)$ admits the identity matrix as a solution to the Lyapunov equation and, hence, it is stable. \square

3.7 Applications and Examples

3.7.1 Fixed-Pole Assignment

Consider the case in which the compensator transfer function is designed so as to locate the closed-loop poles always in the same place independently of the values of the plant parameters, that is, the closed-loop system

$$\Sigma_{CL}(w) = \left[\begin{array}{c|c} \frac{A(w) + B(w)K(w)C(w)}{G(w)C(w)} & \frac{B(w)H(w)}{F(w)} \end{array} \right]$$

exhibits fixed poles. This implies that the Youla–Kucera parameter has fixed poles. To achieve this result, the procedures illustrated in Sect. 3.4 can be used. For simplicity, assume that the desired closed-loop eigenvalues are distinct. Then, the transformation matrix $R(w)$ can be chosen in such a way that $F^{(T)}(w) = F^{(T)} = \text{const}$. The following proposition formalizes this result.

Proposition 3.4. *Assume that the plant is LPV-stable and that the assigned compensator transfer function $N(s, w)/d(s)$ locates the poles of the closed-loop transfer function in fixed positions. Then, an LPV stabilizing realization of the form (3.3) with F constant can be obtained for this compensator.*

If the plant is LPV-stable, the compensator can be structured as in Fig. 3.5, and the sensitivity function can be written as

$$S(s, w) = 1 - [C(w)(sI - A(w))^{-1}B(w)]T(s, w). \quad (3.51)$$

Pole assignment can be accomplished by making $T(s, w)$ cancel all of the plant eigenvalues and replace them by its own poles. In this way, stability is obviously guaranteed for every constant value of w . Instead, to achieve LPV stability, $T(s, w)$ must be realized properly. Since the poles of $T(s, w)$ are fixed, a constant state matrix F can be chosen so that no transformation $R(w)$ is needed.

Example 3.3 (Example 3.1 revisited). Consider again (3.7). The compensator (3.8) locates the closed-loop poles at the roots of (3.9). An *ad hoc* LPV stabilizing realization was already derived in Example 3.1. However, the controller transfer function (3.8) can also be realized according to (3.32) with

$$T(s, w) = \frac{\kappa(w)(s + \alpha)}{(s + \alpha)(s + \beta) + \kappa(w)w} = \frac{(\kappa_0/w)(s + \alpha)}{(s + \alpha)(s + \beta) + \kappa_0}$$

leading to a compensator that ensures closed-loop LPV stability for the desired poles.

3.7.2 Dead-beat LPV Control Problem

A remarkable difference between the discrete- and continuous-time case is that, for w constant, in the former it is possible to achieve a closed-loop system with finite impulse response (FIR); as is known, this can be accomplished by placing all of its poles in the origin. Instead, it is not possible, in general, to make the overall control system FIR in the case of LPV discrete-time systems. It is possible, however, to make finite the impulse response between the reference signal and the control input.

To this purpose, assume for simplicity that the discrete-time plant is SISO and LPV-stable and that a discrete-time compensator is connected with it according to the discrete-time structure analogous to the one depicted in Fig. 3.5 for the continuous-time case. Let $T(z, w)$ be the Youla–Kucera parameter and let $W_C(z, w)$ be a dead-beat compensator transfer function. From the sensitivity function

$$S(z, w) = 1 - [C(w)(zI - A(w))^{-1}B(w)]T(z, w)$$

it is apparent that, under parameter variations, the impulse response is not finite. However the reference-to-control input transfer function is

$$F_{ru}(z, w) = \frac{W_C(z, w)}{1 + W_C(z, w)P(z, w)} = T(z, w).$$

Hence, if the compensator is dead-beat, then all of the poles of $T(z, w)$ must be in the origin.

According to the pole-placement technique described above, $T(z, w)$ can be realized by means of a nilpotent state matrix. Suppose that

$$\{F^{(T)}, G^{(T)}(w), H^{(T)}(w), K^{(T)}(w)\}$$

is a realization of $T(z, w)$ with $F^{(T)}$ constant and nilpotent. Since $x(0) = 0$ and $\hat{x}(0) = 0$ imply $\hat{y}(k) = y(k)$, for all k , then the control $u(k)$ —which is the output of the compensator corresponding to an impulse at one of the inputs d and r —necessarily has finite support.

Consider the strictly proper LPV plant described by the matrices

$$A(w) = \begin{bmatrix} 0 & 1 \\ -w & 1 \end{bmatrix}, \quad B = \begin{bmatrix} 0 \\ 1 \end{bmatrix}, \quad C = [-1.6 \ 1], \quad (3.52)$$

with $w \in [0.125, 0.875]$, that has been tested to be LPV-stable by means of the procedure suggested in [11], and the first-order compensator

$$W_C(z) = \frac{\alpha z + \beta}{z + \gamma},$$

that places all of the closed-loop poles in the origin for fixed values of w . The parameters $\alpha(w)$, $\beta(w)$, and $\gamma(w)$ are the solution of the Diophantine equation

$$(z + \gamma)(z^2 - z + w) + (\alpha z + \beta)(z - 1.6) = z^3.$$

The implementation of the compensator $\{F_c = -\gamma, H_c = \beta - \gamma\alpha, G_c = 1, K_c = \alpha\}$ may lead to instability. On the contrary, the technique described in Sect. 3.6 ensures LPV stability. Simulations with random jumps of w from an extremum to the other of the interval $[0.125, 0.875]$ are shown in Fig. 3.6.

3.7.3 Online Tuning for LTI Plants

The procedures conceived for LPV plants can profitably be used to synthesize parametric compensators for LTI plants. Precisely, to improve the system performance, some parameters of the controller can be tuned online according to the scheme of Fig. 3.7.

Assume that $P(s)$ is stabilizable in the LTI sense and $W_C(s, w)$ is a family of compensator transfer functions, parametrized with respect to w , that ensure the internal stability of the closed-loop system for all constant $w \in \mathscr{W}$. Then, there always exists a realization of $W_C(s, w)$ that guarantees LPV stability too. The result is valid no matter how the parameter tuning is carried out, manually or automatically.

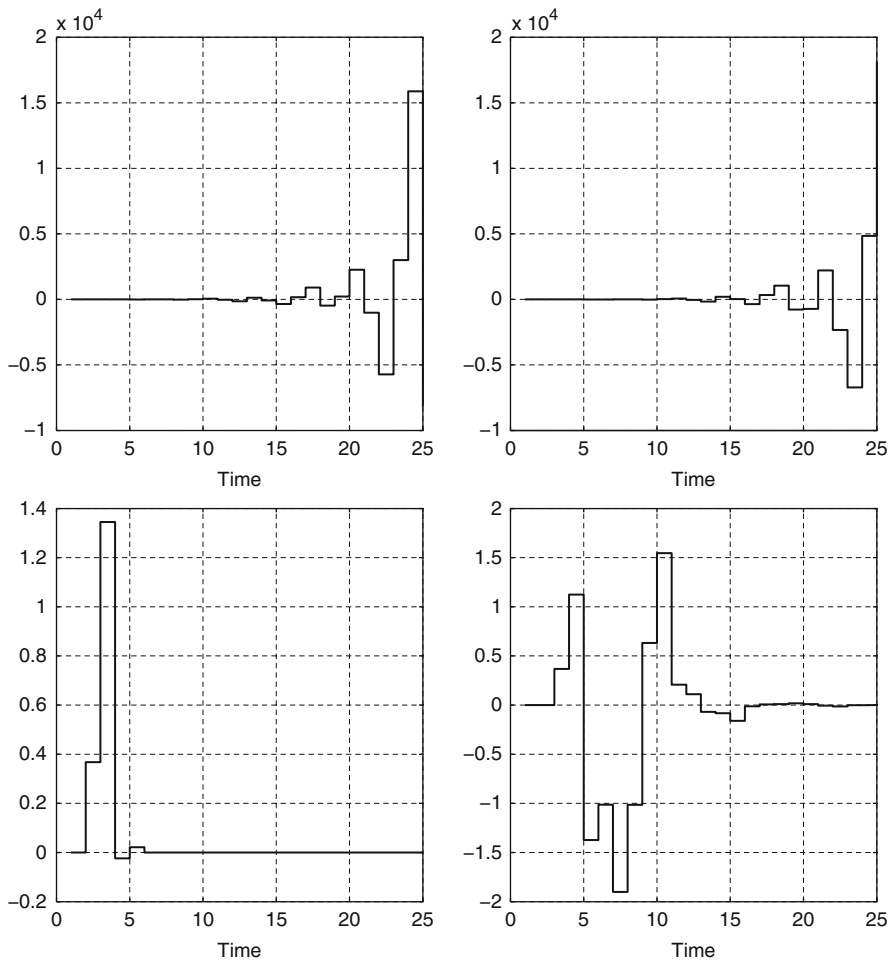


Fig. 3.6 Dead-beat control problem. *Top left:* (unstable) control signal of the direct implementation. *Top right:* the corresponding (unstable) output. *Bottom left:* the FIR control signal of the LPV-stable implementation. *Bottom right:* the (non-FIR) corresponding output

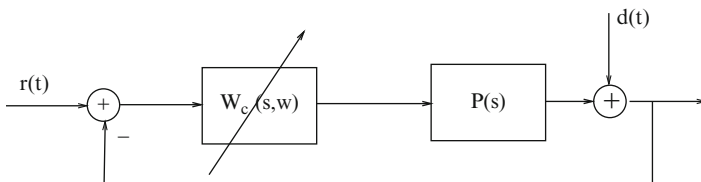


Fig. 3.7 LTI plant with LPV compensator © IEEE 2010 [9]

Example 3.4. Let $P(s)$ in Fig. 3.7 be

$$P(s) = \frac{1}{s + \mu}. \quad (3.53)$$

To (partly) suppress a disturbance $d(t)$ with a (dominant) sinusoidal component of frequency ω_0 , the controller transfer function can be chosen as

$$W_c(s) = \frac{\kappa\omega^2(s + \alpha)}{s^2 + 2\xi\omega s + \omega^2}, \quad (3.54)$$

with $\omega = \omega_0$ and ξ small, which admits the following minimal realization:

$$\left[\begin{array}{c|c} F_{\min} & G_{\min} \\ \hline H_{\min} & K_{\min} \end{array} \right] = \left[\begin{array}{cc|c} 0 & 1 & 0 \\ -\omega^2 & -2\xi\omega & 1 \\ \hline \kappa\alpha\omega^2 & \kappa\omega^2 & 0 \end{array} \right]. \quad (3.55)$$

If the frequency of the disturbance varies in an interval, say $\omega^- \leq \omega \leq \omega^+$, as is often the case in practice, the parameter ω in (3.54) must be adjusted accordingly (which, of course, requires measuring the disturbance frequency) and the control system becomes an LPV system whose stability depends on the controller realization. By considering the above companion realization of the controller, the state, input, and output matrices of the resulting closed-loop system turn out to be:

$$\left[\begin{array}{c|c} A_{\text{CL}} & B_{\text{CL}} \\ \hline C_{\text{CL}} & 0 \end{array} \right] = \left[\begin{array}{ccc|c} -\mu & \kappa\omega^2\alpha & \kappa\omega^2 & 0 \\ 0 & 0 & 1 & 0 \\ -1 & -\omega^2 & -2\xi\omega & 1 \\ \hline 1 & 0 & 0 & 0 \end{array} \right].$$

If we assume for simplicity $\alpha = \mu$ in (3.54) to cancel the pole of (3.53), then the preceding realization is non-minimal and, indeed, equivalent to

$$\left[\begin{array}{c|c} A_{\text{CL}} & B_{\text{CL}} \\ \hline C_{\text{CL}} & 0 \end{array} \right] = \left[\begin{array}{cc|c} 0 & 1 & 0 \\ -(\kappa + 1)\omega^2 & -2\xi\omega & 1 \\ \hline \kappa\omega^2 & 0 & 0 \end{array} \right].$$

It is known that this system is unstable for ξ small and ω varying with time. However, the compensator can be realized in such a way that, for any fixed w , its transfer function matches the desired one and, at the same time, LPV stability is guaranteed. According to Sect. 3.5, the compensator can be given the form

$$W_c(s, w) = -\frac{T(s, w)}{1 - T(s, w)P(s)}, \quad (3.56)$$

from which:

$$T(s, w) = \frac{W_c}{1 + W_c P} = \frac{\kappa \omega^2 (s + \mu)}{s^2 + 2\xi \omega s + (1 + \kappa) \omega^2}.$$

Therefore, the problem can be solved by finding an LPV-stable realization of $T(s, w)$. According to Procedure 3.4.1 and assuming complex eigenvalues, one such realization is

$$\Sigma^{(T)} = \left[\begin{array}{c|c} F^{(T)} & G^{(T)} \\ \hline H^{(T)} & 0 \end{array} \right] = \left[\begin{array}{cc|c} -\xi \omega & \omega \sqrt{1 + \kappa - \xi^2} & 0 \\ -\omega \sqrt{1 + \kappa - \xi^2} & -\xi \omega & 1 \\ \hline h_1(w) & h_2(w) & 0 \end{array} \right],$$

where $h_1(w)$ and $h_2(w)$ are given by

$$h_1(w) = \kappa \omega (\mu - \xi \omega) / \sqrt{1 + \kappa - \xi^2}, \quad h_2(w) = \kappa \omega^2.$$

Thus, (3.56) can be realized as

$$\begin{aligned} \dot{x}_c &= \begin{bmatrix} -\xi \omega & \omega \sqrt{1 + \kappa - \xi^2} & 0 \\ -\omega \sqrt{1 + \kappa - \xi^2} & -\xi \omega & 1 \\ h_1(w) & h_2(w) & -\mu \end{bmatrix} x_c + \begin{bmatrix} 0 \\ 1 \\ 0 \end{bmatrix} e, \\ u &= [h_1(w) \ h_2(w) \ 0] e. \end{aligned} \quad (3.57)$$

Figure 3.8 shows the evolutions of the output y_{lpv} with the controller realized in this way and of the output y_{min} with the same controller realized in the minimal form (3.55) for $\mu = 1$, $\kappa = 10$, and $\xi = 0.01$. The latter clearly leads to instability (note that the scales for y_{lpv} and y_{min} are quite different). The evolution of the tuning parameter ω is also shown in Fig. 3.8.

3.7.4 LPV Stability Within the Hurwitz Region

In most practical cases, given a parametric plant and a parametric compensator, the stability region in the parameter space can be determined by using standard analysis tools, such as the Routh–Hurwitz table. Obviously, this kind of analysis is valid if the parameters are constant in time. However, using the procedure previously outlined, LPV stability can be ensured for all possible parameter variations within the aforementioned stability region.

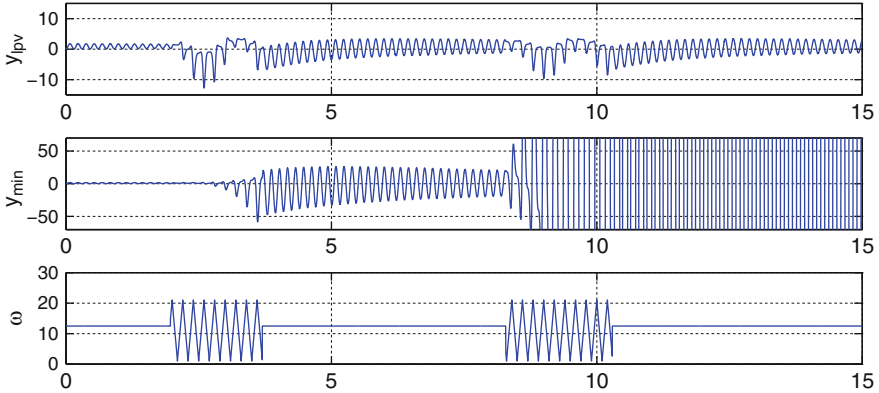


Fig. 3.8 y_{pv} : output with the proposed realization; y_{min} : output corresponding to the unstable closed-loop produced by the minimal realization of the compensator; ω : tuning parameter subject to a piecewise sinusoidal variation © IEEE 2010 [9]

Example 3.5. Consider the plant

$$\left[\begin{array}{c|c} A(w) & B(w) \\ \hline C(w) & 0 \end{array} \right] = \left[\begin{array}{cc|c} 0 & 1 & 0 \\ -(1+\rho w) & -\xi & 1 \\ \hline 1 & 0 & 0 \end{array} \right],$$

with ξ small and positive and ρ slightly less than 1, and assume that the controller must satisfy the following specifications:

- For any fixed value of $w \in [0, 1]$, the controller transfer function has the PI structure:

$$W_c(s) = k + \frac{h}{s}. \quad (3.58)$$

- The closed-loop system is LPV-stable when w varies in time within the interval $[0, 1]$.
- The proportional gain k and the integral gain h can be changed online within the region for which stability is guaranteed for any fixed w .
- The closed-loop system is stable independently of how k and h vary.

Trivial computations based on the Routh–Hurwitz array show that the closed-loop system is stable for every fixed $w \in [0, 1]$, if and only if $h > 0$ and $h \leq \xi(1+k)$. Therefore, for fixed w the stability region in the (k, h) -plane is

$$\mathcal{R} = \{h \geq \varepsilon \quad \text{and} \quad h \leq \xi(1+k) - \varepsilon\},$$

with ε positive and arbitrarily small.

This system is quadratically stabilizable. Possible gains $J(w)$ and $L(w)$ of the observer-based controller (see (3.14)–(3.15)) are

$$J(w) = [\rho w \ -1], \quad L(w) = [0 \ \rho w]^T.$$

Correspondingly, the compensator equations turn out to be

$$\frac{d}{dt} \begin{bmatrix} \hat{x}_1 \\ \hat{x}_2 \end{bmatrix} = \begin{bmatrix} 0 & 1 \\ -(1 + \rho w + k) & -\xi \end{bmatrix} \begin{bmatrix} \hat{x}_1 \\ \hat{x}_2 \end{bmatrix} + \begin{bmatrix} 0 \\ \rho w \end{bmatrix} y(t) + \begin{bmatrix} 0 \\ 1 \end{bmatrix} v(t),$$

$$u(t) = [\rho w \ -1] \begin{bmatrix} \hat{x}_1 \\ \hat{x}_2 \end{bmatrix} + v(t),$$

$$o(t) = -[1 \ 0] \begin{bmatrix} \hat{x}_1 \\ \hat{x}_2 \end{bmatrix} + y(t),$$

$$v(s) = T(s, w) o(s).$$

The Youla–Kucera parameter $T(s, w)$ can be realized starting from any realization of the compensator. A simple realization of (3.58) is given by: $F = 0$, $G = 1$, $H = h$, and $K = k$. In this case:

$$\left[\begin{array}{c|c} F^{(T)}(w) & G^{(T)}(w) \\ \hline H^{(T)}(w) & K^{(T)}(w) \end{array} \right] = \left[\begin{array}{c|c} R(w) & 0 \\ \hline 0 & I \end{array} \right] \left[\begin{array}{c|c|c} 0 & 1 & 0 \\ \hline -(1 + \rho w + k) & -\xi & h \\ \hline -1 & 0 & 0 \end{array} \middle| \begin{array}{c} 0 \\ -(\rho w - k) \\ 1 \end{array} \right] \left[\begin{array}{c|c} R^{-1}(w) & 0 \\ \hline 0 & I \end{array} \right],$$

where $R(w)$ is the upper-triangular Cholesky factor of the solution $P = R^T R = [p_{ij}]$ of the Lyapunov equation:

$$\left(F^{(T)}(w) \right)^T P + P F^{(T)}(w) = -I. \quad (3.59)$$

By setting $\alpha = \xi$, $\beta = (1 + \rho w + k)$, and $\gamma = h$, (3.59) entails the solution of the linear equations:

$$\begin{bmatrix} 0 & 0 & 0 & -2\beta & 0 & -2 \\ 0 & -2\alpha & 0 & 2 & 0 & 0 \\ 0 & 0 & 0 & 0 & 2\gamma & 0 \\ 1 & -\beta & 0 & -\alpha & -1 & 0 \\ 0 & 0 & -1 & \gamma & -\beta & 0 \\ 0 & \gamma & 0 & 0 & -\alpha & 1 \end{bmatrix} \begin{bmatrix} p_{11} \\ p_{22} \\ p_{33} \\ p_{12} \\ p_{23} \\ p_{31} \end{bmatrix} = \begin{bmatrix} -1 \\ -1 \\ -1 \\ 0 \\ 0 \\ 0 \end{bmatrix}.$$

The non-zero entries of $R = [r_{ij}]$ turn out to be

$$\begin{aligned} r_{11} &= \sqrt{p_{11}}, \quad r_{12} = p_{12}/r_{11}, \quad r_{13} = p_{13}/r_{11}, \\ r_{22} &= \sqrt{p_{22} - r_{12}^2}, \quad r_{23} = (p_{23} - r_{12}r_{13})/r_{22}, \\ r_{33} &= \sqrt{p_{33} - r_{13}^2 - r_{23}^2}. \end{aligned}$$

The matrix $R^{-1} = [s_{ij}]$ is also upper-triangular. Its non-zero entries are

$$\begin{aligned} s_{11} &= 1/r_{11}, \quad s_{22} = 1/r_{22}, \quad s_{33} = 1/r_{33}, \\ s_{12} &= -r_{12}/(r_{11}r_{22}), \quad s_{13} = -(r_{22}s_{12} + r_{13}/r_{33}), \\ s_{23} &= -r_{23}/(r_{22}r_{33}). \end{aligned}$$

All of the previous operations can easily be implemented online.

3.7.5 Pointwise Optimality and LPV Stability

The following example shows how LPV stability can be combined with pointwise optimality.

Example 3.6. The LPV system described by

$$\dot{x}(t) = \begin{bmatrix} 0 & 1 & 0 & 0 \\ 0 & 0 & 1 & 0 \\ 0 & 0 & 0 & 1 \\ w(t) & 0 & 0 & 0 \end{bmatrix} x(t) + \begin{bmatrix} 0 \\ 0 \\ 0 \\ 1 \end{bmatrix} u(t), \quad (3.60)$$

$$y(t) = [1 \ 0 \ 0 \ 0] x(t), \quad (3.61)$$

with $w(t) \in [20, 980]$, satisfies Assumption 3.1 and is LPV stabilized by the constant observer and state-feedback gains

$$J(w) = J = [-5442.8 \ -1886.3 \ -352.84 \ -32.57]$$

and

$$L(w) = L = [-32.57 \ -352.84 \ -1886.3 \ -5442.8].$$

Suppose that the LQG controller is designed, for the current value of w , according to the cost function

$$\mathcal{J} = \int_0^\infty \|x(t)\|^2 + 0.01|u(t)|^2 dt$$

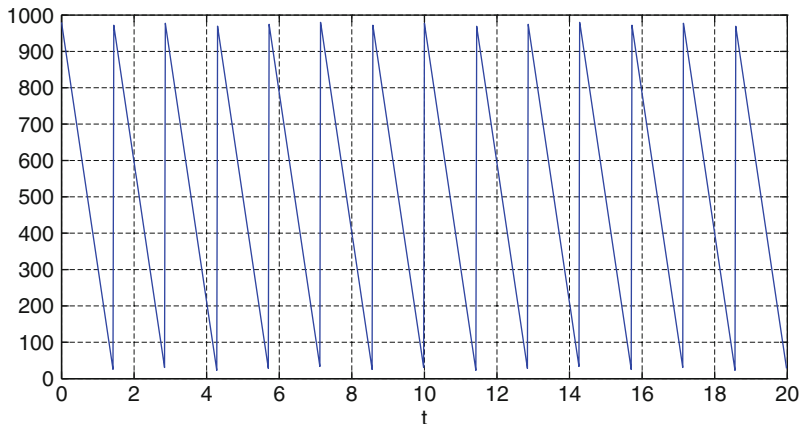


Fig. 3.9 Time course $w(t)$ of the parameter ©IEEE 2010 [9]

and assuming identity state and measurement noise covariance matrices. Suppose also that $w(t)$ is a sawtooth signal spanning the interval from 980 to 20 with a period $T_w = 1.428$ s, as depicted in Fig. 3.9. The direct application of the pointwise controller may lead to instability (see Fig. 3.10, solid line). However, LPV stability can be obtained (see Fig. 3.10, dashed line) without affecting pointwise optimality by following the procedure explained in the previous sections.

3.8 Future Directions

The above-mentioned results lend themselves to interesting extensions. Since the suggested realization procedure is independent of the design criterion, they can be combined with any LTI synthesis technique. It seems particularly suited to the online tuning of standard controllers. Moreover, it could profitably be associated with existing parametric design techniques such as those in [21].

We have seen that pointwise optimality can be ensured along with LPV stability. However, nothing can yet be said about time-varying performance. In this respect, the present chapter follows a path opposite to that followed in [1, 5], where LPV performance has been considered without pointwise optimality. The problem of realizing a pointwise optimal compensator so as to ensure a guaranteed performance is still open.

Another open problem concerns the possibility of “adapting” some robust stability conditions for uncertain LTI systems based on parametric Lyapunov functions [6, 7, 17–19, 26], (for a survey see [20]) so as to ensure LPV stability, too.

In the preceding sections, explicit, yet cumbersome, formulas have been derived for finding a controller by assuming a polyhedral Lyapunov function. It would be interesting to see whether other classes of Lyapunov functions, such as the polynomial [20, 41] and composite ones [25], can lead to simpler formulations.

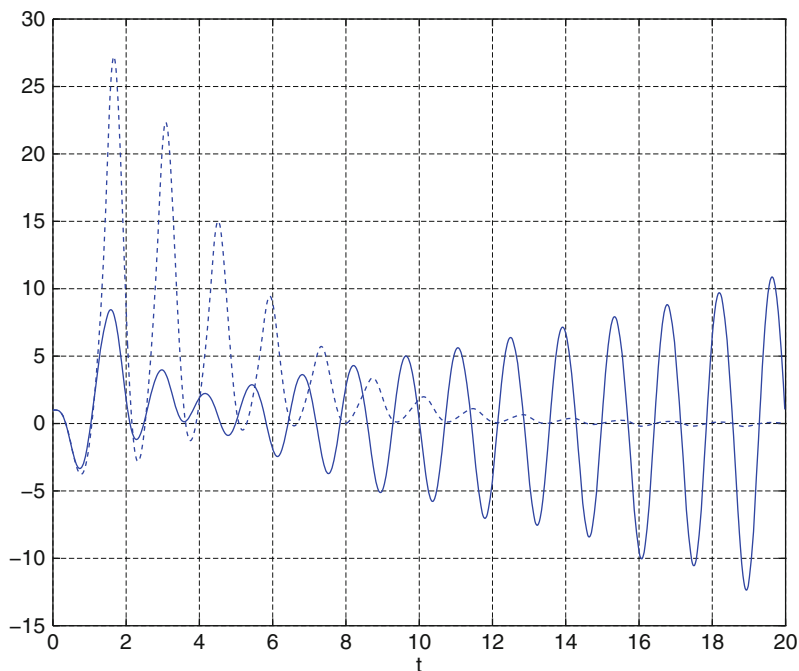


Fig. 3.10 System output with the LQG controller applied directly (*solid line*) and with the LQG controller realized according to the proposed technique (*dashed line*) © IEEE 2010 [9]

References

1. Apkarian P, Gahinet P (1995) A convex characterization of gain-scheduled \mathcal{H}_∞ controllers. *IEEE Trans Automat Contr* 40(5):853–863
2. Barabanov NE (1988) Lyapunov indicator of discrete inclusion. I. *Autom Remote Contr* 49(2):152–157
3. Barabanov NE (1988) Lyapunov indicator of discrete inclusion. II. *Autom Remote Contr* 49(4):283–287
4. Barabanov NE (1988) Lyapunov indicator of discrete inclusion. III. *Autom Remote Contr* 49(5):558–566
5. Becker G, Packard A (1994) Robust performance of linear parametrically varying systems using parametrically-dependent linear feedback. *Syst Contr Lett* 23(3):205–215
6. Bliman PA (2003) Stabilization of LPV systems. In: *Proceedings of 42nd IEEE Conf decision and control*, Maui, HW, pp 6103–6108
7. Bliman PA (2004) A convex approach to robust stability for linear systems with uncertain scalar parameters. *SIAM J Contr Optim* 42(6):2016–2042
8. Blanchini F (1995) Nonquadratic Lyapunov functions for robust control. *Automatica* 31(3):451–461
9. Blanchini F, Casagrande D, Miani S, Viaro U (2010) Stable LPV realization of parametric transfer functions and its application to gain-scheduling control design. *IEEE Trans Automat Contr* 55(10):2271–2281
10. Blanchini F, Miani S (2003) Stabilization of LPV systems: state feedback, state estimation and duality. *SIAM J Contr Optim* 42(1):76–97

11. Blanchini F, Miani S (2008) Set-theoretic methods in control, Birkhäuser, Boston, MA
12. Blanchini F, Miani S, Mesquine F (2009) A separation principle for linear switching systems and parametrization of all stabilizing controllers. *IEEE Trans Automat Contr* 54(2):279–292
13. Blanchini F, Miani S, Savorgnan C (2007) Stability results for linear parameter varying and switching systems. *Automatica* 43(10):1817–1823
14. Boyd S, El Ghaoui L, Feron E, Balakrishnan V (2004) Linear matrix inequalities in system and control theory, SIAM, Philadelphia, PA
15. Brayton RK, Tong CH (1979) Stability of dynamical systems: a constructive approach. *IEEE Trans Circ Syst* 26(4):224–234
16. Brayton RK, Tong CH (1980) Constructive stability and asymptotic stability of dynamical systems. *IEEE Trans Circ Syst* 27(11):1121–1130
17. Chesi G (2003) Robust analysis of linear systems affected by time-invariant hypercubic parameter uncertainty. In: *Proceedings of 42nd IEEE Conf decision and control*, Maui, HI, pp 5019–5024
18. Chesi G, Garulli A, Tesi A, Vicino A, (2007) Robust stability of polytopic systems via polynomially parameter-dependent Lyapunov functions. *Automatica* 43(2):309–316
19. Chesi G, Garulli A, Tesi A, Vicino A, (2005) Polynomially parameter-dependent Lyapunov functions for robust stability of polytopic systems: an LMI approach. *IEEE Trans Automat Contr* 50(3):365–370
20. Chesi G, Garulli A, Tesi A, Vicino A, (2009) Homogeneous polynomial forms for robustness analysis of uncertain systems. Springer, Berlin Heidelberg
21. Dinh M, Scorletti G, Fromion V, Magarotto E (2005) Parameter dependent \mathcal{H}_∞ control by finite dimensional LMI optimization: application to trade-off dependent control. *Int J Robust Nonlin Contr* 15(9):383–406
22. Feron E, Apkarian P, Gahinet P (1996) Analysis and synthesis of robust control systems via parameter-dependent Lyapunov functions. *IEEE Trans Automat Contr* 41(7):1041–1046
23. Helmersson A (1998) μ synthesis and LFT gain scheduling with real uncertainties. *Int J Robust Nonlin Contr* 8(7):631–642
24. Hespanha J, Morse AS (2002) Switching between stabilizing controllers. *Automatica* 38(11):1905–1917
25. Hu T, Huang B, Lin Z (2004) Absolute stability with a generalized sector condition. *IEEE Trans Automat Contr* 49(4):535–548
26. Iwasaki T, Tsiotras P, Zhang X (2005) State-feedback controller synthesis for parameter-dependent LTI systems. In: *Proceedings of american control conference*, Portland, OR, pp 593–597
27. Kucera V (1991) Analysis and design of discrete linear control systems. Prentice Hall, Englewood Cliffs, NJ
28. Lawrence DA, Rugh WJ (1995) Gain scheduling dynamic controllers for a nonlinear plant. *Automatica* 31(3):381–390
29. Liberzon D (2003) Switching in systems and control, systems and control: foundations & applications, Birkhäuser, Boston, MA
30. Molchanov AP, Pyatnitskii ES (1986) Lyapunov functions that define necessary and sufficient conditions for absolute stability of nonlinear nonstationary control systems. I. *Autom Remote Contr* 47:344–354
31. Molchanov AP, Pyatnitskii ES (1986) Lyapunov functions that define necessary and sufficient conditions for absolute stability of nonlinear nonstationary control systems. II. *Autom Remote Contr* 47:443–451
32. Molchanov AP, Pyatnitskii ES (1986) Lyapunov functions that define necessary and sufficient conditions for absolute stability of nonlinear nonstationary control systems. III. *Autom Remote Contr* 47:620–630
33. Rugh WJ, Shamma JS (2000) Research on gain scheduling. *Automatica* 36(10):1401–1425
34. Sanchez-Pena R, Szafer M (1998) Robust systems, theory and applications. Wiley, New York
35. Scorletti G, El Ghaoui L (1992) Improved LMI conditions for gain scheduling and related control problems. *Int J Robust Nonlin Contr* 8(10):845–877

36. Shahruz SM, Behtash S (1992) Designing controllers for linear parameter-varying systems by the gain scheduling technique. *J Math Anal Appl* 168(1):195–217
37. Shamma JS (1996) Linearization and gain scheduling. In: Levine W (ed) *The control handbook*, CRC Press, pp 388–396
38. Shamma JS, Athans M (1990) Analysis of gain scheduled control for nonlinear plants. *IEEE Trans Automat Contr* 35(8):898–907
39. Shamma JS, Athans M (1991) Guaranteed properties of gain scheduled control for linear parameter-varying plants. *Automatica* 27(3):559–564
40. Youla D, Jabr H, Bongiorno J (1976) Modern Wiener–Hopf design of optimal controllers. ii. The multivariable case. *IEEE Trans Automat Contr* 21(3):319–338
41. Zelentsowsky AL (1994) Nonquadratic Lyapunov functions for robust stability analysis of linear uncertain system. *IEEE Trans Automat Contr* 39(1):135–138
42. Zhou K, Doyle J, Glover K (1996) *Robust and optimal control*, Prentice Hall, Englewood, Cliffs, NJ

Chapter 4

Explicit Controller Parametrizations for Linear Parameter-Varying Affine Systems Using Linear Matrix Inequalities

Maurício C. de Oliveira

Abstract In this chapter, we derive explicit controller parametrizations for the design of output feedback controllers for *affine Linear Parametrically Varying* (LPV) systems in the form of Linear Matrix Inequalities (LMIs). The main feature is that variables related to the LPV controller parameters are retained in the design inequalities, a fact that can be used to impose a simpler structure to the resulting controller as well as to develop applications in a number of control problems, such as mixed objective control problems and delay systems. We develop formulas using two approaches: one based on polytopes and another based on norm-bounded uncertainty models. We provide a comparison between these two approaches and their relation to existing results in the literature.

4.1 Problem Formulation

Consider the following continuous-time time-varying linear system described in state space form by the equations

$$\begin{aligned}\dot{x}(t) &= A(\delta(t))x(t) + B_w w(t) + B_u u(t), \\ z(t) &= C_z(\delta(t))x(t) + D_{zw} w(t) + D_{zu} u(t), \\ y(t) &= C_y(\delta(t))x(t) + D_{yw} w(t).\end{aligned}\tag{4.1}$$

where all matrices have dimensions compatible with the signals $x \in \mathbb{R}^n$, $u \in \mathbb{R}^m$, $w \in \mathbb{R}^p$, $z \in \mathbb{R}^q$, $y \in \mathbb{R}^r$, respectively, the state, the control input, an exogenous disturbance, the controlled output, and the measurement output.

M.C. de Oliveira (✉)

Department of Mechanical and Aerospace Engineering, University of California, San Diego, 9500 Gilman Dr., La Jolla, CA 92093-0411, USA
e-mail: mauricio@ucsd.edu

Throughout this chapter, the vector $\delta(t) \in \mathbb{R}^s$ is assumed to be a measurable parameter that will be used by a controller in order to provide stability and performance guarantees to the resulting time-varying linear system. Such systems are often called *Linear Parametrically Varying* systems, or LPV systems, for short. As it is standard in the LPV literature, the parameter $\delta(t)$ is assumed to lie in a compact set Δ which is known a priori even though the actual trajectory $\delta(t)$ is only measured at run-time. In the present chapter, we assume that the dependence of A , C_z , and C_y on $\delta(t)$ is affine, that is,

$$\begin{aligned} A(\delta(t)) &:= A_0 + \sum_{i=1}^s \delta_i(t) A_i, \\ C_z(\delta(t)) &:= C_{z0} + \sum_{i=1}^s \delta_i(t) C_{zi}, \\ C_y(\delta(t)) &:= C_{y0} + \sum_{i=1}^s \delta_i(t) C_{yi}. \end{aligned} \quad (4.2)$$

There are results in the literature that can handle more general forms of dependence on $\delta(t)$, in particular, explicit or implicit rational dependence on $\delta(t)$ are commonly found. A common thread among those approaches is the use of the Elimination Lemma [5, 16] that is used to remove the dependence of the synthesis condition on the controller parameters. See, for instance [1, 2, 4, 12, 13, 15]. Consequently, in these works, the controller does not directly appear on the design inequalities. The main contribution of the present chapter is to derive LMIs for the design of LPV controllers in which the controller parameters appear explicitly, represented by a number of transformed variables. Such feature will enable the application of these formulas in a number of problems, as we will discuss in Sect. 4.4.

In the present chapter, we will determine the parameters of an LPV controller that has the exact same form as the LPV plant, that is,

$$\begin{aligned} \dot{\hat{x}}(t) &= \hat{A}(\delta(t))\hat{x}(t) + \hat{B}y(t), \\ u(t) &= \hat{C}(\delta(t))\hat{x}(t) + \hat{D}y(t), \end{aligned} \quad (4.3)$$

where $\hat{x} \in \mathbb{R}^{n_c}$ and

$$\hat{A}(\delta(t)) := \hat{A}_0 + \sum_{i=1}^s \delta_i(t) \hat{A}_i, \quad \hat{C}(\delta(t)) := \hat{C}_0 + \sum_{i=1}^s \delta_i(t) \hat{C}_i. \quad (4.4)$$

The above controller makes use of the measurement input $y(t)$ as well as the measurable parameter vector $\delta(t)$. We shall assume that $n_c = n$, that is, the controller is *full order*. Note that many LPV methods in the literature produce controllers which are *rational* functions of the parameter $\delta(t)$ even when the plant is affine on the parameter [12, 13] or with a different affine structure [2].

4.2 Closed Loop Stability Analysis

The closed loop connection of the LPV plant (4.1) with the LPV controller (4.3) produces a closed loop LPV system of the form

$$\begin{aligned}\dot{\tilde{x}}(t) &= \mathcal{A}(\delta(t))\tilde{x}(t) + \mathcal{B}w(t), \\ z(t) &= \mathcal{C}(\delta(t))\tilde{x}(t) + \mathcal{D}w(t),\end{aligned}\tag{4.5}$$

where

$$\tilde{x}(t) := \begin{bmatrix} x(t) \\ \hat{x}(t) \end{bmatrix},\tag{4.6}$$

and

$$\begin{aligned}\mathcal{A}(\delta(t)) &:= \begin{bmatrix} A(\delta(t)) + B_u \hat{D}C_y(\delta(t)) & B_u \hat{C}(\delta(t)) \\ \hat{B}C_y(\delta(t)) & \hat{A}(\delta(t)) \end{bmatrix}, & \mathcal{B} &:= \begin{bmatrix} B_w + B_u \hat{D}D_{yw} \\ \hat{B}D_{yw} \end{bmatrix}, \\ \mathcal{C}(\delta(t)) &:= \begin{bmatrix} C_z(\delta(t)) + D_{zu} \hat{D}C_y(\delta(t)) & D_{zu} \hat{C}(\delta(t)) \end{bmatrix}, & \mathcal{D} &:= D_{zw} + D_{zu} \hat{D}D_{yw}.\end{aligned}\tag{4.7}$$

Under the assumption of an affine LPV plant (4.2) as well as an affine LPV controller (4.4), the matrices $\mathcal{A}(\delta(t))$ and $\mathcal{C}(\delta(t))$ are also affine functions of the parameter $\delta(t)$.

As mentioned earlier, we will treat the parameter $\delta(t)$ as an uncertainty in the compact set Δ at each instant of time t . In the present chapter, we consider that Δ is the unit hypercube

$$\Delta_R := \{(\delta_1, \dots, \delta_s) : |\delta_i| \leq 1 \text{ for all } i = 1, \dots, s\}$$

hypercubes with different sizes can be obtained by simply scaling the problem data.

In the next sections, we develop sufficient conditions based on the concept of quadratic stability [3] that will later be used to design the LPV controller. We simultaneously develop two of the most popular approaches found in the literature: one based on *polytopes* and the other on *norm-bounded* uncertainties in the spirit of μ -analysis. In Sect. 4.4, we compare and discuss possible applications for the two sets of conditions.

4.2.1 Polytopic Approach

The LPV controller will be obtained by ensuring that the linear time-varying closed loop system (4.5) is asymptotically stable and, in addition, that it has a bounded L_2 to L_2 gain from the exogenous input w to the controlled output z for all $\delta(t) \in \Delta_R$. After properly scaling the system, this corresponds to asking that $\|z\|_2 < 1$ whenever

$\|w\|_2 < 1$. In this case, a well-known sufficient condition [2] is that the following inequalities, derived from the *Bounded-Real Lemma* [5] using quadratic stability [3], be satisfied

$$\begin{bmatrix} A_j^T \mathcal{P} + \mathcal{P} A_j & \mathcal{P} \mathcal{B} & C_j^T \\ \mathcal{B}^T \mathcal{P} & -I & \mathcal{D}^T \\ C_j & \mathcal{D} & -I \end{bmatrix} \prec 0 \quad \text{for all } j = 1, \dots, 2^s, \quad (4.8)$$

for some matrix $\mathcal{P} = \mathcal{P}^T \succ 0$ where \mathcal{B} , \mathcal{D} are as in (4.7) and the matrices A_j and C_j are constructed by taking all possible combinations of sums and differences of matrices of the form

$$\mathcal{A}_i := \begin{bmatrix} A_i + B_u \hat{D} C_{yi} & B_u \hat{C}_i \\ \hat{B} C_{yi} & \hat{A}_i \end{bmatrix}, \quad \mathcal{C}_i := [C_{zi} + D_{zu} \hat{D} C_{yi} \quad D_{zu} \hat{C}_i], \quad i = 0, \dots, s. \quad (4.9)$$

Indeed

$$A_j = \mathcal{A}_0 + \sum_{i=1}^s e_i^j \mathcal{A}_i, \quad C_j = \mathcal{C}_0 + \sum_{i=1}^s e_i^j \mathcal{C}_i, \quad (4.10)$$

where e^j , $j = 1, \dots, 2^s$, are vectors representing each of the 2^s vertices of the hypercube Δ_R . All entries of a particular e^j are either “1” or “−1”.

Clearly one disadvantage of the polytopic approach is the exponential number of inequalities, which grow with 2^s . The above setup is very close to the one in [2]. However, there are significant differences related to the structure of the controller (4.4), which we will discuss later in Sect. 4.4.

4.2.2 Norm-Bounded Approach

As with the polytopic approach, we wish to enforce that the linear time-varying closed loop system (4.5) be asymptotically stable and that the L_2 to L_2 gain from w to z be bounded for all $\delta(t) \in \Delta_R$. This will be achieved by using tools from μ -analysis with real and mixed-type uncertainties [6, 17]. We start by introducing the following auxiliary LTI plant

$$\begin{aligned} \dot{x}(t) &= A_0 x(t) + \sum_{i=1}^s A_i v_i(t) + B_w w(t) + B_u u(t), \\ r_1(t) &= r_2(t) = \dots = r_s(t) = x(t), \\ z(t) &= C_{z0} x(t) + \sum_{i=1}^s C_{zi} v_i(t) + D_{zw} w(t) + D_{zu} u(t), \\ y(t) &= C_{y0} x(t) + \sum_{i=1}^s C_{yi} v_i(t) + D_{yw} w(t), \end{aligned} \quad (4.11)$$

and the auxiliary LTI controller

$$\begin{aligned}\dot{\hat{x}}(t) &= \hat{A}_0 \hat{x}(t) + \sum_{i=1}^s \hat{A}_s \hat{v}_i(t) + \hat{B}_y u(t), \\ \hat{r}_1(t) &= \hat{r}_2(t) = \dots = \hat{r}_s(t) = \hat{x}(t), \\ u(t) &= \hat{C}_0 \hat{x}(t) + \sum_{i=1}^s \hat{C}_i \hat{v}_i(t) + \hat{D} y(t).\end{aligned}\quad (4.12)$$

As we shall see later, it is essential that the outputs r_i 's and \hat{r}_i 's be copies of the plant and controller state. Defining $\tilde{x}(t)$ as in (4.6) and

$$\tilde{r}_i(t) := \begin{bmatrix} r_i(t) \\ \hat{r}_i(t) \end{bmatrix}, \quad \tilde{v}_i(t) := \begin{bmatrix} v_i(t) \\ \hat{v}_i(t) \end{bmatrix}, \quad i = 1, \dots, s,$$

the closed loop connection of the auxiliary LTI system (4.11) and the auxiliary LTI controller (4.12) produces the LTI closed loop plant

$$\begin{aligned}\dot{\tilde{x}}(t) &= \mathcal{A}_0 \tilde{x}(t) + \sum_{i=1}^s \mathcal{A}_i \tilde{v}_i(t) + \mathcal{B} w(t), \\ \tilde{r}_1(t) &= \tilde{r}_2(t) = \dots = \tilde{r}_s(t) = \tilde{x}(t), \\ z(t) &= \mathcal{C}_0 \tilde{x}(t) + \sum_{i=1}^s \mathcal{C}_i \tilde{r}_i(t) + \mathcal{D} w(t),\end{aligned}\quad (4.13)$$

where $\mathcal{A}_i, \mathcal{C}_i$ are defined in (4.9) and \mathcal{B}, \mathcal{D} are as in (4.7).

The above closed loop LTI system is related to the closed loop LPV system (4.5) through the standard feedback interconnection depicted in the diagram of Fig. 4.1, where

$$r(t) = \begin{bmatrix} \tilde{r}_1(t) \\ \vdots \\ \tilde{r}_s(t) \end{bmatrix}, \quad v(t) = \begin{bmatrix} \tilde{v}_1(t) \\ \vdots \\ \tilde{v}_s(t) \end{bmatrix},$$

P is the LTI system (4.13), and $\Delta = \Delta_R$ represents the time-varying and norm-bounded scheduled parameter.

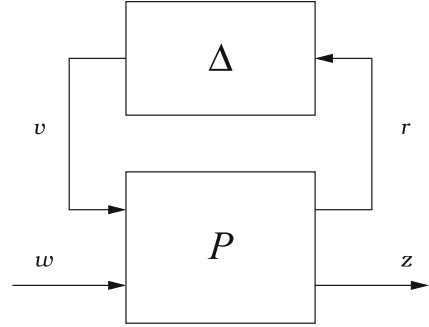
In order to handle the bounded L_2 to L_2 gain requirement, we augment the set Δ_R as follows:

$$\Delta_N := \{(\delta, \Delta) : \delta \in \Delta_R, \quad \|\Delta\| \leq 1\},$$

and ask that the following inequality, which is derived from the Bounded-Real Lemma with the addition of (D, G) scalings [6], be satisfied

$$\begin{bmatrix} \mathcal{A}_0^T & \mathcal{P} & \mathcal{P} \mathcal{A}_0 & \mathcal{P} \mathcal{F} \\ \mathcal{F}^T & \mathcal{P} & & 0 \end{bmatrix} + \begin{bmatrix} \mathcal{G} & \mathcal{H} \\ 0 & I \end{bmatrix}^T \begin{bmatrix} \mathcal{W} & \mathcal{S} \\ -\mathcal{S} & -\mathcal{W} \end{bmatrix} \begin{bmatrix} \mathcal{G} & \mathcal{H} \\ 0 & I \end{bmatrix} < 0 \quad (4.14)$$

Fig. 4.1 Loop interconnection



for some matrices $\mathcal{P} = \mathcal{P}^T \succ 0$, $W = W^T \succ 0$ and $S = -S^T$, where the matrices F , G , and H are defined as

$$\begin{bmatrix} \star & F \\ G & H \end{bmatrix} := \left[\begin{array}{c|cccc} \star & \mathcal{A}_1 & \cdots & \mathcal{A}_s & \mathcal{B} \\ \hline I & 0 & \cdots & 0 & 0 \\ \vdots & \vdots & \ddots & \vdots & \vdots \\ I & 0 & \cdots & 0 & 0 \\ \mathcal{C}_0 & \mathcal{C}_1 & \cdots & \mathcal{C}_s & \mathcal{D} \end{array} \right] \quad (4.15)$$

and the scalings W and S have the particular structure

$$W = \begin{bmatrix} \mathcal{W}_1 & & 0 \\ & \ddots & \\ 0 & & \mathcal{W}_s \\ & & & I \end{bmatrix}, \quad S = \begin{bmatrix} \mathcal{S}_1 & & 0 \\ & \ddots & \\ 0 & & \mathcal{S}_s \\ & & & 0 \end{bmatrix}. \quad (4.16)$$

The LMI (4.14) can be interpreted in the light of standard results in μ -analysis with mixed parametric uncertainty, where the structure of the scalings W and S used above is that of block diagonal (D, G) scalings [6].

4.3 LMIs for Control Design

We now derive LMIs for the design of LPV controllers for affine LPV systems in which the variables associated with the controller parameters appear explicitly, in the spirit of [14]. Let us first define the linear functions

$$\mathbf{A}_i(X, Y, F, R, Q_i, L_i) := \begin{bmatrix} A_i X + B_u L_i & A_i + B_u R C_{yi} \\ Q_i & Y A_i + F C_{yi} \end{bmatrix},$$

$$\begin{aligned}
\mathbf{C}_i(X, R, L_i) &:= [C_{zi}X + D_{zu}L_i \ C_{zi} + D_{zu}RC_{yi}], \\
\mathbf{B}(Y, F, R) &:= \begin{bmatrix} B_w + B_uRD_{yw} \\ YB_w + FD_{yw} \end{bmatrix}, \\
\mathbf{D}(R) &:= D_{zw} + D_{zu}RD_{yw},
\end{aligned} \tag{4.17}$$

for $i = 0, \dots, s$. The dependence on the indicated variables will often be omitted in the interest of a more compact presentation.

In the next sections, we will derive LMIs involving the above functions. Once these LMIs have been solved, the controller parameters can be calculated by first computing square matrices U and V such that

$$YX + VU = I. \tag{4.18}$$

It is always possible to compute matrices U and V which are square and nonsingular from the matrices X and Y obtained from the LMIs, which should satisfy $X \succ Y^{-1}$ (see [14] for details). The controller matrices appearing in (4.3)–(4.4) can then be computed as

$$\begin{aligned}
\begin{bmatrix} \hat{A}_0 \cdots \hat{A}_s & \hat{B} \\ \hat{C}_0 \cdots \hat{C}_s & \hat{D} \end{bmatrix} &= \begin{bmatrix} V & YB_u \\ 0 & I \end{bmatrix}^{-1} \\
&\times \left(\begin{bmatrix} Q_0 \cdots Q_s & F \\ L_0 \cdots L_s & R \end{bmatrix} - \begin{bmatrix} YA_0X \cdots YA_sX & 0 \\ 0 & \cdots & 0 & 0 \end{bmatrix} \right) \begin{bmatrix} U & \cdots & 0 & 0 \\ \vdots & \ddots & \vdots & \vdots \\ 0 & \cdots & U & 0 \\ C_{y0}X \cdots C_{ys}X & I \end{bmatrix}^{-1}, \tag{4.19}
\end{aligned}$$

for both the polytopic model as well as the norm-bounded model. The matrices X , Y , F , R , Q_i , F_i , $i = 0, \dots, s$, come from the solution to the LMIs to be introduced in the next theorems.

Theorem 4.1 (Polytopic). *Consider the linear functions \mathbf{A}_i , \mathbf{B} , \mathbf{C}_i , \mathbf{D} , $i = 0, \dots, s$, defined in (4.17). If there exists matrices $X = X^T$, $Y = Y^T$, F , R , Q_i , F_i , $i = 0, \dots, s$, such that the LMIs*

$$\begin{bmatrix} X & I \\ I & Y \end{bmatrix} \succ 0, \tag{4.20}$$

$$\begin{bmatrix} \mathbf{A}_0 + \mathbf{A}_0^T + \sum_{i=1}^s e_i^j (\mathbf{A}_i + \mathbf{A}_i^T) & \mathbf{B} & \mathbf{C}_0^T + \sum_{i=1}^s e_i^j \mathbf{C}_i^T \\ \mathbf{B}^T & -I & \mathbf{D}^T \\ \mathbf{C}_0 + \sum_{i=1}^s e_i^j \mathbf{C}_i & \mathbf{D} & -I \end{bmatrix} \prec 0, \quad \text{for all } j = 1, \dots, 2^s, \tag{4.21}$$

have a feasible solution then the feedback connection of the LPV system (4.1)–(4.2) with the LPV controller (4.3)–(4.4), where the controller matrices are computed using (4.18)–(4.19), is asymptotically stable and the L_2 to L_2 gain from the exogenous input w to the controlled output z is less than one for all time-varying $\delta(t) \in \Delta_R$.

Theorem 4.2 (Norm-bounded). Consider the linear functions $\mathbf{A}_i, \mathbf{B}, \mathbf{C}_i, \mathbf{D}$, $i = 0, \dots, s$, defined in (4.17). If there exists matrices $X = X^T$, $Y = Y^T$, F, R, Q_i, F_i , $i = 0, \dots, s$, and $W_i = W_i, S_i = -S_i^T$, $i = 1, \dots, s$, such that the LMIs

$$\begin{bmatrix} X & I \\ I & Y \end{bmatrix} \succ 0, \quad W_i \succ 0, \quad \text{for all } i = 1, \dots, s, \quad (4.22)$$

$$\begin{bmatrix} \mathbf{A}_0^T + \mathbf{A}_0 + \sum_{i=1}^s W_i & \mathbf{A}_1 + S_1 & \cdots & \mathbf{A}_s + S_s & \mathbf{B} & \mathbf{C}_0^T \\ \mathbf{A}_1^T - S_1 & -W_1 & \cdots & 0 & 0 & \mathbf{C}_1^T \\ \vdots & \vdots & \ddots & \vdots & \vdots & \vdots \\ \mathbf{A}_s^T - S_s & 0 & \cdots & -W_s & 0 & \mathbf{C}_s^T \\ \mathbf{B}^T & 0 & \cdots & 0 & -I & \mathbf{D}^T \\ \mathbf{C}_0 & \mathbf{C}_1 & \cdots & \mathbf{C}_s & \mathbf{D} & -I \end{bmatrix} \prec 0, \quad (4.23)$$

have a feasible solution then the feedback connection of the LPV system (4.1)–(4.2) with the LPV controller (4.3)–(4.4), where the controller matrices are computed using (4.18)–(4.19), is asymptotically stable and the L_2 to L_2 gain from the exogenous input w to the controlled output z is less than one for all time-varying $\delta(t) \in \Delta_R$.

A sketch of the proof of the above theorems can be found in Sect. 4.5.

4.4 Discussion

In this section, we discuss relations between the LMIs appearing in Theorems 4.1 and 4.2 and with existing results in the literature, as well as applications to other problems, such as mixed objective synthesis and delay systems.

4.4.1 Comparison Between the Polytopic and Norm-Bounded Approaches

We start by comparing Theorem 4.1 with Theorem 4.2. It is often hard to draw a clear-cut comparison between results obtained using the polytopic and the norm-bound approaches. One element that complicates a comparison in the case of LPV

control design is that the resulting controllers often have different structures in each case. The explicit controller parametrization developed in the present chapter enforces the exact same structure to the controller in both approaches, which facilitates a comparison. Indeed, it is easy to prove the following result.

Lemma 4.1. *If there exists matrices $X = X^T$, $Y = Y^T$, F , R , Q_i , F_i , $i = 0, \dots, s$, and $W_i = W_i^T$, $S_i = -S_i^T$, $i = 1, \dots, s$, satisfying the LMIs (4.22)–(4.23) from Theorem 4.2, then the same matrices also satisfy the LMIs (4.20)–(4.21) from Theorem 4.1.*

The lemma implies that the polytopic approach is always *less conservative* than the norm-bounded approach. However, as noted before, this comes at the expense of an exponential growth in the number of inequalities, which might render the norm-bounded inequalities from Theorem 4.2 attractive in the case of a large number of scheduled parameters $\delta(t)$. Theorem 4.2 might also be preferred in the case of other types of parameter scheduling, e.g., as in Sect. 4.4.5.

Lemma 4.1 can be proved simply by multiplying the inequality (4.23) by matrices

$$R^j = \begin{bmatrix} e^j \otimes I & 0 & 0 \\ 0 & I & 0 \\ 0 & 0 & I \end{bmatrix}, \quad \text{for all } j = 1, \dots, 2^s,$$

where the vectors e^j 's are the vertices of the hypercube Δ_R , to obtain inequalities (4.21).

4.4.2 Comparison with Existing Polytopic Results

Start by noting that Theorem 4.1 is not simply an application of the controller parametrization of [14] in the context of [2]. The main difference is that the controller obtained in Theorem 4.1 has the structure (4.4), whereas the controller obtained in [2] is of the form

$$\begin{bmatrix} \hat{A}(\theta(t)) & \hat{B}(\theta(t)) \\ \hat{C}(\theta(t)) & \hat{D}(\theta(t)) \end{bmatrix} = \sum_{j=1}^{2^s} \theta_j(t) \begin{bmatrix} \hat{A}_j & \hat{B}_j \\ \hat{C}_j & \hat{D}_j \end{bmatrix}, \quad (4.24)$$

where the controller parameters \hat{A}_j , \hat{B}_j , \hat{C}_j , \hat{D}_j , $j = 1, \dots, 2^s$, are computed from 2^s inequalities which are similar to (4.21), and θ is a convex combination parameter satisfying

$$\delta(t) = \sum_{j=1}^{2^s} \theta_j(t) e^j, \quad \sum_{j=1}^{2^s} \theta_j(t) = 1, \quad \theta_j(t) \geq 0. \quad (4.25)$$

Note that by imposing the structure (4.4) we might be losing some generality but have dramatically reduced the number of controller parameters (from 4×2^s matrices to $2s + 4$ matrices) as well as achieved a much simpler, i.e., practical, implementation. Indeed, the controller in Theorem 4.1 uses $\delta(t)$ directly while the controller from [2] needs an extra online computation of the convex combination parameter $\theta(t)$ as in (4.25). Note that computing (4.25) requires, in general, that a linear optimization program be solved.

Furthermore, the methods of [2] cannot be used to compute a controller with the structure (4.4). Indeed, because the controller parameters are eliminated from the inequalities, it is impossible to account for the coupling between the controller structure (4.4) and the 2^s inequalities (4.21) (see the proof in Sect. 4.5 for more details). The converse, however, is perfectly fine. That is, it is possible to modify the inequalities in Theorem 4.1 to compute a controller with the structure (4.24).

4.4.3 Comparison with Existing Norm-Bounded Results

The LMIs in Theorem 4.2 can provide explicit parametrizations for the controllers developed in [1, 4, 15] under their respective setup *and* the assumption that the dependence on the parameter $\delta(t)$ is affine. The latter assumption seems to be essential. This is unfortunate, since one of the advantages of the norm-bounded approach is precisely the possibility of handling fairly general rational dependence on the parameter $\delta(t)$ [11]. However, at this point, it seems to be impossible to generalize Theorem 4.2 to cope with rational dependence on $\delta(t)$ without sacrificing linearity of the resulting inequalities. This is even more so in the case of Theorem 4.1, which relies on the machinery of convex combinations that are hard if not impossible to generalize to rational dependence on $\delta(t)$ without convexity.

4.4.4 Mixed Objective Synthesis

Perhaps the main advantage of having LMIs involving explicit parametrizations of LPV controllers is to open the door to a host of control problems with mixed objectives, as done by [14] in the case of standard LTI systems. This is indeed one of our motivations. Once a controller parametrization such as the one proposed in the present chapter is available, one can combine many different performance specifications that should be satisfied simultaneously by a single LPV controller by adding linear constraints on the auxiliary problem variables, e.g., Lyapunov and slack matrices, as done in [14]. For discrete-time systems, it is possible to go even further and introduce additional variables that lead to very effective synthesis conditions, as shown in [10]. The derivation of such conditions starting from the ones provided in the present chapter is a straightforward exercise, which we leave to the interested reader.

4.4.5 Application to Delay Systems

The LMIs derived in Theorem 4.2 can have a rather unexpected application to the control of systems with delays. Indeed, from the point of view of μ -analysis, if the uncertainties in the loop interconnection of Fig. 4.1 are norm-bounded complex linear time-invariant operators, one shall arrive at the exact same conditions of Theorem 4.2 with the extra constraint that the skew-symmetric variables S_i be all zero. But this is precisely the case when the δ 's are replaced by time delays, which are complex linear operators in the unit circle. The conclusion is that one can state the following lemma.

Lemma 4.2 (Delay systems). *If there exists matrices $X = X^T$, $Y = Y^T$, F , R , Q_i , F_i , $i = 0, \dots, s$, and $W_i = W_i^T$, $S_i = 0$, $i = 1, \dots, s$, such that the LMIs (4.22)–(4.23) have a feasible solution then the feedback connection of the linear delay-system*

$$\begin{aligned}\dot{x}(t) &= A_0x(t) + \sum_{i=1}^s A_ix(t - \tau_i) + B_w w(t) + B_u u(t), \\ z(t) &= C_{z0}x(t) + \sum_{i=1}^s C_{zi}x(t - \tau_i) + D_{zw}w(t) + D_{zu}u(t), \\ y(t) &= C_{y0}x(t) + \sum_{i=1}^s C_{yi}x(t - \tau_i) + D_{yw}w(t),\end{aligned}$$

with the linear delay-controller

$$\begin{aligned}\dot{\hat{x}}(t) &= \hat{A}_0\hat{x}(t) + \sum_{i=1}^s \hat{A}_s\hat{x}(t - \tau_i) + \hat{B}_y u(t), \\ u(t) &= \hat{C}_0\hat{x}(t) + \sum_{i=1}^s \hat{C}_i\hat{x}(t - \tau_i) + \hat{D}y(t),\end{aligned}$$

where the controller matrices are computed using (4.18)–(4.19), is asymptotically stable and the H_∞ of the closed loop transfer function from the exogenous input w to the controlled output z is less than one for all time-invariant $\tau_i \geq 0$, $i = 1, \dots, s$.

The above condition is a generalization of the result of [8] for multiple delays. Note that the quantity that is assumed to be measured online in this case is the time delay $\tau_i \geq 0$. In this sense, the controller in Lemma 4.2 can be thought as scheduling the time-invariant norm-bounded delay in much the same way that the LPV controller is scheduling the norm-bounded time-varying parameter $\delta(t) \in \Delta_R$. It is interesting to note that it does not seem possible to directly apply the less-conservative polytopic condition in Theorem 4.1 to delay systems. Indeed, the convex combination machinery prevents the application of Theorem 4.1 to complex parameters.

4.4.6 Robust Control

The fact that we were able to impose the structure (4.4) on the controller might lead one to believe that additional constraints other than the ones discussed above can also be imposed on the controller. Unfortunately this is not the case. Consider for example that one would like to use the present setup to design a *robust controller*, that is, a controller that does not depend on $\delta(t)$. By inspection of (4.4), this corresponds simply to the linear constraints $\hat{A}_i = 0, \hat{C}_i = 0$, for $i = 1, \dots, s$. However, such constraints, when translated in terms of the design variables, become highly nonlinear. In particular, note that if we set $Q_i = 0, L_i = 0$, for $i = 1, \dots, s$, in (4.19) we still obtain $\hat{A}_i \neq 0, \hat{C}_i \neq 0$, for $i = 1, \dots, s$. See [7, 9] for additional discussions on the robust control problem.

4.5 Proofs of the Theorems

The proof of Theorems 4.1 and 4.2 follow the ideas in [14]. Here, we sketch the necessary steps required to prove Theorem 4.2. Theorem 4.1 can be proved along the same lines. We provide some comments regarding Theorem 4.1 at the end of the section.

Define the partitions associated with the symmetric matrix \mathcal{P} , its inverse and the related nonsingular matrix \mathcal{T} as

$$\mathcal{P} := \begin{bmatrix} Y & V \\ V^T & \hat{Y} \end{bmatrix}, \quad \mathcal{P}^{-1} := \begin{bmatrix} X & U^T \\ U & \hat{P} \end{bmatrix}, \quad \mathcal{T} := \begin{bmatrix} X & I \\ U & 0 \end{bmatrix}.$$

Matrix \mathcal{T} is square and nonsingular because U can be assumed to be nonsingular in the case of full order controllers (see discussion in [14] for more details). Now, introduce the variables

$$\begin{bmatrix} Q_0 & \cdots & Q_s & F \\ L_0 & \cdots & L_s & R \end{bmatrix} := \begin{bmatrix} V & Y B_u \\ 0 & I \end{bmatrix} \begin{bmatrix} \hat{A}_0 & \cdots & \hat{A}_s & \hat{B} \\ \hat{C}_0 & \cdots & \hat{C}_s & \hat{D} \end{bmatrix} \begin{bmatrix} U & \cdots & 0 & 0 \\ \vdots & \ddots & \vdots & \vdots \\ 0 & \cdots & U & 0 \\ C_{y0} X & \cdots & C_{ys} X & I \end{bmatrix} \quad (4.26)$$

$$+ \begin{bmatrix} Y A_0 X & \cdots & Y A_s X & 0 \\ 0 & \cdots & 0 & 0 \end{bmatrix} \quad (4.27)$$

and

$$W_i := \mathcal{T}^T \mathcal{W}_i \mathcal{T}, \quad S_i := \mathcal{T}^T \mathcal{S}_i \mathcal{T}, \quad i = 1, \dots, s.$$

These relations are all that are needed to derive the LMIs (4.22)–(4.23). As in [14], the driving force is the fact that

$$\begin{aligned}\mathcal{T}^T \mathcal{P} \mathcal{A}_i \mathcal{T} &= \mathbf{A}_i(X, Y, F, R, Q_i, L_i), & \mathcal{T}^T \mathcal{P} \mathcal{B} &= \mathbf{B}(Y, F, R), \\ \mathcal{C}_i \mathcal{T} &= \mathbf{C}_i(X, R, L_i), & \mathcal{D} &= \mathbf{D}(R),\end{aligned}$$

where $\mathbf{A}_i, \mathbf{B}, \mathbf{C}_i, \mathbf{D}, i = 0, \dots, s$, are as defined in (4.17).

Now expand (4.14) using (4.9) and (4.15)–(4.16) to obtain

$$\begin{bmatrix} \mathcal{A}_0^T \mathcal{P} + \mathcal{P} \mathcal{A}_0 + \sum_{i=1}^s \mathcal{W}_i \mathcal{P} \mathcal{A}_i + \mathcal{S}_1 \cdots \mathcal{P} \mathcal{A}_s + \mathcal{S}_s & \mathcal{P} \mathcal{B} & \mathcal{C}_0^T \\ \mathcal{A}_1^T \mathcal{P} - \mathcal{S}_1 & -\mathcal{W}_1 & \cdots & 0 & 0 & \mathcal{C}_1^T \\ \vdots & \vdots & \ddots & \vdots & \vdots & \vdots \\ \mathcal{A}_s^T \mathcal{P} - \mathcal{S}_s & 0 & \cdots & -\mathcal{W}_s & 0 & \mathcal{C}_s^T \\ \mathcal{B}^T \mathcal{P} & 0 & \cdots & 0 & -I & \mathcal{D}^T \\ \mathcal{C}_0 & \mathcal{C}_1 & \cdots & \mathcal{C}_s & \mathcal{D} & -I \end{bmatrix} \prec 0$$

after applying the Schur Complement formula (see [5, 16]). Using the nonsingularity of \mathcal{T} , the above inequality is equivalent by congruence to the inequality

$$\begin{bmatrix} \left(\begin{array}{c} \mathcal{T}^T \mathcal{A}_0^T \mathcal{P} \mathcal{T} + \\ \mathcal{T}^T \mathcal{P} \mathcal{A}_0 \mathcal{T} + \\ \sum_{i=1}^s \mathcal{T}^T \mathcal{W}_i \mathcal{T} \end{array} \right) & \left(\begin{array}{c} \mathcal{T}^T \mathcal{P} \mathcal{A}_1 \mathcal{T} + \\ \mathcal{T}^T \mathcal{S}_1 \mathcal{T} \end{array} \right) & \cdots & \left(\begin{array}{c} \mathcal{T}^T \mathcal{P} \mathcal{A}_s \mathcal{T} + \\ \mathcal{T}^T \mathcal{S}_s \mathcal{T} \end{array} \right) & \mathcal{T}^T \mathcal{P} \mathcal{B} & \mathcal{T}^T \mathcal{C}_0^T \\ \left(\begin{array}{c} \mathcal{T}^T \mathcal{A}_1^T \mathcal{P} \mathcal{T} - \\ \mathcal{T}^T \mathcal{S}_1 \mathcal{T} \end{array} \right) & -\mathcal{T}^T \mathcal{W}_1 \mathcal{T} & \cdots & 0 & 0 & \mathcal{T}^T \mathcal{C}_1^T \\ \vdots & \vdots & \ddots & \vdots & \vdots & \vdots \\ \left(\begin{array}{c} \mathcal{T}^T \mathcal{A}_s^T \mathcal{P} \mathcal{T} - \\ \mathcal{T}^T \mathcal{S}_s \mathcal{T} \end{array} \right) & 0 & \cdots & -\mathcal{T}^T \mathcal{W}_s \mathcal{T} & 0 & \mathcal{T}^T \mathcal{C}_s^T \\ \mathcal{B}^T \mathcal{P} & 0 & \cdots & 0 & -I & \mathcal{D}^T \\ \mathcal{C}_0 & \mathcal{C}_1 & \cdots & \mathcal{C}_s & \mathcal{D} & -I \end{bmatrix} \prec 0$$

which is precisely (4.23) after substituting for the new variables and linear functions introduced above. Likewise, inequality (4.22) comes from

$$0 \prec \mathcal{T}^T \mathcal{P} \mathcal{T} = \begin{bmatrix} X & I \\ I & Y \end{bmatrix}.$$

Note how important it is that the terms of the form $\mathcal{P} \mathcal{A}_i$ and the variables \mathcal{W}_i and \mathcal{S}_i be multiplied by \mathcal{T} on the right and by its transpose on the left. Indeed, this is the main reason why the multipliers \mathcal{W}_i and \mathcal{S}_i can be fully incorporated in the optimization.

Theorem 4.1 can be proved similarly. However, note the important fact that each inequality of the form (4.8) involves a different affine function of the matrices \mathcal{A}_i as defined in (4.9)–(4.10). It should not be taken for granted that the reason why the change-of-variables (4.26) still works is because of the remarkable property that the right-hand side of (4.26) is simultaneously affine on the controller matrices \hat{A}_i, \hat{C}_i , and the problem data A_i, C_i , for all $i = 1, \dots, s$.

References

1. Apkarian P, Gahinet P (1995) A convex characterization of gain-scheduled h-infinity controllers. *IEEE Trans Automat Contr* 40(5):853–864
2. Apkarian P, Gahinet P, Becker G (1995) Self-scheduled H_∞ control of linear parameter-varying systems—a design example. *Automatica* 31(9):1251–1261
3. Barmish BR (1985) Necessary and sufficient conditions for quadratic stabilizability of an uncertain system. *J Optim Theory Applicat* 46:399–408
4. Becker G, Packard A (1994) Robust performance of linear parametrically varying systems using parametrically-dependent linear feedback. *Syst Contr Lett* 23(3):205–215
5. Boyd SP, El Ghaoui L, Feron E, Balakrishnan V (1994) *Linear matrix inequalities in system and control theory*. SIAM, Philadelphia, PA
6. Fans MKH, Tits AL, Doyle JC (1991) Robustness in the presence of mixed parametric uncertainty and unmodeled dynamics. *IEEE Trans Automat Contr* 36(1):25–38
7. Geromel JC, Bernussou J, de Oliveira MC (1999) H_2 norm optimization with constrained dynamic output feedback controllers: decentralized and reliable control. *IEEE Trans Automat Contr* 44(7):1449–1454
8. de Oliveira MC, Geromel JC (2004) Synthesis of nonrational controllers for linear delay-systems. *Automatica* 40(2):171–181
9. de Oliveira MC, Geromel JC, Bernussou J (2000) Design of dynamic output feedback decentralized controllers via a separation procedure. *Int J Contr* 73(5):371–381
10. de Oliveira MC, Geromel JC, Bernussou J (2002) Extended H_2 and H_∞ norm characterizations and controller parametrizations for discrete-time systems. *Int J Contr* 75(9):666–679
11. Packard A (1994) Gain scheduling via linear fractional transformations. *Syst Contr Lett* 22(2):79–92
12. Scherer CW (2000) Robust mixed control and linear parameter-varying control with full block scalings. In: El Gahoui L, Niculesco SL (eds) *Advances in linear matrix inequality methods in control*, SIAM, Philadelphia, PA, pp 187–207
13. Scherer CW (2001) LPV control and full block multipliers. *Automatica* 37(3):361–375
14. Scherer CW, Gahinet P, Chilali M (1997) Multiobjective output-feedback control via LMI optimization. *IEEE Trans Automat Contr* 42(7):896–911
15. Scorletti G, EL Ghaoui L (1998) Improved LMI conditions for gain scheduling and related control problems. *Int J Robust Nonlin Contr* 8(10):845–877
16. Skelton RE, Iwasaki T, Grigoriadis K (1998) *A unified algebraic approach to control design*. Taylor & Francis, London, UK
17. Zhou K, Doyle JC, Glover K (1996) *Robust and optimal control*. Prentice Hall, Inc., Englewood Cliffs, NJ

Chapter 5

A Parameter-Dependent Lyapunov Approach for the Control of Nonstationary LPV Systems

Mazen Farhood

Abstract The chapter deals with the control of nonstationary linear parameter varying (NSLPV) systems, and is motivated by interest in the control of nonlinear systems along trajectories, particularly prespecified eventually periodic ones. The synthesis objective is to find a feedback parameter-dependent, time-varying controller, where the controller parameters are the same as those of the plant, such that the closed-loop system is asymptotically stable and the ℓ_2 -induced norm of the closed-loop input–output mapping is less than some ℓ_2 -gain performance level γ . The analysis and synthesis results are given in terms of parameterized linear matrix inequalities (PLMIs), and some of the PLMI relaxation methods available in the literature, such as the sum of squares (SOS) decomposition method and the multiconvexity relaxation technique, are discussed. A fast and easy-to-implement algorithm for online controller construction is also provided.

5.1 Introduction

The chapter deals with the control of nonlinear systems along trajectories, particularly prespecified eventually periodic ones. Such trajectories can be arbitrary for a finite amount of time before setting into periodic orbits. Linear parameter-varying (LPV) models will be used to capture the nonlinear dynamics of the system. Specifically, the plant models we consider are of the form

$$\begin{aligned}x(k+1) &= A(\delta(k), k)x(k) + B(\delta(k), k)u(k) \\ y(k) &= C(\delta(k), k)x(k) + D(\delta(k), k)u(k),\end{aligned}\tag{5.1}$$

M. Farhood (✉)
Aerospace and Ocean Engineering Department, Virginia Tech, Blacksburg, VA 24061, USA
e-mail: farhood@vt.edu

where $A(\cdot, \cdot)$, $B(\cdot, \cdot)$, $C(\cdot, \cdot)$, and $D(\cdot, \cdot)$ are matrix-valued functions that are known a priori. The variable k is time, and $\delta(k) := (\delta_1(k), \dots, \delta_r(k))$ is a vector of real scalar parameters. Models of the form in (5.1) are called nonstationary LPV (NSLPV) models, and some work on these models formulated in a linear fractional transformation (LFT) framework can be found in [11, 12]. These models differ from the standard (stationary) LPV ones in that the state-space matrices of NSLPV models have *explicit dependence on time* in addition to the parameters. In the context of control of nonlinear systems along *prespecified* trajectories, NSLPV models arise naturally as a means to capture the nonlinear dynamics while maintaining a model that is amenable to control synthesis. Furthermore, in such a context, an NSLPV model is potentially far less conservative than a corresponding stationary one since, with an NSLPV model, we do not have to parameterize time-varying terms in the system equations, which are associated with the prespecified trajectory and hence known a priori. Note also that hybrid LPV systems are directly linked to NSLPV ones, as will be evident in Sect. 5.4. In the case of hybrid systems, reference trajectories do not have to be prespecified as long as the reference states and controls are within the covered state-space region.

The synthesis objective in this chapter is to find a feedback NSLPV controller, where the controller parameters are the same as those of the plant, such that the closed-loop system is asymptotically stable and the ℓ_2 -induced norm of the closed-loop input-output mapping is less than some ℓ_2 -gain performance level $\gamma > 0$. There are two ways to go about solving this control problem. The first involves the use of a *parameter-independent* Lyapunov function; namely, the Lyapunov function will only have explicit dependence on time. The second is by employing a *parameter-dependent* Lyapunov function with explicit dependence both on time and the parameters. This chapter focuses on the parameter-dependent Lyapunov approach, assuming that the bounds on the rates of variation of the parameters are given. The analysis and synthesis conditions will be provided in terms of linear matrix inequalities (LMIs). Solving the control problem via a parameter-independent Lyapunov function is conservative; whereas, by allowing the Lyapunov function to be parameter dependent, this conservatism is likely to diminish but at the expense of added computational complexity. Also, the type of scheduling parameter dependence, be it linear, polynomial, or rational, influences, in general, the conservatism and computational complexity of the approach. The more complicated the Lyapunov function is allowed to be, the more intensive the computational problem becomes and the less conservative the approach is in general. So, there is a trade-off between conservatism and computational complexity. In this chapter, we will eventually assume polynomial parameter dependence; this is not a limitation as it is always possible to approximate or even equivalently represent a nonlinear function with a polynomial one though additional parameters may be needed.

While in some cases, the attained improvement in performance may not justify the added computational complexity, there are certain control problems where the use of parameter-dependent Lyapunov functions is necessary irrespective of the performance betterment. One such problem is trajectory regulation in the presence

of obstacles [14]. Here, the penalty weights on the tracking errors can be viewed as scheduling parameters. Then, the position of the vehicle in the obstacle environment will dictate the penalty weights on the tracking errors, and accordingly the control strategy will significantly change in order to prioritize the regulation of certain outputs over others. In this case, the use of a parameter-independent Lyapunov function is unfavorable because then all scheduled controllers will be inclined for worst-case-scenario behavior. Instead, a parameter-dependent Lyapunov function should be used, and, furthermore, the rates of variation of the parameters should be of relatively small magnitude by design.

The use of parameter-dependent Lyapunov functions in the context of generalized LMI-based H_∞ control results in analysis and synthesis conditions in the form of parameterized LMIs (PLMIs). Some PLMI relaxation methods available in the literature are the sum of squares (SOS) decomposition method given in [28, 29] and the multiconvexity relaxation technique given in [2], to name a few. A brief discussion of these PLMI relaxation methods will be given. A fast algorithm for online controller construction based on the results of [16] will also be provided.

The literature on stationary LPV models and nonstationary systems is vast; see for instance, [17, 18, 32] and the references therein. Note that, as the Lyapunov function is constructed from the solutions of the synthesis conditions, a parameter-independent Lyapunov function implies that we are only interested in time-varying solutions with no dependence on the parameters. One technique that falls under this approach is given in [12], where gain scheduling is based on LFT models. The results therein are generalizations of those in [27], and are achieved using the framework developed in [6] for linear time-varying systems. No specific bounds, other than the trivial ones, are imposed on the parameter increments in this case. The technique requires that the state-space matrices have rational dependence on the parameters so that the system equations can be formulated in an LFT framework, and it also allows for complex parameters which is a drawback when the parameters are known to be real. This disadvantage is absent, for instance, in the method of [1] for stationary LPV (SLPV) systems, though the parameter dependence in this case can only be affine; see [7] for the generalization of the results of [1] to the NSLPV case.

The outline of the chapter is as follows: in Sect. 5.2, we formulate the control problem; in Sect. 5.3, we give analysis and synthesis results for eventually periodic NSLPV systems; in Sect. 5.4, we give a result on hybrid LPV control; in Sect. 5.5, we briefly list a number of PLMI relaxation techniques; and last, in Sect. 5.6, we present a fast algorithm for online controller construction. The notation is somewhat standard. We denote the set of nonnegative integers by \mathbb{N} and that of real $n \times m$ matrices by $\mathbb{R}^{n \times m}$. If S_i is a sequence of matrices, then $\text{diag}(S_i)$ denotes their block-diagonal augmentation. We use I_n to denote an $n \times n$ identity matrix and $0_{n \times m}$ to denote an $n \times m$ zero matrix. We denote the space of continuous functions by \mathcal{C}^0 . The adjoint of an operator X is written X^* , and we use $X \prec 0$ to mean it is negative definite. The normed space of square summable vector-valued sequences is denoted by ℓ_2 . It consists of elements $x = (x_0, x_1, x_2, \dots)$, with each $x_k \in \mathbb{R}^{n_k}$ for some n_k , having a finite 2-norm $\|x\|$ defined by $\|x\|^2 = \sum_{k=0}^{\infty} \|x_k\|^2 < \infty$, where $\|x_k\|^2 = x_k^* x_k$.

5.2 NSLPV Plant and Controller

Let G be an NSLPV model defined by the following state-space equation:

$$\begin{bmatrix} x(k+1) \\ z(k) \\ y(k) \end{bmatrix} = \begin{bmatrix} A(\delta(k),k) & B_1(\delta(k),k) & B_2(\delta(k),k) \\ C_1(\delta(k),k) & D_{11}(\delta(k),k) & D_{12}(\delta(k),k) \\ C_2(\delta(k),k) & D_{21}(\delta(k),k) & 0 \end{bmatrix} \begin{bmatrix} x(k) \\ w(k) \\ u(k) \end{bmatrix}, \quad (5.2)$$

$x(0) = 0$, for $w \in \ell_2$. The signals $w(k)$ and $z(k)$ denote the exogenous disturbances and errors, respectively, whereas $u(k)$ denotes the applied control and $y(k)$ the measurements. The vectors $x(k)$, $z(k)$, $w(k)$, $y(k)$, and $u(k)$ are real and have time-varying dimensions which we denote by $n(k)$, $n_z(k)$, $n_w(k)$, $n_y(k)$, and $n_u(k)$ respectively. Like in [40], we assume the parameters $\delta(k) = (\delta_1(k), \dots, \delta_r(k))$ and parameter increments $d\delta(k) = \delta(k+1) - \delta(k)$ such that $(\delta(k), d\delta(k)) \in \Gamma$ for all $k \in \mathbb{N}$, where Γ is a polytope defined as

$$\Gamma := \{(p, dp) \in \mathbb{R}^r \times \mathbb{R}^r \mid f_{i,j}(p_i, dp_i) \geq 0 \text{ for all } i=1, \dots, r \text{ and } j=1, 2, 3\}, \quad (5.3)$$

with $f_{i,1} = (p_i - \underline{p}_i)(\bar{p}_i - p_i)$, $f_{i,2} = (dp_i - \underline{dp}_i)(\bar{dp}_i - dp_i)$, $f_{i,3} = (p_i + dp_i - \underline{p}_i)(\bar{p}_i - p_i - dp_i)$, and $\underline{p}_i, \bar{p}_i, \underline{dp}_i, \bar{dp}_i \in \mathbb{R}$, $\underline{dp}_i \leq 0$, $\bar{dp}_i \geq 0$.

Notice that, for each $i = 1, \dots, r$, the set of points satisfying $f_{i,j}(p_i, dp_i) \geq 0$ for $j = 1, 2, 3$ defines a polygon which constitutes the projection of polytope Γ on the (p_i, dp_i) -plane, as shown in Fig. 5.1. Thus, the allowable parameter trajectories δ reside in the set

$$\Delta_\Gamma := \{\delta : \mathbb{N} \rightarrow \mathbb{R}^r \mid (\delta(k), d\delta(k)) \in \Gamma \text{ for all } k \in \mathbb{N}\}. \quad (5.4)$$

It is important at this point to properly characterize the state-space matrix-valued functions. As the following applies to each of the state-space operators, for simplicity we will focus the discussion on the A -matrix only. First, we assume

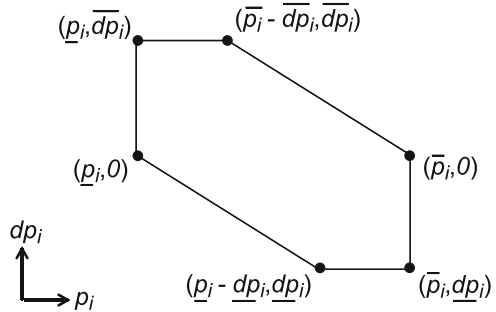


Fig. 5.1 Parameter space in (p_i, dp_i) -plane

that the state-space matrices have continuous dependence on the parameters and are uniformly bounded for all admissible values of time and parameters. Then, setting $\mathcal{A}_k(p) = A(p, k)$, the matrix-valued function $A(p, k)$ can be viewed as a family of continuous functions of the parameter vector p , denoted \mathcal{A} , namely,

$$\mathcal{A} = \left\{ \mathcal{A}_k \in \mathcal{C}^0 \left(\mathbb{R}^r, \mathbb{R}^{n(k+1) \times n(k)} \right) : k \in \mathbb{N} \right\}.$$

Furthermore, \mathcal{A} is uniformly bounded, meaning that there exists a positive scalar λ such that $\|\mathcal{A}_k(p)\| \leq \lambda$ for all $p_i \in [\underline{p}_i, \bar{p}_i]$ and $k \in \mathbb{N}$. Alternatively, setting $A_\delta(k) = A(\delta(k), k)$, the function $A(\delta(k), k)$ can be regarded as a set of sequences, where, for each $\delta \in \Delta_\Gamma$, the corresponding bounded sequence $A_\delta(k)$ is reminiscent of the A -sequence of a standard linear time-varying (LTV) system. Hence, for each $\delta \in \Delta_\Gamma$, the NSLPV model G reduces to a standard LTV system, say, G_δ ; in other words, $G = \{G_\delta : \delta \in \Delta_\Gamma\}$. The uniform boundedness here ensures that there exists a positive scalar λ such that $\|A_\delta(k)\| \leq \lambda$ for all $\delta \in \Delta_\Gamma$ and $k \in \mathbb{N}$.

We say an NSLPV model G , as defined in the preceding, is ℓ_2 -stable if, for each $\delta \in \Delta_\Gamma$, the resulting LTV system is exponentially stable. In the sequel, we will assume that both $\delta(k)$ and $d\delta(k)$ are measurable at each time instant k . As for computing the parameter increment $d\delta(k)$ online, it is reasonable to assume that the parameter function is continuously differentiable, and then, assuming a measurable derivative $\dot{\delta}(k)$ at each k and a sufficiently small sampling time T , the value of $d\delta(k)$ can be obtained from the Euler approximation $d\delta(k) \approx T\dot{\delta}(k)$.

Suppose plant G is controlled by a controller K whose state-space equation is

$$\begin{bmatrix} x_K(k+1) \\ u(k) \end{bmatrix} = \begin{bmatrix} A_K(\delta(k), d\delta(k), k) & B_K(\delta(k), d\delta(k), k) \\ C_K(\delta(k), d\delta(k), k) & D_K(\delta(k), d\delta(k), k) \end{bmatrix} \begin{bmatrix} x_K(k) \\ y(k) \end{bmatrix}, \quad x_K(0) = 0,$$

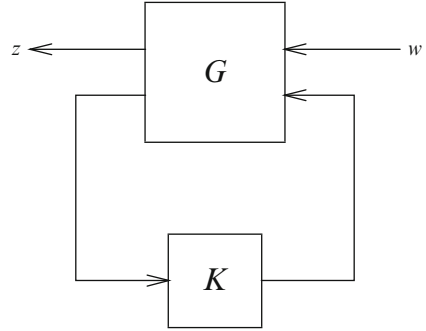
where $x_K(k) \in \mathbb{R}^{m(k)}$. The parameters $\delta_i(k)$ here are the same as those in the plant equations. It goes without saying that, when constructing the controller from the synthesis solutions as discussed later, we will make sure that its system matrices are uniformly bounded functions, with continuous dependence on the parameters and their increments. The feedback interconnection of G and K is shown in Fig. 5.2. We denote this closed-loop system by L and write its realization as

$$\begin{bmatrix} x_L(k+1) \\ z(k) \end{bmatrix} = \begin{bmatrix} A_L(\delta(k), d\delta(k), k) & B_L(\delta(k), d\delta(k), k) \\ C_L(\delta(k), d\delta(k), k) & D_L(\delta(k), d\delta(k), k) \end{bmatrix} \begin{bmatrix} x_L(k) \\ w(k) \end{bmatrix}, \quad (5.5)$$

where column vector $x_L(k) = (x(k), x_K(k)) \in \mathbb{R}^{n(k)+m(k)}$, and the closed-loop state-space matrices are given by

$$\begin{bmatrix} A_L & B_L \\ C_L & D_L \end{bmatrix} = \begin{bmatrix} A + B_2 D_K C_2 & B_2 C_K & B_1 + B_2 D_K D_{21} \\ B_K C_2 & A_K & B_K D_{21} \\ C_1 + D_{12} D_K C_2 & D_{12} C_K & D_{11} + D_{12} D_K D_{21} \end{bmatrix}. \quad (5.6)$$

We now state the synthesis objective.

Fig. 5.2 Closed-loop system

Definition 5.1. A controller K is a γ -admissible synthesis for NSLPV plant G if the closed-loop system in Fig. 5.2 is ℓ_2 -stable and the performance inequality $\|w \mapsto z\|_{\ell_2 \rightarrow \ell_2} < \gamma$ is achieved for all $\delta \in \Delta_\Gamma$.

Before concluding this section, we need to introduce the special class of eventually periodic NSLPV systems. In this case, the explicit time variation in the system realization is eventually periodic. Eventually periodic systems arise in two basic scenarios. The first is when parameterizing the nonlinear system equations about an eventually periodic trajectory, and the second is when the plant has an uncertain initial condition [13]. An eventually periodic trajectory can be arbitrary for an initial amount of time, but then settles into a periodic orbit; a special case of this is when a system transitions between two operating points. Both finite horizon and periodic systems are subclasses of eventually periodic systems.

Definition 5.2. An NSLPV system G is (h, q) -eventually periodic for some integers $h \geq 0$, $q \geq 1$ if each of its state-space matrix-valued functions is (h, q) -eventually periodic with respect to the explicit time dependence; for instance, $A(\delta, k)$ would be of the form

$$\underbrace{A(\delta, 0), A(\delta, 1), \dots, A(\delta, h-1)}_{h \text{ terms}}, \underbrace{A(\delta, h), \dots, A(\delta, h+q-1)}_{q \text{ terms}},$$

$$\underbrace{A(\delta, h), \dots, A(\delta, h+q-1), \dots}_{q \text{ terms}}$$

5.3 Analysis and Synthesis Results

We now state the following analysis and synthesis results from [8].

Theorem 5.1. *Closed-loop system L , defined in (5.5), is ℓ_2 -stable and $\|w \mapsto z\|_{\ell_2 \rightarrow \ell_2} < \gamma$ for all $\delta \in \Delta_\Gamma$, as defined in (5.4), if there exists a uniformly bounded matrix-valued function $X(p, k) \succ 0$, continuous in p , such that*

$$\begin{bmatrix} A_L & B_L \\ C_L & D_L \end{bmatrix}^* \begin{bmatrix} X(p + dp, k + 1) & 0 \\ 0 & \frac{1}{\gamma^2} I \end{bmatrix} \begin{bmatrix} A_L & B_L \\ C_L & D_L \end{bmatrix} - \begin{bmatrix} X(p, k) & 0 \\ 0 & I \end{bmatrix} \prec -\beta I, \quad (5.7)$$

for all $(p, dp) \in \Gamma$ as defined in (5.3), $k \in \mathbb{N}$, and some positive scalar β , where the dependence of the state-space matrices on (p, dp, k) is suppressed for simplicity.

A special case of this analysis result for the stationary LPV case is given in [40].

Proof. To start, consider any $\delta \in \Delta_\Gamma$. Then, given the time-varying parameter trajectory δ , NSLPV system L reduces to a standard discrete-time LTV system, say, L_δ . Suppose that inequality (5.7) holds for all $(p, dp) \in \Gamma$ and $k \in \mathbb{N}$. Then, given $\delta \in \Delta_\Gamma$, the following inequality is valid:

$$\begin{aligned} & F_L^*(\delta(k), d\delta(k), k) \begin{bmatrix} X(\delta(k) + d\delta(k), k + 1) & 0 \\ 0 & \frac{1}{\gamma^2} I \end{bmatrix} \\ & \times F_L(\delta(k), d\delta(k), k) - \begin{bmatrix} X(\delta(k), k) & 0 \\ 0 & I \end{bmatrix} \prec -\beta I, \end{aligned}$$

with $F_L = \begin{bmatrix} A_L & B_L \\ C_L & D_L \end{bmatrix}$, for all $k \in \mathbb{N}$ and some positive scalar β ; this immediately follows from the definition of Δ_Γ , which ensures that $(\delta(k), d\delta(k)) \in \Gamma$ for all $k \in \mathbb{N}$. Then, as $\delta(k + 1) = \delta(k) + d\delta(k)$, we obtain that the sequence $X(\delta(k), k) \succ 0$, bounded above and below, satisfies the Kalman–Yakubovich–Popov (KYP) Lemma condition, with ℓ_2 -gain performance level γ , for the LTV system L_δ , which, by [6, Corollary 12], implies that L_δ is stable and $\|L_\delta\|_{\ell_2 \rightarrow \ell_2} < \gamma$. \square

Theorem 5.2. *Given the NSLPV plant G defined in (5.2) with $\delta \in \Delta_\Gamma$, suppose that*

(A1) *the matrices $[B_2^*(\delta(k), k) \ D_{12}^*(\delta(k), k)]$ and $[C_2(\delta(k), k) \ D_{21}(\delta(k), k)]$ have full-row rank uniformly for all $k \in \mathbb{N}$ and $\delta \in \Delta_\Gamma$.*

Then there exists a γ -admissible NSLPV synthesis K to G according to Definition 5.1 for some scalar γ if there exist uniformly bounded matrix-valued functions $R(p, k) \succ 0$, $S(p, k) \succ 0$, continuous in p , and some positive scalar σ such that

$$\begin{bmatrix} ARA^* - R^+ & ARC_1^* & B_1 \\ C_1RA^* & -\gamma I + C_1RC_1^* & D_{11} \\ B_1^* & D_{11}^* & -\gamma I \end{bmatrix} - \sigma \begin{bmatrix} B_2 \\ D_{12} \\ 0 \end{bmatrix} \begin{bmatrix} B_2 \\ D_{12} \\ 0 \end{bmatrix}^* \prec -\beta I$$

$$\begin{bmatrix} A^*S^+A - S & A^*S^+B_1 & C_1^* \\ B_1^*S^+A & -\gamma I + B_1^*S^+B_1 & D_{11}^* \\ C_1 & D_{11} & -\gamma I \end{bmatrix} - \sigma \begin{bmatrix} C_2^* \\ D_{21}^* \\ 0 \end{bmatrix} \begin{bmatrix} C_2^* \\ D_{21}^* \\ 0 \end{bmatrix}^* \prec -\beta I$$

$$\begin{bmatrix} R & I \\ I & S \end{bmatrix} \succeq 0 \quad (5.8)$$

for all $(p, dp) \in \Gamma$, $k \in \mathbb{N}$, and some positive scalar β , where the dependence of R , S , and the state-space matrices on (p, k) is suppressed for simplicity, and

$$R^+ = R(p + dp, k + 1), \quad S^+ = S(p + dp, k + 1).$$

Proof. As in the proof of Theorem 5.1, for each trajectory $\delta \in \Delta_\Gamma$, NSLPV system G reduces to an LTV system. Then, invoking [6, Theorem 19] along with applications of Finsler's lemma and a similar argument to that in the proof of Theorem 5.2 (iii) in [2] complete the proof. \square

It will be convenient to write the synthesis conditions in (5.8) as

$$\begin{aligned} \mathcal{F}_1(R(p, k), R(p + dp, k + 1), \sigma, p, k) &\prec -\beta I, \\ \mathcal{F}_2(S(p, k), S(p + dp, k + 1), \sigma, p, k) &\prec -\beta I, \\ \mathcal{F}_3(R(p, k), S(p, k)) &\succeq 0, \end{aligned} \quad (5.9)$$

respectively, where \mathcal{F}_i are defined in the obvious way.

We assume henceforth that the state-space matrices have *polynomial* dependence on the parameters. Moreover, we will only seek solutions with polynomial parameter dependence for the synthesis inequalities. Specifically, we define the family of functions \mathcal{X} to consist of all the uniformly bounded matrix-valued functions $X(p, k) \succ 0$, for all $p_i \in [p_i, \bar{p}_i]$ and $k \in \mathbb{N}$, with polynomial dependence on the parameters, namely, with $v = (v_1, v_2, \dots, v_r)$ and $J_\tau := \{(v_1, v_2, \dots, v_r) \mid v_i \in \mathbb{N} \text{ and } \sum_{i=1}^r v_i \leq \tau\}$, we have

$$X(p, k) = \sum_{v \in J_\tau} p_1^{v_1} p_2^{v_2} \dots p_r^{v_r} X_v(k), \quad (5.10)$$

for some $\tau \in \mathbb{N}$, where, for each $v \in J_\tau$, the sequence $X_v(k)$ is bounded above and below. Next in this section, we will be focussing on eventually periodic plants which are presented in Definition 5.2. Thus, it will be convenient to specify (N, q) -eventually periodic matrix-valued functions in \mathcal{X} . Namely, given $X \in \mathcal{X}$

as aforementioned, we say X is (N, q) -eventually periodic if, for each $v \in J_\tau$, the sequence $X_v(k)$ is (N, q) -eventually periodic, i.e., $X_v(k)$ is of the form

$$\underbrace{X_v(0), X_v(1), \dots, X_v(N-1)}_{N \text{ terms}}, \underbrace{X_v(N), \dots, X_v(N+q-1)}_{q \text{ terms}}, \\ \underbrace{X_v(N), \dots, X_v(N+q-1)}_{q \text{ terms}}, \dots$$

The synthesis conditions in (5.8) are convex but infinite dimensional both in time and parameters. However, if the NSLPV plant G is (h, q) -eventually periodic as in Definition 5.2, then the infinite dimensionality with respect to the explicit time dependence can be avoided as shown in the next results.

Proposition 5.1. *Given the NSLPV plant G defined in (5.2) with $\delta \in \Delta_\Gamma$, suppose that G is q -periodic (i.e., $(0, q)$ -eventually periodic), with assumptions (A1) and (A2) the state-space matrices of G have polynomial dependence on the parameters $\delta \in \Delta_\Gamma$.*

Then there exist solutions in \mathcal{X} to synthesis conditions (5.8) if and only if there exist q -periodic solutions in \mathcal{X} .

The proof is given in [8] and is inspired by that of a similar result for standard periodic systems in [6]. Also, a similar averaging technique is used in [5] in the context of time-varying control analysis.

Proposition 5.2. *Suppose NSLPV plant G is (h, q) -eventually periodic, along with assumptions (A1)–(A2). Then there exist solutions in \mathcal{X} to synthesis conditions (5.8) if and only if there exist (N, q) -eventually periodic solutions in \mathcal{X} for some $N \geq h$.*

The proof of this result is also given in [8]. The result states that, in the case of eventually periodic NSLPV plants, a solution to the synthesis conditions, if existent, can always be chosen to be eventually periodic, having the same periodicity as the plant but probably exhibiting a longer finite horizon. From a practical perspective, the preceding means that, given an eventually periodic plant, it may be possible to improve the closed-loop performance by allowing for eventually periodic controllers with longer finite horizons than the plant. This is also the case for standard LTV systems as shown in [9, 10].

We conclude this section with the following summarizing corollary.

Corollary 5.1. *Given the NSLPV plant G defined in (5.2) with $\delta \in \Delta_\Gamma$, suppose that G is (h, q) -eventually periodic, along with assumptions (A1)–(A2). Then, with $N \geq h$, there exists a γ -admissible (N, q) -eventually periodic NSLPV synthesis K to G for some scalar γ if there exist polynomial matrix-valued functions $R_0(p), \dots, R_{N+q-1}(p) \succ 0$, $S_0(p), \dots, S_{N+q-1}(p) \succ 0$, and some positive scalar σ such that*

$$\begin{aligned}
\mathcal{F}_1(R_0(p), R_1(p+dp), \sigma, p, 0) &< 0, \\
\mathcal{F}_1(R_1(p), R_2(p+dp), \sigma, p, 1) &< 0, \\
&\vdots \\
\mathcal{F}_1(R_{N+q-2}(p), R_{N+q-1}(p+dp), \sigma, p, N+q-2) &< 0, \\
\mathcal{F}_1(R_{N+q-1}(p), R_N(p+dp), \sigma, p, N+q-1) &< 0,
\end{aligned} \tag{5.11}$$

and similarly, for $k = 0, 1, \dots, N+q-1$,

$$\mathcal{F}_2(S_k(p), S_{k+1}(p+dp), \sigma, p, k) < 0 \quad \text{and} \quad \mathcal{F}_3(R_k(p), S_k(p)) \geq 0 \tag{5.12}$$

for all $(p, dp) \in \Gamma$, where $S_{N+q}(p) \equiv S_N(p)$. In the event that G is q -periodic, i.e., $h = 0$, then N can be set equal to zero with no added conservatism.

Thus, when the explicit time dependence in the system equations is of an eventually periodic nature, the infinite dimensionality of the synthesis PLMIs with respect to time k can be bypassed, as evident from Corollary 5.1. This PLMI problem though remains infinitely constrained. Fortunately, several PLMI relaxation methods are available in the literature, and a discussion of some of these methods will be presented in Sect. 5.5. With this said, applying the aforesaid corollary to an NSLPV plant with numerous sampling points ($h, q \gg 0$) may result in a formidable computational problem, regardless of the PLMI relaxation method employed. The next section presents a way to reduce the computational complexity of such a problem.

5.4 NSLPV Control of Switched Systems

In many scenarios where time-varying system parameters are known a priori, the use of NSLPV models instead of stationary ones is quite advantageous as a means for less conservative representations. The tradeoff, however, is an added computational complexity to the synthesis approach; this is by the same token that an LTV approach is computationally more expensive than an LTI one. The computational issue is even more severe when a parameter-dependent Lyapunov function is sought since then each PLMI in a stationary LPV (SLPV) problem would correspond to at least $N+q$ PLMIs in an (N, q) -eventually periodic NSLPV problem. It might be possible to avoid a list of PLMIs if the explicit time dependence can be approximated by polynomial functions, bearing in mind that the larger the polynomial degree is, the more computationally intensive the problem becomes. In general, obtaining polynomial approximations can be a very challenging task, and a practical solution to this computational predicament is to divide the state-space region into a number of divisions in which the explicit time variation becomes very

small and the plant dynamics, as a result, can be fairly represented by a stationary LPV model. In other words, we propose to work with switched stationary LPV systems as an alternative to NSLPV models so as to reduce the computational complexity of the synthesis problem to a manageable level. We note that the approach here requires that each of the stationary LPV models of the switched system be strongly stabilizable, as defined next.

Definition 5.3. We say an SLPV system, defined by the state equation

$$x(k+1) = A(\delta(k))x(k) + B(\delta(k))u(k),$$

with $\delta \in \Delta_\Gamma$, is strongly stabilizable by a feedback operator $F(\delta(k), d\delta(k))$ for all $\delta \in \Delta_\Gamma$ if there exists a bounded polynomial function $X(p) \succ 0$ such that

$$\left(A(p) + B(p)F(p, dp) \right) X(p) \left(A(p) + B(p)F(p, dp) \right)^* - X(p + dp) \prec 0,$$

for all $(p, dp) \in \Gamma$.

Consider a nonlinear system and a corresponding NSLPV model G which captures the nonlinear system dynamics over some state-space region \mathcal{E} . Suppose it is possible to divide \mathcal{E} into N subregions $\mathcal{E}^{(i)}$ for $i = 1, 2, \dots, N$ such that, over each subregion $\mathcal{E}^{(i)}$, the explicit time variation of the NSLPV model G is sufficiently small that the system dynamics can be satisfactorily represented by a strongly stabilizable SLPV model $G^{(i)}$. The resulting SLPV models constitute a switched system denoted by $G_s := \{G^{(1)}, \dots, G^{(N)}\}$. We also denote the boundary between subregions $\mathcal{E}^{(i)}$ and $\mathcal{E}^{(j)}$ by \mathcal{B}_{ij} ; a nonexistent boundary is set equal to the empty set.

It is obvious that switched systems are special cases of NSLPV systems; so the results of the previous section are still usable here. As mentioned before, the aim here is to simplify the time-varying nature of the plant in order to render the associated computational problem practicable. This is indeed possible as long as each of the constituent SLPV models of the switched system is strongly stabilizable, as evident from the next result.

Theorem 5.3. *Given a switched SLPV system $G_s = \{G^{(1)}, \dots, G^{(N)}\}$ with $\delta \in \Delta_\Gamma$, suppose that each of the constituent SLPV models is strongly stabilizable along with assumptions (A1)–(A2). Then there exists a γ -admissible switched SLPV synthesis K_s to plant G_s if, for $i, j = 1, 2, \dots, N$, $i \neq j$, there exist polynomial matrix-valued functions $R_i(p) \succ 0$, $S_i(p) \succ 0$, and some positive scalar σ such that*

$$\begin{aligned} \mathcal{F}_1^{(i)}(R_i(p), R_i(p + dp), \sigma, p) &\prec 0, \\ \mathcal{F}_2^{(i)}(S_i(p), S_i(p + dp), \sigma, p) &\prec 0, \\ \mathcal{F}_3^{(i)}(R_i(p), S_i(p)) &\succeq 0, \end{aligned} \tag{5.13}$$

and, across each existent boundary \mathcal{B}_{ij} ,

$$\mathcal{F}_1^{(i)}(R_i(p), R_j(p+dp), \sigma, p) \prec 0, \quad \mathcal{F}_2^{(i)}(S_i(p), S_j(p+dp), \sigma, p) \prec 0, \quad (5.14)$$

for all $(p, dp) \in \Gamma$, where the notation $\mathcal{F}_x^{(y)}$ is as defined in (5.9) with the superscript y indicating that the SLPV state-space data used correspond to subsystem $G^{(y)}$, and the explicit dependence on k is dropped.

Proof. Given a trajectory $\delta \in \Delta_\Gamma$, say the state-space subregions covered are $\mathcal{E}^{(1)}, \dots, \mathcal{E}^{(N)}$, where the time intervals in which the system stays in these subregions are $[0, k_1], [k_1 + 1, k_2], \dots, [k_{N-1}, \infty[$, respectively. Then, the matrix-valued functions $R(p, k) \equiv R_i(p)$, $S(p, k) \equiv S_i(p)$ for $i = 1, \dots, N$, $k = k_{i-1} + 1, \dots, k_i$, with $k_0 = -1$ and $k_N = \infty$, and the positive scalar σ solve the synthesis conditions for the NSLPV system G , whose A -matrix, for example, is defined as $A(p, k) \equiv A^{(i)}(p)$ for i, k as aforementioned. Invoking Corollary 5.1 completes the proof. \square

Remark 5.1. In the preceding result, the switching takes place over one discrete-time instant. It is not difficult to rewrite the conditions so that the switching occurs over several time instants, bearing in mind that this would incur additional PLMIs and hence increase the computational complexity. More work needs to be done to further realize the switching logic and link it to what is currently available in the literature, for instance, [4, 23, 26].

5.5 Parameterized LMI Relaxation

To start, consider the following feasibility problem: for some $\tau \in \mathbb{N}$, find a uniformly bounded matrix-valued polynomial function $X(p)$ of degree τ , as defined in (5.10) for fixed k , such that $X(p) = \sum_{v \in J_\tau} p_1^{v_1} p_2^{v_2} \cdots p_r^{v_r} X_v \succ 0$ and the parameterized LMI $\mathcal{G}(X_v, \tilde{p}) \prec 0_{e \times e}$ hold for all $\tilde{p} = (p, dp) \in \Gamma$. This is an infinitely constrained LMI problem since, for each $\tilde{p} \in \Gamma$, there corresponds an LMI constraint. The parameterized LMI aforementioned can be equivalently written as a polynomial inequality, namely,

$$g(X_v, c, \tilde{p}) = c^* \mathcal{G}(X_v, \tilde{p}) c < 0 \text{ for all } c \in \mathbb{R}^e / \{0\}, \tilde{p} \in \Gamma. \quad (5.15)$$

In the following, we briefly present two of the available relaxation techniques which can potentially render such a problem computationally tractable.

5.5.1 Sum of Squares Method

The first relaxation technique we present here is the sum of squares (SOS) decomposition method given in [28, 29]. As argued in [29], testing global nonnegativity

of a polynomial function of degree greater than or equal to four is an NP-hard problem. One way to circumvent this difficulty is to replace the nonnegativity constraint with an SOS condition. We say a polynomial $h(c_1, \dots, c_e)$ is SOS if it can be written as a sum of squares, namely, $h(c_1, \dots, c_e) = \sum_{i=1}^N h_i^2(c_1, \dots, c_e)$ for some positive integer N , where h_i are real polynomials. The existence of an SOS decomposition is clearly sufficient for guaranteeing global nonnegativity of a polynomial function, but it is *not necessary*; in other words, not every nonnegative polynomial is SOS. There are three cases, however, as shown by Hilbert, where the existence of an SOS decomposition is equivalent to global nonnegativity, notably when the polynomial is: (1) in one variable; (2) quadratic; or (3) quartic in two variables. The appealing feature about SOS conditions is that they can be reformulated as semidefinite programming problems. Specifically, as stated in [29, Theorem 3.3], a dense polynomial function $h(c_1, \dots, c_e)$ of degree $2d$ is SOS if and only if there exists a $\binom{e+d}{d} \times \binom{e+d}{d}$ matrix $Q \succeq 0$ such that $h(c) = Z^*(c)QZ(c)$, where $Z(c)$ is a column vector consisting of all the monomials in the variables c_i having a degree less than or equal to d , namely,

$$Z(c) = [1 \quad c_1 \quad c_2 \quad \cdots \quad c_e \quad c_1c_2 \quad \cdots \quad c_e^d]^*.$$

The size of the semidefinite program is polynomial in the number of variables e for a fixed degree d and also polynomial in d for a fixed e (though not jointly polynomial in both). Note that, as discussed in [30], it may be possible to improve the size and numerical conditioning of the resulting semidefinite program by exploiting several algebraic properties of the polynomial system such as sparsity and structural symmetries.

Going back to (5.15), suppose there exists a solution $X(p) = \sum_{v \in J_\tau} p_1^{v_1} \cdots p_r^{v_r} X_v$ satisfying the polynomial inequality and that $g_x(c, \tilde{p}) := g(X_v, c, \tilde{p})$. Appealing to the definition of Γ in (5.3), we can equivalently write (5.15) as

$$f_{i,j}(p_i, dp_i) \geq 0 \quad \text{for } i = 1, \dots, r \text{ and } j = 1, 2, 3 \implies g_x(c, \tilde{p}) < 0 \quad \forall c \in \mathbb{R}^e, c \neq 0.$$

This implication holds if and only if the set

$$\mathcal{A} = \left\{ (c, p, dp) \in \mathbb{R}^e \times \mathbb{R}^r \times \mathbb{R}^r \mid g_x(c, \tilde{p}) \geq 0, f_{i,j}(p_i, dp_i) \geq 0 \right. \\ \left. \text{for } i = 1, \dots, r, j = 1, 2, 3, \text{ and } l(c) = c^*c - 1 = 0 \right\}$$

is empty. Then, invoking the Positivstellensatz [35], stated for \mathbb{R} (as opposed to the real closed fields), we can provide exact conditions to ascertain that this semialgebraic set is empty; see [3, Theorem 4.4.2] or [29, Theorem 4.6]. Specifically, \mathcal{A} is empty if and only if there exist solutions from certain classes of polynomials to the Positivstellensatz equation. These solutions serve as infeasibility certificates and are not polynomial time verifiable in general. Nevertheless, by restricting the degree of the certificates, it is possible to provide the solutions in terms of semidefinite programs, as demonstrated in the proof of [29, Theorem 5.1]. This theorem further asserts that, if the semialgebraic set is indeed empty, then, by selecting a sufficiently large degree bound, the resulting semidefinite program will be feasible.

For simplicity, set $f_1 = g_x(c, \tilde{p})$, $f_k = f_{i,j}(p_i, dp_i)$ for $i = 1, \dots, r$ and $j = 1, 2, 3$, where $k = i + 1 + (j - 1)r$. We outline next the algorithm for constructing the certificates, as given in the proof of [29, Theorem 5.1]:

- (1) Choose the degree d to be some positive integer;
- (2) Write

$$f = s_0 + s_1 f_1 + s_2 f_2 + \dots + s_{3r+1} f_{3r+1} + s_{12} f_1 f_2 + \dots + s_{12\dots(3r+1)} f_1 \dots f_{3r+1},$$

where s_i are polynomials in (c, \tilde{p}) of degree $\deg(s_i) \leq d$;

- (3) Write $h = t(c^*c - 1)$, where t is a polynomial in (c, \tilde{p}) of degree $\deg(t) \leq d$;
- (4) Solve the convex feasibility problem: find f, h such that s_i are SOS and $f + 1 + h = 0$.

As mentioned before, if the set \mathcal{A} is empty, then we can obtain infeasibility certificates using the preceding algorithm for some sufficiently large degree d . Note that there are some available results that give upper bounds on d ; see, for instance, [22].

At this point, consider again the feasibility problem: find $X(p) \succ 0$ such that (5.15) holds. It is not difficult to see from the preceding that this problem can be reformulated (though not equivalently) as a semidefinite program. To elaborate, consider the aforementioned algorithm, where $f_1 = g(X_v, c, \tilde{p})$ in this case. As X is a variable here and since the goal is to construct a semidefinite programming problem, not all the multipliers s_i in step 2 of the algorithm can be variable; specifically, those multiplying f_1 have to be assigned some nonnegative constant values. With this said, the feasibility problem in question can be cast as a semidefinite program, namely: for some positive integer degree d , find $X(p) \succ 0$, SOS multipliers $s_i(c, \tilde{p})$ of degree $\deg(s_i) \leq d$ for some i as previously noted, and polynomial $t(c, \tilde{p})$ of degree $\deg(t) \leq d$ such that the equality $f + 1 + h = 0$ holds, where all the functions are defined as in the previous algorithm with $f_1 = g(X_v, c, \tilde{p})$. Clearly, the computational complexity can become quite prohibitive in this case. We can, however, construct sufficient SOS conditions which are computationally manageable. For instance, for some sufficiently small positive scalar ε , set $t = 1$, $s_1 = \frac{1}{\varepsilon}$, $s_i = \frac{1}{\varepsilon} q_i$ for $i = 0, 2, 3, \dots, 3r + 1$ and zero for all other i , where q_i are also variable SOS multipliers. Then, the condition

$$-g(X_v, c, \tilde{p}) - \varepsilon c^*c - \sum_{j=1}^3 \sum_{i=1}^r q_k(c, \tilde{p}) f_{i,j}(p_i, dp_i) \text{ is SOS } (k = i + 1 + r(j - 1))$$

implies (5.15). This is exactly the type of SOS conditions used in [41]. This SOS problem can be solved using a third-party MATLAB toolbox called SOS-TOOLS [31], which in turn uses SeDuMi [36] or SDPT3 [37] as the semidefinite program solver.

5.5.2 Multiconvexity Relaxation Technique

This method uses directional convexity concepts to transform (potentially conservatively) a parameterized LMI problem into a standard LMI one. A key result in this regard is [2, Corollary 3.4], which we include next for completeness.

Proposition 5.3 (Multiconvexity). *Consider a twice continuously differentiable function $f(x)$, a polytope Π , and the directions d_1, d_2, \dots, d_q determined by the edges of Π . Then, if f is multiconvex along the directions d_1, \dots, d_q , i.e.,*

$$\left. \frac{\partial^2 f(x + \lambda d_i)}{\partial \lambda^2} \right|_{\lambda=0} \geq 0, \text{ for all } x \in \Pi, i = 1, 2, \dots, q, \quad (5.16)$$

then, f has a maximum over Π at a vertex of Π .

It is not difficult to see from the preceding result that, given a solution $X(p)$ as defined in (5.10) for fixed k , if for each $c \in \mathbb{R}^e / \{0\}$ the polynomial $g(X_v, c, \bar{p})$ from (5.15) is multiconvex along parallels to the edges of the polytope Γ , then $\mathcal{G}(X_v, \bar{p}) \prec 0$ for all $\bar{p} \in \Gamma$ if and only if $\mathcal{G}(X_v, \bar{p}) \prec 0$ for all $\bar{p} \in \text{vert}\Gamma$, where $\text{vert}\Gamma$ denotes the set of vertices of Γ . The multiconvexity condition is not trivial, but it is conceivable that there exists a subset of the set of solutions $X(p)$ such that any solution from this subset would render the polynomial g (or an appropriately modified version of g) multiconvex. Then, appealing to (5.16), it may be possible to enforce multiconvexity by means of additional LMI constraints that would restrict the solution to the aforesaid subset.

To elaborate, consider the following example. Suppose that we have only one parameter p and the associated parameter increment dp , and that

$$X(p) = \sum_{v=0}^2 p^v X_v \succ 0, \quad \mathcal{G}(X_v, \bar{p}) = M_0(X_v) + p^2 dp M_1(X_v) + p^3 M_2(X_v) \prec 0, \quad (5.17)$$

where the $M_i(\cdot)$ are symmetric matrix-valued affine functions of X_v . The edges of the polytope Γ in this case define the directions: $d_1 = [1, 0]$, $d_2 = [0, 1]$, and $d_3 = [1, -1]$. To enforce multiconvexity along these directions, the solution, expressed in terms of the matrix sequence X_v , has to satisfy the constraints

$$(1) \frac{\partial^2 (-w^* X(p) w)}{\partial p^2} \geq 0 \quad \text{and} \quad (2) \left. \frac{\partial^2 g(X_v, c, \bar{p} + \lambda d_i)}{\partial \lambda^2} \right|_{\lambda=0} \geq 0$$

for all $\bar{p} \in \Gamma, i = 1, 2, 3, c \in \mathbb{R}^e / \{0\}$, and $w \in \mathbb{R}^n / \{0\}$, where $n = \dim X$; namely,

$$X_2 \preceq 0, \quad dp M_1(X_v) + 3p M_2(X_v) \succeq 0, \quad (dp - 2p) M_1(X_v) + 3p M_2(X_v) \succeq 0, \quad (5.18)$$

for all $\bar{p} \in \Gamma$. The last two constraints in (5.18) are infinite dimensional but have linear dependence on the parameters; hence, these conditions hold for all $\bar{p} \in \Gamma$

if and only if they hold for all $\tilde{p} \in \text{vert}\Gamma$ since linear functions are trivially multiconvex. As discussed in [2], it is possible to relax the multiconvexity requirements slightly by strengthening the conditions in (5.17), for instance, replacing the condition $\mathcal{G}(X_v, \tilde{p}) \prec 0$ with $\mathcal{G}(X_v, \tilde{p}) \prec -(\kappa_0 + \kappa_1 p^2 + \kappa_2 d p^2)I$, for some nonnegative variables κ_i . Concerning the computational cost, notice that the number of LMIs grows exponentially with the number of parameters.

In the preceding, we briefly discussed some PLMI relaxation results available in the literature. There are many other important results. See, for instance, the work of Lasserre in [20] and the associated MATLAB software GloptiPoly [19], which builds and solves semidefinite programming relaxations for the generalized problem of moments. The latest features of YALMIP [24, 25] are also quite useful for solving PLMIs. The reader is referred to [21] for a comprehensive survey on the hierarchies of semidefinite relaxations and their main properties, and to the papers [33, 34] which focus on PLMI problems with polynomial or rational dependence on uncertainties and their important role in robust control. Note that the S-procedure [15, 42] can be seen as a special case of the SOS methods. The authors behind the multiconvexity technique explore other convexification methods yielding standard LMI problems in [38]; in [39], a relaxation method using monotonicity concepts is provided, where in this case the resulting finite family of LMI constraints is of polynomial order with respect to the number of parameters.

5.6 Controller Construction

Given an (h, q) -eventually periodic plant, suppose that, for some integer $N \geq h$, the (N, q) -eventually periodic matrix-valued continuous functions $R(p, k)$ and $S(p, k)$ satisfy the synthesis conditions (5.8) for all $(p, dp) \in \Gamma$, $k \in \mathbb{N}$, and that the last condition in (5.8) holds with strict inequality, namely,

$$\begin{bmatrix} R(p, k) & I \\ I & S(p, k) \end{bmatrix} \succ 0. \quad (5.19)$$

As in the standard H_∞ case, the controller is constructed from the solutions of the synthesis conditions, namely, $R(\delta(k), k)$ and $S(\delta(k), k)$ for some $\delta \in \Delta_\Gamma$, $k \in \mathbb{N}$. Since these solutions are parameter dependent in this case and as the parameter vector $\delta(k)$ is not known a priori but only available for measurement at each time k , the controller has to be constructed online and, in this section, we will give an algorithm to do so. Clearly, the time taken to compute the controller realization at each instant k has to be insignificant relative to the sampling time.

For simplicity, in the following we will suppress the dependence of the system matrices as well as the controller realization on the parameters, their increments, and time. As aforementioned, at each instant k , the values of $\delta(k)$ and $d\delta(k)$ will be available for measurement. To construct the controller realization at time k , we

will require the matrices $R(\delta(k), k)$, $R(\delta(k+1), k+1)$, $S(\delta(k), k)$, and $S(\delta(k+1), k+1)$, where $\delta(k+1) = \delta(k) + d\delta(k)$. For simplicity, given any matrix-valued function $F(p, k)$, we will use the notations $F_k := F(\delta(k), k)$ and $F_{k+1} = F(\delta(k+1), k+1)$ whenever convenient.

The following algorithm is a generalized version of the one given in [16]. To start, applying the Schur complement formula twice along with an appropriate permutation, the KYP inequality (5.7) can be equivalently written as

$$\begin{bmatrix} -X^{-1}(p+dp, k+1) & A_L & B_L & 0 \\ A_L^* & -X(p, k) & 0 & C_L^* \\ B_L^* & 0 & -\gamma I & D_L^* \\ 0 & C_L & D_L & -\gamma I \end{bmatrix} \prec 0, \quad (5.20)$$

for all $(p, dp) \in \Gamma$, $k \in \mathbb{N}$, where $X(p, k)$ is a positive definite matrix-valued continuous function in the variable p (not necessarily polynomial). Since $X(p, k)$ is constructed from $R(p, k)$ and $S(p, k)$, it is also (N, q) -eventually periodic and so are A_L , B_L , C_L , and D_L . As in the standard H_∞ case, $X(p, k)$ and its inverse satisfy

$$X = \begin{bmatrix} S & N \\ N^* & Z \end{bmatrix}, \quad X^{-1} = \begin{bmatrix} R & M \\ M^* & Y \end{bmatrix}, \quad MN^* = I - RS,$$

where the dependence of X and constituent elements on (p, k) is suppressed. It is also easy to verify that $X(p, k)\Pi_1(p, k) = \Pi_2(p, k)$ and $X^{-1}(p, k)\Pi_3(p, k) = \Pi_4(p, k)$, where

$$\Pi_1 = \begin{bmatrix} R & I \\ M^* & 0 \end{bmatrix}, \quad \Pi_2 = \begin{bmatrix} I & S \\ 0 & N^* \end{bmatrix}, \quad \Pi_3 = \begin{bmatrix} S & I \\ N^* & 0 \end{bmatrix}, \quad \Pi_4 = \begin{bmatrix} I & R \\ 0 & M^* \end{bmatrix}.$$

Pre- and post-multiplying inequality (5.20) by $\text{diag}(\Pi_3^*(p+dp, k+1), \Pi_1^*(p, k), I, I)$ and its transpose, respectively, we get the equivalent inequality

$$\begin{bmatrix} -S(p+dp, k+1) & -I & \hat{A}_{11} & \hat{A}_{12} & \hat{B}_1 & 0 \\ -I & -R(p+dp, k+1) & \hat{A}_{21} & \tilde{A} & \tilde{B} & 0 \\ \hat{A}_{11}^* & \hat{A}_{21}^* & -R(p, k) & -I & 0 & \hat{C}_1^* \\ \hat{A}_{12}^* & \tilde{A}^* & -I & -S(p, k) & 0 & \tilde{C}^* \\ \hat{B}_1^* & \tilde{B}^* & 0 & 0 & -\gamma I & D_L^* \\ 0 & 0 & \hat{C}_1 & \tilde{C} & D_L & -\gamma I \end{bmatrix} \prec 0, \quad (5.21)$$

where $\tilde{A} = A + B_2 D_K C_2$, $\tilde{B} = B_1 + B_2 D_K D_{21}$, $\tilde{C} = C_1 + D_{12} D_K C_2$, $\hat{A}_{11} = S(p+dp, k+1)\tilde{A}R(p, k) + S(p+dp, k+1)B_2 C_K M^*(p, k) + N(p+dp, k+1)B_K C_2 R(p, k) + N(p+dp, k+1)A_K M^*(p, k)$,

$$\begin{aligned}
\hat{A}_{12} &= S(p+dp, k+1)\tilde{A} + N(p+dp, k+1)B_K C_2, \\
\hat{B}_1 &= S(p+dp, k+1)\tilde{B} + N(p+dp, k+1)B_K D_{21}, \\
\hat{A}_{21} &= \tilde{A}R(p, k) + B_2 C_K M^*(p, k), \\
\hat{C}_1 &= \tilde{C}R(p, k) + D_{12} C_K M^*(p, k).
\end{aligned} \tag{5.22}$$

Define the permutation P as

$$P = \begin{bmatrix} 0 & 0 & 0 & 0 & 0 & I \\ I & 0 & 0 & 0 & 0 & 0 \\ 0 & 0 & 0 & 0 & I & 0 \\ 0 & 0 & I & 0 & 0 & 0 \\ 0 & 0 & 0 & I & 0 & 0 \\ 0 & I & 0 & 0 & 0 & 0 \end{bmatrix}.$$

Then, pre- and post-multiplying (5.21) by P^* and P , respectively, we get

$$\begin{bmatrix} \Omega & L_R & L_S \\ L_R^* & -R(p, k) & \hat{A}_{11}^* \\ L_S^* & \hat{A}_{11} & -S(p+dp, k+1) \end{bmatrix} \prec 0, \tag{5.23}$$

where

$$\Omega = \begin{bmatrix} -R(p+dp, k+1) & 0 & \tilde{A} & \tilde{B} \\ 0 & -\gamma I & \tilde{C} & D_L \\ \tilde{A}^* & \tilde{C}^* & -S(p, k) & 0 \\ \tilde{B}^* & D_L^* & 0 & -\gamma I \end{bmatrix},$$

$$L_R = \begin{bmatrix} \hat{A}_{21} \\ \hat{C}_1 \\ -I \\ 0 \end{bmatrix}, \quad L_S = \begin{bmatrix} -I \\ 0 \\ \hat{A}_{12}^* \\ \hat{B}_1^* \end{bmatrix}.$$

Appealing to (5.22), we can write L_R and L_S as

$$L_R = \begin{bmatrix} AR(p, k) + B_2 K_C \\ C_1 R(p, k) + D_{12} K_C \\ -I \\ 0 \end{bmatrix}, \quad L_S = \begin{bmatrix} -I \\ 0 \\ A^* S(p+dp, k+1) + C_2^* K_B \\ B_1^* S(p+dp, k+1) + D_{21}^* K_B \end{bmatrix},$$

where

$$K_C = D_K C_2 R(p, k) + C_K M^*(p, k), \tag{5.24}$$

$$K_B = D_K^* B_2^* S(p+dp, k+1) + B_K^* N^*(p+dp, k+1). \tag{5.25}$$

By the Schur complement formula, inequality (5.23) holds if and only if the following inequalities are valid:

$$\Omega \prec 0 \quad \text{and} \quad \begin{bmatrix} \Delta_R & \Delta_{21}^* \\ \Delta_{21} & \Delta_S \end{bmatrix} \prec 0,$$

where $\Delta_R = -R(p, k) - L_R^* \Omega^{-1} L_R$, $\Delta_S = -S(p + dp, k + 1) - L_S^* \Omega^{-1} L_S$, and $\Delta_{21} = \hat{A}_{11} - L_S^* \Omega^{-1} L_R$. It is always possible to choose the A -matrix of the controller, $A_K(p, dp, k)$, such that $\Delta_{21} = 0$ for all $(p, dp) \in \Gamma$, $k \in \mathbb{N}$. With this being the case, the validity of the KYP inequality becomes equivalent to the validity of $\Omega \prec 0$, $\Delta_R \prec 0$, and $\Delta_S \prec 0$. Observe that $\Omega \prec 0$ is a PLMI in the variable D_K , and so using one of the relaxation techniques presented in the previous section, we can solve offline for a polynomial function $D_K(p, dp, k)$ satisfying $\Omega \prec 0$ for all $(p, dp) \in \Gamma$, $k = 0, 1, \dots, N + q - 1$. Once D_K is computed, then we can apply the Schur complement formula to turn inequalities $\Delta_R \prec 0$ and $\Delta_S \prec 0$ into the PLMIs

$$\begin{bmatrix} -R(p, k) & L_R^* \\ L_R & \Omega \end{bmatrix} \prec 0 \quad \text{and} \quad \begin{bmatrix} -S(p + dp, k + 1) & L_S^* \\ L_S & \Omega \end{bmatrix} \prec 0 \quad (5.26)$$

in the variables K_C and K_B , respectively. Again, the relaxation techniques of the previous section can be used to solve for polynomial functions $K_C(p, dp, k)$ and $K_B(p, dp, k)$ satisfying the preceding two PLMIs for all $(p, dp) \in \Gamma$, $k = 0, 1, \dots, N + q - 1$. The three PLMIs may also be solved simultaneously. It is worth noting that, if the state-space matrices are of large dimensions, then the large size of the aforementioned PLMI problems may prohibit the use of the SOS relaxation method; in such a case, the multiconvexity relaxation technique may be very effective.

With D_K , K_C , and K_B calculated offline, the online computation of the controller realization at time k can be summarized as follows:

- (1) Compute the following factorizations: $M_k N_k^* = I - R_k S_k$ and $M_{k+1} N_{k+1}^* = I - R_{k+1} S_{k+1}$. For instance, choose $N_k = I$ and $M_k = I - R_k S_k$ for all k ; observe from (5.19) that this choice of M_k is invertible.
- (2) Evaluate D_K , K_C , and K_B at $(\delta(k), d\delta(k), k)$. Then, from (5.24) and (5.25), we have

$$C_K = (K_C - D_K C_2 R_k) (M_k^*)^{-1}, \quad B_K = (N_{k+1})^{-1} (K_B^* - S_{k+1} B_2 D_K).$$

- (3) Set $\Delta_{21} = 0$ to compute A_K ; namely,

$$A_K = (N_{k+1})^{-1} (L_S^* \Omega^{-1} L_R - S_{k+1} \tilde{A} R_k - S_{k+1} B_2 C_K M_k^* - N_{k+1} B_K C_2 R_k) (M_k^*)^{-1}.$$

An alternative to solving the PLMIs (5.26) offline for K_C and K_B is to compute online at each instant k the least-norm solutions $\begin{bmatrix} K_B \\ \star \end{bmatrix}$ and $\begin{bmatrix} K_C \\ \star \end{bmatrix}$ of the linear equations

$$\begin{bmatrix} 0 & 0 & 0 & C_2 & D_{21} \\ 0 & -R_{k+1} & 0 & \tilde{A} & \tilde{B} \\ 0 & 0 & -\gamma I & \tilde{C} & D_L \\ C_2^* & \tilde{A}^* & \tilde{C}^* & -S_k & 0 \\ D_{21}^* & \tilde{B}^* & D_L^* & 0 & -\gamma I \end{bmatrix} \begin{bmatrix} K_B \\ \star \end{bmatrix} = - \begin{bmatrix} 0 \\ -I \\ 0 \\ A^* S_{k+1} \\ B_1^* S_{k+1} \end{bmatrix},$$

$$\begin{bmatrix} 0 & B_2^* & D_{12}^* & 0 & 0 \\ B_2 & -R_{k+1} & 0 & \tilde{A} & \tilde{B} \\ D_{12} & 0 & -\gamma I & \tilde{C} & D_L \\ 0 & \tilde{A}^* & \tilde{C}^* & -S_k & 0 \\ 0 & \tilde{B}^* & D_L^* & 0 & -\gamma I \end{bmatrix} \begin{bmatrix} K_C \\ \star \end{bmatrix} = - \begin{bmatrix} 0 \\ AR_k \\ C_1 R_k \\ -I \\ 0 \end{bmatrix}.$$

The reader is referred to [8] for an additional algorithm for constructing the controller online, which is based on the results of [27]. Note that online implementation simplifies significantly when all the states are exactly measurable, i.e., $C_2 = I$ and $D_{21} = 0$, as evident from [8, Theorem 8].

5.7 Conclusions

The chapter presents a parameter-dependent Lyapunov approach for the control of eventually periodic NSLPV and switched SLPV systems, using the ℓ_2 -induced norm as the performance measure. The analysis and synthesis conditions are in the form of PLMIs, and a discussion of some of the PLMI relaxation techniques available in the literature is provided. The chapter also gives a fast and easy-to-implement algorithm for online controller construction.

References

1. Apkarian P, Gahinet P (1995) A convex characterization of gain-scheduled H_∞ controllers. IEEE Trans Automat Contr 40:853–864
2. Apkarian P, Tuan HD (2000) Parameterized LMIs in control theory. SIAM J Contr Optim 38(4):1241–1264
3. Bochnak J, Coste M, Roy MF (1998) Real algebraic geometry. Springer-Verlag, Berlin

4. Branicky MS (1995) Studies in hybrid systems: modeling, analysis, and control. PhD thesis, Massachusetts Institute of Technology
5. Chapellat H, Dahleh M (1992) Analysis of time-varying control strategies for optimal disturbance rejection and robustness. *IEEE Trans Automat Contr* 37:1734–1745
6. Dullerud GE, Lall SG (1999) A new approach to analysis and synthesis of time-varying systems. *IEEE Trans Automat Contr* 44(8):1486–1497
7. Farhood M (2010) Trajectory regulation of a double pendulum using a nonstationary LPV approach. In: Proceedings of the American Control Conference
8. Farhood M (2012) LPV control of nonstationary systems: a parameter-dependent Lyapunov approach. *IEEE Trans Automat Contr* 57(1):209–215
9. Farhood M, Dullerud GE (2002) LMI tools for eventually periodic systems. *Syst Contr Lett* 47(5):417–432
10. Farhood M, Dullerud GE (2005) Duality and eventually periodic systems. *Int J Robust Nonlin Contr* 15(13):575–599
11. Farhood M, Dullerud GE (2007) Model reduction of nonstationary LPV systems. *IEEE Trans Automat Contr* 52(2):181–196
12. Farhood M, Dullerud GE (2008) Control of nonstationary LPV systems. *Automatica* 44(8):2108–2119
13. Farhood M, Dullerud GE (2008) Control of systems with uncertain initial conditions. *IEEE Trans Automat Contr* 53(11):2646–2651
14. Farhood M, Feron E (2011) Obstacle-sensitive trajectory regulation via gain scheduling and semidefinite programming. *IEEE Trans Contr Syst Technol*, to appear, doi: 10.1109/TCST.2011.2159718, <http://ieeexplore.ieee.org/stamp/stamp.jsp?tp=&arnumber=5960813&isnumber=4389040>
15. Fradkov AL, Yakubovich VA (1979) The S-procedure and duality relations in nonconvex problems of quadratic programming. *Vestnik Leningrad Univ Math* 6:101–109. (In Russian 1973)
16. Gahinet P (1996) Explicit controller formulas for LMI-based H_∞ synthesis. *Automatica* 32(7):1007–1014
17. Green M, Limebeer D (1995) Linear robust control. Prentice Hall, Englewood Cliffs, NJ
18. Halanay A, Ionescu V (1994) Time-varying discrete linear systems. Birkhäuser, Boston, MA
19. Henrion D, Lasserre JB, Lofberg J (2009) GloptiPoly 3: moments, optimization and semidefinite programming. *Optim Meth Software* 24:761–779
20. Lasserre J (2008) A semidefinite programming approach to the generalized problem of moments. *Math Program* 112:65–92
21. Laurent M (2009) Sums of squares, moment matrices and optimization over polynomials. In: Putinar M, Sullivant S (eds) Emerging applications of algebraic geometry. IMA volumes in mathematics and its applications, vol 149. Springer, pp 157–270
22. Lavaei J, Aghdam AG (2008) Robust stability of LTI systems over semialgebraic sets using sum-of-squares matrix polynomials. *IEEE Trans Automat Contr* 53(1):417–423
23. Liberzon D (2003) Switching in systems and control. Birkhäuser, Boston, MA
24. Lofberg J (2004) YALMIP: a toolbox for modeling and optimization in MATLAB. In: Proceedings of the CACSD Conference. Taipei, Taiwan. <http://control.ee.ethz.ch/~joloef/wiki/pmwiki.php>
25. Lofberg J, Parrilo PA (2004) From coefficients to samples: a new approach to SOS optimization. In: Proceedings of IEEE conference on decision and control, pp 3154–3159
26. Lu B, Wu F (2004) Switching LPV control designs using multiple parameter-dependent Lyapunov functions. *Automatica* 40(11):1973–1980
27. Packard A (1994) Gain scheduling via linear fractional transformations. *Syst Contr Lett* 22:79–92
28. Parrilo PA (2000) Structured semidefinite programs and semialgebraic geometry methods in robustness and optimization. PhD thesis, California Institute of Technology. <http://www.cds.caltech.edu/pablo/>
29. Parrilo PA (2003) Semidefinite programming relaxations for semialgebraic problems. *Math Program Ser B* 96(2):293–320

30. Parrilo PA (2005) Exploiting algebraic structure in sum of squares programs. In: Henrion D, Garulli A (eds) Positive polynomials in control. Lecture notes in control and information sciences, vol. 312, Springer, Berlin/Heidelberg, pp 181–194
31. Prajna S, Papachristodoulou A, Seiler P, Parrilo PA (2004) SOSTOOLS: sum of squares optimization toolbox for MATLAB. Optim Meth Software. <http://www.cds.caltech.edu/sostools> and <http://www.mit.edu/~parrilo/sostools>
32. Rugh WJ, Shamma JS (2000) Research on gain scheduling. *Automatica* 36(10):1401–1425
33. Scherer CW (2006) LMI relaxations in robust control. *Euro J Contr* 12(1)
34. Scherer CW, Hol CWJ (2006) Matrix sum-of-squares relaxations for robust semi-definite programs. *Math Program* 107:189–211
35. Stengle G (1973) A nullstellensatz and a positivstellensatz in semialgebraic geometry. *Math Annal* 207:87–97
36. Sturm JF (1999) Using SeDuMi 1.02, a MATLAB toolbox for optimization over symmetric cones. *Optim Meth Software* 11–12:625–653. Version 1.05. <http://fewcal.kub.nl/sturm>
37. Toh KC, Todd MJ, Tutuncu RH (1999) SDPT3—a Matlab software package for semidefinite programming. *Optim Meth Software* 11:545–581
38. Tuan HD, Apkarian P (1999) Relaxations of parameterized LMIs with control applications. *Int J Robust Nonlin Contr* 9:59–84
39. Tuan HD, Apkarian P (2002) Monotonic relaxations for robust control: new characterizations. *IEEE Trans Automat Contr* 47(2):378–384
40. Wu F, Dong K (2006) Gain-scheduling control of LFT systems using parameter-dependent Lyapunov functions. *Automatica* 42:39–50
41. Wu F, Prajna S (2005) SOS-based solution approach to polynomial LPV system analysis and synthesis problems. *Int J Contr* 78(8):600–611
42. Yakubovich VA (1977) The S-procedure in nonlinear control theory. *Vestnik Leningrad Univ Math* 4. (In Russian 1971)

Chapter 6

Generalized Asymptotic Regulation for LPV Systems with Additional Performance Objectives

Hakan Köroğlu

Abstract A generalized version of the asymptotic output regulation problem is considered for an LPV plant subject to bounded (yet infinite-energy) disturbances generated by an LPV exogenous system. The uncertain parameters affecting the plant are all assumed to be measurable during online operation. On the other hand, the exogenous system is allowed to have dependence on measurable as well as unmeasurable parameters. The goal in the basic generalized asymptotic regulation problem is to synthesize an LPV controller that guarantees the internal stability of the closed loop and that ensures a bound on the steady-state peak of an output for all admissible parameter trajectories. A solution can be obtained for this problem based on a set of parameter-dependent LMIs. This chapter provides the LMI conditions that guarantee the satisfaction of an additional performance objective imposed on a (possibly) different output signal. Two different types of additional constraints are considered: (1) a bound on the \mathcal{L}_2 -gain from a finite-energy disturbance input to the considered output; (2) an \mathcal{H}_2 -type average energy constraint on the considered output in response to impulsive disturbance inputs in different directions.

6.1 Introduction

The classical theory of asymptotic output regulation is concerned with perfect cancelation of infinite-energy disturbances (or perfect tracking of infinite-energy references) in steady-state (see [26] for a modern account). Within the framework of this theory, the disturbances that influence the plant to be controlled are viewed as the outputs an unexcited and anti-stable (exogenous) system. A key result

H. Köroğlu (✉)

Electrical Engineering Department, King Fahd University of Petroleum and Minerals,
P.O. Box 983, Dhahran 31261, Saudi Arabia
e-mail: hkoroglu@kfupm.edu.sa

established by [4] (and known as the Internal Model Principle) states that the exact asymptotic regulation problem can be solved by replicating the dynamics of the exo-system in the feedback loop. This imposes a particular structure on the candidate controllers, which need to be stabilizing as well to provide a solution to the asymptotic regulation problem. In fact, it is possible to aim for more and synthesize a controller that achieves additional performance objectives expressed in the form of \mathcal{H}_∞ or \mathcal{H}_2 norm constraints [26, 29, 30].

A useful generalization of the asymptotic regulation problem is possible when the disturbance and references are restricted to be sinusoidal or constant signals. In this formulation that we refer to as generalized asymptotic regulation (GAR), the goal is to ensure that the peak-to-peak gain from the exo-system state to the output to be regulated is as small as possible or desirable (rather than zero, see [10]). Such a formulation is possible in the case of unbounded disturbances as well, but might be of little use for practical purposes. The multi-objective version of the GAR problem was considered in [16] and [20] with \mathcal{H}_∞ and \mathcal{H}_2 norm constraints, respectively. These works clarified how generalized asymptotic regulation constraints can be integrated into \mathcal{H}_∞ and \mathcal{H}_2 (as well as various other) synthesis problems that can be solved based on linear matrix inequality (LMI) optimization.

Due to the increased interest in parameter-dependent models known as linear parameter-varying (LPV) systems, it is natural to consider the asymptotic regulation problem for such systems as well. But the key motivation originates from practical engineering systems that are subject to sinusoidal disturbances whose frequencies show variations in time [1, 3, 8, 9, 11, 13, 23]. Such non-stationary sinusoidal disturbances can clearly be generated by parameter-dependent exo-system models. The existence of parameter dependence in the plant or the exo-system introduces a significant challenge in the solution of the standard asymptotic regulation problem. As a matter of fact, one is faced with a differential algebraic constraint when there is time variation in the plant or the exo-system [12, 32]. The exact asymptotic regulation objective then becomes too ambitious and is achievable under restrictive assumptions (see, e.g., [15]). The problem becomes even more complicated when the exo-system has dependence on unmeasurable parameters as well, which is also a case of significant practical relevance. For this reason, the generalized formulation of the asymptotic regulation problem becomes particularly convenient for parameter-dependent plants and exo-systems.

The GAR problem was considered for LPV systems with online-measurable parameters in [17] and an observer-based solution was derived within the framework of LMI optimization. This solution was extended by [22] in a way to optimize the transient behavior with a controller of general structure. The case of uncertain exo-system with unmeasurable uncertainty was considered in [18, 19] for a linear time invariant (LTI) plant. Based on the achievements of these works, a solution was derived by [21] for the case in which the plant has dependence only on online-measurable parameters, while the exo-system is allowed to depend on unmeasurable parameters as well (see also [14] on avoidance of parameter-derivative dependence in the LPV controller).

This chapter basically summarizes the results of [21] and extends them in a way to handle additional performance objectives as well. The problem setup described in Sect. 6.2 is slightly more general than that of [21] in that it facilitates the use of the knowledge concerning the rates-of-variation of the unmeasurable parameters. The basic problem that we refer to as robust GAR is formulated and studied in Sect. 6.3. The contents of this section are basically adapted and shortened from [21]. As the main novel content, this chapter provides solutions to the robust GAR problem with additional performance objectives. Section 6.4 considers the problem with an \mathcal{L}_2 -gain constraint, whereas Sect. 6.5 elaborates on the problem with an \mathcal{H}_2 -type performance objective. In addition to providing LMI-based solutions, these sections also specialize them to LTI plants/exo-systems and thus establish links to the relevant works [16] and [20], respectively. Illustrative simulation results are also provided for the course control problem inherited from [21, 22]. The chapter is concluded with a brief discussion of interesting and challenging research directions.

6.2 Problem Setup

The problems considered in this chapter are formulated for a parameter-dependent plant whose dynamics are described as

$$\Sigma_p : \begin{bmatrix} \dot{x} \\ e \\ z \\ y \end{bmatrix} = \begin{bmatrix} A(\mu) & B_r(\delta) & B_p(\delta) & B(\mu) \\ C_r(\delta) & D_r(\delta) & D_{rp}(\delta) & D_{rc}(\delta) \\ C_p(\delta) & D_{pr}(\delta) & D_p(\delta) & D_{pc}(\delta) \\ C(\mu) & D_{cr}(\delta) & D_{cp}(\delta) & 0 \end{bmatrix} \begin{bmatrix} x \\ w \\ v \\ u \end{bmatrix}, \quad (6.1)$$

where $x(t) \in \mathbb{R}^k$ denotes the state vector. The design goal is to generate the control input vector $u(t) \in \mathbb{R}^n$ by processing the measurements $y(t) \in \mathbb{R}^m$ in a way to achieve a generalized regulation objective for the error signal $e(t) \in \mathbb{R}^r$ and an additional objective for the performance output $z \in \mathbb{R}^q$. This is to be done in the face of a finite-energy disturbance $v(t) \in \mathbb{R}^p$ and an infinite-energy disturbance $w(t) \in \mathbb{R}^l$. The infinite-energy disturbance is assumed to be generated by a neutrally stable exogenous system from nonzero initial states as

$$\dot{w} = A_e(\delta)w. \quad (6.2)$$

In our setting, the full vector of uncertain parameters is represented by

$$\delta = \begin{bmatrix} \mu \\ v \end{bmatrix} = \begin{bmatrix} \theta^m \\ v^m \\ \theta^u \\ v^u \end{bmatrix}; \quad \begin{array}{l} \theta^m : \text{vector of measurable parameters} \\ v^m : \text{derivative of } \theta^m \text{ (measurable)} \\ \theta^u : \text{vector of unmeasurable parameters} \\ v^u : \text{derivative of } \theta^u \text{ (unmeasurable).} \end{array} \quad (6.3)$$

The uncertain parameter vector $\theta \triangleq (\theta^m, \theta^u)$ is allowed to vary in time in a compact (i.e., closed and bounded) region \mathcal{R} in such a way that its derivative $v \triangleq \dot{\theta}$ stays within \mathcal{D} . We represent the set of admissible values for the full parameter vector δ as \mathcal{U} . Note that \mathcal{U} is necessarily a subset of $\mathcal{R} \times \mathcal{D}$, yet it can be a smaller set depending on the set of admissible parameter trajectories, which we denote as \mathcal{T} . When the uncertainty is described directly by the sets \mathcal{R} and \mathcal{U} , the set of admissible parameter trajectories is identified as $\mathcal{T} = \{\theta(\cdot) : [0, \infty) \rightarrow \mathcal{R} \mid (\theta(t), \dot{\theta}(t)) \in \mathcal{U}\}$, which should clearly be nonempty for a nontrivial problem formulation. In order to restrict our interest to the set of measurable parameters or parameter trajectories, we use \mathcal{R}_m , \mathcal{U}_m , and \mathcal{T}_m .

We assume that all the system matrices in (6.1) and (6.2), as well as all the design variables that will come into the scene in the sequel, depend continuously on the uncertain parameter vectors. For some design elements, we also assume differentiability with respect to θ and use

$$\partial S(\delta) \triangleq \sum_{i=1}^{n_m} \frac{\partial S}{\partial \theta_i^m} v_i^m + \sum_{i=1}^{n_u} \frac{\partial S}{\partial \theta_i^u} v_i^u, \quad (6.4)$$

where θ_i^m , v_i^m , θ_i^u , and v_i^u represent the i th elements of the relevant vectors. When a design element, say Y , depends only on θ^m , we write $\partial Y(\mu)$. We completely suppress the parameter dependency whenever it is inferrable from the context. To reduce the redundancy of notation, we represent the symmetric part of a matrix as $\text{He}A \triangleq A + A^T$ and use $*$ to indicate the blocks of a matrix that are uniquely identifiable from symmetry.

For the sake of a concise notation, we express the dynamics of the extended plant by appending the dynamics of the exo-system to the dynamics of the plant as

$$\begin{aligned} \dot{\tilde{x}} &= \underbrace{\begin{bmatrix} A(\mu) & B_r(\delta) \\ 0 & A_e(\delta) \end{bmatrix}}_{\tilde{A}(\delta)} \underbrace{\begin{bmatrix} x \\ w \end{bmatrix}}_{\tilde{x}} + \underbrace{\begin{bmatrix} B_p(\delta) \\ 0 \end{bmatrix}}_{\tilde{B}_p(\delta)} v + \underbrace{\begin{bmatrix} B(\mu) \\ 0 \end{bmatrix}}_{\tilde{B}(\mu)=\tilde{B}(\mu)} u, \\ e &= \underbrace{\begin{bmatrix} C_r(\delta) & D_r(\delta) \end{bmatrix}}_{\tilde{C}_r(\delta)} \tilde{x} + D_{rp}(\delta)v + D_{rc}(\delta)u, \\ z &= \underbrace{\begin{bmatrix} C_p(\delta) & D_{pr}(\delta) \end{bmatrix}}_{\tilde{C}_p(\delta)} \tilde{x} + D_p(\delta)v + D_{pc}(\delta)u, \\ y &= \underbrace{\begin{bmatrix} C(\mu) & D_{cr}(\delta) \end{bmatrix}}_{\tilde{C}(\delta)} \tilde{x} + D_{cp}(\delta)v. \end{aligned} \quad (6.5)$$

In order to avoid the dependence of the synthesized controller on the unmeasurable parameter vector v , we will use the decompositions of some δ -dependent extended plant matrices as

$$\tilde{A}(\delta) = \underbrace{\begin{bmatrix} A(\mu) & B_r^m(\mu) \\ 0 & A_e^m(\mu) \end{bmatrix}}_{\hat{A}(\mu)} + \underbrace{\begin{bmatrix} B_r^u(\delta) \\ A_e^u(\delta) \end{bmatrix}}_{\tilde{B}_r^u(\delta)} \underbrace{\begin{bmatrix} 0_{l \times k} & I_l \end{bmatrix}}_E, \quad (6.6)$$

$$\tilde{C}(\delta) = \underbrace{\begin{bmatrix} C(\mu) & D_{cr}^m(\mu) \end{bmatrix}}_{\hat{C}(\mu)} + D_{cr}^u(\delta)E. \quad (6.7)$$

We note here that the hats should remind the reader of no dependence on the unmeasurable parameters, if the parameter dependencies are suppressed for simplicity. Hence, any decomposition in which this is respected will in fact be admissible in our derivations (the simplest can be obtain with $B_r^m = 0$, $A_e^m = 0$, and $D_{cr}^m = 0$). Since such a decomposition is not needed when there are no unmeasurable parameters (i.e., when ν is void), we will use

$$\hat{A} = \tilde{A}, \quad \hat{C} = \tilde{C} \quad \text{and} \quad \tilde{B}_r^u = 0, \quad D_{cr}^u = 0, \quad \text{if} \quad \delta = \mu. \quad (6.8)$$

We adapt the common assumptions in asymptotic regulation problems (see, e.g., [26]) to our setting together with the introduction of some additional notation as follows:

(A.1) *Neutrally Stable Exo-System*: There exists a symmetric positive-definite map $S_0 : \mathcal{R} \rightarrow \mathbb{S}_+^l$ such that

$$\mathcal{L}_e(S_0, \delta) \triangleq \partial S_0(\delta) + \text{He}(S_0(\theta)A_e(\delta)) = 0, \quad \forall \delta \in \mathcal{U}. \quad (6.9)$$

(A.2) *Stabilizability*: There exist $Y : \mathcal{R}_m \rightarrow \mathbb{S}_+^k$, $N : \mathcal{U}_m \rightarrow \mathbb{R}^{n \times k}$, and $\rho \in \mathbb{R}_+$ such that

$$\begin{aligned} \mathcal{L}_s(Y, N, \mu) &\triangleq -\partial Y(\mu) + \text{He}(A(\mu)Y(\theta^m) + B(\mu)N(\mu)) \\ &\preceq -2\rho Y(\theta^m), \quad \forall \mu \in \mathcal{U}_m. \end{aligned} \quad (6.10)$$

(A.3) *Detectability*: There exist $X : \mathcal{R}_m \rightarrow \mathbb{S}_+^{k+l}$, $M : \mathcal{U}_m \rightarrow \mathbb{R}^{(k+l) \times m}$, and $\rho \in \mathbb{R}_+$ such that

$$\begin{aligned} \mathcal{L}_d(X, M, \delta) &\triangleq \underbrace{\partial X(\mu) + \text{He}(X(\theta^m)\hat{A}(\mu) + M(\mu)\hat{C}(\mu))}_{\mathcal{L}_d^m(X, M, \mu)} \\ &\quad + \text{He}(X(\theta^m)\tilde{B}_r^u(\delta)E + M(\mu)\tilde{D}_{cr}^u(\delta)E) \\ &= \partial X(\mu) + \text{He}(X(\theta^m)\tilde{A}(\delta) + M(\mu)\tilde{C}(\delta)) \\ &\preceq -2\rho X(\theta^m), \quad \forall \delta \in \mathcal{U}. \end{aligned} \quad (6.11)$$

The considered class of infinite-energy disturbances are basically formed by bounded non-stationary sinusoidal signals. In order to clarify this, we first introduce

the positive-definite function $\mathcal{V}_e(w, \theta) \triangleq w^T S_0(\theta)w$ and infer from (A.1) that it remains constant along the trajectories of (6.2). In other words, we have for all admissible parameter trajectories that

$$w(t)^T S_0(\theta(t))w(t) = w(0)^T S_0(\theta(0))w(0), \quad \forall t \geq 0. \quad (6.12)$$

With the uniform lower and upper bounds on the eigenvalues of S_0 expressed as

$$\lambda_{\min} I \preceq S_0(\theta) \preceq \lambda_{\max} I, \quad \forall \theta \in \mathcal{R}, \quad (6.13)$$

the norm of w can be shown to be bounded from below and above as

$$\sqrt{\lambda_{\min}/\lambda_{\max}} \|w(0)\| \leq \|w(t)\| \leq \sqrt{\lambda_{\max}/\lambda_{\min}} \|w(0)\|. \quad (6.14)$$

As a representative example, let us now consider

$$\begin{bmatrix} \dot{w}_1(t) \\ \dot{w}_2(t) \end{bmatrix} = \begin{bmatrix} 0 & -\varpi(t) \\ \varpi(t) & 0 \end{bmatrix} \begin{bmatrix} w_1(t) \\ w_2(t) \end{bmatrix}, \quad (6.15)$$

where $\varpi(t)$ serves as a time-varying frequency, which might depend on measurable as well as unmeasurable parameters. We can obtain the explicit expression for the states of this system as

$$\begin{bmatrix} w_1(t) \\ w_2(t) \end{bmatrix} = \begin{bmatrix} \cos(\int_0^t \varpi(\tau) d\tau) & -\sin(\int_0^t \varpi(\tau) d\tau) \\ \sin(\int_0^t \varpi(\tau) d\tau) & \cos(\int_0^t \varpi(\tau) d\tau) \end{bmatrix} \begin{bmatrix} w_1(0) \\ w_2(0) \end{bmatrix}. \quad (6.16)$$

Since the exo-system matrix in this example is skew symmetric, (A.1) is satisfied with $S_0 = I$.

The problems considered in this chapter aim at designing a controller whose dynamics depend on the measurable parameter vector as

$$\Sigma_c : \begin{bmatrix} \dot{\xi} \\ u \end{bmatrix} = \begin{bmatrix} A_c(\mu) & B_c(\mu) \\ C_c(\mu) & D_c(\mu) \end{bmatrix} \begin{bmatrix} \xi \\ y \end{bmatrix}. \quad (6.17)$$

We consider full-order synthesis, which means in this case that the order of the controller is equal to the order of the plant plus the order of the exo-system (i.e., $\xi(t) \in \mathbb{R}^{k+l}$). The generalized asymptotic regulation objective will be imposed on the error signal e when $v = 0$. In this case, the closed-loop dynamics can be expressed as

$$\begin{aligned} \dot{\tilde{x}} &= \underbrace{\begin{bmatrix} \tilde{A} + \tilde{B}D_c\tilde{C} & \tilde{B}C_c \\ B_c\tilde{C} & A_c \end{bmatrix}}_{\mathcal{A}_r(\delta)} \underbrace{\begin{bmatrix} \tilde{x} \\ \xi \end{bmatrix}}_{\tilde{x}}, \\ e &= \underbrace{[\tilde{C}_r + D_{rc}D_c\tilde{C} \quad D_{rc}C_c]}_{\mathcal{C}_r(\delta)} \tilde{x}. \end{aligned} \quad (6.18)$$

On the other hand, the additional performance objectives will be imposed on the signal z when $w = 0$. The closed loop evolves in this case according to

$$\begin{aligned} \dot{z} &= \underbrace{\begin{bmatrix} A + BD_c C & BC_c \\ B_c C & A_c \end{bmatrix}}_{\mathcal{A}_p(\mu)} \underbrace{\begin{bmatrix} x \\ \xi \\ \zeta \end{bmatrix}}_{z} + \underbrace{\begin{bmatrix} B_p + BD_c D_{cp} \\ B_c D_{cp} \end{bmatrix}}_{\mathcal{B}_p(\delta)} v, \\ z &= \underbrace{\begin{bmatrix} C_p + D_{pc} D_c C & D_{pc} C_c \end{bmatrix}}_{\mathcal{C}_p(\delta)} z + \underbrace{\begin{bmatrix} D_p + D_{pc} D_c D_{cp} \end{bmatrix}}_{\mathcal{D}_p(\delta)} v. \end{aligned} \quad (6.19)$$

Due to the linearity of the system for a fixed parameter trajectory, the closed loop is expected to have a desirable behavior with the synthesized controller when w and v are both nonzero. Since this will be the case especially for $z = e$, the performance output should be chosen to include the error signal as well. A typical choice would be $z = [e^T \lambda u^T]^T$, where λ is a (small) positive scalar that is properly tuned to adjust the required control effort.

6.3 Robust Generalized Asymptotic Regulation (GAR)

6.3.1 Robust GAR Problem

Based on the problem setup described in the previous section, the robust generalized asymptotic regulation problem is formulated as follows:

Problem 6.1. Given the plant in (6.1), the exo-system in (6.2) and the uncertainty regions (\mathcal{R} , \mathcal{D} , \mathcal{U} , etc.), design a controller as in (6.17) such that:

(C.1) *Robust Internal Stability:* There exist $\varphi, \rho \in \mathbb{R}_+$ such that, in the closed-loop system of (6.18) with $w(0) = 0$ (i.e., for $\dot{z} = \mathcal{A}_p(\mu)z$), we have

$$\|z(t)\|^2 \leq \varphi \|z(0)\|^2 e^{-2\rho t}, \quad \forall t \geq 0, \quad \forall \theta^m(\cdot) \in \mathcal{T}_m. \quad (6.20)$$

(C.2) *Robust GAR of Level $\kappa \in \mathbb{R}_+$:* There exist $\alpha, \rho \in \mathbb{R}_+$ such that, in the closed-loop system of (6.18), we have

$$\|e(t)\|^2 \leq \alpha \|\tilde{z}(0)\|^2 e^{-2\rho t} + \kappa^2 w(t)^T \Phi(\theta(t)) w(t), \quad \forall t \geq 0, \quad \forall \theta(\cdot) \in \mathcal{T}, \quad (6.21)$$

where $\Phi(\cdot)$ represents a positive semi-definite attenuation profile.

The generalized asymptotic regulation constraint in (C.2) is adapted from [10]. Recall that the classical asymptotic regulation problem is formulated with $\kappa = 0$. Since we consider an uncertain exo-system, the exact asymptotic regulation problem will usually be unsolvable. For this reason, the goal in the robust generalized asymptotic regulation problem would be to keep κ as small as possible or desirable.

We have introduced $\Phi(\cdot)$ as an additional design element. Recalling from (A.1) the existence of a positive-definite map S_0 for which $\mathcal{L}_e(S_0, \delta) = 0$ and $\|S_0(\theta)\| \leq 1$, we can view $\Phi(\theta) = S_0(\theta)$ as an alternative choice to $\Phi = I$. In fact, it is quite reasonable to allow for a graceful degradation on the attenuation level if the uncertain parameters deviate from their nominal values. In view of this, Φ can be chosen in the general form

$$\Phi(\theta) = (1 + \zeta(\|\theta\|))S_0(\theta), \quad (6.22)$$

where $\zeta(\cdot)$ is a scalar-valued, preferably monotone nondecreasing function that is zero at zero. A simple and convenient choice would be $\zeta(\|\theta\|) = \zeta_0\|\theta\|^2$, where ζ_0 is a nonnegative scalar that determines the admissible rate of degradation in the level of steady-state attenuation with increasing deviations from the nominal parameter vector $\theta = 0$.

6.3.2 A Sufficient Condition for Robust GAR

A necessary and sufficient condition is provided for generalized asymptotic regulation in LTI systems by [10]. This condition can be rephrased as a sufficient condition for parameter-dependent systems considered in this chapter as follows:

Lemma 6.1. *The closed-loop system in (6.18) satisfies (C.1) and (C.2) if there exist $\rho, \phi \in \mathbb{R}_+$ and $\mathcal{X} : \mathcal{R} \rightarrow \mathbb{S}_+^{2(k+l)}$ for which*

$$\mathcal{N}(\delta) = \partial \mathcal{X}_r(\delta) + 2\rho \mathcal{X}_r(\theta) + \text{He}(\mathcal{X}_r(\theta)\mathcal{A}_r(\delta)) \preceq 0, \quad \forall \delta \in \mathcal{U}, \quad (6.23)$$

$$\mathcal{P}(\delta) = \begin{bmatrix} \mathcal{X}(\theta) & \mathcal{E}_r(\delta)^T \\ \mathcal{E}_r(\delta) & \phi I \end{bmatrix} \succ 0, \quad \forall \delta \in \mathcal{U}, \quad (6.24)$$

with

$$\mathcal{X}_r \triangleq \mathcal{X} - \phi^{-1} \kappa^2 \mathcal{J}^T \Phi \mathcal{J}, \quad (6.25)$$

where

$$\mathcal{J} \triangleq \begin{bmatrix} E & 0_{l \times (k+l)} \end{bmatrix} = \begin{bmatrix} 0_{l \times k} & I_l & 0_{l \times (k+l)} \end{bmatrix}. \quad (6.26)$$

We then have for the closed-loop system of (6.18) for any admissible parameter variation that

$$\|e(t)\|^2 \leq \phi \tilde{z}(0)^T \mathcal{X}_r(\theta(0)) \tilde{z}(0) e^{-2\rho t} + \kappa^2 w(t)^T \Phi(\theta(t)) w(t), \quad \forall t \geq 0. \quad (6.27)$$

Proof. We first infer from (6.23) that the function $\mathcal{V}(\tilde{z}, \theta) \triangleq \tilde{z}^T \mathcal{X}_r(\theta) \tilde{z}$ satisfies

$$\frac{d}{dt} (e^{2\rho t} \mathcal{V}(\tilde{z}(t), \theta(t))) = e^{2\rho t} \tilde{z}(t)^T \mathcal{N}(\delta(t)) \tilde{z}(t) \leq 0, \quad \forall t \geq 0, \quad (6.28)$$

along the trajectories of the extended closed-loop system in (6.18) for any admissible parameter variation. It hence stays bounded in time from above according to

$$\underbrace{\tilde{z}(t)^T \mathcal{X}(\theta(t)) \tilde{z}(t) - \phi^{-1} \kappa^2 w(t)^T \Phi(\theta(t)) w(t)}_{\mathcal{V}(\tilde{z}(t), \theta(t))} \leq \underbrace{\tilde{z}(0)^T \mathcal{X}_r(\theta(0)) \tilde{z}(0)}_{\mathcal{V}(\tilde{z}(0), \theta(0))} e^{-2\rho t}. \quad (6.29)$$

We thus conclude for all $t \geq 0$ that

$$\underbrace{\phi \tilde{z}(t)^T \mathcal{X}(\theta(t)) \tilde{z}(t)}_{\geq \varepsilon \|\tilde{z}(t)\|^2} \leq \underbrace{\phi \tilde{z}(0)^T \mathcal{X}_r(\theta(0)) \tilde{z}(0)}_{\leq \alpha \|\tilde{z}(0)\|^2 e^{-2\rho t}} e^{-2\rho t} + \kappa^2 w(t)^T \Phi(\theta(t)) w(t), \quad (6.30)$$

where ε and α are any positive scalars that satisfy

$$\varepsilon I \preceq \phi \mathcal{X}(\theta) \preceq \phi \mathcal{X}_r(\theta) \preceq \alpha I, \quad \forall \theta \in \mathcal{R}. \quad (6.31)$$

When $w(0) = 0$, we have $w(t) = 0$, as a result of which $\|\mathcal{z}(t)\| = \|\tilde{z}(t)\|$ obeys (6.20) with $\varphi = \alpha/\varepsilon$. For general $w(0)$, we infer from (6.24) that

$$\phi \tilde{z}(t)^T \mathcal{X}(\theta(t)) \tilde{z}(t) - \|e(t)\|^2 = \chi(t)^T \mathcal{P}(\delta(t)) \chi(t) \geq 0, \quad \forall t \geq 0, \quad (6.32)$$

where $\chi(t)^T = [\phi^{1/2} \tilde{z}(t)^T - \phi^{-1/2} e(t)^T]$. This clearly implies (6.27) and thus (6.21). \square

Conditions (6.23) and (6.24) are also necessary if θ is time invariant and fixed, i.e., when the problem is considered for an LTI system with no uncertainty (see [10]). Note that in this case $\partial \mathcal{X}_r$ is to be replaced with zero. We can then also fix the value of ϕ (e.g., as $\phi = \kappa$) without introducing any conservatism. The condition is potentially conservative in the general case since it is based on the construction of a Lyapunov function with only quadratic state dependence. Further conservatism might also be introduced when the parameter-dependent conditions are relaxed into finitely many LMIs. In fact, the value of ϕ might affect the level of conservatism introduced at the stage of relaxation. When additional performance objectives are considered, ϕ will again serve as a parameter that might potentially reduce conservatism.

6.3.3 A Solution to the Robust GAR Problem

A solution is obtained by [21] for Problem 6.1 based on LMI optimization. This solution is derived by first expressing the conditions of Lemma 6.1 equivalently (and with the parameter dependencies suppressed for simplicity) as

$$\mathcal{Y}^T (\partial \mathcal{X}_r) \mathcal{Y} + 2\rho \mathcal{Y}^T \mathcal{X}_r \mathcal{Y} + \text{He} (\mathcal{Y}^T \mathcal{X}_r \mathcal{A}_r \mathcal{Y}) \preceq 0, \quad (6.33)$$

$$\begin{bmatrix} \mathcal{Y}^T & \mathcal{X} & \mathcal{Y} & \mathcal{Y}^T \mathcal{C}_r^T \\ \mathcal{C}_r & \mathcal{Y} & & \phi I \end{bmatrix} \succ 0. \quad (6.34)$$

Here, $\mathcal{Y} : \mathcal{R} \rightarrow \mathbb{R}^{2(k+l) \times 2(k+l)}$ represents a nonsingular map, the choice of which forms the key step. The suitable choice of \mathcal{Y} in this case is derived in [21] by combining the transformations of [27, 29] similarly to [2]. The equivalent matrix inequality conditions obtained in this fashion are then rendered affine in all free matrix variables through a bijective transformation of the controller realization matrices into a set of new matrix variables. The design ingredients are chosen in such a way that the resulting controller has no dependence on the unmeasurable parameters.

Let us now summarize the solution of [21] by first partitioning \mathcal{X} and its inverse compatibly with \mathcal{A}_r in (6.18) as

$$\mathcal{X} = \begin{bmatrix} P & U \\ U^T & U^T (P - Q^{-1})^{-1} U \end{bmatrix}, \quad \mathcal{X}^{-1} = \begin{bmatrix} Q & V \\ V^T & V^T (Q - P^{-1})^{-1} V \end{bmatrix}. \quad (6.35)$$

We assume without loss of generality that U and V are invertible and note that they are required to satisfy

$$PQ + UV^T = I, \quad (6.36)$$

as follows from $\mathcal{X} \mathcal{X}^{-1} = I$. Without loss of generality, the matrix Q is chosen to be of the form

$$Q = \begin{bmatrix} Q_{11} & Q_{12} \\ Q_{12}^T & Q_{22} \end{bmatrix} = \begin{bmatrix} I & \Omega \\ 0 & W \end{bmatrix}^{-1} \begin{bmatrix} Y & 0 \\ 0 & W \end{bmatrix} \begin{bmatrix} I & \Omega \\ 0 & W \end{bmatrix}^{-T}, \quad (6.37)$$

where the partition is compatible with \tilde{A} in (6.6). The first set of design variables are defined by

$$W \triangleq Q_{22}^{-1}, \quad (6.38)$$

$$\Omega \triangleq -Q_{12}W, \quad (6.39)$$

$$Y \triangleq Q_{11} - \Omega W^{-1} \Omega^T, \quad (6.40)$$

$$X \triangleq P - E^T W E, \quad (6.41)$$

where E is the constant matrix introduced in (6.26). We will omit W in the final design conditions and instead use

$$S \triangleq \phi^{-1} \kappa^2 \Phi - W. \quad (6.42)$$

With T formed as

$$T \triangleq \left[\begin{array}{c|c} \hat{\Omega} & \\ \hline WE & \end{array} \right] = \left[\begin{array}{c|c} I & \Omega \\ \hline 0 & W \end{array} \right], \quad (6.43)$$

the suitable choice of \mathcal{Y} is given by

$$\mathcal{Y}^T = \left[\begin{array}{c|c} TQ & TV \\ \hline I & 0 \end{array} \right]. \quad (6.44)$$

The second set of design variables are introduced by the transformation

$$\left[\begin{array}{c|c} L & -\Theta & M \\ \hline N & -\Psi & D \end{array} \right] \triangleq \left[\begin{array}{c|c} U & X\hat{B} \\ \hline 0 & I \end{array} \right] \left[\begin{array}{c|c} A_c & B_c \\ \hline C_c & D_c \end{array} \right] \left[\begin{array}{c|c} V^T \hat{\Omega}^T & V^T E^T W \\ \hline \hat{C} Q \hat{\Omega}^T & \hat{C} Q E^T W \\ \hline 0 & I \end{array} \right] \\ + \left[\begin{array}{c|c} (X\hat{A}Q + (\partial X)Q + (\partial U)V^T) & \hat{\Omega}^T \\ \hline 0 & 0 \end{array} \right] \left[\begin{array}{c|c} (X\hat{A}Q + (\partial X)Q + (\partial U)V^T) & E^T W \\ \hline 0 & 0 \end{array} \right]. \quad (6.45)$$

The controller realization matrices can be obtained from the design ingredients via the inverse transformation

$$\left[\begin{array}{c|c} A_c & B_c \\ \hline C_c & D_c \end{array} \right] = \left[\begin{array}{c|c} U^{-1} & -U^{-1}X\hat{B} \\ \hline 0 & I \end{array} \right] \left[\begin{array}{c|c} \hat{L} & M \\ \hline \hat{N} & D \end{array} \right] \left[\begin{array}{c|c} T^{-T}V^{-T} & 0 \\ \hline -\hat{C}QV^{-T} & I \end{array} \right], \quad (6.46)$$

where

$$\hat{L} = [L - \Theta] - X\hat{A}QT^T - (\partial X)QT^T - (\partial U)V^T T^T \quad \text{and} \quad \hat{N} = [N - \Psi]. \quad (6.47)$$

Thanks to the use of \hat{A} and \hat{C} from the decompositions in (6.6) and (6.7) rather than \tilde{A} and \tilde{C} , it will be possible to synthesize the controller realization matrices from the inverse transformation in a way to depend only on the measurable parameters. For this, one will have to use design elements with no dependence on the unmeasurable parameters. The only exception to this restriction is S , on which the controller turns out to have no dependence.

With the design ingredients introduced above, one arrives at the following solution of [21] to Problem 6.1:

Theorem 6.1. *There is a solution to Problem 6.1 if there exist $\rho, \phi \in \mathbb{R}_+$ and*

$$Y : \mathcal{R}_m \rightarrow \mathbb{S}_+^k, X : \mathcal{R}_m \rightarrow \mathbb{S}_+^{k+l}, \Omega : \mathcal{R}_m \rightarrow \mathbb{R}^{k \times l}, \\ K : \mathcal{U}_m \rightarrow \mathbb{R}^{(k+l) \times k}, M : \mathcal{U}_m \rightarrow \mathbb{R}^{(k+l) \times m}, N : \mathcal{U}_m \rightarrow \mathbb{R}^{n \times k}, \\ D : \mathcal{U}_m \rightarrow \mathbb{R}^{n \times m}, \Psi : \mathcal{U}_m \rightarrow \mathbb{R}^{n \times l}, \Theta : \mathcal{U}_m \rightarrow \mathbb{R}^{(k+l) \times l} \quad \text{and} \quad S : \mathcal{R} \rightarrow \mathbb{S}^l, \quad (6.48)$$

with which

$$\begin{bmatrix} \mathcal{L}_s(Y, N) & * & * \\ K - \partial \hat{\Omega}^T & \mathcal{L}_d^m(X, M) + \text{He}(\Theta E) & * \\ \mathcal{L}_{se}(\Omega, \Psi_r)^T & -\Theta_r^T & -\mathcal{L}_e(S) \end{bmatrix} \preccurlyeq -2\rho \begin{bmatrix} Y & \hat{\Omega} & 0 \\ \hat{\Omega}^T & X & 0 \\ 0 & 0 & -S \end{bmatrix}, \quad (6.49)$$

$$\begin{bmatrix} Y & * & * & * \\ \hat{\Omega}^T & X & * & * \\ 0 & 0 & \phi^{-1} \kappa^2 \Phi - S & * \\ C_r Y + D_{rc} N & C_r \hat{\Omega} + D_{rc} (D\hat{C} + \Psi E) & \mathcal{L}_{re}(\Omega, \Psi_r) & \phi I \end{bmatrix} \succ 0, \quad (6.50)$$

are satisfied for all $\delta \in \mathcal{U}$, where

$$\mathcal{L}_{se}(\Omega, \Psi) \triangleq \partial \Omega + \Omega A_e + B_r - A \Omega - B \Psi, \quad (6.51)$$

$$\mathcal{L}_{re}(\Omega, \Psi) \triangleq C_r \Omega + D_{rc} \Psi - D_r, \quad (6.52)$$

and

$$\Theta_r \triangleq \Theta - X \hat{B}_r^u - M D_{cr}^u, \quad (6.53)$$

$$\Psi_r \triangleq \Psi - D D_{cr}^u, \quad (6.54)$$

In terms of

$$H \triangleq X - \hat{\Omega}^T Y^{-1} \hat{\Omega}, \quad (6.55)$$

$$F \triangleq N Y^{-1} \hat{\Omega} - \Psi E, \quad (6.56)$$

$$G \triangleq X^{-1} M, \quad (6.57)$$

$$L \triangleq K - (A \hat{\Omega} + B (D\hat{C} + \Psi E))^T, \quad (6.58)$$

$$Z = X^{-1} ((\partial X) X^{-1} \hat{\Omega}^T - L) Y^{-1}, \quad (6.59)$$

a controller that solves the problem can then be constructed with $U = -X$ and $V^T = X^{-1} H Q$ as

$$\begin{bmatrix} A_c & B_c \\ C_c & D_c \end{bmatrix} = \left[\begin{array}{c|c} (\hat{A} + \hat{B}F + G\hat{C} - \hat{B}D\hat{C} + Z\hat{\Omega} + X^{-1}\Theta E)H^{-1}X & \hat{B}D - G \\ \hline (F - D\hat{C})H^{-1}X & D \end{array} \right]. \quad (6.60)$$

Proof. The proof consists of expressing the conditions of Lemma 6.1 in terms of the design variables introduced above. The construction of the controller is based on the inversion of (6.45) as in (6.46). For further details, we refer the reader to [21]. \square

Conditions (6.49) and (6.50) read as infinitely many matrix inequalities in finite number of variables, once ρ and ϕ are chosen and the parameter dependencies of the matrix variables (affine, quadratic, general polynomial, or rational) are fixed. They can be replaced with finitely many LMIs by employing the relaxation schemes that are suitable for the considered uncertainty regions. For further information on robust optimization problems and common relaxation schemes, we refer the reader to [28] and the references therein.

6.3.4 On Avoiding Parameter Derivative Dependence in the Controller

The dependence of the controller on the derivatives of the online-measurable parameters might be undesirable due to implementation issues. If there is no $v^m = \hat{\theta}^m$ dependence in the system matrices A , B , and C , it is possible to eliminate v^m dependence in the controller. For this, we need to remove the v^m -dependent term from Z and form it as

$$Z = -X^{-1}LY^{-1}. \quad (6.61)$$

As a result of this, there will emerge in condition (6.49) a dependence on the nonlinear term $(\partial X)X^{-1}\hat{\Omega}^T$. Based on (6.50), a sufficient condition can be derived for the new version of (6.49) as

$$\begin{bmatrix} \mathcal{L}_s(Y, N) & * & * & * \\ K + 2\rho\hat{\Omega}^T - \partial\hat{\Omega}^T \mathcal{L}_d^m(X, M) + \text{He}(\Theta E) & * & * & * \\ \mathcal{L}_{se}(\Omega, \Psi_r)^T & -\Theta_r^T & -\mathcal{L}_e(S) & * \\ 0 & \partial X & 0 & 0 \end{bmatrix} \preceq -2\rho \text{blockdiag}((1 + \psi)Y, X, -S, -\psi X). \quad (6.62)$$

Clearly, a line search over $\psi \geq 0$ will be needed when using this new condition for controller synthesis. We refer the reader to [14] for further details and an alternative condition obtained with a different realization of the controller.

6.3.5 Synthesis in the Absence of Unmeasurable Parameters

When there is no unmeasurable parameter (i.e., when θ^u is void and hence $\delta = \mu$), simplified conditions can be derived for robust generalized asymptotic regulation by recalling (6.8) and setting $\Theta = 0$. Note also from (6.53) and (6.54) that we then have

$\Theta_r = \Theta = 0$ and $\Psi_r = \Psi$. By choosing $K = \partial \hat{\Omega}^T$, we can reduce condition (6.49) to (6.11) and

$$\begin{bmatrix} \mathcal{L}_s(Y, N) + 2\rho Y & * \\ \mathcal{L}_{se}(\Omega, \Psi)^T & -\mathcal{L}_e(S) - 2\rho S \end{bmatrix} \preceq 0, \forall \mu \in \mathcal{R}_m. \quad (6.63)$$

We emphasize that no conservatism is introduced by choosing Θ and K as described above. This result is summarized as follows:

Corollary 6.1. *When there are no unmeasurable parameters (i.e., θ^u is void), Problem 6.1 admits a solution if there exist maps as in (6.48) and positive scalars ρ, ϕ with which (6.11), (6.50), and (6.63) are satisfied with $\Psi_r = \Psi$. With H, F, G, L , and Z obtained as in (6.55)–(6.59) using $K = \partial \hat{\Omega}^T$, a controller that solves the problem can then be constructed as in (6.60) by setting $\Theta = 0$.*

As a further simplification, we can also set $D = 0$ in the conditions without introducing any conservatism, since any particular solution X can always be magnified together with the associated M as desired (i.e., as βX and βM with a sufficiently large positive scalar β) to render (6.50) feasible for any D . In fact, based on the idea of magnifying the particular solutions, we can also obtain an observer-based controller. Such a controller can be constructed by replacing $H^{-1}X$ and Z in (6.60) with I and 0 , respectively.

At this point, we should also mention the alternative solution derived in [17, 22] for the GAR problem (with $\Phi = I$) in the absence of unmeasurable parameters. In this alternative approach, the problem is shown to be solvable under the existence of bounded time-varying matrices Π and Γ that satisfy

$$\dot{\Pi} = A\Pi + B\Gamma - \Pi A_e - B_r \quad \text{and} \quad \limsup_{t \rightarrow \infty} \|\mathcal{L}_{re}(\Pi(t), \Gamma(t))\| \leq \kappa. \quad (6.64)$$

Interestingly, such Π and Γ are then shown to exist under similar LMI conditions (more clearly, (6.50) with third row/column blocks removed and (6.63)). On the other hand, the synthesis of the controller is more complicated since its state vector includes the matrix Π as well, which is to be obtained online from the solution of a differential equation. For a more detailed comparison, we refer the reader to [21].

Let us now restrict our attention to the case of a fixed $\delta = \mu$, i.e., the GAR problem for a known LTI system. This problem has been considered by [16], the solvability condition of which can be expressed in our setting as the existence of matrices Ω and Ψ that satisfy

$$A\Omega + B\Psi - \Omega A_e - B_r = 0, \quad (6.65)$$

$$\begin{bmatrix} \kappa\Phi & (C_r\Omega + D_{rc}\Psi - D_r)^T \\ C_r\Omega + D_{rc}\Psi - D_r & \kappa I \end{bmatrix} \succ 0. \quad (6.66)$$

The sufficiency of these conditions can easily be observed from (6.50) and (6.63), while their necessity is not easily inferrable. Intuitively, reducing the value of ρ is expected to reduce the conservatism, since this facilitates a slow decay of the tran-

sients. In the limit as $\rho \rightarrow 0$, the choices of S that ensure the feasibility of (6.63) will approach 0 since $\mathcal{L}_e(S)$ cannot be positive definite. This will also force Ω and Ψ to satisfy condition (6.65). Condition (6.66) will then follow from (6.50) with $S \rightarrow 0$.

We emphasize that the conditions of Theorem 6.1 are especially suitable when the exo-system has dependence on the unmeasurable parameters. As a matter of fact, it is quite hard (if not impossible) to find design elements that satisfy the differential equation in (6.64) or the equality constraint of (6.65), when the exo-system depends on some unmeasurable parameters. The scalar ρ plays an important role in this case and cannot be set to zero. It also facilitates the shaping of the transient behavior.

6.3.6 Shaping the Transient Behavior

It is easy to observe from (6.27) that faster convergence to steady-state behavior can be achieved by larger ρ values. However, this might come at the price of an increased initial peaking of the error, which is clearly undesirable. It is also easy to avoid this simply by keeping the maximum eigenvalue of \mathcal{X}_r small. An \mathcal{H}_2 -type problem would allow us to adjust the trade-off between fast convergence and high initial peaking of the error. Note, however, that e will not decay to zero as time goes to infinity, unless $w = 0$ or $\kappa = 0$. It is hence not possible to formulate the transient response shaping problem as the minimization of the energy of e . In an effort to formulate an \mathcal{H}_2 -type problem, one might instead think of ensuring

$$\begin{aligned} \mathcal{J}_{\text{tr}}(e(\cdot), w(\cdot), \theta(\cdot), t; \tilde{x}(0)) &\triangleq \int_0^t (\|e(\tau)\|^2 - \kappa^2 w(\tau)^T \Phi(\theta(\tau)) w(\tau)) d\tau \\ &\leq \sigma^2 \|\tilde{x}(0)\|^2, \quad \forall \tilde{x}(0) \in \mathbb{R}^{k+l}, \quad \forall t \geq 0, \quad \forall \theta(\cdot) \in \mathcal{T}. \end{aligned} \quad (6.67)$$

For small values of κ , the transient behavior of the error output can be improved by minimizing σ .

In order to derive a condition that guarantees (6.67), we first recall (6.27) which is implied by the LMI conditions in Lemma 6.1. By a simple integration, we can establish with zero initial controller states (i.e., $\xi(0) = 0$) for all $t \geq 0$ that

$$\mathcal{J}_{\text{tr}}(e(\cdot), w(\cdot), \theta(\cdot), t; \tilde{x}(0)) \leq \frac{\phi}{2\rho} \tilde{x}(0)^T (X(\theta^m(0)) - E^T S(\theta(0)) E) \tilde{x}(0) (1 - e^{-2\rho t}). \quad (6.68)$$

A condition that guarantees (6.67) is then obviously given by

$$X(\theta^m) - E^T S(\theta) E \prec \frac{2\rho}{\phi} \sigma^2 I, \quad \forall \theta \in \mathcal{R}. \quad (6.69)$$

We emphasize again that this additional condition will ensure (6.67) only when the initial controller states are set to zero.

When shaping the transient behavior, it might be convenient to restrict the interest to a particular set of initial conditions, $\tilde{x}_0^j \in \mathbb{R}^{k+l}$, collected in the matrix

$$B_i = \begin{bmatrix} B_p \\ B_c \end{bmatrix} = \begin{bmatrix} x_0^1 \cdots x_0^p \\ w_0^1 \cdots w_0^p \end{bmatrix} = [\tilde{x}_0^1 \cdots \tilde{x}_0^p]. \quad (6.70)$$

In this case, it would be reasonable to ensure a condition of the form

$$\sum_{j=1}^p \mathcal{J}_{\text{tr}} \left(e(\cdot), w(\cdot), \theta(\cdot), t; \tilde{x}_0^j \right) < \sigma^2. \quad (6.71)$$

Since the norms of the initial state vectors are now absorbed in the total cost σ^2 , it makes sense to choose \tilde{x}_0^j in such a way that their norms are close to each other. In order to guarantee (6.71), one needs to impose the trace condition

$$\text{trace} B_i^T (X(\theta^m) - E^T S(\theta) E) B_i < \frac{2\rho}{\phi} \sigma^2, \quad \forall \theta \in \mathcal{R}. \quad (6.72)$$

It might also be necessary to shape the transient behavior of the control input u , since the transient behavior of e can typically be improved at the cost of extra control effort. One might in fact consider imposing (6.67) or (6.71) for a different output z (formed, for instance, as $z = [e^T \lambda u^T]^T$ with a properly tuned $\lambda > 0$). In that case, it would be necessary to impose a generalized asymptotic regulation constraint on z , together with the transient response-shaping constraints derived above. The conditions derived based on these alternative approaches can be found in [21]. We will also comment briefly on how to use the multi-objective design problems considered in the sequel for shaping the transient behavior as well.

6.4 Robust GAR Under an \mathcal{L}_2 -Gain Constraint

6.4.1 Robust GAR Problem with an \mathcal{L}_2 -Gain Constraint

In this section, we consider a multi-objective GAR problem formulated as follows:

Problem 6.2. Given the plant in (6.1), the exo-system in (6.2) and the uncertainty regions, synthesize a controller as in (6.17) that ensures (C.1) and (C.2) as well as the following \mathcal{L}_2 -gain constraint:

(C.3) When the initial states are zero, i.e., $\tilde{x}(0) = 0$, one can find a positive scalar ε such that the closed-loop system in (6.19) satisfies for all admissible parameter trajectories that

$$\int_0^\infty \|z(t)\|^2 dt \leq (\gamma - \varepsilon)^2 \int_0^\infty \|v(t)\|^2 dt, \quad \forall v(\cdot) : \int_0^\infty \|v(t)\|^2 dt < \infty, \quad (6.73)$$

where $\gamma > 0$ represents the level of \mathcal{L}_2 -gain performance.

6.4.2 Robust GAR with \mathcal{L}_2 -Gain Performance

In an effort to derive a solution to Problem 6.2, we first recall the well-known matrix inequality condition for \mathcal{L}_2 -gain performance:

Lemma 6.2. *The closed-loop system in (6.18) satisfies (C.1) and (C.3) if there exist $\mathcal{X}_p : \mathcal{R} \rightarrow \mathbb{S}_+^{2k+l}$ and $\psi \in \mathbb{R}_+$ that satisfy*

$$\begin{bmatrix} \partial \mathcal{X}_p(\delta) + \text{He}(\mathcal{X}_p(\theta), \mathcal{A}_p(\delta)) & \mathcal{X}_p(\theta) \mathcal{B}_p(\delta) & \mathcal{C}_p(\delta)^T \\ \mathcal{B}_p(\delta)^T \mathcal{X}_p(\theta) & -\psi^{-1} \gamma I & \mathcal{D}_p(\delta)^T \\ \mathcal{C}_p(\delta) & \mathcal{D}_p(\delta) & -\psi \gamma I \end{bmatrix} \prec 0, \quad \forall \delta \in \mathcal{U}. \quad (6.74)$$

When the initial state $\varkappa(0)$ is nonzero, this condition will ensure

$$\int_0^\infty \|z(t)\|^2 dt < \gamma^2 \int_0^\infty \|v(t)\|^2 dt + \psi \gamma \varkappa(0)^T \mathcal{X}_p(\delta(0)) \varkappa(0). \quad (6.75)$$

Proof. For the sake of completeness and the clarity of some ensuing discussions, we sketch the proof that is already available in the literature. We first use the continuity of the maps and the compactness of \mathcal{U} to assert the existence of a (small) positive scalar ε such that (6.74) is still satisfied when γ is replaced with $\gamma - \varepsilon$ and \prec is changed to \preceq . After a multiplication from the left by $\varkappa_p^T = [\psi^{1/2} \varkappa^T \quad \psi^{1/2} v^T \quad \psi^{-1/2} (\gamma - \varepsilon)^{-1} z^T]$ and from the right by \varkappa_p , we conclude that

$$\frac{d}{dt} (\psi \varkappa(t)^T \mathcal{X}_p(\delta(t)) \varkappa(t)) - (\gamma - \varepsilon) \|v(t)\|^2 + (\gamma - \varepsilon)^{-1} \|z(t)\|^2 \leq 0. \quad (6.76)$$

Multiplying both sides by $\gamma - \varepsilon > 0$ and integrating from $t = 0$ to $t = \tau$, we obtain

$$\begin{aligned} \int_0^\tau \|z(t)\|^2 dt &\leq (\gamma - \varepsilon)^2 \int_0^\tau \|v(t)\|^2 dt \\ &+ \psi (\gamma - \varepsilon) (\varkappa(0)^T \mathcal{X}_p(\delta(0)) \varkappa(0) - \varkappa(\tau)^T \mathcal{X}_p(\delta(\tau)) \varkappa(\tau)). \end{aligned} \quad (6.77)$$

Since the negative definiteness of the (1, 1) block in (6.74) ensures internal stability, we have $\lim_{\tau \rightarrow \infty} \varkappa(\tau) = 0$ for any finite energy $v(\cdot)$. We then easily infer (6.73) and (6.75) for the cases of zero and nonzero initial state vector $\varkappa(0)$, respectively. \square

As is also the case for various other multi-objective synthesis problems, the challenge in solving Problem 6.2 is to choose the design ingredients in such a way that the resulting controller ensures the conditions of Lemma 6.1 as well as those of Lemma 6.2. Since it is not easy (if not impossible) to obtain the same controller by using different design elements, we think of constructing \mathcal{X}_p by using the design elements introduced in the partitions of \mathcal{X} and \mathcal{X}^{-1} in Subsect. 6.3.3. The next challenge then becomes the determination of a suitable \mathcal{D}_p in such a way that

a congruence transformation applied to (6.74) with $\text{blockdiag}(\mathcal{Y}_p, I, I)$ renders the condition affine in all of the design ingredients.

Let us now describe the choices with which we are able to provide solutions to the multi-objective synthesis problems considered in this chapter. Since the exo-system is excluded from the closed-loop dynamics in (6.19), we consider removing the corresponding parts from \mathcal{X} and choosing \mathcal{X}_p as

$$\mathcal{X}_p = \begin{bmatrix} I_{(k+l) \times k}^T P I_{(k+l) \times k} & I_{(k+l) \times k}^T U \\ U^T I_{(k+l) \times k} & U^T (P - Q^{-1})^{-1} U \end{bmatrix}, \quad (6.78)$$

where $I_{(k+l) \times k} \triangleq [I_{k \times k} \ 0_{k \times l}]^T$. Note that the presence of ψ in (6.74) eliminates the need for the introduction of a scalar in the choice of \mathcal{X}_p for purposes of reduction of conservatism. In fact, we have two scalars (ϕ and ψ) to search over for reducing the potential conservatism originating from parameter dependence and multi-objective design constraints. We will be commenting further on their roles in the sequel. Once the choice of \mathcal{X}_p is fixed in this fashion, the challenge is reduced to the determination of \mathcal{Y}_p . Note that it is not possible to derive the appropriate choice in a similar fashion from \mathcal{Y} . In fact, the suitable choice turns out to be

$$\mathcal{Y}_p^T = \begin{bmatrix} Y & \hat{\Omega} V \\ \hat{\Omega}^T & -E^T W E V \end{bmatrix}. \quad (6.79)$$

This is a legitimate choice since its inverse exists and is given explicitly by

$$\mathcal{Y}_p^{-T} = \begin{bmatrix} 0 & I_{(k+l) \times k}^T \\ V^{-1} I_{(k+l) \times k} & U^T (P - Q^{-1})^{-1} \end{bmatrix}. \quad (6.80)$$

With the choices we have just described, one is able to obtain the following solution to Problem 6.2:

Theorem 6.2. *There is a controller of the form in (6.60) that solves Problem 6.2 if there exist $\rho, \phi, \psi \in \mathbb{R}_+$ and maps as in (6.48) with which (6.49), (6.50) and*

$$\begin{bmatrix} \mathcal{L}_s(Y, N) & * & * & * \\ K - \partial \hat{\Omega}^T & \mathcal{L}_d^m(X, M) + \text{He}(\Theta E) & * & * \\ (B_p + B D D_{cp})^T & (X \tilde{B}_p + M D_{cp})^T & -\psi^{-1} \gamma I & * \\ C_p Y + D_{pc} N & C_p \hat{\Omega} + D_{pc} (D \hat{C} + \Psi E) & D_p + D_{pc} D D_{cp} - \psi \gamma I & \end{bmatrix} \prec 0, \quad (6.81)$$

are satisfied for all $\delta \in \mathcal{U}$.

Proof. To establish the proof, we only need to show that (6.74) is expressed equivalently as in (6.81) after a congruence transformation with $\text{blockdiag}(\mathcal{Y}_p, I, I)$.

For this purpose, we have to express the terms in the transformed matrix inequality in terms of the design elements introduced in Subject. 6.3.3. To this end, we first compute

$$\mathcal{Y}_p^T \mathcal{X}_p = \begin{bmatrix} I & 0 \\ PI_{(k+l) \times k} & U \end{bmatrix}, \quad \mathcal{Y}_p^T \mathcal{X}_p \mathcal{Y}_p = \begin{bmatrix} Y & \hat{\Omega} \\ \hat{\Omega}^T & X \end{bmatrix}. \quad (6.82)$$

Using these, the transformed differential term is obtained as

$$\begin{aligned} \mathcal{Y}_p^T (\partial \mathcal{X}_p) \mathcal{Y}_p &= \underbrace{\begin{bmatrix} \partial Y & \partial \hat{\Omega} \\ \partial \hat{\Omega}^T & \partial X \end{bmatrix}}_{\partial(\mathcal{Y}_p^T \mathcal{X}_p \mathcal{Y}_p)} - \text{He} \underbrace{\begin{bmatrix} I & 0 \\ PI_{(k+l) \times l} & U \end{bmatrix}}_{\mathcal{Y}_p^T \mathcal{X}_p} \underbrace{\begin{bmatrix} \partial Y & \partial \hat{\Omega} \\ \partial(V^T \hat{\Omega}^T) & -\partial(V^T E^T W E) \end{bmatrix}}_{\partial \mathcal{Y}_p} \\ &= \begin{bmatrix} -\partial Y & * \\ -\partial \hat{\Omega}^T + ((\partial X)Q + (\partial U)V^T) \hat{\Omega}^T & \partial X - \text{He}(((\partial X)Q + (\partial U)V^T) E^T W E) \end{bmatrix}. \end{aligned} \quad (6.83)$$

In order to facilitate the final computations, we first express some transformed controller parameters introduced in (6.45) more explicitly as

$$M = X \hat{B} D + U B_c, \quad (6.84)$$

$$N = C_c V^T \hat{\Omega}^T + D C Y, \quad (6.85)$$

$$\Psi = -(C_c V^T E^T W + D(D_{cr}^m - C \Omega)), \quad (6.86)$$

where $D \triangleq D_c$. To simplify the later expressions with the differential terms, we next introduce

$$\begin{aligned} L_d &\triangleq L - ((\partial X)Q + (\partial U)V^T) \hat{\Omega}^T \\ &= X \hat{A} Q \hat{\Omega}^T + X \hat{B} N + U (A_c V^T \hat{\Omega}^T + B_c C Y), \end{aligned} \quad (6.87)$$

$$\begin{aligned} \Theta_d &\triangleq \Theta + ((\partial X)Q + (\partial U)V^T) E^T W \\ &= X \hat{A} Q E^T W + X \hat{B} \Psi - U (A_c V^T E^T W + B_c (D_{cr}^m - C \Omega)). \end{aligned} \quad (6.88)$$

We can now use the expressions provided so far together with the realization of the closed-loop dynamics as in (6.19) to derive

$$\mathcal{Y}_p^T \mathcal{X}_p \mathcal{A}_p \mathcal{Y}_p = \begin{bmatrix} AY + BN & A \hat{\Omega} + B(D_c \hat{C} + \Psi E) \\ L_d & X \hat{A} + M \hat{C} + \Theta_d E \end{bmatrix}, \quad (6.89)$$

$$\mathcal{B}_p^T \mathcal{X}_p \mathcal{Y}_p = [(B_p + B D D_{cp})^T (X \hat{B}_p + M D_{cp})^T], \quad (6.90)$$

$$\mathcal{C}_p \mathcal{Y}_p = [C_p Y + D_{pc} N \quad C_p \hat{\Omega} + D_{pc} (D \hat{C} + \Psi E)]. \quad (6.91)$$

By combining these expressions and performing some final cancelations, one arrives at the matrix inequality in (6.81). We also note that $\mathcal{Y}_p^T \mathcal{X}_p \mathcal{Y}_p \succ 0$ is not added as an extra condition since it is already implied by (6.50). \square

6.4.3 GAR with \mathcal{H}_∞ Performance for LTI Systems

The LTI version of the multi-objective synthesis problem that we have formulated in Subject. 6.4.1 was considered in [16]. In this section, we obtain the solvability conditions of [16] by specializing Theorem 6.2 to the case $\rho = 0$. Recall that, in this case S has to be set to zero, which forces Ω and Ψ to be chosen in a way to satisfy (6.65) and Θ to be set to zero. It then becomes unnecessary to impose (6.49) since it is already implied by (6.81). By applying the Schur complement and noting that ϕ can be chosen arbitrarily large, we can express (6.50) equivalently as (6.66) and

$$\begin{bmatrix} Y & \hat{\Omega} \\ \hat{\Omega}^T & X \end{bmatrix} \succ 0. \quad (6.92)$$

The solvability of the GAR problem with \mathcal{H}_∞ performance is hence guaranteed under (6.65), (6.66), (6.81) with $\Theta = 0$ and (6.92). We can also set $\psi = 1$ without introducing any conservatism.

Since the transformed controller matrices appear in a single LMI in the solution we have just derived, they can be eliminated by a routine application of the projection theorem [6]. In this fashion, we arrive at the following conditions derived in [16]:

Theorem 6.3. *Problem 6.2 admits a solution in the LTI case if and only if there exist $Y \in \mathbb{S}_+^k$, $X \in \mathbb{S}_+^{k+l}$, $\Omega \in \mathbb{R}^{k \times l}$, and $\Psi \in \mathbb{R}^{n \times l}$ that satisfy (6.65), (6.66), (6.92), and*

$$\begin{bmatrix} \mathcal{N}_s & 0 \\ 0 & I \end{bmatrix}^T \begin{bmatrix} AY + YA^T & * & * \\ C_p Y & -\gamma I & * \\ B_p^T & D_p^T & -\gamma I \end{bmatrix} \begin{bmatrix} \mathcal{N}_s & 0 \\ 0 & I \end{bmatrix} \prec 0, \quad (6.93)$$

$$\begin{bmatrix} \mathcal{N}_d & 0 \\ 0 & I \end{bmatrix}^T \begin{bmatrix} X\tilde{A} + \tilde{A}^T X & * & * \\ X\tilde{B}_p & -\gamma I & * \\ C_p \hat{\Omega} + D_{pc} \Psi E & D_p & -\gamma I \end{bmatrix} \begin{bmatrix} \mathcal{N}_d & 0 \\ 0 & I \end{bmatrix} \prec 0, \quad (6.94)$$

where \mathcal{N}_s and \mathcal{N}_d represent any bases for the null spaces of $[B^T \ D_{pc}^T]$ and $[\tilde{C} \ D_{cp}]$, respectively.

With the design variables that satisfy the conditions expressed in Theorem 6.3, one can construct \mathcal{X}_p as in (6.78) (with preferred U and V) and then solve (6.74) for the controller realization matrices (A_c, B_c, C_c, D_c) . Alternatively, one can develop

a procedure for a more explicit construction of the controller realization matrices along similar lines to [5]. It is also possible to use (6.81) with $\Theta = 0$ (instead of (6.93), (6.94)) and then synthesize the controller as in (6.60).

6.4.4 Shaping the Transient Behavior with an \mathcal{L}_2 -Gain Constraint

It is possible to shape the transient behavior in the generalized asymptotic regulation problem partially by the help of the \mathcal{L}_2 -gain constraint. To this end, one needs to set $D_p = 0$, $D_{cp} = 0$ and choose the columns of B_p as the initial plant state vectors of interest (i.e., $x(0)$) or simply as the identity matrix. The resulting controller should be used with zero initial states. When v is a vector signal whose j th element is an impulse at $t = 0$ while the other entries are all zero, the closed loop in (6.19) will generate the same $z(t)$ as the system in (6.18) with $w(0) = 0$ and $x(0) = B_p^j$, i.e., the j th column of B_p . This means that the energy of z can be viewed as an indicator of the quality of the transient behavior resulting from the initial plant states of interest. One hence needs to impose the \mathcal{L}_2 -gain constraint with a sufficiently small γ to (partially) improve the transient behavior. Note, however, that this should be done without leading to an explosion in the second term in the right-hand side of (6.75). In order to avoid such an explosion, one might bound the trace of $\tilde{B}_p^T X \tilde{B}_p = \tilde{B}_p^T P \tilde{B}_p$ from above by a desirably small scalar. Note that the constraint in (6.72) also serves the same purpose. Typically, one needs to run several optimizations to decide on the suitable values of the bounds in the constraints discussed above.

6.5 Robust GAR Under an \mathcal{H}_2 -Type Constraint

6.5.1 Robust GAR Problem with an \mathcal{H}_2 -Type Constraint

In this section, we consider a multi-objective GAR problem formulated as follows:

Problem 6.3. Given the plant in (6.1), the exo-system in (6.2) and the uncertainty regions, synthesize a controller as in (6.17) that ensures (C.1) and (C.2) as well as the following \mathcal{H}_2 -type constraint:

(C.4) When the initial states are zero, i.e., $\tilde{z}(0) = 0$, the closed-loop system of (6.19) satisfies for all admissible parameter trajectories that

$$\sum_{j=1}^p \int_0^{\infty} \|z^j(\tau)\|^2 d\tau < \gamma^2, \quad (6.95)$$

where $\gamma > 0$ indicates the performance level and z^j represents the performance output obtained in response to

$$v^j(t) \triangleq [0 \cdots 0 \delta_D(t) 0 \cdots 0]^T, \quad (6.96)$$

with the Dirac's delta function $\delta_D(\cdot)$ being located in the j th position.

6.5.2 Robust GAR with \mathcal{H}_2 Performance

We adapt the LMI conditions for \mathcal{H}_2 performance (in the sense explained above) to our case as follows:

Lemma 6.3. *The closed-loop system in (6.18) satisfies (C.1) and (C.4) with $\gamma = \sum_{j=1}^p \sigma_j$, if $\mathcal{D}_p = 0$ and there exist $\mathcal{X}_p : \mathcal{R} \rightarrow \mathbb{S}_+^{2k+l}$ and $\psi \in \mathbb{R}_+$ that satisfy*

$$\begin{bmatrix} \partial \mathcal{X}_p(\delta) + \text{He}(\mathcal{X}_p(\theta) \mathcal{A}_p(\delta)) & \mathcal{C}_p(\delta)^T \\ \mathcal{C}_p(\delta) & -\psi \gamma I \end{bmatrix} \prec 0, \quad \forall \delta \in \mathcal{U}, \quad (6.97)$$

$$\begin{bmatrix} \mathcal{X}_p(\theta) & \mathcal{X}_p(\theta) \mathcal{B}_p^j(\delta) \\ \mathcal{B}_p^j(\delta)^T \mathcal{X}_p(\theta) & \psi^{-1} \sigma_j I \end{bmatrix} \succ 0, \quad \forall \delta \in \mathcal{U}; \quad j = 1, \dots, p, \quad (6.98)$$

where \mathcal{B}_p^j represents the j th column of \mathcal{B}_p .

Proof. We first briefly note that the internal stability, i.e., (C.1), is ensured by the negative definiteness of the (1,1) block in the left-hand side of (6.97). When $x(0) = 0$, $v = v^j$ and $\mathcal{D}_p = 0$, the dynamics of the closed-loop system in (6.19) can equivalently be expressed as

$$\begin{aligned} \dot{x}^j &= \mathcal{A}_p(\mu) x^j, \\ x^j(0) &= \mathcal{B}_p^j(\delta(0)), \\ z^j &= \mathcal{C}_p(\mu) x^j, \end{aligned} \quad (6.99)$$

where x^j and z^j represent the state and the output vectors obtained in response to $v = v^j$. Through multiplication from the left by $(x_p^j)^T \triangleq [\psi^{1/2} (x^j)^T \quad \psi^{-1/2} \gamma^{-1} (z^j)^T]$ and from the right by x_p^j , we then infer from condition (6.97) that

$$\frac{d}{dt} (\psi x^j(t)^T \mathcal{X}_p(\theta(t)) x^j(t)) + \gamma^{-1} \|z^j(t)\|^2 \leq 0. \quad (6.100)$$

After multiplying both sides with γ , we integrate over time and sum over j to obtain

$$\begin{aligned} \sum_{j=1}^p \int_0^\infty \|z^j(t)\|^2 dt &\leq \gamma \sum_{j=1}^p \lim_{\tau \rightarrow \infty} \int_\tau^0 \frac{d}{dt} (\psi \varkappa^j(t)^T \mathcal{X}_p(\theta(t)) \varkappa^j(t)) dt \\ &= \psi \gamma \sum_{j=1}^p \mathcal{B}_p^j(\delta(0))^T \mathcal{X}_p(\theta(0)) \mathcal{B}_p^j(\delta(0))^T, \end{aligned} \quad (6.101)$$

where we used $\varkappa^j(0) = \mathcal{B}_p^j(\delta(0))$ and the fact that $\lim_{\tau \rightarrow \infty} \varkappa^j(\tau) = 0$, which follows from internal stability. By an application of the Schur-complement lemma, we next infer from (6.98) that

$$\psi \mathcal{B}_p^j(\delta)^T \mathcal{X}_p(\theta) \mathcal{B}_p^j(\delta)^T < \sigma_j, \quad \forall \delta \in \mathcal{U}. \quad (6.102)$$

Using this result in (6.101) and recalling $\gamma = \sum_{j=1}^p \sigma_j$, we conclude that (C.6.3) is satisfied. \square

A solution can be obtained for Problem 6.3 by applying congruence transformations to (6.97) and (6.98) via $\text{blockdiag}(\mathcal{A}_p, I)$. Since the suitable choice for \mathcal{A}_p and the resulting expressions in the transformed conditions are already explained in Subsect. 6.4.1, we directly provide the resulting solution as follows:

Theorem 6.4. *There is a controller of the form in (6.60) that solves Problem 6.3, if there exist $\rho, \phi, \psi \in \mathbb{R}_+$ and maps as in (6.48) with which (6.49), (6.50) and*

$$\sum_{j=1}^p \sigma_j - \gamma = 0, \quad (6.103)$$

$$D_p + D_{pc} D D_{cp} = 0, \quad (6.104)$$

$$\begin{bmatrix} \mathcal{L}_s(Y, N) & * & * \\ K - \partial \hat{\Omega}^T & \mathcal{L}_d^m(X, M) + \text{He}(\Theta E) & * \\ C_p Y + D_{pc} N & C_p \hat{\Omega} + D_{pc}(D \hat{C} + \Psi E) - \psi \gamma I \end{bmatrix} < 0, \quad (6.105)$$

$$\begin{bmatrix} Y & * & * \\ \hat{\Omega}^T & X & * \\ (B_p^j + B D D_{cp}^j)^T & (X \bar{B}_p^j + M D_{cp}^j)^T & \psi^{-1} \sigma_j \end{bmatrix} \succ 0, \quad j = 1, \dots, p, \quad (6.106)$$

are satisfied for all $\delta \in \mathcal{U}$, where the superscript j is used to represent the j th column of the relevant matrix.

Proof. The proof consists of expressing the conditions of Lemma 6.3 in terms of the design variables. This is done simply by using (6.89)–(6.91). \square

6.5.3 GAR with \mathcal{H}_2 Performance for LTI Systems

A solution was derived by [20] for the solution of the GAR problem with \mathcal{H}_2 performance in the case of LTI systems (with no uncertainty). In fact, the \mathcal{H}_2 performance objective was formulated in [20] based on a stochastic interpretation, which turns out to be somewhat inconvenient to use for LPV systems. The result of Theorem 6.4 can be specialized to LTI systems as well. For this purpose, we only need to adapt the lines of reasoning in Subsect. 6.4.3. In this fashion, we obtain the following LMI conditions that are dual to those derived in [20]:

Theorem 6.5. *Problem 6.3 admits a solution in the LTI case with no uncertainty if and only if there exist $Y \in \mathbb{S}_+^k$, $X \in \mathbb{S}_+^{k+l}$, $\Omega \in \mathbb{R}^{k \times l}$, and $\Psi \in \mathbb{R}^{n \times l}$ that satisfy (6.65), (6.66), (6.103), (6.104), (6.105), and (6.106) with $\Theta = 0$ and $\psi = 1$.*

A controller that solves the GAR problem with \mathcal{H}_2 performance can then be constructed again as in (6.60). It is also possible to derive conditions in which part of the transformed controller parameters are eliminated. For instance, K and N can be eliminated from (6.105). This might be useful especially for performance analysis, since it will basically complicate the construction of the controller. The dual LMI conditions (6.5) were also discussed in [20], especially in the context of GAR problem with suboptimal transient response. We establish further links to [20] in the following discussion on how to shape the transient response by an \mathcal{H}_2 -type constraint.

6.5.4 Shaping the Transient Behavior with an \mathcal{H}_2 -Type Constraint

We have already discussed in Subsect. 6.4.4 how the performance channel matrices can be chosen to (partially) shape the transient behavior. In fact, an \mathcal{H}_2 -type performance is more suitable for shaping the transient response. This is due to the fact that the effect of nonzero initial conditions can be expressed equivalently with impulsive disturbance inputs. In this context, we recall from Subsect. 6.4.4 that when the performance channel matrices are chosen as

$$D_p = 0, D_{cp} = 0, B_p = [x_0^1 \cdots x_0^p], \quad (6.107)$$

the closed loop in (6.19) with $v = v^j$ (see (6.96)) will generate the same $z(t)$ as the system in (6.18) with $w(0) = 0$ and $x(0) = x_0^j$. Hence, by imposing (C.4), we can ensure that the total energy of the performance output z resulting from the different initial conditions of interest is desirably small.

The particular choices of the performance channel matrices in (6.107) facilitate some simplification in the conditions of (6.106). In order to derive a new condition in the same vein as [20], we first take the Schur complement with respect to the (2, 2)

block and thus rewrite (6.106) with the performance channel matrices of (6.107) equivalently as

$$\begin{bmatrix} Y - \hat{\Omega}X^{-1}\hat{\Omega}^T & B_p^j - \hat{\Omega}\tilde{B}_p^j \\ (B_p^j - \hat{\Omega}\tilde{B}_p^j)^T & \psi^{-1}\sigma_j - (\tilde{B}_p^j)^T X \tilde{B}_p^j \end{bmatrix} \succ 0. \quad (6.108)$$

Recalling the expressions of \tilde{B}_p and $\hat{\Omega}$, respectively, from (6.5) and (6.43), we observe that $\hat{\Omega}\tilde{B}_p^j = B_p^j$. Since the cross-diagonal terms are zero, this condition reduces to the positive definiteness of the diagonal blocks. The positive definiteness of the (1, 1) block in (6.108) can be expressed equivalently as in (6.92) since $X \succ 0$. We next combine the positive definiteness of the (2, 2) block for $j = 1, \dots, p$ together with (6.103) to obtain an equivalent trace condition as

$$\text{trace} \tilde{B}_p^T X \tilde{B}_p < \psi^{-1} \gamma. \quad (6.109)$$

Since the equality constraint in (6.104) is automatically satisfied with the performance channel matrices in (6.107), we obtain the conditions to impose for shaping the transient behavior as (6.92), (6.105), and (6.109).

When we specialize the above derivation to the case of LTI systems with no uncertainty, we basically obtain the LMI conditions derived in [20] for the GAR problem with suboptimal transient response. Nevertheless, the particular line of derivation employed in [20] facilitates a problem formulation in which $w(0)$ need not be zero. As a result of this, the trace condition in (6.109) is expressed with $\tilde{B}_p \rightarrow \tilde{B}_i$, where B_i is an initial condition matrix of the form (6.70).

It is also interesting to note the resemblance of the trace condition in (6.109) to the one in (6.72), which was introduced for shaping the transient behavior as well. There are, however, several differences between the two conditions, which are essentially the results of different problem formulations. We emphasize that, in both cases, the resulting LMI conditions facilitate a partial shaping of the transient behavior.

6.6 Illustrative Example

In this section, we consider a plant with a state-space description as

$$\begin{bmatrix} \dot{x}_1 \\ \dot{x}_2 \\ \dot{x}_3 \end{bmatrix} = \begin{bmatrix} -\omega_2 & 0 & 0 \\ -\omega_1 k_{vr} & -\omega_1 & 0 \\ 0 & 1 & 0 \end{bmatrix} \begin{bmatrix} x_1 \\ x_2 \\ x_3 \end{bmatrix} + \begin{bmatrix} 0 \\ \omega_1 \\ 0 \end{bmatrix} d + \begin{bmatrix} 0 \\ \omega_1^0 \\ 0 \end{bmatrix} v + \begin{bmatrix} \omega_2 k_{dv} \\ \omega_1 k_{dr} \\ 0 \end{bmatrix} u. \quad (6.110)$$

This is a slightly modified expression of the course dynamics adapted from [25] and considered before by [21, 22]. The states are identified as follows: x_1 is the sway

velocity (in m/s), x_3 is the yaw angle (in degrees) and x_2 is its rate. The control problem is to adjust the rudder deflection u (in degrees), so that the yaw angle $y = e = x_3$ follows zero reference as good as possible in the face of a sinusoidal wave disturbance d and a finite-energy disturbance v . The dynamics depend on the velocity of the ship

$$V_s(t) = V_0(1 + \theta^m(t)); \quad \theta^m(t) \in [-\theta_{\max}^m, \theta_{\max}^m], \quad (6.111)$$

through the velocity-dependent system parameters

$$k_{vr} = -0.46, \quad k_{dr} = 0.0027V_s, \quad k_{dv} = 0.01V_s, \quad \omega_1 = 0.0769V_s, \quad \omega_2 = 0.0128V_s. \quad (6.112)$$

For the sake of simplicity in the design phase, we used a constant term $\omega_1^0 = 0.0769V_0$ in the input matrix associated with the disturbance v . The sinusoidal wave disturbance has an uncertain frequency expressed as

$$\omega_w = \omega_w^0(1 + \theta^u(t)); \quad \theta^u(t) \in [-\theta_{\max}^u, \theta_{\max}^u]. \quad (6.113)$$

Due to the velocity of the ship, such a disturbance effects the ship with a frequency shifted as

$$\bar{\omega} = \omega_w - g^{-1}\omega_w^2 \cos \chi_s V_s, \quad (6.114)$$

where g is the gravitational constant and χ_s is the angle between the heading and the direction of the wave. The sinusoidal wave disturbance $d = w_2$ is hence generated by (6.15) with $\bar{\omega}$ given as in (6.114). The acceleration of the ship is assumed to be bounded according to $\dot{\theta}^m(t) \in [-v_{\max}^m, v_{\max}^m]$, while no bound is assumed for $\dot{\theta}^u(t)$.

We performed three different designs in MATLAB[®] for a system with

$$\omega_w = 1 \text{ rad/s}, \quad \chi_s = 45^\circ, \quad V_0 = 10 \text{ m/s}, \quad \theta_{\max}^m = 0.2, \quad v_{\max}^m = 0.01\pi\theta_{\max}^m, \quad \theta_{\max}^u = 0.2.$$

The performance output is formed as $z = [x_3 \ \lambda u]^T$ with $\lambda = 10^{-5}$. The feed-through terms of the controllers are all set to zero. The design variables are chosen to have affine dependence on θ^m , except for K and Θ , which are chosen to depend on $(\theta^m)^2$ and $(\theta^m)^3$ as well. We briefly note that the parameter-dependent LMIs are relaxed based on the partial convexity approach [7] and refer the reader to [21] for the relevant details. The LMI problems are coded by using the Yalmip [24] interface and the optimizations are performed with the SDP solver SeDuMi [31]. All of the three controllers are designed with $\Phi = I$ and $\kappa = 0.003$. This value of κ is observed to be feasible (with $\phi = \kappa$) for $\rho = 0.125$, which is also kept the same in all the designs. The first controller is designed to shape the transient behavior of z , in the way described in [21]. On the other hand, the second and third controllers are designed to achieve, respectively, the \mathcal{L}_2 -gain and \mathcal{H}_2 -type performance objectives described in Sects. 6.4 and 6.5. The minimum γ levels are found in these designs by a search over $\psi \in [0.01, 100]$ as $\gamma = 0.0015$ for Σ_c^2 (with $\psi = 2.9151$) and $\gamma = 0.0073$ for Σ_c^3 (with

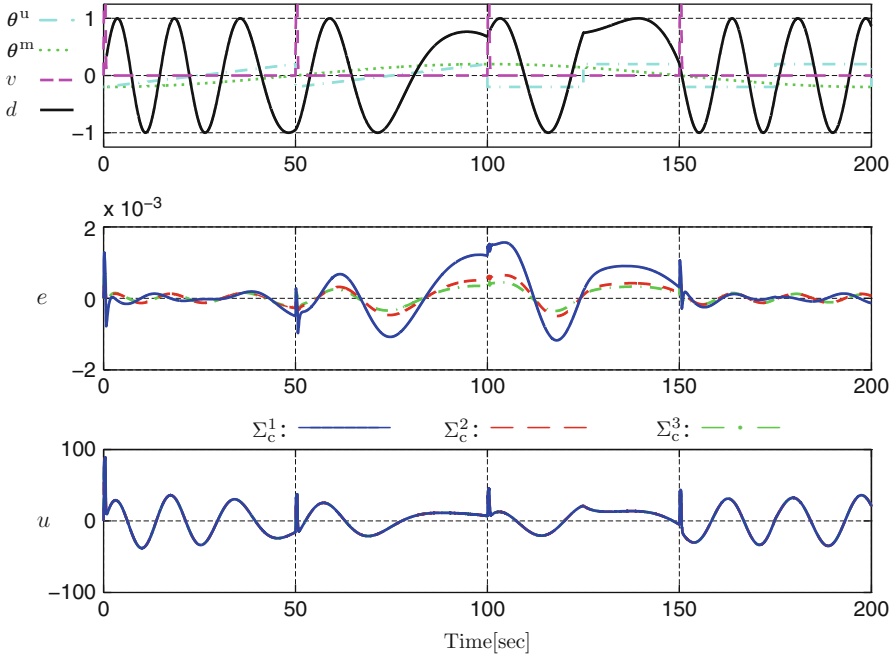


Fig. 6.1 Illustrative designs for course control

$\psi = 0.0443$). After this step, the controllers are designed by setting γ to 1.1 times its optimum value (for a fixed ψ) and by then minimizing the maximum eigenvalue of X (as motivated for the shaping of the transient response). In all the designs, some frozen-parameter pole-placement constraints are also imposed to avoid large simulation times. We should note that this typically leads to some increase in the minimum performance levels.

The simulation results obtained for the initial state vector $\tilde{x}(0) = [0 \ 0 \ 0 \ 1 \ 0]^T$ and a sinusoidal θ^m trajectory $\theta^m(t) = -\theta_{\max}^m \cos(v_{\max}^m t / \theta_{\max}^m)$ are presented in Fig. 6.1. Note from the top plot that the unmeasurable parameter increases linearly with time from -0.2 to 0.2 during $[0, 50]$ and $[50, 100]$, with a jump from maximum to minimum value at $t = 50$. In the remaining time interval, it exhibits switches between -0.2 and 0.2 once in every 50 s. The shape of the sinusoidal signal is deformed especially due to the jumps of the unmeasurable parameter. The finite energy disturbance is formed by short pulses of duration 1–2 s that occur once in 50 s as well. The timing of the pulses are chosen to coincide with the switches in θ^u . This is done to observe the response of the system to the combined challenges of the unmeasurable parameter and the finite-energy disturbance. As can be observed from the middle plot, the multi-objective designs Σ_c^2 and Σ_c^3 lead to better disturbance attenuation than Σ_c^1 , especially within the time range $[50, 150]$. We could verify this better by zooming in the plot around the instants of impulsive disturbances. In

fact, the performance of Σ_c^3 is also quite acceptable. This is not too surprising since it is designed to shape the transient behavior in a desirable way. The disturbance attenuation performances of Σ_c^2 and Σ_c^3 are very similar to each other. The control inputs generated by the three different controllers are not distinguishable within the scale of the bottom plot in the figure. Looking closely, we noticed slight differences around the instants at which the impulsive disturbances occur. This shows that the disturbance attenuation performance can be improved by slightly different control inputs. We should also note from the bottom plot that the rudder deflection reaches its natural limit during the start-up period. In fact, practical saturation limits are much smaller and pose a serious challenge for all of the designs, as we encountered in our simulation exercises.

6.7 Concluding Remarks

The generalized asymptotic regulation problem is a particular version of the peak-to-peak gain minimization, since the disturbances are restricted to be generated by known exo-systems. We have provided LMI solutions to the basic as well as multi-objective versions of this problem in a parameter-dependent setting. A key feature of the solutions is that they are applicable when the exo-system depends on unmeasurable parameters as well. For potential reduction of conservatism, one needs to perform searches over various scalars. It would be quite convenient to eliminate—at least—the search over the decay rate ρ in the LMIs for GAR. The problem becomes quite challenging when there are saturation constraints on the control inputs. Integration of LPV designs with a parameter estimation scheme is another interesting research direction in robust and adaptive control. This seems to be challenging for general LPV synthesis problems, but might be promising for the GAR problem with an LTI plant and an LPV exo-system.

Acknowledgments The author acknowledges the support of King Fahd University of Petroleum and Minerals. He would also like to thank Prof. Carsten W. Scherer for many fruitful discussions.

References

1. Dettori M (2001) LMI techniques for control with application to a compact disc player mechanism. PhD thesis, Delft University of Technology, The Netherlands
2. Dietz SG, Scherer CW, Koroğlu H (2007) Robust control against disturbance model uncertainty: a convex solution. In: Proceedings of 46th IEEE Conference on Decision and Control, New Orleans, LA, pp 842–847
3. Du H, Zhang L, Shi X (2003) LPV technique for the rejection of sinusoidal disturbance with time-varying frequency. IEE Proc D Contr Theory Applicat 150(2):132–138
4. Francis B, Sebakhy OA, Wonham WM (1974) Synthesis of multivariable regulators: the internal model principle. Appl Math Optim 1(1):64–86

5. Gahinet P (1996) Explicit controller formulas for LMI-based \mathcal{H}_∞ synthesis. *Automatica* 32(7):1007–1014
6. Gahinet P, Apkarian P (1994) A linear matrix inequality approach to \mathcal{H}_∞ control. *Int J Robust Nonlin Contr* 4(4):421–448
7. Gahinet P, Apkarian P, Chilali M (1996) Affine parameter-dependent Lyapunov functions and real parametric uncertainty. *IEEE Trans Automat Contr* 41(3):436–442
8. Gan WC, Qiu L, Wang J (2008) An adaptive sinusoidal disturbance rejection controller for single-input-single-output systems. In: *Proceedings 17th IFAC Triennial World Congress, Seoul, Korea*, pp 15684–15689
9. Gruenbacher E, Furtmueller C, del Re L (2007) Suppression of frequency varying periodic disturbances in continuous casting using an internal model predictor. In: *Proceedings of American Control Conference, New York*, pp 4142–4147
10. Hu T, Teel AR, Lin Z (2005) Lyapunov characterization of forced oscillations. *Automatica* 41(10):1723–1735
11. Hüttner C, Rieber JM, Allgöwer F, Hugel J (2005) Compensation of time-varying harmonic disturbances on nonlinear bearingless slice motors. In: *Proceedings of 16th IFAC Triennial World Congress, Prague, Czech Republic*
12. Ichikawa A, Katayama H (2006) Output regulation of time-varying systems. *Syst Contr Lett* 55(12):999–1005
13. Narikiyo T, Fuwa K, Kandoh H (2008) A construction of disturbance observer to cope with frequency variation and its application to vibration suppression control system. In: *Proceedings of 17th IFAC Triennial World Congress, Seoul, Korea*, pp 2697–2701
14. Köroğlu H (2010) Robust generalized asymptotic regulation via an LPV controller without parameter derivative dependence. In: *Proceedings of 49th IEEE Conference on Decision and Control, Georgia, Atlanta*, pp 4965–4971
15. Köroğlu H, Scherer CW (2007) An LPV control approach to asymptotic rejection of non-stationary disturbances with guaranteed worst-case performance. In: *Proceedings of American Control Conference, New York*, pp 6085–6090
16. Köroğlu H, Scherer CW (2008) An LMI approach to \mathcal{H}_∞ synthesis subject to almost asymptotic regulation constraints. *Syst Contr Lett* 57(4):300–308
17. Köroğlu H, Scherer CW (2008) LPV control for robust attenuation of non-stationary sinusoidal disturbances with measurable frequencies. In: *Proceedings of 17th IFAC Triennial World Congress*, pp 4928–4933
18. Köroğlu H, Scherer CW (2008) Robust attenuation of non-stationary sinusoidal disturbances with uncertain frequencies. In: *Proceedings of 17th IFAC Triennial World Congress*, pp 14115–14120
19. Köroğlu H, Scherer CW (2008) Robust generalized asymptotic regulation against non-stationary sinusoidal disturbances. In: *Proceedings 47th IEEE Conference on Decision and Control, Cancun, Mexico*, pp 5426–5431
20. Köroğlu H, Scherer CW (2009) Generalized asymptotic regulation with guaranteed \mathcal{H}_2 performance: An LMI solution. *Automatica* 45(3):823–829
21. Köroğlu H, Scherer CW (2011) Robust generalized asymptotic regulation against non-stationary sinusoidal disturbances with uncertain frequencies. *Int J Robust Nonlin Contr* 21(8):883–903
22. Köroğlu H, Scherer CW (2011) Scheduled control for robust attenuation of non-stationary sinusoidal disturbances with measurable frequencies. *Automatica* 47(3):504–514
23. Kulkarni VV, Pao LY, Zhong H (2005) Robust rejection of periodic and almost periodic disturbances. In: *Proceedings of 16th IFAC Triennial World Congress, Prague, Czech Republic*
24. Löfberg J (2004) YALMIP: A toolbox for modeling and optimization in MATLAB. In: *Proceedings of CACSD Conference*. <http://control.ee.ethz.ch/~joleof/yalmip.php>
25. Mackenroth U (2004) *Robust control systems: Theory and case studies*. Springer, Berlin
26. Saberi A, Stoorvogel AA, Sannuti P (2000) *Control of linear systems with regulation and input constraints*. Springer, London

27. Scherer CW (2000) An efficient solution to multi-objective control with LMI objectives. *Syst Contr Lett* 40(1):43–57
28. Scherer CW (2006) LMI relaxations in robust control. *Euro J Contr* 12(1):3–29
29. Scherer CW, Gahinet P, Chilali M (1997) Multiobjective output-feedback control via LMI optimization. *IEEE Trans Automat Contr* 42(7):896–911
30. Stoorvogel AA, Saberi A, Sannuti P (2000) Performance with regulation constraints. *Automatica* 36(10):1443–1456
31. Sturm JF (1998) Using SeDuMi 1.02: A MATLAB toolbox for optimization over symmetric cones. *Optim Math Software* 11–12:625–653 <http://sedumi.mcmaster.ca/>
32. Zhang Z, Serrani A (2006) The linear periodic output regulation problem. *Syst Contr Lett* 55(7):518–529

Chapter 7

Robust Stabilization and Disturbance Attenuation of Switched Linear Parameter-Varying Systems in Discrete Time

Ji-Woong Lee and Geir E. Dullerud

Abstract Nonconservative analysis of discrete-time switched linear parameter-varying systems is achieved via switching path-dependent Lyapunov and Kalman–Yakubovich–Popov inequalities. Exact convex conditions for the synthesis of a class of state-feedback controllers are then expressed in terms of nested unions of linear matrix inequalities. The resulting controllers are robust in the sense that their coefficients depend solely on a finite number of the most recent past modes and parameters, but not on the current mode or parameter.

7.1 Introduction

A linear parameter-varying (LPV) system is defined by a parameterized collection of linear state-space models and a set of admissible parameter trajectories [1, 2, 13]. An LPV system typically arises from the abstraction of a nonlinear model, where the precise nonlinear dependence on trajectories is replaced by a covering abstraction given in terms of varying parameters. The attraction with such abstracted models is that they can be significantly simpler to analyze, while at the same time—because they admit more behaviors than the original nonlinear system—can be used to infer guaranteed properties about the original system. Counterbalancing this potential ease of analysis is that, if the abstraction is too coarse or conservative, it may not be

J.-W. Lee (✉)

Department of Electrical Engineering, The Pennsylvania State University, University Park, PA 16802, USA

e-mail: jiwoong@psu.edu

G.E. Dullerud

Department of Mechanical Science and Engineering, The University of Illinois at Urbana-Champaign, Urbana, IL 61801, USA

e-mail: dullerud@illinois.edu

possible to prove anything about the abstracted model even though the nonlinear system on which it is based has all the properties sought. In particular, such conservatism can occur in the situation where the underlying nonlinear dynamics are operating about several different equilibrium points. Although frequently possible to use a pure LPV model to abstract the nonlinear dynamics in this scenario, there is potentially much to gain in terms of reducing conservatism of the abstraction by explicitly modeling the logical switches between equilibrium points. This motivates the class of *switched* LPV systems considered in this chapter.

Further motivating the switched LPV class, even when simply operating around a single equilibrium point, is the situation where a nonlinear system to be analyzed exhibits multiple modes of operation due to jumps in the dynamics; in this case, it is natural to abstract the system by multiple LPV models and a switching logic between them, so that a switch from one LPV model to another corresponds to a jump from one nonlinear dynamical equation to another. Whenever such a switched LPV abstraction of a nonlinear system satisfies certain stability and performance specifications over all admissible parameter trajectories and mode switching sequences, the original nonlinear system is expected to satisfy the same stability and performance requirements. For these reasons, switched LPV approaches have found applications to a variety of nonlinear analysis and control problems such as gain-scheduled missile autopilot [10], active magnetic bearing system design [11], high-performance aircraft control [12], and multi-objective control of a wind turbine [9].

In this chapter, we focus on discrete-time switched LPV systems, where each LPV model is associated with a parameter polytope. Such systems have already been considered in the literature in the context of stabilization, \mathcal{H}_∞ -type disturbance attenuation, and model reduction [14, 15]. However, these results are based on a conservative analysis of stability and disturbance attenuation properties. Thus, our first objective is to present a nonconservative, convex analysis of these properties by extending the existing nonconservative analysis results for LPV systems [6] and switched linear systems [7, 8] to switched LPV systems. The resulting analysis conditions are expressed in terms of an increasing union of Lyapunov inequalities (for stability) and Kalman–Yakubovich–Popov inequalities (for disturbance attenuation performance) indexed by the number of most recent past system modes and parameters that the associated quadratic Lyapunov function depends on.

Our next objective is to use these analysis conditions to obtain nonconservative, convex synthesis conditions for a certain type of robust state-feedback controllers that guarantee stability and disturbance attenuation bounds. These controllers are robust in the sense that they do not depend on the current system mode or parameter value. However, we assume that the system mode and parameter become available to the controller with a unit delay, and that the state-feedback gain matrix is parameterized by a finite number of past modes and parameters. Our synthesis conditions thus complement existing results, which are limited to controllers that do not recall past modes or parameters.

The organization of the chapter is as follows. In Sects. 7.2 and 7.3, we present stability analysis and robust stabilization results. Then these results are generalized

to disturbance attenuation problems in Sects. 7.4 and 7.5. The analysis and synthesis results are illustrated and compared with existing results via numerical examples in Sect. 7.6. Then a concluding remark is made in Sect. 7.7.

Notation

Denoted by \mathbb{R} , \mathbb{N} , and \mathbb{N}_0 are the spaces of real numbers, positive integers, and nonnegative integers, respectively. For $x \in \mathbb{R}^n$, denoted by $\|x\|$ is the Euclidean norm of x defined by $\|x\| = (x^T x)^{1/2}$. For $\mathbf{X} \in \mathbb{R}^{n \times n}$, we write $\mathbf{X} > \mathbf{0}$ (resp. $\mathbf{X} < \mathbf{0}$) to indicate that \mathbf{X} is symmetric and positive definite (resp. negative definite). The identity matrix (resp. zero matrix) is denoted by \mathbf{I} (resp. $\mathbf{0}$) with its dimension understood.

7.2 Stability

Let $N, M_1, \dots, M_N \in \mathbb{N}$ be given. Let

$$\Theta \subset \{1, \dots, N\}^\infty$$

be a nonempty set of infinite sequences in $\{1, \dots, N\}$. For each $i \in \{1, \dots, N\}$ let Λ_i be the set of all probability distributions on $\{1, \dots, M_i\}$; namely,

$$\Lambda_i = \left\{ \lambda = \left(\lambda^{(1)}, \dots, \lambda^{(M_i)} \right) \in \mathbb{R}^{M_i} : \lambda^{(1)}, \dots, \lambda^{(M_i)} \geq 0 \text{ and } \sum_{j=1}^{M_i} \lambda^{(j)} = 1 \right\}.$$

Then, for each $\theta = (\theta(0), \theta(1), \dots) \in \Theta$, define

$$\Lambda^\theta = \Lambda_{\theta(0)} \times \Lambda_{\theta(1)} \times \dots = \{(\sigma(0), \sigma(1), \dots) : \sigma(t) \in \Lambda_{\theta(t)} \text{ for all } t \in \mathbb{N}_0\},$$

so that Λ^θ is the space of all infinite sequences $(\sigma(0), \sigma(1), \dots)$, where $\sigma(t)$ is a probability distribution on $\{1, \dots, M_{\theta(t)}\}$ for each $t \in \mathbb{N}_0$.

Let $n \in \mathbb{N}$ and $\mathbf{A}_{ij} \in \mathbb{R}^{n \times n}$ be given for $i = 1, \dots, N$ and $j = 1, \dots, M_i$. Write

$$\mathbf{A}_{i\lambda} = \sum_{j=1}^{M_i} \lambda^{(j)} \mathbf{A}_{ij}$$

for $i \in \{1, \dots, N\}$ and $\lambda = \left(\lambda^{(1)}, \dots, \lambda^{(M_i)} \right) \in \Lambda_i$. Then the polytope (i.e., bounded polyhedron) defined by

$$\mathcal{A}_i = \{\mathbf{A}_{i\lambda} : \lambda \in \Lambda_i\} \subset \mathbb{R}^{n \times n}$$

is the convex hull of matrices $\mathbf{A}_{i1}, \dots, \mathbf{A}_{iM_i}$ for each $i = 1, \dots, N$. With

$$\mathcal{A} = \{\mathcal{A}_1, \dots, \mathcal{A}_N\},$$

the pair (\mathcal{A}, Θ) defines the discrete-time *switched polytopic linear parameter-varying (or switched LPV) system*, whose state-space description takes the form

$$x(t+1) = \mathbf{A}_{\theta(t)\sigma(t)}x(t), \quad t \in \mathbb{N}_0, \quad (7.1)$$

for *mode sequences* $\theta = (\theta(0), \theta(1), \dots) \in \Theta$ and *parameter sequences* $\sigma = (\sigma(0), \sigma(1), \dots) \in \Lambda^\theta$. In the special case of $N = 1$ (i.e., single mode), the switched LPV system reduces to an LPV system \mathcal{A}_1 , where the time-varying parameter $\sigma(t)$ determines the state matrix $\mathbf{A}_{1\sigma(t)}$ for (7.1) from a polytope of matrices (i.e., the convex hull of $\mathbf{A}_{11}, \dots, \mathbf{A}_{1M_1}$). On the other hand, in the special case of $M_1 = \dots = M_N = 1$, the switched LPV system (\mathcal{A}, Θ) reverts to the switched linear system $(\{\mathbf{A}_{11}, \dots, \mathbf{A}_{N1}\}, \Theta)$, where the time-varying mode $\theta(t)$ determines the state matrix $\mathbf{A}_{\theta(t)1}$ for (7.1) from a finite set of matrices.

Our stability requirement for the switched LPV system is that the state $x(t)$ of the state-space model (7.1) converges to the origin with a single exponential decay rate uniformly in time and also uniformly over mode sequences and parameter sequences.

Definition 7.1. The switched LPV system (\mathcal{A}, Θ) is said to be *uniformly exponentially stable* if there exist $c \geq 1$ and $\lambda \in (0, 1)$ such that the state-space model (7.1) satisfies

$$\|x(t)\| \leq c\lambda^{t-t_0}\|x(t_0)\| \quad (7.2)$$

for all $t, t_0 \in \mathbb{N}_0$ with $t \geq t_0$, for all $x(t_0) \in \mathbb{R}^n$, for all $\theta \in \Theta$, and for all $\sigma \in \Lambda^\theta$.

The stability of the switched LPV system (\mathcal{A}, Θ) is closely related to that of an associated switched linear system. Let

$$\widehat{\mathcal{A}} = \{\mathbf{A}_{11}, \dots, \mathbf{A}_{1M_1}, \dots, \mathbf{A}_{N1}, \dots, \mathbf{A}_{NM_N}\}.$$

An infinite sequence of (pairs of) indices (i_0j_0, i_1j_1, \dots) is a switching sequence for $\widehat{\mathcal{A}}$ if $i_t \in \{1, \dots, N\}$ and $j_t \in \{1, \dots, M_{i_t}\}$ for all $t \in \mathbb{N}_0$. Let $\widehat{\Theta}$ be the set of all switching sequences for $\widehat{\mathcal{A}}$ restricted to the mode sequences in Θ ; that is,

$$\widehat{\Theta} = \{(i_0j_0, i_1j_1, \dots) : (i_0, i_1, \dots) \in \Theta, j_t = 1, \dots, M_{i_t}, t \in \mathbb{N}_0\}.$$

Then the pair $(\widehat{\mathcal{A}}, \widehat{\Theta})$ defines the discrete-time *switched linear system* whose state-space description is given by (7.1) for switching sequences $(\theta, \sigma) = (\theta(0)\sigma(0), \theta(1)\sigma(1), \dots) \in \widehat{\Theta}$. The stability requirement for this switched linear system is consistent with that for the linear LPV system.

Definition 7.2. The switched linear system $(\widehat{\mathcal{A}}, \widehat{\Theta})$ is said to be *uniformly exponentially stable* if there exist $c \geq 1$ and $\lambda \in (0, 1)$ such that the state-space model (7.1) satisfies (7.2) for all $t, t_0 \in \mathbb{N}_0$ with $t \geq t_0$, for all $x(t_0) \in \mathbb{R}^n$, and for all $(\theta, \sigma) \in \widehat{\Theta}$.

To simplify notation, set $\theta(t) = 0$ and $\sigma(t) = 1$ (i.e., $\Lambda_0 = \{1\}$) for $t < 0$ whenever $\theta \in \Theta$ and $\sigma \in \Lambda^\theta$. Define $\mathcal{L}_M(\Theta)$ (resp. $\mathcal{L}_M(\widehat{\Theta})$) as the set of all switching paths of length $M \in \mathbb{N}_0$ that appear in at least one of the mode sequences in Θ (resp. switching sequences in $\widehat{\Theta}$):

$$\mathcal{L}_M(\Theta) = \{(\theta(t-M), \dots, \theta(t)) : \theta \in \Theta, t \in \mathbb{N}_0\}, \quad (7.3a)$$

$$\mathcal{L}_M(\widehat{\Theta}) = \{(\hat{\theta}(t-M), \dots, \hat{\theta}(t)) : \hat{\theta} \in \widehat{\Theta}, t \in \mathbb{N}_0\}. \quad (7.3b)$$

Then let $\mathcal{N}_M(\Theta)$ be the largest subset of $\mathcal{L}_M(\Theta)$ satisfying the following: For each $(i_0, \dots, i_M) \in \mathcal{N}_M(\Theta)$, there exist $K \in \mathbb{N}$ with $K > M$ and (i_{M+1}, \dots, i_K) such that $(i_{K-M}, \dots, i_K) = (i_0, \dots, i_M)$ and $(i_k, \dots, i_{k+M}) \in \mathcal{N}_M(\Theta)$ for $0 \leq k \leq K - M$. Similarly, let $\mathcal{N}_M(\widehat{\Theta})$ be the largest subset of $\mathcal{L}_M(\widehat{\Theta})$ satisfying the following: For each $(i_0 j_0, \dots, i_M j_M) \in \mathcal{N}_M(\widehat{\Theta})$, there exist $K \in \mathbb{N}$ with $K > M$ and $(i_{M+1} j_{M+1}, \dots, i_K j_K)$ such that $(i_{K-M} j_{K-M}, \dots, i_K j_K) = (i_0 j_0, \dots, i_M j_M)$ and $(i_k j_k, \dots, i_{k+M} j_{k+M}) \in \mathcal{N}_M(\widehat{\Theta})$ for $0 \leq k \leq K - M$.

We will use the convention that $(i_k, \dots, i_l) = 0$ (resp. $(i_k j_k, \dots, i_l j_l) = 01$) if $k > l$; otherwise, (i_k, \dots, i_l) (resp. $(i_k j_k, \dots, i_l j_l)$) is a switching path of length $l - k$. The following theorem gives an exact convex condition for the stability of switched LPV systems in terms of linear matrix inequalities.

Theorem 7.1. *The following are equivalent:*

- (a) *The switched LPV system (\mathcal{A}, Θ) is uniformly exponentially stable.*
- (b) *The switched linear system $(\widehat{\mathcal{A}}, \widehat{\Theta})$ is uniformly exponentially stable.*
- (c) *There exist a path length $M \in \mathbb{N}_0$ and an indexed (finite) family of matrices $\mathbf{Y}_{(i_1 j_1, \dots, i_M j_M)} \in \mathbb{R}^{n \times n}$ such that*

$$\mathbf{Y}_{(i_0 j_0, \dots, i_{M-1} j_{M-1})} > \mathbf{0}, \quad (7.4a)$$

$$\mathbf{A}_{i_M j_M} \mathbf{Y}_{(i_0 j_0, \dots, i_{M-1} j_{M-1})} \mathbf{A}_{i_M j_M}^\top - \mathbf{Y}_{(i_1 j_1, \dots, i_M j_M)} < \mathbf{0} \quad (7.4b)$$

for all $(i_0 j_0, \dots, i_M j_M) \in \mathcal{N}_M(\widehat{\Theta})$.

- (d) *There exist a path length $M \in \mathbb{N}_0$, real numbers $\alpha, \beta > 0$, and an indexed (uncountably infinite) family of matrices $\mathbf{Y}_{(i_1 \lambda_1, \dots, i_M \lambda_M)} \in \mathbb{R}^{n \times n}$ such that*

$$\alpha \mathbf{I} \leq \mathbf{Y}_{(i_0 \lambda_0, \dots, i_{M-1} \lambda_{M-1})} \leq \beta \mathbf{I}, \quad (7.5a)$$

$$\mathbf{A}_{i_M \lambda_M} \mathbf{Y}_{(i_0 \lambda_0, \dots, i_{M-1} \lambda_{M-1})} \mathbf{A}_{i_M \lambda_M}^\top - \mathbf{Y}_{(i_1 \lambda_1, \dots, i_M \lambda_M)} \leq -\alpha \mathbf{I} \quad (7.5b)$$

for all $(i_0, \dots, i_M) \in \mathcal{N}_M(\Theta)$ and for all $(\lambda_0, \dots, \lambda_M) \in \Lambda_{i_0} \times \dots \times \Lambda_{i_M}$.

Moreover, if (c) holds with $M \in \mathbb{N}$, then (d) is satisfied with

$$\mathbf{Y}_{(i_0 j_0, \dots, i_{M-1} j_{M-1})} = \sum_{j_0=1}^{M_{i_0}} \cdots \sum_{j_{M-1}=1}^{M_{i_{M-1}}} \lambda_0^{(j_0)} \cdots \lambda_{M-1}^{(j_{M-1})} \mathbf{Y}_{(i_0 j_0, \dots, i_{M-1} j_{M-1})}, \quad (7.6a)$$

$$\mathbf{Y}_{(i_1 \lambda_1, \dots, i_M \lambda_M)} = \sum_{j_1=1}^{M_{i_1}} \cdots \sum_{j_M=1}^{M_{i_M}} \lambda_1^{(j_1)} \cdots \lambda_M^{(j_M)} \mathbf{Y}_{(i_1 j_1, \dots, i_M j_M)} \quad (7.6b)$$

for $(\lambda_0, \dots, \lambda_M) \in \Lambda_{i_0} \times \cdots \times \Lambda_{i_M}$, where $\lambda_k = \left(\lambda_k^{(1)}, \dots, \lambda_k^{(M_{i_k})} \right)$, $k = 0, \dots, M$. If (c) holds with $M = 0$, then (d) is satisfied with

$$\mathbf{Y}_{(i_0 \lambda_0, \dots, i_{M-1} \lambda_{M-1})} = \mathbf{Y}_{(i_1 \lambda_1, \dots, i_M \lambda_M)} = \mathbf{Y}_{01}.$$

Proof. The proof extends that of [6, Theorem 1]. We will show that (a) \Rightarrow (b) \Rightarrow (c) \Rightarrow (a); the equivalence (c) \Leftrightarrow (d) will follow as a by-product. It is clear that (a) implies (b). Due to [7, Corollary 3.4], condition (b) implies the existence of an $M \in \mathbb{N}_0$ and matrices $\mathbf{X}_{(i_1 j_1, \dots, i_M j_M)} > \mathbf{0}$ such that

$$\mathbf{A}_{i_M j_M}^T \mathbf{X}_{(i_1 j_1, \dots, i_M j_M)} \mathbf{A}_{i_M j_M} - \mathbf{X}_{(i_0 j_0, \dots, i_{M-1} j_{M-1})} < \mathbf{0}$$

for all $(i_0 j_0, \dots, i_M j_M) \in \mathcal{N}_M(\hat{\Theta})$. The Schur complement formula, along with

$$\mathbf{Y}_{(i_1 j_1, \dots, i_M j_M)} = \mathbf{X}_{(i_1 j_1, \dots, i_M j_M)}^{-1},$$

then yields (c).

Suppose (c) holds true, so that (7.4) is satisfied for all $(i_0 j_0, \dots, i_M j_M) \in \mathcal{N}_M(\hat{\Theta})$. Similarly to the proof of [7, Corollary 3.4], run the following algorithm to enlarge the set $\mathcal{N}_M(\hat{\Theta})$ to $\mathcal{L}_M(\hat{\Theta})$:

Step 0. Set $\mathcal{L} = \mathcal{N}_M(\hat{\Theta})$.

Step 1. If $\mathcal{L} = \mathcal{L}_M(\hat{\Theta})$, then stop; otherwise, choose a switching path $(i_0 j_0, \dots, i_M j_M) \in \mathcal{L}_M(\hat{\Theta}) \setminus \mathcal{L}$ such that $(i_1 j_1, \dots, i_{M+1} j_{M+1}) \in \mathcal{L}$ for some $i_{M+1} \in \{1, \dots, N\}$ and $j_{M+1} \in \{1, \dots, M_{i_{M+1}}\}$.

Step 2. If $(i_0 j_0, \dots, i_{M-1} j_{M-1}, \hat{k}_M \hat{l}_M) \notin \mathcal{L}$ for any $\hat{k}_M \in \{1, \dots, M\}$ and $\hat{l}_M \in \{1, \dots, M_{\hat{k}_M}\}$, then choose a $\mathbf{Y} > \mathbf{0}$ such that

$$\mathbf{A}_{i_M j_M} \mathbf{Y} \mathbf{A}_{i_M j_M}^T - \mathbf{Y}_{(i_1 j_1, \dots, i_M j_M)} < \mathbf{0},$$

put $\mathbf{Y}_{(i_0 j_0, \dots, i_{M-1} j_{M-1})} = \mathbf{Y}$, and go to *Step 4*.

Step 3. Choose an $\varepsilon > 0$ such that

$$\varepsilon \mathbf{A}_{i_M j_M} \mathbf{Y}_{(i_0 j_0, \dots, i_{M-1} j_{M-1})} \mathbf{A}_{i_M j_M}^T - \mathbf{Y}_{(i_1 j_1, \dots, i_M j_M)} < \mathbf{0}$$

and substitute $\mathbf{Y}_{(i_0 j_0, \dots, i_{M-1} j_{M-1})}$ with $\varepsilon \mathbf{Y}_{(i_0 j_0, \dots, i_{M-1} j_{M-1})}$. Whenever there exist $K \in \mathbb{N}$ and $(i_{-K} j_{-K}, \dots, i_{-1} j_{-1})$ such that $(i_{k-K} j_{k-K}, \dots, i_{k-K+M} j_{k-K+M}) \in \mathcal{L}$ for all $k = 0, \dots, K$, then scale $\mathbf{Y}_{(i_{k-K} j_{k-K}, \dots, i_{k-K+M} j_{k-K+M})}$ with the same scaling factor ε for all $k = 0, \dots, K$ as well.

Step 4. Substitute \mathcal{L} with $\mathcal{L} \cup \{(i_0 j_0, \dots, i_M j_M)\}$ and go to *Step 1*.

By the definition of $\mathcal{N}_M(\widehat{\Theta})$, each step of this algorithm (including *Step 3*) is well defined. Moreover, the algorithm produces an extended set of matrices $\mathbf{Y}_{(i_1 j_1, \dots, i_M j_M)}$ such that (7.4) holds for all $(i_0 j_0, \dots, i_M j_M) \in \mathcal{L}_M(\widehat{\Theta})$. Assume $M \in \mathbb{N}$ without loss of generality. Since $\mathcal{L}_M(\widehat{\Theta})$ is a finite set, there exist $\alpha, \beta > 0$ such that

$$\alpha \mathbf{I} \leq \mathbf{Y}_{(i_0 j_0, \dots, i_{M-1} j_{M-1})} \leq \beta \mathbf{I} \quad (7.7a)$$

and

$$\mathbf{A}_{i_M j_M} \mathbf{Y}_{(i_0 j_0, \dots, i_{M-1} j_{M-1})} \mathbf{A}_{i_M j_M}^T - \mathbf{Y}_{(i_1 j_1, \dots, i_M j_M)} < -\alpha \mathbf{I}$$

for all $(i_0 j_0, \dots, i_M j_M) \in \mathcal{L}_M(\widehat{\Theta})$. Applying the Schur complement formula to the last inequality yields

$$\begin{bmatrix} \alpha \mathbf{I} - \mathbf{Y}_{(i_1 j_1, \dots, i_M j_M)} & \mathbf{A}_{i_M j_M} \mathbf{Y}_{(i_0 j_0, \dots, i_{M-1} j_{M-1})} \\ * & -\mathbf{Y}_{(i_0 j_0, \dots, i_{M-1} j_{M-1})} \end{bmatrix} < \mathbf{0}. \quad (7.7b)$$

Given $(i_0, \dots, i_M) \in \mathcal{L}_M(\Theta)$, choose $(\lambda_0, \dots, \lambda_M) \in \Lambda_{i_0} \times \dots \times \Lambda_{i_M}$ with $\lambda_k = (\lambda_k^{(1)}, \dots, \lambda_k^{(M_{i_k})})$ for $k = 0, \dots, M$, where $\Lambda_0 = \{1\}$. Define $\mathbf{Y}_{(i_0 \lambda_0, \dots, i_{M-1} \lambda_{M-1})}$ and $\mathbf{Y}_{(i_1 \lambda_1, \dots, i_M \lambda_M)}$ as in (7.6). Taking the weighted sum of (7.7) with weights given by $(\lambda_0, \dots, \lambda_M)$ then yields (7.5a) and

$$\begin{bmatrix} \alpha \mathbf{I} - \mathbf{Y}_{(i_1 \lambda_1, \dots, i_M \lambda_M)} & \mathbf{A}_{i_M \lambda_M} \mathbf{Y}_{(i_0 \lambda_0, \dots, i_{M-1} \lambda_{M-1})} \\ * & -\mathbf{Y}_{(i_0 \lambda_0, \dots, i_{M-1} \lambda_{M-1})} \end{bmatrix} < \mathbf{0}.$$

Taking the Schur complement of $-\mathbf{Y}_{(i_0 \lambda_0, \dots, i_{M-1} \lambda_{M-1})}$ from this inequality, we obtain (7.5b). This shows that, if (c) holds, then (7.5) is satisfied for all $(i_0, \dots, i_M) \in \mathcal{L}_M(\Theta)$ and $(\lambda_0, \dots, \lambda_M) \in \Lambda_{i_0} \times \dots \times \Lambda_{i_M}$. Because this implies (d) and because (c) is a special case of (d), it is immediate that (c) and (d) are equivalent.

To complete the proof, we will show (a) holds true given that (7.5) is satisfied for all $(i_0, \dots, i_M) \in \mathcal{L}_M(\Theta)$ and $(\lambda_0, \dots, \lambda_M) \in \Lambda_{i_0} \times \dots \times \Lambda_{i_M}$. Choose a mode sequence $\theta \in \Theta$ and a parameter sequence $\sigma \in \Lambda^\theta$. Put

$$\mathbf{A}(t) = \mathbf{A}_{\theta(t)\sigma(t)},$$

$$\mathbf{Y}(t) = \mathbf{Y}_{(\theta(t-M)\sigma(t-M), \dots, \theta(t-1)\sigma(t-1))}$$

for all $t \in \mathbb{N}_0$, so that

$$\begin{aligned}\alpha \mathbf{I} &\leq \mathbf{Y}(t) \leq \beta \mathbf{I}, \\ \mathbf{A}(t) \mathbf{Y}(t) \mathbf{A}(t)^\top - \mathbf{Y}(t+1) &\leq -\alpha \mathbf{I}\end{aligned}$$

for all $t \in \mathbb{N}_0$. If we put $\mathbf{X}(t) = \mathbf{Y}(t)^{-1}$, then there exists an $\eta > 0$, independent of θ and σ , such that

$$\begin{aligned}\beta^{-1} \mathbf{I} &\leq \mathbf{X}(t) \leq \alpha^{-1} \mathbf{I}, \\ \mathbf{A}(t)^\top \mathbf{X}(t+1) \mathbf{A}(t) - \mathbf{X}(t) &\leq -\eta \mathbf{I}\end{aligned}$$

for all $t \in \mathbb{N}_0$. Thus, by specializing [5, Corollary 12] to pure stability analysis, we deduce that there exist $c \geq 1$ and $\lambda \in (0, 1)$ such that the linear time-varying system (7.1) satisfies (7.2) for all $t, t_0 \in \mathbb{N}_0$ with $t \geq t_0$. Since $\theta \in \Theta$ and $\sigma \in \Lambda^\theta$ are arbitrary, and since the constants c and λ can be determined solely from α^{-1} , β^{-1} , and η (see, e.g., [8, Lemma 4]), we conclude that (a) holds true. \square

According to Theorem 7.1, only the mode switching paths in $\mathcal{N}_M(\Theta)$ are relevant to stability. This is because the switching paths outside $\mathcal{N}_M(\Theta)$ cannot appear more than once in any mode sequence in Θ , and because the number of such switching paths is finite for each path length M .

Although there is no upper bound on the path length M that is required for our stability test, it is usually the case in practice that one only needs to try the first few path lengths M . This agrees with the fact that the common Lyapunov function approach (i.e., the case of $M = 0$) and the multiple Lyapunov function approaches (i.e., versions of the case of $M = 1$) have been very useful in practice. What Theorem 7.1 gives us is the option to go beyond $M = 0$ and $M = 1$ if we are willing and able to pay additional computational cost in return for potentially better stability analysis.

7.3 Stabilization

Let $m, n \in \mathbb{N}$, $\mathbf{A}_{ij} \in \mathbb{R}^{n \times n}$, and $\mathbf{B}_{ij} \in \mathbb{R}^{n \times m}$ be given for $i = 1, \dots, N$ and $j = 1, \dots, M_i$. Write

$$\mathbf{A}_{i\lambda} = \sum_{j=1}^{M_i} \lambda^{(j)} \mathbf{A}_{ij} \quad \text{and} \quad \mathbf{B}_{i\lambda} = \sum_{j=1}^{M_i} \lambda^{(j)} \mathbf{B}_{ij}$$

whenever $i \in \{1, \dots, N\}$ and $\lambda = (\lambda^{(1)}, \dots, \lambda^{(M_i)}) \in \Lambda_i$. The polytopes defined by

$$\begin{aligned}\mathcal{A}_i &= \{\mathbf{A}_{i\lambda} : \lambda \in \Lambda_i\} \subset \mathbb{R}^{n \times n}, \\ \mathcal{B}_i &= \{\mathbf{B}_{i\lambda} : \lambda \in \Lambda_i\} \subset \mathbb{R}^{n \times m}\end{aligned}$$

are the convex hulls of $\mathbf{A}_{i1}, \dots, \mathbf{A}_{iM_i}$ and $\mathbf{B}_{i1}, \dots, \mathbf{B}_{iM_i}$, respectively, for each $i = 1, \dots, N$. As in the previous section, let $\Theta \subset \{1, \dots, N\}^\infty$ be a nonempty set of mode sequences. Then, with

$$\mathcal{G} = \{(\mathcal{A}_1, \mathcal{B}_1), \dots, (\mathcal{A}_N, \mathcal{B}_N)\},$$

the pair (\mathcal{G}, Θ) defines the controlled version of the discrete-time switched LPV system described by

$$x(t+1) = \mathbf{A}_{\theta(t)\sigma(t)}x(t) + \mathbf{B}_{\theta(t)\sigma(t)}u(t), \quad t \in \mathbb{N}_0, \quad (7.8)$$

for mode sequences $\theta \in \Theta$, parameter sequences $\sigma \in \Lambda^\theta$, and control sequences $u = (u(0), u(1), \dots)$.

We will consider all linear state-feedback controllers that generate the control input $u(t)$ at each time $t \in \mathbb{N}_0$ based on a finite number $L \in \mathbb{N}_0$ of past mode sequences $\theta(t-L), \dots, \theta(t-1)$ and parameter sequences $\sigma(t-L), \dots, \sigma(t-1)$ as well as the perfectly observed current state $x(t)$. As in the previous section, let $\theta(t) = 0$ and $\sigma(t) = 1$ for $t < 0$ whenever $\theta \in \Theta$ and $\sigma \in \Lambda^\theta$. Also, write

$$\begin{aligned} (\theta\sigma)_L(t) &= (\theta(t-L)\sigma(t-L), \dots, \theta(t)\sigma(t)), \\ (\theta\sigma)_L(t)_- &= (\theta(t-L)\sigma(t-L), \dots, \theta(t-1)\sigma(t-1)), \\ (\theta\sigma)_L(t)_+ &= (\theta(t-L+1)\sigma(t-L+1), \dots, \theta(t)\sigma(t)) \end{aligned}$$

for $L, t \in \mathbb{N}_0$, $\theta \in \Theta$, and $\sigma \in \Lambda^\theta$. For a fixed path length $L \in \mathbb{N}_0$, let $\Lambda_0 = \{1\}$ and

$$\mathcal{K} = \{\mathbf{K}_{(i_1\lambda_1, \dots, i_L\lambda_L)} : \lambda_k \in \Lambda_{i_k}, i_k = 0, 1, \dots, N, k = 1, \dots, L\} \subset \mathbb{R}^{m \times n}$$

if $L > 0$, and let $\mathcal{K} = \{\mathbf{K}_{01}\} \subset \mathbb{R}^{m \times n}$ be a singleton if $L = 0$. Then \mathcal{K} defines a *robust L -path-dependent state-feedback controller* described by

$$u(t) = \mathbf{K}_{(\theta\sigma)_L(t)_-}x(t), \quad t \in \mathbb{N}_0, \quad (7.9)$$

if $L > 0$, and $u(t) = \mathbf{K}_{01}x(t)$, $t \in \mathbb{N}_0$, if $L = 0$. For example, if $L = 2$, then

$$\begin{aligned} u(0) &= \mathbf{K}_{(01,01)}x(0), \\ u(1) &= \mathbf{K}_{(01,\theta(0)\sigma(0))}x(1), \end{aligned}$$

and

$$u(t) = \mathbf{K}_{(\theta(t-2)\sigma(t-2), \theta(t-1)\sigma(t-1))}x(t)$$

for $t \geq 2$. Clearly, the case of $L = 0$ corresponds to the robust state-feedback controller in the usual sense; if $L > 0$, on the other hand, the controller perfectly observes the mode and parameter sequences with a unit delay (or less) and performs gain scheduling based on the most recent past L modes and parameters.

The feedback interconnection of the controlled system (\mathcal{G}, Θ) , described by (7.8), and a robust path-dependent controller \mathcal{K} , described by (7.9), gives rise to a closed-loop system whose state evolves according to

$$x(t+1) = (\mathbf{A}_{\theta(t)\sigma(t)} + \mathbf{B}_{\theta(t)\sigma(t)} \mathbf{K}_{(\theta\sigma)_L(t-)}) x(t), \quad t \in \mathbb{N}_0. \quad (7.10)$$

We now present an exact convex condition for the existence of a stabilizing robust path-dependent controller, and a synthesis procedure guaranteed to yield such a controller, if it exists.

Definition 7.3. The switched LPV system (\mathcal{G}, Θ) is said to be *uniformly exponentially stabilizable* if there exist $c \geq 1$, $\lambda \in (0, 1)$, $L \in \mathbb{N}_0$, and a robust L -path-dependent state-feedback controller such that the closed-loop state-space model (7.10) satisfies (7.2) for all t , $t_0 \in \mathbb{N}_0$ with $t \geq t_0$, for all $x(t_0) \in \mathbb{R}^n$, for all $\theta \in \Theta$, and for all $\sigma \in \Lambda^\theta$.

Theorem 7.2. *The switched LPV system (\mathcal{G}, Θ) is uniformly exponentially stabilizable if and only if there exist a path length $M \in \mathbb{N}_0$ and indexed (finite) families of matrices $\mathbf{W}_{(i_1 j_1, \dots, i_M j_M)} \in \mathbb{R}^{m \times n}$ and $\mathbf{Y}_{(i_1 j_1, \dots, i_M j_M)} \in \mathbb{R}^{n \times n}$ such that*

$$\begin{bmatrix} -\mathbf{Y}_{(i_1 j_1, \dots, i_M j_M)} & \mathbf{A}_{i_M j_M} \mathbf{Y}_{(i_0 j_0, \dots, i_{M-1} j_{M-1})} + \mathbf{B}_{i_M j_M} \mathbf{W}_{(i_0 j_0, \dots, i_{M-1} j_{M-1})} \\ * & -\mathbf{Y}_{(i_0 j_0, \dots, i_{M-1} j_{M-1})} \end{bmatrix} < \mathbf{0} \quad (7.11)$$

for all $(i_0 j_0, \dots, i_M j_M) \in \mathcal{N}_M(\widehat{\Theta})$. Moreover, if (7.11) holds with $M \in \mathbb{N}$, then a robust M -path-dependent state-feedback controller \mathcal{K} that uniformly exponentially stabilizes the system (\mathcal{G}, Θ) is given by

$$\mathbf{K}_{(i_0 \lambda_0, \dots, i_{M-1} \lambda_{M-1})} = \mathbf{W}_{(i_0 \lambda_0, \dots, i_{M-1} \lambda_{M-1})} \mathbf{Y}_{(i_0 \lambda_0, \dots, i_{M-1} \lambda_{M-1})}^{-1} \quad (7.12a)$$

for all $(i_0, \dots, i_M) \in \mathcal{N}_M(\Theta)$ and for all $(\lambda_0, \dots, \lambda_M) \in \Lambda_{i_0} \times \dots \times \Lambda_{i_M}$, where

$$\mathbf{Y}_{(i_0 \lambda_0, \dots, i_{M-1} \lambda_{M-1})} = \sum_{j_0=1}^{M_{i_0}} \dots \sum_{j_{M-1}=1}^{M_{i_{M-1}}} \lambda_0^{(j_0)} \dots \lambda_{M-1}^{(j_{M-1})} \mathbf{Y}_{(i_0 j_0, \dots, i_{M-1} j_{M-1})}, \quad (7.12b)$$

$$\mathbf{W}_{(i_0 \lambda_0, \dots, i_{M-1} \lambda_{M-1})} = \sum_{j_0=1}^{M_{i_0}} \dots \sum_{j_{M-1}=1}^{M_{i_{M-1}}} \lambda_0^{(j_0)} \dots \lambda_{M-1}^{(j_{M-1})} \mathbf{W}_{(i_0 j_0, \dots, i_{M-1} j_{M-1})} \quad (7.12c)$$

for $(\lambda_0, \dots, \lambda_{M-1}) \in \Lambda_{i_0} \times \dots \times \Lambda_{i_{M-1}}$ with $\lambda_k = (\lambda_k^{(1)}, \dots, \lambda_k^{(M_{i_k})})$, $k = 0, \dots, M-1$. If (7.11) holds with $M = 0$, then a robust uniformly exponentially stabilizing state-feedback controller \mathcal{K} is given by

$$\mathbf{K}_{01} = \mathbf{W}_{01} \mathbf{Y}_{01}^{-1}.$$

Proof. The proof is an extension of [6, Theorem 2]. Suppose that the closed-loop system with a robust L -path-dependent controller \mathcal{K} is uniformly exponentially stable. Then there exist $c \geq 1$ and $\lambda \in (0, 1)$ such that (7.2) holds for all $t, t_0 \in \mathbb{N}_0$ with $t \geq t_0$, for all $x(t_0) \in \mathbb{R}^n$, for all $\theta \in \Theta$, and for all $\sigma \in \Lambda^\theta$. Following the proof of [8, Lemma 4(a)], it is readily seen that there exists an $M \geq L$, constants $\alpha, \beta > 0$ (which depend solely on c and λ), and matrices $\mathbf{Y}_{(i_1 j_1, \dots, i_M j_M)} > \mathbf{0}$ such that

$$\begin{aligned} \alpha \mathbf{I} &\leq \mathbf{Y}_{(\theta \sigma)_M(t)_-} \leq \beta \mathbf{I}, \\ \widehat{\mathbf{A}}_{(\theta \sigma)_L(t)} \mathbf{Y}_{(\theta \sigma)_M(t)_-} \widehat{\mathbf{A}}_{(\theta \sigma)_L(t)}^\top - \mathbf{Y}_{(\theta \sigma)_M(t)_+} &< -\alpha \mathbf{I} \end{aligned}$$

for all $t \in \mathbb{N}_0$, $\theta \in \Theta$, and $\sigma \in \Lambda^\theta$, where

$$\widehat{\mathbf{A}}_{(\theta \sigma)_L(t)} = \mathbf{A}_{\theta(t)\sigma(t)} + \mathbf{B}_{\theta(t)\sigma(t)} \mathbf{K}_{(\theta \sigma)_L(t)_-}$$

are the closed-loop state matrices. In particular, this holds whenever $\theta_M(t) \in \mathcal{N}_L(\Theta)$ and $\sigma_M(t) \in \Lambda_{\theta(t-M)} \times \dots \times \Lambda_{\theta(t)}$, and so

$$\alpha \mathbf{I} \leq \mathbf{Y}_{(i_0 \lambda_0, \dots, i_{M-1} \lambda_{M-1})} \leq \beta \mathbf{I} \quad (7.13a)$$

and

$$\begin{aligned} \widehat{\mathbf{A}}_{(i_{M-L} \lambda_{M-L}, \dots, i_M \lambda_M)} \mathbf{Y}_{(i_0 \lambda_0, \dots, i_{M-1} \lambda_{M-1})} \widehat{\mathbf{A}}_{(i_{M-L} \lambda_{M-L}, \dots, i_M \lambda_M)}^\top \\ - \mathbf{Y}_{(i_1 \lambda_1, \dots, i_M \lambda_M)} &< -\alpha \mathbf{I} \end{aligned}$$

for all $(i_0, \dots, i_M) \in \mathcal{N}_M(\Theta)$ and $(\lambda_0, \dots, \lambda_M) \in \Lambda_{i_0} \times \dots \times \Lambda_{i_M}$. As $M \geq L$, the L -path-dependent controller \mathcal{K} can be taken to be M -path-dependent, so we can assume $L = M > 0$ without loss of generality. Now, applying the Schur complement formula to the last inequality gives

$$\left[\begin{array}{c} \alpha \mathbf{I} - \mathbf{Y}_{(i_1 \lambda_1, \dots, i_M \lambda_M)} \\ * \\ \mathbf{A}_{i_M \lambda_M} + \mathbf{B}_{i_M \lambda_M} \mathbf{K}_{(i_0 \lambda_0, \dots, i_{M-1} \lambda_{M-1})} \\ \mathbf{Y}_{(i_0 \lambda_0, \dots, i_{M-1} \lambda_{M-1})} \\ - \mathbf{Y}_{(i_0 \lambda_0, \dots, i_{M-1} \lambda_{M-1})} \end{array} \right] < \mathbf{0} \quad (7.13b)$$

for all $(i_0, \dots, i_M) \in \mathcal{N}_M(\Theta)$ and $(\lambda_0, \dots, \lambda_M) \in \Lambda_{i_0} \times \dots \times \Lambda_{i_M}$. Specializing (7.13) to the associated switched linear system over all switching sequences in $\widehat{\Theta}$, and using (7.12a), we obtain (7.11) for all $(i_0 j_0, \dots, i_M j_M) \in \mathcal{N}_M(\widehat{\Theta})$. This establishes necessity.

To show sufficiency, suppose (7.11) holds for all $(i_0 j_0, \dots, i_M j_M) \in \mathcal{N}_M(\widehat{\Theta})$. Since (7.11) defines a finite number of inequalities over a finite number of matrix variables, there exist $\alpha, \beta > 0$ such that, along with (7.12), we have (7.13) for

all $(i_0, \dots, i_M) \in \mathcal{N}_M(\Theta)$ and $(\lambda_0, \dots, \lambda_M) \in \Lambda_{i_0} \times \dots \times \Lambda_{i_M}$. Taking the Schur complement of $-\mathbf{Y}_{(i_0\lambda_0, \dots, i_{M-1}\lambda_{M-1})}$ in (7.13b) gives

$$\begin{aligned} \alpha \mathbf{I} &\leq \mathbf{Y}_{(i_0\lambda_0, \dots, i_{M-1}\lambda_{M-1})} \leq \beta \mathbf{I}, \\ \widehat{\mathbf{A}}_{(i_0\lambda_0, \dots, i_M\lambda_M)} \mathbf{Y}_{(i_0\lambda_0, \dots, i_{M-1}\lambda_{M-1})} \widehat{\mathbf{A}}_{(i_0\lambda_0, \dots, i_M\lambda_M)}^T - \mathbf{Y}_{(i_1\lambda_1, \dots, i_M\lambda_M)} &\leq -\alpha \mathbf{I} \end{aligned}$$

for all $(i_0, \dots, i_M) \in \mathcal{N}_M(\Theta)$ and $(\lambda_0, \dots, \lambda_M) \in \Lambda_{i_0} \times \dots \times \Lambda_{i_M}$, where

$$\widehat{\mathbf{A}}_{(i_0\lambda_0, \dots, i_M\lambda_M)} = \mathbf{A}_{i_M\lambda_M} + \mathbf{B}_{i_M\lambda_M} \mathbf{K}_{(i_0\lambda_0, \dots, i_{M-1}\lambda_{M-1})}$$

are the closed-loop state matrices. Now, the equivalence of (a) and (d) in Theorem 7.1 implies that the closed-loop system is uniformly exponentially stable. \square

According to Theorem 7.2, only the feedback gain matrices $\mathbf{K}_{(\theta\sigma)_{M(t)-}}$ over $\theta_{M(t)} \in \mathcal{N}_M(\Theta)$, $t \in \mathbb{N}_0$, and $\theta \in \Theta$ are relevant to the stability of the closed-loop system. The remaining feedback gain matrices can be chosen arbitrarily. Note that Theorem 7.2 gives an exact synthesis condition, but that it is limited to the cases where the mode and parameter are observed with a unit delay. If either the current mode or the current parameter is available for measurement, then one can use the results in [15].

7.4 Performance Analysis

In this section, we will address the problem of evaluating the worst-case ℓ_2 -induced norm (i.e., the disturbance attenuation property) of a switched LPV system. Given $l, m, n \in \mathbb{N}$, and given $\mathbf{A}_{ij} \in \mathbb{R}^{n \times n}$, $\mathbf{B}_{ij} \in \mathbb{R}^{n \times m}$, $\mathbf{C}_{ij} \in \mathbb{R}^{l \times n}$, and $\mathbf{D}_{ij} \in \mathbb{R}^{l \times m}$ for $i = 1, \dots, N$ and for $j = 1, \dots, M_i$, consider the state-space model

$$\begin{aligned} x(t+1) &= \mathbf{A}_{\theta(t)\sigma(t)} x(t) + \mathbf{B}_{\theta(t)\sigma(t)} w(t), \quad t \in \mathbb{N}_0; \\ z(t) &= \mathbf{C}_{\theta(t)\sigma(t)} x(t) + \mathbf{D}_{\theta(t)\sigma(t)} w(t), \quad t \in \mathbb{N}_0, \end{aligned} \quad (7.14)$$

over mode sequences $\theta \in \Theta$, parameter sequences $\sigma \in \Lambda^\theta$, and disturbance sequences $w = (w(0), w(1), \dots)$; the error output sequence is given by $z = (z(0), z(1), \dots)$. Writing

$$\begin{aligned} \mathcal{A}_i &= \{\mathbf{A}_{i\lambda} : \lambda \in \Lambda_i\} \subset \mathbb{R}^{n \times n}, \\ \mathcal{B}_i &= \{\mathbf{B}_{i\lambda} : \lambda \in \Lambda_i\} \subset \mathbb{R}^{n \times m}, \\ \mathcal{C}_i &= \{\mathbf{C}_{i\lambda} : \lambda \in \Lambda_i\} \subset \mathbb{R}^{l \times n}, \\ \mathcal{D}_i &= \{\mathbf{D}_{i\lambda} : \lambda \in \Lambda_i\} \subset \mathbb{R}^{l \times m} \end{aligned}$$

for $i \in \{1, \dots, N\}$, let

$$\mathcal{S} = \{(\mathcal{A}_1, \mathcal{B}_1, \mathcal{C}_1, \mathcal{D}_1), \dots, (\mathcal{A}_N, \mathcal{B}_N, \mathcal{C}_N, \mathcal{D}_N)\}.$$

If Θ is a nonempty subset of $\{1, \dots, N\}^\infty$, then the pair (\mathcal{S}, Θ) defines the discrete-time switched LPV system whose ℓ_2 -induced norm under given $\theta \in \Theta$ and $\sigma \in \Lambda^\theta$ is defined by the supremum of the square root of $\sum_{t=0}^\infty \|z(t)\|^2 / \sum_{t=0}^\infty \|w(t)\|^2$ over all w with $\sum_{t=0}^\infty \|w(t)\|^2 < \infty$. We are concerned with evaluating the worst-case ℓ_2 -induced norm over all θ and σ . The system (\mathcal{S}, Θ) shall be said to be uniformly exponentially stable if (\mathcal{S}, Θ) is uniformly exponentially stable.

Definition 7.4. A uniformly exponentially stable switched LPV system (\mathcal{S}, Θ) is said to satisfy *uniform disturbance attenuation level* $\gamma > 0$ if there exists $\tilde{\gamma} \in (0, \gamma)$ such that

$$\sum_{t=0}^\infty \|z(t)\|^2 \leq \tilde{\gamma}^2 \sum_{t=0}^\infty \|w(t)\|^2 \quad (7.15)$$

for all $\theta \in \Theta$, for all $\sigma \in \Lambda^\theta$, and for all w with $\sum_{t=0}^\infty \|w(t)\|^2 < \infty$.

As in the case of pure stability, the disturbance attenuation property of the switched LPV system (\mathcal{S}, Θ) is closely related to that of the switched linear system $(\widehat{\mathcal{S}}, \widehat{\Theta})$, where

$$\begin{aligned} \widehat{\mathcal{S}} &= \{(\mathbf{A}_{ij}, \mathbf{B}_{ij}, \mathbf{C}_{ij}, \mathbf{D}_{ij}) : i = 1, \dots, N, j = 1, \dots, M_i\}, \\ \widehat{\Theta} &= \{(i_0 j_0, i_1 j_1, \dots) : (i_0, i_1, \dots) \in \Theta, j_t = 1, \dots, M_{i_t}, t \in \mathbb{N}_0\}. \end{aligned}$$

The state-space description of the switched linear system $(\widehat{\mathcal{S}}, \widehat{\Theta})$ is given by (7.14), and hence the same as that of the switched LPV system (\mathcal{S}, Θ) , except that it is restricted to switching sequences $(\theta, \sigma) = (\theta(0)\sigma(0), \theta(1)\sigma(1), \dots) \in \widehat{\Theta}$. The system $(\widehat{\mathcal{S}}, \widehat{\Theta})$ is said to be uniformly exponentially stable if $(\widehat{\mathcal{S}}, \widehat{\Theta})$ is uniformly exponentially stable. The performance requirement for $(\widehat{\mathcal{S}}, \widehat{\Theta})$ is consistent with that for (\mathcal{S}, Θ) .

Definition 7.5. A uniformly exponentially stable switched linear system $(\widehat{\mathcal{S}}, \widehat{\Theta})$ is said to satisfy *uniform disturbance attenuation level* $\gamma > 0$ if there exists $\tilde{\gamma} \in (0, \gamma)$ such that (7.15) holds for all $(\theta, \sigma) \in \widehat{\Theta}$ and for all w with $\sum_{t=0}^\infty \|w(t)\|^2 < \infty$.

We will continue to use the convention that $\theta(t) = 0$ and $\sigma(t) = 1$ (i.e., $\Lambda_0 = \{1\}$) for $t < 0$ whenever $\theta \in \Theta$ and $\sigma \in \Lambda^\theta$. Let $\mathcal{L}_M(\Theta)$ and $\mathcal{L}_M(\widehat{\Theta})$ be as in (7.3) for path lengths $M \in \mathbb{N}_0$. The following theorem gives an exact convex condition for the stability and performance of switched LPV systems in terms of linear matrix inequalities.

Theorem 7.3. *Let $\gamma > 0$. The following are equivalent:*

- (a) *The switched LPV system (\mathcal{S}, Θ) is uniformly exponentially stable and satisfies uniform disturbance attenuation level γ .*
- (b) *The switched linear system $(\widehat{\mathcal{S}}, \widehat{\Theta})$ is uniformly exponentially stable and satisfies uniform disturbance attenuation level γ .*
- (c) *There exist a path length $M \in \mathbb{N}_0$ and an indexed (finite) family of matrices $\mathbf{Y}_{(i_1 j_1, \dots, i_M j_M)} \in \mathbb{R}^{n \times n}$ such that*

$$\mathbf{Y}_{(i_0 j_0, \dots, i_{M-1} j_{M-1})} > \mathbf{0}, \quad (7.16a)$$

$$\begin{aligned} & \begin{bmatrix} \mathbf{A}_{i_M j_M} & \mathbf{B}_{i_M j_M} \\ \mathbf{C}_{i_M j_M} & \mathbf{D}_{i_M j_M} \end{bmatrix} \begin{bmatrix} \mathbf{Y}_{(i_0 j_0, \dots, i_{M-1} j_{M-1})} & \mathbf{0} \\ \mathbf{0} & \mathbf{I} \end{bmatrix} \begin{bmatrix} \mathbf{A}_{i_M j_M} & \mathbf{B}_{i_M j_M} \\ \mathbf{C}_{i_M j_M} & \mathbf{D}_{i_M j_M} \end{bmatrix}^T \\ & - \begin{bmatrix} \mathbf{Y}_{(i_1 j_1, \dots, i_M j_M)} & \mathbf{0} \\ \mathbf{0} & \gamma^2 \mathbf{I} \end{bmatrix} < \mathbf{0} \end{aligned} \quad (7.16b)$$

for all $(i_0 j_0, \dots, i_M j_M) \in \mathcal{L}_M(\widehat{\Theta})$.

- (d) *There exist a path length $M \in \mathbb{N}_0$, real numbers $\alpha, \beta > 0$, and an indexed (uncountably infinite) family of matrices $\mathbf{Y}_{(i_1 \lambda_1, \dots, i_M \lambda_M)} \in \mathbb{R}^{n \times n}$ such that*

$$\alpha \mathbf{I} \leq \mathbf{Y}_{(i_0 \lambda_0, \dots, i_{M-1} \lambda_{M-1})} \leq \beta \mathbf{I}, \quad (7.17a)$$

$$\begin{aligned} & \begin{bmatrix} \mathbf{A}_{i_M \lambda_M} & \mathbf{B}_{i_M \lambda_M} \\ \mathbf{C}_{i_M \lambda_M} & \mathbf{D}_{i_M \lambda_M} \end{bmatrix} \begin{bmatrix} \mathbf{Y}_{(i_0 \lambda_0, \dots, i_{M-1} \lambda_{M-1})} & \mathbf{0} \\ \mathbf{0} & \mathbf{I} \end{bmatrix} \begin{bmatrix} \mathbf{A}_{i_M \lambda_M} & \mathbf{B}_{i_M \lambda_M} \\ \mathbf{C}_{i_M \lambda_M} & \mathbf{D}_{i_M \lambda_M} \end{bmatrix}^T \\ & - \begin{bmatrix} \mathbf{Y}_{(i_1 \lambda_1, \dots, i_M \lambda_M)} & \mathbf{0} \\ \mathbf{0} & \gamma^2 \mathbf{I} \end{bmatrix} \leq -\alpha \mathbf{I} \end{aligned} \quad (7.17b)$$

for all $(i_0, \dots, i_M) \in \mathcal{L}_M(\Theta)$ and for all $(\lambda_0, \dots, \lambda_M) \in \Lambda_{i_0} \times \dots \times \Lambda_{i_M}$.

Moreover, if (c) holds with $M \in \mathbb{N}$, then (d) is satisfied with (7.6) for $(\lambda_0, \dots, \lambda_M) \in \Lambda_{i_0} \times \dots \times \Lambda_{i_M}$, where $\lambda_k = (\lambda_k^{(1)}, \dots, \lambda_k^{(M_k)})$, $k = 0, \dots, M$. If (c) holds with $M = 0$, then (d) is satisfied with $\mathbf{Y}_{(i_0 \lambda_0, \dots, i_{M-1} \lambda_{M-1})} = \mathbf{Y}_{(i_1 \lambda_1, \dots, i_M \lambda_M)} = \mathbf{Y}_{01}$.

Proof. We will show (a) \Rightarrow (b) \Rightarrow (c) \Rightarrow (d) \Rightarrow (a). Clearly (a) implies (b). Suppose (b) holds. Then, due to the proof of the necessity part of [7, Theorem 3.3] and a simple scaling argument to take into account $\gamma \neq 1$, there exist $\mathbf{X}_{(i_0 j_0, \dots, i_{M-1} j_{M-1})} > \mathbf{0}$ satisfying

$$\begin{aligned} & \begin{bmatrix} \mathbf{A}_{i_M j_M} & \mathbf{B}_{i_M j_M} \\ \mathbf{C}_{i_M j_M} & \mathbf{D}_{i_M j_M} \end{bmatrix}^T \begin{bmatrix} \mathbf{X}_{(i_1 j_1, \dots, i_M j_M)} & \mathbf{0} \\ \mathbf{0} & \mathbf{I} \end{bmatrix} \begin{bmatrix} \mathbf{A}_{i_M j_M} & \mathbf{B}_{i_M j_M} \\ \mathbf{C}_{i_M j_M} & \mathbf{D}_{i_M j_M} \end{bmatrix} \\ & - \begin{bmatrix} \mathbf{X}_{(i_0 j_0, \dots, i_{M-1} j_{M-1})} & \mathbf{0} \\ \mathbf{0} & \gamma^2 \mathbf{I} \end{bmatrix} < \mathbf{0} \end{aligned}$$

for all $(i_0 j_0, \dots, i_M j_M) \in \mathcal{L}_M(\widehat{\Theta})$. Then the Schur complement formula, along with

$$\mathbf{Y}_{(i_0 j_0, \dots, i_{M-1} j_{M-1})} = \gamma^2 \mathbf{X}_{(i_0 j_0, \dots, i_{M-1} j_{M-1})}^{-1},$$

gives (c). Suppose (c) holds, and assume $M \in \mathbb{N}$ without loss of generality. Since $\mathcal{L}_M(\widehat{\Theta})$ is a finite set, there exist $\alpha, \beta > 0$ such that

$$\alpha \mathbf{I} \leq \mathbf{Y}_{(i_0 j_0, \dots, i_{M-1} j_{M-1})} \leq \beta \mathbf{I} \quad (7.18a)$$

and

$$\begin{bmatrix} \mathbf{A}_{i_M j_M} & \mathbf{B}_{i_M j_M} \\ \mathbf{C}_{i_M j_M} & \mathbf{D}_{i_M j_M} \end{bmatrix} \begin{bmatrix} \mathbf{Y}_{(i_0 j_0, \dots, i_{M-1} j_{M-1})} & \mathbf{0} \\ \mathbf{0} & \mathbf{I} \end{bmatrix} \begin{bmatrix} \mathbf{A}_{i_M j_M} & \mathbf{B}_{i_M j_M} \\ \mathbf{C}_{i_M j_M} & \mathbf{D}_{i_M j_M} \end{bmatrix}^T \\ - \begin{bmatrix} \mathbf{Y}_{(i_1 j_1, \dots, i_M j_M)} & \mathbf{0} \\ \mathbf{0} & \gamma^2 \mathbf{I} \end{bmatrix} < - \begin{bmatrix} \alpha \mathbf{I} & \mathbf{0} \\ \mathbf{0} & \alpha \mathbf{I} \end{bmatrix}$$

for all $(i_0 j_0, \dots, i_M j_M) \in \mathcal{L}_M(\widehat{\Theta})$. Applying the Schur complement formula to the last inequality yields

$$\begin{bmatrix} \alpha \mathbf{I} - \mathbf{Y}_{(i_1 j_1, \dots, i_M j_M)} & \mathbf{0} & \mathbf{A}_{i_M j_M} \mathbf{Y}_{(i_0 j_0, \dots, i_{M-1} j_{M-1})} & \mathbf{B}_{i_M j_M} \\ * & \alpha \mathbf{I} - \gamma^2 \mathbf{I} & \mathbf{C}_{i_M j_M} \mathbf{Y}_{(i_0 j_0, \dots, i_{M-1} j_{M-1})} & \mathbf{D}_{i_M j_M} \\ * & * & -\mathbf{Y}_{(i_0 j_0, \dots, i_{M-1} j_{M-1})} & \mathbf{0} \\ * & * & * & -\mathbf{I} \end{bmatrix} < \mathbf{0}. \quad (7.18b)$$

Given $(i_0, \dots, i_M) \in \mathcal{L}_M(\Theta)$, choose $(\lambda_0, \dots, \lambda_M) \in \Lambda_{i_0} \times \dots \times \Lambda_{i_M}$ with $\lambda_k = (\lambda_k^{(1)}, \dots, \lambda_k^{(M_{i_k})})$ for $k = 0, \dots, M$, where $\Lambda_0 = \{1\}$. Define $\mathbf{Y}_{(i_0 \lambda_0, \dots, i_{M-1} \lambda_{M-1})}$ and $\mathbf{Y}_{(i_1 \lambda_1, \dots, i_M \lambda_M)}$ as in (7.6). Taking the weighted sum of (7.18) with weights given by $(\lambda_0, \dots, \lambda_M)$ then yields (7.17a) and

$$\begin{bmatrix} \alpha \mathbf{I} - \mathbf{Y}_{(i_1 \lambda_1, \dots, i_M \lambda_M)} & \mathbf{0} & \mathbf{A}_{i_M \lambda_M} \mathbf{Y}_{(i_0 \lambda_0, \dots, i_{M-1} \lambda_{M-1})} & \mathbf{B}_{i_M \lambda_M} \\ * & \alpha \mathbf{I} - \gamma^2 \mathbf{I} & \mathbf{C}_{i_M \lambda_M} \mathbf{Y}_{(i_0 \lambda_0, \dots, i_{M-1} \lambda_{M-1})} & \mathbf{D}_{i_M \lambda_M} \\ * & * & -\mathbf{Y}_{(i_0 \lambda_0, \dots, i_{M-1} \lambda_{M-1})} & \mathbf{0} \\ * & * & * & -\mathbf{I} \end{bmatrix} < \mathbf{0}.$$

Using the Schur complement formula once more, we obtain (7.17b). Thus, (d) holds true.

It remains to show (d) implies (a). Suppose (d) holds, so that (7.17) is satisfied for all $(i_0, \dots, i_M) \in \mathcal{L}_M(\Theta)$ and $(\lambda_0, \dots, \lambda_M) \in \Lambda_{i_0} \times \dots \times \Lambda_{i_M}$. Assume $M \in \mathbb{N}$ without loss of generality, and fix a $\theta \in \Theta$ and a $\sigma \in \Lambda^\theta$. Put

$$\mathbf{A}(t) = \mathbf{A}_{\theta(t)\sigma(t)}, \quad \mathbf{B}(t) = \mathbf{B}_{\theta(t)\sigma(t)}, \quad \mathbf{C}(t) = \mathbf{C}_{\theta(t)\sigma(t)}, \quad \mathbf{D}(t) = \mathbf{D}_{\theta(t)\sigma(t)},$$

and

$$\mathbf{Y}(t) = \mathbf{Y}_{(\theta(t-M)\sigma(t-M), \dots, \theta(t-1)\sigma(t-1))}$$

for $t \in \mathbb{N}_0$, so that

$$\alpha \mathbf{I} \leq \mathbf{Y}(t) \leq \beta \mathbf{I},$$

$$\begin{bmatrix} \mathbf{A}(t) & \mathbf{B}(t) \\ \mathbf{C}(t) & \mathbf{D}(t) \end{bmatrix} \begin{bmatrix} \mathbf{Y}(t) & \mathbf{0} \\ \mathbf{0} & \mathbf{I} \end{bmatrix} \begin{bmatrix} \mathbf{A}(t) & \mathbf{B}(t) \\ \mathbf{C}(t) & \mathbf{D}(t) \end{bmatrix}^T - \begin{bmatrix} \mathbf{Y}(t+1) & \mathbf{0} \\ \mathbf{0} & \gamma^2 \mathbf{I} \end{bmatrix} \leq -\alpha \mathbf{I}$$

for all $t \in \mathbb{N}_0$. If we put $\mathbf{X}(t) = \gamma^2 \mathbf{Y}(t)^{-1}$, then there exists an $\eta > 0$, independent of θ and σ , such that

$$\gamma^2 \beta^{-1} \mathbf{I} \leq \mathbf{X}(t) \leq \gamma^2 \alpha^{-1} \mathbf{I},$$

$$\begin{bmatrix} \mathbf{A}(t) & \mathbf{B}(t) \\ \mathbf{C}(t) & \mathbf{D}(t) \end{bmatrix}^T \begin{bmatrix} \mathbf{X}(t+1) & \mathbf{0} \\ \mathbf{0} & \mathbf{I} \end{bmatrix} \begin{bmatrix} \mathbf{A}(t) & \mathbf{B}(t) \\ \mathbf{C}(t) & \mathbf{D}(t) \end{bmatrix} - \begin{bmatrix} \mathbf{X}(t) & \mathbf{0} \\ \mathbf{0} & \gamma^2 \mathbf{I} \end{bmatrix} \leq -\eta \mathbf{I}$$

for all $t \in \mathbb{N}_0$. Thus, by [5, Corollary 12] with an appropriate scaling argument, the linear time-varying system (7.14) is uniformly exponentially stable and satisfies uniform disturbance attenuation level γ . Since $\theta \in \Theta$ and $\sigma \in \Lambda^\theta$ are arbitrary, and since α^{-1} , β^{-1} , and η can be chosen independently of (θ, σ) , we conclude that (a) holds true. \square

Note that, in Theorem 7.3, the Kalman–Yakubovich–Popov (KYP) inequality (7.16) is required to be satisfied over all switching paths in $\mathcal{L}_M(\hat{\Theta})$, including the transient paths that contain the dummy mode-parameter pair 01. Compare this with Theorem 7.1, where the Lyapunov inequality (7.4) is required over a smaller set of switching paths $\mathcal{N}_M(\hat{\Theta})$. If the mode sequence and parameter sequence are fixed, then this agrees with the intuition that, while only the switching paths that occur infinitely many times in the mode sequence is relevant to uniform exponential stability, every switching path including those that never occur more than once in the mode sequence counts as far as disturbance attenuation performance is concerned. Theorems 7.1 and 7.3 make this intuition precise for the case where the mode and parameter sequences are nondeterministic.

7.5 Performance Optimization

Given $l, m_1, m_2, n \in \mathbb{N}$, and given $\mathbf{A}_{ij} \in \mathbb{R}^{n \times n}$, $\mathbf{B}_{1,ij} \in \mathbb{R}^{n \times m_1}$, $\mathbf{B}_{2,ij} \in \mathbb{R}^{n \times m_2}$, $\mathbf{C}_{ij} \in \mathbb{R}^{l \times n}$, $\mathbf{D}_{1,ij} \in \mathbb{R}^{l \times m_1}$, and $\mathbf{D}_{2,ij} \in \mathbb{R}^{l \times m_2}$ for $i = 1, \dots, N$ and for $j = 1, \dots, M_i$, consider the controlled state-space model

$$\begin{aligned} x(t+1) &= \mathbf{A}_{\theta(t)\sigma(t)} x(t) + \mathbf{B}_{1,\theta(t)\sigma(t)} w(t) + \mathbf{B}_{2,\theta(t)\sigma(t)} u(t), & t \in \mathbb{N}_0; \\ z(t) &= \mathbf{C}_{\theta(t)\sigma(t)} x(t) + \mathbf{D}_{1,\theta(t)\sigma(t)} w(t) + \mathbf{D}_{2,\theta(t)\sigma(t)} u(t), & t \in \mathbb{N}_0. \end{aligned} \quad (7.19)$$

Our objective in this section is to extend the result of the previous section to the problem of designing a state-feedback controller that optimizes the disturbance attenuation performance of the closed-loop system. Defining matrix polytopes

$$\begin{aligned}\mathcal{A}_i &= \{\mathbf{A}_{i\lambda} : \lambda \in \Lambda_i\} \subset \mathbb{R}^{n \times n}, \\ \mathcal{B}_{1,i} &= \{\mathbf{B}_{1,i\lambda} : \lambda \in \Lambda_i\} \subset \mathbb{R}^{n \times m_1}, \quad \mathcal{B}_{2,i} = \{\mathbf{B}_{2,i\lambda} : \lambda \in \Lambda_i\} \subset \mathbb{R}^{n \times m_2}, \\ \mathcal{C}_i &= \{\mathbf{C}_{i\lambda} : \lambda \in \Lambda_i\} \subset \mathbb{R}^{l \times n}, \\ \mathcal{D}_{1,i} &= \{\mathbf{D}_{1,i\lambda} : \lambda \in \Lambda_i\} \subset \mathbb{R}^{l \times m_1}, \quad \mathcal{D}_{2,i} = \{\mathbf{D}_{2,i\lambda} : \lambda \in \Lambda_i\} \subset \mathbb{R}^{l \times m_2}\end{aligned}$$

for $i = 1, \dots, N$, let

$$\mathcal{T} = \{(\mathcal{A}_1, \mathcal{B}_{1,1}, \mathcal{B}_{2,1}, \mathcal{C}_1, \mathcal{D}_{1,1}, \mathcal{D}_{2,1}), \dots, (\mathcal{A}_N, \mathcal{B}_{1,N}, \mathcal{B}_{2,N}, \mathcal{C}_N, \mathcal{D}_{1,N}, \mathcal{D}_{2,N})\}.$$

If Θ is a nonempty subset of $\{1, \dots, N\}^\infty$, then the pair (\mathcal{T}, Θ) defines the controlled version of the discrete-time switched LPV system (\mathcal{S}, Θ) considered in the previous section. The system (\mathcal{T}, Θ) is said to be uniformly exponentially stable if (\mathcal{A}, Θ) is uniformly exponentially stable.

We will consider all linear state-feedback controllers that recall L most recent past modes and parameters for some $L \in \mathbb{N}_0$. Let

$$\mathcal{K} = \{\mathbf{K}_{(i_1 \lambda_1, \dots, i_L \lambda_L)} : \lambda_k \in \Lambda_{i_k}, i_k = 0, 1, \dots, N, k = 1, \dots, L\} \subset \mathbb{R}^{m_2 \times n}$$

if $L > 0$, and let $\mathcal{K} = \{\mathbf{K}_{01}\} \subset \mathbb{R}^{m_2 \times n}$ be a singleton if $L = 0$. Then \mathcal{K} defines such a controller, which we call a robust L -path-dependent state-feedback controller. The feedback interconnection of the controlled system (\mathcal{T}, Θ) and a robust path-dependent controller \mathcal{K} gives rise to a closed-loop system of the form

$$\begin{aligned}x(t+1) &= (\mathbf{A}_{\theta(t)\sigma(t)} + \mathbf{B}_{2,\theta(t)\sigma(t)} \mathbf{K}_{(\theta\sigma)_L(t)_-})x(t) + \mathbf{B}_{1,\theta(t)\sigma(t)}w(t), \quad t \in \mathbb{N}_0; \\ z(t) &= (\mathbf{C}_{\theta(t)\sigma(t)} + \mathbf{D}_{2,\theta(t)\sigma(t)} \mathbf{K}_{(\theta\sigma)_L(t)_-})x(t) + \mathbf{D}_{1,\theta(t)\sigma(t)}w(t), \quad t \in \mathbb{N}_0.\end{aligned}\tag{7.20}$$

Definition 7.6. Let $\gamma > 0$ and $L \in \mathbb{N}_0$. A robust L -path-dependent state-feedback controller \mathcal{K} is said to achieve *uniform disturbance attenuation level* γ for the switched LPV system (\mathcal{T}, Θ) if there exists $\tilde{\gamma} \in (0, 1)$ such that the closed-loop state-space model (7.20) is uniformly exponentially stable and satisfies (7.15) for all $\theta \in \Theta$, for all $\sigma \in \Lambda^\theta$, and for all w with $\sum_{t=0}^\infty \|w(t)\|^2 < \infty$.

Theorem 7.4. Let $\gamma > 0$. There exists a robust finite-path-dependent state-feedback controller that stabilizes and achieves uniform disturbance attenuation level γ for the switched LPV system (\mathcal{T}, Θ) if and only if there exist a path length $M \in \mathbb{N}_0$ and indexed (finite) families of matrices $\mathbf{W}_{(i_1 j_1, \dots, i_M j_M)} \in \mathbb{R}^{m_2 \times n}$ and $\mathbf{Y}_{(i_1 j_1, \dots, i_M j_M)} \in$

$\mathbb{R}^{n \times n}$ such that

$$\begin{bmatrix} -\mathbf{Y}_{(i_1 j_1, \dots, i_M j_M)} & \mathbf{0} & \mathbf{F}_{(i_0 j_0, \dots, i_M j_M)} & \mathbf{B}_{1, i_M j_M} \\ * & -\gamma^2 \mathbf{I} & \mathbf{G}_{(i_0 j_0, \dots, i_M j_M)} & \mathbf{D}_{1, i_M j_M} \\ * & * & -\mathbf{Y}_{(i_0 j_0, \dots, i_{M-1} j_{M-1})} & \mathbf{0} \\ * & * & * & -\mathbf{I} \end{bmatrix} < \mathbf{0}, \quad (7.21a)$$

with

$$\mathbf{F}_{(i_0 j_0, \dots, i_M j_M)} = \mathbf{A}_{i_M j_M} \mathbf{Y}_{(i_0 j_0, \dots, i_{M-1} j_{M-1})} + \mathbf{B}_{2, i_M j_M} \mathbf{W}_{(i_0 j_0, \dots, i_{M-1} j_{M-1})}, \quad (7.21b)$$

$$\mathbf{G}_{(i_0 j_0, \dots, i_M j_M)} = \mathbf{C}_{i_M j_M} \mathbf{Y}_{(i_0 j_0, \dots, i_{M-1} j_{M-1})} + \mathbf{D}_{2, i_M j_M} \mathbf{W}_{(i_0 j_0, \dots, i_{M-1} j_{M-1})} \quad (7.21c)$$

for all $(i_0 j_0, \dots, i_M j_M) \in \mathcal{L}_M(\widehat{\Theta})$. Moreover, if (7.21) holds with $M \in \mathbb{N}$, then a robust M -path-dependent state-feedback controller \mathcal{K} that achieves uniform disturbance attenuation level γ for the system (\mathcal{T}, Θ) is given by (7.12) for all $(i_0, \dots, i_M) \in \mathcal{L}_M(\Theta)$ and for all $(\lambda_0, \dots, \lambda_M) \in \Lambda_{i_0} \times \dots \times \Lambda_{i_M}$. If (7.21) holds with $M = 0$, then a robust uniformly exponentially stabilizing state-feedback controller \mathcal{K} is given by $\mathbf{K}_{01} = \mathbf{W}_{01} \mathbf{Y}_{01}^{-1}$.

Proof. The proof is based on Theorem 7.3 but otherwise parallels that of Theorem 7.2, so it is omitted. \square

Theorem 7.4 gives an exact, convex condition for the existence of suboptimal robust finite-path-dependent state-feedback controllers. If an optimal (stabilizing) controller exists, then one can run the sequence of semidefinite programs that minimize γ^2 subject to linear matrix inequalities (7.21) for path lengths $M = 0, 1, \dots$. As in the case of pure stabilization, the minimal value of γ^2 saturates fast as one goes down this sequence of semidefinite programs, and thus trying only the first few path lengths M often suffices in practice.

Theorem 7.4 is a direct extension of Theorem 7.2 to performance optimization, and, hence, it is limited to the synthesis of robust state-feedback controllers that observe the mode and parameter with a unit delay. Again, if the current mode or parameter is available for measurement, then the results in [15] can be used instead.

7.6 Illustrative Examples

Example 1

In this example, we will apply Theorem 7.1 to analyze the stability of a simple switched LPV system (\mathcal{A}, Θ) . Let $N = 2$, $M_1 = M_2 = 2$, and $\Theta = \{1, 2\}^\infty$ (i.e., the mode sequence is unconstrained). Let \mathcal{A} have

$$\mathbf{A}_{11} = \begin{bmatrix} 0.1 & 0.9 \\ 0.0 & 0.1 \end{bmatrix}, \quad \mathbf{A}_{12} = \begin{bmatrix} \alpha & 0 \\ 1 & \alpha \end{bmatrix}, \quad \mathbf{A}_{21} = \mathbf{A}_{11}, \quad \text{and} \quad \mathbf{A}_{22} = \mathbf{A}_{12},$$

where $\alpha > 0$. Since $\mathbf{A}_{11} = \mathbf{A}_{21}$ and $\mathbf{A}_{12} = \mathbf{A}_{22}$, it is easily seen that the switched LPV system (\mathcal{A}, Θ) is equivalent to the LPV system $\{\mathbf{A}_{1\lambda} : \lambda \in \Lambda_1\}$ considered in [6, Example 1], which in turn is equivalent to the switched linear system $(\{\mathbf{A}_{11}, \mathbf{A}_{12}\}, \Theta)$. For each path length $M \in \mathbb{N}_0$, let α_M denote the largest value of α such that the system of Lyapunov inequalities (7.4) is feasible for all $(i_0 j_0, \dots, i_M j_M) \in \mathcal{N}_M(\widehat{\Theta})$, where

$$\mathcal{N}_0(\widehat{\Theta}) = \{11, 12, 21, 22\},$$

$$\mathcal{N}_1(\widehat{\Theta}) = \{(11, 11), (11, 12), (11, 21), (11, 22), (12, 11), \dots, \\ (21, 22), (22, 11), (22, 12), (22, 21), (22, 22)\},$$

and so on. Then, we obtain $\alpha_0 = 0.301$, $\alpha_1 = 0.478$, and $\alpha_2 = \alpha_3 = \dots = 0.513$. Thus, we conclude that $\alpha = 0.513$ is the largest value of α for which the switched LPV system is uniformly exponentially stable. This result agrees with that of [6, Example 1]. Restricting our attention to parameter-dependent Lyapunov functions as in [4] and [3] would yield suboptimal stability bounds $\alpha = 0.422$ and $\alpha = 0.478$, respectively.

Example 2

We will borrow an example from [14] and use Theorem 7.4 to illustrate how optimal disturbance attenuation is achieved for switched LPV systems. Let $N = 6$, $M_1 = \dots = M_6 = 2$, and $\Theta = \{\theta\}$ be a singleton, where

$$\theta = (1, 2, 3, 4, 5, 6, 5, 4, 3, 2, 1, 2, 3, 4, 5, 6, 5, 4, 3, 2, \dots)$$

is of period 10. Let \mathcal{T} have

$$\mathbf{A}_{i1} = \begin{bmatrix} 0.95 & 0.86 \\ -0.1 & -0.02 \end{bmatrix} + \rho_i \begin{bmatrix} -0.19 & -0.5 \\ -0.17 & 0.49 \end{bmatrix}, \quad \mathbf{B}_{1,i1} = \begin{bmatrix} -0.14 \\ -1.58 \end{bmatrix} + \rho_i \begin{bmatrix} -10.5 \\ 10.9 \end{bmatrix}, \\ \mathbf{C}_{i1} = [-0.58 \quad -0.6] + \rho_i [-0.04 \quad -0.05], \\ \mathbf{B}_{2,i1} = \mathbf{B}_{1,i1}, \quad \mathbf{D}_{1,i1} = \mathbf{D}_{2,i1} = 0,$$

and

$$\begin{aligned}\mathbf{A}_{i2} &= \begin{bmatrix} 0.74 & 0.69 \\ 0.08 & 0.13 \end{bmatrix} + \rho_i \begin{bmatrix} -0.18 & -0.21 \\ -0.16 & 0.18 \end{bmatrix}, & \mathbf{B}_{1,i2} &= \begin{bmatrix} -0.51 \\ -0.9 \end{bmatrix} + \rho_i \begin{bmatrix} -1.34 \\ 1.27 \end{bmatrix}, \\ \mathbf{C}_{i2} &= [-0.62 \quad -0.65] + \rho_i [-0.02 \quad -0.03], \\ \mathbf{B}_{2,i2} &= \mathbf{B}_{1,i2}, & \mathbf{D}_{1,i2} &= \mathbf{D}_{2,i2} = 0,\end{aligned}$$

where $\rho_i = \cos((i-1)\pi/5)$ for $i = 1, \dots, 6$. Our objective is to achieve optimal disturbance attenuation performance for the switched LPV system (\mathcal{T}, Θ) via robust finite-path-dependent state feedback. We have

$$\begin{aligned}\mathcal{L}_0(\Theta) &= \{1, 2, 3, 4, 5, 6\}, \\ \mathcal{L}_1(\Theta) &= \{(0, 1), (1, 2), (2, 3), (3, 4), (4, 5), (5, 6), (6, 5), \dots, (2, 1)\}, \\ \mathcal{L}_2(\Theta) &= \{(0, 0, 1), (0, 1, 2), (1, 2, 3), (2, 3, 4), (3, 4, 5), (4, 5, 6), \\ &\quad (5, 6, 5), (6, 5, 4), (5, 4, 3), (4, 3, 2), (3, 2, 1), (2, 1, 2)\},\end{aligned}$$

and so on. It is readily seen that, for this particular Θ , no path length $M > 2$ needs to be considered because all path lengths $M \geq 2$ result in the same system of linear matrix inequalities. It is straightforward to obtain

$$\begin{aligned}\mathcal{L}_2(\hat{\Theta}) &= \{(01, 01, 11), (01, 01, 12), (01, 11, 21), (01, 11, 22), (01, 12, 21), \dots, \\ &\quad (21, 12, 22), (22, 11, 21), (22, 11, 22), (22, 12, 21), (22, 12, 22)\}.\end{aligned}$$

This set contains 86 switching paths. If $\mathbf{B}_{2,i1}$ and $\mathbf{B}_{2,i2}$ were zero for $i = 1, \dots, 6$, then minimizing γ^2 subject to the system of KYP inequalities (7.16), with $\mathbf{B}_{ij} = \mathbf{B}_{1,ij}$ and $\mathbf{D}_{ij} = \mathbf{D}_{1,ij}$, over all $(i_0 j_0, i_1 j_1, i_2 j_2) \in \mathcal{L}_2(\hat{\Theta})$ would yield $\gamma = 7.44$. This is the minimum disturbance attenuation level of the uncontrolled system. However, minimizing γ^2 subject to the system of linear matrix inequalities (7.21) over all $(i_0 j_0, i_1 j_1, i_2 j_2) \in \mathcal{L}_2(\hat{\Theta})$ gives $\gamma = 1.55$, which is the minimum performance bound achievable by a robust finite-path-dependent state-feedback controller. An optimal solution to (7.21) is given by 43 pairs of $\mathbf{W}_{(i_0 j_0, i_1 j_1)}$ and $\mathbf{Y}_{(i_0 j_0, i_1 j_1)}$. The resulting optimal controller takes the form

$$u(t) = \begin{cases} \mathbf{K}_{(01,01)}x(0) & \text{if } t = 0; \\ \mathbf{K}_{(01,\theta(0)\sigma(0))}x(1) & \text{if } t = 1; \\ \mathbf{K}_{(\theta(t-2)\sigma(t-2),\theta(t-1)\sigma(t-1))}x(t), & \text{if } t \geq 2, \end{cases}$$

where, whenever

$$\begin{aligned}\theta(t-2) &= i_0, & \sigma(t-2) &= \lambda_0 = (\lambda_0^{(1)}, \lambda_0^{(2)}), \\ \theta(t-1) &= i_1, & \sigma(t-1) &= \lambda_1 = (\lambda_1^{(1)}, \lambda_1^{(2)}),\end{aligned}$$

we have

$$\begin{aligned}\mathbf{K}_{(01,\theta(0)\sigma(0))} &= \mathbf{W}_{(01,i_0\lambda_0)} \mathbf{Y}_{(01,i_0\lambda_0)}^{-1}, \\ \mathbf{K}_{(\theta(t-2)\sigma(t-2),\theta(t-1)\sigma(t-1))} &= \mathbf{W}_{(i_0\lambda_0,i_1\lambda_1)} \mathbf{Y}_{(i_0\lambda_0,i_1\lambda_1)}^{-1}\end{aligned}$$

with

$$\begin{aligned}\mathbf{Y}_{(01,i_0\lambda_0)} &= \lambda_0^{(1)} \mathbf{Y}_{(01,i_01)} + \lambda_0^{(2)} \mathbf{Y}_{(01,i_02)}, \\ \mathbf{W}_{(01,i_0\lambda_0)} &= \lambda_0^{(1)} \mathbf{W}_{(01,i_01)} + \lambda_0^{(2)} \mathbf{W}_{(01,i_02)}, \\ \mathbf{Y}_{(i_0\lambda_0,i_1\lambda_1)} &= \lambda_0^{(1)} \lambda_1^{(1)} \mathbf{Y}_{(i_01,i_11)} + \cdots + \lambda_0^{(2)} \lambda_1^{(2)} \mathbf{Y}_{(i_02,i_12)}, \\ \mathbf{W}_{(i_0\lambda_0,i_1\lambda_1)} &= \lambda_0^{(1)} \lambda_1^{(1)} \mathbf{W}_{(i_01,i_11)} + \cdots + \lambda_0^{(2)} \lambda_1^{(2)} \mathbf{W}_{(i_02,i_12)}.\end{aligned}$$

Example 3

We will now consider the example studied in [15, Sect. 5]. Let $N = 2$, $M_1 = M_2 = 2$, and $\Theta = \{1, 2\}^\infty$. Let \mathcal{S} have

$$\begin{aligned}\mathbf{A}_{11} &= \begin{bmatrix} 0 & 1 & 0 \\ 0 & 0 & 1 \\ 0.0341 & -0.2571 & 0.7769 \end{bmatrix}, \quad \mathbf{B}_{1,11} = \begin{bmatrix} 0.3 \\ 0.1 \\ 0.8 \end{bmatrix}, \quad \mathbf{B}_{2,11} = \begin{bmatrix} 0 \\ -0.1 \\ -0.5 \end{bmatrix}, \\ \mathbf{C}_{11} &= [0.2 \ 0.1 \ 1], \quad \mathbf{D}_{1,11} = \mathbf{D}_{2,11} = 0, \\ \mathbf{A}_{12} &= \begin{bmatrix} 0 & 1 & 0 \\ 0 & 0 & 1 \\ -0.0341 & -0.2571 & -0.7769 \end{bmatrix}, \quad \mathbf{B}_{1,12} = \begin{bmatrix} 0.3 \\ 0.1 \\ -0.8 \end{bmatrix}, \quad \mathbf{B}_{2,12} = \begin{bmatrix} 0 \\ -0.2 \\ -0.3 \end{bmatrix}, \\ \mathbf{C}_{12} &= [-0.2 \ 0.1 \ 1], \quad \mathbf{D}_{1,12} = \mathbf{D}_{2,12} = 0, \\ \mathbf{A}_{21} &= \begin{bmatrix} 0 & -1 & 0 \\ 0 & 0 & 1 \\ 0.0341 & -0.2571 & 0.7769 \end{bmatrix}, \quad \mathbf{B}_{1,21} = \begin{bmatrix} -0.3 \\ 0.1 \\ 0.8 \end{bmatrix}, \quad \mathbf{B}_{2,21} = \begin{bmatrix} 0 \\ -0.1 \\ -0.8 \end{bmatrix}, \\ \mathbf{C}_{21} &= [0.2 \ 0.1 \ -1], \quad \mathbf{D}_{1,21} = \mathbf{D}_{2,21} = 0, \\ \mathbf{A}_{22} &= \begin{bmatrix} 0 & -1 & 0 \\ 0 & 0 & 1 \\ -0.0341 & -0.2571 & -0.7769 \end{bmatrix}, \quad \mathbf{B}_{1,22} = \begin{bmatrix} -0.3 \\ 0.1 \\ -0.8 \end{bmatrix}, \quad \mathbf{B}_{2,22} = \begin{bmatrix} 0 \\ -1 \\ -0.5 \end{bmatrix}, \\ \mathbf{C}_{22} &= [-0.2 \ 0.1 \ -1], \quad \mathbf{D}_{1,22} = \mathbf{D}_{2,22} = 0.\end{aligned}$$

The objective is to obtain a robust finite-path-dependent state-feedback controller that achieves a desired disturbance attenuation performance for the switched LPV system (\mathcal{F}, Θ) . We have

$$\begin{aligned}\mathcal{L}_0(\Theta) &= \{1, 2\}, \\ \mathcal{L}_1(\Theta) &= \{(0, 1), (0, 2), (1, 1), (1, 2), (2, 1), (2, 2)\}, \\ \mathcal{L}_2(\Theta) &= \{(0, 0, 1), (0, 0, 2), (0, 1, 1), (0, 1, 2), (0, 2, 1), (0, 2, 2), (1, 1, 1), \\ &\quad (1, 1, 2), (1, 2, 1), (1, 2, 2), (2, 1, 1), (2, 1, 2), (2, 2, 1), (2, 2, 2)\},\end{aligned}$$

and so on. With path length $M = 0$, minimizing γ^2 subject to (7.21) for all mode-parameter pairs in $\mathcal{L}_0(\hat{\Theta})$ gives $\gamma = 4.38$, and a robust state-feedback controller $u(t) = \mathbf{K}_{01}x(t)$, $t \in \mathbb{N}_0$, that achieves this performance level is given by

$$\begin{aligned}\mathbf{K}_{01} &= \mathbf{W}_{01} \mathbf{Y}_{01}^{-1} = [-5.03 \quad -26.6 \quad 2.13] \begin{bmatrix} 85.0 & 10.2 & -4.84 \\ 10.2 & 54.4 & -3.68 \\ -4.84 & -3.68 & 3.33 \end{bmatrix}^{-1} \\ &= [0.00483 \quad -0.481 \quad 0.115].\end{aligned}$$

This result coincides with that in [15, Sect. 5]. However, if past modes and parameters are available to the controller, then a better-performing controller can be obtained by considering a path length $M > 0$. Indeed, if γ_M denotes the minimum achievable disturbance attenuation level by a robust M -path-dependent state-feedback controller, then we have $\gamma_0 = 4.38, \gamma_1 = 4.28, \gamma_2 = 4.14, \gamma_3 = 4.14, \dots$. Moreover, if either the current mode or the current parameter is available to the controller, then one can lower the performance level further by using mode-dependent and parameter-dependent controllers as in [15].

7.7 Conclusion

We extended existing nonconservative analysis and synthesis results for switched linear systems and polytopic LPV systems to switched LPV systems. These extensions are again nonconservative, and provide convex analysis and synthesis conditions in terms of linear matrix inequalities. In particular, the stability and performance analysis conditions cover existing but conservative results in the literature, and allow us to pay additional computational cost in return for a better analysis. On the other hand, the controller synthesis conditions are useful for the case where neither the system mode nor the system parameter is observed without delay, and thus complements existing results. We envision that the results of this work could play an important role in automated analysis and synthesis for control of nonlinear systems.

References

1. Apkarian P, Gahinet P (1995) A convex characterization of gain-scheduled H_∞ controllers. *IEEE Trans Automat Contr* 40(5):853–864
2. Blanchini F, Miani S (2003) Stabilization of LPV systems: state feedback, state estimation, and duality. *SIAM J Contr Optim* 42(1):76–97
3. Daafouz J, Bernussou J (2001) Parameter dependent Lyapunov functions for discrete time systems with time varying parametric uncertainties. *Syst Contr Lett* 43(5):355–359
4. de Oliveira MC, Bernussou J, Geromel JC (1999) A new discrete-time robust stability condition. *Syst Contr Lett* 37(4):261–265
5. Dullerud GE, Lall S (1999) A new approach for analysis and synthesis of time-varying systems. *IEEE Trans Automat Contr* 44(8):1486–1497
6. Lee J-W (2006) On uniform stabilization of discrete-time linear parameter-varying control systems. *IEEE Trans Automat Contr* 51(10):1714–1721
7. Lee J-W, Dullerud GE (2006) Optimal disturbance attenuation for discrete-time switched and Markovian jump linear systems. *SIAM J Contr Optim* 45(4):1329–1358
8. Lee J-W, Dullerud GE (2006) Uniform stabilization of discrete-time switched and Markovian jump linear systems. *Automatica* 42(2):205–218
9. Lescher F, Zhao JY, Borne P (2006) Switching LPV controllers for a variable speed pitch regulated wind turbine. *Int J Comp Commun Contr* 1(4):73–84
10. Lim S, How JP (2003) Modeling and H_∞ control for switched linear parameter-varying missile autopilot. *IEEE Trans Contr Syst Technol* 11(6):830–838
11. Lu B, Wu F (2004) Switching LPV control designs using multiple parameter-dependent Lyapunov functions. *Automatica* 40(11):1973–1980
12. Lu B, Wu F, Kim SW (2006) Switching LPV control of an F-16 aircraft via controller state reset. *IEEE Trans Contr Syst Technol* 14(2):267–277
13. Shamma JS, Athans M (1991) Guaranteed properties of gain scheduled control for linear parameter-varying plants. *Automatica* 27(3):559–564
14. Zhang L, Shi P (2008) $\ell_2 - \ell_\infty$ model reduction for switched LPV systems with average-dwell time. *IEEE Trans Automat Contr* 53(10):2443–2448
15. Zhang L, Shi P, Boukas EK, Wang C (2006) H_∞ control of switched linear discrete-time systems with polytopic uncertainties. *Optim Contr Applicat Meth* 27(5):273–291

Chapter 8

Gain-Scheduled Output-Feedback Controllers with Good Implementability and Robustness

Masayuki Sato and Dimitri Peaucelle

Abstract This article addresses the design problem of gain-scheduled output-feedback (GSOF) controllers, which depend on inexactly provided scheduling parameters, for continuous-time linear parameter-varying (LPV) systems via parameter-dependent Lyapunov functions (PDLFs). We successfully propose a new design method for our problem. That is, in stark contrast to conventional design methods, our method produces practical GSOF controllers being independent of the derivatives of scheduling parameters, i.e., good implementability is assured, and depending only on inexactly provided scheduling parameters, i.e., robustness against the uncertainties on the scheduling parameters is also assured. For further good implementability of GSOF controllers, we show that it is always possible to obtain polynomially parameter-dependent GSOF controllers if rationally parameter-dependent GSOF controllers can be designed for LPV systems under a very mild constraint.

8.1 Introduction

It has been demonstrated by many researchers that gain-scheduled (GS) controllers have better performance than robust linear time-invariant (LTI) controllers when scheduling parameters, which describe changes of plant dynamics, are available. Therefore, many researchers have already tackled the design problem of GS output-feedback (GSOF) controllers for linear parameter-varying (LPV) systems using

M. Sato (✉)

Japan Aerospace Exploration Agency, 6-13-1 Osawa, Mitaka, Tokyo 181-0015, Japan
e-mail: sato.masayuki@jaxa.jp

D. Peaucelle

CNRS; LAAS; 7, avenue du Colonel Roche, F-31077 Toulouse, France

Universite de Toulouse; UPS, INSA, INP, ISAE, UTM, UT1; LAAS; F-31077 Toulouse, France
e-mail: peaucelle@laas.fr

Table 8.1 Classification of existing design methods

		Exact scheduling parameters	Inexact scheduling parameters
PiDLFs		[3–5, 27]	[12, 20, 30, 32]
PDLFs	GSOFC controllers <i>depending</i> on derivatives of scheduling parameters	[1, 2, 35, 41, 42]	[17]
	GSOFC controllers <i>independent</i> of derivatives of scheduling parameters	[1, 14, 18, 33, 34]	Our target

linear matrix inequalities (LMIs), e.g., [1–5, 15, 21, 28, 35, 41, 42] and references therein. Furthermore, some applications of GSOFC controllers to real systems have been reported [22, 23, 40]. Thus, the design technique for GSOFC controllers seems to be matured like H_∞ controller design [44].

Existing design methods of GSOFC controllers for continuous-time LPV systems are classified in Table 8.1 according to the parameter dependency of the adopted Lyapunov functions in the design process and to the exactness of the exploited scheduling parameters in the GSOFC controllers. In Table 8.1, “PiDLFs” and “PDLFs” respectively denote “Parameter-independent Lyapunov Functions” and “Parameter-Dependent Lyapunov Functions”.

When GS controllers are designed to real systems, the following requirements should be considered:

- Reduction of conservatism
- Good implementability of controllers
- Robustness against uncertainties in the provided scheduling parameters

When GS state-feedback (GSSF) controllers are considered, these requirements are easily met by the conventional change-of-variable method [6] with controller matrix and the inverse of Lyapunov matrix being dependent on uncertain scheduling parameters instead of actual scheduling parameters [31]. (For reference, the method is shown in the appendix.) However, when GSOFC controllers are considered, meeting these requirements is not so easy.

We review existing methods of GSOFC controllers from viewpoints of these requirements.

For the first requirement, several methods using PDLFs have been proposed [1, 35, 41, 42]. Those methods successfully reduce conservatism due to PiDLFs used in [3–5]; that is, the first requirement is met by applying the methods in [1, 35, 41, 42]. However, the designed controllers require not only the scheduling parameters but also their derivatives. Generally speaking, the derivatives of scheduling parameters cannot be obtained in the real world. This property contradicts the second requirement. Several remedies for this issue have been proposed with the first requirement being simultaneously considered, e.g., controller implementation incorporating filters for provided scheduling parameters [18], controller design via PDLFs with structured parameter dependency [1], and controller design using sufficient conditions in which the term including the derivatives of scheduling

parameters is overbounded by another tractable term [14,33,34]. Sato and Peaucelle [34] is an extended version of [33]. Incorporating filters is an attractive method from a theoretical point of view, as the method recovers the best achievable performance by the methods in [1, 35, 42] if the time constants of the filters are set to be sufficiently small. However, this remedy is not so good from a practical point of view because the incorporated filters increase the online calculations. The structured PDLFs used in the remedy in [1] are not recommended from the standpoint of the first requirement. The methods in [14, 34] are attractive because there are no restrictions on the parameter dependency of PDLFs, which is different from the remedy in [1], and designed controllers introduce no additional systems, which is different from the method in [18]. A numerical example in [34] demonstrates that the performance degradation from the method in [1], which is caused by overbounding the derivative term, is very small (less than 5%). Thus, the methods in [14, 34] are recommended from the standpoints of the first and the second requirements.

There have been several papers for tackling the third requirement, e.g., [12, 17, 20, 30, 32]. The methods in [17, 20] evaluate the effect of the uncertainties in provided scheduling parameters by introducing an additional uncertain block in the H_∞ control problem. However, in general, multiple uncertain blocks lead to conservative controllers. The problem setting in [12] is slightly impractical because the uncertainties are supposed to be proportional to the actual scheduling parameters. In other words, if some scheduling parameters are almost zeros, then the related uncertainties are also assumed to be almost zeros. Thus, bias errors cannot be addressed by the method in [12]. On the other hand, the method in [30] (the journal version is [32]) is attractive because it can design GSOF controllers which are robust against bias-type uncertainties, and recovers the conventional design method when the exact values of scheduling parameters are provided. Thus, if the provided scheduling parameters have bias-type uncertainties, then the method in [30, 32] is recommended. However, PiDLFs were adopted in those papers for deriving the design method, which contradicts the first requirement.

This article tackles the design problem of GSOF controllers exploiting inexact scheduling parameters for continuous-time LPV systems via PDLFs with the controllers incorporating no additional systems (such as filters) and being independent of the derivatives of the provided scheduling parameters. That is, the controllers to be designed are required to have good implementability as well as robustness against uncertainties on the scheduling parameters. To meet these requirements, the methods in [32,34] are combined, and a new design method is successfully proposed in this article. Our method is formulated in terms of parameter-dependent bilinear matrix inequalities (PDBMIs). As well known, it is very hard to obtain the optima of the problems formulated with PDBMIs, two tractable algorithms for suboptimal solutions by solving parameter-dependent LMIs (PDLMI) are shown.

This article is organized as follows: Section 8.2 first defines LPV systems and GSOF controllers to be designed, then defines our problem, and finally shows basic lemmas related to our problem. Section 8.3 first shows our method, then gives some remarks on conservatism of the method, and finally shows that it is always possible to obtain polynomially parameter-dependent GSOF controllers if rationally

parameter-dependent GSOF controllers can be designed. Section 8.4 shows design results for numerical examples borrowed from the literature to support our results. Finally, Sect. 8.5 gives concluding remarks.

As mentioned above, solving PDLMI are required in our method. Several books and many papers on this topic have been published, e.g., [8–10, 13]. Considering that sum-of-squares (SOS) techniques [9, 24, 37] is one of the powerful methods for solving PDLMI and that the slack variable (SV) approach encompasses SOS techniques [25], this article adopts the SV approach for solving PDLMI. Thus, a very brief description of the SV approach is given in the appendix.

In this article, we use the following notations: $\text{He}\{X\}$ is a shorthand notation for $X + X^T$, I_n , \mathbf{I} and $\mathbf{0}$, respectively, denote an $n \times n$ dimensional identity matrix, an identity matrix and a zero matrix of appropriate dimensions, \mathbb{R}^n , $\mathbb{R}^{n \times m}$ and \mathbb{S}^n respectively denote sets of n dimensional real vectors, $n \times m$ dimensional real matrices and $n \times n$ dimensional symmetric real matrices, \otimes denotes the Kronecker product, $*$ denotes an abbreviated off-diagonal block in a symmetric matrix, $\text{Tr}(X)$ for a square matrix X denotes the matrix trace, and $\text{diag}(X_1, \dots, X_k)$ denotes a block-diagonal matrix composed of X_1, \dots, X_k .

8.2 Preliminaries

8.2.1 System Definitions

Suppose that a continuous-time LPV system $G(\theta)$ with k independent scheduling parameters $\theta = [\theta_1 \ \dots \ \theta_k]^T$ is given as follows:

$$G(\theta) : \begin{cases} \dot{x} = A(\theta)x + B_1(\theta)w + B_2u \\ z = C_1(\theta)x + D_{11}(\theta)w + D_{12}(\theta)u \\ y = C_2x + D_{21}(\theta)w \end{cases}, \quad (8.1)$$

where $x \in \mathbb{R}^n$, $w \in \mathbb{R}^{n_w}$, $u \in \mathbb{R}^{n_u}$, $z \in \mathbb{R}^{n_z}$, and $y \in \mathbb{R}^{n_y}$ respectively denote the state with $x = \mathbf{0}$ at $t = 0$, the disturbance input, the control input, the controlled output, and the measurement output. The state-space matrices in (8.1) are supposed to have compatible dimensions.

As indicated in (8.1), we make the following assumption:

Assumption 8.1. *Matrices B_2 and C_2 are constant.*

This assumption slightly restricts the applicability of the method exposed hereafter. One of the simplest methods to satisfy this assumption is to incorporate strictly proper LTI filters to the original signals u and y [4]. If not adding filters and if only one of B_2 or C_2 is indeed parameter dependent, the method we expose remains valid with appropriate modifications, although more complex. (See Remark 8.5 in the next section.)

The parameter dependency of $G(\theta)$ may be quite general. Nevertheless, we address the design problem assuming that the state-space matrices of $G(\theta)$ are polynomial with respect to θ . This assumption plus the choice of polynomially parameter-dependent decision variables makes it possible to solve the PDLMIIs that we will encounter, for example by using SOS techniques [9, 24, 37] or the SV approach [25].

Assumption 8.2. *All state-space matrices of LPV system $G(\theta)$ are supposed to be polynomial with respect to the parameters θ_i ; that is, their values are supposed to be continuous and bounded in the domain defined hereafter.*

The scheduling parameters θ_i and the derivatives of the scheduling parameters with respect to time $\dot{\theta}_i$ are supposed to lie in a priori given hyper-rectangles Ω_θ and Λ_θ , respectively; that is, the following holds for θ and $\dot{\theta} = [\dot{\theta}_1 \cdots \dot{\theta}_k]^T$:

$$\begin{cases} \theta(t) \in \Omega_\theta, \forall t \geq 0 \\ \dot{\theta}(t) \in \Lambda_\theta, \forall t \geq 0 \end{cases}. \quad (8.2)$$

It is supposed that Λ_θ includes the origin.

We consider a full-order GSOF controller for LPV system $G(\theta)$. In stark contrast to conventional problem setting, it is supposed that the values of the scheduling parameters are provided not accurately but with some uncertainties; that is, the i -th scheduling parameter is provided as $\theta_i + \delta_i$ with its uncertainty δ_i . In this practical situation, we define a full-order GSOF controller $K(\theta + \delta)$ as follows:

$$K(\theta + \delta) : \begin{cases} \dot{x}_K = A_K(\theta + \delta)x_K + B_K(\theta + \delta)y \\ u = C_K(\theta + \delta)x_K + D_K(\theta + \delta)y \end{cases}, \quad (8.3)$$

where $x_K \in \mathbb{R}^n$ denotes the state with $x_K = \mathbf{0}$ at $t = 0$, and matrices $A_K(\theta + \delta)$, etc. are appropriately dimensioned parameter-dependent matrices to be designed. Vector $\delta = [\delta_1 \cdots \delta_k]^T$ denotes the uncertainties on the scheduling parameters. It is supposed that the bounds of the uncertainties are given a priori; that is, the uncertainties δ_i are supposed to lie in a hyper-rectangle Ω_δ which is known in advance.

$$\delta(t) \in \Omega_\delta, \forall t \geq 0. \quad (8.4)$$

Furthermore, the derivatives of the uncertainties with respect to time $\dot{\delta}_i$ are also supposed to lie in a priori given hyper-rectangle Λ_δ ; that is, the following holds for $\dot{\delta} = [\dot{\delta}_1 \cdots \dot{\delta}_k]^T$:

$$\dot{\delta}(t) \in \Lambda_\delta, \forall t \geq 0. \quad (8.5)$$

It is also supposed that Λ_δ includes the origin.

This assumption seems to be impractical; however, if there are several occasions to measure scheduling parameters before designing controllers, it is possible to estimate the bounds of the derivatives of the uncertainties. Otherwise, the bounds should be set to be sufficiently large.

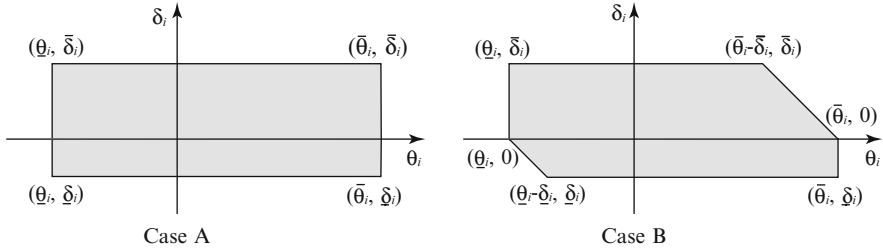


Fig. 8.1 Region of pair of (θ_i, δ_i) (Case A: δ_i is independent of θ_i , Case B: δ_i depends on θ_i and provided scheduling parameter $\theta_i + \delta_i$ is bounded by $\underline{\theta}_i$ and $\bar{\theta}_i$, where $\underline{\delta}_i \leq 0 \leq \bar{\delta}_i$ is supposed)

The closed-loop system $G_{\text{cl}}(\theta, \theta + \delta)$ comprising $G(\theta)$ in (8.1) and $K(\theta + \delta)$ in (8.3) is given as follows:

$$G_{\text{cl}}(\theta, \theta + \delta) : \begin{cases} \dot{x}_{\text{cl}} = A_{\text{cl}}(\theta, \theta + \delta)x_{\text{cl}} + B_{\text{cl}}(\theta, \theta + \delta)w \\ z = C_{\text{cl}}(\theta, \theta + \delta)x_{\text{cl}} + D_{\text{cl}}(\theta, \theta + \delta)w \end{cases}, \quad (8.6)$$

where $x_{\text{cl}} = [x^T \ x_K^T]^T$, and

$$\begin{cases} A_{\text{cl}}(\theta, \theta + \delta) = \bar{A}(\theta) + \bar{B}_2 \bar{K}(\theta + \delta) \bar{C}_2 \\ B_{\text{cl}}(\theta, \theta + \delta) = \bar{B}_1(\theta) + \bar{B}_2 \bar{K}(\theta + \delta) \bar{D}_{21}(\theta) \\ C_{\text{cl}}(\theta, \theta + \delta) = \bar{C}_1(\theta) + \bar{D}_{12}(\theta) \bar{K}(\theta + \delta) \bar{C}_2 \\ D_{\text{cl}}(\theta, \theta + \delta) = \bar{D}_{11}(\theta) + \bar{D}_{12}(\theta) \bar{K}(\theta + \delta) \bar{D}_{21}(\theta) \end{cases} \quad (8.7)$$

with $\bar{K}(\theta + \delta) = \begin{bmatrix} A_K(\theta + \delta) & B_K(\theta + \delta) \\ C_K(\theta + \delta) & D_K(\theta + \delta) \end{bmatrix}$ and the following matrices:

$$\begin{bmatrix} \bar{A}(\theta) & \bar{B}_1(\theta) & \bar{B}_2 \\ \bar{C}_1(\theta) & \bar{D}_{11}(\theta) & \bar{D}_{12}(\theta) \\ \bar{C}_2 & \bar{D}_{21}(\theta) & \end{bmatrix} = \begin{bmatrix} A(\theta) & \mathbf{0} & B_1(\theta) & \mathbf{0} & B_2 \\ \mathbf{0} & \mathbf{0} & \mathbf{0} & I_n & \mathbf{0} \\ \bar{C}_1(\theta) & \mathbf{0} & \bar{D}_{11}(\theta) & \mathbf{0} & \bar{D}_{12}(\theta) \\ \mathbf{0} & I_{n_1} & \mathbf{0} & & \\ C_2 & \mathbf{0} & \bar{D}_{21}(\theta) & & \end{bmatrix}.$$

Remark 8.1. In the problem setting above, the uncertainties on scheduling parameters are supposed to be independent of the scheduling parameters. (See Case A in Fig. 8.1 where θ_i and δ_i are supposed to satisfy $\underline{\theta}_i \leq \theta_i \leq \bar{\theta}_i$ and $\underline{\delta}_i \leq \delta_i \leq \bar{\delta}_i$ respectively.) However, if the provided scheduling parameter $\theta_i + \delta_i$ with its uncertainty δ_i satisfying $\underline{\delta}_i \leq \delta_i \leq \bar{\delta}_i$ does not exceed the physically defined bounds $\underline{\theta}_i$ and $\bar{\theta}_i$, i.e., $\underline{\theta}_i \leq \theta_i + \delta_i \leq \bar{\theta}_i$, then the region of the pair (θ_i, δ_i) should be revised to conform the physical bounds; that is, the pair (θ_i, δ_i) should lie in the gray region depicted in Case B in Fig. 8.1. This revision conforms the physical bounds of the scheduling parameter, but also increases the number of vertices compared to Case A.

8.2.2 Problem Definitions

We tackle the following problems.

Problem 8.1 (H_∞ control-type problem). For a given positive number γ_∞ , design a GSOF controller $K(\theta + \delta)$ depending solely on the provided scheduling parameters $\theta_i + \delta_i$ which stabilizes the closed-loop system $G_{cl}(\theta, \theta + \delta)$ and satisfies (8.8) for all admissible quadruplets $(\theta, \dot{\theta}, \delta, \dot{\delta}) \in \Omega_\theta \times \Lambda_\theta \times \Omega_\delta \times \Lambda_\delta$.

$$\sup_{w \in \mathcal{L}_2, w \neq \mathbf{0}} \frac{\|z\|_2}{\|w\|_2} < \gamma_\infty. \quad (8.8)$$

Problem 8.2 (H_2 control-type problem). Suppose that $D_{11}(\theta) = \mathbf{0}$ holds for all θ . For a given positive number γ_2 , design a GSOF controller $K(\theta + \delta)$ depending solely on the provided scheduling parameters $\theta_i + \delta_i$ with $D_K(\theta + \delta) = \mathbf{0}$ which stabilizes the closed-loop system $G_{cl}(\theta, \theta + \delta)$ and satisfies (8.9) for all admissible quadruplets $(\theta, \dot{\theta}, \delta, \dot{\delta}) \in \Omega_\theta \times \Lambda_\theta \times \Omega_\delta \times \Lambda_\delta$.

$$\mathcal{E} \left(\int_0^\infty z^T z dt \right) < \gamma_2^2 \text{ for } w = \begin{cases} w_0 (t=0) \\ \mathbf{0} (t \neq 0) \end{cases}, \quad (8.9)$$

with a random variable w_0 satisfying $\mathcal{E}(w_0 w_0^T) = I_{n_w}$.

These problem settings above are natural and practical, because the designed controllers are required to be independent of the derivatives of the scheduling parameters, i.e., good implementability is required, and the provided scheduling parameters are supposed to be inexact, i.e., robustness against the uncertainties on the scheduling parameters is also required.

8.2.3 Basic Lemmas

We show basic lemmas related to our problems.

Hereafter, for continuously differentiable parameter-dependent matrices $X(\theta)$ and $X(\theta + \delta)$, $\dot{X}(\theta)$ and $\dot{X}(\theta + \delta)$, respectively, denote $\frac{d}{dt}X(\theta) = \sum_{i=1}^k \frac{d\theta_i}{dt} \frac{\partial X(\theta)}{\partial \theta_i}$ and $\frac{d}{dt}X(\theta + \delta) = \sum_{i=1}^k \left(\frac{d\theta_i}{dt} \frac{\partial X(\theta + \delta)}{\partial \theta_i} + \frac{d\delta_i}{dt} \frac{\partial X(\theta + \delta)}{\partial \delta_i} \right)$.

Suppose that some controller $K(\theta + \delta)$ defined in (8.3) is given. Then, the following lemmas are directly derived from the results in [39, 42] by considering the uncertainty vector δ in $K(\theta + \delta)$ to be an additional parameter vector.

Lemma 8.1 ([31]). For a given positive number γ_∞ , if there exists a continuously differentiable parameter-dependent matrix $X_{cl}(\theta + \delta) \in \mathbb{S}^{2n}$ such that (8.10) and

(8.11) hold, then the closed-loop system $G_{\text{cl}}(\theta, \theta + \delta)$ is exponentially stable and satisfies (8.8) for all admissible quadruplets $(\theta, \dot{\theta}, \delta, \dot{\delta}) \in \Omega_\theta \times \Lambda_\theta \times \Omega_\delta \times \Lambda_\delta$.

$$X_{\text{cl}}(\theta + \delta) > 0, \quad \forall (\theta, \delta) \in \Omega_\theta \times \Omega_\delta, \quad (8.10)$$

$$\left[\begin{array}{cc} \text{He}\{A_{\text{cl}}(\theta, \theta + \delta)X_{\text{cl}}(\theta + \delta)\} - \dot{X}_{\text{cl}}(\theta + \delta) & * & B_{\text{cl}}(\theta, \theta + \delta) \\ C_{\text{cl}}(\theta, \theta + \delta)X_{\text{cl}}(\theta + \delta) & -\gamma_\infty I_{n_z} & D_{\text{cl}}(\theta, \theta + \delta) \\ * & * & -\gamma_\infty I_{n_w} \end{array} \right] < 0, \\ \forall (\theta, \dot{\theta}, \delta, \dot{\delta}) \in \Omega_\theta \times \Lambda_\theta \times \Omega_\delta \times \Lambda_\delta. \quad (8.11)$$

Lemma 8.2 ([31]). Suppose that $D_{\text{cl}}(\theta, \theta + \delta) = \mathbf{0}$ holds for all pairs (θ, δ) . For a given positive number γ_2 , if there exist a continuously differentiable parameter-dependent matrix $X_{\text{cl}}(\theta + \delta) \in \mathbb{S}^{2n}$ and a parameter-dependent matrix $Q(\theta, \theta + \delta) \in \mathbb{S}^{n_w}$ such that (8.12), (8.13) and (8.14) hold, then the closed-loop system $G_{\text{cl}}(\theta, \theta + \delta)$ is exponentially stable and satisfies (8.9) for all admissible quadruplets $(\theta, \dot{\theta}, \delta, \dot{\delta}) \in \Omega_\theta \times \Lambda_\theta \times \Omega_\delta \times \Lambda_\delta$.

$$\left[\begin{array}{cc} \text{He}\{A_{\text{cl}}(\theta, \theta + \delta)X_{\text{cl}}(\theta + \delta)\} - \dot{X}_{\text{cl}}(\theta + \delta) & * \\ C_{\text{cl}}(\theta, \theta + \delta)X_{\text{cl}}(\theta + \delta) & -I_{n_z} \end{array} \right] < 0, \\ \forall (\theta, \dot{\theta}, \delta, \dot{\delta}) \in \Omega_\theta \times \Lambda_\theta \times \Omega_\delta \times \Lambda_\delta, \quad (8.12)$$

$$\left[\begin{array}{cc} Q(\theta, \theta + \delta) & * \\ B_{\text{cl}}(\theta, \theta + \delta) & X_{\text{cl}}(\theta + \delta) \end{array} \right] > 0, \quad \forall (\theta, \delta) \in \Omega_\theta \times \Omega_\delta, \quad (8.13)$$

$$\gamma_2^2 > \text{Tr}(Q(\theta, \theta + \delta)), \quad \forall (\theta, \delta) \in \Omega_\theta \times \Omega_\delta. \quad (8.14)$$

Results we derive in the next section are based on the linearizing change-of-variables in [11, 36] and its simplified version in [19] for LTI controller design. The result relies on a factorization of the inverse of the Lyapunov matrix such that $X_{\text{cl}} = \Pi_1 \Pi_2^{-1}$ with $\Pi_1 = \begin{bmatrix} \mathcal{X} & I_n \\ \mathcal{Y}^T & \mathbf{0} \end{bmatrix}$ and $\Pi_2 = \begin{bmatrix} I_n & \mathcal{Z} \\ \mathbf{0} & \mathcal{N}^T \end{bmatrix}$, where \mathcal{Y} and \mathcal{N} are any matrices such that $I_n - \mathcal{X}\mathcal{Z} = \mathcal{Y}\mathcal{N}^T$. One possible choice of these \mathcal{Y} and \mathcal{N} matrices is $\mathcal{Y} = \mathcal{X} - \mathcal{Z}^{-1}$ and $\mathcal{N} = -\mathcal{Z}$ (details about this choice in GS controller design can be found in [29]). For this choice, the invertible change-of-variables amounts to replacing the control gain matrices by

$$\bar{K} = \begin{bmatrix} -\mathcal{Z}^{-1} & B_2 \\ \mathbf{0} & I_{n_u} \end{bmatrix} \left(\mathcal{K} - \begin{bmatrix} \mathcal{Z}A\mathcal{X} & \mathbf{0} \\ \mathbf{0} & \mathbf{0} \end{bmatrix} \right) \begin{bmatrix} \mathcal{Y}^{-1} & \mathbf{0} \\ -C_2\mathcal{X}\mathcal{Y}^{-1} & I_{n_y} \end{bmatrix}, \quad (8.15)$$

where \mathcal{K} is a full matrix containing the new decision variables. Other choices of \mathcal{Y} and \mathcal{N} are modifications of the basis in which the state-space matrices of the

controller are defined. The adopted choice allows to have a simplified expression of the inverse of Lyapunov matrix

$$X_{\text{cl}} = \begin{bmatrix} \mathcal{X} & \mathcal{Y} \\ \mathcal{Y} & \mathcal{Y} \end{bmatrix}. \quad (8.16)$$

We adopt exactly this change-of-variables in the next section with the objective to get a parameter-dependent $\bar{K}(\theta + \delta)$ that should depend only on the provided scheduling parameters with uncertainties $\theta_i + \delta_i$ and not on the actual scheduling parameters θ_i . For this reason, we impose the inverse of Lyapunov matrix $X_{\text{cl}}(\theta + \delta)$ to depend only on the provided scheduling parameters (thus $\mathcal{X}(\theta + \delta)$, $\mathcal{Y}(\theta + \delta)$ and $\mathcal{Z}(\theta + \delta)$ are also functions of these provided scheduling parameters) and the matrix A in the formulation of (8.15) is chosen to be $A(\theta + \delta)$ and not the actual $A(\theta)$. More precisely we use the following formulas:

$$X_{\text{cl}}(\theta + \delta) = \begin{bmatrix} \mathcal{X}(\theta + \delta) & * \\ \mathcal{Y}(\theta + \delta) & \mathcal{Y}(\theta + \delta) \end{bmatrix}, \quad (8.17)$$

$$\begin{aligned} \bar{K}(\theta + \delta) = & \begin{bmatrix} -\mathcal{Z}(\theta + \delta)^{-1} B_2 \\ \mathbf{0} & I_{n_u} \end{bmatrix} \left(\mathcal{K}(\theta + \delta) - \begin{bmatrix} \mathcal{Z}(\theta + \delta)A(\theta + \delta)\mathcal{X}(\theta + \delta) & \mathbf{0} \\ \mathbf{0} & \mathbf{0} \end{bmatrix} \right) \\ & \times \begin{bmatrix} \mathcal{Y}(\theta + \delta)^{-1} & \mathbf{0} \\ -C_2\mathcal{X}(\theta + \delta)\mathcal{Y}(\theta + \delta)^{-1} & I_{n_y} \end{bmatrix}. \end{aligned} \quad (8.18)$$

To cope with the term introduced by the choice of $A(\theta + \delta)$ in the change-of-variables, a technical lemma is used. It is a variation on the celebrated properties $\text{He}\{X^T Y\} \leq \varepsilon X^T X + \varepsilon^{-1} Y^T Y$, $\forall \varepsilon > 0$ (see [26]) and $\text{He}\{X^T Y\} \leq X^T \mathcal{E} X + Y^T \mathcal{E}^{-1} Y$, $\forall \mathcal{E} = \mathcal{E}^T > 0$ (see [43]). Combined to a Schur complement, the result is used in the context of this article to approximate in a linear fashion some products of parameter-dependent decision matrices.

Lemma 8.3. *Suppose that symmetric matrices Y_0, Γ and matrices Y_1, Y_2 with compatible dimensions are given. If one of the following two inequalities holds for some symmetric positive definite matrix \mathcal{E} with compatible dimensions satisfying $\mathcal{E}^{1/2}\Gamma = \Gamma\mathcal{E}^{1/2}$:*

$$\begin{bmatrix} Y_0 & * \\ [Y_1 \ \mathcal{E}Y_2] & -\mathcal{E}\Gamma \end{bmatrix} < 0, \quad (8.19)$$

$$\begin{bmatrix} Y_0 & * \\ \text{diag}(Y_1, \mathcal{E}Y_2) & -\text{diag}(\mathcal{E}\Gamma, \mathcal{E}\Gamma) \end{bmatrix} < 0, \quad (8.20)$$

then $Y_0 + \begin{bmatrix} \mathbf{0} & * \\ Y_2^T \Gamma^{-1} Y_1 & \mathbf{0} \end{bmatrix} < 0$ holds.

Proof. Applying Schur complement to (8.19) gives

$$\Upsilon_0 + \begin{bmatrix} \mathbf{0} & * \\ \Upsilon_2^\top \Gamma^{-1} \Upsilon_1 & \mathbf{0} \end{bmatrix} < - \begin{bmatrix} \Upsilon_1^\top (\mathcal{E}^{1/2} \Gamma \mathcal{E}^{1/2})^{-1} \Upsilon_1 & \mathbf{0} \\ \mathbf{0} & \Upsilon_2^\top \mathcal{E}^{1/2} \Gamma^{-1} \mathcal{E}^{1/2} \Upsilon_2 \end{bmatrix}.$$

The right-hand side is negative semidefinite. Thus, it proves the lemma for (8.19). Similarly,

$$\Upsilon_0 + \begin{bmatrix} \mathbf{0} & * \\ \Upsilon_2^\top \Gamma^{-1} \Upsilon_1 & \mathbf{0} \end{bmatrix} < - \begin{bmatrix} \Upsilon_1^\top \\ -\Upsilon_2^\top \mathcal{E} \end{bmatrix} (\mathcal{E}^{1/2} \Gamma \mathcal{E}^{1/2})^{-1} [\Upsilon_1 \ -\mathcal{E} \Upsilon_2] \leq 0$$

is obtained from (8.20) by applying Schur complement. Thus, it proves the lemma for (8.20). \square

8.3 Main Results

8.3.1 Proposed Methods

For both H_∞ control-type and H_2 control-type problems, we define the following notations:

$$\Upsilon_A(\theta, \theta + \delta) = \begin{bmatrix} A(\theta) \mathcal{X}(\theta + \delta) & A(\theta) \\ \mathbf{0} & \mathcal{Z}(\theta + \delta) A(\theta) \end{bmatrix} + \begin{bmatrix} \mathbf{0} & B_2 \\ I_n & \mathbf{0} \end{bmatrix} \mathcal{K}(\theta + \delta) \begin{bmatrix} I_n & \mathbf{0} \\ \mathbf{0} & C_2 \end{bmatrix},$$

$$\Upsilon_B(\theta, \theta + \delta) = \begin{bmatrix} B_1(\theta) \\ \mathcal{Z}(\theta + \delta) B_1(\theta) \end{bmatrix} + \begin{bmatrix} \mathbf{0} & B_2 \\ I_n & \mathbf{0} \end{bmatrix} \mathcal{K}(\theta + \delta) \begin{bmatrix} \mathbf{0} \\ D_{21}(\theta) \end{bmatrix},$$

$$\Upsilon_C(\theta, \theta + \delta) = [C_1(\theta) \mathcal{X}(\theta + \delta) \ C_1(\theta)] + [\mathbf{0} \ D_{12}(\theta)] \mathcal{K}(\theta + \delta) \begin{bmatrix} I_n & \mathbf{0} \\ \mathbf{0} & C_2 \end{bmatrix},$$

$$\Upsilon_D(\theta, \theta + \delta) = D_{11}(\theta) + [\mathbf{0} \ D_{12}(\theta)] \mathcal{K}(\theta + \delta) \begin{bmatrix} \mathbf{0} \\ D_{21}(\theta) \end{bmatrix},$$

$$\Upsilon_X(\theta, \dot{\theta}, \delta, \dot{\delta}) = \begin{bmatrix} -\dot{\mathcal{X}}(\theta + \delta) & \mathbf{0} \\ \mathbf{0} & \dot{\mathcal{Z}}(\theta + \delta) \end{bmatrix}.$$

We also define two choices of the pair of matrices (Υ_d, Γ_d) as follows:

$$\begin{array}{c} \hline \hline \Upsilon_d(\theta, \dot{\theta}, \delta, \dot{\delta}) \qquad \qquad \Gamma_d(\theta, \delta) \\ \hline \hline \text{(i)} \quad [I_n \ \varepsilon_1 \dot{\mathcal{Z}}(\theta + \delta)] \qquad \qquad -\varepsilon_1 \dot{\mathcal{Z}}(\theta + \delta) \\ \hline \hline \text{(ii)} \quad \text{diag}(I_n, \varepsilon_1 \dot{\mathcal{Z}}(\theta + \delta)) \quad \text{diag}(-\varepsilon_1 \dot{\mathcal{Z}}(\theta + \delta), -\varepsilon_1 \dot{\mathcal{Z}}(\theta + \delta)) \\ \hline \hline \end{array} \quad (8.21)$$

and four choices of the pair of matrices (Υ_u, Γ_u) as follows:

	$\Upsilon_u(\theta, \delta)$	Γ_u
(a)	$[\mathcal{X}(\theta + \delta) \quad \mathcal{E}_2(A(\theta) - A(\theta + \delta))^T \mathcal{Z}(\theta + \delta)]$	$-\mathcal{E}_2$
(b)	$[(A(\theta) - A(\theta + \delta)) \mathcal{X}(\theta + \delta) \quad \mathcal{E}_2 \mathcal{Z}(\theta + \delta)]$	$-\mathcal{E}_2$
(c)	$\text{diag}(\mathcal{X}(\theta + \delta) \quad \mathcal{E}_2(A(\theta) - A(\theta + \delta))^T \mathcal{Z}(\theta + \delta))$	$-\text{diag}(\mathcal{E}_2, \mathcal{E}_2)$
(d)	$\text{diag}((A(\theta) - A(\theta + \delta)) \mathcal{X}(\theta + \delta) \quad \mathcal{E}_2 \mathcal{Z}(\theta + \delta))$	$-\text{diag}(\mathcal{E}_2, \mathcal{E}_2)$

(8.22)

8.3.1.1 H_∞ Control-Type Problem

Let the parameter-dependent matrix

$$\Upsilon_\infty(\theta, \dot{\theta}, \delta, \dot{\delta}) = \begin{bmatrix} \text{He}\{\Upsilon_\lambda(\theta, \theta + \delta)\} + \Upsilon_X(\theta, \dot{\theta}, \delta, \dot{\delta}) & * & \Upsilon_B(\theta, \theta + \delta) \\ \Upsilon_C(\theta, \theta + \delta) & -\gamma I_{n_z} & \Upsilon_D(\theta, \theta + \delta) \\ * & * & -\gamma I_{n_w} \end{bmatrix}. \quad (8.23)$$

Theorem 8.1. *For a given positive number γ_∞ , suppose that there exist a positive scalar ε_1 , a positive definite matrix $\mathcal{E}_2 \in \mathbb{S}^n$, continuously differentiable parameter-dependent matrices $\mathcal{X}(\theta + \delta), \mathcal{Z}(\theta + \delta) \in \mathbb{S}^n$, and a parameter-dependent matrix $\mathcal{K}(\theta + \delta) \in \mathbb{R}^{(n+n_u) \times (n+n_y)}$ such that the following conditions hold for all quadruplets $(\theta, \dot{\theta}, \delta, \dot{\delta}) \in \Omega_\theta \times \Lambda_\theta \times \Omega_\delta \times \Lambda_\delta$:*

$$\begin{bmatrix} \mathcal{X}(\theta + \delta) & I_n \\ I_n & \mathcal{Z}(\theta + \delta) \end{bmatrix} > 0, \quad (8.24)$$

$$\begin{bmatrix} \Upsilon_\infty(\theta, \dot{\theta}, \delta, \dot{\delta}) & * \\ \left[\begin{array}{cc} \Upsilon_d(\theta, \dot{\theta}, \delta, \dot{\delta}) & \mathbf{0} \\ \Upsilon_u(\theta, \delta) & \mathbf{0} \end{array} \right] & \left[\begin{array}{cc} \Gamma_d(\theta, \delta) & \mathbf{0} \\ \mathbf{0} & \Gamma_u \end{array} \right] \end{bmatrix} < 0, \quad (8.25)$$

where $(\Upsilon_d(\theta, \dot{\theta}, \delta, \dot{\delta}), \Gamma_d(\theta, \delta))$ is any pair chosen from (8.21) and $(\Upsilon_u(\theta, \delta), \Gamma_u)$ is any pair chosen from (8.22), then the GS controller $K(\theta + \delta)$, whose state-space matrices are constructed using (8.18), stabilizes the closed-loop system $G_{\text{cl}}(\theta, \theta + \delta)$ and satisfies (8.8) for all admissible quadruplets $(\theta, \dot{\theta}, \delta, \dot{\delta}) \in \Omega_\theta \times \Lambda_\theta \times \Omega_\delta \times \Lambda_\delta$.

Proof. Pre- and postmultiply (8.24) by $\begin{bmatrix} I_n & \mathbf{0} \\ I_n - \mathcal{Z}(\theta + \delta)^{-1} \end{bmatrix}$ and its transpose, respectively, to get that $X_{\text{cl}}(\theta + \delta)$ defined in (8.17) is positive definite. Thus, (8.10) holds.

Lemma 8.3 is applied twice to (8.25). First it is applied with respect to the pair $(\Upsilon_u(\theta, \delta), \Gamma_u)$ and whatever its choice among those defined in (8.22) one gets

$$\begin{bmatrix} \Upsilon_{\infty,1}(\theta, \dot{\theta}, \delta, \dot{\delta}) & * \\ [\Upsilon_d(\theta, \dot{\theta}, \delta, \dot{\delta}) \mathbf{0} \mathbf{0}] & \Gamma_d(\theta, \delta) \end{bmatrix} < 0, \quad (8.26)$$

where $\Upsilon_{\infty,1}(\theta, \dot{\theta}, \delta, \dot{\delta})$ has the same definition as (8.23) except for the term $\Upsilon_A(\theta, \theta + \delta)$ which is replaced by

$$\begin{aligned} \Upsilon_{A,1}(\theta, \theta + \delta) &= \begin{bmatrix} A(\theta) \mathcal{X}(\theta + \delta) & A(\theta) \\ \mathcal{Z}(\theta + \delta) (A(\theta) - A(\theta + \delta)) \mathcal{X}(\theta + \delta) & \mathcal{Z}(\theta + \delta) A(\theta) \end{bmatrix} \\ &+ \begin{bmatrix} \mathbf{0} & B_2 \\ I_n & \mathbf{0} \end{bmatrix} \mathcal{K}(\theta + \delta) \begin{bmatrix} I_n & \mathbf{0} \\ \mathbf{0} & C_2 \end{bmatrix}. \end{aligned}$$

This replacement allows to cope with the fact that the controller is defined using $A(\theta + \delta)$ and not the actual $A(\theta)$. Lemma 8.3 is then applied to (8.26) with respect to the pair $(\Upsilon_d(\theta, \dot{\theta}, \delta, \dot{\delta}), \Gamma_d(\theta, \delta))$ and whatever its choice among those defined in (8.21) one gets:

$$\Upsilon_{\infty,2}(\theta, \dot{\theta}, \delta, \dot{\delta}) < 0, \quad (8.27)$$

where $\Upsilon_{\infty,2}(\theta, \dot{\theta}, \delta, \dot{\delta})$ has the same definition as $\Upsilon_{\infty,1}(\theta, \dot{\theta}, \delta, \dot{\delta})$ except for the term $\Upsilon_X(\theta, \dot{\theta}, \delta, \dot{\delta})$ which is replaced by

$$\Upsilon_{X,2}(\theta, \dot{\theta}, \delta, \dot{\delta}) = \begin{bmatrix} -\dot{\mathcal{X}}(\theta + \delta) & * \\ \dot{\mathcal{Z}}(\theta + \delta) \mathcal{Z}(\theta + \delta)^{-1} \dot{\mathcal{Z}}(\theta + \delta) & \end{bmatrix}.$$

This replacement thus introduces some derivative dependent terms which are not available for constructing controller matrices.

Similarly to [30, 32–34], applying the change-of-variables, which amounts to the inverse of formula (8.18), one proves that (8.11) holds with the $X_{cl}(\theta + \delta)$ defined in (8.17). From Lemma 8.1, the assertions are proved. \square

8.3.1.2 H_2 Control-Type Problem

Let the parameter-dependent matrix

$$\Upsilon_2(\theta, \dot{\theta}, \delta, \dot{\delta}) = \begin{bmatrix} \text{He} \{ \Upsilon_A(\theta, \theta + \delta) \} + \Upsilon_X(\theta, \dot{\theta}, \delta, \dot{\delta}) & * \\ \Upsilon_C(\theta, \theta + \delta) & -I_{n_z} \end{bmatrix}. \quad (8.28)$$

Theorem 8.2. *For a given positive number γ_2 , suppose that there exist a positive scalar ε_1 , a positive definite matrix $\mathcal{E}_2 \in \mathbb{S}^n$, continuously differentiable parameter-dependent matrices $\mathcal{X}(\theta + \delta), \mathcal{Z}(\theta + \delta) \in \mathbb{S}^n$, and parameter-dependent matrices*

$\mathcal{Q}(\theta, \theta + \delta) \in \mathbb{S}^{n_w}$, $\mathcal{K}(\theta + \delta) \in \mathbb{R}^{(n+n_u) \times (n+n_y)}$ such that the following conditions hold for all quadruplets $(\theta, \dot{\theta}, \delta, \dot{\delta}) \in \Omega_\theta \times \Lambda_\theta \times \Omega_\delta \times \Lambda_\delta$:

$$[\mathbf{0} \ I_{n_u}] \mathcal{K}(\theta + \delta) \begin{bmatrix} \mathbf{0} \\ I_{n_y} \end{bmatrix} = \mathbf{0}, \quad (8.29)$$

$$\begin{bmatrix} \Upsilon_2(\theta, \dot{\theta}, \delta, \dot{\delta}) & * \\ \left[\begin{array}{c|c} \Upsilon_d(\theta, \dot{\theta}, \delta, \dot{\delta}) & \mathbf{0} \\ \hline \Upsilon_u(\theta, \delta) & \mathbf{0} \end{array} \right] & \left[\begin{array}{c|c} \Gamma_d(\theta, \delta) & \mathbf{0} \\ \hline \mathbf{0} & \Gamma_u \end{array} \right] \end{bmatrix} < 0, \quad (8.30)$$

$$\begin{bmatrix} \mathcal{Q}(\theta, \theta + \delta) & * \\ \Upsilon_B(\theta, \theta + \delta) & \left[\begin{array}{c|c} \mathcal{X}(\theta + \delta) & I_n \\ \hline I_n & \mathcal{Z}(\theta + \delta) \end{array} \right] \end{bmatrix} > 0, \quad (8.31)$$

$$\gamma_2^2 - \text{Tr}(\mathcal{Q}(\theta, \theta + \delta)) > 0, \quad (8.32)$$

where $(\Upsilon_d(\theta, \dot{\theta}, \delta, \dot{\delta}), \Gamma_d(\theta, \delta))$ is any pair chosen from (8.21) and $(\Upsilon_u(\theta, \delta), \Gamma_u)$ is any pair chosen from (8.22), then the GS controller $K(\theta + \delta)$, whose state-space matrices are constructed using (8.18), stabilizes the closed-loop system $G_{cl}(\theta, \theta + \delta)$ and satisfies (8.9) for all admissible quadruplets $(\theta, \dot{\theta}, \delta, \dot{\delta}) \in \Omega_\theta \times \Lambda_\theta \times \Omega_\delta \times \Lambda_\delta$.

The proof is omitted here as it is very similar to that of Theorem 8.1.

Remark 8.2. In Theorem 8.1 and Theorem 8.2, PDLFs are set as $x_{cl}^T X_{cl}(\theta + \delta)^{-1} x_{cl}$ using $X_{cl}(\theta + \delta)$ defined in (8.17) with $\mathcal{Y}(\theta + \delta) = \mathcal{X}(\theta + \delta) - \mathcal{Z}(\theta + \delta)^{-1}$.

Remark 8.3. Theorems 8.1 and 8.2 have eight different formulations for the same conclusions. At the current stage, it is not certain which is the best with respect to conservatism. However, concerning the numerical complexity for designing controllers, formulations using matrices with small numbers of rows are always preferred, i.e., choice (i) in (8.21), and choice (a) or (b) in (8.22) are recommended.

Remark 8.4. As (8.21) and (8.22) indicate, both inequalities (8.25) and (8.30) have multiplications of decision variables, i.e., $\varepsilon_1 \mathcal{Y}(\theta + \delta)$ and $\varepsilon_1 \mathcal{Z}(\theta + \delta)$, and terms involving \mathcal{E}_2 and $\mathcal{Z}(\theta + \delta)$. That is, those inequalities are PDBMIs and are PDLMI for fixed values of ε_1 and \mathcal{E}_2 .

Remark 8.5. Theorems 8.1 and 8.2 introduce a positive definite matrix \mathcal{E}_2 to address the gap between the actual $A(\theta)$ and its uncertain value $A(\theta + \delta)$ used to define the controller matrix $A_K(\theta + \delta)$. Applying the same technique exposed above, we can derive similar formulations for designing GSOF controllers for LPV system $G(\theta)$ with Assumption 8.1 being relaxed. However, in this case, the gap between $B_2(\theta)$ and $B_2(\theta + \delta)$, or between $C_2(\theta)$ and $C_2(\theta + \delta)$ should be also considered thus introducing a new bilinear term dependent on a new matrix. This would consequently increase both the conservatism and the numerical complexity.

8.3.1.3 Algorithm for Solving PDBMIs

As noted in Remark 8.4, our method is formulated in terms of PDBMIs which are not tractable compared to PDLMIs. We show hereafter two algorithms used in this article to solve the PDBMIs. Both these algorithms assume that we are able to solve PDLMIs which is indeed possible with either SOS techniques [9, 24, 37] or with the SV approach [25]. The main assumption for applying these results is that the data and the decision variables are polynomially dependent with respect to θ , $\hat{\theta}$, δ , and $\hat{\delta}$.

The bilinear terms in (8.21) are $\varepsilon_1 \mathcal{L}(\theta + \delta)$ and $\varepsilon_1 \mathcal{Z}(\theta + \delta)$. If ε_1 is fixed a priori then the bilinear terms become linear with respect to the decision variables. Thus, line search for ε_1 circumvents the difficulty.

On the other hand, the bilinear terms in (8.22) are complicated. However, if \mathcal{E}_2 is set as $\varepsilon_2 I_n$ with a priori fixed positive scalar ε_2 , then the bilinear terms become linear with respect to the decision variables. Similarly to the above discussion for ε_1 , line search for ε_2 circumvents the difficulty. Thus, the following algorithm is proposed.

Algorithm I (line search algorithm) Solve the conditions of Theorem 8.1 or Theorem 8.2 with two line search parameters ε_1 and ε_2 ($\mathcal{E}_2 = \varepsilon_2 I_n$).

Although the above algorithm is simple and works well, the numerical complexity is huge because of two line search parameters. In addition, restricting \mathcal{E}_2 to be $\varepsilon_2 I_n$ introduces conservatism. Note that if either a pair $(\varepsilon_1, \mathcal{E}_2)$ or $\mathcal{L}(\theta + \delta)$ is fixed a priori, the conditions of Theorems 8.1 and 8.2 are formulated with tractable PDLMIs. Thus, the following algorithm, in which “Theorem” and “ γ ”, respectively, denote “Theorem 8.1” and “ γ_∞ ” when Problem 8.1 is addressed or “Theorem 8.2” and “ γ_2 ” when Problem 8.2 is addressed, is proposed to overcome the bilinear terms.

Algorithm II (iterative algorithm)

- Step 0 Set $i = 0$, $\gamma_i = \infty$, $\varepsilon_1 = \varepsilon_{10}$, and $\mathcal{E}_2 = \mathcal{E}_{20} = \varepsilon_{20} I_n$ with some given positive scalars ε_{10} and ε_{20} , e.g., 1.
- Step i.1 Set $i = i + 1$. Minimize γ under the conditions of Theorem with fixed $\varepsilon_{1_{i-1}}$ and $\mathcal{E}_{2_{i-1}}$, and set $\mathcal{L}(\theta + \delta)_{i-1}$ be the optimum of $\mathcal{L}(\theta + \delta)$.
- Step i.2 Minimize γ under the conditions of Theorem with fixed $\mathcal{L}(\theta + \delta)_{i-1}$, and set ε_{1_i} , \mathcal{E}_{2_i} , and γ_i be the optima of ε_1 , \mathcal{E}_2 , and γ , respectively.
- Step i.3 If $\gamma_{i-1} - \gamma_i$ is below some predefined threshold ρ , then stop the iteration. Otherwise, return to Step i.1.

Although this algorithm does not guarantee the convergence to the global optima, conservatism reduction is expected compared to Algorithm I since the structural constraint for \mathcal{E}_2 is relaxed.

8.3.1.4 Extension: LPV Systems with Unmeasurable Parameters

Theorems 8.1 and 8.2 address the design problem of GSOF controllers in which all parameters of the plant are available for the controllers, although with some

uncertainties δ_i . We shall now extend the results to the design problem of robust GSOF controllers in which some of the parameters are available and others are not. The controller gains then should depend on the available parameters and the closed-loop system should be robust against the others, which stand for uncertainties.

Let us assume that the parameters $\theta_1 \dots \theta_k$ are ordered in such a way that the first k_1 elements are scheduling parameters and the $k - k_1$ last elements are uncertainties. Enforcing that parameters θ_i ($i = k + 1, \dots, k$) is uncertain, and thus not available for tuning the controller, amounts to stating that uncertainties δ_i ($i = k + 1, \dots, k$) on their measurements are as large as their actual values: $\delta_i = -\theta_i$, ($i = k + 1, \dots, k$). Thus, the robust GSOF controller design problem suits the above described framework by simply rewriting the vector of uncertainties on the parameters as $\delta_{[1,k_1]} = [\delta_1 \dots \delta_{k_1} - \theta_{k_1+1} \dots - \theta_k]^T$ and the vector of available parameters becomes:

$$\theta + \delta_{[1,k_1]} = [\theta_1 + \delta_1 \dots \theta_{k_1} + \delta_{k_1} \ 0 \dots 0]^T. \quad (8.33)$$

According to these notations, we appropriately define the sets of admissible uncertainties $\Omega_{\delta_{[1,k_1]}}$ and of their derivatives $\Lambda_{\delta_{[1,k_1]}}$. With these notations, Theorems 8.1 and 8.2 can be easily extended to handle the robust GSOF controller design problem. We only give the formulation of that result for the H_∞ control-type problem. A similar one can trivially be derived for the H_2 control-type problem.

Corollary 8.1. *For a given positive number γ_∞ , suppose that there exist a positive scalar ε_1 , a positive definite matrix $\mathcal{E}_2 \in \mathbb{S}^n$, continuously differentiable parameter-dependent matrices $\mathcal{X}(\theta + \delta_{[1,k_1]})$, $\mathcal{Z}(\theta + \delta_{[1,k_1]}) \in \mathbb{S}^n$, and a parameter-dependent matrix $\mathcal{K}(\theta + \delta_{[1,k_1]}) \in \mathbb{R}^{(n+n_u) \times (n+n_y)}$ such that the conditions (8.24) and (8.25) hold for all quadruplets $(\theta, \dot{\theta}, \delta_{[1,k_1]}, \dot{\delta}_{[1,k_1]}) \in \Omega_\theta \times \Lambda_\theta \times \Omega_{\delta_{[1,k_1]}} \times \Lambda_{\delta_{[1,k_1]}}$, where $(\Upsilon_d(\theta, \dot{\theta}, \delta, \dot{\delta}), \Gamma_d(\theta, \delta))$ and $(\Upsilon_u(\theta, \delta), \Gamma_u)$ are, respectively, any pairs chosen from (8.21) and (8.22) with δ and $\dot{\delta}$ being, respectively, replaced by $\delta_{[1,k_1]}$ and $\dot{\delta}_{[1,k_1]}$, then the GS controller $K(\theta + \delta_{[1,k_1]})$, whose state-space matrices are constructed using (8.18), stabilizes the closed-loop system $G_{cl}(\theta, \theta + \delta_{[1,k_1]})$ and satisfies (8.8) for all admissible quadruplets $(\theta, \dot{\theta}, \delta_{[1,k_1]}, \dot{\delta}_{[1,k_1]}) \in \Omega_\theta \times \Lambda_\theta \times \Omega_{\delta_{[1,k_1]}} \times \Lambda_{\delta_{[1,k_1]}}$.*

Remark 8.6. Since the controller matrices are constructed using the matrices $\mathcal{X}(\theta + \delta_{[1,k_1]})$ and $\mathcal{Z}(\theta + \delta_{[1,k_1]})$, the method imposes to enforce these to be independent of the uncertainties $\theta_{k_1+1}, \dots, \theta_k$. This clearly brings some conservatism with respect to the robustness issues. The conservatism is similar to that of the methods in [30] (Proposition 2 and Proposition 3), in which PiDLFs are adopted for designing robust controllers.

8.3.2 Recovery of Conventional Design Methods

In this section, we show that Theorems 8.1 and 8.2 recover the design methods in [32, 34]. Although we only show the result for Theorem 8.1, similar assertions hold for Theorem 8.2. Our claims to be proved here are as follows:

- Consider Problem 8.1 in which PiDLFs are adopted instead of PDLFs. Then, Theorem 8.1 recovers the method in [32] for an ε_1 taken sufficiently large.
- Consider Problem 8.1 in which scheduling parameters are exactly provided. Then, Theorem 8.1 recovers the method in [34] for an $\mathcal{E}_2 = \varepsilon_2 I_n$ taken either sufficiently large or close to zero depending on the choices of the pair $(\Upsilon_u(\theta, \delta), \Gamma_u)$.

Let us first address the first assertion. In [32], the design problem is considered for a parametrically affine GSOF controller $K(\theta + \delta)$ for LPV system $G(\theta)$ with some mild constraints.¹ Nevertheless, these assumptions can be removed and results of [32] may be extended to LPV system (8.1). This extended version is given below.

Lemma 8.4. *For a given positive number γ_∞ , suppose that there exist a positive definite matrix $\mathcal{E}_2 \in \mathbb{S}^n$, parameter independent matrices $\mathcal{X}, \mathcal{Z} \in \mathbb{S}^n$, and a parameter-dependent matrix $\mathcal{K}(\theta + \delta) \in \mathbb{R}^{(n+n_u) \times (n+n_y)}$ such that the following conditions hold for all pairs $(\theta, \delta) \in \Omega_\theta \times \Omega_\delta$:*

$$\begin{bmatrix} \mathcal{X} & I_n \\ I_n & \mathcal{Z} \end{bmatrix} > 0, \quad (8.34)$$

$$\begin{bmatrix} \Upsilon_\infty^c(\theta, \theta + \delta) & * \\ [\Upsilon_u(\theta, \delta) \ \mathbf{0} \ \mathbf{0}] & \Gamma_u \end{bmatrix} < 0, \quad (8.35)$$

where $\Upsilon_\infty^c(\theta, \theta + \delta)$ stands for the matrix defined in (8.23) with $\Upsilon_X(\theta, \dot{\theta}, \delta, \dot{\delta})$ set to $\mathbf{0}$, and $(\Upsilon_u(\theta, \delta), \Gamma_u)$ is any pair chosen from (8.22), then the GS controller $K(\theta + \delta)$, whose state-space matrices are constructed using (8.18), stabilizes the closed-loop system $G_{cl}(\theta, \theta + \delta)$ and satisfies (8.8) for all admissible pairs $(\theta, \delta) \in \Omega_\theta \times \Omega_\delta$.

We make the following assertion for Theorem 8.1 and Lemma 8.4. It clearly states that Theorem 8.1 is less conservative since it allows PDLFs.

Theorem 8.3. *Let any performance level γ_∞ , the following two propositions are equivalent:*

- 1- *There exists a solution $(\mathcal{E}_2, \mathcal{X}, \mathcal{Z}, \mathcal{K}(\theta + \delta))$ to the conditions of Lemma 8.4.*
- 2- *There exists a solution $(\varepsilon_1, \mathcal{E}_2, \mathcal{X}, \mathcal{Z}, \mathcal{K}(\theta + \delta))$ to the conditions of Theorem 8.1 with parameter-independent matrices \mathcal{X} and \mathcal{Z} .*

¹In addition to Assumption 8.1, matrices $A(\theta)$, $B_1(\theta)$, $C_1(\theta)$ and $D_{11}(\theta)$ are supposed to be parametrically affine, and matrices $D_{12}(\theta)$ and $D_{21}(\theta)$ are supposed to be constant.

Proof. Let us first prove that -2- implies -1-. For parameter-independent matrices \mathcal{X} and \mathcal{Z} , condition (8.24) is exactly (8.34). Pre- and postmultiply (8.25) with parameter-independent \mathcal{X} and \mathcal{Z} by $\begin{bmatrix} I_{2n+n_z+n_w} & \mathbf{0} \\ \mathbf{0} & [\mathbf{0} \ I_n] \end{bmatrix}$ and its transpose, respectively, one exactly gets condition (8.35). Thus -1- indeed holds with exactly the same values of the solution $(\mathcal{E}_2, \mathcal{X}, \mathcal{Z}, \mathcal{K}(\theta + \delta))$ of Theorem 8.1.

We now prove that -1- implies -2-. The condition (8.35) holds for all pairs $(\theta, \delta) \in \Omega_\theta \times \Omega_\delta$, i.e. (8.35) holds on a compact set. There, therefore, exists a positive scalar ε , potentially very small, such that for all pairs $(\theta, \delta) \in \Omega_\theta \times \Omega_\delta$

$$\begin{bmatrix} \Upsilon_\infty^c(\theta, \theta + \delta) & * \\ [\Upsilon_u(\theta, \delta) \ \mathbf{0} \ \mathbf{0}] & \Gamma_u \end{bmatrix} < -\text{diag}(\varepsilon \mathcal{Z}^{-1}, \mathbf{0}, \mathbf{0}, \mathbf{0}, \mathbf{0}). \quad (8.36)$$

Take $\varepsilon_1 = \varepsilon^{-1}$, the right-hand term of (8.36) can be factorized either as

$$[I_n \ \mathbf{0} \ \mathbf{0} \ \mathbf{0} \ \mathbf{0}]^T (\varepsilon_1 \mathcal{Z})^{-1} [I_n \ \mathbf{0} \ \mathbf{0} \ \mathbf{0} \ \mathbf{0}]$$

or as

$$\begin{bmatrix} I_n \ \mathbf{0} \ \mathbf{0} \ \mathbf{0} \ \mathbf{0} \\ \mathbf{0} \ \mathbf{0} \ \mathbf{0} \ \mathbf{0} \ \mathbf{0} \end{bmatrix}^T \begin{bmatrix} \varepsilon_1 \mathcal{Z} & \mathbf{0} \\ \mathbf{0} & \varepsilon_1 \mathcal{Z} \end{bmatrix}^{-1} \begin{bmatrix} I_n \ \mathbf{0} \ \mathbf{0} \ \mathbf{0} \ \mathbf{0} \\ \mathbf{0} \ \mathbf{0} \ \mathbf{0} \ \mathbf{0} \ \mathbf{0} \end{bmatrix}.$$

A Schur complement applied to (8.36) with either these factorizations gives (8.25) for the two possible choices of the pair (Υ_d, Γ_d) with $\mathcal{X} = \mathcal{Z} = \mathbf{0}$. \square

Remark 8.7. The proof indicates that when looking for a matrix $\mathcal{Z}(\theta + \delta)$ with fast variations of scheduling parameters, an appropriate choice of ε_1 is to take it large. Smaller values of ε_1 in Theorem 8.1 may reduce the conservatism due to having a constant \mathcal{Z} .

In the proof given above, the reasoning does not depend at all on \mathcal{X} , it is, therefore, also possible to give the following intermediate result which is trivially more conservative than Theorem 8.1, but has the advantage of not involving bilinear terms with scalar ε_1 . This result is directly related to the result of [1] using structured PDLFs.

Lemma 8.5. *For a given positive number γ_∞ , suppose that there exist a positive definite matrix $\mathcal{E}_2 \in \mathbb{S}^n$, a continuously differentiable parameter-dependent matrix $\mathcal{X}(\theta + \delta) \in \mathbb{S}^n$, a parameter-independent matrix $\mathcal{Z} \in \mathbb{S}^n$, and a parameter-dependent matrix $\mathcal{K}(\theta + \delta) \in \mathbb{R}^{(n+n_u) \times (n+n_y)}$ such that the following conditions hold for all quadruplets $(\theta, \dot{\theta}, \delta, \dot{\delta}) \in \Omega_\theta \times \Lambda_\theta \times \Omega_\delta \times \Lambda_\delta$:*

$$\begin{bmatrix} \mathcal{X}(\theta + \delta) & I_n \\ I_n & \mathcal{Z} \end{bmatrix} > 0, \quad (8.37)$$

$$\begin{bmatrix} \Upsilon_\infty^X(\theta, \dot{\theta}, \delta, \dot{\delta}) & * \\ [\Upsilon_u(\theta, \delta) \ \mathbf{0} \ \mathbf{0}] & \Gamma_u \end{bmatrix} < 0, \quad (8.38)$$

where $\Upsilon_\infty^X(\theta, \dot{\theta}, \delta, \dot{\delta})$ stands for the matrix defined in (8.23) with $\Upsilon_X(\theta, \dot{\theta}, \delta, \dot{\delta})$ being replaced by $\text{diag}(-\mathcal{X}(\theta + \delta), \mathbf{0})$ and $(\Upsilon_u(\theta, \delta), \Gamma_u)$ is any pair chosen from (8.22), then the GS controller $K(\theta + \delta)$, whose state-space matrices are constructed using (8.18), stabilizes the closed-loop system $G_{\text{cl}}(\theta, \theta + \delta)$ and satisfies (8.8) for all admissible quadruplets $(\theta, \dot{\theta}, \delta, \dot{\delta}) \in \Omega_\theta \times \Lambda_\theta \times \Omega_\delta \times \Lambda_\delta$.

We now address the second assertion. The method in [34] is applicable for LPV system (8.1) with Assumption 8.1 not being made. Thus, we show a slightly revised version of the method in [34], which is for LPV system (8.1) with Assumption 8.1.

Lemma 8.6. *For a given positive number γ_∞ , suppose that there exist a positive scalar ε_1 , continuously differentiable parameter-dependent matrices $\mathcal{X}(\theta), \mathcal{Z}(\theta) \in \mathbb{S}^n$, and a parameter-dependent matrix $\mathcal{K}(\theta) \in \mathbb{R}^{(n+n_u) \times (n+n_y)}$ such that the following conditions hold for all pairs $(\theta, \dot{\theta}) \in \Omega_\theta \times \Lambda_\theta$:*

$$\begin{bmatrix} \mathcal{X}(\theta) & I_n \\ I_n & \mathcal{Z}(\theta) \end{bmatrix} > 0, \quad (8.39)$$

$$\begin{bmatrix} \Upsilon_\infty(\theta, \dot{\theta}) & * \\ [\Upsilon_d(\theta, \dot{\theta}) \ \mathbf{0} \ \mathbf{0}] & \Gamma_d(\theta) \end{bmatrix} < 0, \quad (8.40)$$

where $\Upsilon_\infty(\theta, \dot{\theta})$ stands for the matrix defined in (8.23) with both δ and $\dot{\delta}$ being set to be $\mathbf{0}$ and $(\Upsilon_d(\theta, \dot{\theta}), \Gamma_d(\theta))$ is any pair chosen from (8.21), then the GS controller $K(\theta)$, whose state-space matrices are constructed using (8.18), stabilizes the closed-loop system $G_{\text{cl}}(\theta)$ and satisfies (8.8) for all pairs $(\theta, \dot{\theta}) \in \Omega_\theta \times \Lambda_\theta$

We make the following assertion for Theorem 8.1 and Lemma 8.6. It clearly states that Theorem 8.1 extends Lemma 8.6 to the design problem with uncertainties on scheduling parameters, without additional conservatism with respect to the parameter-dependency of Lyapunov functions.

Theorem 8.4. *Let any performance level γ_∞ , the following two propositions are equivalent:*

- 1- *There exists a solution $(\varepsilon_1, \mathcal{X}(\theta), \mathcal{Z}(\theta), \mathcal{K}(\theta))$ to the conditions of Lemma 8.6.*
- 2- *There exists a solution $(\varepsilon_1, \varepsilon_2, \mathcal{X}(\theta), \mathcal{Z}(\theta), \mathcal{K}(\theta))$, i.e., with uncertainties δ being set to zero, to the conditions of Theorem 8.1.*

Proof. The proof that -2- implies -1- is similar to that in the proof of Theorem 8.3. We thus concentrate on proving that -1- implies -2-.

Condition (8.40) holds for all pairs $(\theta, \dot{\theta}) \in \Omega_\theta \times \Lambda_\theta$, i.e., (8.40) holds on a compact set. There, therefore, exists a positive scalar ε , potentially very small, such that for all pairs $(\theta, \dot{\theta}) \in \Omega_\theta \times \Lambda_\theta$

$$\begin{bmatrix} \Upsilon_\infty(\theta, \dot{\theta}) & * \\ [\Upsilon_d(\theta, \dot{\theta}) \ \mathbf{0} \ \mathbf{0}] & \Gamma_d(\theta) \end{bmatrix} < -\text{diag}(\varepsilon \mathcal{X}(\theta)^2, \mathbf{0}, \mathbf{0}, \mathbf{0}, \mathbf{0}). \quad (8.41)$$

Take $\mathcal{E}_2 = \varepsilon^{-1}I_n$, the right-hand term of (8.41) can be factorized either as

$$[\mathcal{X}(\theta) \mathbf{0} \mathbf{0} \mathbf{0} \mathbf{0}]^T \mathcal{E}_2^{-1} [\mathcal{X}(\theta) \mathbf{0} \mathbf{0} \mathbf{0} \mathbf{0}]$$

or as

$$\begin{bmatrix} \mathcal{X}(\theta) \mathbf{0} \mathbf{0} \mathbf{0} \mathbf{0} \\ \mathbf{0} \mathbf{0} \mathbf{0} \mathbf{0} \end{bmatrix}^T \begin{bmatrix} \mathcal{E}_2 & \mathbf{0} \\ \mathbf{0} & \mathcal{E}_2 \end{bmatrix}^{-1} \begin{bmatrix} \mathcal{X}(\theta) \mathbf{0} \mathbf{0} \mathbf{0} \mathbf{0} \\ \mathbf{0} \mathbf{0} \mathbf{0} \mathbf{0} \end{bmatrix}.$$

A Schur complement applied to (8.41) with either these factorizations gives (8.25) for the two choices (a) and (c) of the pair (Y_u, Γ_u) , respectively. The formulas for choices (b) and (d) are obtained in a similar way but starting from the existence of $\varepsilon > 0$ potentially very small such that

$$\begin{bmatrix} Y_\infty(\theta, \dot{\theta}) & * \\ [\gamma_d(\theta, \dot{\theta}) \mathbf{0} \mathbf{0}] & \Gamma_d(\theta) \end{bmatrix} < -\text{diag}(\mathbf{0}, \varepsilon \mathcal{L}(\theta)^2, \mathbf{0}, \mathbf{0}, \mathbf{0}), \quad (8.42)$$

and choosing $\mathcal{E}_2 = \varepsilon I_n$. □

Remark 8.8. The proof indicates that when the uncertainties on the scheduling parameters are small, an appropriate choice of \mathcal{E}_2 is to have it proportional to the identity matrix $\mathcal{E}_2 = \varepsilon_2 I_n$ and to take ε_2 large in case of choices (a) and (c) of the pair (Y_u, Γ_u) , and to take ε_2 small for choices (b) and (d). Other choices of \mathcal{E}_2 in Theorem 8.1 can potentially reduce conservatism when uncertainties δ_i are large.

Remark 8.9. Combining Theorems 8.3 and 8.4, one can easily prove that our proposed method includes conventional design method either with PiDLFs or structured PDLFs as in [1].

8.3.3 Polynomially Parameter-Dependent GSOF Controllers

The GSOF controllers designed by our methods, i.e., Theorem 8.1, Theorem 8.2, and Corollary 8.1, meet our design requirements: robustness against the uncertainties on scheduling parameters as well as good implementability being independent of their derivatives. However, as shown in (8.18), the state-space matrices of designed GSOF controllers are rationally parameter dependent and require complicated online calculations. From a practical point of view, implementability would be much better if GSOF controllers are polynomially parameter dependent. Related to this issue, we formulate the following two design problems.

Problem 8.3. Suppose that a polynomially parameter-dependent solution $(\varepsilon_1, \mathcal{E}_2, \mathcal{X}(\theta + \delta), \mathcal{L}(\theta + \delta), \mathcal{K}(\theta + \delta))$ to the conditions of Theorem 8.1 is

given for some γ_∞ . Find a polynomially parameter-dependent $\bar{K}(\theta + \delta)$ solution of (8.11) with the same γ_∞ using the matrix $X_{\text{cl}}(\theta + \delta)$ defined in (8.17) for all quadruplets $(\theta, \dot{\theta}, \delta, \dot{\delta}) \in \Omega_\theta \times \Lambda_\theta \times \Omega_\delta \times \Lambda_\delta$.

Problem 8.4. Suppose that a polynomially parameter-dependent solution $(\varepsilon_1, \varepsilon_2, \mathcal{X}(\theta + \delta), \mathcal{Z}(\theta + \delta), \mathcal{Q}(\theta, \theta + \delta), \mathcal{K}(\theta + \delta))$ to the conditions of Theorem 8.2 is given for some γ_2 . Find a polynomially parameter-dependent $\bar{K}(\theta + \delta)$ solution of (8.12) and (8.13) with the same $\mathcal{Q}(\theta, \theta + \delta)$ using the matrix $X_{\text{cl}}(\theta + \delta)$ defined in (8.17) for all quadruplets $(\theta, \dot{\theta}, \delta, \dot{\delta}) \in \Omega_\theta \times \Lambda_\theta \times \Omega_\delta \times \Lambda_\delta$.

Having chosen the order of the polynomially parameter-dependent matrix $\bar{K}(\theta + \delta)$, these problems are formulated in terms of PDLMI that can be solved with some numerical methods. If a feasible solution is found, one may be satisfied and use the obtained implementable controller. If not, a strategy may be to increase the order of the polynomially parameter-dependent matrix $\bar{K}(\theta + \delta)$ and solve again the problem. The question then becomes whether it is guaranteed to get a feasible solution, eventually at the expense of sufficiently high-order polynomially parameter-dependent matrix $\bar{K}(\theta + \delta)$. The answer is positive and relies on Weierstrass approximation theorem. Such reasoning can be found in [7] and is reproduced here for our problems.

For this assertion, we make the following very mild assumption:

Assumption 8.3. Matrices $[B_2^T D_{12}^T(\theta)]^T$ and $[C_2 D_{21}(\theta)]$ have at least single non-zero entries for all admissible $\theta \in \Omega_\theta$.

Matrices B_2 and C_2 usually have at least single non-zero entries. Otherwise, controllability or observability is, or both are not satisfied. Thus, this assumption is not restrictive at all.

Under this very mild constraint, we give a proof for our assertion.

Proof. Suppose that a polynomially parameter-dependent solution $(\varepsilon_1, \varepsilon_2, \mathcal{X}(\theta + \delta), \mathcal{Z}(\theta + \delta), \mathcal{K}(\theta + \delta))$ to the conditions of Theorem 8.1 is given. From formulas (8.17) and (8.18), there exist rationally parameter-dependent matrices $X_{\text{cl}}(\theta + \delta)$ and $\bar{K}^r(\theta + \delta)$ satisfying (8.11). This inequality is satisfied for all quadruplets $(\theta, \dot{\theta}, \delta, \dot{\delta}) \in \Omega_\theta \times \Lambda_\theta \times \Omega_\delta \times \Lambda_\delta$, i.e., on a compact set and all functions are continuous; therefore, there exists a positive scalar μ , possibly very small, such that $\forall (\theta, \dot{\theta}, \delta, \dot{\delta}) \in \Omega_\theta \times \Lambda_\theta \times \Omega_\delta \times \Lambda_\delta$

$$\begin{bmatrix} \text{He}\{A_{\text{cl}}(\theta, \theta + \delta)X_{\text{cl}}(\theta + \delta)\} - \dot{X}_{\text{cl}}(\theta + \delta) & * & B_{\text{cl}}(\theta, \theta + \delta) \\ C_{\text{cl}}(\theta, \theta + \delta)X_{\text{cl}}(\theta + \delta) & -\gamma_\infty I_{n_z} & D_{\text{cl}}(\theta, \theta + \delta) \\ * & * & -\gamma_\infty I_{n_w} \end{bmatrix} < -\mu \mathbf{I}.$$

Matrices A_{cl} , B_{cl} , C_{cl} , and D_{cl} are affine with respect to $\bar{K}^r(\theta + \delta)$, thus this inequality can be written as

$$\Xi_0(\theta, \dot{\theta}, \delta, \dot{\delta}) + \text{He}\{\Xi_1(\theta)\bar{K}^r(\theta + \delta)\Xi_2(\theta, \delta)\} < -\mu\mathbf{I},$$

where $\Xi_1(\theta) = [\bar{B}_2^T \bar{D}_{12}^T(\theta) \mathbf{0}]^T$ and $\Xi_2(\theta, \delta) = [\bar{C}_2 X_{cl}(\theta + \delta) \mathbf{0} \bar{D}_{21}(\theta)]$. Due to Assumption 8.3 and the fact that $\Xi_1(\theta)$ and $\Xi_2(\theta, \delta)$ are continuous bounded functions on a compact set (Assumption 8.2), there exists a positive scalar α such that $0 < \|\Xi_1(\theta)\|_2 \|\Xi_2(\theta, \delta)\|_2 \leq \alpha$ holds for all pairs $(\theta, \delta) \in \Omega_\theta \times \Omega_\delta$ where $\|\cdot\|_2$ stands for the spectral norm.

Each coefficient of the matrix $\bar{K}^r(\theta + \delta) = [k_{ij}^r(\theta + \delta)]_{i=1 \dots (n+n_u), j=1 \dots (n+n_y)}$ is a rational real-valued function. By Weierstrass approximation theorem, there exists a polynomial function that is as close as needed to the rational function on the compact set $\Omega_\theta \times \Omega_\delta$. Thus, for any positive scalar η , there exist polynomial real-valued functions $k_{ij}^p(\theta + \delta)$ such that $|k_{ij}^p(\theta + \delta) - k_{ij}^r(\theta + \delta)| \leq \eta$ hold for all pairs $(\theta, \delta) \in \Omega_\theta \times \Omega_\delta$. From Lemma 8.7 in the appendix, the following holds for all pairs $(\theta, \delta) \in \Omega_\theta \times \Omega_\delta$.

$$\|\bar{K}^p(\theta + \delta) - \bar{K}^r(\theta + \delta)\|_2 \leq \eta \sqrt{(n+n_u)(n+n_y)}.$$

Take $\eta \leq \mu / (2\alpha \sqrt{(n+n_u)(n+n_y)})$. One then gets that:

$$\begin{aligned} \Xi_0(\theta, \dot{\theta}, \delta, \dot{\delta}) + \text{He}\{\Xi_1(\theta)\bar{K}^p(\theta + \delta)\Xi_2(\theta, \delta)\} \\ &< -\mu\mathbf{I} + \text{He}\{\Xi_1(\theta)(\bar{K}^p(\theta + \delta) - \bar{K}^r(\theta + \delta))\Xi_2(\theta, \delta)\} \\ &\leq (-\mu + \|\text{He}\{\Xi_1(\theta)(\bar{K}^p(\theta + \delta) - \bar{K}^r(\theta + \delta))\Xi_2(\theta, \delta)\}\|_2)\mathbf{I} \\ &\leq (-\mu + 2\|\Xi_1(\theta)\|_2 \|\bar{K}^p(\theta + \delta) - \bar{K}^r(\theta + \delta)\|_2 \|\Xi_2(\theta, \delta)\|_2)\mathbf{I} \\ &\leq 0. \end{aligned}$$

Equation (8.11) thus holds for the polynomially parameter-dependent matrix $\bar{K}^p(\theta + \delta) = [k_{ij}^p(\theta + \delta)]_{i=1, \dots, (n+n_u), j=1, \dots, (n+n_y)}$. \square

The same result can be obtained for the H_2 control-type problem.

8.4 Numerical Examples

To demonstrate the effectiveness of our method, we show design results of H_∞ control-type problem for two numerical examples from the literature. All our results are obtained by using YALMIP [16] and SeDuMi [38].

The PDLMI in Algorithm I and Algorithm II in the design process are solved by applying Lemma 8.8 in the appendix if they are not parametrically affine.

8.4.1 Example in [12]

The state-space matrices of LPV system $G(\theta)$ are given as follows:

$$\begin{bmatrix} \underline{A}(\theta) & \underline{B}_1(\theta) & \underline{B}_2 \\ \underline{C}_1(\theta) & \underline{D}_{11}(\theta) & \underline{D}_{12}(\theta) \\ \underline{C}_2 & \underline{D}_{21}(\theta) & \underline{D}_{22} \end{bmatrix} = \begin{bmatrix} -0.89 - 0.89\theta & 1 & 0.01 & -0.119 \\ -142.6 - 178.25\theta & 0 & 0 & -130.8 \\ 0 & 1 & 0 & 1 \\ -1.52 & 0 & 0.01 & 1 \end{bmatrix}, \quad (8.43)$$

where scheduling parameter θ is bounded as $|\theta| \leq 1$, the variation rate of θ is bounded as $|\dot{\theta}| \leq \zeta$, the uncertainty δ in the provided scheduling parameter is bounded as $|\delta| \leq \xi$, and the variation rate of δ is bounded as $|\dot{\delta}| \leq 10 \times \zeta$. We consider the following sets for ζ and ξ :

$$\begin{aligned} \zeta &\in \{0, 1, 100, 10,000\}, \\ \xi &\in \{0, 0.1, 0.5, 1\}. \end{aligned}$$

We omit the results for $\zeta = 10,000$ when $\xi \neq 0$ holds, because they are almost the same as those for $\zeta = 100$.

In the design results shown below, parameter-dependent decision matrices are all set to be affine with respect to the parameter. Although we designed GSOF controllers using quadratically parameter-dependent decision matrices, the results are almost the same as using parametrically affine decision matrices. Thus, they are omitted here.

Table 8.2 shows the design results using Theorem 8.1 with Algorithm I in which line search algorithm for ε_1 and ε_2 were conducted with all combinations of six points linearly gridded over a logarithmic scale in the interval $[10^{-5}, 10^5]$ for each parameter. For reference, the values of the line search parameters for optimal controllers are also given in parentheses.

Table 8.3 shows the design results using Theorem 8.1 with Algorithm II in which threshold ρ was set as 0.001.

Table 8.4 shows the design results using Lemma 8.4 with matrix \mathcal{E}_2 being set to be $\varepsilon_2 I_n$ with a positive scalar ε_2 and all parameter-dependent decision matrices being set to be parametrically affine. In this case, the conditions of Lemma 8.4 are all parametrically affine. Thus, they were solved without Lemma 8.8 being applied. The line search for ε_2 was conducted with six points linearly gridded over a logarithmic scale in the interval $[10^{-5}, 10^5]$.

Table 8.5 shows the design results using Lemma 8.6 but with δ being set to 0. The line search for ε_1 was conducted with six points linearly gridded over a logarithmic scale in the interval $[10^{-5}, 10^5]$.

We first examine the conservatism of two algorithms, line search algorithm and iterative algorithm. Comparison of Tables 8.2 and 8.3 for $\xi \neq 0$ confirms that the iterative algorithm has a good potential to produce less conservative controllers

Table 8.2 Optimal γ_∞ when designing GSOF controllers using Theorem 8.1 with Algorithm I

ζ	(i), (a)	(i), (b)	(i), (c)	(i), (d)	(ii), (a)	(ii), (b)	(ii), (c)	(ii), (d)
0	0.111	0.111	0.111	0.111	0.111	0.111	0.111	0.111
	(1.0e+3, 1.0e+5)	(1.0e+3, 1.0e-5)	(1.0e+5, 1.0e+5)	(1.0e+3, 1.0e-5)	(1.0e+3, 1.0e+5)	(1.0e+5, 1.0e-5)	(1.0e+5, 1.0e+5)	(1.0e+3, 1.0e-5)
	1	0.119	0.119	0.119	0.118	0.118	0.118	0.118
100	(1.0e-1, 1.0e+5)	(1.0e-1, 1.0e-5)	(1.0e-1, 1.0e+5)	(1.0e-1, 1.0e-5)	(1.0e-1, 1.0e+5)	(1.0e-1, 1.0e-5)	(1.0e-1, 1.0e+5)	(1.0e-1, 1.0e-5)
	100	0.152	0.152	0.152	0.152	0.152	0.152	0.152
	(1.0e+5, 1.0e+5)	(1.0e+5, 1.0e-5)	(1.0e+5, 1.0e+5)	(1.0e+5, 1.0e-5)	(1.0e+5, 1.0e+5)	(1.0e+5, 1.0e-5)	(1.0e+5, 1.0e+5)	(1.0e+5, 1.0e-5)
10,000	0.153	0.153	0.153	0.153	0.153	0.153	0.153	0.153
	(1.0e+5, 1.0e+5)	(1.0e+5, 1.0e-5)	(1.0e+5, 1.0e+5)	(1.0e+5, 1.0e-5)	(1.0e+5, 1.0e+5)	(1.0e+5, 1.0e-5)	(1.0e+5, 1.0e+5)	(1.0e+5, 1.0e-5)
	0.1	0.177	0.247	0.240	0.177	0.247	0.161	0.240
0.1	(1.0e+5, 1.0e-1)	(1.0e+5, 1.0e-1)	(1.0e+5, 1.0e-1)	(1.0e+5, 1.0e-1)	(1.0e+5, 1.0e-1)	(1.0e+5, 1.0e-1)	(1.0e+5, 1.0e-1)	(1.0e+5, 1.0e-1)
	1	0.209	0.310	0.302	0.209	0.310	0.193	0.301
	(1.0e+1, 1.0e-1)	(1.0e-1, 1.0e-1)	(1.0e+1, 1.0e-1)	(1.0e+1, 1.0e-1)	(1.0e+1, 1.0e-1)	(1.0e-1, 1.0e-1)	(1.0e+1, 1.0e-1)	(1.0e+1, 1.0e-1)
100	0.218	0.314	0.205	0.307	0.218	0.314	0.205	0.307
	(1.0e+5, 1.0e-1)	(1.0e+5, 1.0e-1)	(1.0e+5, 1.0e-1)	(1.0e+5, 1.0e-1)	(1.0e+5, 1.0e-1)	(1.0e+5, 1.0e-1)	(1.0e+5, 1.0e-1)	(1.0e+5, 1.0e-1)
	100	0.218	0.314	0.307	0.218	0.314	0.205	0.307
100	(1.0e+5, 1.0e-1)	(1.0e+5, 1.0e-1)	(1.0e+5, 1.0e-1)	(1.0e+5, 1.0e-1)	(1.0e+5, 1.0e-1)	(1.0e+5, 1.0e-1)	(1.0e+5, 1.0e-1)	(1.0e+5, 1.0e-1)
	100	0.218	0.314	0.307	0.218	0.314	0.205	0.307
	100	0.218	0.314	0.307	0.218	0.314	0.205	0.307

(continued)

Table 8.2. (continued)

ξ	ζ	(i), (a)	(i), (b)	(i), (c)	(i), (d)	(ii), (a)	(ii), (b)	(ii), (c)	(ii), (d)
0.5	0	0.711	1.582	0.646	1.537	0.711	1.582	0.646	1.537
		(1.0e+5, 1.0e-1)	(1.0e+5, 1.0e-1)	(1.0e+5, 1.0e-1)	(1.0e+5, 1.0e-1)	(1.0e+5, 1.0e-1)	(1.0e+5, 1.0e-1)	(1.0e+5, 1.0e-1)	(1.0e+5, 1.0e-1)
1	1	0.717	1.652	0.653	1.623	0.717	1.653	0.652	1.622
		(1.0e+1, 1.0e-1)	(1.0e-1, 1.0e-1)	(1.0e+1, 1.0e-1)	(1.0e+1, 1.0e-1)	(1.0e+1, 1.0e-1)	(1.0e-1, 1.0e-1)	(1.0e+1, 1.0e-1)	(1.0e+1, 1.0e-1)
1.0	100	0.734	1.675	0.670	1.629	0.734	1.675	0.670	1.629
		(1.0e+5, 1.0e-1)	(1.0e+5, 1.0e-1)	(1.0e+5, 1.0e-1)	(1.0e+5, 1.0e-1)	(1.0e+5, 1.0e-1)	(1.0e+5, 1.0e-1)	(1.0e+5, 1.0e-1)	(1.0e+5, 1.0e-1)
1.0	0	1.549	4.556	1.436	4.503	1.549	4.556	1.436	4.503
		(1.0e+5, 1.0e-1)	(1.0e+5, 1.0e-1)	(1.0e+5, 1.0e-1)	(1.0e+5, 1.0e-1)	(1.0e+5, 1.0e-1)	(1.0e+5, 1.0e-1)	(1.0e+5, 1.0e-1)	(1.0e+5, 1.0e-1)
1	1	1.549	4.556	1.436	4.503	1.549	4.556	1.436	4.503
		(1.0e+5, 1.0e-1)	(1.0e+5, 1.0e-1)	(1.0e+5, 1.0e-1)	(1.0e+5, 1.0e-1)	(1.0e+5, 1.0e-1)	(1.0e+5, 1.0e-1)	(1.0e+5, 1.0e-1)	(1.0e+5, 1.0e-1)
100	100	1.549	4.556	1.436	4.503	1.549	4.556	1.436	4.503
		(1.0e+5, 1.0e-1)	(1.0e+5, 1.0e-1)	(1.0e+5, 1.0e-1)	(1.0e+5, 1.0e-1)	(1.0e+5, 1.0e-1)	(1.0e+5, 1.0e-1)	(1.0e+5, 1.0e-1)	(1.0e+5, 1.0e-1)

“(i), (a),” etc. in the first row denote the choices of (8.21) and (8.22), and the numbers in parentheses denote the values of line search parameters, ϵ_1 and ϵ_2 , in order, for optimal controllers

Table 8.3 Optimal γ_∞ when designing GSOF controllers using Theorem 8.1 with Algorithm II

ξ	ζ	(i), (a)	(i), (b)	(i), (c)	(i), (d)	(ii), (a)	(ii), (b)	(ii), (c)	(ii), (d)
0	0	0.111	0.118	0.111	0.119	0.111	0.119	0.111	0.120
	1	0.118	0.120	0.118	0.121	0.118	0.130	0.118	0.130
	100	0.153	0.155	0.153	0.159	0.153	0.155	0.153	0.159
	10,000	0.153	0.156	0.153	0.160	0.153	0.156	0.153	0.160
0.1	0	0.130	0.136	0.183	0.128	0.130	0.135	0.183	0.128
	1	0.159	0.163	0.191	0.155	0.158	0.159	0.189	0.153
	100	0.172	0.171	0.258	0.173	0.172	0.171	0.256	0.173
0.5	0	0.212	0.212	0.533	0.276	0.212	0.212	0.532	0.277
	1	0.230	0.233	0.461	0.309	0.231	0.231	0.439	0.311
	100	0.235	0.235	0.433	0.310	0.235	0.235	0.397	0.311
1.0	0	0.290	0.474	1.221	0.503	0.290	0.477	1.214	0.503
	1	0.290	0.474	1.466	0.504	0.290	0.471	0.900	0.504
	100	0.290	0.477	1.195	0.503	0.290	0.479	1.304	0.503

“(i), (a)”, etc. in the first row denote the choices of (8.21) and (8.22)

Table 8.4 Optimal γ_∞ when designing GSOF controllers using Lemma 8.4

ξ	(a)	(b)	(c)	(d)
0	0.153	0.153	0.153	0.153
	(1.0e+5)	(1.0e-5)	(1.0e+5)	(1.0e-5)
0.1	0.218	0.314	0.205	0.307
	(1.0e-1)	(1.0e-1)	(1.0e-1)	(1.0e-1)
0.5	0.734	1.675	0.670	1.629
	(1.0e-1)	(1.0e-1)	(1.0e-1)	(1.0e-1)
1.0	1.549	4.556	1.436	4.503
	(1.0e-1)	(1.0e-1)	(1.0e-1)	(1.0e-1)

“(a)”, etc. in the first row denote the choice of (8.22), and the numbers in parentheses denote the values of line search parameter ε_2 for optimal controllers

than the line search algorithm. This fact is reasonable as the iterative algorithm uses matrix \mathcal{E}_2 instead of scalar ε_2 . However, the iterative algorithm sometimes, in particular $\xi = 0$, produces more conservative controllers than the line search algorithm. This may be caused by the rough stopping criterion as $\rho = 0.001$.

We next examine the recovery of Theorem 8.1 to Lemma 8.4. Comparison of Table 8.2 for large values of ζ and Table 8.4 confirms that Theorem 8.3 holds.

We finally examine the recovery of Theorem 8.1 to Lemma 8.6. Comparison of Table 8.2 for $\xi = 0$ and Table 8.5 confirms that Theorem 8.4 holds.

Table 8.5 Optimal γ_∞ when designing GSOF controllers using Lemma 8.6 with δ being set to 0

ζ	(i)	(ii)
0	0.111 (1.0e+5)	0.111 (1.0e+5)
1	0.119 (1.0e-1)	0.118 (1.0e-1)
100	0.152 (1.0e+5)	0.152 (1.0e+5)
10,000	0.153 (1.0e+5)	0.153 (1.0e+5)

“(i)” and “(ii)” in the first row denote the choice of (8.21), and the numbers in parentheses denote the values of line search parameter ϵ_1 for optimal controllers

8.4.2 Example in [18]

The state-space matrices of LPV system $G(\theta)$ are given as

$$\left[\begin{array}{c|c|c} A(\theta) & B_1(\theta) & B_2(\theta) \\ \hline C_1(\theta) & D_{11}(\theta) & D_{12}(\theta) \\ \hline C_2(\theta) & D_{21}(\theta) & \end{array} \right] = \left[\begin{array}{ccc|cc} -4 & 3 & 5 & 1 & 0 \\ 0 & 7 & -5 & -2 & 16 \\ 0.1 & -2 & -3 & 1 & -10 \\ \hline 1 & 1 & 0 & 0 & 1 \\ \hline 0 & 1 & 0 & 2 & \end{array} \right] + \theta \left[\begin{array}{ccc|cc} 1 & 0 & 1 & 0 & 1 \\ 2 & 0 & -5 & 0 & -5 \\ 2.5 & 1.5 & 0 & 0 & 3.5 \\ \hline 0 & 0 & 0 & 0 & 0 \\ \hline 0 & 0 & 0 & 0 & \end{array} \right], \tag{8.44}$$

where scheduling parameter θ is bounded as $|\theta| \leq 3$, the variation rate of θ is bounded as $|\dot{\theta}| \leq \zeta$, the uncertainty δ in the provided scheduling parameter is bounded as $|\delta| \leq \xi$, and the variation rate of δ is bounded as $|\dot{\delta}| \leq 10 \times \zeta$. We consider the following sets for ζ and ξ :

$$\zeta \in \{0, 1, 10\},$$

$$\xi \in \{0, 0.01, 0.05\}.$$

Since the state-space matrices in (8.44) do not satisfy Assumption 8.1, a strictly proper LTI filter $1/(0.01s + 1)$ is implemented to control input u .

Hereafter, “ ∞ ” in tables denotes that no stabilizing controllers were obtained.

We first design GSOF controllers with δ being set to 0 using the method in [1], in which all parameter-dependent decision matrices apart from $X(\theta)$ and $Y(\theta)$ are set to be affine with respect to θ . The results are shown in Table 8.6. Note that the controllers designed using parameter-dependent $X(\theta)$ and $Y(\theta)$ depend on the derivative of the scheduling parameter $\dot{\theta}$.

For reference, we design GSSF controllers using Lemma 8.9 in the appendix. The results are shown in Table 8.7. Considering that the method in Lemma 8.9 is a

Table 8.6 Optimal γ_∞ when designing GSOF controllers using method in [1] with δ being set to 0

ζ	Parametrically affine $X(\theta), Y(\theta)$	Parametrically affine $X(\theta)$ and constant Y	Constant X and parametrically affine $Y(\theta)$	Constant X, Y
0	19.291	∞	26.071	∞
1	21.383	∞	27.500	∞
10	32.043	∞	37.291	∞

Table 8.7 Optimal γ_∞ when designing GSSF controllers using Lemma 8.9

ξ	ζ	Parametrically affine decision matrices	Quadratically parameter-dependent decision matrices
0	0	1.068	1.045
	1	1.144	1.087
	10	1.796	1.445
0.01	0	1.093	1.058
	1	1.907	1.509
	10	∞	∞
0.05	0	1.174	1.100
	1	1.956	1.536
	10	∞	∞

Table 8.8 Optimal γ_∞ when designing GSOF controllers using Theorem 8.1 with Algorithm II and parametrically affine decision matrices

ξ	ζ	(i), (a)	(i), (b)	(i), (c)	(i), (d)	(ii), (a)	(ii), (b)	(ii), (c)	(ii), (d)
0	0	∞	19.302	574.876	21.071	∞	21.070	574.934	19.333
	1	707.225	22.357	707.225	22.115	706.637	22.384	706.631	23.472
	10	1,802.908	38.072	1,802.839	36.919	1,822.564	37.473	1,822.579	38.689
0.01	0	∞	22.964	612.772	21.819	∞	22.965	612.770	22.553
	1	∞	43.109	∞	45.381	∞	46.747	∞	44.454
	10	∞	∞	∞	∞	∞	∞	∞	∞
0.05	0	∞	72.698	826.937	55.589	∞	72.697	∞	60.873
	1	∞	485.940	∞	243.284	∞	479.622	∞	∞
	10	∞	∞	∞	∞	∞	∞	∞	∞

“(i), (a)”, etc. in the first row denote the choices of (8.21) and (8.22)

direct extension of the conventional method of GSSF controllers and no additional conservatism is consequently introduced, the results in Table 8.7 for $\zeta = 10$ and $\xi \neq 0$ reveal the difficulty for designing GS controllers which are robust against the uncertainties on the scheduling parameters.

We next design GSOF controllers using Theorem 8.1, in which iterative algorithm was conducted with threshold $\rho = 0.001$, with parametrically affine decision matrices and quadratically parameter-dependent decision matrices. The results are given in Tables 8.8 and 8.9.

Table 8.9 Optimal γ_∞ when designing GSOF controllers using Theorem 8.1 with Algorithm II and quadratically parameter-dependent decision matrices

ξ	ζ	(i), (a)	(i), (b)	(i), (c)	(i), (d)	(ii), (a)	(ii), (b)	(ii), (c)	(ii), (d)
0	0	401.295	17.750	401.298	17.751	401.342	16.352	401.346	16.345
	1	477.443	19.509	480.690	19.513	478.102	18.541	475.105	18.665
	10	1,339.922	31.767	1,339.905	31.785	1,323.187	31.579	1,323.236	31.582
0.01	0	431.811	19.281	417.931	18.859	431.805	19.276	417.875	18.859
	1	∞	35.993	∞	37.311	∞	35.597	∞	37.101
	10	∞	∞	∞	∞	∞	∞	∞	∞
0.05	0	673.785	53.386	544.276	44.844	673.778	53.388	544.288	44.842
	1	∞	199.587	∞	147.354	∞	196.162	∞	146.467
	10	∞	∞	∞	∞	∞	∞	∞	∞

“(i), (a)”, etc. in the first row denote the choices of (8.21) and (8.22)

We first examine the conservatism of our method compared to the conventional method in [1]. The least γ_∞ 's in Table 8.8 for $\xi = 0$ are 19.302, 22.115, and 36.919, respectively for $\zeta = 0, 1$, and 10. Although they are worse than the least conservative results in Table 8.6, i.e. 19.291, 21.383, and 32.043, by about 0.06%, 3.4%, and 15.2%, respectively, our controllers have good implementability as being independent of θ . On the other hand, those values are better than the γ_∞ 's obtained using the method in [1] with constant X and parametrically affine $Y(\theta)$. That is, this example illustrates that our method can produce good compromised controllers between conservatism and implementability.

We next examine the conservatism with respect to the parameter dependency of decision matrices. The values in Table 8.9 are all smaller than the corresponding values in Table 8.8. Thus, high-order parameter-dependent decision matrices are recommended to obtain controllers with small conservatism. However, the GSOF controllers in Table 8.9 become more complicated than those in Table 8.8. To obtain practical GSOF controllers, Problem 8.3 is then solved.

Let us consider the case of $\xi = 0.01$ and $\zeta = 1$. Table 8.9 implies that the controller designed using the choices of (ii) and (b) has the best performance $\gamma_\infty = 35.597$.

We solve Problem 8.3 using the solution $(\mathcal{L}(\theta + \delta), \mathcal{L}(\theta + \delta))$ to the conditions of Theorem 8.1 with the choices of (ii) and (b). As the matrix $X_{c1}(\theta + \delta)$ defined in (8.17) is complicated as rational, PDLMI (8.11) is solved at all combinations of linearly gridded ten points in the intervals of $\theta, \hat{\theta}, \delta$ and $\hat{\delta}$, i.e., at 10,000 combinations of these variables. We first set the parameter-dependent matrix $\bar{K}(\theta + \delta)$ to be affine, then it is found that the problem is infeasible. We then set $\bar{K}(\theta + \delta)$ to be quadratically parameter-dependent, then a feasible solution is found. We further set $\bar{K}(\theta + \delta)$ to be cubically parameter-dependent, then a feasible solution is also found.

For reference, we check the H_∞ performance of the closed-loop system using the quadratically and rationally parameter-dependent GSOF controllers with the assumption that the scheduling parameter and the uncertainty are both frozen in their intervals. The maximum H_∞ performance of the closed-loop system using

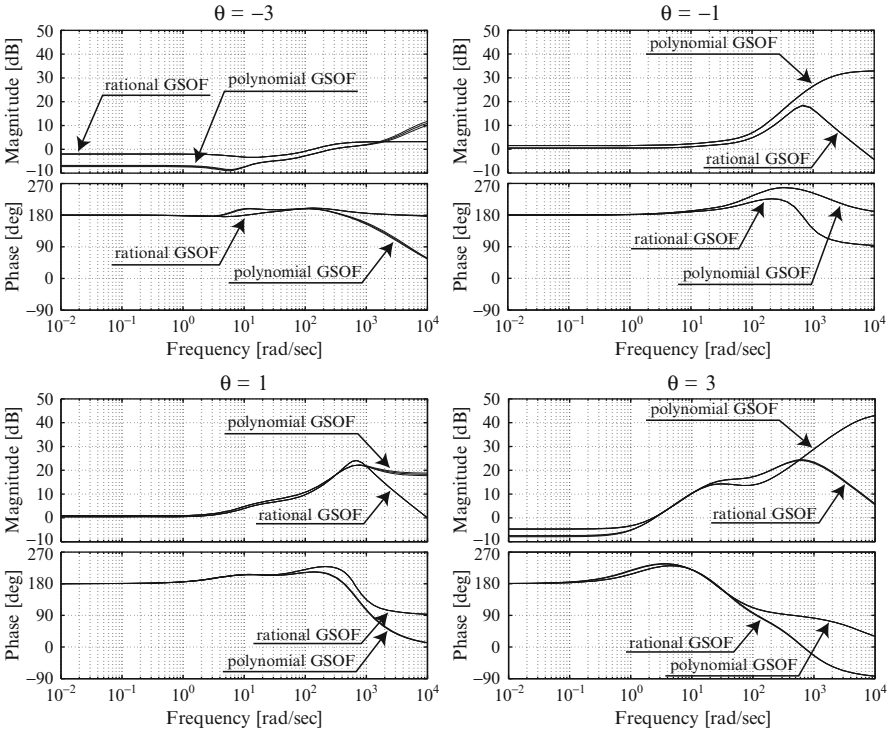


Fig. 8.2 Bode plots of rationally parameter-dependent GSOF controller and quadratically parameter-dependent GSOF controller (three lines corresponding to $\delta = -0.01, 0, 0.01$ are drawn for each controller)

the quadratically parameter-dependent GSOF controller among all combinations of linearly gridded 1,000 points in the intervals of θ and δ , i.e., of 10^6 combinations of these variables, is obtained as 21.573, and the corresponding value using the rationally parameter-dependent GSOF controller is 20.235. It is confirmed that these values are smaller than the value of γ_∞ when designing the rationally parameter-dependent GSOF controller.

Figure 8.2 shows the Bode plots of the two controllers, i.e., quadratically and rationally parameter-dependent GSOF controllers at frozen values of θ as $-3, -1, 1,$ and 3 , and Fig. 8.3 shows the gain plots of the closed-loop systems with the two controllers at the same values of the frozen θ . Figure 8.2 confirms that frequency responses of the two controllers at frozen scheduling parameters are similar to each other in the low frequencies, and Fig. 8.3 confirms that the gain properties of the closed-loop systems are also similar to each other.

This example indicates that we can design simple GSOF controllers by solving Problem 8.3 after designing rationally parameter-dependent GSOF controllers using Theorem 8.1.

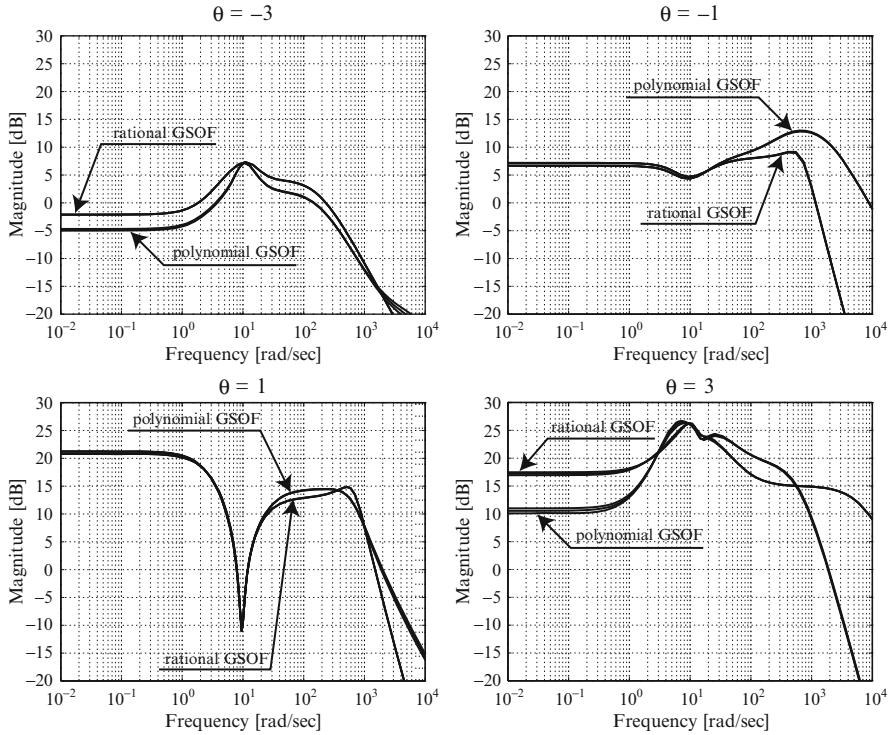


Fig. 8.3 Gain plots of closed-loop systems with rationally parameter-dependent GSOF controller and quadratically parameter-dependent GSOF controller (three lines corresponding to $\delta = -0.01, 0, 0.01$ are drawn for each controller)

8.5 Conclusions

This article tackles the design problem of gain-scheduled output-feedback (GSOF) controllers for continuous-time LPV systems via parameter-dependent Lyapunov functions (PDLFs). In stark contrast to conventional problem setting, GSOF controllers are required to have the following properties: robustness against uncertainties in the provided scheduling parameters and independence from the derivatives of the provided scheduling parameters. We successfully propose a new design method for our problem in terms of PDBMIs. We show two algorithms for solving the PDBMIs, i.e., line search algorithm and iterative algorithm. It is also proved that our method recovers conventional methods when scheduling parameters are precisely provided, or parameter-independent Lyapunov functions (PiDLFs) or structured PDLFs are adopted.

For further good implementability of designed GSOF controllers, we show that it is always possible to design polynomially parameter-dependent GSOF controllers if rationally parameter-dependent GSOF controllers can be designed under a very mild constraint for LPV systems.

The design results for numerical examples borrowed from the literature well support our results.

Acknowledgments This work was supported by the Ministry of Education, Culture, Sports, Science and Technology of Japan under Grant-in-Aid for Young Scientists (B) No. 20760287.

Appendix 1

Lemma 8.7. *For a given matrix $[X_{ij}] \in \mathbb{R}^{p \times q}$, all the elements of which satisfy $|X_{ij}| \leq \kappa$ for a given positive number κ , the following inequality holds:*

$$\|[X_{ij}]\|_2 \leq \kappa \sqrt{pq}. \quad (8.45)$$

Note that $\|x\|_2 = \left\| \begin{bmatrix} \|x_1\|_2 \\ \vdots \\ \|x_q\|_2 \end{bmatrix} \right\|_2 = \left\| \begin{bmatrix} |x_1| \\ \vdots \\ |x_q| \end{bmatrix} \right\|_2$ holds for $x \in \mathbb{R}^q$ [44].

Proof. $\|[X_{ij}]\|_2$ is defined as $\sup_{\|x\|_2=1, x \in \mathbb{R}^q} \|[X_{ij}]x\|_2$. Then,

$$\begin{aligned} \|[X_{ij}]\|_2 &= \sup_{\substack{\|x\|_2=1, \\ x \in \mathbb{R}^q}} \left\| \begin{bmatrix} \sum_{j=1}^q X_{1j}x_j \\ \vdots \\ \sum_{j=1}^q X_{pj}x_j \end{bmatrix} \right\|_2 = \sup_{\substack{\|x\|_2=1, \\ x \in \mathbb{R}^q}} \left\| \begin{bmatrix} \left\| \sum_{j=1}^q X_{1j}x_j \right\|_2 \\ \vdots \\ \left\| \sum_{j=1}^q X_{pj}x_j \right\|_2 \end{bmatrix} \right\|_2 \\ &\leq \sup_{\substack{\|x\|_2=1, \\ x \in \mathbb{R}^q}} \left\| \begin{bmatrix} \sum_{j=1}^q |X_{1j}||x_j| \\ \vdots \\ \sum_{j=1}^q |X_{pj}||x_j| \end{bmatrix} \right\|_2 = \sup_{\substack{\|x\|_2=1, \\ x \in \mathbb{R}^q}} \sqrt{\sum_{i=1}^p \left(\sum_{j=1}^q |X_{ij}||x_j| \right)^2} \\ &\leq \sup_{\substack{\|x\|_2=1, \\ x \in \mathbb{R}^q}} \sqrt{\sum_{i=1}^p \left(\sum_{j=1}^q \kappa |x_j| \right)^2} = \sup_{\substack{\|x\|_2=1, \\ x \in \mathbb{R}^q}} \left\| \begin{bmatrix} \kappa \cdots \kappa \\ \vdots \\ \kappa \cdots \kappa \end{bmatrix} \begin{bmatrix} |x_1| \\ \vdots \\ |x_q| \end{bmatrix} \right\|_2 \\ &\leq \sup_{\substack{\|x\|_2=1, \\ x \in \mathbb{R}^q}} \left\| \begin{bmatrix} \sqrt{\kappa} \\ \vdots \\ \sqrt{\kappa} \end{bmatrix} \right\|_2 \left\| [\sqrt{\kappa} \cdots \sqrt{\kappa}] \right\|_2 \|x\|_2 = \kappa \sqrt{pq}. \end{aligned}$$

Thus, $\|[X_{ij}]\|_2 \leq \kappa \sqrt{pq}$ is proved. \square

Appendix 2

The general form of the SV approach for solving PDLMI is given in [25]. However, the PDLMI to solve in this article include scheduling parameter vector θ as well as uncertainty parameter vector δ . Thus, the approach in [25] is revised as shown below.

Suppose that the state-space matrices of LPV system $G(\theta)$ are parametrically affine and that either $D_{12}(\theta)$ or $D_{21}(\theta)$ is constant. If the decision matrices in our propositions are set to be affinely or quadratically parameter dependent, then the related PDLMI can be written as follows:

$$\begin{aligned} & \left(\begin{bmatrix} 1 \\ \theta + \delta \end{bmatrix} \otimes \mathbf{I} \right)^T \Phi(\theta, \dot{\theta}, \delta, \dot{\delta}) \left(\begin{bmatrix} 1 \\ \theta + \delta \end{bmatrix} \otimes \mathbf{I} \right) < 0, \\ & \forall (\theta, \dot{\theta}, \delta, \dot{\delta}) \in \Omega_\theta \times \Lambda_\theta \times \Omega_\delta \times \Lambda_\delta, \end{aligned} \quad (8.46)$$

where $\Phi(\theta, \dot{\theta}, \delta, \dot{\delta})$ is defined as

$$\Phi(\theta, \dot{\theta}, \delta, \dot{\delta}) = \Phi_0 + \sum_{i=1}^k \theta_i \Phi_i + \sum_{i=1}^k \dot{\theta}_i \hat{\Phi}_i + \sum_{i=1}^k \delta_i \Psi_i + \sum_{i=1}^k \dot{\delta}_i \hat{\Psi}_i$$

with appropriately dimensional matrices Φ_0 , Φ_i , $\hat{\Phi}_i$, Ψ_i , and $\hat{\Psi}_i$ which include decision variables.

The SV approach for solving PDLMI (8.46) is given below.

Lemma 8.8. *If there exists a constant matrix M of appropriate dimensions such that (8.47) holds, then (8.46) holds.*

$$\begin{aligned} & \Phi(\theta, \dot{\theta}, \delta, \dot{\delta}) + \text{He} \left\{ \left(\begin{bmatrix} \theta^T + \delta^T \\ -I_k \end{bmatrix} \otimes \mathbf{I} \right) M \right\} < 0, \\ & \forall (\theta, \dot{\theta}, \delta, \dot{\delta}) \in \text{ver}(\Omega_\theta) \times \text{ver}(\Lambda_\theta) \times \text{ver}(\Omega_\delta) \times \text{ver}(\Lambda_\delta), \end{aligned} \quad (8.47)$$

where $\text{ver}(\cdot)$ denotes the vertex set of the corresponding set.

This lemma is easily proved by multiplying $[1 \ \theta^T + \delta^T] \otimes \mathbf{I}$ and its transpose to (8.47) from the left and the right, respectively.

When $\delta = \mathbf{0}$ holds, the condition of Lemma 8.8 has only to be checked for all pairs $(\theta, \dot{\theta}) \in \text{ver}(\Omega_\theta) \times \text{ver}(\Lambda_\theta)$.

Appendix 3

Here, we show the design methods of GSSF controllers for Problem 8.1 and Problem 8.2.

Lemma 8.9 ([31]). *For LPV system $G(\theta)$ in (8.1), suppose that matrix B_2 is parameter-dependent $B_2(\theta)$, and that C_2 and $D_{21}(\theta)$ are respectively I_n and $\mathbf{0}$. For a given positive number γ_∞ , suppose that there exist a continuously differentiable parameter-dependent matrix $\mathcal{X}_{SF}(\theta + \delta) \in \mathbb{S}^n$ and a parameter-dependent matrix $\mathcal{K}_{SF}(\theta + \delta) \in \mathbb{R}^{n_u \times n}$ such that the following conditions hold for all quadruplets $(\theta, \dot{\theta}, \delta, \dot{\delta}) \in \Omega_\theta \times \Lambda_\theta \times \Omega_\delta \times \Lambda_\delta$:*

$$\mathcal{X}_{SF}(\theta + \delta) > 0, \quad (8.48)$$

$$\begin{aligned} & \left[\begin{array}{cc} \text{He}\{A(\theta)\mathcal{X}_{SF}(\theta + \delta) + B_2(\theta)\mathcal{K}_{SF}(\theta + \delta)\} - \dot{\mathcal{X}}_{SF}(\theta + \delta) & * \\ C_1(\theta)\mathcal{X}_{SF}(\theta + \delta) + D_{12}(\theta)\mathcal{K}_{SF}(\theta + \delta) & -\gamma_\infty^2 I_{n_z} \end{array} \right] \\ & + \begin{bmatrix} B_1(\theta) \\ D_{11}(\theta) \end{bmatrix} [B_1(\theta)^T \ D_{11}(\theta)^T] < 0, \end{aligned} \quad (8.49)$$

then the GSSF controller $u = K_{SF}(\theta + \delta)x$ with $K_{SF}(\theta + \delta) = \mathcal{K}_{SF}(\theta + \delta)\mathcal{X}_{SF}(\theta + \delta)^{-1}$ stabilizes the closed-loop system and satisfies (8.8) for all admissible quadruplets $(\theta, \dot{\theta}, \delta, \dot{\delta}) \in \Omega_\theta \times \Lambda_\theta \times \Omega_\delta \times \Lambda_\delta$.

Lemma 8.10 ([31]). *For LPV system $G(\theta)$ in (8.1), suppose that matrix B_2 is parameter-dependent $B_2(\theta)$, and that $D_{11}(\theta)$, C_2 and $D_{21}(\theta)$ are, respectively, $\mathbf{0}$, I_n and $\mathbf{0}$. For a given positive number γ_2 , suppose that there exist a continuously differentiable parameter-dependent matrix $\mathcal{X}_{SF}(\theta + \delta) \in \mathbb{S}^n$, and parameter-dependent matrices $\mathcal{K}_{SF}(\theta + \delta) \in \mathbb{R}^{n_u \times n}$ and $\mathcal{Q}(\theta, \theta + \delta) \in \mathbb{S}^{n_w}$ such that the following conditions hold for all quadruplets $(\theta, \dot{\theta}, \delta, \dot{\delta}) \in \Omega_\theta \times \Lambda_\theta \times \Omega_\delta \times \Lambda_\delta$:*

$$\left[\begin{array}{cc} \text{He}\{A(\theta)\mathcal{X}_{SF}(\theta + \delta) + B_2(\theta)\mathcal{K}_{SF}(\theta + \delta)\} - \dot{\mathcal{X}}_{SF}(\theta + \delta) & * \\ C_1(\theta)\mathcal{X}_{SF}(\theta + \delta) + D_{12}(\theta)\mathcal{K}_{SF}(\theta + \delta) & -I_{n_z} \end{array} \right] < 0, \quad (8.50)$$

$$\left[\begin{array}{cc} \mathcal{Q}(\theta, \theta + \delta) & * \\ B_1(\theta) & \mathcal{X}_{SF}(\theta + \delta) \end{array} \right] > 0, \quad (8.51)$$

$$\gamma_2^2 - \text{Tr}(\mathcal{Q}(\theta, \theta + \delta)) > 0, \quad (8.52)$$

then the GSSF controller $u = K_{SF}(\theta + \delta)x$ with $K_{SF}(\theta + \delta) = \mathcal{K}_{SF}(\theta + \delta)\mathcal{X}_{SF}(\theta + \delta)^{-1}$ stabilizes the closed-loop system and satisfies (8.9) for all admissible quadruplets $(\theta, \dot{\theta}, \delta, \dot{\delta}) \in \Omega_\theta \times \Lambda_\theta \times \Omega_\delta \times \Lambda_\delta$.

References

1. Apkarian P, Adams RJ (1998) Advanced gain-scheduling techniques for uncertain systems. *IEEE Trans Contr Syst Technol* 6(1):21–32
2. Apkarian P, Adams RJ (2000) Advanced gain-scheduling techniques for uncertain systems. In: Ghaoui LE, Niculescu S (eds) *Advances in linear matrix inequality methods in control*. SIAM, Philadelphia, pp 209–228
3. Apkarian P, Gahinet P (1995) A convex characterization of gain-scheduled H_∞ controllers. *IEEE Trans Automat Contr* 40(5):853–864
4. Apkarian P, Gahinet P, Becker G (1995) Self-scheduled H_∞ control of linear parameter-varying systems: a design example. *Automatica* 31(9):1251–1261
5. Becker G, Packard A (1994) Robust performance of linear parametrically varying systems using parametrically-dependent linear feedback. *Syst Contr Lett* 23(3):205–215
6. Bernussou J, Peres PLD, Geromel JC (1989) A linear programming oriented procedure for quadratic stabilization of uncertain systems. *Syst Contr Lett* 13:65–72
7. Bliman PA (2004) An existence result for polynomial solutions of parameter-dependent LMIs. *Syst Contr Lett* 51(3-4):165–169
8. Chesi G (2010) LMI techniques for optimization over polynomials in control: a survey. *IEEE Trans Automat Contr* 55(11):2500–2510
9. Chesi G, Garulli A, Tesi A, Vicino A (2009) *Homogeneous polynomial forms for robustness analysis of uncertain systems*. Springer, Berlin
10. Chesi G, Henrion D (eds) (2009) *Special issue on positive polynomials in control*. *IEEE Trans Automat Contr* 54(5):935–1064
11. Chilali M, Gahinet P (1996) H_∞ design with pole placement constraints: an LMI approach. *IEEE Trans Automat Contr* 41(3):358–367
12. Daafouz J, Bernussou J, Geromel JC (2008) On inexact LPV control design of continuous-time polytopic systems. *IEEE Trans Automat Contr* 53(7):1674–1678
13. Henrion D, Garulli A (eds) (2005) *Positive polynomials in control*. Springer, Berlin
14. Köroğlu H (2010) Robust generalized asymptotic regulation via an LPV controller without parameter derivative dependence. In: *Proceedings of the 49th IEEE conference on decision and control*, Atlanta, Georgia, pp 4965–4971
15. Leith DJ, Leithead WE (2000) Survey of gain-scheduling analysis and design. *Int J Control* 73(11):1001–1025
16. Löfberg J (2004) YALMIP: a toolbox for modeling and optimization in MATLAB. In: *Proceedings of the CACSD conference*, Taipei, Taiwan, pp 284–289. <http://control.ee.ethz.ch/~joloef/yalmip.php>
17. Masubuchi I, Kato J, Saeki M, Ohara A (2004) Gain-scheduled controller design based on descriptor representation of LPV systems: application to flight vehicle control. In: *Proceedings of the 43rd IEEE conference on decision and control*, Atlantis, Paradise Island, Bahamas, pp 815–820
18. Masubuchi I, Kurata I (2009) Gain-scheduled control synthesis by using filtered scheduling parameters. In: *Proceedings of the 48th IEEE conference on decision and control*, Shanghai, P.R. China, pp 2180–2185
19. Masubuchi I, Ohara A, Suda N (1998) LMI-based output feedback controller design: a unified formulation and solution. *Int J Robust Nonlinear Contr* 8(8):669–686
20. Ohara A, Yamaguchi Y, Morito T (2001) LPV modeling and gain scheduled control of re-entry vehicle in approach and landing phase. In: *AIAA guidance, navigation, and control conference and exhibit*, AIAA 2001-4038, Montreal, Canada
21. Packard A (1994) Gain scheduling via linear fractional transformations. *Syst Contr Lett* 22(2):79–92
22. Papageorgiou G, Glover K (1999) Design of a robust gain scheduled controller for the high incidence research model. In: *AIAA guidance, navigation, and control conference and exhibit*, AIAA-1999-4276, Portland, Oregon

23. Papageorgiou G, Glover K, D’Mello G, Patel Y (2000) Taking robust LPV control into flight on the VAAC harrier. In: Proceedings of the 39th IEEE conference on decision and control, Sydney, Australia, pp 4558–4564
24. Parrilo PA (2003) Semidefinite programming relaxations for semialgebraic problems. *Math Program Ser B* 96(2):293–320
25. Peaucelle D, Sato M (2009) LMI tests for positive definite polynomials: slack variable approach. *IEEE Trans Automat Contr* 54(4):886–891
26. Petersen IR (1987) A stabilization algorithm for a class of uncertain linear systems. *Syst Contr Lett* 8(4):351–357
27. Prempain E, Postlethwaite I (2008) L_2 and H_2 performance analysis and gain-scheduling synthesis for parameter-dependent systems. *Automatica* 44(8):2081–2089
28. Rugh WJ, Shamma J (2000) Research on gain scheduling. *Automatica* 36(10):1401–1425
29. Sato M (2008) Design method of gain-scheduled controllers not depending on derivatives of parameters. *Int J Contr* 81(6):1013–1025
30. Sato M (2010) Gain-scheduled output-feedback controllers using inexactly measured scheduling parameters. In: Proceedings of the 49th IEEE conference on decision and control, Atlanta, Georgia, pp 3174–3080
31. Sato M, Ebihara Y, Peaucelle D (2010) Gain-scheduled state-feedback controllers using inexactly measured scheduling parameters: H_2 and H_∞ problems. In: Proceedings of the American control conference, Baltimore, Maryland, pp 3094–3099
32. Sato M, Peaucelle D Gain-scheduled output feedback controllers using inexact scheduling parameters for continuous-time LPV systems. (submitted)
33. Sato M (2011) Gain-scheduled output feedback controllers depending solely on scheduling parameters via parameter-dependent Lyapunov functions. *Automatica* 47(12):2786–2790
34. Sato M, Peaucelle D (2011) Gain-scheduled H_∞ controllers being derivative-free of scheduling parameters via parameter-dependent Lyapunov functions. In: Proceedings of the 18th IFAC world congress, Milano, Italy, pp 7951–7956
35. Scherer CW (1996) Mixed H_2/H_∞ control for time-varying and linear parametrically-varying systems. *Int J Robust Nonlinear Contr* 6(9-10):929–952
36. Scherer C, Gahinet P, Chilali M (1997) Multiobjective output-feedback control via LMI optimization. *IEEE Trans Automat Contr* 42(7):896–911
37. Scherer CW, Hol CWJ (2006) Matrix sum-of-squares relaxations for robust semi-definite programs. *Math Program Ser B* 107(1-2):189–211
38. Sturm JS (1999) Using SeDuMi 1.02, a MATLAB toolbox for optimization over symmetric cones. *Optim Method Softw* 11:625–653
39. Sznaier M (1999) Receding horizon: an easy way to improve performance in LPV systems. In: Proceedings of the American control conference, San Diego, California, pp 2257–2261
40. Witte J, Balini HMNK, Scherer CW (2010) Robust and LPV control of an AMB system. In: Proceedings of the American control conference, Baltimore, Maryland, pp 2194–2199
41. Wu F, Dong K (2006) Gain-scheduling control of LFT systems using parameter-dependent Lyapunov functions. *Automatica* 42(1):39–50
42. Wu F, Yang XH, Packard A, Becker G (1996) Induced L_2 -norm control for LPV systems with bounded parameter variation rates. *Int J Robust Nonlinear Contr* 6(9-10):983–998
43. Xie L, de Souza CE (1992) Robust H_∞ control for linear systems with norm-bounded time-varying uncertainty. *IEEE Trans Automat Contr* 37(8):1188–1191
44. Zhou K, Doyle JC, Glover K (1996) Robust and optimal control. Prentice Hall, Upper Saddle River, New Jersey

Chapter 9

Decentralised Model Predictive Control of Time-Varying Splitting Parallel Systems

Tri Tran, H.D. Tuan, Q.P. Ha, and Hung T. Nguyen

Abstract This chapter is devoted to the development of a decentralised model predictive control (MPC) strategy for splitting parallel systems that have *time-varying* and *unknown splitting ratios*. The large-scale system in consideration consists of several dynamically-coupled modular subsystems. Each subsystem is regulated by a dedicated multivariable controller employing the open-loop MPC algorithms in conjunction with stability constraints. The connection topology of the large-scale systems includes serial, parallel and recirculated configurations. The solution to splitting parallel systems in this chapter is not only an alternative to the hybrid approach for duty-standby modes, but also a novel approach that accommodates the concurrent operations of splitting parallel systems. The effectiveness of this approach rests on the newly introduced *asymptotically positive real constraint* (APRC) which prescribes an approaching characteristic towards a positive real property of the system under control. The asymptotic attribute of APRC smooths out all significant wind-up actions in the control trajectories. The APRCs are developed into a one-time-step quadratic constraint on the local control vectors, which plays the role of a stability constraint for the decentralised MPC. The recursive feasibility is assured by characterizing the APRC with dynamic multiplier matrices. Numerical simulations for two typical modular systems in an alumina refinery are provided to illustrate the theoretical results.

T. Tran • H.D. Tuan (✉) • Q.P. Ha • H.T. Nguyen
Faculty of Engineering and Information Technology, University of Technology,
Sydney, 15 Broadway, Ultimo, NSW-2007, Australia
e-mail: TCTran@ieee.org; Tuan.Hoang@uts.edu.au; h.d.tuan@unsw.edu.au;
Quang.Ha@eng.uts.edu.au; Hung.Nguyen@uts.edu.au

9.1 Industrial Plant-Wide Process Control and Time-Varying Splitting Systems

9.1.1 Departmentalisation and Mixed Operational Mode

In industrial plant-wide process system design, it is admirable to have the design strategy of departmentalised systems for the entire large-scale plant. One department having some redundant process streams is dedicated to a processing area where at least one unit operation is involved. Departmentalisation is a method of decomposing the large-scale plant under the perspective of process system designs, operational scheduling, and production planning and management. To increase the operability, maintainability and business continuity, the principle of reliable system designs using parallel redundant subsystems [24] are prevailing in many process industries. The redundancy management within a department can be executed by parallel or duty-standby operations. It can also vary between full-capacity duty-standby and shared-capacity parallel operations. The processing areas are normally connected in a serial configuration with some recirculated paths as conceptually depicted in Fig. 9.1.

In the plant-wide process control and optimisation design, it is common to implement one centralised multivariable MPC for a single subsystem of a department, due to the intricate interaction between its state variables. There are thus several MPCs implemented for different subsystems and departments in a large-scale processing plant in a distributed or decentralised manner. The envisaged issues arising from running the whole plant with such disparate MPCs may come from the department start-ups and warm re-starts after a shutdown, or from the process stream switch-overs and operational mode changes. Specifically, the issues faced by plant operations can be listed as

- The synchronisation between local MPCs during the starting up and warm restarting periods
- The start-up of a process stream while the others are running

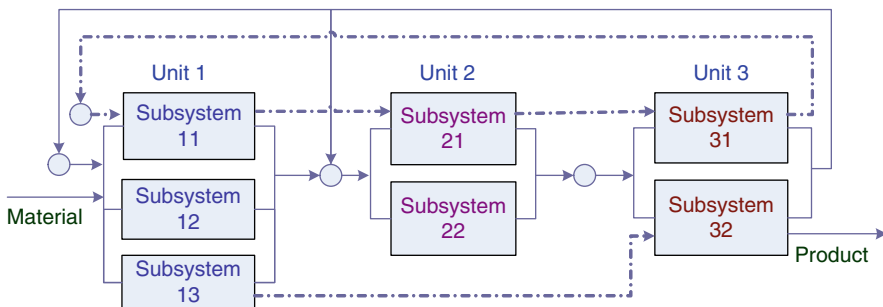


Fig. 9.1 Mixed connection topology of an interconnected system

- The switch-over between the duty and standby process streams within one department while the downstream and remaining departments are in full or reduced-capacity operations
- The operational mode change of a downstream department (e.g. from Automatic to Manual control mode) while the upstream departments are operating in their Automatic control mode

These activities are always costly to the plant operations due to the complexity of shutting down, restarting or switching over tasks. Sometimes they even cause a plant-wide shutdown because of the system instability. The operational efficiency is therefore heavily degraded. Automating these activities by having some forms of orchestrations between the local MPCs will profoundly and ultimately improve the operational performances. Such automation will reduce the down time, as well as shorten the startup, restart, and switching over time, yet maintain the operation at a highest achievable efficiency. A stability assurance measure for the overall system in different operational scenarios will, therefore, be up-most important.

9.1.2 *Time-Varying Splitting Parallel Systems*

The parallel connection of parallel redundancies is universal in process system designs for increasing the reliability, availability and business continuity. The parallel connections, which may destroy the guaranteed-stability property of an existing strategy, are explicitly addressed in our proposed interconnection stabilisability condition. The special requirement in parallelism comes from the splitting ratios of parallel subsystems, which are *unknown* and *time varying*, because of which the existing centralised methods cannot provide efficient solutions. The control of complex interconnection structures which are involved with both serial and parallel configurations have been designed using different hybrid approaches. Whilst being effective with duty-standby operations, wherein a standby subsystem is switched on or off, the hybrid solution cannot be adopted for parallel operations. Furthermore, a centralised controller for parallel connections systems will not be accepted due to reliability and maintainability requirements. Decentralised controllers will thus be desirable. The parallel connections and operations are widespread in the process system designs and process control applications, wherein both duty and standby subsystems are run concurrently to share a common production rate. A continuous control strategy must therefore be employed instead of hybrid strategies. In a continuous control strategy, the changing-overs between duty and standby parallel subsystems are assumed being smooth, i.e., state jumps will not incur due to the changing-over operations.

This chapter presents a continuous control strategy as an alternative to hybrid approaches for splitting parallel systems, which effectively stabilise the plant-wide process in all operational scenarios, including concurrent operation and duty-standby modes. We have addressed the stabilisation for interconnected systems in

a decentralised architecture using a segregated approach of the so-called stabilizing agent [29, 30, 32]. The stability of semi-automatic control systems that are involved with the closed-loop control and man-in-the-loop regulations is achieved in that approach. An alternative and progressing approach to the constructive method for stabilizing controllers based on the asymptotically positive realness constraint (APRC) and its employment in decentralised MPC problems is presented in this chapter. The formulation of MPC is developed in conjunction with the APRC-based quadratic stability constraint, which can be solved by a convex quadratic programming (QP) numerical method. The stabilisability and feasibility conditions are rendered by the linear matrix inequalities (LMI) [4, 7]. Parts of the multiplier matrices of quadratic stability constraints are updated online in this approach to guarantee the recursive feasibility of MPC problems [31].

9.1.3 Novelty and Chapter Contents

A decentralised perspective on the predictive control of modular systems with application in the mineral processes is presented as an essential constituent of this chapter. Special treatments for parallel connections of time-varying and unknown splitting ratios are provided to stabilise the large-scale system having an arbitrary connection topology and mixed operational modes. This decentralised control strategy is cutting edge by employing only decoupled control vectors and precluding artificial constraints on the coupling variables. The former improves the system reliability. The latter mitigates any conservativeness of limiting the energy or material flows between dynamically coupled subsystems. Moreover, a continuous control strategy is proposed for parallel redundant systems as an alternative to the hybrid approaches, which effectively stabilise the plant-wide process in all operational scenarios, including concurrently parallel and duty-standby modes. The special requirement in parallelism comes from the splitting ratios of parallel subsystems, which are *unknown* and *time varying*, because of which the existing centralised methods cannot provide an efficient solution. The mixed connection configuration is dealt with by explicitly incorporating the two types of connections, serial and parallel, into the state space models. The input and output attributes are then capitalised to derive a new interconnection stabilisability condition in the time domain. The issue of unknown and time-varying splitting ratios is tackled by having a combined solution, wherein the quadratic constraint is developed for each individual subsystem while the dissipativity criteria are derived for the whole bulk of subsystems in parallel.

Decentralised control strategies, prevalently used in the field of large-scale interconnected systems, have been comprehensively described in the literature; see, e.g., [16, 18, 27]. In a decentralised architecture, the quadratic optimal control synthesis has been identified with major difficulties. The obstacles around the constructive methods of H_2 or H_∞ decentralised optimal control lie in the nonconvex

nature of optimisation problems. Different results have been presented in the past, such as the computations for uplifting the H_∞ performance based on the finite horizon optimisation in [28], or convex relaxation for decentralised H_2 control [22].

Decentralised model predictive control strategies, the non-communication versions of distributed MPCs have been successfully developed for both dynamically coupled and decoupled systems in the literature; see, e.g., [23]. Albeit being provided with different solutions including coordinative, cooperative, iterative and hierarchical methods, the field of orchestrating disparate MPCs for large interconnected systems is still in its infancy stage [21]. Generic approaches that are applicable to different types of systems and industries are still open for research.

An existence condition for the constrained stabilisation of interconnected systems in the discrete time domain will be derived in this chapter based on the newly introduced APRC [32]. The APRC-based stabilisability conditions are subsequently developed into *stability constraints* for the local MPCs in a decentralised configuration. The recursive feasibility is guaranteed by characterizing the APRC with dynamic multiplier matrices. With the asymptotic attribute, the APRC-based stability constraint smooths out all wind-up control actions. LMI-based stability and feasibility conditions are obtained as a result of the developments. It is well known that if a system is quadratically dissipative with respect to its inputs and outputs then the positive real constraint (PRC) derived from the integral quadratic constraint (IQC) in the time domain (see, e.g., [2, 14, 19]), is sufficient for its stabilisability. The stabilizing control can then be found from those satisfying the positive real condition. However, its lack of correlations between the recursive control states causes unacceptably non-smooth behaviors to the control. As a consequence, it cannot be implemented in constrained control applications. The variations of asymptotic approximation parameters in APRC will make the recursive control states well correlated, thus leads to an efficiently implemented controllers. In other words, the fundamental result of a stabilisable positive real system is not always accompanied by a realisable controller, due to the fact that an infinitely power control may be required. This chapter addresses the issue by introducing the APRC concept for use with constrained control problems. The APRC represents an approaching characteristic towards the positive real property of the system under control.

This chapter is organised as follows. In Sect. 9.2, the system and control models for interconnected systems having splitting parallel subsystems are provided. The interaction-oriented models [16] are used in this chapter. The APRC and a constructive method of quadratic constraints for decentralised model predictive controllers based on the APRC are introduced in Sect. 9.3. Handling parallel redundant subsystems that have time-varying and unknown splitting ratios is another essential part of this section. The control applications of the counter-current washing circuit and the predesilication unit operation in a typical alumina refinery are simulated in Sect. 9.4 to illustrate the viability of the APRC-based decentralised MPC for time-varying splitting parallel systems.

9.1.4 Notation

Capital letters denote matrices. Lower-case alphabet and Greek letters denote column vectors and scalars, respectively.

$(\cdot)^T$ denote matrix transpose operations, respectively.

I_n is the identity matrix of dimension $n \times n$. 0_n is the zero matrix of dimension $n \times n$.

$\text{diag}[A_i]_1^N$ is the block diagonal matrix with diagonal entries $A_i, i = 1, 2, \dots, N$.

$\text{diag}[Q_{jic}]_{j=1\dots h, i=1\dots g_j}$ is the block diagonal matrix with diagonal entries $Q_{jic}, j = 1, \dots, h, i = 1, \dots, g_j$.

$\|v\|$ denotes the L_2 -norm of vector v .

$\|Q\|$ is the induced 2-norm of the matrix Q , which is defined as
 $\|Q\| = \max \{ \|Qv\|_2 : v \in \mathbb{R}^n, \|v\|_2 \leq 1 \}$, $\|v\|_2$ is the L_2 -norm of v .

The ℓ th element of a vector $u_i(k)$ is denoted as $u_i^{(\ell)}(k)$.

The notation $u_i \in [\underline{u}_i, \bar{u}_i]$ is component-wise understood, i.e. $u_i^{(\ell)} \in [\underline{u}_i^{(\ell)}, \bar{u}_i^{(\ell)}]$ ($\underline{u}_i^{(\ell)} \leq u_i^{(\ell)} \leq \bar{u}_i^{(\ell)} \forall \ell$).

In symmetric block matrices or long matrix expressions, we use $*$ as an ellipsis for terms that are induced by symmetry, e.g.,

$$(*) \begin{bmatrix} (*) + R & S \\ (*) & Q \end{bmatrix} K = K^T \begin{bmatrix} R^T + R & S \\ S^T & Q \end{bmatrix} K.$$

In the discrete-time domain, the time index is denoted by $k, k \in \mathbb{Z}$.

In a proof, when the time index k is omitted for conciseness, $v(-\tau)$ denotes the vector $v(k - \tau)$.

\hat{u} denotes a sequence of predictive vectors of $u(j)$ starting from the current time step.

\check{u} denotes a sequence of $u(-j)$ representing the historical data of u .

The boldface style for letters is used in optimisation formulations to emphasise that they are variables.

9.2 Model Development and Problem Statement

The interaction-oriented state space model defined by Lunze (1992) in [16] is adopted in this section as it is well suited to the input and output nature of interconnected systems. This type of models is also known as two-port model. The denotations for subsystems, units and the large-scale system is given in Fig. 9.2, wherein a large-scale system is viewed as consisting of two layers, Units and Subsystems.

9.2.1 Control and System Model

Consider a large-scale system Σ consisting of h units, denoted as $\mathcal{G}_j, j = 1 \dots h$. Each unit \mathcal{G}_j has g_j subsystems, denoted as $\mathcal{S}_{ji}, i = 1 \dots g_j$. The hierarchical tree representing the nested subsystems is given in Fig. 9.2 to illustrate subsystem denotations in this section. Each subsystem \mathcal{S}_{ji} is represented by the discrete-time state space model of the form

$$\mathcal{S}_{ji} : \begin{cases} x_{ji}(k+1) = A_{ji} x_{ji}(k) + B_{ji} u_{ji}(k) + E_{ji} v_{ji}(k), \\ y_{ji}(k) = C_{ji} x_{ji}(k), \quad w_{ji}(k) = F_{ji} x_{ji}(k), \end{cases} \quad (9.1)$$

where $E_{ji} = [E_{\pi_{ji}} \ E_{\sigma_{ji}}]$, $v_{ji}^T = [v_{\pi_{ji}}^T \ v_{\sigma_{ji}}^T]$, $F_{ji} = [F_{\pi_{ji}} \ F_{\sigma_{ji}}]$, $w_{ji}^T = [w_{\pi_{ji}}^T \ w_{\sigma_{ji}}^T]$, in which $v_{\sigma_{ji}} \in \mathbb{R}^{m_{\sigma_{ji}}}$ and $w_{\sigma_{ji}} \in \mathbb{R}^{q_{\sigma_{ji}}}$ are *serial coupling* input and output vectors respectively, while $v_{\pi_{ji}} \in \mathbb{R}^{m_{\pi_{ji}}}$ and $w_{\pi_{ji}} \in \mathbb{R}^{q_{\pi_{ji}}}$ are *parallel coupling* input and output vectors; $x_{ji} \in \mathbb{R}^{n_{ji}}$ is the state vector, $y_{ji} \in \mathbb{R}^{q_{ji}}$ is the measurement output vector, $u_{ji} \in \mathbb{U}_{ji} \subset \mathbb{R}^{m_{ji}}$ is the control input vector. It is notably that, there are $h_{\Sigma} := \sum_{j=1}^h g_j$ subsystems \mathcal{S}_{ji} in Σ .

Serial Connections: Two subsystems $\mathcal{S}_{\xi i}$ and $\mathcal{S}_{\zeta o}$ are said to be *serially connected* (SC) if the coupling input vector $v_{\sigma_{\xi i}}$ of $\mathcal{S}_{\xi i}$ is the coupling output vector $w_{\sigma_{\zeta o}}$ of $\mathcal{S}_{\zeta o}$, i.e.

$$(SC) \ v_{\sigma_{\xi i}}(k) = w_{\sigma_{\zeta o}}(k). \quad (9.2)$$

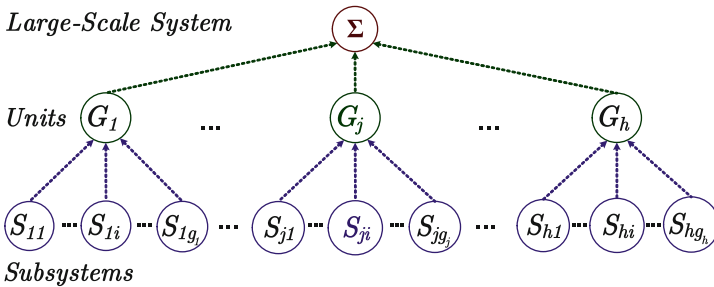


Fig. 9.2 Denotations for subsystems, units and the large-scale system

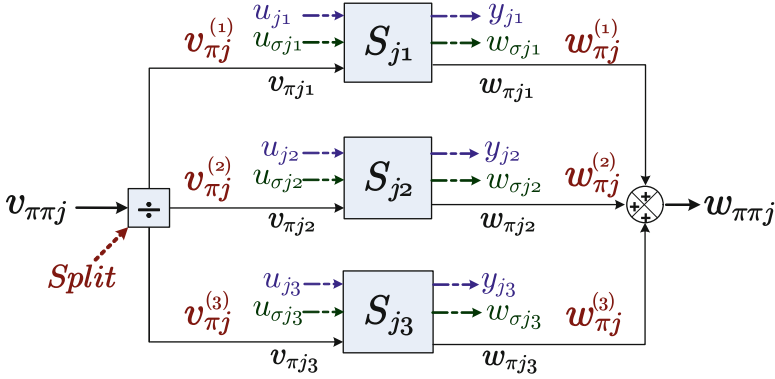


Fig. 9.3 Parallel connections of a unit \mathcal{G}_j having three subsystems

In the following, M_j (of unit \mathcal{G}_j) denotes the diagonal matrix $\text{diag}[M_{ji}]_1^{g_j}$, and v_{*j} denotes the stacking vector $[v_{*j1}^T \dots v_{*jg_j}^T]^T$ (i.e., unit subscript j remains). A unit \mathcal{G}_j is represented by the block diagonal system formed by g_j parallel subsystems \mathcal{S}_{ji} as

$$\mathcal{G}_j : \begin{cases} x_j(k+1) = A_j x_j(k) + B_j u_j(k) + E_j v_j(k), \\ y_j(k) = C_j x_j(k), \quad w_j(k) = F_j x_j(k), \end{cases} \quad (9.3)$$

where $E_j = [E_{\pi j} \ E_{\sigma j}]$, $v_j^T = [v_{\pi j}^T \ v_{\sigma j}^T]$, $F_j = [F_{\pi j} \ F_{\sigma j}]$, $w_j^T = [w_{\pi j}^T \ w_{\sigma j}^T]$.

Specifically, $A_j = \text{diag}[A_{ji}]_1^{g_j}$, $B_j = \text{diag}[B_{ji}]_1^{g_j}$, $C_j = \text{diag}[C_{ji}]_1^{g_j}$, $E_{\pi j} = \text{diag}[E_{\pi ji}]_1^{g_j}$, $F_{\pi j} = \text{diag}[F_{\pi ji}]_1^{g_j}$, $E_{\sigma j} = \text{diag}[E_{\sigma ji}]_1^{g_j}$, $F_{\sigma j} = \text{diag}[F_{\sigma ji}]_1^{g_j}$, $x_j^T = [x_{j1}^T \dots x_{jg_j}^T]$, $u_j^T = [u_{j1}^T \dots u_{jg_j}^T]$, $y_j^T = [y_{j1}^T \dots y_{jg_j}^T]$, $v_{\pi j}^T = [v_{\pi j1}^T \dots v_{\pi jg_j}^T]$, $w_{\pi j}^T = [w_{\pi j1}^T \dots w_{\pi jg_j}^T]$, $v_{\sigma j}^T = [v_{\sigma j1}^T \dots v_{\sigma jg_j}^T]$, $w_{\sigma j}^T = [w_{\sigma j1}^T \dots w_{\sigma jg_j}^T]$.

Parallel Connections within One Unit: The parallel coupling vectors $v_{\pi ji}$ and $w_{\pi ji}$ of all subsystems \mathcal{S}_{ji} belonging to a unit \mathcal{G}_j are assumed, without loss of generality, having the same size. If there is only one parallel signal, the block diagram of the parallel connections within a unit \mathcal{G}_j having three subsystems ($g_j = 3$) is given in Fig. 9.3. The divider operator at $v_{\pi\pi j}$ in this figure represents the splitting of $v_{\pi\pi j}$ into $v_{\pi j}^{(\ell)}$.

Two new signals, $v_{\pi\pi j}$ and $w_{\pi\pi j}$ are introduced here. While the outputs $w_{\pi j}$ are summed up to become $w_{\pi\pi j}$, the input $v_{\pi\pi j}$ is split up into $v_{\pi j}$. Their relationships are represented by two matrices Ψ_{v_j} and Ψ_{w_j} , which are defined as

$$\begin{aligned} \text{(PC)} \quad v_{\pi\pi j} &= v_{\pi j1} + \dots + v_{\pi jg_j} := \Psi_{v_j} v_{\pi j}, \\ w_{\pi\pi j} &= w_{\pi j1} + \dots + w_{\pi jg_j} := \Psi_{w_j} w_{\pi j}, \end{aligned} \quad (9.4)$$

where $v_{\pi j}^T = [v_{\pi j1}^T \dots v_{\pi jg_j}^T]$, $w_{\pi j}^T = [w_{\pi j1}^T \dots w_{\pi jg_j}^T]$.

In the parallel redundant configuration, where the material or energy flows are split into smaller flows to each subsystems, it is impossible to have a constant splitting ratio at all time, but rather dynamic ratios. The splitting ratios between $v_{\pi ji}$ of $v_{\pi j}$ should, therefore, be *time varying* and *unknown*. Due to these unknown splitting ratios of parallel subsystems, the connectivity of the large-scale interconnection process can not be established on the basis of subsystems. In later sections, we tackle this issue by establishing the dissipativity criteria for a unit consisting of parallel subsystems, i.e., the open-loop subsystems are not necessarily dissipative, but only their auspice unit is. It is noted here that the common input and output vectors, $v_{\pi\pi j}$ and $w_{\pi\pi j}$, of parallel connections are involved in the connection processes, instead of $v_{\pi j}$ and $w_{\pi j}$.

In the following, M (of Σ) denotes the diagonal matrix $\text{diag}[M_j]_1^h$, and v_* denotes the stacking vector $[v_{*1}^T \dots v_{*h}^T]^T$ (unit subscripts j vanish). The large-scale system Σ is represented by the block diagonal system formed by h diagonal units \mathcal{G}_j (or h_Σ subsystems \mathcal{S}_{ji}), and the large-scale interconnection processes $H_\sigma, H_{\pi\pi}$ as

$$\Sigma : \begin{cases} x(k+1) = Ax(k) + Bu(k) + Ev(k), \\ y(k) = Cx(k), w(k) = Fx(k), \\ v_{\pi\pi}(k) = H_{\pi\pi} w_{\pi\pi}(k), v_\sigma(k) = H_\sigma w_\sigma(k), \end{cases} \quad (9.5)$$

where $E = [E_\pi \ E_\sigma]$, $F = [F_\pi \ F_\sigma]$, $v^T = [v_\pi^T \ v_\sigma^T]$, $w^T = [w_\pi^T \ w_\sigma^T]$. Specifically, $A = \text{diag}[A_j]_1^h$, $B = \text{diag}[B_j]_1^h$, $C = \text{diag}[C_j]_1^h$, $E_\pi = \text{diag}[E_{\pi j}]_1^h$, $F_\pi = \text{diag}[F_{\pi j}]_1^h$, $E_\sigma = \text{diag}[E_{\sigma j}]_1^h$, $F_\sigma = \text{diag}[F_{\sigma j}]_1^h$, $x^T = [x_1^T \dots x_h^T]$, $u = [u_1^T \dots u_h^T]$, $y = [y_1^T \dots y_h^T]$, $v_\pi = [v_{\pi 1}^T \dots v_{\pi h}^T]$, $w_\pi = [w_{\pi 1}^T \dots w_{\pi h}^T]$, $v_{\pi\pi} = [v_{\pi\pi 1}^T \dots v_{\pi\pi h}^T]$, $w_{\pi\pi} = [w_{\pi\pi 1}^T \dots w_{\pi\pi h}^T]$, $v_\sigma = [v_{\sigma 1}^T \dots v_{\sigma h}^T]$, $w_\sigma = [w_{\sigma 1}^T \dots w_{\sigma h}^T]$.

The parallel connection process inside Σ is as follows:

$$v_{\pi\pi}(k) = \Psi_v v_\pi(k), w_{\pi\pi}(k) = H_{\pi\pi} \Psi_w w_\pi(k), \quad (9.6)$$

where $\Psi_v = \text{diag}[\Psi_{v_j}]_1^h$, $\Psi_w = \text{diag}[\Psi_{w_j}]_1^h$.

The interconnections between units and subsystems are specified by the interconnection matrices $H_{\pi\pi}$ and H_σ , respectively. The elements of $H_{\pi\pi}$ and H_σ are zero or one only. The block diagrams of the large-scale system Σ from the unit and subsystem perspectives are depicted in Figs. 9.4 and 9.5, respectively. It is notably that the parallel connections cause a disconnection at $v_{\pi\pi}$ in Fig. 9.5 because of the unknown splitting ratios. It is, therefore, preferable to use the block diagram on the basis of units \mathcal{G}_j in Fig. 9.4.

The following bounded control constraint is considered:

$$\mathbb{U}_{ji} := \{u_{ji} : u_{ji} \in [\underline{u}_{ji}, \bar{u}_{ji}], \quad \forall k \in \mathbb{Z}\}, \quad (9.7)$$

where \underline{u}_{ji} and \bar{u}_{ji} are the lower and upper bounds of u_{ji} deduced from the physical limit of the actuators corresponding to the control vector u_{ji} .

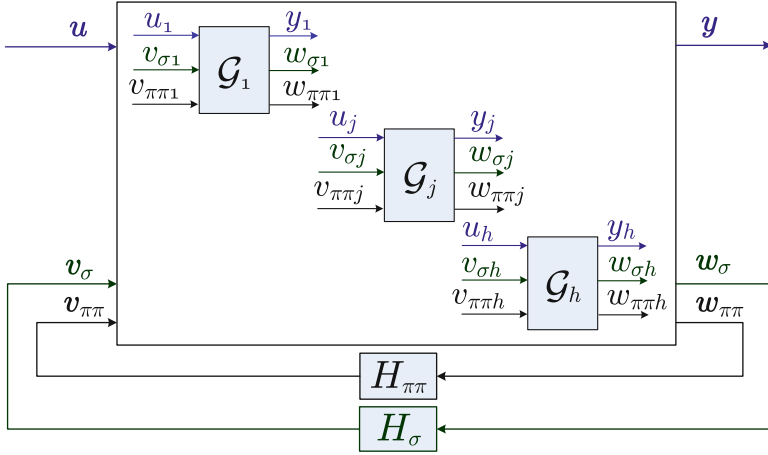


Fig. 9.4 Block diagram of the large-scale system Σ on the basis of units \mathcal{G}_j

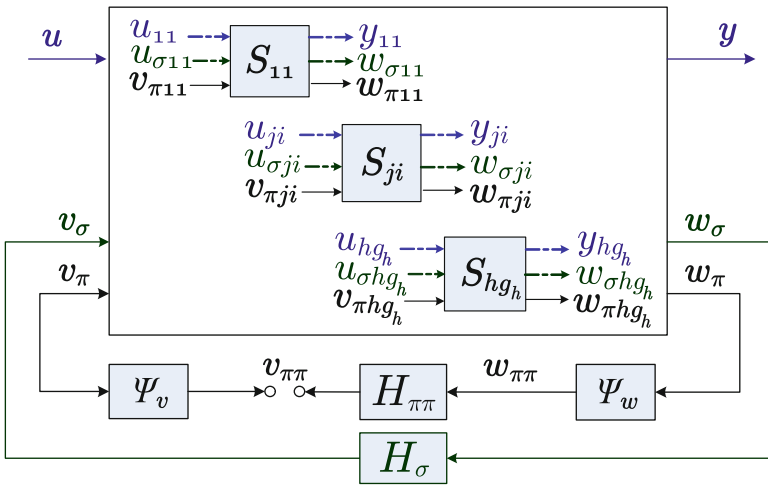


Fig. 9.5 Block diagram of the large-scale system Σ on the basis of subsystems \mathcal{S}_{ji}

It is clear that (9.5) belongs to the class of time-varying uncertain linear systems. The difficulty there is that the time-varying parameter $E\nu(k)$ is unknown and thus cannot be treated as gain-scheduling ones. Consequently, the popular gain-scheduling control techniques for time-varying systems [1, 3, 33, 34] cannot be applied. It should be also noted that the gain-scheduling techniques could hardly address the control-bounded constraints in time domain such as (9.7).

In a decentralised architecture, the stand-alone subsystem model (when all coupling inputs and outputs vanish: $v_{ji} = 0, w_{ji} = 0$) is also requisite, which is represented by

$$\mathcal{S}_{ji}^s : \begin{cases} x_{ji}(k+1) = A_{ji} x_{ji}(k) + B_{ji} u_{ji}(k), \\ y_{ji}(k) = C_{ji} x_{ji}(k). \end{cases} \quad (9.8)$$

Assumption 9.1. (i) *The large-scale system is observable (zero-state observable) and controllable.*

(ii) *The updating instants and all invocations are synchronised between all subsystems and their controllers.*

Assumption 9.2. *The changing-over between the duty and standby subsystems within one unit is smooth, i.e., state jumps will not incur due to the changing-over operations. The fault-tolerant controls for duty and standby subsystems, and the distributed optimisation schemes for parallel operations within one unit, if there are any, are regarded as internal activities of that unit.*

9.2.2 Problem Description and Rationale

The large-scale interconnected system processing a mixed connection configuration presented in Sect. 9.2 is considered herein. The subsystem models (9.1) in Sect. 9.2.1 are employed to derive the stabilisability condition. The open-loop model predictive control algorithm is implemented for each subsystem \mathcal{S}_{ji} using the stand-alone model (9.8) associated with (9.1). As mentioned in the introduction, the given MPC vectors $\hat{u}_{ji}(k)$ may destabilise the large-scale system Σ (9.5), defined in Sect. 9.2. Our problem is to redesign these controllers on-the-fly to stabilise it. We are concerned with the design of h_Σ disparate dynamic stability constraints for these decentralised MPCs. The online and historical data of \mathcal{C}_{ji} and \mathcal{S}_{ji} are used to characterise the stability constraint on the outputs of \mathcal{C}_{ji} (i.e., control inputs for \mathcal{S}_{ji}). The stability constraints ensure that Σ remains within a stabilisable region recursively. There are not any assumed constraints on the coupling vectors between subsystems and units. The inter-subsystem communication between subsystem controllers are not available for control updates.

9.3 Asymptotically Positive Realness Constraint and Interconnection Stabilisability Condition

This section presents the main results of this chapter on establishing a new stabilisability condition for the large-scale interconnected systems. Let us first introduce the APRC for each subsystem \mathcal{S}_{ji} (9.1).

9.3.1 Asymptotically Positive Realness Constraint

Define a quadratic supply rate

$$\xi_{jic} = (u_{ji}(k), y_{ji}(k)) \begin{bmatrix} u_{ji}(k) \\ y_{ji}(k) \end{bmatrix}^T \begin{bmatrix} Q_{jic}(k) & S_{jic}(k) \\ S_{jic}^T(k) & R_{jic}(k) \end{bmatrix} \begin{bmatrix} u_{ji}(k) \\ y_{ji}(k) \end{bmatrix}, \quad (9.9)$$

where $Q_{jic}(k), R_{jic}(k), S_{jic}(k)$ are multiplier matrices with symmetric $Q_{jic}(k)$ and $R_{jic}(k)$. For conciseness, $\xi_{jic}(u_{ji}(k), y_{ji}(k))$ is denoted as ξ_{jic}^k and the time index k is represented by a superscript typeface without brackets where appropriated.

Definition 9.1. An input–output pair $(u_{ji}(k), y_{ji}(k))$ of subsystem \mathcal{S}_{ji} is said to satisfy the *asymptotically positive real constraint* (APRC) if

$$\xi_{jic}^k \geq 0 \quad \text{as } k \rightarrow +\infty. \quad (9.10)$$

Lemma 9.1. If there are $k_0 \in \mathbb{Z}^+$ and $0 \leq \gamma_{ji}(k) < 1 - \varepsilon_{ji}$ ($0 < \varepsilon_{ji} < 1$) such that whenever $k > k_0$, ξ_{jic}^k satisfies the following inequality

$$\xi_{jic}^k > \gamma_{ji}(k) \xi_{jic}^{k-1}, \quad (9.11)$$

then (9.10) holds true.

Proof. There are two possibilities:

- $\xi_{jic}^{k_0} \geq 0$. Then (9.11) means $\xi_{jic}^k > 0 \forall k > k_0$.
- $\xi_{jic}^{k_0} < 0$ and $0 < \gamma_{ji}(k) < 1 - \varepsilon_{ji}$ then

$$\begin{aligned} \xi_{jic}^k &\geq \xi_{jic}^{k_0} \prod_{\ell=k_0}^k \gamma_{ji}(\ell) \\ &\geq \xi_{jic}^{k_0} (1 - \varepsilon_{ji})^{k-k_0-1} \rightarrow 0 \quad \text{as } k \rightarrow \infty. \end{aligned} \quad \square$$

Now, rewrite (9.11) as the following constraint in \mathbf{u}_{ji}^k ,

$$\mathbf{u}_{ji}^k (-Q_{jic}^k) \mathbf{u}_{ji}^k - 2y_{ji}^{kT} S_{jic}^k \mathbf{u}_{ji}^k < y_{ji}^{kT} \mathbf{R}_{jic}^k y_{ji}^k - \gamma_{ji}^k \xi_{jic}^{k-1}, \quad (9.12)$$

which is convex if and only if $Q_{jic}^k \prec 0$. Then, by rewriting

$$\begin{aligned} \xi_{jic}^k &= -(u_{ji} - (Q_{jic}^k)^{-1} S_{jic} y_{ji})^T (-Q_{jic}^k) (u_{ji} - (Q_{jic}^k)^{-1} S_{jic} y_{ji}) \\ &\quad + y_{ji}^T (\mathbf{R}_{jic}^k - S_{jic}^{kT} (Q_{jic}^k)^{-1} S_{jic}^k) y_{ji}, \end{aligned}$$

the feasibility of (9.12) in \mathbf{u}_{ji}^k requires $Q_{jic}^k \prec 0$, and

$$y_{ji}^{kT} (\mathbf{R}_{jic}^k - S_{jic}^{kT} (Q_{jic}^k)^{-1} S_{jic}^k) y_{ji}^k - \gamma_{ji}^k \xi_{jic}^{k-1} > 0. \quad (9.13)$$

Here, we would like to further elaborate the concept of APRC informally. It is well known that if a system is positive real, then it can be stabilised. However, this fundamental result is not always realisable, due to the fact that an infinitely power control may be required. On the other hand, a positive realness constraint can be treated as a quantity representing the transience of the positive realness property relatively to the positivity of $\xi_{jic}(k)$ (9.9). It is natural that, if a system does not satisfy the positive realness constraint (or $\xi_{jic}(k)$ is negative at some time instant k), one cannot make it bounded by the PRC immediately because the control is also power constrained. Therefore, an immediate step to make the system tend to satisfy the PRC is more realistic and desirable.

9.3.2 Stability and Feasibility Conditions

As mentioned in the first section, the issue of unknown and time-varying splitting ratios in parallel subsystems is tackled by having a combined solution, wherein the APRC is developed for each individual subsystem \mathcal{S}_{ji} while the dissipativity criteria are derived for the unit \mathcal{G}_j consisting of g_j subsystems \mathcal{S}_{ji} in parallel.

A unit \mathcal{G}_j is said to be quadratically dissipative with respect to the quadratic supply rate $\xi_j(y_{jD}, u_{jD})$ defined as,

$$\xi_j(y_{jD}(k), u_{jD}(k)) := \begin{bmatrix} y_{jD}(k) \\ u_{jD}(k) \end{bmatrix}^T \begin{bmatrix} Q_j & S_j \\ S_j^T & R_j \end{bmatrix} \begin{bmatrix} y_{jD}(k) \\ u_{jD}(k) \end{bmatrix}, \tag{9.14}$$

where $y_{jD}^T = [y_j^T w_{\pi\pi_j}^T w_{\sigma_j}^T]$, $u_{jD}^T = [u_j^T v_{\pi\pi_j}^T v_{\sigma_j}^T]$, the multiplier matrices Q_j, S_j, R_j are block diagonal of the form

$$Q_j = \text{diag}\{Q_{11j}, Q_{22j}, Q_{33j}\}, S_j = \text{diag}\{S_{11j}, S_{22j}, S_{33j}\}, R_j = \text{diag}\{R_{11j}, R_{22j}, R_{33j}\},$$

in which each block element has a block diagonal structure corresponding to subsystem dimensions, with symmetric Q_j and R_j , if there exists a nonnegative C^1 function, addressed as storage function, $V_j(x_j(k))$, $V_j(0) = 0$, such that for all u_{jD} and all $k \in \mathbb{Z}^+$, the following dissipation inequality is satisfied irrespectively of the initial value of the state $x_j(0)$:

$$V_j(x_j(k+1)) - V_j(x_j(k)) \leq \xi_j(y_{jD}(k), u_{jD}(k)). \tag{9.15}$$

The square storage function of the form $V_j(x(k)) = x_j(k)^T P_j x_j(k)$, $P_j = P_j^T \succ 0$, is considered in this section. Define:

- The dissipativity matrices of the large-scale system Σ as $Q_{11} := \text{diag}[Q_{11j}]_1^h$, $S_{11} := \text{diag}[S_{11j}]_1^h$, $R_{11} := \text{diag}[R_{11j}]_1^h$, $Q_{22} := \text{diag}[Q_{22j}]_1^h$, $S_{22} := \text{diag}[S_{22j}]_1^h$, $R_{22} := \text{diag}[R_{22j}]_1^h$, $Q_{33} := \text{diag}[Q_{33j}]_1^h$, $S_{33} := \text{diag}[S_{33j}]_1^h$, $R_{33} := \text{diag}[R_{33j}]_1^h$.
- The dissipativity matrices of unit \mathcal{G}_j as $Q_{11j} := \text{diag}[Q_{11ji}]_1^{g_j}$, $Q_{22j} := \text{diag}[Q_{22ji}]_1^{g_j}$, $Q_{33j} := \text{diag}[Q_{33ji}]_1^{g_j}$, $S_{11j} := \text{diag}[S_{11ji}]_1^{g_j}$, $S_{22j} := \text{diag}[S_{22ji}]_1^{g_j}$, $S_{33j} := \text{diag}[S_{33ji}]_1^{g_j}$, $R_{11j} := \text{diag}[R_{11ji}]_1^{g_j}$, $R_{22j} := \text{diag}[R_{22ji}]_1^{g_j}$, $R_{33j} := \text{diag}[R_{33ji}]_1^{g_j}$, where Q_{11ji}, R_{11ji} are symmetric matrices of dimensions $q_{ji} \times q_{ji}, m_{ji} \times m_{ji}$, respectively, Q_{22ji}, R_{22ji} are symmetric matrices of dimensions $q_{w_{\pi j}} \times q_{w_{\pi j}}, m_{v_{\pi j}} \times m_{v_{\pi j}}$, respectively, Q_{33ji}, R_{33ji} are symmetric matrices of dimensions $q_{w_{\sigma j}} \times q_{w_{\sigma j}}, m_{v_{\sigma j}} \times m_{v_{\sigma j}}$, respectively, S_{11ji} are rectangular matrices of $q_{ji} \times m_{ji}$ dimensions, S_{22ji} are rectangular matrices of $q_{w_{\pi j}} \times m_{v_{\pi j}}$ dimensions, S_{33ji} are rectangular matrices of $q_{w_{\sigma j}} \times m_{v_{\sigma j}}$ dimensions.
- The multiplier matrices for the APRC of the large-scale diagonal controller as $Q_c^k := \text{diag}[Q_{jic}^k]_{j=1\dots h, i=1\dots g_j}$, $S_c^k := \text{diag}[S_{jic}^k]_{j=1\dots h, i=1\dots g_j}$, $R_c^k := \text{diag}[R_{jic}^k]_{j=1\dots h, i=1\dots g_j}$.

The interconnection stabilisability condition for the large-scale system based on the APRC is stated next.

Theorem 9.1. *Suppose that*

- (i) *The following LMIs are feasible in $P_j, Q_{jic}^{k_0}, S_{jic}^{k_0}, Q_{11j}, S_{11j}, R_{11j}, Q_{22j}, S_{22j}, R_{22j}, Q_{33j}, S_{33j}, R_{33j}$:*

$$\begin{bmatrix} Q_{11j} & S_{11j} + S_{jic}^{k_0} \\ * & R_{11j} + Q_{jic}^{k_0} \end{bmatrix} \prec 0, \quad \mathcal{Q}_j \prec 0, \quad \mathcal{Q}_j \sigma \prec 0, \quad Q_{jic}^{k_0} \prec 0, \quad (9.16a)$$

$$\begin{bmatrix} \mathcal{Q}_j & M_{12} & M_{13} & M_{14} \\ * & M_{22} & B_j^T P_j E_{\pi j} & B_j^T P_j E_{\sigma j} \\ * & * & M_{33} & 0 \\ * & * & * & M_{44} \end{bmatrix} \preccurlyeq 0, \quad P_j \succ 0, \quad (9.16b)$$

$j = 1 \dots h, i = 1 \dots g_j,$

where

$$\begin{aligned} M_{12} &:= A_j^T P_j B_j - C_j^T S_{11j}, \\ M_{13} &:= A_j^T P_j E_{\pi j} - F_{\pi j}^T \Psi_{w_j}^T S_{22j} \Psi_{v_j}, \\ M_{14} &:= A_j^T P_j E_{\sigma j} - F_{\sigma j}^T S_{33j}, \\ M_{22} &:= B_j^T P_j B_j - R_{11j}, \\ M_{33} &:= E_{\pi j}^T P_j E_{\pi j} - \Psi_{v_j}^T R_{22j} \Psi_{v_j}, \\ M_{44} &:= E_{\sigma j}^T P_j E_{\sigma j} - R_{33j}, \end{aligned}$$

$$\begin{aligned} \mathcal{Q}_j &:= A_j^T \mathbf{P}_j A_j - \mathbf{P}_j - C_j^T \mathbf{Q}_{11j} C_j - F_{\sigma j}^T \mathbf{Q}_{33j} F_{\sigma j} - F_{\pi j}^T \Psi_{w_j}^T \mathbf{Q}_{22j} \Psi_{w_j} F_{\pi j}, \\ \mathcal{Q}_{j\pi} &:= \Psi_w^T \mathbf{Q}_{22} \Psi_w + \Psi_w H_{\pi\pi}^T \mathbf{R}_{22} H_{\pi\pi} \Psi_w + \Psi_w^T \mathbf{S}_{22} H_{\pi\pi} \Psi_w + \Psi_w^T H_{\pi\pi}^T \mathbf{S}_{22}^T \Psi_w, \\ \mathcal{Q}_{j\sigma} &:= \mathbf{Q}_{33} + \mathbf{S}_{33} H_{\sigma} + H_{\sigma}^T \mathbf{S}_{33}^T + H_{\sigma}^T \mathbf{R}_{33} H_{\sigma}; \end{aligned}$$

- (ii) With $\mathcal{Q}_{jic}^k \equiv \mathcal{Q}_{jic}^{k_0}$, $S_{jic}^k \equiv S_{jic}^{k_0}$, where $\mathcal{Q}_{jic}^{k_0}$ and $S_{jic}^{k_0}$ are a feasible solution pair to (9.16), the system of linear inequality constraints (9.13) and $\mathbf{R}_{jic}^k \prec 0$ for $j = 1 \dots h$, $i = 1 \dots g_j$ are feasible in R_{jic}^k ;

Then there exist h_{Σ} unconstrained control vectors $u_{ji}(k)$, $k > 0$, that stabilise the system Σ (9.5).

Proof. (a) The supposition (ii) and $\mathcal{Q}_{jic}^{k_0} \prec 0$ in (9.16a) guarantee the feasibility of a convex constraint (9.12) in unconstrained u_{ji} .

(b) *Quadratical Dissipativity of Unit \mathcal{G}_j* : By substituting the model of \mathcal{G}_j (9.3) and the parallel connections of (9.4) into the dissipation inequality of (9.15), it follows that \mathcal{G}_j is quadratically dissipative w.r.t the supply rate (9.14) (i.e., with respect to the output and input pair of $y_{jD} = (y_j^T, (\Psi_{w_j} w_{\pi j})^T, w_{\sigma j}^T)^T$, $u_{jD} = (u_j^T, (\Psi_{v_j} v_{\pi j})^T, v_{\sigma j}^T)^T$) if and only if LMI (9.16b) holds (see, e.g., [6]). Thus (9.15) is verified for all (y_{jD}, u_{jD}) .

(c) *Stability*: Define

$$\xi_c^k := u(k)^T \mathcal{Q}_c^k u(k) + 2y(k)^T S_c^k u(k) + y(k)^T R_c^k y(k).$$

Under the condition (ii), there are unconstrained $u_{ji}(k)$ feasible to (9.12), thus by Lemma 9.1

$$\xi_c^k \geq 0 \quad \text{as } k \rightarrow +\infty. \tag{9.17}$$

Therefore, such $u_{ji}(k)$ will make

$$\xi_c^k \geq 0 \quad \text{for } k \geq \bar{k} < +\infty. \tag{9.18}$$

Using (9.15) and the diagonality of $\mathcal{Q}_{11}, \mathcal{Q}_{22}, \mathcal{Q}_{33}, S_{11}, S_{22}, S_{33}, R_{11}, R_{22}, R_{33}$ we obtain for $V(x(k)) := \sum_{j=1}^h V_j(x_j(k))$,

$$V(x(k+1)) - V(x(k)) \leq \xi((y^k, w_{\pi\pi}^k, w_{\sigma}^k), (u^k, v_{\pi\pi}^k, v_{\sigma}^k)),$$

where

$$\begin{aligned} \xi((y^k, w_{\pi\pi}^k, w_{\sigma}^k), (u^k, v_{\pi\pi}^k, v_{\sigma}^k)) &= (y^{kT} \mathcal{Q}_{11} y^k + 2y^{kT} S_{11} u^k + u^{kT} R_{11} u^k) \\ &\quad + (w_{\pi\pi}^{kT} \mathcal{Q}_{22} w_{\pi\pi}^k + 2w_{\pi\pi}^{kT} S_{22} v_{\pi\pi}^k + v_{\pi\pi}^{kT} R_{22} v_{\pi\pi}^k) \\ &\quad + (w_{\sigma}^{kT} \mathcal{Q}_{33} w_{\sigma}^k + 2w_{\sigma}^{kT} S_{33} v_{\sigma}^k + v_{\sigma}^{kT} R_{33} v_{\sigma}^k). \end{aligned}$$

Then, due to (9.18) and (9.6), it follows that

$$V(k+1) - V(k) \leq \sigma^k,$$

where

$$\begin{aligned} \sigma^k &:= \xi((y^k, w_{\pi\pi}^k, w_{\sigma}^k), (u^k, v_{\pi\pi}^k, v_{\sigma}^k)) + \xi_c(u^k, y^k) \\ &= w_{\pi\pi}^{kT} \mathcal{Q}_{j\pi} w_{\pi\pi}^k + w_{\sigma}^{kT} \mathcal{Q}_{j\sigma} w_{\sigma}^k \\ &\quad + \sum_{j=1\dots h, i=1\dots g_j} (*) \begin{bmatrix} \mathcal{Q}_{11ji} + R_{jic}^k & S_{11ji} + S_{jic}^k \\ (S_{11ji} + S_{jic}^k)^T & R_{11ji} + \mathcal{Q}_{jic}^k \end{bmatrix} \begin{bmatrix} y_{ji}^k \\ u_{ji}^k \end{bmatrix}. \end{aligned}$$

Using (9.16a) and $R_{jic}^k \prec 0$ in (ii) yields

$$V(k+1) - V(k) \leq \sigma^k < 0, \text{ for all } (y^T, w^T, u^T) \neq 0.$$

As Σ is observable, if $(y^T, w^T, u^T) = 0$ we also have $x = 0$, the origin is globally asymptotically stable. \square

In the following Theorem, the feasibility condition for constraint satisfactions that will be used to guarantee the optimizing feasibility for the MPC is stated.

Theorem 9.2. *Suppose that, with the measurement output $y_{ji}(k)$ at the current step k and $\mathcal{Q}_{jic}^{k_0}$ from the offline LMIs (9.16),*

(i) *The following linear inequality constraint holds:*

$$(\mathcal{Q}_{jic}^{k_0})^{-1} \mathbf{S}_{jic}^k y_{ji}^k \in [\underline{u}_{ji}, \bar{u}_{ji}]; \quad (9.19)$$

(ii) *With a feasible solution of S_{jic}^k in (9.19) and $\mathcal{Q}_{jic}^k = \mathcal{Q}_{jic}^{k_0}$, the linear inequality constraint (9.13) holds;*

Then, the intersection of \mathbb{U}_{ji} and the feasible set of (9.12) is nonempty recursively in k .

Proof. Due to $\mathcal{Q}_{jic}^{k_0} \prec 0$ and (ii), (9.12) is an ellipsoid region having the center at $\tilde{u}_{ji}(k) = (\mathcal{Q}_{jic}^{k_0})^{-1} S_{jic}^k y_{ji}^k$, and not shrinking to a point. If this center point lies inside \mathbb{U}_{ji} , i.e. if $\tilde{u}_{ji}(k) \in [\underline{u}_{ji}, \bar{u}_{ji}]$, which is fulfilled by (9.19), the intersection of \mathbb{U}_{ji} and (9.12) will be nonempty. \square

To ensure that both results of stability and optimizing feasibility are obtained simultaneously, LMIs (9.16) in Theorem 9.1 will be initially solved *offline* for the dissipativity matrices $\mathcal{Q}_{11}, \mathcal{Q}_{22}, \mathcal{Q}_{33}, S_{11}, S_{22}, S_{33}, R_{11}, R_{22}, R_{33}$, and $\mathcal{Q}_{jic}^{k_0}$. Subsequently, using those resulting offline matrices, the linear inequality constraint (9.19) in Theorem 9.2 will be solved *online* together with the first LMI of (9.16a) in Theorem 9.1 (that has S_{jic}^k as a variable only) for the multiplier matrix S_{jic}^k at every step $k > k_0$. The multiplier matrix \mathbf{R}_{jic}^k is then updated by (9.13) using the resulting online matrix S_{jic}^k and the offline matrix $\mathcal{Q}_{jic}^{k_0}$.

We have shown that the issue of unknown and time-varying splitting ratios have been solved by applying the common input and output vectors ($v_{\pi\pi_j}(k), w_{\pi\pi_j}(k)$) representing the sums of parallel coupling vectors in the supply rates of dissipative units. The present stabilisability condition thus naturally eliminates any conservativeness caused by the fixed splitting ratios of material or energy flows of dynamically-coupled subsystems. In this section, the optimisation problem of each local MPC is additionally imposed with the convex quadratic constraint w.r.t $u_{ji}(k)$ of (9.12) as a stability constraint, to guarantee the stability of Σ , as outlined in the next section.

9.3.3 APRC-Based Decentralised Model Predictive Control

Consider a conventional quadratic objective function with respect to the state and control input vectors and adequately chosen weighting matrices $\mathcal{Q}_{ji}, \mathcal{R}_{ji}$ over a predictive horizon N for subsystem \mathcal{S}_{ji}^s (9.8):

$$\mathcal{J}_{ji}^k = \sum_{\ell=1}^{N+1} x_{ji}^T(k+\ell) \mathcal{Q}_{ji} x_{ji}(k+\ell) + \sum_{\ell=0}^N u_{ji}^T(k+\ell) \mathcal{R}_{ji} u_{ji}(k+\ell). \quad (9.20)$$

According to the MPC literature, see, e.g. [17], the constrained optimisation problem for a stand-alone MPC at step k is as follows:

$$\min_{\hat{\mathbf{u}}_{ji}(k)} \hat{\mathbf{u}}_{ji}^T(k) \Phi_{ji} \hat{\mathbf{u}}_{ji}(k) + 2\Upsilon_{ji}(k) \hat{\mathbf{u}}_{ji}(k) + \delta_{ji}(k) \quad \text{subject to} \quad \hat{\mathbf{u}}_{ji}(k) \in \hat{\mathbb{U}}_{ji}, \quad (9.21)$$

where

$$\Phi_{ji} := \Gamma_{ji}^T \tilde{\mathcal{Q}}_{jiN} \Gamma_{ji} + \tilde{\mathcal{R}}_{jiN}, \Upsilon_{ji}(k) := \mathbf{r}_{ji}^T(k) \tilde{\mathcal{Q}}_{jiN} \Gamma_{ji}, \delta_{ji}(k) := \mathbf{r}_{ji}^T(k) \tilde{\mathcal{Q}}_{jiN} \mathbf{r}_{ji}(k),$$

$$\mathbf{r}_{ji}(k) := \Theta_{ji} \mathbf{x}_{ji}(k), \tilde{\mathcal{Q}}_{jiN} := \text{diag}[\mathcal{Q}_{ji}]_1^{N_{ji}}, \tilde{\mathcal{R}}_{jiN} := \text{diag}[\mathcal{R}_{ji}]_1^{N_{ji}},$$

$$\Gamma_{ji} := \begin{bmatrix} B_{ji} & \dots & 0 & 0 \\ A_{ji} B_{ji} & \dots & 0 & 0 \\ \dots & \dots & \dots & \dots \\ A_{ji}^N B_{ji} & \dots & A_{ji} B_{ji} & B_{ji} \end{bmatrix}, \Theta_{ji} := \begin{bmatrix} A_{ji} \\ A_{ji}^2 \\ \dots \\ A_{ji}^{N+1} \end{bmatrix},$$

and $\hat{\mathbb{U}}_{ji}$ is the constraint set for the variable $\hat{\mathbf{u}}_{ji}$, which is deduced from the constraint set \mathbb{U}_{ji} (9.7). Specifically,

$$\hat{\mathbb{U}}_{ji} := \{\hat{\mathbf{u}}_{ji} = [u_{ji}^T(k), u_{ji}^T(k+1), \dots, u_{ji}^T(k+N)]^T : u_{ji}(\cdot) \in [\underline{u}_{ji}, \bar{u}_{ji}]\}. \quad (9.22)$$

Using the inequality of APRC (9.12), the decentralised MPC problem with the APRC-based one-time-step control constraint is given below:

$$\begin{aligned} \min_{\hat{\mathbf{u}}_{ji}(k)} \quad & \hat{\mathbf{u}}_{ji}^T(k) \Phi_{ji} \hat{\mathbf{u}}_{ji}(k) + 2Y_{ji}^T(k) \hat{\mathbf{u}}_{ji}(k) + \delta_{ji}(k) \quad \text{subject to} \quad \hat{\mathbf{u}}_{ji}(k) \in \hat{\mathcal{U}}_{ji} \quad \text{and} \\ & \hat{\mathbf{u}}_{ji}^k M_{ji}^T (-Q_{jic}^k) M_{ji} \hat{\mathbf{u}}_{ji}^k - 2y_{ji}^{kT} S_{jic}^k M_{ji} \hat{\mathbf{u}}_{ji}^k - y_{ji}^{kT} R_{jic}^k y_{ji}^k + \gamma_{ji}^k \xi_{jic}^{k-1} < 0, \end{aligned} \quad (9.23)$$

where $M_{ji} = [I_{m_{ji}} \ 0_{m_{ji}} \dots \ 0_{m_{ji}}]$.

The problem (9.23) is solved by the local controller for the minimising vector sequence $\hat{\mathbf{u}}_{ji}(k)$ which consists of N elements of $u_{ji}(k)$. Only the first element $u_{ji}(k)$ of the sequence $\hat{\mathbf{u}}_{ji}(k)$ is outputted to \mathcal{S}_{ji} . This rolling process is repeated at the next time step, and continues thereon. This problem can be solved any optimisers using the convex quadratic programming (QP) numerical methods.

From Theorems 9.1 and 9.2, the corollary below provides the stabilisability condition for constrained control problems.

Corollary 9.1. *Suppose that*

- (i) *The LMIs (9.16) are feasible in $P_j, Q_{jic}^{k_0}, S_{jic}^{k_0}, Q_{11ji}, S_{11ji}, R_{11ji}, Q_{22j}, S_{22j}, R_{22j}, Q_{33j}, S_{33j}, R_{33j}$;*
- (ii) *Initialised from feasible matrices $Q_{11ji}, S_{11ji}, R_{11ji}, Q_{jic}^{k_0}, S_{jic}^{k_0}$ of LMIs (9.16) and a feasible solution $R_{jic}^{k_0}$ of the LMIs $S_{jic}^{k_0T} (Q_{jic}^{k_0})^{-1} S_{jic}^{k_0} \prec R_{jic}^{k_0} \prec 0$, the following conditions are fulfilled recursively in $k > k_0$:*
 - (iia) *The following LMIs are feasible in S_{jic}^k for $j = 1, 2, \dots, h, i = 1, 2, \dots, g_j$:*

$$\begin{bmatrix} Q_{11ji} & S_{11ji} + S_{jic}^{kT} \\ S_{11ji}^T + S_{jic}^k & R_{jic}^k + Q_{jic}^k \end{bmatrix} \prec 0, \quad (Q_{jic}^{k_0})^{-1} S_{jic}^k y_{ji}^k \in [\underline{u}_{ji}, \bar{u}_{ji}]; \quad (9.24)$$

- (iib) *With feasible matrices S_{jic}^k from LMIs (9.24) and $Q_{jic}^k \equiv Q_{jic}^{k_0}$, the system of linear inequality constraints (9.13) is feasible in R_{jic}^k for $j = 1, 2, \dots, h, i = 1, 2, \dots, g_j$;*

Then there exist controls $u_{ji}(k), j = 1 \dots h, i = 1 \dots g_j$ satisfying the constraint (9.7) that stabilise the system Σ (9.5).

Proof. This is a direct result of Theorems 1 and 2. □

Based on Corollary 9.1, the control algorithm is summarised in Procedures 1 and 2 below.

Procedure 1—Offline Calculations:

- (A.1) *Initiate $\xi_{ji}^0, y_{ji}(0), Y_{ji}(0), \delta_{ji}(0), x_{ji}(1)$, and select the coefficient γ_{ji} (only time-invariant γ_{ji} is used in this procedure).*

- (A.2) Determine the multiplier matrices Q_{jic}^0, S_{jic}^0 for all h_{Σ} local controllers of h_{Σ} subsystems \mathcal{S}_{ji} using offline LMIs (9.16) in Theorem 9.1, and R_{jic}^0 subsequently using (9.13). Calculate the constant Φ_{ji} .

Procedure 2—Online Calculations:

At every synchronised step $k > 0$ of the local controllers,

- (A.1) Using the measurement outputs $y_{ji}(k)$ and Q_{jic}^0 to solve LMIs (9.24) for the multiplier matrix S_{jic}^k . Then chose R_{jic}^k from (9.13) using the resulting S_{jic}^k and Q_{jic}^0 .
- (A.2) Using $x_{ji}(k)$ and calculating ξ_{jic}^{k-1} to update $Y_{ji}(k)$ and $\delta_{ji}(k)$. Then verify the positive condition of $\xi_{jic}^{k-1} > 0$. If true, set $\gamma_{ji} = 0$.
- (A.3) Using the resulting multiplier matrices $Q_{jic}^k, S_{jic}^k, R_{jic}^k$ to formulate, then solve the optimisation problem (9.23) to yield the local control sequence $\hat{\mathbf{u}}_{ji}(k)$. The first vector element $u_{ji}(k)$ is applied to control \mathcal{S}_{ji} .

Remark 9.1. The choice of γ_{ji}^k is crucial to the convergence to zero of solutions. When γ_{ji}^k approaches 1, the controllers will tend to be smoother but are slower to converge to zero, and reversely otherwise. This can be seen clearly in the output trends in Figs. 9.12 and 9.13 in the first example of Sect. 5, wherein all outputs converge to zero after time step 80 with $\gamma_{ji} = 0.99$ in Fig. 9.12 compared to time step 120 with $\gamma_{ji} \simeq 1$ (0.998 or 0.999) in Fig. 9.13. It is notably that, a time-invariant γ can be employed, as it is in this procedure, to simplify the implementation.

Remark 9.2. The first step of Procedure 2, which is for updating the multiplier matrices S_{jic}^k and R_{jic}^k online, can be ignored if the offline multiplier matrices S_{jic}^0 and R_{jic}^0 of the APRC-based stability constraints are sufficient for feasible solutions.

9.4 Case Studies: Process Control in Alumina Refineries

In the production of alumina from the bauxite ores, the Bayer cycle is recognised as a unique processing technology (patented by Karl Bayer with Pechiney in 1887). A simplified block diagram of the Bayer process is illustrated in Fig. 9.6, whereby there are four main departments, namely Digestion, Clarification, Precipitation, and Evaporation.

The production basically dilutes the bauxite ore in certain forms, most popularly is solid Gibbsite–Trihydrate ($\text{Al}_2\text{O}_3 \cdot 3\text{H}_2\text{O}$), Boehmite–Monohydrate ($\text{Al}_2\text{O}_3 \cdot \text{H}_2\text{O}$) and Kaolinite ($\text{Al}_2\text{O}_3 \cdot 2\text{SiO}_2 \cdot 2\text{H}_2\text{O}$), together with some impurities, such as, Silica (SiO_2), Iron Oxide (Fe_2O_3), and Titania (TiO_2), in heated soda solutions with the basic reactions of



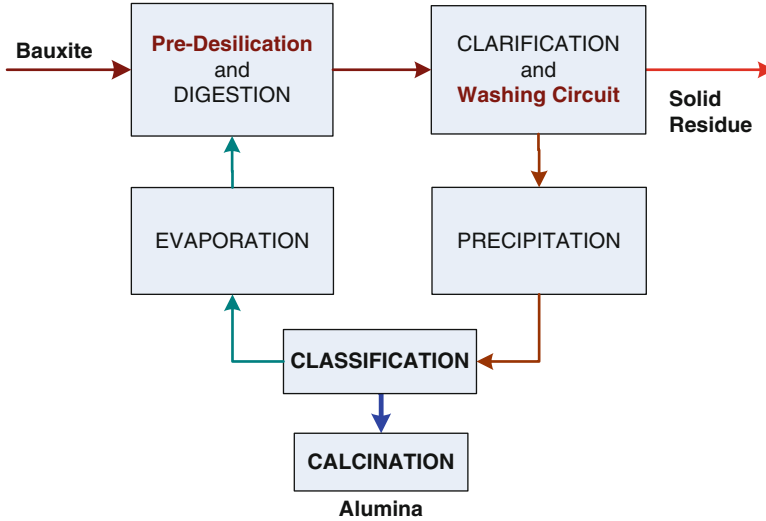


Fig. 9.6 The departments of Bayer process



to obtain the soluble NaAlO_2 and the solid desilication product $3\text{Na}_2\text{O} \cdot 3\text{Al}_2\text{O}_3 \cdot 5\text{SiO}_2 \cdot 5\text{H}_2\text{O}$ (in the Digesters). It is then going through a series of crystallisation (in the Thickeners) and precipitation (in the Precipitators) stages, then the classification stage (through various Filters) and the calcination stage (via Kilns) to become the final product of Al_2O_3 in white powder form, called alumina. The residue liquor that still contains certain levels of Al_2O_3 will be recirculated to the Digestion stage via the Evaporators where water condensates are recovered from the evaporated steam. The residue mud is washed to eliminate all toxic NaOH before being put into security ponds. The typical equilibrium curve of the Bayer process, the Bayer cycle, is provided in Fig. 9.7 for information.

The alumina refining challenges are to maximise yield (defined as the ratio of Weight of Al_2O_3 recovered over Volume of liquor circulating— $\text{g}(\text{Al}_2\text{O}_3)/\text{litre}$) subject to constraints on caustic concentration (expressed in terms of $\text{g}(\text{Na}_2\text{CO}_3)/\text{litre}$), particle size distribution in precipitation, and to robustly maintain liquor inventories and surge volumes within the optimal operating range [26]. Automatic control requirements for this process used to be considered as simple and there were no rooms for advanced process controls in the past. It is, nonetheless, becoming a promising candidate for modern control theories since the modular approach for process system designs have been deployed in the recently built plants. They are not only equipped with high-tech instrumentations, but also allow ultra-complex interconnections and ultra-flexible parallel operations of several sub-processes, especially in the Brownfield plants. These complexities do not exist previously (see Fig. 9.8).

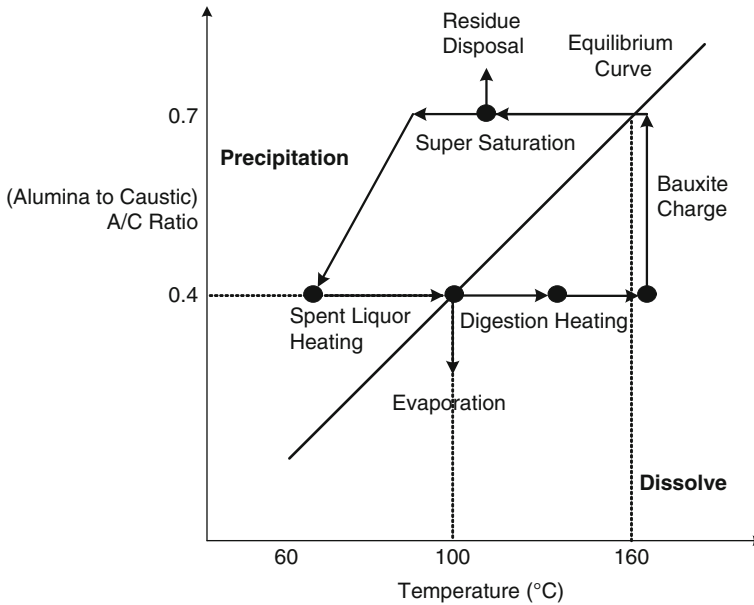


Fig. 9.7 Typical equilibrium curve of Bayer process: the alumina/caustic ratio ($\frac{\text{Al}_2\text{O}_3}{\text{Na}_2\text{CO}_3}$) vs. temperature

9.4.1 Plant-Wide Process Control for Alumina Refineries

With the ever increasing demands of aluminium around the world in the next 15 years, as evaluated by the visionary experts [9], and the widespread approach of modular assemblies and constructions in the fast-track projects of both Greenfield and Brownfield alumina refineries [10], the dynamic control of reticulated systems become imminently requisite and in great needs. With the maturity of optimisation methods and information technologies, the plant-wide dynamic operation and control, which have been considered as emerging applications for the mining industry about a decade ago [11, 26], are playing important roles in reducing the operational costs for large complex mineral processing plants nowadays [13].

While having appeared in open publications since the early days, the applications of dynamic modeling and control in this field emphasised on process simulations using empirical models for the caustic cycle or for the whole plant [12, 15], and on phenomenological models for different unit operations, see [5] and references therein, the multivariable control and optimisation-based techniques have only been attracted to lately [20]. Albeit gradually appreciated, the multivariable control designs have only been proposed and implemented to the individual unit operation as a single system [26]. In this chapter, we present a novel distributed and decentralised model predictive control, as well as online centric stabilisation strategies that are readily applied to the complex reticulated systems arising in the alumina refineries.

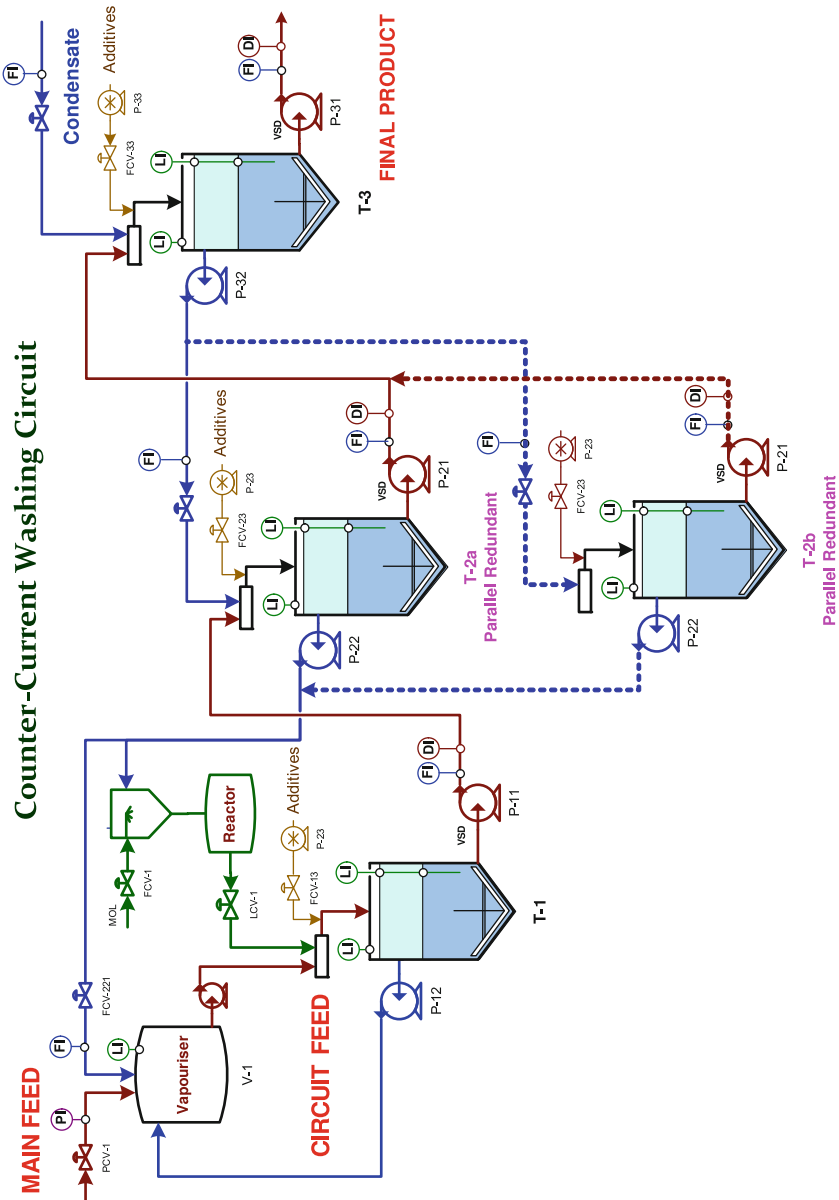


Fig. 9.8 The mud washing department in an alumina refinery

In this chapter, two sub-processes are taken from such a complex refinery for use in the illustrative examples. They are the inlet department of Predesilications and the final stage of Counter-Current Washing Circuits. The positions of these two department within the Bayer process is described in Fig. 9.6. Albeit simulating with simplified process systems and models, typically serial, parallel and cycle connections are all represented in these process systems. The developed methods are applicable to other sub-processes within the refinery and potentially to the entire Bayer cycle itself. The process descriptions here will only focus on the information relevant to the control design problem. The process system designs are not under the scope of this chapter.

9.4.2 *The Counter-Current Washing Circuit*

The counter-current washing technology is popularly used in the mineral processing industry. The process flow diagram of a typical washing circuit with a parallel redundant washing stage T-2b is given in Fig. 9.9. In an alumina refinery, the washing circuit recovers caustic soda from the residues of the upstream thickeners and clarifiers. Three residue washers are normally in operation. The inlet slurry is fed into the first washing stage while fresh condensates (water) are added to the final stage. The level of liquor on the top and the level of residue solids in the bottom of each washing tank will be continuously measured and controlled. Each washing stage (a tank) will have an underflow and overflow pump (e.g., P-11 and P-12, respectively, of the first tank). The main inlets of a washing tank will be from the upstream underflow and downstream overflow. The mixing of underflow and overflow streams will occur in a mixer prior to feeding into each tank. Flocculants are added after the slurry is mixed to enhance the settling conditions. The settled residue which has lower levels of caustic is raked to the tank perimeter where it is removed and pumped to the next downstream stage. The overflow liquor which has higher levels of caustic is pumped to the next upstream tank. The caustic content is thus reduced as residues move down the washing circuit.

For increasing the system reliability and operational availability, the second washing stage is installed with two parallel tanks which unevenly share the overflow and underflow from the downstream and upstream stages.

A modular control strategy is applied to this washing circuit instead of a plant-wide strategy, wherein the regulations of the underflow and overflow pumps depend only on the liquor and residue levels of the same stage. The underflow rates are thus linearly proportional to the residue levels while the overflow rates are proportional to the liquor levels. A washing stage is represented by a subsystem state space model. The nested system models, consisting of Units and Subsystems, will be deployed for the large-scale system having mixed connection configurations like this one. The large-scale process is grouped into three Units. Unit 2 has two Subsystems. Units 1 and 3 each has one Subsystem. Three controlled variables (plant outputs, y_i) of each subsystems correspond to the residue level, liquor level and slurry density.

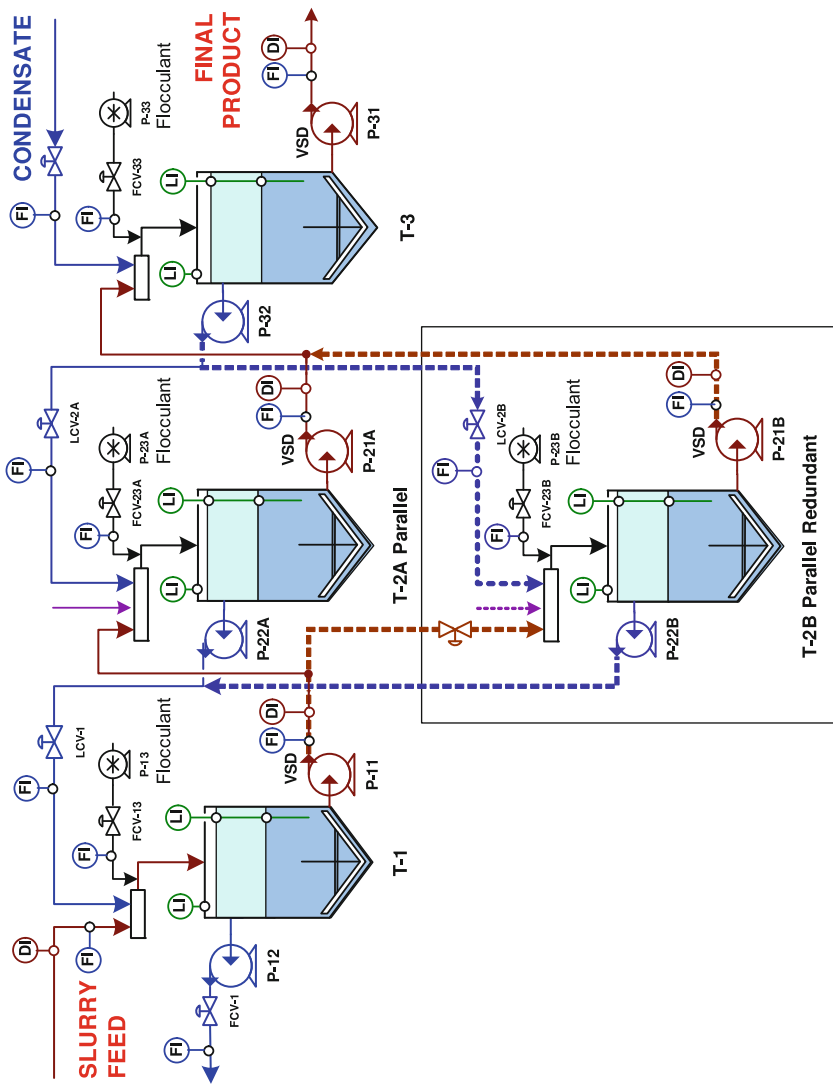


Fig. 9.9 Counter-current washing circuit with a parallel redundant subsystem in hydro-metallurgical processes

The manipulated variables (u_i) of the first tank are the feeding slurry and flocculant flow rates, of the second tank is the flocculant flow rate, and of the third tank are the condensate and flocculant flow rates. The lumped parameter models [8,25] have been developed for this process. The state space realisation matrices of the linearised models are given in the following:

$$\begin{aligned}
 A_{11} &= \begin{bmatrix} -29 & 0 & 0 \\ 17 & -6 & 0.5 \\ -8 & 0 & 0 \end{bmatrix}, B_{11} = \begin{bmatrix} 1 & 0 \\ 0 & 0 \\ 0 & 1 \end{bmatrix}, C_{11} = \begin{bmatrix} 1 & 0 & 0 \\ 0 & 1 & 0 \end{bmatrix}, \\
 A_{21} &= \begin{bmatrix} -14 & 0 & 0 \\ 18 & -0.5 & 0 \\ -3 & 0 & 0.2 \end{bmatrix}, B_{21} = \begin{bmatrix} 0 \\ 0 \\ 1 \end{bmatrix}, C_{21} = \begin{bmatrix} 1 & 0 & 0 \\ 0 & 1 & 0 \end{bmatrix}, \\
 A_{22} &= \begin{bmatrix} -13 & 0 & 0 \\ 16 & -0.5 & 0 \\ -5 & 0 & 0.2 \end{bmatrix}, B_{22} = \begin{bmatrix} 0 \\ 0 \\ 1 \end{bmatrix}, C_{22} = \begin{bmatrix} 1 & 0 & 0 \\ 0 & 1 & 0 \end{bmatrix}, \\
 A_{31} &= \begin{bmatrix} -16 & 0 & 1 \\ 12 & -0.7 & 0 \\ -6 & 0 & 0 \end{bmatrix}, B_{31} = \begin{bmatrix} -0.1 & 0 \\ 1 & 0 \\ 0 & 1 \end{bmatrix}, C_{31} = \begin{bmatrix} 1 & 0 & 0 \\ 0 & 1 & 0 \end{bmatrix}
 \end{aligned}$$

$$\begin{aligned}
 E_{\pi 11} &= \begin{bmatrix} 0 & -0.4 \\ 0 & 2 \\ 0 & 0 \end{bmatrix}, E_{\pi 31} = \begin{bmatrix} 2 & 0 \\ 0 & 0.8 \\ 0 & 0 \end{bmatrix}, \\
 E_{\pi 21} &= \begin{bmatrix} 2 & 0 & -1 & 0 \\ 0 & 0 & 0 & 0 \\ 0 & 0.8 & 0 & 0 \end{bmatrix}, E_{\pi 22} = \begin{bmatrix} 1.8 & 0 & -1.3 & 0 \\ 0 & 0 & 0 & 0 \\ 0 & 0.9 & 0 & 0 \end{bmatrix},
 \end{aligned}$$

$$F_{\pi 11} = \begin{bmatrix} 0.1 & 0 & 0 \\ 0 & 0 & 1 \end{bmatrix}, F_{\pi 21} = \begin{bmatrix} 0.1 & 0 & 0 \\ 0 & 0 & 0.5 \end{bmatrix}, F_{\pi 22} = \begin{bmatrix} 0.1 & 0 & 0 \\ 0 & 0 & 0.5 \end{bmatrix}, F_{\pi 31} = [0 \ 0.7 \ 0],$$

$$H_{\pi} = \begin{bmatrix} 0 & 0 & 1 & 0 & 0 \\ 0 & 0 & 0 & 1 & 0 \\ \hline 1 & 0 & 0 & 0 & 1 \\ 0 & 1 & 0 & 0 & 0 \\ \hline 0 & 0 & 1 & 0 & 0 \\ 0 & 0 & 0 & 1 & 0 \end{bmatrix}, H_{\sigma} = 0.$$

The control purpose is to track the set points of the controlled variables, which in this case, are transformed into the stabilizing problem of the linearised system subject to the control constraints on u_i and the decentralised architecture.

Short predictive horizons of $N_{11} = N_{21} = N_{22} = 3$ have been chosen for the first three subsystems, while a longer horizon of $N_{31} = 12$ is chosen for the fourth one. They all have the same sampling time of 0.4 min. The weighting coefficients for the control inputs, their increments and measurement outputs in the objective functions of three MPCs are as follows: $\mathcal{R}_{11} = \text{diag}\{2, 1\}$, $\mathcal{R}_{\Delta 11} = \text{diag}\{5, 1\}$, $\mathcal{Q}_{11} = \text{diag}\{5, 1, 2\}$, $\mathcal{R}_{21} = 1$, $\mathcal{R}_{\Delta 21} = 0.3$, $\mathcal{Q}_{21} = \text{diag}\{1, 1, 2\}$,

$\mathcal{R}_{22} = 1$, $\mathcal{R}_{\Delta 22} = 0.3$, $\mathcal{Q}_{22} = \text{diag}\{1, 1, 2\}$, $\mathcal{R}_{31} = \text{diag}\{0.5, 1\}$, $\mathcal{R}_{\Delta 31} = \text{diag}\{0.2, 0.7\}$, $\mathcal{Q}_{31} = \text{diag}\{4, 1, 5\}$. The control increments are included in the objective function (the weighting matrices are subscripted with Δ) and their constraints are also considered in this simulation. The constraints on the control inputs are setup as, $\bar{u}_{11} = -\underline{u}_{11} = [2 \ 2]^T$, $\bar{u}_{21} = -\underline{u}_{21} = [2 \ 2]^T$, $\bar{u}_{22} = -\underline{u}_{22} = [2 \ 2]^T$, $\bar{u}_{31} = -\underline{u}_{31} = [15 \ 15]^T$. The output constraints are ignored to emulate the control system instability.

When the multiplier matrices of the APRC are updated online (i.e., the first step in Procedure 2 is now active), the trends of plant outputs and control inputs are shown in Fig. 9.10, also indicating clearly a stabilised interconnected system. The APRC-based stability constraints have been imposed from step 20 in this simulation. It shows a monotonous increasing $\min(\xi_{jic})$ after which. And this implies a better control performance and a smoother control trajectory. The values of multiplier matrices S_{jic}^k at steps $k = 30, 45$ and 54 are listed below.

Subsystem 11:

$$S_{11c}^{30} = 10^8 \times \begin{bmatrix} 5.2984 & 0.8103 \\ -0.76381 & -4.4362 \end{bmatrix},$$

$$S_{11c}^{45} = 10^8 \times \begin{bmatrix} 6.1578 & 0.98013 \\ -0.8154 & -5.4738 \end{bmatrix}, S_{11c}^{54} = 10^8 \times \begin{bmatrix} 6.1456 & 0.9248 \\ -0.9012 & -5.1768 \end{bmatrix},$$

Subsystem 31:

$$S_{31c}^{30} = 10^8 \times \begin{bmatrix} 5.2346 & 0.9575 \\ -0.66474 & -4.7956 \end{bmatrix},$$

$$S_{31c}^{45} = 10^8 \times \begin{bmatrix} 5.1235 & 0.91714 \\ -0.6019 & -5.1279 \end{bmatrix}, S_{31c}^{54} = 10^8 \times \begin{bmatrix} 5.1780 & 0.9562 \\ -0.6346 & -5.2355 \end{bmatrix}.$$

Simulation results in this section have verified the effectiveness of the developed APRC-based stability constraints in a decentralised MPC strategy. In terms of operability and reliability, the proposed modular control strategy in this example is much better than the ad hoc plant-wide strategy usually implemented for this plant, wherein the downstream overflows (e.g., of tank 3) depend on the upstream liquor levels (e.g., of tank 2). By employing this modular strategy, the MPC controller relating to a single tank can be set up individually and built-in at the construction stage. The final control design for the interconnected system is just simply setting up the multiplier matrices for the APRC-based stability constraints.

9.4.3 Predesilication Process

In the predesilication department, the extracted bauxite ores are fed into grinding machines, then preheated and circulated through a system of settling and

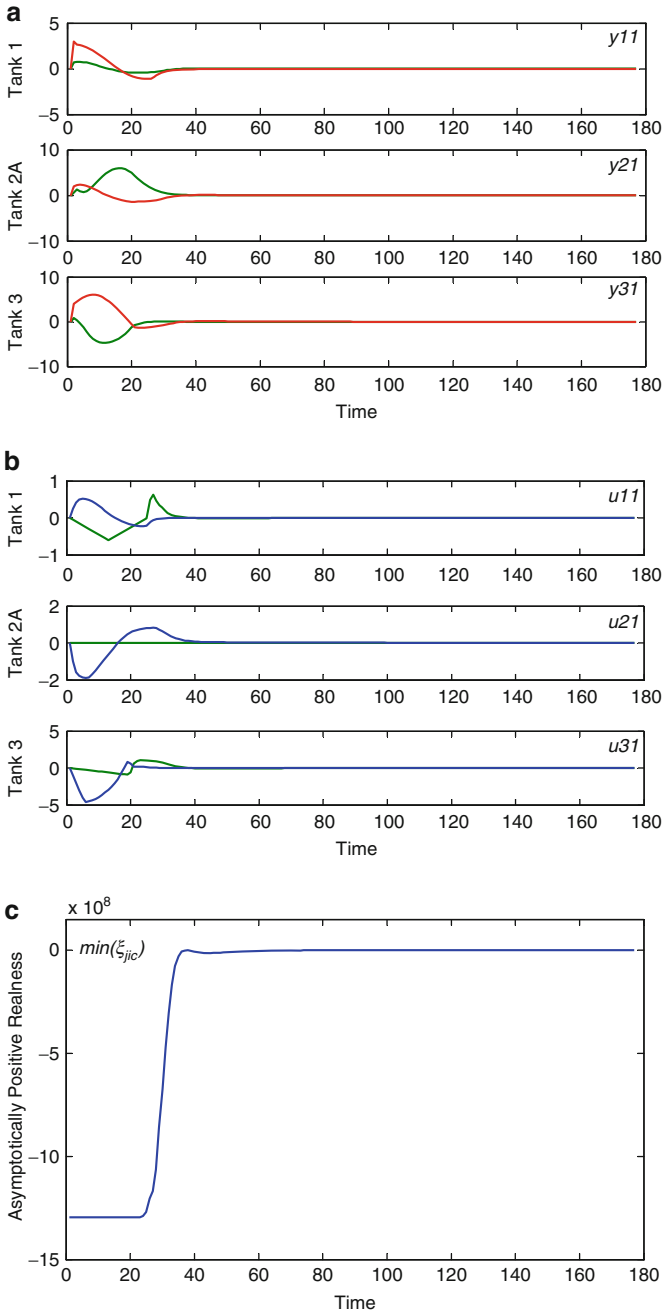


Fig. 9.10 APRC-based decentralised MPCs with quadratic programming of the counter-current washing circuit—time responses (a) Online updated multiplier matrices—plant outputs (b) Online updated multiplier matrices—control inputs (c) Online updated multiplier matrices— ξ_{jic}

predesilicating tanks before being mixed with heated soda in the digesters. The predesilication area of an alumina refinery is typical with parallel subsystems. A simplified process diagram of an actual plant is given in Fig. 9.11. The large-scale process is grouped into three Units. Unit 1 has two subsystems. Units 2 and 3 each has one subsystem. There are two mill grinding subsystems in this case. The mill grinding area (Unit 1) has two grinding mills (ML-1,-2) built with belt weighers (W-11,-12), mill slurry tanks (T-11,-12), and relay tanks (T-21, -22). Each mill is installed with an independent inching control system. The heating and predesilication area (Unit 2) has three steam heaters (H-31, 32-33) built with mill slurry pumps (P-31, -32, 33), booster pumps (P-34, -35, -36) and three predesilicating tanks (T-31, -32, -33) built with transfer and recirculation pumps (P-41, -42, -43). The saturated liquor from R-51 in Unit 3 is extracted and recirculated back to the mill grinding area via the reheater H-51. The large-scale system is modeled as four subsystems grouped into three units in this example. Units two and three each has only one subsystem, whereas unit one has two parallel subsystems. The control input of each subsystem in Unit 1 is the mill feed solid flow rate via the belt weigher (W-11/W-12). The control for this unit (1 only) is preferable with on/off (bang-bang) control. The levels in the mill, slurry and relay tanks are its states. The control inputs for the predesilication tanks in Unit 2 are the transfer and recirculation flow rates (P-41/42/-43). The levels in three predesilication tanks are its states. The temperature and flow control loops in Unit 2 are not included in this scheme. The two control inputs of the subsystem in Unit 3 are steam and caustic soda flow rates feeding to the top of R-51. The level and temperature in the reactor R-51 are its states. The state space realisation matrices are provided in the following:

$$\begin{aligned}
 A_{11} &= \begin{bmatrix} -1.4 & 0.3 & 0 \\ 0 & -1.8 & 1.5 \\ 0.1 & -2.7 & 1.06 \end{bmatrix}, B_{11} = \begin{bmatrix} 0 \\ 0 \\ 1 \end{bmatrix}, E_{\pi 11} = \begin{bmatrix} 0.48 \\ 0 \\ 0.48 \end{bmatrix}, \\
 A_{12} &= \begin{bmatrix} -1.6 & 0.2 & 0 \\ 0 & -2.1 & 1.7 \\ 0.3 & -1.8 & 0.9 \end{bmatrix}, B_{12} = \begin{bmatrix} 0 \\ 0 \\ 1 \end{bmatrix}, E_{\pi 12} = \begin{bmatrix} 0.5 \\ 0 \\ 0.5 \end{bmatrix}, \\
 A_{21} &= \begin{bmatrix} -0.76 & 0 & 0.25 \\ 0.48 & -0.56 & 0 \\ 0 & 0.2 & -0.34 \end{bmatrix}, B_{21} = - \begin{bmatrix} 1 & 0 & 0 \\ 0 & 1 & 0 \\ 0 & 0 & 1 \end{bmatrix}, E_{\pi 21} = \begin{bmatrix} 0.8 \\ 0 \\ 0 \end{bmatrix}, \\
 A_{31} &= \begin{bmatrix} -4.3 & 5.9 \\ -1.8 & 2.7 \end{bmatrix}, B_{31} = \begin{bmatrix} 1 & 0 \\ 0 & 1 \end{bmatrix}, E_{\sigma 31} = \begin{bmatrix} 0.5 \\ 0 \end{bmatrix}, \\
 C_{11} &= \begin{bmatrix} 1 & 0 & 0 \\ 0 & 1 & 0 \end{bmatrix}, F_{\pi 11} = [1 \ 0 \ 0], C_{12} = \begin{bmatrix} 1 & 0 & 0 \\ 0 & 1 & 0 \end{bmatrix},
 \end{aligned}$$

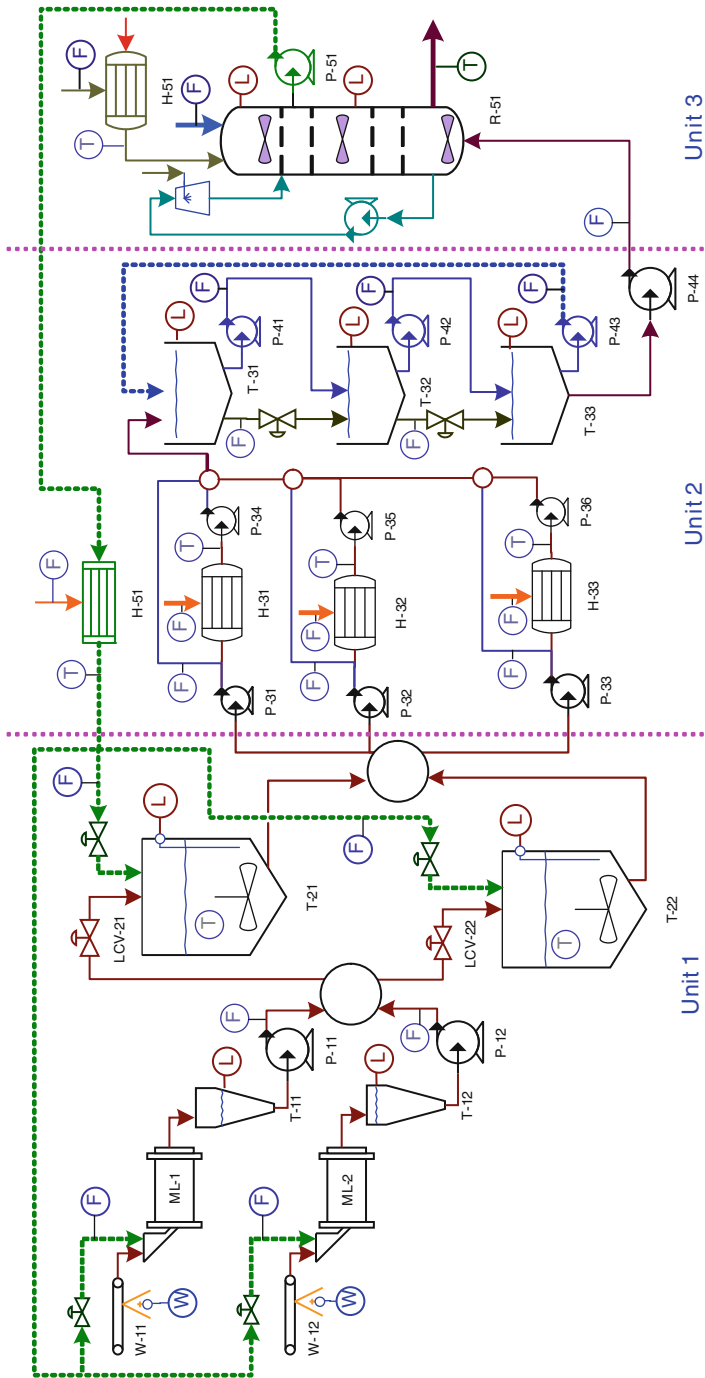


Fig. 9.11 Pre-desiccation process with parallel subsystems

$$\begin{aligned}
 F_{\pi 12} &= [1 \ 0 \ 0], \quad C_{21} = \begin{bmatrix} 1 & 0 & 0 \\ 0 & 1 & 0 \end{bmatrix}, \quad F_{\sigma 21} = [0 \ 0 \ 1], \\
 C_{31} &= \begin{bmatrix} 1 & 0 \\ 0 & 1 \end{bmatrix}, \quad F_{\pi 31} = [1 \ 0], \\
 H_{\pi\pi} &= \begin{bmatrix} 0 & 0 & 1 \\ 1 & 0 & 0 \\ 0 & 0 & 0 \end{bmatrix}, \quad H_{\sigma} = \begin{bmatrix} 0 & 0 & 0 \\ 0 & 0 & 0 \\ 0 & 1 & 0 \end{bmatrix}.
 \end{aligned}$$

The control purpose is to track the set points of the controlled variables, which in this case, are transformed into the stabilizing problem of the linearised state space model. The controlled variables (or plant outputs) are the two out of three states of subsystems 11 (levels of slurry and relay tanks, T-11 and T-21, respectively), 12 (levels of tanks T-12 and T-22) and 21 (levels of tanks T-31 and T-32), and the two states of subsystem 31 (temperature and level of R-51), respectively. The control problem is subject to the constraints on the control vectors u_i and the decentralised architecture.

The subsystem MPCs are formulated with the chosen predictive horizons, weighting matrices, initial state and control vectors, and the control constraints. The predictive horizons of four subsystems are as follows: $N_{11} = N_{12} = 6$, $N_{21} = 8$, $N_{31} = 6$. The weighting matrices are set up as, $\mathcal{L}_{11} = \text{diag}\{1, 1, 2\}$, $\mathcal{R}_{11} = [0.2]$, $\mathcal{L}_{12} = \text{diag}\{1, 1, 2\}$, $\mathcal{R}_{12} = [0.2]$, $\mathcal{L}_{21} = \text{diag}\{1.5, 2.4, 1.6\}$, $\mathcal{R}_{21} = \text{diag}\{0.2, 0.2, 0.2\}$, $\mathcal{L}_{31} = \text{diag}\{1, 3\}$, $\mathcal{R}_{31} = \text{diag}\{0.5, 0.5\}$. The initial state and control vectors are chosen as, $x_{11}^0 = [-1 \ -1 \ -1]^T$, $u_{11}^0 = -1$, $x_{12}^0 = [-1 \ -1 \ -1]^T$, $u_{12}^0 = -1$, $x_{21}^0 = [-1 \ 1 \ -1]^T$, $u_{21}^0 = [1 \ -1 \ 1]^T$, $x_{31}^0 = [1 \ -1]^T$, $u_{31}^0 = [-1 \ 1]^T$. The constraints on the control input vectors are as follows: $\bar{u}_{11} = -\underline{u}_{11} = 0.15$, $\bar{u}_{12} = -\underline{u}_{12} = 0.15$, $\bar{u}_{21} = -\underline{u}_{21} = [10 \ 10]^T$, $\bar{u}_{21} = -\underline{u}_{21} = [1 \ 1]^T$. The constraints of 10% \bar{u}_{ij} on the control increments are also setup here.

The multipliers are firstly determined offline using Procedure 1. When the local MPCs are imposed with the APRC-based stability constraints in the control algorithm of Procedure 2, the measurement output and control input trends are given in Fig. 9.12a,b, respectively. For asymptotical positive realness, two different sets of $\gamma_{ij}(k)$ are chosen for the simulations. Only time-invariant γ_{ji} is employed in this example. The coefficients $\gamma_{11} = 0.99$, $\gamma_{12} = 0.99$, $\gamma_{21} = 0.99$, $\gamma_{31} = 0.99$ in this simulation. If the coefficients are increased as $\gamma_{11} = 0.999$, $\gamma_{12} = 0.999$, $\gamma_{21} = 0.998$, $\gamma_{31} = 0.998$, the responses are given in Fig. 9.13a,b, respectively. From these two simulations, it is clearly that, there is a trade-off between the convergent rate of solutions and γ_{ij} . When γ_{ij} approaches 1, the control tends to be smoother, as shown by trends in Fig. 9.13 compared to those in Fig. 9.12 with smaller γ_{ij} . The settling times are, however, longer in Fig. 9.13 when γ_{ij} approaches 1.

To demonstrate the efficacy of the proposed approach, only offline multiplier matrices $Q_{jic}^0, S_{jic}^0, R_{jic}^0$ have been used in this example (i.e., the first online step in Procedure 2 is omitted). They are listed below.

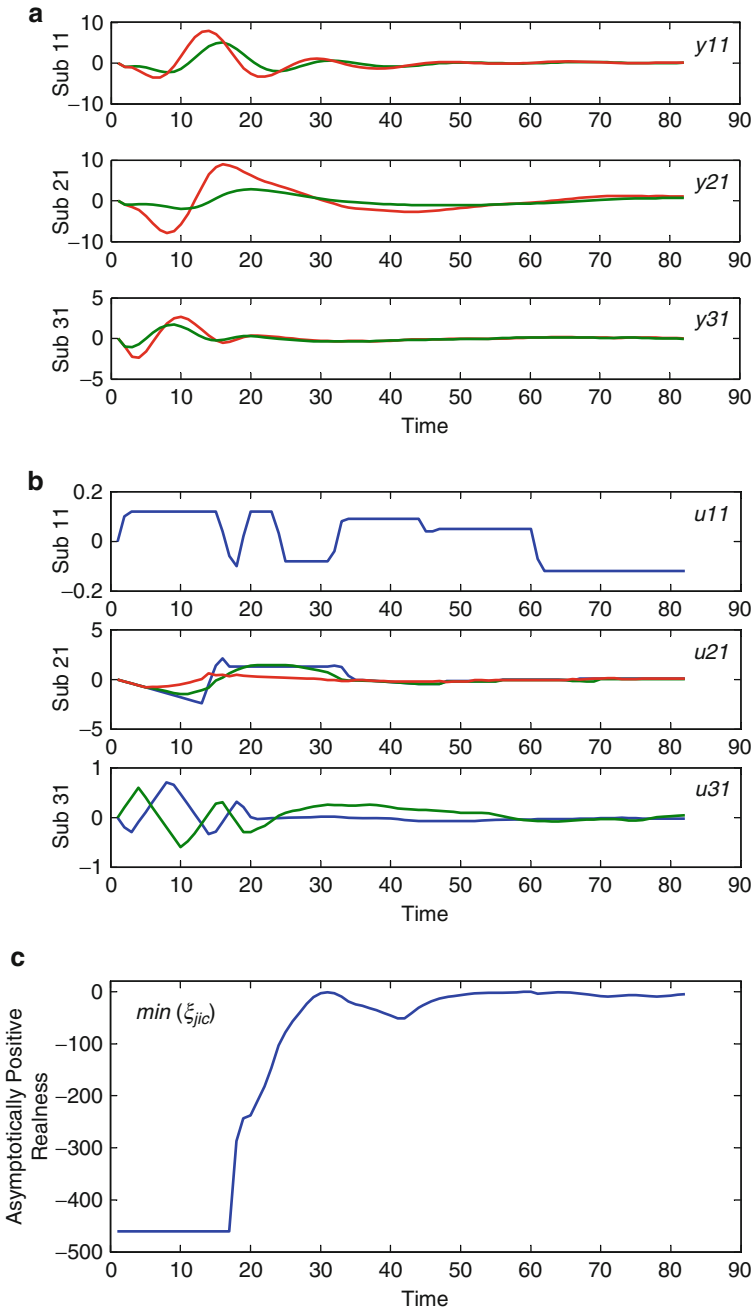


Fig. 9.12 Decentralised MPC with quadratic programming, and smaller γ_{ji} -time responses (a) With APRC-based stability constraints—plant outputs (b) With APRC-based stability constraints—control inputs (c) With APRC-based stability constraints— ξ_{jic}

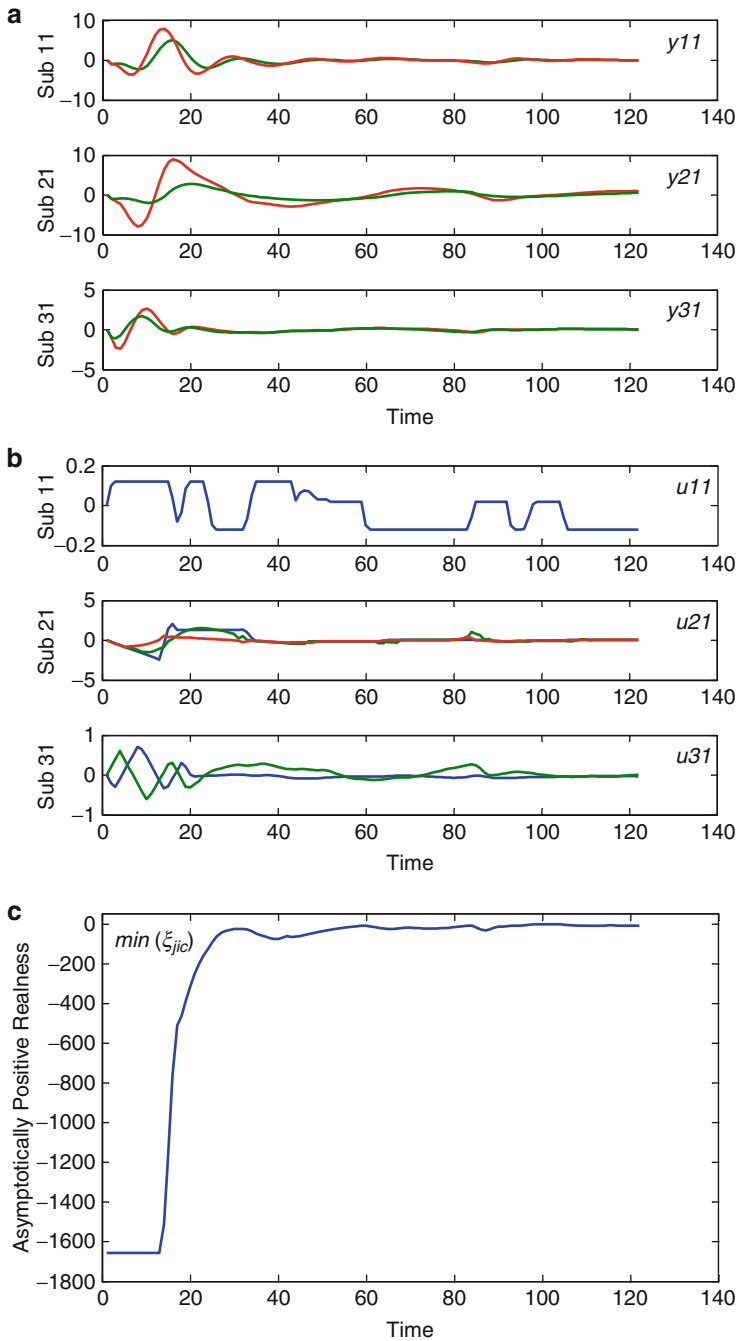


Fig. 9.13 Decentralised MPC with quadratic programming, $\gamma_{ji} \simeq 1$ —time responses (a) With APRC-based stability constraints—plant outputs (b) With APRC-based stability constraints—control inputs (c) With APRC-based APRC-based stability constraints— ξ_{jic}

$$\begin{aligned}
Q_{11c}^0 &= [-5.0161], Q_{21c}^0 = \begin{bmatrix} -4.3430 & -0.0036 & -0.5936 \\ -0.0036 & -4.3187 & -0.0821 \\ -0.5936 & -0.0821 & -6.8165 \end{bmatrix}, \\
Q_{31c}^0 &= \begin{bmatrix} -4.0614 & 0.1716 \\ 0.1716 & -4.2755 \end{bmatrix}, \\
S_{11c}^0 &= 10^2 \begin{bmatrix} -0.0639 \\ 0.4198 \end{bmatrix}, S_{21c}^0 = 10^2 \begin{bmatrix} 1.1024 & 0.0607 & 0.5236 \\ 0.0695 & 1.3737 & 0.5001 \end{bmatrix}, \\
S_{31c}^0 &= 10^2 \begin{bmatrix} 1.68 & -0.75 \\ 0.68 & -2.24 \end{bmatrix}, \\
R_{11c}^0 &= \begin{bmatrix} 50.499 & -1.922 \\ -1.922 & 42.016 \end{bmatrix}, R_{21c}^0 = 10^2 \begin{bmatrix} 0.2843 & -0.0380 \\ -0.0380 & 0.4379 \end{bmatrix}, \\
R_{31c}^0 &= 10^2 \begin{bmatrix} 0.4745 & -0.6883 \\ -0.6883 & 1.0104 \end{bmatrix}.
\end{aligned}$$

In this illustrative example, the APRC-based stability constraints are only imposed on the optimisation problems from step 15. It is observed that the minimum of ξ_{jic} , $j = 1, 2, 3$; $i = 1, 2$, increases monotonously towards zero without any fluctuations (Fig. 9.12c), compared to that in Fig. 9.13c. This is also equivalent to a smoother control trend, as analyzed above.

9.5 Conclusion

This chapter has provided a decentralised perspective on the control of time-varying splitting parallel systems. We have started with a brief overview on the industrial plant-wide process control with parallel redundant configurations and mixed operational modes. They are the basis for introducing the issues around the parallel systems that have time-varying and unknown splitting ratios. The state space models of complex interconnected systems with parallel and serial coupling vectors have been delineated in the subsequent section. Special treatments for parallel connections of time-varying and unknown splitting ratios are outlined in details in this section. A decentralised model predictive control strategy for such complex interconnected systems presented afterwards constituted an essential part of this chapter. There are not any requirements for the additional constraints on, or local measurements for, the vectors of coupling inputs and outputs in this approach. More importantly, a continuous control strategy for time-varying splitting parallel systems has been presented as an alternative to the hybrid control strategies. From the theoretical perspective, we have introduced the notion of APRC and its employment in a constructive method of approaching the positive real property for the

system under control. The APRC-based stabilisability conditions are developed into stability constraints for the local MPCs. These stability constraints are characterised dynamically to guarantee the recursive feasibility of the convex optimisations. Two case studies of typical modular systems in an alumina refinery have verified the efficacy of the presented decentralised MPC strategy. With the deployment of this decentralised MPC, the plant-wide control implementation for time-varying splitting parallel systems can now be facilitated by a simple plug-and-play function.

References

1. Apkarian P, Adams R (2000) Advanced gain-scheduling techniques for uncertain systems. In: Ghaoui L El, Niculescu S (eds) *Advanced in linear matrix inequality methods in control*. SIAM, Philadelphia, pp 971–981
2. Apkarian P, Noll D (2006) IQC analysis and synthesis via nonsmooth optimization. *Syst Contr Lett* 55(12):971–981
3. Apkarian P, Pellanda P, Tuan H (2000) Mixed h_2/h_∞ multi-channel linear parameter-varying control in discrete time. *Syst Contr Lett* 41:333–346
4. Apkarian P, Tuan HD (2003) Parameterized linear matrix inequalities in control theory. *SIAM J Contr Optim* 38(4):1241–1264
5. Bao L, Nguyen AV (2010) Developing a physically consistent model for gibbsite leaching kinetics. *Hydrometallurgy* 104:86–98
6. Brogliato B, Lozano R, Maschke B, Egeland O (2006) *Dissipative systems analysis and control: theory and applications*. Springer, London
7. El Ghaoui L, Niculescu S (2000) *Advances in linear matrix inequality methods in control*. Society for Industrial and Applied Mathematics, Philadelphia, PA, USA
8. Hangos KM, Cameron IT (2001) *Process modelling and model analysis*. Academic Press, London
9. Harder J (2010) Trends in the extraction of bauxite and alumina. *Aufbereitungs-Technik/Mineral Processing* 51(5):44–57
10. Henrickson L (2010) The need for energy efficiency in Bayer refining. In: *Proceedings of TMS annual meeting - light metals'10*, Seattle pp 173–178
11. Hodouin D, Jämsä-Jounela SL, Carvalhoc MT, Bergh L (2001) State of the art and challenges in mineral processing control. *Contr Eng Pract* 9(1):995–1005
12. Hoffman T, Hutchinson HP (1975) The simulation of the Bayer process for extracting alumina from bauxite ore. In: *Proceedings of symposium on computer design and erection of chemical plants*, Czechoslovakia, pp 451–485
13. Jämsä-Jounela SL (2007) Future trends in process automation. *Annu Rev Contr* 31:211–220
14. Koroğlu H, Scherer CW (2007) Robust performance analysis for structured linear time-varying perturbations with bounded rates-of-variation. *IEEE Trans Automat Contr* 52(3):197–211
15. Leslie RA, Blair JR (1975) The dynamic modelling of caustic concentration in the Bayer process. In: *Proceedings of APCOM symposium 5*, pp 137–14
16. Lunze J (1992) *Feedback control of large scale systems*. Prentice Hall, London
17. Maciejowski JM (2002) *Predictive control with constraints*. Prentice Hall, Harlow
18. Mahmoud MS (2010) *Decentralized control and filtering in interconnected dynamical systems*. CRC Press, New York
19. Megretski A, Rantzer A (1997) System analysis via integral quadratic constraints. *IEEE Trans Automat Contr* 42(6):819–830

20. Ouellet V, Bergeron S, Verville D (2007) Bayer process control at Alcan Vaudreuil works. In: Proceedings of 12th IFAC symposium on automation in mining, mineral and metal processing 12(1):Quebec
21. Rawlings JB, Stewart BT (2008) Coordinating multiple optimization-based controllers: New opportunities and challenges. *J Process Control* 18:839–845
22. Rotkowitz M, Lall S (2006) A characterization of convex problems in decentralized control. *IEEE Trans Automat Contr* 51:274–286
23. Scattolini R (2009) Architectures for distributed and hierarchical model predictive control - A Review. *J Process Control* 19:723–731
24. Schooman ML (2001) Reliability of computer systems and networks: fault tolerance, analysis and design. Wiley-Interscience, New York
25. Seborg DE, Edgar TF, Mellichamp DA, III FJD (2010) Process dynamics and control, 3rd edn. Wiley, New York
26. Sidrak YL (2001) Dynamic simulation and control of the Bayer process—a review. *Ind Eng Chem Res* 40:1146–1156
27. Siljak DD (1991) Decentralized control of complex systems. Academic, New York
28. Sourlas DD, Manousiouthakis V (2003) Best achievable decentralized performance. *IEEE Trans Automat Contr* 40(11):1858–1871
29. Tran T (2010) Overriding control for stability with manifest variables. In: Proceedings of IEEE international conference on control, automation, robotics and vision ICARCV'10, pp 236–241
30. Tran T, Nguyen HT, Ha QP (2010) Stability of complex systems with mixed connection configurations under shared control. In: Proceedings of IEEE international conference on control, automation, robotics and vision ICARCV'10, pp 513–517
31. Tran T, Tuan HD, Ha QP, Nguyen HT (2011) Toward plant-wide control of reticulated systems arising in alumina refineries with online stabilisation. In: Proceedings of the 18th IFAC World Congress, Milano, Italy
32. Tran T, Tuan HD, Ha QP, Nguyen HT (2011) Stabilising agent design for the control of interconnected systems. *Int J Contr* 84:1140–1156
33. Tuan HD, Apkarian P, Narikyio T, Yamamoto Y (2001) Parametrized linear matrix inequalities in fuzzy control system design. *IEEE Trans Fuzzy Syst* 9:324–332
34. Tuan HD, Apkarian P, Narikyio T, Kanota M (2004) New fuzzy control model and dynamic output feedback parallel distributed compensation. *IEEE Trans Fuzzy Syst* 12:13–21

Chapter 10

Robust Estimation with Partial Gain-Scheduling Through Convex Optimization

Joost Veenman, Carsten W. Scherer, and I. Emre Köse

Abstract The problem of robust estimation for uncertain dynamical systems with a linear fractional dependence on uncertainties is considered. It is assumed that some of the parametric uncertainties affecting the system are available online and the estimator is scheduled on these parameters. The integral quadratic constraint (IQC) framework is considered for handling the uncertainties. Full-block static multipliers are used for capturing the properties of the measured parameters in the system while no structural or dynamic restrictions are placed on the multipliers used for the nonmeasured uncertainties. Sufficient existence conditions for constructing such robustly stabilizing, partially gain-scheduled estimators with guaranteed \mathcal{L}_2 -gain bounds are given in terms of finite dimensional linear matrix inequalities. A numerical example illustrates the advantages of gain-scheduling in robust estimation whenever possible.

10.1 Introduction

The online estimation of nonmeasured variables in a dynamical system constitutes one of the most important problems in systems and control theory. When the mathematical model represents the physical system exactly, the estimation problem is solved efficiently within the framework of \mathcal{H}_2 - or \mathcal{H}_∞ -control theory and the solutions are expressed in terms of convex optimization problems (see, e.g., [4]).

J. Veenman (✉) • C.W. Scherer
Department of Mathematics, University of Stuttgart, Stuttgart, Germany
e-mail: joost.veenman@mathematik.uni-stuttgart.de;
carsten.scherer@mathematik.uni-stuttgart.de

I.E. Köse
Department of Mechanical Engineering, Boğazici University, Istanbul, Turkey
e-mail: koseemre@boun.edu.tr

It has recently been observed that in the presence of modeling uncertainties, the robust estimation problem also yields a convex solution [7], which is certainly not the case for a general robust control design problem.

Since then, a number of papers have appeared investigating different uncertainty structures in the plant and different methods of solution. As is typical of all theoretical studies in the literature, the results vary with the dependence of the plant on the uncertainties. For instance, systems with affine dependence on uncertain parameters that take values in a convex polytope were studied in [7, 8]. The conservatism of the techniques presented in these papers was reduced by the use of parametric Lyapunov functions in [9] and also in [1, 24]. On the other hand, assuming a linear fractional (i.e., LFT) dependence on uncertain parameters that is familiar from robust control theory, static and dynamic D/G -scales were considered in [22, 23], respectively. For dynamical systems involving uncertainties that are captured by integral quadratic constraints (IQCs) as in [16], a full solution for the robust estimation problem was given in [19].

In this chapter, we focus on a linear fractional transformation (LFT) representation of the uncertain system and assume that the uncertainties affecting the system fall into two categories. In the first category are the uncertainties whose characteristics are known, but which are not measured online, and, therefore, cannot be used for scheduling the estimator. The second category consists of parametric variations that are measurable online, with a priori known bounds and arbitrarily fast rates-of-variation. The estimator we seek is scheduled on the uncertainties in this second category and, hence, is only partially gain-scheduled. The objective is to find such an estimator that is robustly stable and yields a guaranteed \mathcal{L}_2 -gain bound from the disturbance to the estimation error signal. This represents a very realistic engineering scenario and, to the best of our knowledge, has not been addressed in the literature so far.

Our main result is given in terms of convex conditions for the existence of such an estimator, together with a construction of the estimator when these conditions are satisfied. Our solution is based on the robustness analysis of the interconnection of the system with the estimator using IQCs that are defined through “multipliers” that describe the characteristics of a given operator [16]. For each category of the uncertainties, we use the most representative multipliers in the literature. Indeed, for the unmeasured uncertainties, we allow any appropriate, possibly dynamic (i.e., frequency-dependent), multiplier to be included in our solution. In our computations, these multipliers are parameterized through the use of basis functions, enabling us to approximate the IQCs with arbitrary accuracy and simplifying the search for optimal multipliers. For the measured parametric uncertainties, we use full-block static multipliers [17], which are known to yield the least conservative representation of arbitrarily fast parametric variations.

The results in this chapter are based on [17, 19] and the fact that the structure of the estimation problem allows one to take the crucial step of “dualization.” This also allows us to show that the McMillan degree of the estimator can be set to zero and

the design problem will still yield a convex solution. Lastly, completely analogous results can be derived for the design of robust, partially gain-scheduled feedforward controllers employing the techniques here, only in dual form.

The chapter is organized as follows. In Sect. 10.2, we introduce the robust estimation problem with partial gain-scheduling in detail. Robustness analysis of the interconnection of the system with the estimator through the use of IQCs is discussed in Sect. 10.3. Basic results regarding the structure of the multipliers and the issue of nominal stability characterization in state-space are discussed here. The main result of the chapter, namely Theorem 10.4, is given in Sect. 10.4. Due to space limitations, we only give a sketch of the proof of Theorem 10.4 in Sections “Sketch of Proof of Theorem 10.4: Necessity” and “Sketch of Proof of Theorem 10.4: Sufficiency” in the Appendix. The findings of the chapter are highlighted through a numerical example in Sect. 10.5. We conclude the chapter with some remarks in Sect. 10.6. Some technical tools used in this chapter are given in the Appendix.

10.1.1 Notation

The symbol \mathcal{L}_2 denotes the space of vector-valued square integrable functions defined on $[0, \infty)$, with the usual inner product given by $\langle \cdot, \cdot \rangle$. The space of all real-rational and proper (and stable) matrix functions that have no poles on the extended imaginary axis (in the closed right-half complex plane) is denoted by $\mathcal{RL}_\infty^{m \times n}$ ($\mathcal{RH}_\infty^{m \times n}$). By an operator we mean a map $G : \mathcal{L}_2^a \rightarrow \mathcal{L}_2^b$, and for two given operators $G = \begin{pmatrix} G_{11} & G_{12} \\ G_{21} & G_{22} \end{pmatrix}$ and Δ , the LFT $\Delta \star G$ is defined as $G_{22} + G_{21}\Delta(I - G_{11}\Delta)^{-1}G_{12}$, assuming that $(I - G_{11}\Delta)^{-1}$ exists. Realizations of linear time-invariant (LTI) systems are denoted by $G = C(sI - A)^{-1}B + D := \begin{bmatrix} A & B \\ C & D \end{bmatrix}$ and with $G(i\omega)^*$ we mean $G(-i\omega)^T$. If G has no eigenvalues on the extended imaginary axis and P is a symmetric matrix, then, by the KYP Lemma, the frequency domain inequality (FDI) $G(i\omega)^*PG(i\omega) \prec 0 \forall \omega \in \mathbb{R} \cup \{\infty\}$ is equivalent to the existence of a symmetric matrix X , for which the following LMI is feasible:

$$\begin{pmatrix} I & 0 \\ A & B \\ C & D \end{pmatrix}^T \underbrace{\begin{pmatrix} 0 & X & 0 \\ X & 0 & 0 \\ 0 & 0 & P \end{pmatrix}}_{\mathcal{M}(X,P)} \begin{pmatrix} I & 0 \\ A & B \\ C & D \end{pmatrix} \prec 0. \quad (10.1)$$

It is finally convenient to say that X is a certificate for the FDI and to use the abbreviation $(\star)^*PG$ for G^*PG .

10.2 The Robust Gain-Scheduled Estimation Problem

Consider the uncertain LPV plant in Fig. 10.1 where

$$\begin{pmatrix} z_d \\ z_s \\ z_p \\ y \end{pmatrix} = \underbrace{\begin{pmatrix} G_{dd} & G_{ds} & G_{dp} \\ G_{sd} & G_{ss} & G_{sp} \\ G_{pd} & G_{ps} & G_{pp} \\ G_{yd} & G_{ys} & G_{yp} \end{pmatrix}}_{G \in \mathcal{RH}_\infty} \begin{pmatrix} w_d \\ w_s \\ w_p \end{pmatrix} \tag{10.2}$$

represents a proper, stable LTI system that admits a minimal realization of the form

$$G = \begin{bmatrix} A & B_d & B_s & B_p \\ C_d & D_{dd} & D_{ds} & D_{dp} \\ C_s & D_{sd} & D_{ss} & D_{sp} \\ C_p & D_{pd} & D_{ps} & D_{pp} \\ C_y & D_{yd} & D_{ys} & D_{yp} \end{bmatrix}, A \in \mathbb{R}^{n \times n}. \tag{10.3}$$

Here, respectively, $\text{col}(w_d, w_s, w_p) \in \mathcal{L}_2^{n_{w_d} + n_{w_s} + n_{w_p}}$ and $\text{col}(z_d, z_s, z_p, y) \in \mathcal{L}_2^{n_{z_d} + n_{z_s} + n_{z_p} + n_y}$ denote the collection of uncertainty, scheduling and exogenous disturbance input signals and uncertainty, scheduling, performance and measurement output signals.

The plant G is subject to perturbations by the bounded and causal operators Δ_d and Δ_s , also referred to as the uncertainty and scheduling block, respectively. The uncertainty block Δ_d belongs to a given star-convex set $\mathbf{\Delta}_d$ with center zero (i.e., $[0, 1]\mathbf{\Delta}_d \subseteq \mathbf{\Delta}_d$), capturing the properties of the uncertainties and nonlinearities, while the scheduling block $\Delta_s := \hat{\Delta}_s \circ \eta$ is assumed to be a linear function of an

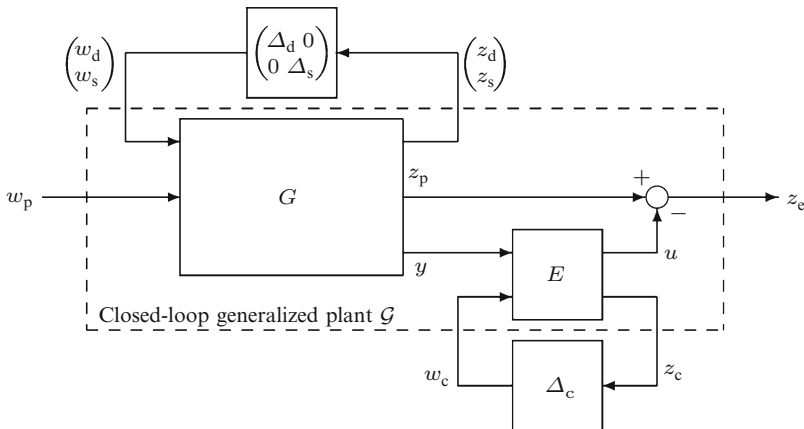


Fig. 10.1 Robust gain-scheduled estimation problem

online measurable time-varying parameter vector $\eta : [0, \infty) \rightarrow \Lambda$. Here the map $\hat{\Delta}_s : \mathbb{R}^k \rightarrow \mathbb{R}^{n_{ws} \times n_{zs}}$ is defined by $\hat{\Delta}_s(\eta) := \sum_{i=1}^k \eta_i H_i$ for some fixed matrices H_i , $\eta \in \mathbb{R}^k$, and we assume that η takes its values in $\Lambda := \text{co}\{\eta^1, \dots, \eta^m\} \subseteq \mathbb{R}^k$, where $\eta^j = (\eta_1^j, \dots, \eta_k^j)$, $j \in \mathbf{J} := \{1, \dots, m\}$ represent the generator points. Without loss of generality, Λ contains the origin. Then the scheduling block Δ_s is contained in the set $\mathbf{\Delta}_s := \{\hat{\Delta}_s \circ \eta : \eta \in \mathbf{C}_p([0, \infty), \Lambda)\}$ (with $\mathbf{C}_p([0, \infty), \Lambda)$ denoting the space of piecewise continuous functions $[0, \infty) \rightarrow \Lambda$) and defines the scheduling operator $w_s(t) = \hat{\Delta}_s(\eta(t))z_s(t)$.

The plant G interacts with Δ_d and Δ_s through an LFT, which we assume to be well-posed. Equivalently, this boils down to

$$\begin{pmatrix} I & 0 \\ 0 & I \end{pmatrix} - \begin{pmatrix} G_{dd} & G_{ds} \\ G_{sd} & G_{ss} \end{pmatrix} \begin{pmatrix} \Delta_d & 0 \\ 0 & \Delta_s \end{pmatrix} \quad (10.4)$$

being well-posed, which means that (10.4) is assumed to have a causal inverse for all $\Delta_d \in \mathbf{\Delta}_d$ and $\Delta_s \in \mathbf{\Delta}_s$.

The main goal in robust gain-scheduled estimation is the synthesis of a filter $E \star \Delta_c$ that dynamically and causally processes the measurement y and the scheduling signal η in order to provide an estimate u of the signal z_p in the sense that the \mathcal{L}_2 -gain from w_p to $z_e = z_p - u$ is rendered less than an a priori given $\gamma > 0$. Here the operator Δ_c represents the so-called scheduling function that is defined with some to-be-constructed $\hat{\Delta}_c : \mathbb{R}^{n_{ws} \times n_{zs}} \rightarrow \mathbb{R}^{n_{wc} \times n_{zc}}$ as $\Delta_c := \hat{\Delta}_c(\Delta_s)$. Again, Δ_c defines the operator $w_c(t) = \hat{\Delta}_c(\hat{\Delta}_s(\eta(t)))z_c(t)$. Moreover, E is a proper and stable LTI system that admits a realization of the form

$$\begin{pmatrix} u \\ z_c \end{pmatrix} = \underbrace{\begin{bmatrix} A_E & B_y & B_c \\ C_u & D_{uy} & D_{uc} \\ C_c & D_{cy} & D_{cc} \end{bmatrix}}_E \begin{pmatrix} y \\ w_c \end{pmatrix}, \quad A_E \in \mathbb{R}^{n \times n}, \quad (10.5)$$

where A_E is Hurwitz and where $\text{col}(y, w_c) \in \mathcal{L}_2^{n_y + n_{wc}}$ and $\text{col}(u, z_c) \in \mathcal{L}_2^{n_u + n_{zc}}$ denote the collection of measurement and scheduling input and the control and scheduling output signals respectively.

Given G , Λ and $\mathbf{\Delta}_d$, the goal of this chapter can now be formally stated as follows: “Design a gain-scheduled estimator $E \star \Delta_c$ such that, for all $\Delta_d \in \mathbf{\Delta}_d$ and $\Delta_s \in \mathbf{\Delta}_s$, the interconnection of Fig. 10.1 is well-posed, stable and the \mathcal{L}_2 -gain from w_p to z_e is rendered less than γ .”

10.3 Robust Stability and Performance Analysis

As a preparation, consider the standard input–output setting for robust stability and performance analysis in Fig. 10.2, where $\mathcal{G} \in \mathcal{RH}_\infty^{(n_K + n_{z_e}) \times (n_\Psi + n_{w_p})}$ represents the nominal and stable closed-loop generalized plant, as represented by the dashed

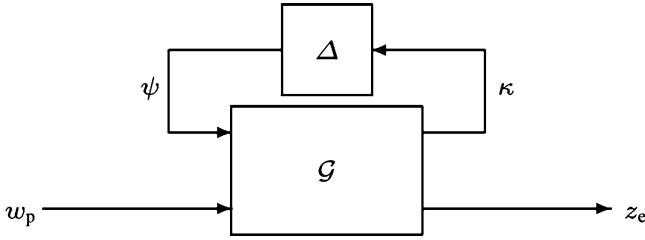


Fig. 10.2 Standard configuration for robust stability and performance analysis

box in Fig. 10.1. Here, $\kappa = \text{col}(z_d, z_s, z_c) \in \mathcal{L}_2^{n_{z_d} + n_{z_s} + n_{z_c}}$ and $\psi = \text{col}(w_d, w_s, w_c) \in \mathcal{L}_2^{n_{w_d} + n_{w_s} + n_{w_c}}$ denote the collection of scheduling and uncertainty signals and G admits the realization

$$\begin{aligned}
 G &:= \begin{pmatrix} \mathcal{G}_{\kappa\psi} & \mathcal{G}_{\kappa p} \\ \mathcal{G}_{e\psi} & \mathcal{G}_{ep} \end{pmatrix} = \begin{pmatrix} \mathcal{G}_{dd} & \mathcal{G}_{ds} & 0 & \mathcal{G}_{dp} \\ \mathcal{G}_{sd} & \mathcal{G}_{ss} & 0 & \mathcal{G}_{sp} \\ \mathcal{G}_{cd} & \mathcal{G}_{cs} & \mathcal{G}_{cc} & \mathcal{G}_{cp} \\ \mathcal{G}_{ed} & \mathcal{G}_{es} & \mathcal{G}_{ec} & \mathcal{G}_{ep} \end{pmatrix} = \left[\begin{array}{c|ccc|c} A & B_d & B_s & B_c & B_p \\ \hline C_d & D_{dd} & D_{ds} & 0 & D_{dp} \\ C_s & D_{sd} & D_{ss} & 0 & D_{sp} \\ \hline C_c & D_{cd} & D_{cs} & D_{cc} & D_{cp} \\ C_e & D_{ed} & D_{es} & D_{ec} & D_{ep} \end{array} \right] = \\
 &= \left[\begin{array}{cc|cc|c|c} A & 0 & B_d & B_s & 0 & B_p \\ \hline B_y C_y & A_E & B_y D_{yd} & B_y D_{ys} & B_c & B_y D_{yp} \\ \hline C_d & 0 & D_{dd} & D_{ds} & 0 & D_{dp} \\ C_s & 0 & D_{sd} & D_{ss} & 0 & D_{sp} \\ \hline D_{cy} C_y & C_c & D_{cy} D_{yd} & D_{cy} D_{ys} & D_{cc} & D_{cy} D_{yp} \\ \hline C_p - D_{uy} C_y & -C_u & D_{pd} - D_{uy} D_{yd} & D_{ps} - D_{uy} D_{ys} & -D_{uc} & D_{pp} - D_{uy} D_{yp} \end{array} \right]. \tag{10.6}
 \end{aligned}$$

As a natural consequence, G is (1) stable if A and A_E are Hurwitz and (2) subject to perturbations by the bounded and causal operator $\Delta := \text{diag}(\Delta_d, \Delta_s, \Delta_c)$ which is contained in the set $\mathbf{\Delta} := \text{diag}(\mathbf{\Delta}_d, \mathbf{\Delta}_s, \hat{\Delta}_c(\mathbf{\Delta}_s))$ and represents the collection of uncertainty and scheduling blocks. The system interconnection of Fig. 10.2 is now said

- (A.1) To be well-posed if the operator $I - \mathcal{G}_{\kappa\psi}\Delta$ has a causal inverse for all $\Delta \in \mathbf{\Delta}$.
- (A.2) To be robustly stable if $I - \mathcal{G}_{\kappa\psi}\Delta$ is well-posed and if its inverse is bounded on \mathcal{L}_2 .
- (A.3) To have a robust \mathcal{L}_2 -gain performance of level γ , if it is robustly \mathcal{L}_2 -stable and if for all $\Delta \in \mathbf{\Delta}$ the \mathcal{L}_2 -gain from w_p to z_e is less than $\gamma > 0$.

By recalling the structure of (10.6), clearly $I - \mathcal{G}_{\kappa\psi}\Delta$ is well-posed if and only if

$$I - \mathcal{G}_{cc}\Delta_c \tag{10.7}$$

and (10.4) are well-posed for all $\Delta_c \in \hat{\Delta}_c(\mathbf{\Delta}_s)$ and for all $\Delta_d \in \mathbf{\Delta}_d$ and $\Delta_s \in \mathbf{\Delta}_s$, respectively. Hence, since (10.4) is well-posed by assumption, we only require (10.7) to have a bounded inverse for all $\Delta_c \in \hat{\Delta}_c(\mathbf{\Delta}_s)$, which in turn just means that $E \star \Delta_c$ must be well-posed.

10.3.1 Analysis with IQCs

Recall that the operator Δ is said to satisfy the IQC defined by the multiplier $\Pi = \Pi^* \in \mathcal{R}\mathcal{L}_\infty^{(n_\kappa+n_\psi) \times (n_\kappa+n_\psi)}$ if the following condition holds true:

$$\left\langle \begin{pmatrix} \kappa \\ \Delta(\kappa) \end{pmatrix}, \Pi \begin{pmatrix} \kappa \\ \Delta(\kappa) \end{pmatrix} \right\rangle \geq 0 \quad \forall \kappa \in \mathcal{L}_2^{n_\kappa}. \quad (10.8)$$

For the correct interpretation of this expression, we refer the reader to [5]. In this chapter, we assume that Π is factorized as $\Phi^* P \Phi$, with P being a symmetric matrix and $\Phi \in \mathcal{R}\mathcal{H}_\infty^{n_\psi \times n_\kappa}$ a typically tall transfer matrix. In applications one constructs a whole family of multipliers $\Pi = \Phi^* P \Phi$ with a suitable set of symmetric matrices $P \in \mathbf{P}$ such that the IQC holds for all $\Delta \in \mathbf{\Delta}$. We do not make use of any particular structure of Φ and P for the uncertainty Δ_d and restrict our attention to static full-block multipliers for the scheduling block $\Delta_{sc} := \text{diag}(\Delta_s, \Delta_c)$. Hence, let us consider the following two IQCs:

$$\left\langle \begin{pmatrix} z_d \\ \Delta_d(z_d) \end{pmatrix}, \Psi^* P_1 \Psi \begin{pmatrix} z_d \\ \Delta_d(z_d) \end{pmatrix} \right\rangle \geq 0 \quad \forall z_d \in \mathcal{L}_2^{n_{z_d}}, \quad (10.9)$$

$$\left\langle \begin{pmatrix} z_{sc} \\ \Delta_{sc} z_{sc} \end{pmatrix}, P_{2e} \begin{pmatrix} z_{sc} \\ \Delta_{sc} z_{sc} \end{pmatrix} \right\rangle \geq 0 \quad \forall z_{sc} := \begin{pmatrix} z_s \\ z_c \end{pmatrix} \in \mathcal{L}_2^{n_{z_s} + n_{z_c}}. \quad (10.10)$$

Here, $\Psi := (\Psi_1 \ \Psi_2) \in \mathcal{R}\mathcal{H}_\infty^{n_\psi \times (n_{w_d} + n_{z_d})}$ is partitioned according to the structure of $\text{col}(z_d, \Delta_d(z_d))$ and $P_1 \in \mathbf{P}_1$ is any suitable (LMIable) set of structured symmetric matrices such that (10.9) holds (see Sect. 10.3.2 for examples). Moreover, (10.10) is satisfied if P_{2e} is confined to

$$\mathbf{P}_{2e} := \left\{ P_{2e} : (\star)^T \underbrace{\begin{pmatrix} Q & Q_{12}^T & S & S_{12} \\ Q_{12}^T & Q_{22} & S_{21} & S_{22} \\ S^T & S_{21}^T & R & R_{12} \\ S_{12}^T & S_{22}^T & R_{12}^T & R_{22} \end{pmatrix}}_{P_{2e}} \begin{pmatrix} I & 0 \\ 0 & I \\ -\hat{\Delta}_s(\eta^j) & 0 \\ 0 & \hat{\Delta}_c(\hat{\Delta}_s(\eta^j)) \end{pmatrix} \succ 0, \begin{pmatrix} R & R_{12} \\ R_{12}^T & R_{22} \end{pmatrix} \prec 0 \forall j \in \mathbf{J} \right\}. \quad (10.11)$$

Hence, with $P_1 \in \mathbf{P}_1$ and $P_{2e} \in \mathbf{P}_{2e}$, we infer that (10.8) is satisfied for all $\Delta \in \mathbf{\Delta}$ with

$$\Pi = \Phi^* P \Phi = \Phi^* \begin{pmatrix} P_1 & 0 \\ 0 & P_{2e} \end{pmatrix} \Phi = (\star)^* \begin{pmatrix} P_1 & 0 & 0 & 0 & 0 \\ 0 & Q & Q_{12} & S & S_{12} \\ 0 & Q_{12}^T & Q_{22} & S_{21} & S_{22} \\ 0 & S^T & S_{21}^T & R & R_{12} \\ 0 & S_{12}^T & S_{22}^T & R_{12}^T & R_{22} \end{pmatrix} \begin{pmatrix} \Psi_1 & 0 & 0 & \Psi_2 & 0 & 0 \\ 0 & I & 0 & 0 & 0 & 0 \\ 0 & 0 & I & 0 & 0 & 0 \\ 0 & 0 & 0 & 0 & I & 0 \\ 0 & 0 & 0 & 0 & 0 & I \end{pmatrix}.$$

It is well known from [16] that robust stability and performance of the system interconnection of Fig. 10.2 can now be characterized as follows.

Theorem 10.1. *Suppose that (10.4) is well-posed and that Δ_d satisfies (10.9) for all $\Delta_d \in \mathbf{\Delta}_d$. Then, for all $\Delta \in \mathbf{\Delta}$ the system interconnection of Fig. 10.2 is well-posed, robustly stable and has a robust \mathcal{L}_2 -gain performance level of γ , if there exists $P_1 \in \mathbf{P}_1$ and $P_{2e} \in \mathbf{P}_{2e}$ for which the following FDI holds:*

$$(\star)^* \underbrace{(\star)^* \begin{pmatrix} P_1 & 0 & 0 \\ 0 & I & 0 \\ 0 & 0 & -\gamma^2 I \end{pmatrix}}_{P_p} \begin{pmatrix} \Phi(i\omega) & 0 & 0 \\ 0 & I & 0 \\ 0 & 0 & I \end{pmatrix} \begin{pmatrix} \mathcal{G}_{\kappa\psi}(i\omega) & \mathcal{G}_{\kappa p}(i\omega) \\ -I & 0 \\ \mathcal{G}_{e\psi}(i\omega) & \mathcal{G}_{ep}(i\omega) \\ 0 & I \end{pmatrix} \prec 0 \quad \forall \omega \in \mathbb{R} \cup \{\infty\}. \quad (10.12)$$

From now on, let us assume that there exists at least one $P_1 \in \mathbf{P}_1$ with

$$\Psi_1(i\omega)^* P_1 \Psi_1(i\omega) \succ 0 \quad \forall \omega \in \mathbb{R} \cup \{\infty\} \quad (10.13)$$

and suppose that Ψ_1 and Ψ_2 , respectively, admit the minimal realizations

$$\Psi_1 = \begin{bmatrix} A_1 & B_1 \\ C_1 & D_1 \end{bmatrix}, \quad \Psi_2 = \begin{bmatrix} A_2 & B_2 \\ C_2 & D_2 \end{bmatrix} \quad (10.14)$$

with A_1 and A_2 being Hurwitz. Then, we can define the controllable realization

$$\Psi = (\Psi_1 \ \Psi_2) = \begin{bmatrix} A_1 & 0 & B_1 & 0 \\ 0 & A_2 & 0 & B_2 \\ C_1 & C_2 & D_1 & D_2 \end{bmatrix} =: \begin{bmatrix} A_\Psi & B_{\Psi_1} & B_{\Psi_2} \\ C_\Psi & D_{\Psi_1} & D_{\Psi_2} \end{bmatrix}, \quad (10.15)$$

where we stress that the specific structure of (10.15) is relevant for the results presented in Sect. 10.3.5. If applying the KYP Lemma, the FDIs (10.12) and (10.13) are equivalent to the existence of some symmetric matrices \mathcal{X} and X_Ψ for which the following LMIs hold:

Example 10.1 (Dynamic D/G-scalings). Consider the block diagonally repeated LTI parametric uncertainty $z_d = \Delta_{DG}w_d$ defined as $z_d(t) := \delta w_d(t)$ with $\delta \in [-1, 1]$. Then, (10.9) holds with

$$\Psi(i\omega)^* P_1 \Psi(i\omega) = \begin{pmatrix} \psi(i\omega) & 0 \\ 0 & \psi(i\omega) \end{pmatrix}^* \begin{pmatrix} D & G \\ G^* & -D \end{pmatrix} \begin{pmatrix} \psi(i\omega) & 0 \\ 0 & \psi(i\omega) \end{pmatrix}, \tag{10.20}$$

for all $\delta \in [-1, 1]$ and Δ_d replaced by Δ_{DG} , if

$$\psi(i\omega)^* D \psi(i\omega) \succ 0, \quad \psi(i\omega)^* G \psi(i\omega) = -\psi(i\omega)^* G^* \psi(i\omega). \tag{10.21}$$

Here, $\psi \in \mathcal{RH}_\infty$ is a basis function which can, for example, be chosen as

$$\psi(i\omega) = I \otimes \left(1 \frac{1}{(i\omega - \alpha)} \cdots \frac{1}{(i\omega - \alpha)^v} \right)^T, \quad \alpha < 0, \quad v \in \mathbb{N}_0 \tag{10.22}$$

with realization

$$\psi = \begin{bmatrix} A_{\psi,v} & B_{\psi,v} \\ C_{\psi,v} & D_{\psi,v} \end{bmatrix}.$$

Example 10.2 (Time-varying parametric uncertainties with bounds on the rate of variation). Consider the block diagonally repeated time-varying parametric uncertainty $z_d = \Delta_{TV}w_d$ defined as $z_d(t) := \delta(t)w_d(t)$ with $(\delta(t), \dot{\delta}(t)) \in \mathbf{R} := [-\bar{\delta}, \bar{\delta}] \times [-\bar{v}, \bar{v}]$. Then (10.9) is satisfied with Δ_d replaced by Δ_{TV} and for all $(\delta(t), \dot{\delta}(t)) \in \mathbf{R}$, if choosing

$$\Psi(i\omega)^* P_1 \Psi(i\omega) = \begin{pmatrix} \psi_1(i\omega) & 0 \\ 0 & \psi_2(i\omega) \end{pmatrix}^* P_1 \begin{pmatrix} \psi_1(i\omega) & 0 \\ 0 & \psi_2(i\omega) \end{pmatrix} \tag{10.23}$$

and P_1 with

$$\begin{pmatrix} I & 0 \\ 0 & I \\ \delta I & 0 \\ 0 & vI \end{pmatrix}^T P_1 \begin{pmatrix} I & 0 \\ 0 & I \\ \delta I & 0 \\ 0 & vI \end{pmatrix} \succ 0 \quad \forall (\delta, v) \in \mathbf{R}. \tag{10.24}$$

Here, respectively, ψ_1 and ψ_2 admit the realizations

$$\psi_1 = \begin{bmatrix} A_{\psi,v} & B_{\psi,v} \\ C_{\psi,v} & D_{\psi,v} \\ I & 0 \end{bmatrix}, \quad \psi_2 = \begin{bmatrix} A_{\psi,v} & B_{\psi,v} & I \\ C_{\psi,v} & D_{\psi,v} & 0 \\ 0 & 0 & I \end{bmatrix}.$$

If $\bar{v} = \infty$ one has to choose $v = 0$, while for finite rate bounds $\bar{v} \geq 0$ one can take $v \geq 0$. Also note that (10.24) is a semi-infinite LMI constraint and should be relaxed into a finite number of LMIs through some relaxation scheme. In our numerical

examples, we use full-block multipliers in combination with a polytopic relaxation (see Example 10.3). We refer the reader to [14] for further details.

It should be emphasized that the length of the basis function (10.22) plays an important role in the analysis problem described in Theorem 10.2. Choosing $v=0$ corresponds to non-dynamic multipliers, which might yield overly conservative results or even lead to infeasibility of the analysis problem. On the other hand, by increasing $v>0$ we allow for (more and more) dynamics and, hence, more freedom in the analysis problem, at the cost of (more and more) computational load. This very often leads to much less conservative results.

Example 10.3 (Static full-block multipliers). Consider the uncertainty $\Delta_s \in \mathbf{\Delta}_s$ as defined in Sect. 10.2. Then, the IQC

$$\left\langle \begin{pmatrix} z_s \\ \Delta_s z_s \end{pmatrix}, P_2 \begin{pmatrix} z_s \\ \Delta_s z_s \end{pmatrix} \right\rangle \geq 0 \quad \forall z_s \in \mathcal{L}_2^{n_{zs}}$$

is satisfied for all $\Delta_s \in \mathbf{\Delta}_s$, if the symmetric matrix P_2 is confined to

$$\mathbf{P}_2 := \left\{ P_2 = \begin{pmatrix} Q & S \\ S^T & R \end{pmatrix} : \begin{pmatrix} I \\ \hat{\Delta}_s(\eta^j) \end{pmatrix}^T P_2 \begin{pmatrix} I \\ \hat{\Delta}_s(\eta^j) \end{pmatrix} \succ 0, R \prec 0 \quad \forall j \in \mathbf{J} \right\}. \quad (10.25)$$

Recall, from Sect. 10.3.1, that (10.10) is satisfied for all $\Delta_{sc} = \text{diag}(\Delta_s, \Delta_c) \in \text{diag}(\mathbf{\Delta}_s, \hat{\Delta}_c(\mathbf{\Delta}_s))$ if $P_{2e} \in \mathbf{P}_{2e}$. As will become clear in the sequel, the results of this chapter rely on the elimination of the realization matrices of E , and, consequently, the elimination of the scheduling function $\hat{\Delta}_c(\Delta_s)$, from the synthesis problem. Therefore, the so-called extended multiplier $P_{2e} \in \mathbf{P}_{2e}$ for analysis results in the reduced multiplier $P_2 \in \mathbf{P}_2$ appearing in the synthesis conditions. For further details, we refer the reader to the proof in Section “Sketch of Proof of Theorem 10.4: Sufficiency” in the Appendix and [17].

10.3.3 From Analysis to Synthesis

Since the system matrices depend on to-be-designed estimator variables, the conditions in (10.19) are no longer affine in all variables, such that LMI solvers are unable to handle the synthesis problem. A common procedure to resolve this problem is to eliminate the estimator variables by applying Lemma 10.5 (see Appendix). However, there are three main issues appearing in the robust gain-scheduling estimator synthesis problem that need to be resolved.

- (A.1) Due to the generality of the multipliers, $\mathcal{X} \succ 0$ is no longer the appropriate condition in order to enforce closed-loop stability [19].
- (A.2) In order to eliminate the estimator variables by applying Lemma 10.5, it is required to formulate a second (dual) solvability condition by applying

Lemma 10.4 (see Appendix). However, the outer factors of the IQC-multiplier factorization $\Psi^* P_1 \Psi$ are generally tall and, hence, cannot be inverted. Since the inverse of $\Psi^* P_1 \Psi$ is essential in order to explicitly formulate the dual of matrix inequality (10.16), the (primal) matrix inequality (10.16) must be reformulated with a square factorization of $\Psi^* P_1 \Psi$ (i.e. $\Psi^* P_1 \Psi = \hat{\Psi}^* \text{diag}(I, -I) \hat{\Psi}$ with $\hat{\Psi}$ being square invertible) [15].

- (A.3) Unlike the standard nominal \mathcal{H}_∞ -controller synthesis problem [6, 11], it is not sufficient to only eliminate the controller/estimator variables. The primal and dual solvability conditions usually induce a nonconvex constraint on the multipliers which are, in general, impossible to convexify.

10.3.4 A Characterization of Nominal Stability

In this section we focus on the first issue, by considering the characterization of nominal stability as presented in [19]. Recall that $P_1 \in \mathbf{P}_1$ is generally indefinite. This implies that positive definiteness of the matrix \mathcal{X} is no longer an appropriate condition in order to enforce stability on the underlying closed-loop system. The following theorem provides a coupling constraint between (10.16) and (10.17), which is equivalent to \mathcal{A} being Hurwitz.

Lemma 10.1. *A_Ψ and \mathcal{A} are Hurwitz and FDIs (10.12) as well as (10.13) hold if and only if there exist solutions \mathcal{X} and X_Ψ of LMIs (10.16) and (10.17) which are coupled as*

$$\mathcal{X} - \begin{pmatrix} X_\Psi & 0 & 0 \\ 0 & 0 & 0 \\ 0 & 0 & 0 \end{pmatrix} = \begin{pmatrix} X_{11} - X_\Psi & X_{12} & U_1 \\ X_{12}^T & X_{22} & U_2 \\ U_1^T & U_2^T & \bar{X} \end{pmatrix} \succ 0. \quad (10.26)$$

Proof. See Appendix. □

It is now possible to exploit Lemma 10.1 in order to state the following result.

Theorem 10.3. *Suppose that (10.4) is well-posed and that Δ_d satisfies (10.9) for all $\Delta_d \in \mathbf{\Delta}_d$. Then there exist a stable and causal estimator $E \star \Delta_c$ such that for all $\Delta \in \mathbf{\Delta}$ the system interconnection of Fig. 10.2 is well-posed, robustly stable and the resulting \mathcal{L}_2 -gain from w_p to z_c is rendered less than γ , if*

$$\text{there exist } \mathcal{X}, X_\Psi, P_1 \in \mathbf{P}_1, P_{2e} \in \mathbf{P}_{2e} \text{ such that (16), (17), (26) hold.} \quad (10.27)$$

10.3.5 Reformulation of the Analysis LMIs of Theorem 10.2

As discussed in Sect. 10.3.3, it is nontrivial to formulate an explicit dual solvability condition, since the outer factors of the multipliers Ψ are generally tall, and, hence, cannot be inverted. In order to resolve this problem we will rely on the results

of [21, 25]. Indeed, one can show, by solving two algebraic Riccati equations, that it is possible to construct a “new” factorization of $\Psi^*P_1\Psi$ that has square and invertible outer factors. Moreover, one can, subsequently, eliminate the initial multiplier factorization $\Psi^*P_1\Psi$ appearing in the FDI (10.12) and replace it by the new one. The key difficulty is how this can be done by using state-space arguments.

Lemma 10.2 (IQC Squaring). *Suppose that (10.19) holds. Then, there exist symmetric matrices Z, W_ε , with $W_\varepsilon \rightarrow 0$ for $\varepsilon \rightarrow 0$ and matrices $\hat{\Psi}_j \in \mathcal{RH}_\infty$, $j = 1, 2, 3$ with $\hat{\Psi}_1^{-*}, \hat{\Psi}_2^{-1} \in \mathcal{RH}_\infty$ such that*

$$\Psi^*P_1\Psi = \begin{pmatrix} \hat{\Psi}_1 & \hat{\Psi}_3 \\ 0 & \hat{\Psi}_2 \end{pmatrix}^* \begin{pmatrix} I & 0 \\ 0 & -I \end{pmatrix} \begin{pmatrix} \hat{\Psi}_1 & \hat{\Psi}_3 \\ 0 & \hat{\Psi}_2 \end{pmatrix} =: \hat{\Psi}^* \hat{P}_1 \hat{\Psi}, \tag{10.28}$$

$\hat{\Psi}$ admits the controllable realization

$$\hat{\Psi} = \begin{pmatrix} \hat{\Psi}_1 & \hat{\Psi}_3 \\ 0 & \hat{\Psi}_2 \end{pmatrix} = \left[\begin{array}{cc|cc} A_1 & 0 & B_1 & 0 \\ 0 & \hat{A}_2 & 0 & \hat{B}_2 \\ \hline \hat{C}_1 & \hat{C}_3 & \hat{D}_1 & \hat{D}_3 \\ 0 & \hat{C}_2 & 0 & \hat{D}_2 \end{array} \right] =: \left[\begin{array}{ccc|ccc} \hat{A}_\Psi & & & \hat{B}_{\Psi_1} & & \hat{B}_{\Psi_2} \\ \hline \hat{C}_{\Psi_1} & & & \hat{D}_{\Psi_1} & & \hat{D}_{\Psi_3} \\ \hat{C}_{\Psi_2} & & & 0 & & \hat{D}_{\Psi_2} \end{array} \right], \tag{10.29}$$

Z satisfies

$$(\star)^T \begin{pmatrix} 0 & | & Z & | & 0 & | & 0 & | & 0 \\ \hline Z & | & 0 & | & 0 & | & 0 & | & 0 \\ 0 & | & 0 & | & I & | & 0 & | & 0 \\ \hline 0 & | & 0 & | & 0 & | & -I & | & 0 \\ \hline 0 & | & 0 & | & 0 & | & 0 & | & -P_1 \end{pmatrix} \begin{pmatrix} I & | & 0 & | & 0 \\ \hline \hat{A}_\Psi & | & \hat{B}_{\Psi_1} & | & \hat{B}_{\Psi_2} \\ \hline \hat{C}_{\Psi_1} & | & \hat{D}_{\Psi_1} & | & \hat{D}_{\Psi_3} \\ \hline \hat{C}_{\Psi_2} & | & 0 & | & \hat{D}_{\Psi_2} \\ \hline C_\Psi(I \ 0) & | & D_{\Psi_1} & | & D_{\Psi_2} \end{pmatrix} = 0 \tag{10.30}$$

and

$$(\star)^T \begin{pmatrix} 0 & | & Z+W_\varepsilon & | & 0 & | & 0 & | & 0 \\ \hline Z+W_\varepsilon & | & 0 & | & 0 & | & 0 & | & 0 \\ 0 & | & 0 & | & I & | & 0 & | & 0 \\ \hline 0 & | & 0 & | & 0 & | & -I & | & 0 \\ \hline 0 & | & 0 & | & 0 & | & 0 & | & -P_1 \end{pmatrix} \begin{pmatrix} I & | & 0 & | & 0 \\ \hline \hat{A}_\Psi & | & \hat{B}_{\Psi_1} & | & \hat{B}_{\Psi_2} \\ \hline \hat{C}_{\Psi_1} & | & \hat{D}_{\Psi_1} & | & \hat{D}_{\Psi_3} \\ \hline \hat{C}_{\Psi_2} & | & 0 & | & \hat{D}_{\Psi_2} \\ \hline C_\Psi(I \ 0) & | & D_{\Psi_1} & | & D_{\Psi_2} \end{pmatrix} \prec 0 \tag{10.31}$$

holds for all small $\varepsilon > 0$.

Proof. The proof is found in [25]. □

It is obvious that the initial “old” multiplier factorization $\Psi^*P_1\Psi$ appearing in the FDI (10.12) can now simply be replaced with the “new” factorization $\hat{\Psi}^*\hat{P}_1\hat{\Psi}$ as in (10.28). However, it has only recently been shown in [21] how this can be done in state-space, by systematically merging (10.16) and (10.31).

Lemma 10.3 (LMI Gluing). *Suppose that (10.19) holds and that Z and W_ε satisfy (10.31) for all small $\varepsilon > 0$. Then, (10.31) and (10.16) imply*

$$(\star)^T \mathcal{M}(\hat{\mathcal{X}}, T_3) \prec 0, \tag{10.32}$$

where

$$\hat{\mathcal{X}} = \begin{pmatrix} \tilde{X} & \tilde{U} \\ \tilde{U}^T & \tilde{X} \end{pmatrix} = \begin{pmatrix} T^T X_{11} T + Z + W_\varepsilon & T^T X_{12} & T^T U_1 \\ X_{12}^T T & X_{22} & U_2 \\ U_1^T T & U_2^T & \tilde{X} \end{pmatrix}, \tag{10.33}$$

$T = \text{diag}(I, (0 I))$ and $T_3 = \text{diag}(\hat{P}_1, P_{2e}, I, -\gamma^2 I)$.

Since the outer factors of the multipliers are now square and invertible, it is possible to eliminate \hat{C}_{Ψ_2} and \hat{D}_{Ψ_2} by transforming (10.32) by congruence into

$$(\star)^T (32) \prec 0. \tag{10.34}$$

This yields

$$(\star)^T \mathcal{M}(\hat{\mathcal{X}}, T_3) \prec 0, \tag{10.35}$$

where

$$\left[\begin{array}{c|ccc|c} \hat{A} & \hat{B}_d & \hat{B}_s & \hat{B}_c & \hat{B}_p \\ \hat{C}_d & \hat{D}_d & \hat{D}_{ds} & 0 & \hat{D}_{dp} \\ \hat{C}_s & \hat{D}_{sd} & \mathcal{D}_{ss} & 0 & \mathcal{D}_{sp} \\ \hat{C}_c & \hat{D}_{cd} & \mathcal{D}_{cs} & \mathcal{D}_{cc} & \mathcal{D}_{cp} \\ \hat{C}_e & \hat{D}_{ed} & \mathcal{D}_{es} & \mathcal{D}_{ec} & \mathcal{D}_{ep} \end{array} \right] := \left[\begin{array}{c|ccc|ccc} \hat{A}_{\Psi_1} - \hat{L}_1 \hat{D}_{\Psi_2}^{-1} \hat{C}_{\Psi_2} & \hat{B}_{\Psi_1} \mathcal{C}_d & \hat{L}_1 \hat{D}_{\Psi_2}^{-1} \hat{B}_{\Psi_1} \mathcal{D}_{ds} & 0 & \hat{B}_{\Psi_1} \mathcal{D}_{dp} \\ -\mathcal{B}_d \hat{D}_{\Psi_2}^{-1} \hat{C}_{\Psi_2} & \mathcal{A} & \mathcal{B}_d \hat{D}_{\Psi_2}^{-1} \mathcal{B}_s & \mathcal{B}_c & \mathcal{B}_p \\ \hat{C}_{\Psi_1} - \hat{L}_2 \hat{D}_{\Psi_2}^{-1} \hat{C}_{\Psi_2} & \hat{D}_{\Psi_1} \mathcal{C}_d & \hat{L}_2 \hat{D}_{\Psi_2}^{-1} \hat{D}_{\Psi_1} \mathcal{D}_{ds} & 0 & \hat{D}_{\Psi_1} \mathcal{D}_{dp} \\ -\mathcal{D}_{sd} \hat{D}_{\Psi_2}^{-1} \hat{C}_{\Psi_2} & \mathcal{C}_s & \mathcal{D}_{sd} \hat{D}_{\Psi_2}^{-1} \mathcal{D}_{ss} & 0 & \mathcal{D}_{sp} \\ -\mathcal{D}_{cd} \hat{D}_{\Psi_2}^{-1} \hat{C}_{\Psi_2} & \mathcal{C}_c & \mathcal{D}_{cd} \hat{D}_{\Psi_2}^{-1} \mathcal{D}_{cs} & \mathcal{D}_{cc} & \mathcal{D}_{cp} \\ -\mathcal{D}_{ed} \hat{D}_{\Psi_2}^{-1} \hat{C}_{\Psi_2} & \mathcal{C}_e & \mathcal{D}_{ed} \hat{D}_{\Psi_2}^{-1} \mathcal{D}_{es} & \mathcal{D}_{ec} & \mathcal{D}_{ep} \end{array} \right], \quad (10.36)$$

$\hat{L}_1 = \hat{B}_{\Psi_1} \mathcal{D}_{dd} + \hat{B}_{\Psi_2}$ and $\hat{L}_2 = \hat{D}_{\Psi_1} \mathcal{D}_{dd} + \hat{D}_{\Psi_3}$. It is now crucial to observe that we have appropriately reformulated (10.16) in order to apply Lemma 10.4:

$$(\star)^T \mathcal{M}(\hat{\mathcal{X}}, T_3)^{-1} \begin{pmatrix} -\hat{\mathcal{A}}_1^T & -\hat{\mathcal{C}}_d^T & -\hat{\mathcal{C}}_s^T & -\hat{\mathcal{C}}_c^T & -\hat{\mathcal{C}}_e^T \\ I & 0 & 0 & 0 & 0 \\ 0 & I & 0 & 0 & 0 \\ -\hat{\mathcal{B}}_d^T & -\hat{\mathcal{D}}_{dd}^T & -\hat{\mathcal{D}}_{sd}^T & -\hat{\mathcal{D}}_{cd}^T & -\hat{\mathcal{D}}_{ed}^T \\ 0 & 0 & I & 0 & 0 \\ 0 & 0 & 0 & I & 0 \\ -\hat{\mathcal{B}}_s^T & -\hat{\mathcal{D}}_{ds}^T & -\mathcal{D}_{ss}^T & -\mathcal{D}_{cs}^T & -\mathcal{D}_{es}^T \\ -\hat{\mathcal{B}}_c^T & 0 & 0 & -\mathcal{D}_{cc}^T & -\mathcal{D}_{ec}^T \\ 0 & 0 & 0 & 0 & I \\ -\hat{\mathcal{B}}_p^T & -\hat{\mathcal{D}}_{dp}^T & -\mathcal{D}_{sp}^T & -\mathcal{D}_{cp}^T & -\mathcal{D}_{ep}^T \end{pmatrix} \succ 0. \quad (10.37)$$

Since (10.35) can be written in the form of (10.44) in the unknown realization matrices of E , we can apply Lemma 10.5. Hence, this resolves the second issue discussed in Sect. 10.3.3.

Remark 10.1. Based on the previous reformulation it is also easily seen that (10.35) implies $\hat{\mathcal{X}} \hat{A} + \hat{A}^T \hat{\mathcal{X}} \prec 0$. Since \hat{A}_{Ψ} is Hurwitz, we conclude that positive definiteness of $\hat{\mathcal{X}}$ is equivalent to \mathcal{A} being Hurwitz. We can thus infer that (10.27) holds if and only if there exists a positive definite matrix $\hat{\mathcal{X}}$ that satisfies (10.35). Moreover, if (10.35) is feasible with $\hat{\mathcal{X}} \succ 0$, the closed-loop system (10.36) is stable.

10.4 Main Result

Before we state the main result, let us define the symmetric matrices

$$P_2 := \begin{pmatrix} Q & S \\ S^T & R \end{pmatrix}, \quad \tilde{P}_2 := \begin{pmatrix} \tilde{Q} & \tilde{S} \\ \tilde{S}^T & \tilde{R} \end{pmatrix},$$

where P_2 and \tilde{P}_2 take their values from the set \mathbf{P}_2 , as well as the matrices

$$T_1 := \text{diag}(P_1, P_2, I, -\gamma^2 I), \quad T_2 := \text{diag}(P_1, \tilde{P}_2, 0, -\gamma^2 I).$$

Let us also define the arbitrary basis matrix Γ of the kernel of $(0 \ C_y \ D_{yd} \ D_{ys} \ D_{yp})$. Then we have introduced all the necessary ingredients in order to provide a finite-dimensional convex feasibility test for the existence of robust gain-scheduled estimators that guarantee a given \mathcal{L}_2 -gain for the system interconnection of Fig. 10.1.

Theorem 10.4. *Statement (10.27) is valid if and only if there exist matrices $X, Y, X_\Psi, P_1 \in \mathbf{P}_1, P_2, \tilde{P}_2 \in \mathbf{P}_2$ for which the following LMIs hold:*

$$\Gamma^T \mathcal{O}^T \mathcal{M}(X, T_1) \mathcal{O} \Gamma \prec 0, \tag{10.38}$$

$$\mathcal{O}^T \mathcal{M}(Y, T_2) \mathcal{O} \prec 0, \tag{10.39}$$

$$\mathcal{O} = \begin{pmatrix} \begin{array}{c|ccc} I & & & 0 \\ \hline A_\Psi & B_{\Psi_1} C_d & B_{\Psi_1} D_{dd} + B_{\Psi_2} & B_{\Psi_1} D_{ds} & B_{\Psi_1} D_{dp} \\ \hline 0 & A & B_d & B_s & B_p \\ \hline C_\Psi & D_{\Psi_1} C_d & D_{\Psi_1} D_{dd} + D_{\Psi_2} & D_{\Psi_1} D_{ds} & D_{\Psi_1} D_{dp} \\ \hline 0 & C_s & D_{sd} & D_{ss} & D_{sp} \\ \hline 0 & 0 & 0 & I & 0 \\ \hline 0 & C_p & D_{pd} & D_{ps} & D_{pp} \\ \hline 0 & 0 & 0 & 0 & I \end{array} \end{pmatrix},$$

$$\begin{pmatrix} A_\Psi^T X_\Psi + X_\Psi A_\Psi + C_\Psi^T P_1 C_\Psi & X_\Psi B_1 + C_\Psi^T P_1 D_{\Psi_1} \\ B_{\Psi_1}^T X_\Psi + D_{\Psi_1}^T P_1 C_\Psi & D_{\Psi_1}^T P_1 D_{\Psi_1} \end{pmatrix} \succ 0, \tag{10.40}$$

$$Y - \begin{pmatrix} X_\Psi & 0 \\ 0 & 0 \end{pmatrix} \succ 0, \quad X - Y \succ 0. \tag{10.41}$$

Here, the matrix $Y = Y^T$ has a block structure identical to that of X .

Once the LMIs (10.38)–(10.41) in the variables $X, Y, X_\Psi, P_1, P_2, \tilde{P}_2$, and γ^2 are feasible, the estimator E and the scheduling function $\hat{\Delta}_c(\Delta_s)$ can be constructed according to the steps taken in the proof which is found in the Appendix.

In summary, we have merged the problem of designing robust LTI estimators using general dynamic IQC multiplier [19] with the problem of designing nominal gain-scheduled estimators using full-block multipliers [17], yielding a convex feasibility test for the existence of robust gain-scheduled estimators. We have resolved the difficulties of enforcing closed-loop stability, eliminating the realization matrices of E and removing the remaining nonconvex constraints as raised in Sect. 10.3.3. It is one of the main differences between the existing results on gain-scheduled controller synthesis and Theorem 10.4 that both P_2 and \tilde{P}_2 can be identified as “primal” multipliers. As a natural consequence, it is interesting to observe that one recovers a special case of the robust estimation problem of [19] by

setting $P_2 = \tilde{P}_2$. Finally, as discussed in Sect. 10.1, we stress that the McMillan degree of the estimator can be set to zero by enforcing $X = Y$ and ignoring the inequality $X - Y \succ 0$.

Although it is very nice to see that the robust estimation problem of [19] can be generalized to gain-scheduling based on static (non-dynamic) full-block multipliers, it remains an open question how to solve the more general case of gain-scheduling based on general dynamic multipliers. First, results in that direction have shown that it is possible to solve the nominal gain-scheduling controller synthesis problem based on dynamic D -scalings [20]. However, it remains a conjecture that the two approaches can be merged. We further remark that it is straightforward to derive a convex feasibility test for the synthesis of robust gain-scheduled feedforward controllers by working with the dual of FDI (10.12) [15]. In fact, it has been recently shown in [18] that the robust estimator and feedforward controller synthesis problems can be unified into the following considerably more general robust controller synthesis problem

$$\begin{pmatrix} z_p \\ y \end{pmatrix} = \begin{pmatrix} \mathcal{P}_{11}(\Delta_{d1}, \Delta_{d2}) & \mathcal{P}_{12}(\Delta_{d2}) \\ \mathcal{P}_{21}(\Delta_{d1}) & \mathcal{P}_{22} \end{pmatrix} \begin{pmatrix} w_p \\ u \end{pmatrix}, \tag{10.42}$$

where only the control channel is not affected by uncertainties. It would be interesting to see how this problem can be generalized to gain-scheduling as well.

10.5 Numerical Example

In order to illustrate our results, let us consider the uncertain LPV system

$$\begin{pmatrix} \dot{x}(t) \\ z_e(t) \\ y(t) \end{pmatrix} = \begin{pmatrix} 0 & -1 + 0.95\delta_d & -2 & 0 \\ 1 & -0.5 + 0.25\eta(t) & 1 & 0 \\ 1 & \eta(t) & 0 & 0 \\ 1 & 0 & 0 & 0.01 \end{pmatrix} \begin{pmatrix} x(t) \\ w_p(t) \end{pmatrix}, \tag{10.43}$$

where $x(t)$ is the state, $\eta(t) = \sin \frac{1}{10}t$ an online measurable scheduling variable, $\delta_d \in [-1, 1]$ a time-invariant parametric uncertainty and $w_p = \text{col}(w_{p1}, w_{p2})$. Then, the operators $\Delta_s, \Delta_d : \mathcal{L}_2 \rightarrow \mathcal{L}_2$ are defined by $w_s(t) = (\Delta_s z_s)(t) = \eta(t)z_d(t)$ and $w_d(t) = (\Delta_d z_d)(t) = \delta_d z_s(t)$, respectively.

In complete analogy to Sect. 10.2, the goal is to design a robust gain-scheduled estimator that dynamically processes the measurement y and the scheduling signal η in order to provide an estimate u of the signal z_p while the \mathcal{L}_2 -gain from w_p to $z_e = z_p - u$ is rendered less than γ . For reasons of comparison, we have designed four estimators:

- (A.1) A nominal LTI estimator E_{nom} , which renders the \mathcal{L}_2 -gain from w_p to z_e less than $\gamma = 0.015$ if δ_d and η are assumed to be zero. Here, we applied standard \mathcal{H}_∞ -synthesis techniques such as in [6, 11].

- (A.2) A robust LTI estimator E_{rob} , which renders the \mathcal{L}_2 -gain from w_p to z_e less than $\gamma=29.19$ for all $\delta_d \in [-1, 1]$, $\eta(t) \in [-1, 1]$ and $\dot{\eta}(t) \in \frac{1}{10}[-1, 1]$. Here, we applied the synthesis results of [19], in combination with multipliers of the form presented in Example 10.2 with basis length $\nu = 2$ and pole location $\alpha = -1$. This allowed us to bound the rate-of-variation of the scheduling variable. Without bounding the rate-of-variation of the scheduling variable (i.e., set $\nu = 0$), the synthesis LMIs are not feasible. Note that Δ_c is nonexistent in this design.
- (A.3) A nominal gain-scheduled estimator $E_{\text{nomgs}}(\Delta_s)$, which renders the \mathcal{L}_2 -gain from w_p to z_e less than $\gamma=0.026$ for all $\eta(t) \in [-1, 1]$ and if δ_d is assumed to be zero. Here, we considered the synthesis results of [17] based on nondynamic full-block multipliers. We remark that gain-scheduling synthesis based on general dynamic multipliers is still an open problem. Bounding the rate-of-variation, like we did for the robust estimator E_{rob} design, is, hence, not yet possible in this framework.
- (A.4) A robust gain-scheduled estimator $E_{\text{robgs}}(\Delta_s)$ which renders the \mathcal{L}_2 -gain from w_p to z_e less than $\gamma=3.67$ for all $\delta_d \in [-1, 1]$ and $\eta(t) \in [-1, 1]$. Here, we considered the main results of this chapter, in combination with dynamic multipliers of the form discussed in Example 10.1, with basis length $\nu = 2$ and pole location $\alpha = -1$ for the LTI parametric uncertainty δ_d and non-dynamic full-block multipliers for the scheduling variable η . Allowing δ_d to vary arbitrarily fast (i.e., set $\nu = 0$) leads to infeasibility of the synthesis LMIs.

Remark 10.2. It is interesting to remark that considering non-dynamic multipliers in this example leads to infeasibility of the synthesis problem. This very nicely illustrates the limitations of non-dynamic multipliers, since allowing for dynamics in the multipliers leads to feasible solutions as well as a considerable improvement of performance.

Conformably with Fig. 10.1, let us now define the four closed-loop plants $z_e := \mathcal{P}_x(\Delta_d, \Delta_s)w_p$, $x \in \mathbf{x}$, where $\mathbf{x} = \{\text{nom}, \text{rob}, \text{nomgs}, \text{robgs}\}$, corresponding to the four designed estimators E_x , and discuss the synthesis results. Figure 10.3 shows the estimation error for $\delta_d = 0$ (left) and $\delta_d = 1$ (right) for a random wave disturbance input w_{p1} (i.e., a sinusoid with a random uniformly distributed frequency) and a random uniformly distributed noise input w_{p2} with an amplitude of 1 and 0.0001, respectively.

It is very satisfactory to see that the gain-scheduled estimators E_{nomgs} and E_{robgs} outperform the LTI estimators E_{nom} and E_{rob} and that the LTI estimator E_{rob} outperforms the LTI estimator E_{nom} (in the sense that the estimation error is rendered small). This reveals that gain-scheduled estimation can be preferable over robust estimation in practice. Nevertheless, if we simulate the system with $\delta_d = 1$, the estimators E_{nom} , E_{rob} and E_{nomgs} show a drastic performance degradation. However, it is again very nice to see that the robust gain-scheduled estimator E_{robgs} keeps the estimation error small, despite the uncertainty in the system.

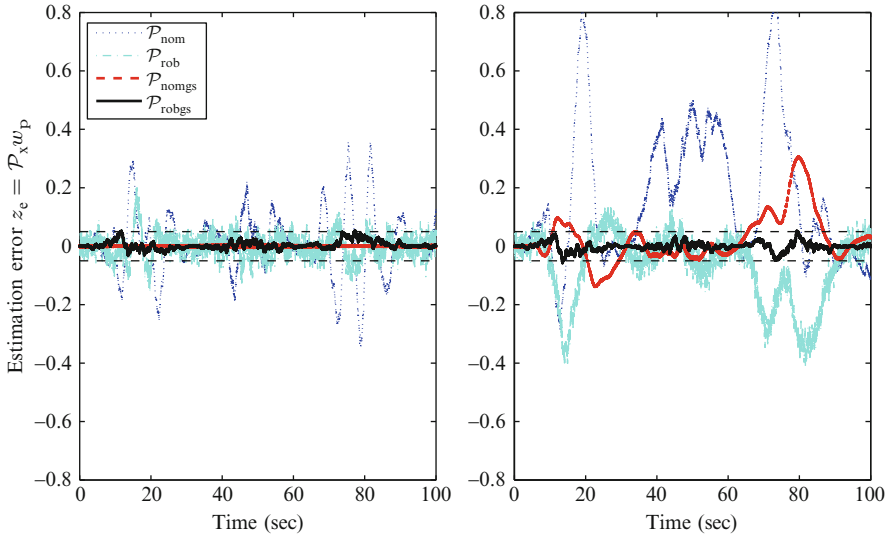


Fig. 10.3 *Left:* estimation error for $\delta_d = 0$. *Right:* estimation error for $\delta_d = 1$

The results are also consistent with the singular value plots from the disturbance input w_p to the estimation error output z_e in Fig. 10.4, if fixing the parameter η to various points in $[-1, 1]$. Indeed, if we compare, for example, Fig. 10.4.1.3 with Fig. 10.4.2.3, it can be seen that the nominal gain-scheduled estimator E_{nomgs} is very sensitive to deviating values of the uncertainty δ_d from zero. Moreover, clearly, this is also the case if we consider the nominal and robust LTI estimator E_{nom} and E_{rob} , respectively, in Fig. 10.4.1.1–Fig. 10.4.2.2, which are sensitive to variations of both η and δ_d . On the other hand, it is very nice to observe that, by comparing Fig. 10.4.1.4 with Fig. 10.4.2.4, this is not the case for the robust gain-scheduled estimator E_{robgs} , which is insensitive to deviating values of the uncertainty δ_s from zero.

10.6 Concluding Remarks

We have considered the robust estimation problem for uncertain LFT systems using the IQC framework. Assuming that some parametric uncertainties are measured online, we have obtained sufficient conditions for the existence of robust estimators that are scheduled on the measured parametric variations. The multipliers for the nonmeasured uncertainties are not restricted by any structural requirements or frequency independence constraints. For the measured parameters, we have used the least conservative class of multipliers in the literature, namely static full-block multipliers. A detailed investigation of the proposed technique on a numerical example demonstrates the advantages of gain-scheduling in the problem of robust estimation for uncertain systems.

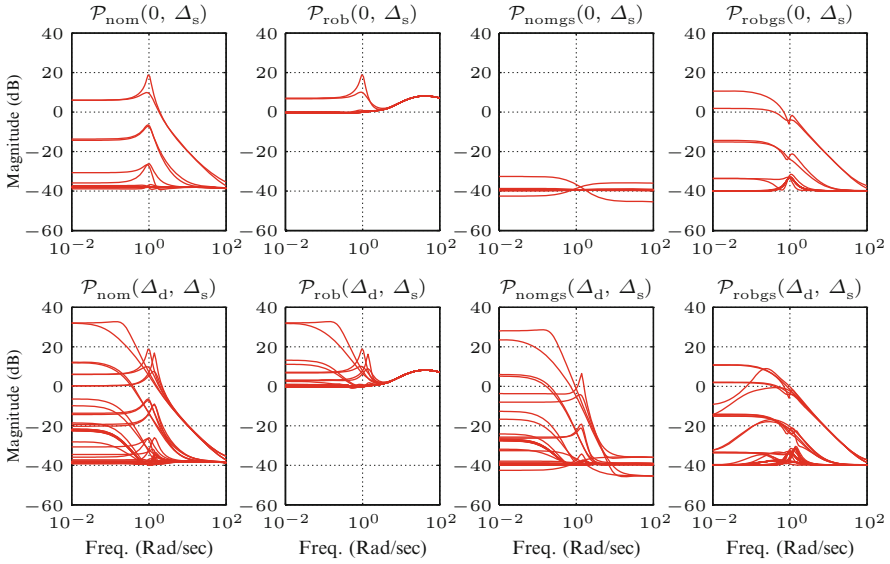


Fig. 10.4 Upper row: Singular value plots of $\mathcal{P}_x(\Delta_d, \Delta_s)$ evaluated at $\Delta_d=0$ and different values of $\Delta_s \in [-1, 1]$. Bottom row: Singular value plots of $\mathcal{P}_x(\Delta_d, \Delta_s)$ evaluated at different values of $\Delta_d \in [-1, 1]$ and $\Delta_s \in [-1, 1]$

Acknowledgments The authors would like to thank the German Research Foundation (DFG) for financial support of the project within the Cluster of Excellence in Simulation Technology (EXC 310/1) at the University of Stuttgart.

Appendix: Dualization and Elimination

Lemma 10.4 ([17]). Let $A \in \mathbb{R}^{(m+n) \times m}$ have full column rank and $X = X^T \in \mathbb{R}^{(m+n) \times (m+n)}$ be nonsingular such that X has m and n negative and positive eigenvalues, respectively. Then $A^T X A \prec 0$ if and only if $A_\perp^T X^{-1} A_\perp \succ 0$, where A_\perp forms a basis for the orthogonal complement of the image of A .

Lemma 10.5 ([17]). Let $C \in \mathbb{R}^{n \times m}$ and $P = P^T \in \mathbb{R}^{(m+n) \times (m+n)}$ has m negative and n positive eigenvalues and consider the matrix inequality

$$\begin{pmatrix} I \\ A^T X B + C \end{pmatrix}^T P \begin{pmatrix} I \\ A^T X B + C \end{pmatrix} \prec 0 \tag{10.44}$$

in the unstructured unknown X . Then, there exists an X for which (10.44) is satisfied, if and only if

$$B_{\perp}^{\top} \begin{pmatrix} I \\ C \end{pmatrix}^{\top} P \begin{pmatrix} I \\ C \end{pmatrix} B_{\perp} \prec 0 \quad \text{and} \quad A_{\perp}^{\top} \begin{pmatrix} -C^{\top} \\ I \end{pmatrix}^{\top} P^{-1} \begin{pmatrix} -C^{\top} \\ I \end{pmatrix} A_{\perp} \succ 0. \quad (10.45)$$

Here, A_{\perp} and B_{\perp} denote arbitrary basis matrices of the kernel of A and B , respectively.

Proof of Lemma 10.1

Observe that (10.16) implies

$$\begin{pmatrix} I & 0 \\ 0 & I \\ \hline A_{\Psi} & B_{\Psi_1} C_d \\ 0 & \mathcal{A} \\ \hline C_{\Psi} & D_{\Psi_1} C_d \end{pmatrix}^{\top} \mathcal{M}(\mathcal{X}, P_1) \begin{pmatrix} I & 0 \\ 0 & I \\ \hline A_{\Psi} & B_{\Psi_1} C_d \\ 0 & \mathcal{A} \\ \hline C_{\Psi} & D_{\Psi_1} C_d \end{pmatrix} \prec 0 \quad (10.46)$$

and that (10.17) can be inflated to

$$\begin{pmatrix} I & 0 \\ 0 & I \\ \hline A_{\Psi} & B_{\Psi_1} C_d \\ 0 & \mathcal{A} \\ \hline C_{\Psi} & D_{\Psi_1} C_d \end{pmatrix}^{\top} \mathcal{M}(\text{diag}(X_{\Psi}, 0, 0), -P_1) \begin{pmatrix} I & 0 \\ 0 & I \\ \hline A_{\Psi} & B_{\Psi_1} C_d \\ 0 & \mathcal{A} \\ \hline C_{\Psi} & D_{\Psi_1} C_d \end{pmatrix} \preceq 0. \quad (10.47)$$

Adding up the two inequalities then yields

$$\begin{pmatrix} I & 0 \\ 0 & I \\ \hline A_{\Psi} & B_{\Psi_1} C_d \\ 0 & \mathcal{A} \\ \hline C_{\Psi} & D_{\Psi_1} C_d \end{pmatrix}^{\top} \mathcal{M}(\mathcal{X} - \text{diag}(X_{\Psi}, 0, 0), 0) \begin{pmatrix} I & 0 \\ 0 & I \\ \hline A_{\Psi} & B_{\Psi_1} C_d \\ 0 & \mathcal{A} \\ \hline C_{\Psi} & D_{\Psi_1} C_d \end{pmatrix} \prec 0, \quad (10.48)$$

which implies

$$\begin{pmatrix} A_{\Psi} & B_{\Psi_1} C_d \\ 0 & \mathcal{A} \end{pmatrix}^{\top} \left(X - \begin{pmatrix} X_{\Psi} & 0 \\ 0 & 0 \end{pmatrix} \right) + \left(X - \begin{pmatrix} X_{\Psi} & 0 \\ 0 & 0 \end{pmatrix} \right) \begin{pmatrix} A_{\Psi} & B_{\Psi_1} C_d \\ 0 & \mathcal{A} \end{pmatrix} \prec 0. \quad (10.49)$$

Positive definiteness of (10.26) is, hence, equivalent to A_{Ψ} and \mathcal{A} being Hurwitz.

Sketch of Proof of Theorem 10.4: Necessity

Let us assume that statement (10.27) is true. Then, there exist matrices \mathcal{X} , X_Ψ , $P_1 \in \mathbf{P}_1$, $P_{2e} \in \mathbf{P}_{2e}$ for which (10.16) and (10.17) as well as (10.26) are feasible. We follow the well-known procedure of eliminating the estimator variables by working with primal and dual matrix inequalities and applying Lemma 10.5 (see, e.g., [17]). However, since Ψ is a tall transfer matrix and, hence, cannot be inverted (e.g., recall (10.22)) it is unknown how to directly apply Lemma 10.4. To overcome this trouble, we reformulate (10.16) as suggested in Sect. 10.3.5 by applying Lemma 10.2 and 10.3. This yields (10.32). Now, observe that (10.32) can be written in the form of (10.44) in the unstructured realization matrices of E . We can, hence, apply Lemma 10.5. Therefore, let us, respectively, choose the basis matrices Γ_e and Γ of the kernels of

$$\begin{pmatrix} 0 & 0 & I & 0 & 0 & 0 & 0 \\ 0 & C_y & 0 & D_{yd} & D_{ys} & 0 & D_{yp} \\ 0 & 0 & 0 & 0 & 0 & I & 0 \end{pmatrix} \quad \text{and} \quad \begin{pmatrix} 0 & C_y & D_{yd} & D_{ys} & D_{yp} \end{pmatrix}. \tag{10.50}$$

It is then easy to verify that, by left-multiplying and right-multiplying (10.32) with Γ_e^T and Γ_e , respectively, we obtain

$$(\star)^T \mathcal{M}(\tilde{X}, T_4) \begin{pmatrix} I & & & & & & 0 \\ \hat{A}_\Psi & \hat{B}_\Psi C_d & \hat{B}_\Psi D_{dd} + \hat{B}_\Psi D_{ds} & \hat{B}_\Psi D_{dp} & & & \\ 0 & A & B_d & B_s & B_p & & \\ \hat{C}_\Psi & \hat{D}_\Psi C_d & \hat{D}_\Psi D_{dd} + \hat{D}_\Psi D_{ds} & \hat{D}_\Psi D_{dp} & & & \\ \hat{C}_\Psi & 0 & \hat{D}_\Psi & 0 & 0 & & \\ 0 & C_s & D_{sd} & D_{ss} & D_{sp} & & \\ 0 & 0 & 0 & I & 0 & & \\ 0 & C_p & D_{pd} & D_{ps} & D_{pp} & & \\ 0 & 0 & 0 & 0 & 0 & I & \end{pmatrix} \Gamma \prec 0, \tag{10.51}$$

where $T_4 = \text{diag}(\hat{P}_1, P_2, I, -\gamma^2 I)$ and where we recall that \tilde{X} is the left-upper block of $\hat{\mathcal{X}}$ in (10.33). It is now possible to apply the steps described in Sect. 10.3.5 in the reverse direction. Hence, we infer, by Lemma 10.2 and 10.3, that (10.51) implies (10.38).

Before we continue with the formulation of the dual solvability condition, let us discuss the following observation first: Since $\hat{\mathcal{X}} \succ 0$, it obviously holds that

$$\hat{\mathcal{X}}^{-1} = \begin{pmatrix} (\tilde{X} - \tilde{U} \tilde{X}^{-1} \tilde{U}^T)^{-1} & \star \\ \star & \star \end{pmatrix} =: \begin{pmatrix} \tilde{Y}^{-1} & \star \\ \star & \star \end{pmatrix}$$

with \star of being no interest. Now, let us define the new variable

$$Y = \begin{pmatrix} Y_{11} & Y_{12} \\ Y_{12}^T & Y_{22} \end{pmatrix} := \begin{pmatrix} X_{11} & X_{12} \\ X_{12}^T & X_{22} \end{pmatrix} - \begin{pmatrix} U_1 \\ U_2 \end{pmatrix} \tilde{X}^{-1} (U_1^T \ U_2^T)$$

and observe that

$$\tilde{Y} = \tilde{X} - \tilde{U}\tilde{X}^{-1}\tilde{U}^T = \begin{pmatrix} T^T Y_{11} T + Z + W_\varepsilon & T^T Y_{12} \\ Y_{12}^T T & Y_{22} \end{pmatrix}, \quad (10.52)$$

where, clearly, the structured partitioning of \tilde{X} as in (10.33) is preserved. This is highly relevant in the sequel. Also observe that since $\hat{\mathcal{X}} \succ 0$, we can infer that $\tilde{X} \succ 0$ and $\tilde{X} \succ 0$, which, hence, implies that $\tilde{Y} \succ 0$.

Let us now apply the congruence transformation (10.34) and apply Lemma 10.4. This yields (10.37). It is now possible to define the basis matrix

$$Y = \begin{pmatrix} I & 0 & 0 & 0 \\ 0 & I & 0 & 0 \\ 0 & 0 & 0 & 0 \\ 0 & 0 & I & 0 \\ 0 & 0 & 0 & I \\ 0 & 0 & 0 & 0 \\ 0 & 0 & 0 & 0 \end{pmatrix}$$

of the kernel of

$$\begin{pmatrix} 0 & 0 & I & 0 & 0 & 0 & 0 \\ 0 & 0 & 0 & 0 & 0 & 0 & -I \\ 0 & 0 & 0 & 0 & 0 & I & 0 \end{pmatrix}.$$

Applying Lemma 10.5, by left-multiplying and right-multiplying, the dual inequality of (10.35) with Y^T and Y then yields

$$\hat{\mathcal{O}}_\perp^T \mathcal{M}(\tilde{Y}, T_5)^{-1} \hat{\mathcal{O}}_\perp \succ 0, \quad (10.53)$$

where $\hat{\mathcal{O}}_\perp$ forms a basis for the orthogonal complement of the image of

$$\hat{\mathcal{O}} =: \begin{pmatrix} & & I & & & & 0 \\ \hat{A}_\Psi - \hat{L}_1 \hat{D}_{\Psi_2}^{-1} \hat{C}_{\Psi_2} & \hat{B}_{\Psi_1} C_d & & \hat{L}_1 \hat{D}_{\Psi_2}^{-1} & \hat{B}_{\Psi_1} D_{ds} & \hat{B}_{\Psi_1} D_{ds} & \\ -B_d \hat{D}_{\Psi_2}^{-1} \hat{C}_{\Psi_2} & A & & B_d \hat{D}_{\Psi_2}^{-1} & B_s & B_p & \\ \hat{C}_{\Psi_1} - \hat{L}_2 \hat{D}_{\Psi_2}^{-1} \hat{C}_{\Psi_2} & \hat{D}_{\Psi_1} C_d & & \hat{L}_2 \hat{D}_{\Psi_2}^{-1} & \hat{D}_{\Psi_1} D_{ds} & \hat{D}_{\Psi_1} D_{dp} & \\ 0 & 0 & & I & 0 & 0 & \\ -D_{sd} \hat{D}_{\Psi_2}^{-1} \hat{C}_{\Psi_2} & C_s & & D_{sd} \hat{D}_{\Psi_2}^{-1} & \hat{D}_{\Psi_1} D_{ss} & \hat{D}_{\Psi_1} D_{sp} & \\ 0 & 0 & & 0 & I & 0 & \\ -D_{pd} \hat{D}_{\Psi_2}^{-1} \hat{C}_{\Psi_2} & C_p & & D_{pd} \hat{D}_{\Psi_2}^{-1} & \hat{D}_{\Psi_1} D_{ps} & \hat{D}_{\Psi_1} D_{pp} & \\ 0 & 0 & & 0 & 0 & 0 & I \end{pmatrix}$$

and where $T_5 = \text{diag}(\hat{P}_1, \tilde{P}_2, 0, -\gamma^2 I)$ with

$$\tilde{P}_2 := \begin{pmatrix} \tilde{Q} & \tilde{S} \\ \tilde{S}^T & \tilde{R} \end{pmatrix} = \begin{pmatrix} Q & S \\ S^T & R \end{pmatrix} - \begin{pmatrix} Q_{12}^T & S_{21} \\ S_{12}^T & R_{12}^T \end{pmatrix}^T \begin{pmatrix} Q_{22} & S_{22} \\ S_{22}^T & R_{22} \end{pmatrix}^{-1} \begin{pmatrix} Q_{12}^T & S_{21} \\ S_{12}^T & R_{12}^T \end{pmatrix}.$$

As the key observation that leads to a convex feasibility test for the synthesis of a robust gain-scheduled estimators, observe that (10.53) has the right structure in order to apply Lemma 10.4 again. Indeed, it is easily verified that (10.53) is equivalent to

$$\hat{O}^T \mathcal{M}(\tilde{Y}, T_5) \hat{O} \prec 0. \tag{10.54}$$

Applying the congruence transformation

$$\begin{pmatrix} I & 0 & 0 \\ \hat{C}_2 & 0 & \hat{D}_2 \\ 0 & 0 & I \end{pmatrix}^T \tag{54} \begin{pmatrix} I & 0 & 0 \\ \hat{C}_2 & 0 & \hat{D}_2 \\ 0 & 0 & I \end{pmatrix} \prec 0,$$

now yields

$$(\star)^T \mathcal{M}(\tilde{Y}, T_5) \begin{pmatrix} I & & & & 0 \\ \hat{A}_\Psi & \hat{B}_\Psi C_d & \hat{B}_\Psi D_{dd} + \hat{B}_\Psi D_{ds} & \hat{B}_\Psi D_{dp} \\ 0 & A & B_d & B_s & B_p \\ \hat{C}_\Psi & \hat{D}_\Psi C_d & \hat{D}_\Psi D_{dd} + \hat{D}_\Psi D_{ds} & \hat{D}_\Psi D_{dp} \\ \hat{C}_\Psi & 0 & \hat{D}_\Psi & 0 & 0 \\ 0 & C_s & D_{sd} & D_{ss} & D_{sp} \\ 0 & 0 & 0 & I & 0 \\ 0 & C_p & D_{pd} & D_{ps} & D_{pp} \\ 0 & 0 & 0 & 0 & I \end{pmatrix} \prec 0. \tag{10.55}$$

Finally, it is again possible to apply the steps described in Sect. 10.3.5 in the reverse direction and infer, by Lemma 10.2 and 10.3, that (10.55) implies (10.39).

Now observe that left-multiplying and right-multiplying (10.11) with $\text{col}(I, 0)$ directly yields (10.25). Moreover, if we apply Lemma 10.4 to inequality (10.11) and subsequently left-multiplying and right-multiplying with $\text{col}(I, 0)$, we find

$$\begin{pmatrix} -\hat{\Delta}_s(\eta^j)^T \\ I \end{pmatrix}^T \begin{pmatrix} \tilde{Q} & \tilde{S} \\ \tilde{S}^T & \tilde{R} \end{pmatrix}^{-1} \begin{pmatrix} -\hat{\Delta}_s(\eta^j)^T \\ I \end{pmatrix} \prec 0, \quad j=1, \dots, m.$$

Clearly, by applying Lemma 10.4, we can infer $\tilde{P}_2 \in \mathbf{P}_2$.

The necessity part of the proof is now completed by showing that (10.41) holds true. Let us, hence, recall by Lemma 10.1 that stability of \mathcal{A} implies and is implied by the existence of some solutions of (10.40) for which

$$\begin{pmatrix} X - \begin{pmatrix} X_\Psi & 0 \\ 0 & 0 \end{pmatrix} U \\ U^T & \bar{X} \end{pmatrix} \succ 0,$$

or equivalently

$$(X - U\bar{X}^{-1}U^T) - \begin{pmatrix} X_\Psi & 0 \\ 0 & 0 \end{pmatrix} \succ 0 \quad \text{and} \quad \bar{X} \succ 0.$$

Since $Y = X - U\bar{X}^{-1}U^T$, we can infer that $\bar{X} \succ 0$ (slightly perturb if necessary) implies $X \succ Y$ and thus (10.41).

In summary, we have shown that (10.16) can be reformulated as (10.32), by using the results described in Sect. 10.3.5. This allowed us eliminate the realization matrices of E by applying Lemma 10.5. Two observations then led to the solvability conditions (10.38) and (10.39) in Theorem 10.4: (1) The matrix inequality (10.53) has the right structure in order to apply Lemma 10.4 and (2) the steps described in Sect. 10.3.5 can be applied in the reverse direction. Finally, the stability enforcing positivity conditions in (10.41) come along very naturally by observing that the structure of \tilde{X} is preserved in (10.52).

Sketch of Proof of Theorem 10.4: Sufficiency

Suppose now that all conditions of Theorem 10.4 hold true. Then, there exist matrices $X, Y, X_\Psi, P_1 \in \mathbf{P}_1, P_2, \tilde{P}_2 \in \mathbf{P}_2$ that render (10.38)–(10.41) feasible.

Let us first consider the nonsingular matrices X and $X - Y$ (slightly perturbed if necessary). Then by defining

$$\mathcal{X} = \begin{pmatrix} X & X - Y \\ X - Y & X - Y \end{pmatrix},$$

we can infer (10.41) thanks to the Schur complement.

For the extension of the scalings we recall from the literature [17] that, given the matrices P_2 and \tilde{P}_2 , it is always possible (slightly perturb if necessary) to find a nonsingular matrix N and a simple permutation matrix \hat{N} such that

$$\mathbf{P}_{2e} \ni P_{2e} = \hat{N}^T \begin{pmatrix} P_2 & N \\ N^T & N^T(P_2 - \tilde{P}_2)^{-1}N \end{pmatrix} \hat{N}.$$

This also yields an explicit scheduling function $\hat{\Delta}_c(\Delta_s)$ which depends smoothly on Δ_s and satisfies (10.11).

The realization matrices of E are finally obtained by substituting the constructed matrices \mathcal{X}, P_1 and P_{2e} in (10.16) and solving the resulting LMI which is, after applying the Schur complement, affine in the realization matrix variables of E .

References

1. Barbosa KA, de Souza CE, Trofino A (2005) Robust \mathcal{H}_2 filtering for uncertain linear systems: LMI based methods with parametric Lyapunov function. *Syst Contr Lett* 54:251–262
2. Chen X, Wen JT (1995) Robustness analysis of LTI systems with structured incrementally sector bounded nonlinearities. *Proc ACC* June:3883–3887
3. D’Amato FJ, Rotea MA, Megretski AV, Jönsson UT (2001) New result for analysis of systems with repeated nonlinearities. *Automatica* 37:739–747
4. Dullerud G, Paganini F (2000) A course in robust control theory. Springer Verlag, New York
5. Francis BA (1987) A course in \mathcal{H}_∞ control theory. Springer, Berlin
6. Gahinet P, Apkarian P (1994) A Linear Matrix Inequality approach to \mathcal{H}_∞ control. *Int J Robust Nonlinear Contr* 4:421–448
7. Geromel JC (1999) Optimal linear filtering under parameter uncertainty. *IEEE Trans Signal process* 47:168–175
8. Geromel JC, de Oliveira MC (2001) \mathcal{H}_2 and \mathcal{H}_∞ robust filtering for convex bounded uncertain systems. *IEEE Trans Automat Contr* 46:100–107
9. Geromel JC, de Oliveira MC, Bernussou J (1999) Robust filtering of discrete-time linear systems with parameter-dependent Lyapunov functions. In: *Proceedings of the 38th CDC*, pp 570–575
10. Helmersson A (1999) An IQC-based stability criterion for systems with slowly varying parameters. In: *Proceedings of the 14th IFAC Trien Cong Beijing, China vol 14*, pp 525–530
11. Iwasaki T, Skelton R (1994) All controllers for the general \mathcal{H}_∞ control problem: LMI existence conditions and state space formulas. *Automatica* 30:1307–1317
12. Jun M, Safonov MG (2000) Stability analysis of a system with time-delayed states. *Proc ACC IL*:949–952
13. Kao C, Rantzer A (2007) Stability analysis of systems with uncertain time-varying delays. *Automatica* 43:959–970
14. Koroğlu H, Scherer CW (2006) Robust stability analysis against perturbations of smoothly time-varying parameters. In: *Proceedings of the 45th IEEE CDC*, pp 2895–2900
15. Köse IE, Scherer CW (2009) Robust \mathcal{L}_2 -gain feedforward control of uncertain systems using dynamic IQCs. *Int J Robust Nonlinear Contr* 19:1224–1247
16. Megretski A, Rantzer A (1997) System analysis via integral quadratic constraints. *IEEE Trans Automat Contr* 42:819–830
17. Scherer CW (2001) LPV control and full-block multipliers. *Automatica* 37:361–375
18. Scherer CW (2009) Robust Controller Synthesis is Convex for Systems without Control Channel Uncertainties. In: Van den Hof PMJ, Scherer CW, Heuberger PSC (eds) *Model based control, bridging rigorous theory and advanced technology*, Springer
19. Scherer CW, Köse IE (2008) Robustness with dynamic Integral Quadratic Constraints: An exact state space characterization of nominal stability with applications to robust estimation. *Automatica* 44:1666–1675
20. Scherer CW, Köse IE (2010) Gain -Scheduled Controller Synthesis using Dynamic D-scales. *IEEE Trans Automat Contr* (Accepted for publication)
21. Scherer CW, Köse IE (2011) From Transfer Matrices to Realizations: Convergence Properties and Parameterization of Robustness Analysis Conditions. Preprint
22. Scorletti G, Fromion V (2006) Further results on the design of robust \mathcal{H}_∞ feedforward controllers and filters. In: *Proceedings of the IEEE CDC*, pp 3560–3565
23. Sun K, Packard A (2005) Robust \mathcal{H}_2 and \mathcal{H}_∞ filters for uncertain lft system. *IEEE Trans Automat Contr* 50:715–720
24. Tuan H, Apkarian P, Nguyen TQ (2003) Robust filtering for uncertain nonlinearly parametrized plants. *IEEE Trans Signal Process* 51:1806–1815
25. Veenman J, Scherer CW (2011) IQC-synthesis with general dynamic multipliers. In: *Proceedings of the 18th IFAC World Congress*
26. Zames G, Falb PL (1968) Stability conditions for systems with monotone and slope-restricted nonlinearities. *SIAM J Contr* 6:89–109

Chapter 11

Delay-Dependent Output Feedback Control of Time-Delay LPV Systems

Rohit Zope, Javad Mohammadpour, Karolos Grigoriadis,
and Matthew Franchek

Abstract Presented in this chapter, is a method for the design of output feedback \mathcal{H}_∞ controllers for linear parameter-varying (LPV) time-delay systems. Towards this goal, a delay-dependent bounded real lemma (BRL) condition is first developed by taking advantage of parameter-dependent Lyapunov–Krasovskii functionals. An existence condition for an output feedback controller with delay in its dynamics is then developed to guarantee a prescribed \mathcal{H}_∞ performance level for the closed loop system by relaxing the obtained BRL through the introduction of additional slack variables. The proposed synthesis condition is formulated in terms of linear matrix inequalities (LMIs) that can be solved using existing efficient interior-point algorithms. A numerical example based on a lumped parameter model of a milling process is finally employed to validate the presented design method of this chapter.

11.1 Introduction

Dynamic systems with time delays appear frequently in engineering and biological systems. Time delays may be constant or time varying, point-wise or distributed, deterministic or stochastic. The most obvious example of time delay in a system is introduced by the interconnection of two subsystems that are separated by a significant physical distance resulting in transport or transmission delays between the subsystems. Delays often describe the time to effect coupling or interconnection between dynamics through propagation or transport phenomena in shared environments, or through heredity and competition in population dynamics. Time delays complicate the controller design process as they often induce instability in the feedback control system [14]. The mathematical formulation of a time-delay system

R. Zope • J. Mohammadpour (✉) • K. Grigoriadis • M. Franchek
Department of Mechanical Engineering, University of Houston, Houston, TX, 77204, USA
e-mail: razope@uh.edu; jmohammadpour@uh.edu; karolos@uh.edu; mfranchek@uh.edu

results in a system of functional differential equations (FDEs) which are infinite dimensional, as opposed to ordinary differential equations (ODEs) that describe finite-dimensional systems. Stability analysis and control of time-delay systems is a subject of great practical and theoretical importance and has been studied extensively in the controls literature for decades. For example, refer the monographs [13, 18, 21, 26, 28, 41, 49] and the numerous references therein. Richard in [32] provides a good overview of some recent advances and open problems in time-delay systems.

Stability of time-delay systems can be broadly studied using either frequency domain or time domain methods. The discussion in this chapter is restricted to the use of time domain methods and more specifically to the employment of Lyapunov-based methods. Existing stabilization results for delay systems are concerned with either one of the following two types of stabilization: delay-independent stabilization or delay-dependent stabilization. Delay-independent stabilization is based on conditions that are independent of the size of the delay and has been studied extensively in the literature [4, 8, 9, 15, 16, 19, 24, 31]. It is well known that delay-independent criteria for stabilization lead to conservative results specially for systems with small time delays, as stability is guaranteed for all nonnegative values of time delays. Delay-dependent criteria ensure stabilization and a prescribed level of performance of the system for magnitudes of the delays smaller than a given bound. This knowledge of a bound on the size of the time delay allows for reduced conservatism compared to the delay-independent approach. Development of the delay-dependent stability conditions and control has been investigated in [11, 17, 23, 25, 27, 33, 39, 45, 46] among many others.

Linear parameter-varying (LPV) systems provide a systematic way of computing gain-scheduled controllers for nonlinear and/or time-varying systems when formulated in the LPV framework. Stability analysis and control synthesis problems for LPV systems have been investigated extensively in the literature [1–3, 29, 44]. The above results, however, do not consider systems with delay in their dynamics. LPV systems with time delays often appear in many engineering applications. In fact, in parameter-varying systems often the magnitude of the delay changes as a function of varying parameters in the system. For instance, the transport delay in an internal combustion engine is a known function of the engine speed and mass air flow. Similarly, parameter-varying time delays also appear in many manufacturing processes such as the milling process, where the changes in system dynamics result in variable time delays. Stability analysis and control of such LPV time-delay systems has attracted a lot of attention in the last decade. One of the first work appeared in [43], where the authors analyzed a time-delay LPV system and developed a delay-independent condition, with an additional restriction of keeping the kernel of the integral term parameter independent. State feedback controller synthesis conditions guaranteeing a desired induced \mathcal{L}_2 gain performance were also presented in [43]. The authors in [48] developed stability tests for LPV time-delay systems using both delay-independent and delay-dependent conditions. However, the delays are assumed to be constant (not parameter varying) and no controller synthesis conditions were provided. The authors in [20] provide

the delay-independent and delay-dependent stability analysis results for quadratic stability and affine quadratic stability and further discuss \mathcal{L}_2 gain state feedback control using delay-independent conditions. Improvements over the result of [43] are presented in [37] along with new results discussing the $\mathcal{L}_2 - \mathcal{L}_\infty$ gain control. Output feedback control synthesis has been discussed in [36, 40] again using the delay-independent conditions. Delay-dependent \mathcal{H}_∞ control result for LPV systems with state delays first appeared in [42]. However, the rate information for the delay variation has not been used resulting in conservative results. The authors in [47] examined state feedback \mathcal{H}_∞ control of LPV time-delay systems with a rate bounded time-varying delay. Their approach uses a model transformation introducing additional dynamics in the system. This shortcoming is overcome in the work of [34], where an equivalent descriptor model transformation first introduced in [10], along with Park's inequality [30] for bounding cross terms is used to derive less conservative results. Additional results concerning control and filtering of LPV time-delay systems appear in [6, 7, 22].

Despite a large number of research articles appeared in the past decade on the control of time-delay LPV systems, \mathcal{H}_∞ control of LPV time-delay systems based on output-feedback is still an open problem with more efforts directed towards reducing the design conservatism. It is well known that the choice of an appropriate Lyapunov–Krasovskii functional is crucial for deriving stability conditions. The conservatism of the existing delay-dependent conditions stems from two sources: one is the model transformation used and the other is the inequality bounding techniques usually employed for some cross terms encountered in the analysis and synthesis conditions. The Lyapunov–Krasovskii functional used in this work is borrowed from [5] and modified to allow for the dependence of the time-varying delay on the scheduling parameter. This type of Lyapunov–Krasovskii functionals avoids any model transformation or any bounding of the cross terms. The only conservatism introduced by this method comes from the initial choice of the Lyapunov–Krasovskii functional and the use of the Jensen's inequality [13] employed to bound an integral term in the derivative of Lyapunov–Krasovskii functional. The main advantage of these functionals is their simplicity and the lower number of matrix variables involved in the Lyapunov–Krasovskii functional, thus reducing products between data matrices and decision variables and making them potentially interesting candidates for the stabilization and control design purposes. In this chapter, a bounded real lemma, which is an LMI analysis condition guaranteeing a prescribed level of \mathcal{H}_∞ performance is derived for the time-delay LPV system. Before substituting the closed-loop system state-space matrices and deriving synthesis conditions, the LMI conditions are relaxed using the approach presented in [38], which introduces *slack* variables. The resulting bilinear matrix inequality (BMI) conditions corresponding to the closed-loop system are linearized using a nonlinear transformation leading to the final delayed-feedback output controller synthesis conditions. The structure of the feedback controller is assumed to have a delay term in its dynamics.

The notation used in this chapter is standard. \mathbb{R} stands for the set of real numbers. \mathbb{R}^n and $\mathbb{R}^{k \times m}$ denote the set of real vectors of dimension n and the set of real $k \times m$

matrices, respectively. The transpose of a real matrix M is denoted as M^T and its null space by $\ker(M)$. \mathbb{S}^n denotes real symmetric $n \times n$ matrices and \mathbb{S}_{++}^n is the set of real symmetric positive definite $n \times n$ matrices. The asterisk (*) in the (i, j) element of a symmetric matrix denotes transpose of the (j, i) submatrix. $\mathcal{C}(J, K)$ denotes the set of continuous functions from a set J to a set K .

11.2 Problem Statement and Preliminaries

Consider the following state-space representation of a time-delay LPV system:

$$\begin{aligned}
 (\Sigma_\rho) : \dot{x}(t) &= A(\rho)x(t) + A_h(\rho)x(t - h(\rho(t))) + B_1(\rho)w(t) + B_2(\rho)u(t), \\
 z(t) &= C_1(\rho)x(t) + C_{1h}(\rho)x(t - h(\rho(t))) + D_{11}(\rho)w(t) + D_{12}(\rho)u(t), \\
 y(t) &= C_2(\rho)x(t) + C_{2h}(\rho)x(t - h(\rho(t))) + D_{21}(\rho)w(t), \\
 x(\theta) &= \phi(\theta), \forall \theta \in [-h(\rho(0)) \ 0],
 \end{aligned}
 \tag{11.1}$$

where $x(t) \in \mathbb{R}^n$ is the system state vector, $w(t) \in \mathbb{R}^{n_w}$ is the vector of exogenous disturbance with finite energy in the space $\mathcal{L}_2[0 \ \infty)$, $u(t) \in \mathbb{R}^{n_u}$ is the input vector, $z(t) \in \mathbb{R}^{n_z}$ is the vector of controlled outputs, $y(t) \in \mathbb{R}^{n_y}$ is the vector of measurable outputs, $\phi(\cdot)$ denotes the initial system condition, and h is a differentiable scalar function representing the parameter-varying time delay. We assume that the delay is bounded and that the function h lies in the set

$$\mathcal{H} := \{h \in \mathcal{C}(\mathbb{R}^s, \mathbb{R}) : 0 \leq h(t) \leq h_{\max} < \infty, \forall t \in \mathbb{R}_+\}.$$

The initial condition function ϕ is a given function in $\mathcal{C}([-h_{\max} \ 0], \mathbb{R}^n)$. Wherever needed, the notation $x_t(\theta)$ is used to denote $x(t + \theta)$ for $\theta \in [-h_{\max} \ 0]$, that is, x_t is the infinite dimensional state of the system. The state-space matrices $A(\cdot), A_h(\cdot), B_1(\cdot), B_2(\cdot), C_1(\cdot), C_{1h}(\cdot), C_2(\cdot), C_{2h}(\cdot), D_{11}(\cdot), D_{12}(\cdot), D_{21}(\cdot)$ are assumed to be known continuous functions of a time-varying parameter vector $\rho(\cdot) \in \mathcal{F}_{\mathcal{P}}^V$, where $\mathcal{F}_{\mathcal{P}}^V$ is the set of allowable parameter trajectories defined as

$$\mathcal{F}_{\mathcal{P}}^V \triangleq \{\rho \in \mathcal{C}(\mathbb{R}_+, \mathbb{R}^s) : \rho(t) \in \mathcal{P}, |\dot{\rho}_i(t)| \leq v_i\},$$

where \mathcal{P} is a compact subset of \mathbb{R}^s , i.e., we consider bounded parameter trajectories with bounded rates for the parameter variation. Notice that, the parametric dependence of the delay on ρ results in a given delay bound h_{\max} , since ρ is restricted to lie in the given parameter set \mathcal{P} . Bounding the rate of variation of the parameter vector ρ allows the use of parameter-dependent Lyapunov–Krasovskii functionals resulting in less conservative analysis and synthesis conditions [1, 44].

In this chapter, we are interested in an \mathcal{H}_∞ design as the performance specification for the closed-loop system. The induced \mathcal{L}_2 gain (or \mathcal{H}_∞ norm) of the LPV system Σ_ρ from w to z considering $u \equiv 0$ is defined by

$$\|T_{zw}\|_\infty = \sup_{\rho \in \mathcal{F}_\rho} \sup_{\|w\|_2 \neq 0} \frac{\|z\|_2}{\|w\|_2},$$

where T_{zw} is the operator mapping w to z , $\|w\|_2$ is the 2-norm of the exogenous input and $\|z\|_2$ is the 2-norm of the desired controlled output vector.

This chapter takes advantage of a number of lemmas to prove some of the technical results. The two important ones are described below.

Lemma 11.1 (Projection Lemma). *Given a symmetric matrix $\Psi \in \mathbb{R}^{m \times m}$ and two matrices \mathcal{C}, \mathcal{D} of appropriate dimensions, the following problem:*

$$\Psi + \mathcal{C}^T \Theta^T \mathcal{D} + \mathcal{D}^T \Theta \mathcal{C} < 0$$

is solvable in a matrix Θ of compatible dimension if and only if

$$\text{Ker}^T(\mathcal{C})\Psi\text{Ker}(\mathcal{C}) < 0, \quad \text{Ker}^T(\mathcal{D})\Psi\text{Ker}(\mathcal{D}) < 0,$$

where $\text{Ker}(\mathcal{C})$ and $\text{Ker}(\mathcal{D})$ are any basis of the kernel or null space of \mathcal{C} and \mathcal{D} , respectively.

Proof. Refer to [12]. □

Lemma 11.2 (Jensen’s Lemma). *Let ϕ be a convex function and $f(x)$ is a function integrable over $[a, b]$, $a < b$. Then, the following inequality holds:*

$$\phi \left(\int_a^b f(x) dx \right) \leq (b-a) \int_a^b \phi(f(x)) dx$$

Proof. Refer to [13]. □

The Jensen’s inequality is often used in the \mathcal{H}_∞ norm analytical computation of integral operators in time-delay systems framework. It is also used in approaches based on Lyapunov–Krasovskii functionals as an efficient bounding technique. An example of one such application is given as follows:

$$\left(\int_{t-h}^t \dot{x}(\theta) d\theta \right)^T P \left(\int_{t-h}^t \dot{x}(\theta) d\theta \right) \leq h \int_{t-h}^t \dot{x}(\theta)^T P \dot{x}(\theta) d\theta$$

with $P = P^T \succ 0$. The convex function is $\phi(z) = z^T P z$ and $f(t) = \dot{x}(t)$.

11.3 \mathcal{H}_∞ Performance Analysis of Time-Delay LPV Systems

Consider the unforced (i.e., $u \equiv 0$) time-delay LPV system

$$\begin{aligned} (\Sigma_{\rho_w}) : \dot{x}(t) &= A(\rho)x(t) + A_h(\rho)x(t - h(\rho(t))) + B_1(\rho)w(t), \\ z(t) &= C_1(\rho)x(t) + C_{1h}(\rho)x(t - h(\rho(t))) + D_{11}(\rho)w(t). \end{aligned} \quad (11.2)$$

The following theorem provides a sufficient condition guaranteeing asymptotic stability along with a prescribed level of disturbance attenuation in an \mathcal{H}_∞ setting.

Theorem 11.1. *The system (Σ_{ρ_w}) is asymptotically stable for all $h \in \mathcal{H}$ and satisfies the condition $\|z\|_2 \leq \gamma\|w\|_2$, if there exists a continuously differentiable matrix function $P : \mathbb{R}^s \rightarrow \mathbb{S}_{++}^n$, constant matrices $Q, R \in \mathbb{S}_{++}^n$, and a scalar $\gamma > 0$ such that the following LMI:*

$$\begin{bmatrix} M(\rho, \nu) & P(\rho)A_h + R & P(\rho)B_1(\rho) & C_1^T(\rho) & h_{\max}A^T(\rho)R \\ * & -\left[1 - \sum_{i=1}^s \pm \left(v_i \frac{\partial h}{\partial \rho_i}\right)\right] Q - R & 0 & C_{1h}^T(\rho) & h_{\max}A_h^T(\rho)R \\ * & * & -\gamma I & D_{11}^T(\rho) & h_{\max}B_1^T(\rho)R \\ * & * & * & -\gamma I & 0 \\ * & * & * & * & -R \end{bmatrix} < 0 \quad (11.3)$$

with $M(\rho, \nu) = A^T(\rho)P(\rho) + P(\rho)A(\rho) + \left[\sum_{i=1}^s \pm \left(v_i \frac{\partial P(\rho)}{\partial \rho_i}\right)\right] + Q - R$ holds for all $\rho \in \mathcal{F}_{\mathcal{D}}^\nu$.

Proof. Consider the following Lyapunov–Krasovskii type functional: □

$$V(x_t, \rho) = V_1(x, \rho) + V_2(x_t, \rho) + V_3(x_t, \rho), \quad (11.4)$$

$$V_1(x, \rho) = x^T(t)P(\rho)x(t), \quad (11.5)$$

$$V_2(x_t, \rho) = \int_{t-h(\rho(t))}^t x^T(\xi)Qx(\xi)d\xi, \quad (11.6)$$

$$V_3(x_t, \rho) = \int_{-h_{\max}}^0 \int_{t+\theta}^t \dot{x}^T(\eta)h_{\max}R\dot{x}(\eta)d\eta d\theta. \quad (11.7)$$

It is easy to show that $V(x_t, \rho)$ is positive definite. To ascertain the asymptotic stability of the system, the time derivative of $V(x_t, \rho)$ is computed along the trajectories of the system as follows:

$$\dot{V}_1(x, \rho) = \dot{x}^T(t)P(\rho)x(t) + x^T(t)P(\rho)\dot{x}(t) + x^T(t)\frac{\partial P(\rho)}{\partial \rho}\dot{\rho}x(t), \quad (11.8)$$

$$\dot{V}_2(x_t, \rho) = \dot{x}^T(t) Q x(t) - \left(1 - \frac{\partial h}{\partial \rho} \dot{\rho}\right) x^T(t - h(\rho(t))) Q x(t - h(\rho(t))), \quad (11.9)$$

$$\dot{V}_3(x_t, \rho) = h_{\max}^2 \dot{x}^T(t) R \dot{x}(t) - \int_{t-h_{\max}}^t \dot{x}^T(\theta) h_{\max} R \dot{x}(\theta) d\theta. \quad (11.10)$$

Since $h(t) \leq h_{\max}$ then

$$- \int_{t-h_{\max}}^t \dot{x}^T(\theta) h_{\max} R \dot{x}(\theta) d\theta \leq - \int_{t-h(t)}^t \dot{x}^T(\theta) h_{\max} R \dot{x}(\theta) d\theta.$$

Using Jensen's inequality in Lemma 11.2, it is possible to bound the integral term in $\dot{V}_3(x_t, \rho)$ as follows:

$$\begin{aligned} \dot{V}_3(x_t, \rho) &\leq h_{\max}^2 \dot{x}^T(t) R \dot{x}(t) - \int_{t-h(t)}^t \dot{x}^T(\theta) h_{\max} R \dot{x}(\theta) d\theta \\ &\leq h_{\max}^2 \dot{x}^T(t) R \dot{x}(t) - \frac{h_{\max}}{h(t)} \left(\int_{t-h(t)}^t \dot{x}(\theta) d\theta \right)^T R \left(\int_{t-h(t)}^t \dot{x}(\theta) d\theta \right) \\ &= h_{\max}^2 \dot{x}^T(t) R \dot{x}(t) - \frac{h_{\max}}{h(t)} [x(t) - x(t - h(\rho(t)))]^T \\ &\quad \times R [x(t) - x(t - h(\rho(t)))]. \end{aligned}$$

Finally bounding $-\frac{h_{\max}}{h(t)}$ by -1 , we get

$$\dot{V}_3(x_t, \rho) \leq h_{\max}^2 \dot{x}^T(t) R \dot{x}(t) - [x(t) - x(t - h(\rho(t)))]^T R [x(t) - x(t - h(\rho(t)))].$$

Gathering all the derivative terms and letting $\dot{V}(x_t, \rho) < 0$, we determine the following inequality condition:

$$\dot{V}(x_t, \rho) \leq \zeta^T(t) \Xi(\rho, \dot{\rho}) \zeta(t) < 0$$

with

$$\Xi(\rho, \dot{\rho}) = \begin{bmatrix} \bar{\Xi}_{11} & P(\rho) A_h(\rho) + R P(\rho) B_1(\rho) \\ * & \bar{\Xi}_{22} & 0 \\ * & * & 0 \end{bmatrix} + h_{\max}^2 T^T(\rho) R T(\rho),$$

$$\zeta(t) = \text{col}[x(t), x(t - h(\rho(t))), w(t)],$$

$$T = [A(\rho) \quad A_h(\rho) \quad B_1(\rho)],$$

$$\bar{\Xi}_{11} = A^T(\rho) P(\rho) + P(\rho) A(\rho) + \frac{\partial P(\rho)}{\partial \rho} \dot{\rho} + Q - R,$$

$$\bar{\Xi}_{22} = - \left(1 - \frac{\partial h}{\partial \rho} \dot{\rho}\right) Q - R.$$

To establish the prescribed \mathcal{H}_∞ performance level γ , we further require [43]

$$\dot{V}(x_t, \rho) - \gamma^2 w^T(t)w(t) + z^T(t)z(t) \leq 0.$$

Substituting $z(t)$ into the inequality above finally leads to the inequality $\zeta^T(t)\Omega(\rho, \dot{\rho})\zeta(t) < 0$ with

$$\Omega = \begin{bmatrix} \Omega_{11} & PA_h + R + h_{\max}^2 A^T RA_h + C_1^T C_{1h} & PB_1 + h_{\max}^2 A^T RB_1 + C_1^T D_{11} \\ * & \Xi_{22} + h_{\max}^2 A_h^T RA_h + C_{1h}^T C_{1h} & h_{\max}^2 A_h^T RB_1 + C_{1h}^T D_{11} \\ * & * & h_{\max}^2 B_1^T RB_1 + D_{11}^T D_{11} - \gamma^2 I \end{bmatrix}$$

with $\Omega_{11} = A^T P + PA + \frac{\partial P}{\partial \rho} \dot{\rho} + Q - R + h_{\max}^2 A^T RA + C_1^T C_1$, and where the explicit dependence on the scheduling parameter vector ρ has been dropped for convenience. Applying Schur complement lemma [4] to the above inequality expression leads to LMI (11.3). Finally noting that $\dot{\rho}$ enters affinely in the LMI, it suffices to check the LMI only at the vertices of $\dot{\rho}$ and hence $\frac{\partial h}{\partial \rho} \dot{\rho}$ and $\frac{\partial P}{\partial \rho} \dot{\rho}$ are replaced by $\sum_{i=1}^s \pm \left(v_i \frac{\partial h}{\partial \rho_i} \right)$ and $\sum_{i=1}^s \pm \left(v_i \frac{\partial P(\rho)}{\partial \rho_i} \right)$, respectively.

Remark 11.1. The notation $\sum_{i=1}^s \pm(\cdot)$ is used to indicate that every combination of $+(\cdot)$ and $-(\cdot)$ should be included in the inequality. That is the inequality actually represents 2^s different inequalities that correspond to the 2^s different combinations in the summation.

Remark 11.2. The LMI condition in (11.3) corresponds to an infinite-dimensional convex optimization problem due to the parametric dependence. To obtain a finite-dimensional optimization problem, the parameter-dependent matrix function $P(\cdot)$ can be approximated using a finite set of basis functions and a finite gridding of the parameter space can be used. As the LMIs are to be solved only at each of the grid points, this results in a set of finite-dimensional LMIs that can be solved numerically using commercial solvers.

11.3.1 LMI Relaxation Using Slack Variables

A drawback of the standard matrix inequality characterization given by Theorem 11.1 is that it involves multiple product terms including PA and RA and was found not to be suitable to derive the synthesis conditions. In this section, a reciprocal variant of Lemma 11.1 is used to derive a relaxed condition. This technique introduces the so-called *slack* variables which bring additional flexibility in the synthesis problem. Moreover, this flexibility is expected to result in far less conservative conditions than with customary approaches. The following theorem will be useful in this respect.

Theorem 11.2. *The system $(\Sigma_{\rho w})$ is asymptotically stable for all $h \in \mathcal{H}$ and satisfies the condition $\|z\|_2 \leq \gamma \|w\|_2$, if there exist a continuously differentiable matrix function $P : \mathbb{R}^s \rightarrow \mathbb{S}_{++}^n$, constant matrices $Q, R \in \mathbb{S}_{++}^n$, matrix functions $V_1, V_2, V_3 : \mathbb{R}^s \rightarrow \mathbb{R}^{n \times n}$ and a scalar $\gamma > 0$ such that the following LMI condition:*

$$\begin{bmatrix} -V_1 - V_1^T & P - V_2^T + V_1 A & -V_3^T + V_1 A_h & V_1 B_1 & 0 & V_1 + h_{\max} R \\ * & \Psi_{22} + A^T V_2^T + V_2 A & R + A^T V_3^T + V_2 A_h & V_2 B_1 & C_1^T & V_2 - P \\ * & * & \Xi_{22} + A_h^T V_3^T + V_3 A_h & V_3 B_1 & C_{1h}^T & V_3 \\ * & * & * & -\gamma I & D_{11}^T & 0 \\ * & * & * & * & -\gamma I & 0 \\ * & * & * & * & * & (-1 - 2h_{\max})R \end{bmatrix} < 0 \quad (11.11)$$

with $\Psi_{22} = \frac{\partial P}{\partial \rho} \dot{\rho} + Q - R$ and Ξ_{22} as defined earlier, holds true for all $\rho \in \mathcal{F}_{\mathcal{D}}^v$.

Proof. The proof is inspired from [38]. We first rewrite (11.11) as

$$\Psi + \mathcal{C}^T \Theta^T \mathcal{D} + \mathcal{D}^T \Theta \mathcal{C} < 0 \quad (11.12)$$

with

$$\Psi = \begin{bmatrix} 0 & P(\rho) & 0 & 0 & 0 & h_{\max} R \\ * & \Psi_{22} & R & 0 & C_1^T(\rho) & -P(\rho) \\ * & * & \Xi_{22} & 0 & C_{1h}^T(\rho) & 0 \\ * & * & * & -\gamma I & D_{11}^T(\rho) & 0 \\ * & * & * & * & -\gamma I & 0 \\ * & * & * & * & * & (-1 - 2h_{\max})R \end{bmatrix}, \quad (11.13)$$

$$\mathcal{C}(\rho) = [-I \ A(\rho) \ A_h(\rho) \ B_1(\rho) \ 0 \ I], \quad (11.14)$$

$$\mathcal{D} = \begin{bmatrix} I & 0 & 0 & 0 & 0 & 0 \\ 0 & I & 0 & 0 & 0 & 0 \\ 0 & 0 & I & 0 & 0 & 0 \end{bmatrix}, \quad (11.15)$$

$$\Theta^T = [V_1^T \ V_2^T \ V_3^T]. \quad (11.16)$$

The explicit bases of the null space of \mathcal{C} and \mathcal{D} are given by

$$\text{Ker}(\mathcal{C}(\rho)) = \begin{bmatrix} A(\rho) & A_h(\rho) & B_1(\rho) & 0 & I \\ I & 0 & 0 & 0 & 0 \\ 0 & I & 0 & 0 & 0 \\ 0 & 0 & I & 0 & 0 \\ 0 & 0 & 0 & I & 0 \\ 0 & 0 & 0 & 0 & I \end{bmatrix}, \quad \text{Ker}(\mathcal{D}) = \begin{bmatrix} 0 & 0 & 0 \\ 0 & 0 & 0 \\ 0 & 0 & 0 \\ I & 0 & 0 \\ 0 & I & 0 \\ 0 & 0 & I \end{bmatrix}.$$

Applying Lemma 11.1 with respect to the variable Θ in (11.12) yields two inequalities, one of which is exactly the characterization given by (11.3) and the other is the LMI given by (11.17)

$$\begin{bmatrix} -\gamma I & D_{11}^T(\rho) & 0 \\ * & \gamma I & 0 \\ * & & (-1 - 2h_{\max})R \end{bmatrix} < 0. \quad (11.17)$$

The above inequality is a relaxed form of the right bottom 3×3 block of the inequality (11.3) and is always satisfied. Hence, the feasibility of (11.11) implies the feasibility of (11.3), which along with the result of Theorem 11.1 concludes the proof. \square

11.4 \mathcal{H}_∞ Output Feedback Control Design

In this section, the analysis results presented in the previous section are used to design a dynamic output feedback controller. The time delay in the system dynamics is assumed to be an exactly known or measurable function of the scheduling parameter ρ . For the system (Σ_ρ) , we seek to design a controller of the following form:

$$\begin{aligned} (K_{\text{delayed}}) : \dot{x}_k(t) &= A_k(\rho)x_k(t) + A_{hk}(\rho)x_k(t - h(\rho(t))) + B_k(\rho)y(t), \\ u(t) &= C_k(\rho)x_k(t) + C_{hk}(\rho)x_k(t - h(\rho(t))) + D_k(\rho)y(t), \end{aligned} \quad (11.18)$$

where $x_k(t) \in \mathbb{R}^n$ is the controller state vector and $x_k(t - h(\rho(t))) \in \mathbb{R}^n$ denotes the delayed state of the controller. The closed loop system formed by the interconnection of (Σ_ρ) and (K_{delayed}) is given by

$$\begin{aligned} (\Sigma_{\rho,\text{cl}}) : \dot{x}_{\text{cl}}(t) &= \underbrace{\begin{bmatrix} A + B_2 D_k C_2 & B_2 C_k \\ B_k C_2 & A_k \end{bmatrix}}_{A_{\text{cl}}} x_{\text{cl}}(t) + \underbrace{\begin{bmatrix} A_h + B_2 D_k C_{2h} & B_2 C_{hk} \\ B_k C_{2h} & A_{hk} \end{bmatrix}}_{A_{\text{hcl}}} x_{\text{cl}_h} \\ &+ \underbrace{\begin{bmatrix} B_1 + B_2 D_k D_{21} \\ B_k D_{21} \end{bmatrix}}_{B_{\text{cl}}} w(t), \\ z(t) &= \underbrace{\begin{bmatrix} C_1 + D_{12} D_k C_2 & D_{12} C_k \end{bmatrix}}_{C_{\text{cl}}} x_{\text{cl}}(t) + \underbrace{\begin{bmatrix} C_{1h} + D_{12} D_k C_{2h} & D_{12} C_{hk} \end{bmatrix}}_{C_{\text{hcl}}} x_{\text{cl}_h} \\ &+ \underbrace{\begin{bmatrix} D_{11} + D_{12} D_k D_{21} \end{bmatrix}}_{D_{\text{cl}}} w(t) \end{aligned}$$

with $x_{\text{cl}}(t) = \text{col}[x(t), x_k(t)]$ and $x_{\text{cl}_h} = x_{\text{cl}}(t - h(\rho(t)))$, where again the dependence on the scheduling parameter has been dropped in order to improve clarity. The following result gives sufficiency conditions for the synthesis of a delayed output feedback controller, such that the closed loop system $\Sigma_{\rho, \text{cl}}$ is asymptotically stable and has an induced \mathcal{L}_2 norm less than γ .

Theorem 11.3. *If there exist continuously differentiable matrix functions $\tilde{P} : \mathbb{R}^s \rightarrow \mathbb{S}_{++}^{2n}$, and $X, Y : \mathbb{R}^s \rightarrow \mathbb{S}_{++}^n$, constant matrices $\tilde{Q}, \tilde{R} \in \mathbb{S}_{++}^{2n}$, parameter-dependent matrices $\hat{A}, \hat{A}_h, \hat{B}, \hat{C}, \hat{C}_h$ and D_k and a scalar $\gamma > 0$ such that the LMI*

$$\begin{bmatrix} -2\tilde{V} & \tilde{P} - \tilde{V} + \mathcal{A} & -\tilde{V} + \mathcal{A}_h & \mathcal{B} & 0 & \tilde{V} + h_{\max}\tilde{R} \\ * & \tilde{\Psi}_{22} + \mathcal{A} + \mathcal{A}^T & \tilde{R} + \mathcal{A}^T + \mathcal{A}_h & \mathcal{B} & \mathcal{C}^T & \tilde{V} - \tilde{P} \\ * & * & \tilde{\Xi}_{22} + \mathcal{A}_h + \mathcal{A}_h^T & \mathcal{B} & \mathcal{C}_h^T & \tilde{V} \\ * & * & * & -\gamma I & \mathcal{D}^T & 0 \\ * & * & * & * & -\gamma I & 0 \\ * & * & * & * & * & (-1 - 2h_{\max})\tilde{R} \end{bmatrix} < 0 \quad (11.19)$$

holds for all $\rho \in \mathcal{F}_{\mathcal{P}}^V$ with

$$\tilde{V} = \begin{bmatrix} Y & I \\ I & X \end{bmatrix},$$

$$\mathcal{A} = \begin{bmatrix} AY + B_2\hat{C} & A + B_2D_kC_2 \\ \hat{A} & XA + \hat{B}C_2 \end{bmatrix},$$

$$\mathcal{A}_h = \begin{bmatrix} A_hY + B_2\hat{C}_h & A_h + B_2D_kC_{2h} \\ \hat{A}_h & XA_h + \hat{B}C_{2h} \end{bmatrix},$$

$$\mathcal{B} = \begin{bmatrix} B_1 + B_2D_kD_{21} \\ XB_1 + \hat{B}D_{21} \end{bmatrix},$$

$$\mathcal{C} = [C_1Y + D_{12}\hat{C} \quad C_1 + D_{12}D_kC_2],$$

$$\mathcal{C}_h = [C_{1h}Y + D_{12}\hat{C}_h \quad C_{1h} + D_{12}D_kC_{2h}],$$

$$\mathcal{D} = [D_{11} + D_{12}D_kD_{21}],$$

$$\tilde{\Psi}_{22} = \tilde{Q} - \tilde{R} + \left[\sum_{i=1}^s \pm \left(v_i \frac{\partial \tilde{P}(\rho)}{\partial \rho_i} \right) \right],$$

$$\tilde{\Xi}_{22} = - \left[1 - \sum_{i=1}^s \pm \left(v_i \frac{\partial h}{\partial \rho_i} \right) \right] \tilde{Q} - \tilde{R}$$

then there exists a controller of the form (K_{delayed}) such that:

(A.1) The closed-loop system $\Sigma_{\rho,\text{cl}}$ with $h \in \mathcal{H}$ is asymptotically stable for any $\rho \in \mathcal{F}_{\mathcal{D}}^{\vee}$.

(A.2) The \mathcal{H}_{∞} norm of the closed loop system is bounded by the positive scalar γ .

Moreover, once the parameter-dependent matrices satisfying the LMI conditions are determined, the delayed output feedback control matrices can be computed using the following steps:

(A.1) Obtain M and N from the factorization problem

$$I - XY = NM^{\text{T}} \quad (11.20)$$

(A.2) Compute the controller matrices by reversing the transformations defined by

$$\begin{aligned} \widehat{A} &= XAY + XB_2D_kC_2Y + NB_kC_2Y + XB_2C_kM^{\text{T}} + NA_kM^{\text{T}}, \\ \widehat{A}_h &= XA_hY + XB_2D_kC_{2h}Y + NB_kC_{2h}Y + XB_2C_{hk}M^{\text{T}} + NA_{hk}M^{\text{T}}, \\ \widehat{B} &= XB_2D_k + NB_k, \\ \widehat{C} &= D_kC_2Y + C_kM^{\text{T}}, \\ \widehat{C}_h &= D_kC_{2h}Y + C_{hk}M^{\text{T}} \end{aligned} \quad (11.21)$$

It is to be noted that the matrices M and N are always square and invertible in the case of full-order controllers.

Proof. The proof uses the result of Theorem 11.2. For simplicity, the slack variable matrix functions are restricted to be equal and symmetric positive definite. Further, we define a partitioned form for the slack variable matrix. Hence,

$$V_1 = V_2 = V_3 = V = \begin{bmatrix} X & N \\ N^{\text{T}} & \star \end{bmatrix}.$$

Define the inverse of V as

$$V^{-1} = \begin{bmatrix} Y & M \\ M^{\text{T}} & \star \end{bmatrix},$$

such that $XY + NM^{\text{T}} = I$, where X and Y are symmetric matrices of dimension $n \times n$. Substituting the closed-loop system matrices in LMI (11.11) and performing a congruence transformation $\mathcal{T} = \text{diag}(Z^{\text{T}}, Z^{\text{T}}, Z^{\text{T}}, I, I, Z^{\text{T}})$, where

$$Z := \begin{bmatrix} Y & I \\ M^{\text{T}} & 0 \end{bmatrix}$$

leads to the inequality

$$\begin{bmatrix} -2Z^T V Z & \tilde{P} - Z^T V Z + Z^T V A_{cl} Z & -Z^T V Z + Z^T V A_{hcl} Z \\ * & \tilde{\Psi}_{22} + Z^T (A_{cl}^T V + V A_{cl}) Z & \tilde{R} + Z^T A_{cl}^T Z + Z^T V A_{hcl} Z \\ * & * & \tilde{\Xi} + Z^T (A_{hcl}^T V + V A_{hcl}) Z \\ * & * & * \\ * & * & * \\ * & * & * \\ Z^T V B_{cl} & 0 & Z^T V Z + h_{\max} \tilde{R} \\ Z^T V B_{cl} & Z^T C_{cl}^T & Z^T V Z - \tilde{P} \\ Z^T V B_{cl} & Z^T C_{hcl}^T & Z^T V Z \\ -\gamma I & D_{cl}^T & 0 \\ * & -\gamma I & 0 \\ * & * & (-1 - 2h_{\max} \tilde{R}) \end{bmatrix} < 0 \quad (11.22)$$

with $\tilde{P} = Z^T P Z$, $\tilde{R} = Z^T R Z$, $\tilde{\Psi}_{22} = Z^T \Psi_{22} Z$ and $\tilde{\Xi}_{22} = Z^T \Xi Z$. Note that

$$Z^T V Z = \begin{bmatrix} Y & I \\ I & X \end{bmatrix} \quad \text{and} \quad Z^T V = \begin{bmatrix} I & 0 \\ X & N \end{bmatrix}.$$

With this, the following identities can be obtained:

$$\begin{aligned} Z^T V A_{cl} Z &= \mathcal{A}, & Z^T V B_{cl} &= \mathcal{B}, \\ Z^T V A_{hcl} Z &= \mathcal{A}_h, & Z^T C_{cl}^T &= \mathcal{C}^T, \\ Z^T C_{hcl}^T &= \mathcal{C}_h^T, & D_{cl} &= \mathcal{D}. \end{aligned}$$

Thus, the inequality has been linearized with respect to the new variables (\hat{A} , \hat{A}_h , \hat{B} , \hat{C} , \hat{C}_h and D_k) and it represents the LMI condition presented in Theorem 11.3. Finally, once the decision matrices are determined, one can use the nonlinear transformations in (11.21) to obtain the controller state-space matrices as follows:

$$\begin{aligned} C_{hk} &= (\hat{C}_h - D_k C_{2h} Y) M^{-T}, \\ C_k &= (\hat{C} - D_k C_2 Y) M^{-T}, \\ B_k &= N^{-1} (\hat{B} - X B_2 D_k), \\ A_{hk} &= -N^{-1} (X A_h Y + X B_2 D_k C_{2h} Y + N B_k C_{2h} Y + X B_2 C_{hk} M^T - \hat{A}_h) M^{-T}, \\ A_k &= -N^{-1} (X A Y + X B_2 D_k C_2 Y + N B_k C_2 Y + X B_2 C_k M^T - \hat{A}) M^{-T}. \end{aligned} \quad (11.23)$$

Remark 11.3. The previous work on \mathcal{H}_∞ control design for LPV time-delay systems in case of a time-varying delay required the rate of variation of the time delay to be less than one, i.e., $|\dot{h}| < 1$. With the presented results in this work, this restriction does not exist and the proposed LMI formulation can even handle unbounded delay rates.

11.5 Simulation Example

In this section, a numerical example is employed to demonstrate the main results of the chapter. The example is motivated by the control of chatter during the milling process [35, 48]. In a milling process, the workpiece is clamped and fed to a rotating multitooth cutter. The geometry of the cutting process of a milling machine is as shown in Fig. 11.1. As shown the cutter has two blades that are used to remove material from the workpiece. The force acting on the tool is a function of not only the current displacement of the tool but also the surface characteristics, and hence the displacement at the previous tool pass. This induces a delay into the system. The force depends also on the angular position of the blade, which plays the role of a time-varying parameter. The equations of motion can be derived as follows:

$$m_1 \ddot{x}_1 + k_1(x_1 - x_2) = f, \quad (11.24)$$

$$m_2 \ddot{x}_2 + c\dot{x}_2 + k_1(x_2 - x_1) + k_2x_2 = u, \quad (11.25)$$

$$f = k \sin(\phi + \beta)l(t) - w, \quad (11.26)$$

$$l(t) = \sin(\phi)[x_1(t - h(t)) - x_1(t)], \quad (11.27)$$

where k_1 and k_2 are the stiffness of the two springs, c is the damping coefficient, m_1 and m_2 are the masses of the blade and the tool, and x_1 and x_2 are the displacements of the blade and the tool. The angle β depends on the particular material and the tool

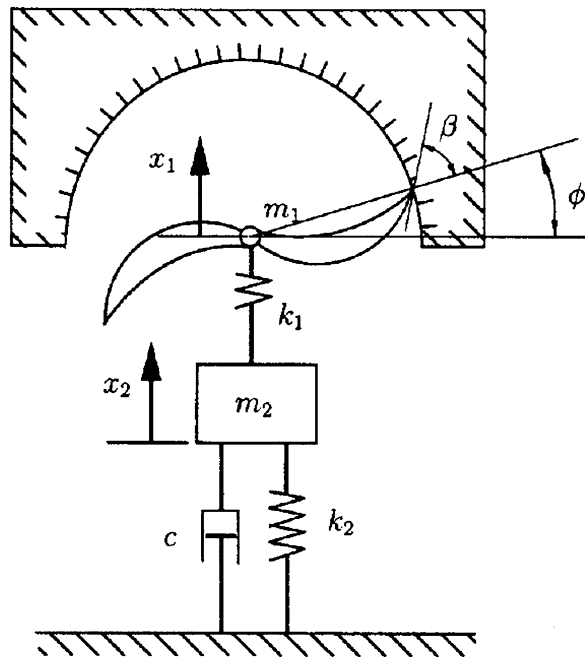


Fig. 11.1 Milling process

used. The angle ϕ denotes the angular position of the blade, k denotes the cutting force coefficient and w denotes the disturbance. The time delay which is the time interval between two successive cuts is denoted by $h(t)$ and is approximated to be $\frac{\pi}{\omega}$ where ω is the rotation speed of the blade. The plant we are considering can be rewritten as

$$\begin{aligned}\ddot{x}_1 &= \frac{1}{m_1}[-k_1x_1 + k_1x_2 - k \sin(\phi + \beta) \sin(\phi)x_1 \\ &\quad + k \sin(\phi + \beta) \sin(\phi)x_1(t - h(t)) - w], \\ \ddot{x}_2 &= \frac{1}{m_2}[k_1x_1 - k_1x_2 - k_2x_2 - c\dot{x}_2 + u].\end{aligned}$$

We consider the following problem data: $m_1 = 1$, $m_2 = 2$, $k_1 = 10$, $k_2 = 20$, $k = 2$, $c = 0.5$, and $\beta = 70^\circ$. It is noted that

$$\sin(\phi + \beta) \sin(\phi) = 0.5 [\cos(\beta) - \cos(2\phi + \beta)] = 0.1710 - 0.5 \cos(2\phi + \beta).$$

The system equations can be put in an LPV form with the scheduling parameter vector $\rho(t) = [\rho_1(t) \ \rho_2(t)]^T$, where $\rho_1(t) = \cos(2\phi + \beta)$ and $\rho_2(t) = \omega$ are measurable in real time and can be used to develop a gain-scheduled controller. The rotation speed of the blade is assumed to be between 200 rpm and 2,000 rpm, and the maximum variation rate is 1,000 rpm/sec. Hence, we have $\rho_1(t) \in [-1 \ 1]$ and $|\frac{d\rho_1}{dt}| = |-2 \sin(2\phi + \beta)\omega| \leq 2 \times 2,000 \times 2\pi/60 = 418.9(\text{rad/s})$, $\rho_2(t) \in [200 \times 2\pi/60 \ 2,000 \times 2\pi/60] = [20.94 \ 209.4](\text{rad/s})$ and $|\frac{d\rho_2}{dt}| = 1,000 \times 2\pi/60 = 52.35(\text{rad/s}^2)$. The delay rate $|\frac{dh(t)}{dt}| = |\frac{-\pi}{\omega^2} \times \frac{d\omega}{dt}| \leq \frac{\pi}{(200 \times 2\pi/60)^2} \times 1,000 \times 2\pi/60 = 0.75 < 1$.

We seek to design an LPV controller to attenuate the effect of the disturbance force w . An output feedback \mathcal{H}_∞ control is to be designed. To this end, we add a control force at mass m_2 . The controlled variable vector z is composed of the displacements of the two masses and the control force. The displacement of the mass m_2 is assumed to be the only measurable output. Considering the state vector to be $x = [x_1 \ x_2 \ \dot{x}_1 \ \dot{x}_2]^T$, the state-space representation of the time-delay LPV plant to be controlled is as follows:

$$\begin{aligned}\dot{x}(t) &= \begin{bmatrix} 0 & 0 & 1 & 0 \\ 0 & 0 & 0 & 1 \\ -10.34 + \rho_1 & 10 & 0 & 0 \\ 5 & -15 & 0 & -0.25 \end{bmatrix} x(t) + \begin{bmatrix} 0 & 0 & 0 & 0 \\ 0 & 0 & 0 & 0 \\ 0.34 - \rho_1 & 0 & 0 & 0 \\ 0 & 0 & 0 & 0 \end{bmatrix} x(t - \pi/\rho_2) \\ &\quad + \begin{bmatrix} 0 \\ 0 \\ -1 \\ 0 \end{bmatrix} w(t) + \begin{bmatrix} 0 \\ 0 \\ 0 \\ 0.5 \end{bmatrix} u(t),\end{aligned}\tag{11.28}$$

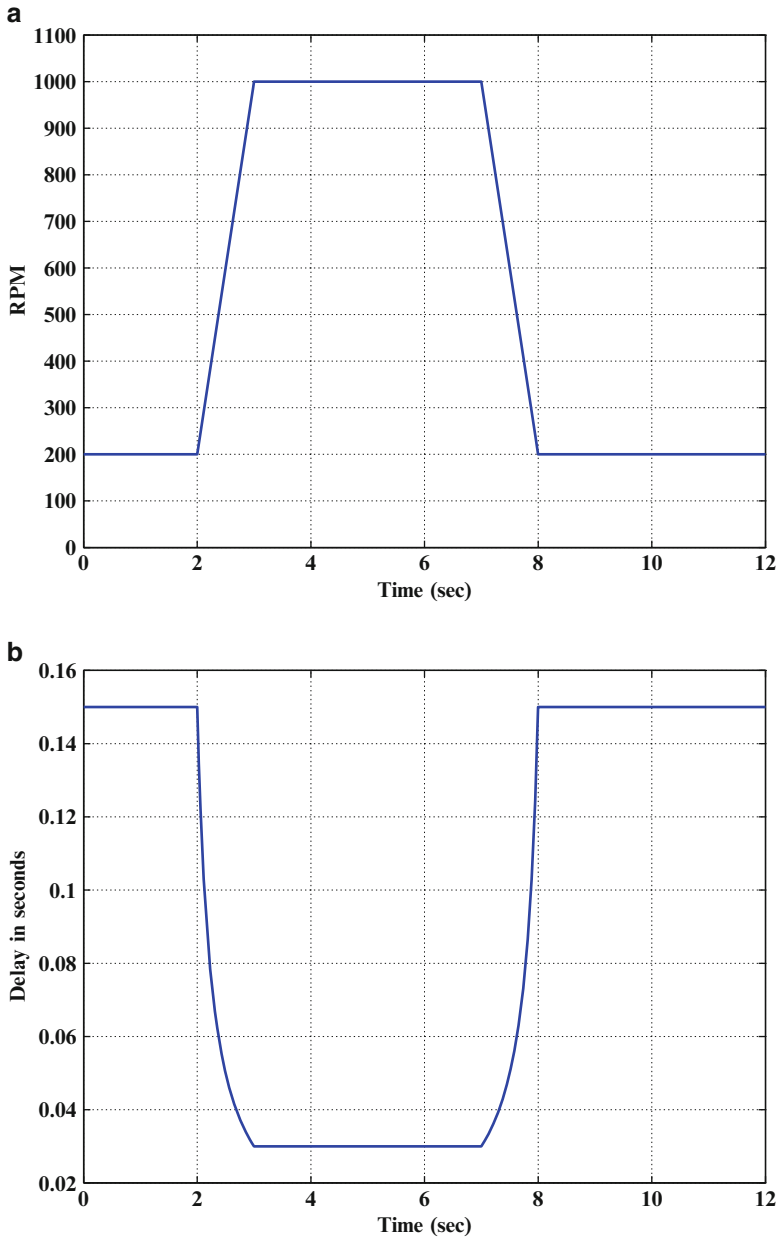


Fig. 11.2 Time varying parameters (a) Blade rotating speed (b) Time-delay

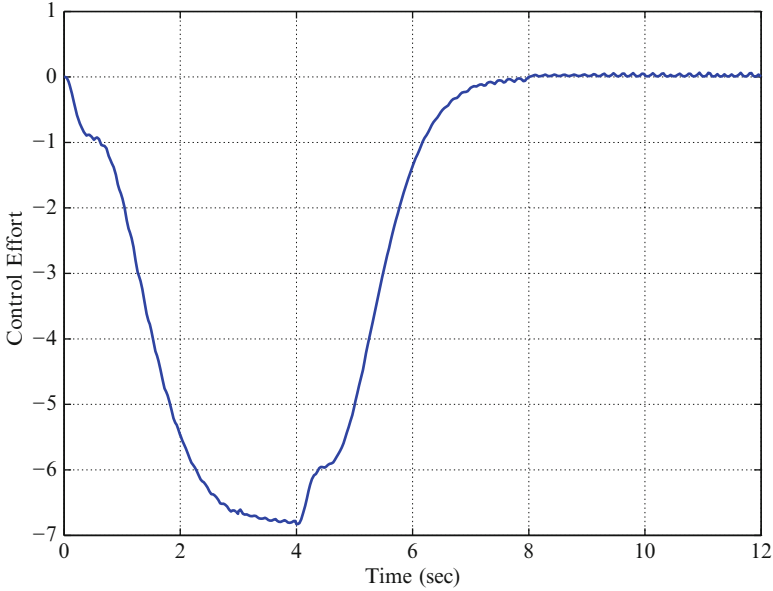


Fig. 11.3 Control effort

$$z(t) = \begin{bmatrix} 1 & 0 & 0 & 0 \\ 0 & 1 & 0 & 0 \\ 0 & 0 & 0 & 0 \end{bmatrix} x(t) + \begin{bmatrix} 0 \\ 0 \\ 0.1 \end{bmatrix} u(t), \quad (11.29)$$

$$y(t) = [0 \ 1 \ 0 \ 0] x(t). \quad (11.30)$$

Note that the penalty on control effort is 0.1. We use the synthesis results presented in this manuscript to design a delayed output feedback controller. For simplicity, both the Lyapunov matrix \tilde{P} and the slack variable matrix \tilde{V} are assumed to be constant matrices. We grid the parameter space using five grid points. Solving the LMI in Theorem 11.3, we obtain an \mathcal{H}_∞ performance bound $\gamma=1.015$. Simulations performed validate the disturbance attenuation performance of the designed controller. The disturbance $w(t)$ used in the simulation is a rectangular signal of unity magnitude for $0 \leq t \leq 4$ and zero elsewhere. The blade rotating speed ω and the resulting time-delay vary as shown in Fig. 11.2. Under the proposed control scheme, the control signal is shown in Fig. 11.3 and the displacements of the two masses in Fig. 11.4. For comparison purposes, we present the displacements of the two masses with and without control and under the same disturbance $w(t)$. As is evident from the plots, the displacements are much larger when no active control is applied.

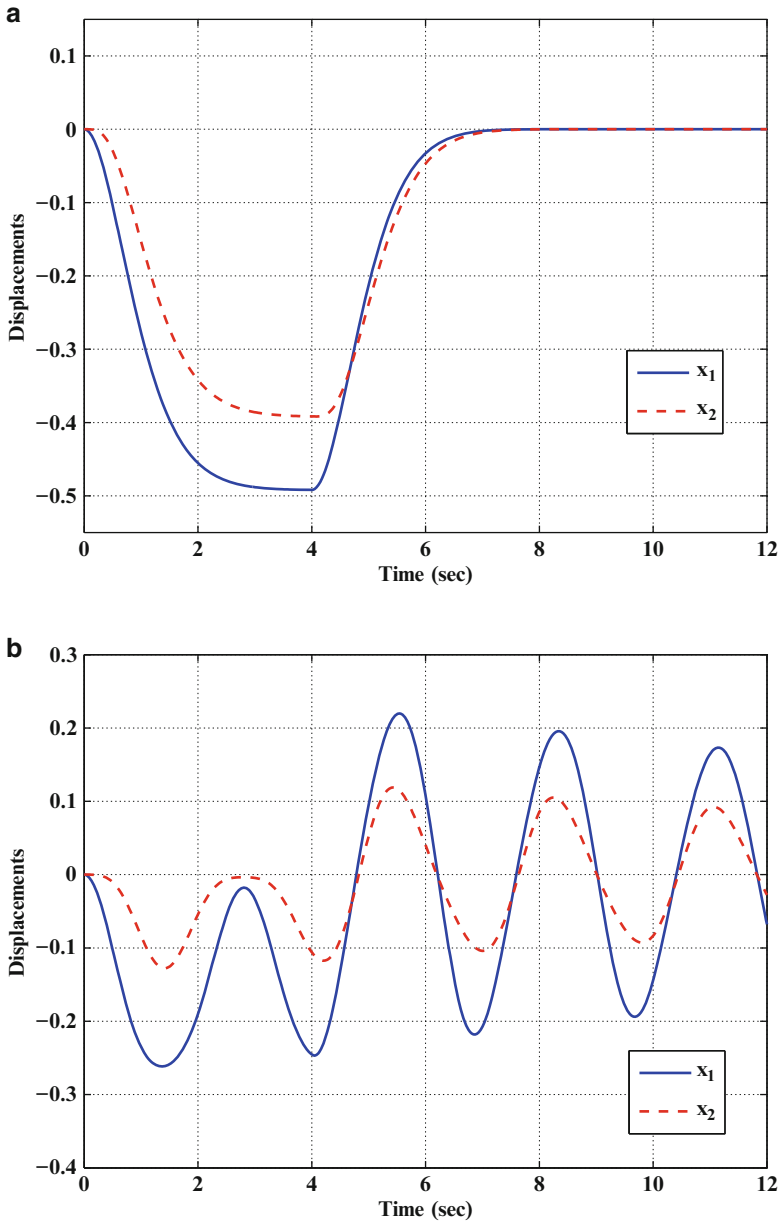


Fig. 11.4 Displacements of the mass and the blade (a) With Control (b) Without Control

11.6 Concluding Remarks

In this chapter, we presented a procedure to design an output feedback controller for LPV systems with parameter-varying time delays. The presented results of this chapter are the first in the literature to provide a solution to the output feedback synthesis problem based on delay-dependent analysis conditions. The developed delay-dependent induced \mathcal{L}_2 gain performance analysis conditions are expressed in terms of LMIs that can be solved efficiently using the commercial solvers. The obtained matrix inequality-based optimization problem is then relaxed by the introduction of additional slack variables that allow the synthesis conditions to be formulated as a convex optimization problem in an LMI form. The proposed systematic procedure for the gain-scheduled output feedback control design leads to less conservative results due to the use of parameter-dependent Lyapunov–Krasovskii functional, inclusion of the delay term in the feedback control dynamics and final delay-dependent synthesis conditions. The developed delay-dependent output feedback design methodology is further validated using simulations on the example of milling process.

Acknowledgment The authors would like to acknowledge the financial support from Qatar Research National Fund under the contract number NPRP 08-398-2-160. Any opinions, findings and conclusions expressed in this material are those of the authors and do not necessarily reflect the views of the sponsor.

References

1. Apkarian P, Adams R (1998) Advanced gain-scheduling techniques for uncertain systems. *IEEE Trans Contr Syst Tech* 6(1):21–32
2. Apkarian P, Gahinet P (1995) A convex characterization of gain-scheduled \mathcal{H}_∞ controllers. *IEEE Trans Automat Contr* 40(5):853–864
3. Becker G, Packard A (1994) Robust performance of linear parametrically varying systems using parametrically-dependent linear feedback. *Syst Contr Lett* 23(3):205–215
4. Boyd S, El Ghaoui L, Feron E, Balakrishnan V (1994) Linear matrix inequalities in system and control theory. Society for Industrial Mathematics
5. Briat C (2008) Robust control and observation of LPV time-delay systems. PhD thesis, Università degli Studi di Siena
6. Briat C, Sename O, Lafay J (2007) A LFT/\mathcal{H}_∞ state-feedback design for linear parameter varying time delay systems. In: European control conference, Kos, Greece
7. Briat C, Sename O, Lafay J (2008) Parameter dependent state-feedback control of LPV time-delay systems with time-varying delays using a projection approach. IFAC world congress, Seoul
8. Brierley S, Chiasson J, Lee E, Zak S (1982) On stability independent of delay for linear systems. *IEEE Trans Automat Contr* 27(1):252–254
9. Chen J, Latchman H (1994) Asymptotic stability independent of delays: simple necessary and sufficient conditions. In: Proceedings of the American control conference, IEEE, pp 1027–1031
10. Fridman E, Shaked U (2002) A descriptor system approach to \mathcal{H}_∞ control of linear time-delay systems. *IEEE Trans Automat Contr* 47(2):253–270

11. Fridman E, Shaked U (2003) Delay-dependent stability and \mathcal{H}_∞ control: constant and time-varying delays. *Int J Contr* 76(1):48–60
12. Gahinet P, Apkarian P (1994) A linear matrix inequality approach to \mathcal{H}_∞ control. *Int J Robust Nonlinear Contr* 4(4):421–448
13. Gu K, Kharitonov V, Chen J (2003) Stability of time-delay systems. Birkhauser, Boston
14. Hale J, Lunel S (1993) Introduction to functional differential equations. Springer, New York
15. Kolmanovskii V, Richard J (1999) Stability of some linear systems with delays. *IEEE Trans Automat Contr* 44(5):984–989
16. Lewis R, Anderson B (1980) Necessary and sufficient conditions for delay-independent stability of linear autonomous systems. *IEEE Trans Automat Contr* 25(4):735–739
17. Li X, De Souza C (1997) Delay-dependent robust stability and stabilization of uncertain linear delay systems: a linear matrix inequality approach. *IEEE Trans Automat Contr* 42(8):1144–1148
18. Mahmoud M (2000) Robust control and filtering for time-delay systems. CRC, New York
19. Mahmoud M, Al-Muthairi N (1994) Design of robust controllers for time-delay systems. *IEEE Trans Automat Contr* 39(5):995–999
20. Mahmoud M, Al-Muthairi N (2003) Linear parameter-varying state-delay (LPVSD) systems: stability and L_2 -gain controllers. *Syst Anal Model Simulat* 43(7):885–915
21. Malek-Zavarei M, Jamshidi M (1987) Time-delay systems: analysis, optimization and applications. Elsevier Science Inc., New York
22. Mohammadpour J, Grigoriadis K (2008) Delay-dependent \mathcal{H}_∞ filtering for time-delayed LPV systems. *Syst Contr Lett* 57(4):290–299
23. Moon Y, Park P, Kwon W, Lee Y (2001) Delay-dependent robust stabilization of uncertain state-delayed systems. *Int J Contr* 74(14):1447–1455
24. Mori T (1985) Criteria for asymptotic stability of linear time-delay systems. *IEEE Trans Automat Contr* 30(2):158–161
25. Mori T, Kokame H (1989) Stability of $x(t) = ax(t) + bx(t - \tau)$. *IEEE Trans Automat Contr* 34(4):460–462
26. Niculescu S (2001) Delay effects on stability: a robust control approach, vol 269. Springer, Heidelberg
27. Niculescu S, Nito T, Dion J, Dugard L (1995) Delay-dependent stability of linear systems with delayed state: an LMI approach. In: Decision and control, proceedings of the 34th IEEE conference on, IEEE, vol 2, pp 1495–1496
28. Niculescu S, Verriest E, Dugard L, Dion J (1998) Stability and robust stability of time-delay systems: a guided tour. *Stability and control of time-delay systems* pp 1–71
29. Packard A (1994) Gain scheduling via linear fractional transformations. *Syst Contr Lett* 22(2):79–92
30. Park P (1999) A delay-dependent stability criterion for systems with uncertain time-invariant delays. *IEEE Trans Automat Contr* 44(4):876–877
31. Phoojaruenchanachai S, Furuta K (1992) Memoryless stabilization of uncertain linear systems including time-varying state delays. *IEEE Trans Automat Contr* 37(7):1022–1026
32. Richard J (2003) Time-delay systems: an overview of some recent advances and open problems. *Automatica* 39(10):1667–1694
33. Su T, Huang C (1992) Robust stability of delay dependence for linear uncertain systems. *IEEE Trans Automat Contr* 37(10):1656–1659
34. Sun M, Jia Y, Du J, Yuan S (2008) Delay-dependent \mathcal{H}_∞ control for LPV systems with time delays. *Int J Syst Contr Commun* 1(2):256–265
35. Tan K (2000) Linear matrix inequality optimization methods for control of parameter varying mechanical systems. PhD thesis, University of Houston
36. Tan K, Grigoriadis K (2000) $L_2 - L_2$ and $L_2 - L_\infty$ output feedback control of time-delayed LPV systems. In: Decision and control, proceedings of the 39th IEEE conference on, IEEE, vol 5, pp 4422–4427
37. Tan K, Grigoriadis K, Wu F (2003) \mathcal{H}_∞ and L_2 -to- L_∞ gain control of linear parameter-varying systems with parameter-varying delays. In: Control theory and applications, IEE proceedings, IET, vol 150, pp 509–17

38. Tuan H, Apkarian P, Nguyen T (2001) Robust and reduced-order filtering: new LMI-based characterizations and methods. *IEEE trans Signal process* 49(12):2975–2984
39. Verriest E (1994) Robust stability of time varying systems with unknown bounded delays. In: *Decision and control, 1994, Proceedings of the 33rd IEEE conference on, IEEE, vol 1, pp 417–422*
40. Wang J, Wang C, Yuan W (2004) A novel \mathcal{H}_∞ output feedback controller design for LPV systems with a state-delay. *Nature Sci* 2(1):53–60
41. Watanabe K, Nobuyama E, Kojima A (1996) Recent advances in control of time delay systems - a tutorial review. In: *Decision and control, 1996, Proceedings of the 35th IEEE, IEEE, vol 2, pp 2083–2089*
42. Wu F (2001) Delay dependent induced L_2 norm analysis and control for LPV systems with state delays. In: *International mechanical engineering congress and exposition, proceedings of the 2001, ASME*
43. Wu F, Grigoriadis K (2001) LPV Systems with parameter-varying time delays: analysis and control. *Automatica* 37(2):221–229
44. Wu F, Yang X, Packard A, Becker G (1996) Induced L_2 -norm control for LPV systems with bounded parameter variation rates. *Int J Robust Nonlinear Contr* 6(9-10):983–998
45. Wu M, He Y, She J, Liu G (2004) Delay-dependent criteria for robust stability of time-varying delay systems. *Automatica* 40(8):1435–1439
46. Xu S, Lam J, Zou Y (2006) New results on delay-dependent robust \mathcal{H}_∞ control for systems with time-varying delays. *Automatica* 42(2):343–348
47. Zhang F, Grigoriadis K (2005) Delay-dependent stability analysis and \mathcal{H}_∞ control for state-delayed lpv system. In: *Intelligent Control, 2005. Proceedings of the 2005 IEEE international symposium on, mediterranean conference on control and automation, IEEE, pp 1532–1537*
48. Zhang X, Tsiotras P, Knospe C (2002) Stability analysis of LPV time-delayed systems. *Int J Contr* 75(7):538–558
49. Zhong Q (2006) *Robust control of time-delay systems*. Springer, London

Part III
Recent Applications of LPV Methods
in the Control of Complex Systems

Chapter 12

Structured Linear Parameter Varying Control of Wind Turbines

Fabiano Daher Adegas, Christoffer Sloth, and Jakob Stoustrup

Abstract High performance and reliability are required for wind turbines to be competitive within the energy market. To capture their nonlinear behavior, wind turbines are often modeled using parameter-varying models. In this chapter, a framework for modelling and controller design of wind turbines is presented. We specifically consider variable-speed, variable-pitch wind turbines with faults on actuators and sensors. Linear parameter-varying (LPV) controllers can be designed by a proposed method that allows the inclusion of faults in the LPV controller design. Moreover, the controller structure can be arbitrarily chosen: static output feedback, dynamic (reduced order) output feedback, decentralized, among others. The controllers are scheduled on an estimated wind speed to manage the parameter-varying nature of the model and on information from a fault diagnosis system. The optimization problems involved in the controller synthesis are solved by an iterative LMI-based algorithm. The resulting controllers can also be easily implemented in practice due to low data storage and simple math operations. The performance of the LPV controllers is assessed by nonlinear simulations results.

12.1 Introduction

Motivated by environmental concerns and the depletion of fossil fuels, as well its mature technological status, wind energy consolidate as a viable sustainable energy source for the decades to come. Over the past 20 years, the global installed capacity

F.D. Adegas (✉) • J. Stoustrup
Department of Electronic Systems, Aalborg Universitet, Fredrik Bajers Vej 7C, Aalborg,
Denmark
e-mail: fda@es.aau.dk; jakob@es.aau.dk

C. Sloth
Department of Computer Science, Aalborg Universitet, Selma Lagerlöfs Vej 300, Aalborg,
Denmark
e-mail: csloth@cs.aau.dk

J. Mohammadpour and C.W. Scherer (eds.), *Control of Linear Parameter Varying Systems with Applications*, DOI 10.1007/978-1-4614-1833-7_12,
© Springer Science+Business Media, LLC 2012

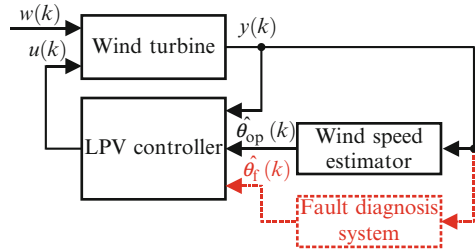
of wind power increased at an average annual growth of more than 25% from around 2.5 GW in 1992 to just under 200 GW at the end of 2010 [14]. Due to ongoing improvements in the wind turbine efficiency and reliability, and higher fuel prices, the cost of electricity produced (COE), which, roughly speaking, takes into account the annual energy production, lifetime of wind turbines, and Operation and Maintenance costs, is becoming economically competitive with conventional power production.

Automatic control is one of the engineering areas that significantly contributed to reduce the cost of wind-generated electricity. In order to reduce COE, a modern wind turbine is not only controlled to maximize energy production but also to minimize mechanical loads. The controlled system also has to comply with external requirements, such as acoustic noise emissions and power quality grid codes. Since many wind turbines are installed at remote locations, the introduction of fault-tolerant control is considered a suitable way of improving reliability/availability and lowering costs of repairs. Finally, the lack of accurate models must be alleviated by robust control strategies capable of securing stability and satisfactory performance despite model uncertainties [19].

From a control point of view, a wind turbine is a challenging system since the wind, which is the energy source driving the machine, is a poorly known stochastic disturbance. Add to that wind turbines inherently exhibit time-varying nonlinear dynamics along their nominal operating trajectory, motivating the use of advanced control techniques such as gain-scheduling, to counteract performance degradation or even instability problems by continuously adapting to the dynamics of the plant. Wind turbine controllers typically consist of multiple gain-scheduled controllers, which are designed to operate in the proximity of a certain operating point. The gain-scheduling approach for industry-standard classical controllers can be either based on switching or interpolation of controller gains [7, 8]. Controller structure may also change by either switching [7] or bumpless transfer [17, 25] according to the wind speed experienced by the wind turbine. The underlying assumption for such control schemes is that parameters only change slowly compared to the system dynamics, which is generally not satisfied in turbulent winds. Additionally, classical gain-scheduling controllers only ensure performance guarantees and stability at the operating points where the linear controllers are designed [22].

A systematic way of designing controllers for systems with linearized dynamics that vary significantly with the operating point is within the framework of linear parameter-varying (LPV) control. An LPV controller can be synthesized after solving an optimization problem subject to linear matrix inequality (LMI) constraints. In control systems for wind turbines, robustness and fault-tolerance capabilities are important properties, which should be considered in the design process, calling for a generic and powerful tool to manage parameter variations and model uncertainties. In this chapter, design procedures for nominal controllers for parameter-varying models as well as active/passive fault-tolerance, are provided. The framework can be trivially extended to design controllers robust to uncertainties in the model [1], e.g., aerodynamic uncertainties [26]. Indeed, handling known parameter dependencies, unknown parameter variations, and faults, constitute the main challenges for the application of wind turbine control.

Fig. 12.1 Block diagram of the controller structures. The black boxes are common to the LPV controllers, while the red dashed box illustrates the fault diagnosis system required by the AFTC



An overview of the proposed control structure is illustrated by the block diagram depicted in Fig. 12.1, where $u(k)$ is the control signal and $w(k)$ is the disturbance. The LPV controllers depend on the measurements $y(k)$ and an estimate of the current operating point, $\hat{\theta}_{\text{op}}(k)$, which is used as scheduling parameter. Additionally, a fault diagnosis system provides the scheduling parameter $\hat{\theta}_{\text{f}}(k)$ for the active fault-tolerant controller (AFTC). The extra degree of freedom added by allowing the AFTC to adapt in case of a fault may introduce less conservatism than for the passive fault-tolerant controller. The AFTC is a conventional LPV controller scheduled on $\theta_{\text{op}}(t)$ and $\theta_{\text{f}}(t)$; the reason for denoting it an active fault-tolerant controller arises from the origin of the scheduling parameters.

The list of faults occurring in wind turbines is extensive, reflecting the complexity of the machines. On a system level, faults occur in sensors, actuators, and system components, ranging from slow gradual faults to abrupt component failures. The occurrence of faults may change the system behavior dramatically. This motivates us to develop methods for fault diagnosis and fault-tolerant control, offering several benefits:

- Prevent catastrophic failures and faults from deteriorating other parts of the wind turbine, by early fault detection and accommodation.
- Reduce maintenance costs by providing remote diagnostic details and avoiding replacement of functional parts, by applying condition-based maintenance instead of time-based maintenance.
- Increase energy production when a fault has occurred by means of fault-tolerant control.

This chapter gives an overview of the most common faults that can be modelled as varying parameters. For a clear exposure, the fault-tolerant controller is designed to cope with the simple case of a single fault: altered dynamics of the hydraulic pitch system due to low hydraulic pressure. The fault is a gradual fault affecting the control actions of the turbine. The method used also applies to fast parameter variations, i.e., abrupt faults in the extreme case [12].

Realizing advanced gain-scheduled controllers can in practice be difficult and may lead to numerical challenges [19, 21]. Several plant and controller matrices must be stored on the controller memory. Moreover, matrix factorizations and inversions are among the operations that must be done online by the controller at each sampling time [4, 5].

The synthesis procedures presented in this chapter are serious candidates for solving a majority of practical wind turbine control problems, provided a sufficiently good model of the wind turbine is available. We believe that the resulting controller can also be easily implemented in practice due to the following reasons:

- (A.1) *Structured controller*: the controller structure can be chosen arbitrarily. Decentralized of any order, dynamic (full or reduced-order) output feedback, static output, and full state feedback are among the possible structures. This is in line with the current control philosophy within wind industry.
- (A.2) *Low data storage*: the required data to be stored in the control computer memory is only the controller matrices, and scalar functions of the scheduling variables representing plant nonlinearities (basis functions).
- (A.3) *Simple math operations*: the mathematical operations needed to compute the controller gains at each sampling time are look-up tables with interpolation, products between a scalar and a matrix, and sums of matrices.

The versatile controller structure and facilitated implementation comes with a price. Due to the (possible) nonconvex characteristics of the synthesis problem, the controller design is solved by an iterative LMI optimization algorithm that may be demanding from a computational point of view. However, the authors consider that it is worth to transfer the computational burden from the controller implementation to the controller design.

The chapter is organized as follows. Section 12.2 describes the LPV wind turbine plant modeling including typical faults and uncertainties. The LPV controller design procedure, based on an iterative LMI optimization algorithm, is presented in Sect. 12.3. Section 12.4 contains a design example on how state of the art industrial controllers can be designed within the LPV framework. A fault-tolerant gain-scheduled PI pitch controller for the full load region is designed and compared to a gain-scheduled controller without fault accommodation capabilities. Simulation results presented in the same section compares the performance of both LPV controllers to show that pitch actuator faults due to low pressure can be accommodated by the fault-tolerant LPV controller, avoiding the shutdown of the wind turbine. Section 12.5 concludes the paper.

12.2 Wind Turbine LPV model

In this section, an LPV model is derived from a nonlinear time-varying wind turbine model. The nonlinear model consists of several subsystems, namely aerodynamics, the tower, the drive train, the generator, the pitch system, and the converter actuator. The interconnection of the wind turbine submodels is illustrated in Fig. 12.2. For simulation purposes, the wind disturbance input, $V(t)$, is provided by a wind model which includes both tower shadow and wind shear [11] together with a turbulence model [13]. The detailed description of the model is provided in [12]. The submodels are individually described in the sequel.

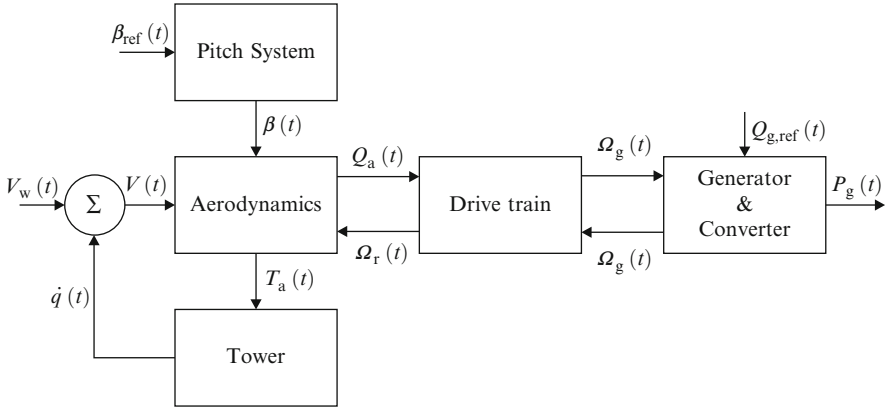


Fig. 12.2 Sub-model-level block diagram of a variable-speed variable-pitch WT

12.2.1 Wind Model

The driving force of a wind turbine is generated by the wind. Therefore, a model of this external input to the wind turbine, $V_w(t)$, has to be provided.

Generally, the wind speed is influenced by several components, which depend on the environment where the wind turbine is located; however, we restrict our model to include only three effects: wind shear, tower shadow, and turbulence. A more thorough wind model can be found in [12]. We will not provide a detailed description of the wind model, but only explain its three components briefly.

Wind shear is caused by the ground and other obstacles in the path of the wind, which cause frictional forces to act on the wind. The frictional forces imply that the mean wind speed becomes dependent on the height above ground level. Therefore, the mean wind speed depends on the location of the three blades. When a blade is located in front of the tower, the lift on that blade decreases because the tower reduces the effective wind speed. This phenomenon is called tower shadow and implies that the force acting on each blade decreases every time a blade is located in front of the tower. Finally, the variations in the wind speed, which are not included in the mean wind speed, are called turbulence and are caused by multiple factors. The utilized turbulence model is based on the Kaimal spectrum that describes the turbulence of a point wind. Since the wind model describes the wind speed averaged over the entire rotor plane, a low-pass filter is applied to smooth the wind speed signal. Figure 12.3 shows an output of the wind model $V_w(t)$. Note that a detailed description of the wind model can be found in [12].

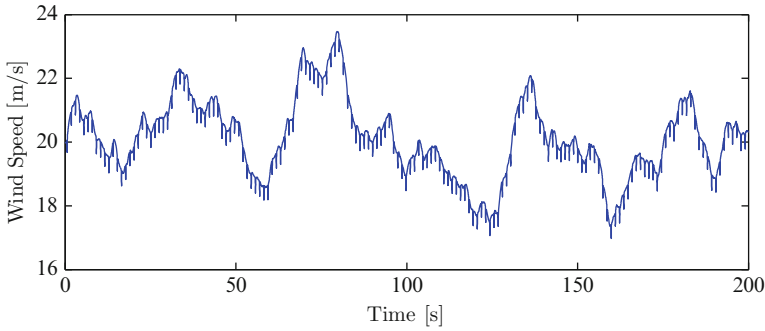


Fig. 12.3 Output of the wind model at a constant rotor speed. The periodic decrease of the wind speed is caused by tower shadow

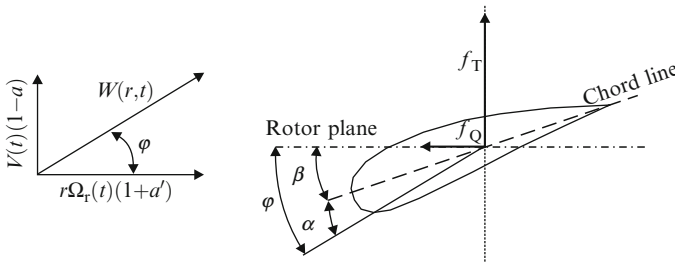


Fig. 12.4 Forces on a blade element

12.2.2 Nonlinear Model

The rotor of a wind turbine converts kinetic energy of the wind into rotational energy of the rotor blades and shaft. Aerodynamic forces over the rotor blades are often determined with the assumptions of blade element momentum (BEM) theory [15]. Figure 12.4 illustrates the forces and velocity vectors on a blade element.

Assuming a symmetric aerodynamic rotor driven by a uniform inflow, and neglecting unsteady aerodynamic effects, the local tangential f_Q and axial f_T forces along the local blade radius r are given by

$$f_Q = \frac{1}{2} \rho c(r) W^2(r,t) \left(C_L(r, \alpha(r,t)) \sin \varphi(r,t) - C_D(r, \alpha(r,t)) \cos \varphi(r,t) \right) \text{ [N]},$$

$$f_T = \frac{1}{2} \rho c(r) W^2(r,t) \left(C_L(r, \alpha(r,t)) \sin \varphi(r,t) + C_D(r, \alpha(r,t)) \cos \varphi(r,t) \right) \text{ [N]}$$

with the squared local inflow velocity $W^2(r, t)$, local angle of attack $\alpha(r, t)$ and local inflow angle $\varphi(r, t)$ described as

$$\begin{aligned} W^2(r, t) &= (V(t)(1 - a(r)))^2 + (r\Omega_r(t)(1 + a'(r)))^2 \quad [\text{m}^2/\text{s}^2], \\ \alpha(r, t) &= \varphi(r, t) - \phi(r) - \beta(t) \quad [^\circ], \\ \varphi(r, t) &= \tan^{-1} \left(V(t)(1 - a(r)) (r\Omega_r(t)(1 + a'(r)))^{-1} \right) \quad [^\circ]. \end{aligned}$$

In the above expressions, ρ is the air density, $c(r)$ is the local chord length, $C_L(r, \alpha)$ and $C_D(r, \alpha)$ are the local steady-state lift and drag coefficients, $V(t)$ is a mean wind speed over the rotor disk, $\Omega_r(t)$ is the rotor speed, $a(r)$ and $a'(r)$ are the axial and tangential flow induction factors, respectively, $\phi(r)$ is the local chord twist angle along the blade, and $\beta(t)$ is the blade pitch angle.

In the aerodynamic model, we assume that a yawing system exists, which always keeps the rotor plane perpendicular to the direction of the wind; hence, $V(t)$ is always perpendicular to the rotor plane. However, as the rotor rotates the resulting wind speed at a blade, called the inflow velocity $W(r, t)$, has an angle φ with respect to the rotor plane. The drag force given by $1/2\rho cW^2C_D$ is defined to point in the opposite direction as $W(r, t)$ and the lift force given by $1/2\rho cW^2C_L$ is perpendicular to drag force. Via projections of these forces, we obtain f_Q and f_T .

The aerodynamic torque Q_a and thrust force T_a produced by the rotor can be expressed as the summation of the forces over the B number of rotor blades

$$Q_a(V, \Omega_r, \beta, a, a') = B \int_0^R f_Q(r, V, \Omega_r, \beta, a(r), a'(r)) r dr \quad [\text{Nm}], \quad (12.1a)$$

$$T_a(V, \Omega_r, \beta, a, a') = B \int_0^R f_T(r, V, \Omega_r, \beta, a(r), a'(r)) dr \quad [\text{N}]. \quad (12.1b)$$

After integration, the aerodynamic torque and thrust are represented as

$$Q_a(t) = \frac{1}{2\Omega_r(t)} \rho AV^3(t) C_P(\lambda(t), \beta(t)) \quad [\text{Nm}], \quad (12.2a)$$

$$T_a(t) = \frac{1}{2} \rho AV^2(t) C_T(\lambda(t), \beta(t)) \quad [\text{N}] \quad (12.2b)$$

with the tip-speed ratio denoting the ratio between the blade tip and the mean wind speed

$$\lambda(t) = \frac{\Omega_r(t)R}{V(t)} \quad [:],$$

where R is the rotor radius and $A = \pi R^2$ is the rotor swept area. The power coefficient $C_P(\lambda, \beta)$ and thrust coefficient $C_T(\lambda, \beta)$ are smooth surfaces usually given in tabular form. Figure 12.5 depicts C_P and C_T surfaces of a typical 2 MW wind turbine.

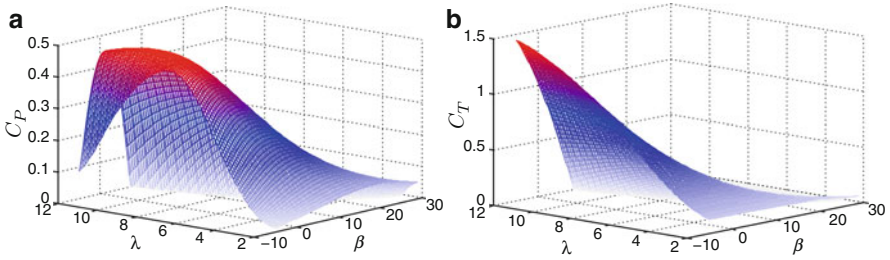


Fig. 12.5 Power and thrust coefficients of a typical utility-scale wind turbine. (a) Power coefficient (b) Thrust coefficient

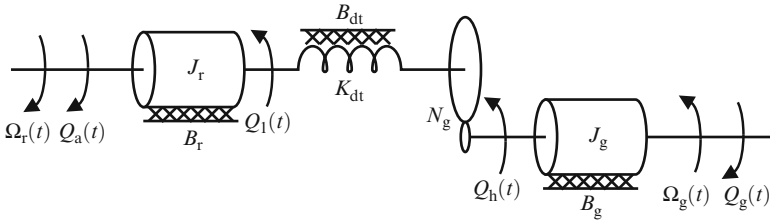


Fig. 12.6 Diagram of the drive train of the wind turbine

Aerodynamic torque Q_a drives a drive train model consisting of a low-speed shaft and a high-speed shaft having inertias J_r and J_g , and friction coefficients B_r and B_g . The shafts are interconnected by a transmission having gear ratio N_g , combined with torsion stiffness K_{dt} , and torsion damping B_{dt} . This results in a torsion angle, $\theta_{\Delta}(t)$, and a torque applied to the generator, $Q_g(t)$, at a speed $\Omega_g(t)$. The model of the drive train is shown in Fig. 12.6 and given by

$$J_r \dot{\Omega}_r(t) = Q_a(t) + \frac{B_{dt}}{N_g} \Omega_g(t) - K_{dt} \theta_{\Delta}(t) - (B_{dt} + B_r) \Omega_r(t) \quad [\text{Nm}], \quad (12.3a)$$

$$J_g \dot{\Omega}_g(t) = \frac{K_{dt}}{N_g} \theta_{\Delta}(t) + \frac{B_{dt}}{N_g} \Omega_r(t) - \left(\frac{B_{dt}}{N_g^2} + B_g \right) \Omega_g(t) - Q_g(t) \quad [\text{Nm}], \quad (12.3b)$$

$$\dot{\theta}_{\Delta}(t) = \Omega_r(t) - \frac{1}{N_g} \Omega_g(t) \quad [\text{rad/s}]. \quad (12.3c)$$

The thrust T_a acting on the rotor introduces fore–aft tower bending described by the axial nacelle linear translation $q(t)$. Sideward movements are ignored by neglecting yawing and drive train reaction torque on the tower. The tower translates in the same direction as the wind; therefore, aerodynamic torque and thrust are in

fact driven by the relative wind speed $V(t) = V_w(t) - \dot{q}(t)$. The tower dynamics is modeled as a mass-spring-damper system

$$M_t \ddot{q}_t(t) = T_a(t) - B_t \dot{q}_t(t) - K_t q_t(t), \quad (12.4)$$

where M_t is the modal mass of the first fore–aft tower bending mode, B_t is structural damping coefficient, and K_t is the modal stiffness for axial nacelle motion due to fore–aft tower bending.

Hydraulic pitch systems are satisfactorily modeled as a second order system with a time delay, t_d , and reference angle $\beta_{\text{ref}}(t)$

$$\ddot{\beta}(t) = -2\zeta \omega_n \dot{\beta}(t) - \omega_n^2 \beta(t) + \omega_n^2 \beta_{\text{ref}}(t - t_d), \quad (12.5)$$

where the natural frequency, ω_n , and damping ratio, ζ , specify the dynamics of the model. To represent the limitations of the pitch actuators, for simulation purposes the model includes constraints on the slew rate and the range of the pitch angle.

Electric power is generated by the generator, while a power converter interfaces the wind turbine generator output with the utility grid and controls the currents in the generator. The generator torque in (12.6) is controlled by the reference $Q_{g,\text{ref}}(t)$. The converter dynamics are approximated by a first order system with time constant τ_g and time delay $t_{g,d}$

$$\dot{Q}_g(t) = -\frac{1}{\tau_g} Q_g(t) + \frac{1}{\tau_g} Q_{g,\text{ref}}(t - t_{g,d}). \quad (12.6)$$

Just as for the model of the pitch system, the slew rate and the operating range of the generator torque are both bounded to match the limitations of the real system. The power produced by the generator can be approximated from the mechanical power calculated in (12.7), where η_g denotes the efficiency of the generator, which is assumed constant

$$P_g(t) = \eta_g \Omega_g(t) Q_g(t). \quad (12.7)$$

12.2.3 Linear Varying Parameters

From the model description, it is clear that a wind turbine is a nonlinear, time-varying system. What is not apparent is how to find an LPV description that captures this dynamic behavior. Wind turbines can be represented as Quasi-LPV models [6, 19] and Linear Fractional Transformation models [19], but the most common approach relies on the classical linearization around equilibrium or operating points resulting in a linearized LPV model [5, 19, 21]. The latter approach is adopted in this chapter.

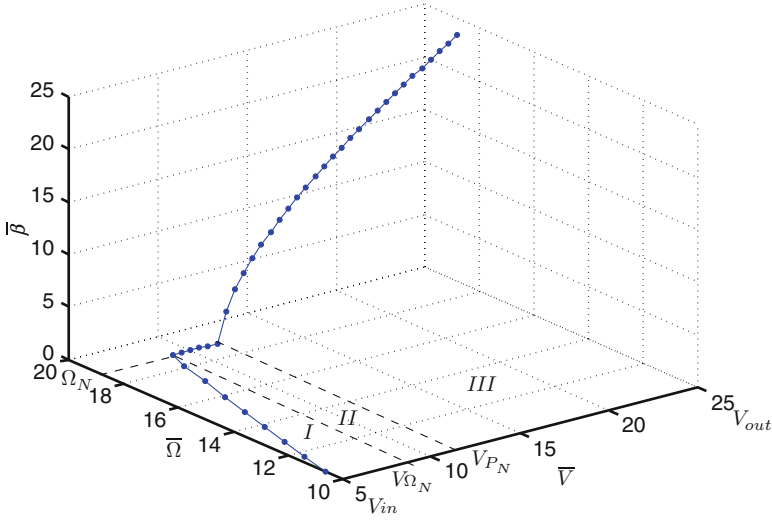


Fig. 12.7 Operating locus of a typical utility-scale wind turbine

12.2.3.1 Aerodynamics

The underlying assumption of a wind turbine LPV model based on linearization is that wind speed, rotor speed, and pitch angle can be described by slow and fast components

$$V(t) = \bar{V}(t) + \hat{V}(t), \quad \Omega_r(t) = \bar{\Omega}_r(t) + \hat{\Omega}_r(t), \quad \beta(t) = \bar{\beta}(t) + \hat{\beta}(t),$$

The collection of operating points $(\bar{V}, \bar{\Omega}, \bar{\beta})$ is what defines the control strategy of a wind turbine, selected to match steady-state requirements such as maximize energy capture, minimize static loads, and limit noise emissions.

A typical control strategy of a generic 2 MW wind turbine is depicted in Fig. 12.7. A more detailed treatment of different operating strategies for wind turbines [5, 7] is outside the scope of this chapter. Three subareas on a typical control strategy can be distinguished:

- (A.1) On Region I (V_{in} to V_{Ω_N}) the energy capture is maximized by keeping the aerodynamic efficiency as high as possible. This can be accomplished by tracking a rotational speed set point using generator torque as the control input variable. Pitch actuation is not utilized for tracking purposes; the pitch angle remains at the value of maximum aerodynamic efficiency. With only one input and one output to be controlled, a multivariable controller is not necessary on this region. Notice that $\bar{\Omega}$ is proportional to \bar{V} as a consequence of optimal aerodynamic efficiency.

- (A.2) On Region II (V_{Ω_N} to V_{P_N}), the wind turbine maintains constant rotational speed at a nominal value Ω_N , by acting on the generator torque. The rotational speed is limited due to acoustic noise emission limits. Pitch actuation remains unused. A multivariable controller is still not needed.
- (A.3) On Region III (V_{P_N} to V_{out}), rated power P_N is reached and the main goal is to minimize power fluctuations. Small fluctuations on the generator torque around rated value add damping to the drive train torsional mode and fine control the electrical power. Therefore, pitch angle should be gradually increased as wind speed rises to limit generated power by lowering the rotor aerodynamic efficiency. In some wind turbines, active tower damping is also implemented on this region.

A linearization-based LPV model is obtained by classical linearization around the operating points given by the control strategy. The aerodynamic model is exclusively the source of time-varying nonlinearities. A first order Taylor series expansion of (12.2) leads to the following linearized representations of torque and thrust:

$$Q_a \approx \bar{Q}_a(\bar{V}, \bar{\Omega}, \bar{\beta}) + \left. \frac{\partial Q_a}{\partial V} \right|_{(\bar{V}, \bar{\Omega}, \bar{\beta})} \hat{V} + \left. \frac{\partial Q_a}{\partial \Omega_r} \right|_{(\bar{V}, \bar{\Omega}, \bar{\beta})} \hat{\Omega}_r + \left. \frac{\partial Q_a}{\partial \beta} \right|_{(\bar{V}, \bar{\Omega}, \bar{\beta})} \hat{\beta}, \quad (12.8a)$$

$$T_a \approx \bar{T}_a(\bar{V}, \bar{\Omega}, \bar{\beta}) + \left. \frac{\partial T_a}{\partial V} \right|_{(\bar{V}, \bar{\Omega}, \bar{\beta})} \hat{V} + \left. \frac{\partial T_a}{\partial \Omega_r} \right|_{(\bar{V}, \bar{\Omega}, \bar{\beta})} \hat{\Omega}_r + \left. \frac{\partial T_a}{\partial \beta} \right|_{(\bar{V}, \bar{\Omega}, \bar{\beta})} \hat{\beta}, \quad (12.8b)$$

where $\bar{Q}_a(\bar{V}, \bar{\Omega}, \bar{\beta})$ and $\bar{T}_a(\bar{V}, \bar{\Omega}, \bar{\beta})$ are equilibrium components of the aerodynamic torque and thrust, respectively. The partial derivatives of Q_a and T_a are given by

$$\begin{aligned} \frac{\partial Q_a}{\partial V} &= \frac{\rho AV^2}{2\Omega_r} \left(3C_P + V \frac{\partial C_P}{\partial \lambda} \frac{\partial \lambda}{\partial V} \right), & \frac{\partial T_a}{\partial V} &= \frac{\rho AV}{2} \left(2C_T + V \frac{\partial C_T}{\partial \lambda} \frac{\partial \lambda}{\partial V} \right), \\ \frac{\partial Q_a}{\partial \Omega_r} &= \frac{\rho AV^3}{2\Omega_r} \left(\frac{\partial C_P}{\partial \lambda} \frac{\partial \lambda}{\partial \Omega_r} - \frac{C_P}{\Omega_r} \right), & \frac{\partial T_a}{\partial \Omega_r} &= \frac{\rho AV^2}{2} \frac{\partial C_T}{\partial \lambda} \frac{\partial \lambda}{\partial \Omega_r}, \\ \frac{\partial Q_a}{\partial \beta} &= \frac{\rho AV^3}{2\Omega_r} \frac{\partial C_P}{\partial \beta}, & \frac{\partial T_a}{\partial \beta} &= \frac{\rho AV^2}{2} \frac{\partial C_T}{\partial \beta}, \end{aligned} \quad (12.9)$$

and must be evaluated at the time-varying equilibrium point $(\bar{V}, \bar{\Omega}, \bar{\beta})$. The partial derivatives of a typical 2 MW wind turbine for the whole operational envelope are depicted in Fig. 12.8. The aerodynamic partial derivatives given by (12.9), hereafter also referred to as aerodynamic gains, are varying parameters in an LPV wind turbine model.

With the assumption that the wind turbine is operating on the nominal trajectory specified in Fig. 12.7, the equilibrium values for pitch angle and rotor/generator speed can be described uniquely by the wind speed, e.g., $\bar{\Omega}(\bar{V})$, $\bar{\beta}(\bar{V})$. This means that the wind turbine can be described by an LPV model scheduled on wind speed only

$$\theta_{op}(t) := \bar{V}(t). \quad (12.10)$$

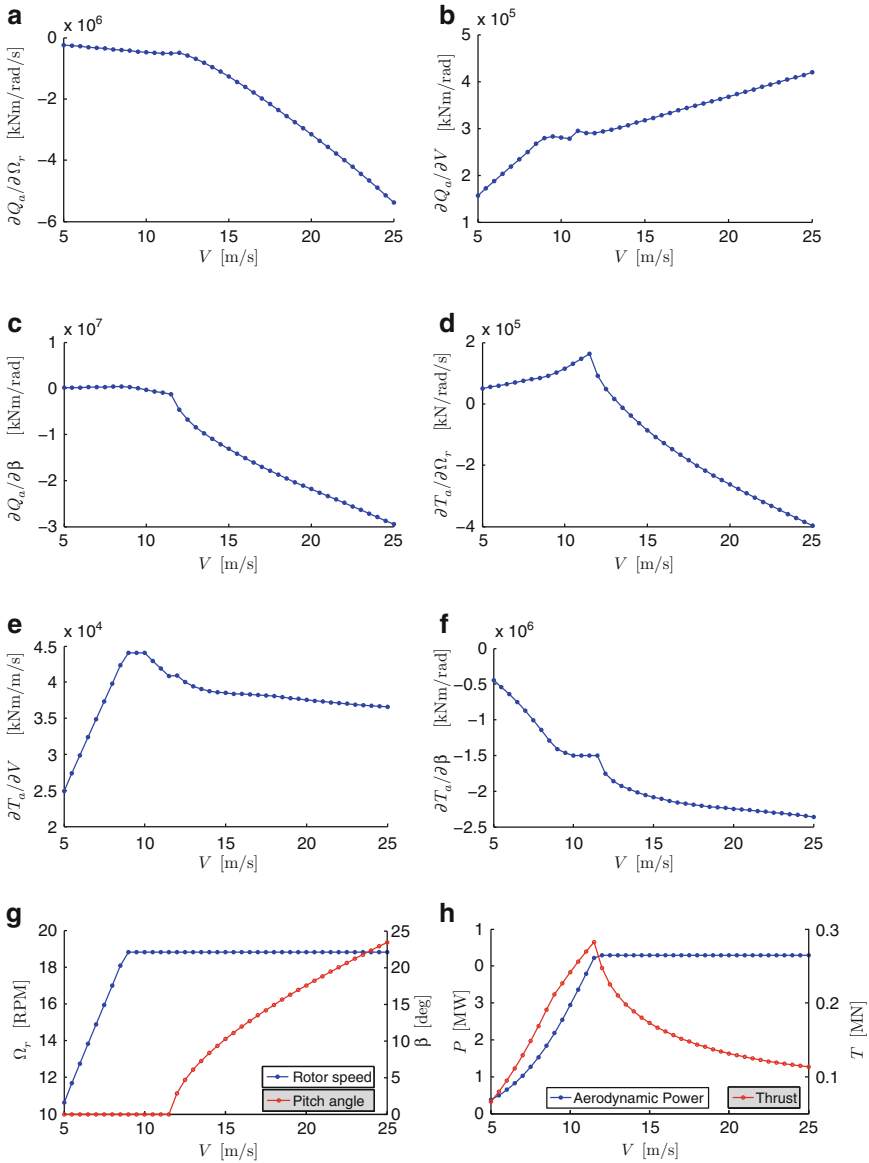


Fig. 12.8 Aerodynamic parameters of a typical 2 MW wind turbine. (a) From rotor speed to torque (b) From wind speed to torque (c) From pitch angle to torque (d) From rotor speed to thrust (e) From wind speed to thrust (f) From pitch angle to thrust (g) Rotor speed and pitch angle (h) Power and thrust

Depending on the region of interest in the control strategy and the model complexity, the varying parameters can be approximated as an explicit function of the scheduling variable. An affine representation is always preferable to diminish the computational cost of solving an LMI-constrained optimization. If tower dynamics are omitted and the aim is to design a controller for Region III, the aerodynamic torque gains can be fairly well approximated by a linear function of the wind speed. In this case, the parameter variations in the nominal LPV plant model are approximated using an affine description in the wind speed [26]. If tower dynamics are taken into account, the aerodynamic gains can be fairly approximated by polynomial functions in Region III. For the most general case, which is the design of a single LPV controller covering the full control strategy locus, representing the aerodynamic gains by polynomials is difficult and one has to resort to grid-based methods at high computational cost [5, 21].

On most wind turbines, the wind speed is measured by an anemometer on the nacelle, which only measures the wind speed at a single point in space and is affected by the presence of the rotor. Therefore, this measurement is not a good estimate of (12.10). To obtain the wind speed for scheduling purposes, an effective wind speed estimator must be designed [20]. The effective wind speed is defined as the spatial average of the wind field over the rotor plane with the wind stream being unaffected by the wind turbine. By inspecting the output of wind models and real field measurements, we determine the rate bounds on the effective wind speed $\hat{\theta}_{\text{op}}(t)$ to be -2 m/s^2 and 2 m/s^2 .

12.2.3.2 Faults

Faults in a wind turbine have different degrees of severity and accommodation requirements. A safe and fast shutdown of the wind turbine is necessary to some of them, while to others the system can be reconfigured to continue power generation. Linear parameter varying control can be applied in the case of failures that gradually change system's dynamics. The most common faults along with their magnitude and the rate at which they can be introduced are summarized in Table 12.1.

Pitch position and generator speed measurements are the sensors most affected by failures. Originated by either electrical or mechanical anomalies, they can result in either a bias or a gain factor on the measurements. A biased pitch sensor measurement affects both the pitch system model and the pitch angle measurement. When the bias is introduced, the pitch actuator model and measurement equation are modified as

$$\ddot{\beta}(t) = -2\zeta\omega_n\dot{\beta}(t) - \omega_n^2(\beta(t) + \beta_{\text{bias}}(t)) + \omega_n^2\beta_{\text{ref}}(t - t_d), \quad (12.11a)$$

$$\beta_{\text{mes}}(k) = \beta(k) + \beta_{\text{bias}}(k) + v_{\beta}(k), \quad (12.11b)$$

where $v_{\beta}(k)$ is a measurement noise. A bias can either be a result of inaccurate calibration of the pitch system or be an gradual fault.

Table 12.1 Specification of ranges and rate limits of gradual faults

Fault	Specification
Pitch sensor	
Bias	$\dot{\beta}_{\text{bias}}(t) \in [-1^\circ/\text{month}, 1^\circ/\text{month}]$ $\beta_{\text{bias}}(t) \in [-7^\circ, 7^\circ]$
Pitch actuator	
High air content	$\dot{\theta}_{\text{ha}}(t) \in [-1/\text{month}, 1/\text{month}]$ $\theta_{\text{ha}}(t) \in [0, 1]$
Pump wear	$\dot{\theta}_{\text{pw}}(t) \in [0, 1/(20 \text{ years})]$ $\theta_{\text{pw}}(t) \in [0, 1]$
Hydraulic leakage	$\dot{\theta}_{\text{hl}}(t) \in [0, 1/(100 \text{ s})]$ $\theta_{\text{hl}}(t) \in [0, 1]$
Pressure drop	$\dot{\theta}_{\text{pd}}(t) \in [-0.033/\text{s}, 0.033/\text{s}]$ $\theta_{\text{pd}}(t) \in [0, 1]$
Generator speed sensor	
Proportional error	$\dot{\theta}_{\text{pe}}(t) \in [-1/\text{month}, 1/\text{month}]$ $\theta_{\text{pe}}(t) \in [-0.1, 0.1]$

A proportional error on the generator speed sensor changes the sensor gain. The measurement equation

$$\Omega_{\text{g,mes}}(k) = (1 + \theta_{\text{pe}}(k)) \Omega_{\text{g}}(k) + v_{\Omega_{\text{g}}}(k) \quad (12.12)$$

is a linear function of the gain deviation θ_{pe} , where $v_{\Omega_{\text{g}}}(k)$ is a measurement noise.

The power converter and pitch systems are the actuators most likely to fail. Power converter faults can result in an offset of the generated torque due to an offset in the internal converter control loops. An offset in the internal converter control loops modifies the generator and converter model as follows:

$$\dot{T}_{\text{g}}(t) = -\frac{1}{\tau_{\text{g}}}(Q_{\text{g}}(t) + Q_{\text{g,bias}}(t)) + \frac{1}{\tau_{\text{g}}}T_{\text{g,ref}}(t - t_{\text{g,d}}), \quad (12.13)$$

where $Q_{\text{g,bias}}(t)$ is an offset of the generated torque.

A fault changes the dynamics of the pitch system by varying the damping ratio and natural frequency from their nominal values ζ_0 and $\omega_{\text{n},0}$ to their faulty values ζ_{f} and $\omega_{\text{n},\text{f}}$. The dynamics of the pitch system can then be represented as

$$\ddot{\beta}(t) = -2\zeta(\theta_{\text{f}})\omega_{\text{n}}(\theta_{\text{f}})\dot{\beta}(t) - \omega_{\text{n}}^2(\theta_{\text{f}})\beta(t) + \omega_{\text{n}}^2(\theta_{\text{f}})\beta_{\text{ref}}(t - t_{\text{d}}) \quad [^\circ/\text{s}^2] \quad (12.14)$$

with the parameters changing according to a convex combination of the vertices of the parameter sets [18]

$$\omega_{\text{n}}^2(\theta_{\text{f}}) = (1 - \theta_{\text{f}})\omega_{\text{n},0}^2 + \theta_{\text{f}}\omega_{\text{n},\text{lp}}^2, \quad (12.15\text{a})$$

$$-2\zeta(\theta_{\text{f}})\omega_{\text{n}}(\theta_{\text{f}}) = -2(1 - \theta_{\text{f}})\zeta_0\omega_{\text{n},0} - 2\theta_{\text{f}}\zeta_{\text{lp}}\omega_{\text{n},\text{lp}}, \quad (12.15\text{b})$$

Table 12.2 Parameters for the pitch system under different conditions

Fault	Parameters
No fault	$\omega_n = 11.11 \text{ rad/s}$, $\zeta = 0.6$
High air content in the oil	$\omega_{n,ha} = 5.73 \text{ rad/s}$, $\zeta_{ha} = 0.45$
Pump wear	$\omega_{n,pw} = 7.27 \text{ rad/s}$, $\zeta_{pw} = 0.75$
Hydraulic leakage	$\omega_{n,hl} = 3.42 \text{ rad/s}$, $\zeta_{hl} = 0.9$
Pressure drop	$\omega_{n,hl} = 3.42 \text{ rad/s}$, $\zeta_{hl} = 0.9$

The normal air content in the hydraulic oil is 7%, whereas high air content in the oil corresponds to 15%. Pump wear represents the situation of 75% pressure in the pitch system while the parameters stated for hydraulic leakage corresponds to a pressure of only 50%

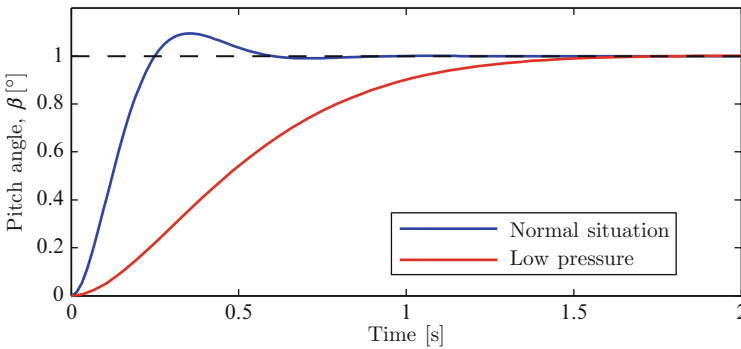


Fig. 12.9 Step responses of hydraulic pitch model under normal (*blue*) and fault (*red*) conditions

where $\theta_f \in [0, 1]$ is an indicator function for the fault with $\theta_f = 0$ and $\theta_f = 1$ corresponding to nominal and faulty conditions, respectively. Pitch system failures are usually occasioned by the following reasons:

- Pump Wear is introduced very slowly and results in low pump pressure. When $\theta_f(t) = 0$ the pump delivers the nominal pressure, but as $\theta_f(t)$ goes to one the pressure drops. Notice that $\dot{\theta}_f(t) \geq 0$ for all t , since the wear is irreversible without replacing the pump. The fault described by $\theta_f = 1$, corresponding to a pressure level of 75%, can emerge after approximately 20 years of operation.
- Hydraulic leakage is introduced considerably faster than pump wear. Again $\dot{\theta}_f(t) \geq 0$ for all t , since a leakage cannot be reversed without repair of the system. Notice that the pressure for $\theta_f = 1$ corresponds to 50% of the nominal pressure.
- High air content in the oil is a fault that, in contrast to pump wear and hydraulic leakage, may disappear; hence, $\dot{\theta}_f(t)$ can be both positive and negative. The extreme values caused by $\theta_f = 0$ and $\theta_f = 1$ correspond to air contents of 7% and 15% in the hydraulic oil.

Values for the natural frequency and damping ratio of the pitch system under faults are described in Table 12.2. Step responses for the normal and fault conditions in the case of high air content in the oil are illustrated in Fig. 12.9.

If a number n_{θ_f} of faults are considered on the modeling, θ_f denotes a vector of scheduling parameters

$$\theta_f = [\theta_{f,1}, \dots, \theta_{f,m}], \quad m = 1, \dots, n_{\theta_f}.$$

12.2.3.3 System Description

The synthesis of LPV controllers are posed similarly to the \mathcal{H}_∞ control of linear systems. The first step is to identify the input variable w known as disturbance or exogenous perturbation, and the fictitious output variable z called performance output or error. Next, weighting functions for these inputs and outputs are chosen, usually rational functions of the Laplace operator s stressing the frequencies of interest. The standard state-space interconnections of the LPV model of the plant and the weighting functions are called augmented plant, given by the general continuous-time LPV system description shown in (12.16)

$$\begin{aligned} \dot{x}(t) &= A(\theta(t))x(t) + B_w(\theta(t))w(t) + B_u(\theta(t))u(t), \\ z(t) &= C_z(\theta(t))x(t) + D_{zw}(\theta(t))w(t) + D_{zu}(\theta(t))u(t), \\ y(t) &= C_y(\theta(t))x(t) + D_{yw}(\theta(t))w(t), \end{aligned} \quad (12.16)$$

where $x(t) \in \mathbb{R}^n$ is the state vector, $w(t) \in \mathbb{R}^{n_w}$ is the vector of exogenous perturbation, $u(t) \in \mathbb{R}^{n_u}$ is the control input, $z(t) \in \mathbb{R}^{n_z}$ is the controlled output, and $y(t) \in \mathbb{R}^{n_y}$ is the measured output. $A(\cdot)$, $B(\cdot)$, $C(\cdot)$, $D(\cdot)$ are continuous functions of the time-varying parameter vector $\theta = [\theta_{\text{op}} \quad \theta_f]$.

Possible types of dependency of the aerodynamic gains on the scheduling parameters have already been discussed in the Aerodynamics subsection. The general case where no restrictions are imposed on the parameter dependence is treated here [4, 5]. It is necessary to choose scalar functions of the varying parameters such that the LPV model of the augmented plant (12.16) is affine in these functions. That is,

$$\begin{aligned} \begin{bmatrix} A(\theta) & B_w(\theta) & B_u(\theta) \\ C_z(\theta) & D_{zw}(\theta) & D_{zu}(\theta) \\ C_y(\theta) & D_{yw}(\theta) & D_{yu}(\theta) \end{bmatrix} &= \begin{bmatrix} A & B_w & B_u \\ C_z & D_{zw} & D_{zu} \\ C_y & D_{yw} & D_{yu} \end{bmatrix}_0 + \sum_i \begin{bmatrix} A & B_w & B_u \\ C_z & D_{zw} & D_{zu} \\ C_y & D_{yw} & D_{yu} \end{bmatrix}_i \rho_i(\theta), \\ &+ \sum_m \begin{bmatrix} A & B_w & B_u \\ C_z & D_{zw} & D_{zu} \\ C_y & D_{yw} & D_{yu} \end{bmatrix}_m \theta_{f,m}, \quad i = 1, \dots, n_\rho, \quad m = 1, \dots, n_{\theta_f}, \end{aligned} \quad (12.17)$$

where $\rho_i(\theta)$ are scalar functions known as basis functions. The aerodynamic partial derivatives are natural candidates for basis functions related to plant nonlinearities [5]

$$\begin{aligned}\rho_1(\theta) &:= \frac{1}{J_r} \left. \frac{\partial Q_a}{\partial \Omega} \right|_{\bar{V}}, & \rho_2(\theta) &:= \frac{1}{J_r} \left. \frac{\partial Q_a}{\partial V} \right|_{\bar{V}}, & \rho_3(\theta) &:= \frac{1}{J_r} \left. \frac{\partial Q_a}{\partial \beta} \right|_{\bar{V}}, \\ \rho_4(\theta) &:= \frac{1}{M_t} \left. \frac{\partial T_a}{\partial \Omega} \right|_{\bar{V}}, & \rho_5(\theta) &:= \frac{1}{M_t} \left. \frac{\partial T_a}{\partial V} \right|_{\bar{V}}, & \rho_6(\theta) &:= \frac{1}{M_t} \left. \frac{\partial T_a}{\partial \beta} \right|_{\bar{V}},\end{aligned}$$

where the division by J_r and M_t is adopted to improve numerical conditioning.

12.3 LPV Controller Design Method

In this section, an LMI-based optimization procedure for designing structured discrete-time LPV controllers is presented. Decentralized controllers of any order, fixed-order, and static output feedback (SOF) are among the possible control structures. Stability is assessed via a parameter-dependent Lyapunov function with varying parameters having their rates of variation contained in a compact closed convex set. A parameter-varying nonconvex condition for an upper bound on the induced \mathcal{L}_2 -norm performance is solved via an iterative LMI-based algorithm [1,2].

An open-loop, discrete-time augmented LPV system with state-space realization of the form

$$\begin{aligned}x(k+1) &= A(\theta)x(k) + B_w(\theta)w(k) + B_u(\theta)u(k), \\ z(k) &= C_z(\theta)x(k) + D_{zw}(\theta)w(k) + D_{zu}(\theta)u(k), \\ y(k) &= C_y(\theta)x(k) + D_{yw}(\theta)w(k)\end{aligned}\tag{12.18}$$

is considered for the purpose of synthesis, where $x(k) \in \mathbb{R}^n$ is the state vector, $w(k) \in \mathbb{R}^{n_w}$ is the vector of disturbance, $u(k) \in \mathbb{R}^{n_u}$ is the control input, $z(k) \in \mathbb{R}^{n_z}$ is the controlled output, and $y(k) \in \mathbb{R}^{n_y}$ is the measured output. $A(\theta)$, $B(\theta)$, $C(\theta)$, $D(\theta)$ are continuous functions of some time-varying parameter vector $\theta = [\theta_1, \dots, \theta_{n_\theta}]$. The same matrix notation to both the continuous-time augmented plant (12.16) and the discrete-time counterpart (12.18) have been adopted. Throughout the text, the context makes it clear when a continuous or discrete system is being referred to.

Assume θ ranges over a hyperrectangle denoted Θ

$$\Theta = \{ \theta : \underline{\theta}_i \leq \theta_i \leq \bar{\theta}_i, i = 1, \dots, n_\theta \}.$$

The rate of variation $\Delta\theta = \theta(k+1) - \theta(k)$ belongs to a hypercube denoted \mathcal{Y}

$$\mathcal{Y} = \{ \Delta\theta : |\Delta\theta_i| \leq v_i, i = 1, \dots, n_\theta \}.$$

The LPV controller has the form

$$\begin{aligned} x_c(k+1) &= A_c(\theta)x_c(k) + B_c(\theta)y(k), \\ u(k) &= C_c(\theta)x_c(k) + D_c(\theta)y(k), \end{aligned} \quad (12.19)$$

where $x_c(k) \in \mathbb{R}^{n_c}$ and the controller matrices are continuous functions of θ . Note that depending on the controller structure, some of the matrices may be zero. The controller matrices can be represented in a compact way

$$K(\theta) := \begin{bmatrix} D_c(\theta) & C_c(\theta) \\ B_c(\theta) & A_c(\theta) \end{bmatrix}. \quad (12.20)$$

The interconnection of system (12.18) and controller (12.19) leads to the following closed-loop LPV system denoted S_{cl} :

$$S_{cl} : \begin{cases} x(k+1) = \mathcal{A}(\theta, K(\theta))x_{cl}(k) + \mathcal{B}(\theta, K(\theta))w(k), \\ z(k) = \mathcal{C}(\theta, K(\theta))x_{cl}(k) + \mathcal{D}(\theta, K(\theta))w(k), \end{cases} \quad (12.21)$$

where the closed-loop matrices are [24]

$$\begin{aligned} \mathcal{A}(\theta, K(\theta)) &= \mathbf{A}(\theta) + \mathbf{B}(\theta)K(\theta)\mathbf{M}(\theta), & \mathcal{B}(\theta, K(\theta)) &= \mathbf{D}(\theta) + \mathbf{B}(\theta)K(\theta)\mathbf{E}(\theta), \\ \mathcal{C}(\theta, K(\theta)) &= \mathbf{C}(\theta) + \mathbf{H}(\theta)K(\theta)\mathbf{M}(\theta), & \mathcal{D}(\theta, K(\theta)) &= \mathbf{F}(\theta) + \mathbf{H}(\theta)K(\theta)\mathbf{E}(\theta), \end{aligned}$$

with

$$\begin{aligned} \mathbf{A}(\theta) &= \begin{bmatrix} A(\theta) & 0 \\ 0 & 0 \end{bmatrix}, & \mathbf{M}(\theta) &= \begin{bmatrix} C_y(\theta) & 0 \\ 0 & I \end{bmatrix}, & \mathbf{B}(\theta) &= \begin{bmatrix} B_u(\theta) & 0 \\ 0 & I \end{bmatrix}, \\ \mathbf{C}(\theta) &= \begin{bmatrix} C_z(\theta) & 0 \end{bmatrix}, & \mathbf{F}(\theta) &= D_{zw}(\theta), & \mathbf{H}(\theta) &= \begin{bmatrix} D_{zu}(\theta) & 0 \end{bmatrix}. \\ \mathbf{E}(\theta) &= \begin{bmatrix} D_{yw}(\theta) \\ 0 \end{bmatrix}, & \mathbf{D}(\theta) &= \begin{bmatrix} B_w(\theta) \\ 0 \end{bmatrix}, \end{aligned}$$

This general system structure can be particularized to some usual control topologies. If $K(\theta)$ is an *unconstrained* matrix and $n_c = 0$, the problem becomes a SOF. The static state feedback (SSF) is a particular case of SOF, when the system output is a full rank linear transformation of the state vector $\forall \theta$. If $n = n_c$, the full-order dynamic output feedback arises. In a structured control context, more elaborate control systems can be designed by constraining $K(\theta)$. A fixed-order dynamic output feedback has $n_c < n$. For decentralized controllers of arbitrary order, the structure of $K(\theta)$ is constrained to be

$$K(\theta) := \begin{bmatrix} \text{diag}(D_c(\theta)) & \text{diag}(C_c(\theta)) \\ \text{diag}(B_c(\theta)) & \text{diag}(A_c(\theta)) \end{bmatrix},$$

where $\text{diag}(\cdot)$ stands that (\cdot) has a block-diagonal structure.

The design of a closed-loop system usually consider performance specifications that can be characterized in different ways. Define $T_{zw}(\theta)$ as the input–output operator that represents the forced response of (12.21) to an input signal $w(k) \in \mathcal{L}_2$ for zero initial conditions. The induced \mathcal{L}_2 -norm of a given input–output operator

$$\|T_{zw}\|_2 := \sup_{(\theta, \Delta) \in \Theta \times \mathcal{V}} \sup_{\|w\|_2 \neq 0} \frac{\|z\|_2}{\|w\|_2}$$

is commonly utilized as a measure of performance of LPV systems and allows formulating the control specification as in \mathcal{H}_∞ control theory. It is of interest to note that an upper bound $\gamma > 0$ on the induced \mathcal{L}_2 -norm $\|T_{zw}\|_2$ can be interpreted in terms of the upper bound on the system's energy gain

$$\lim_{h \rightarrow \infty} \sum_{k=0}^{h-1} z(k)^T z(k) < \gamma^2 \lim_{h \rightarrow \infty} \sum_{k=0}^{h-1} w(k)^T w(k).$$

The LPV system (12.21) is said to have performance level γ when it is exponentially stable and $\|T_{zw}\|_2 < \gamma$ holds. An extension of the bounded real lemma (BRL) for parameter-varying systems provides sufficient conditions to analyze the performance level, by solving a constrained LMI optimization problem [10, 27]. For a given scalar γ and a given LPV controller $K(\theta)$, if there exists a θ -dependent matrix function $\mathcal{P}(\theta) = \mathcal{P}(\theta)^T$ satisfying

$$\begin{bmatrix} \mathcal{P}(\theta + \Delta\theta) & \mathcal{A}(\theta, K(\theta)) & \mathcal{P}(\theta) & \mathcal{B}(\theta, K(\theta)) & 0 \\ * & \mathcal{P}(\theta) & 0 & \mathcal{P}(\theta)\mathcal{C}(\theta, K(\theta))^T & \\ * & * & \gamma I & \mathcal{D}(\theta, K(\theta))^T & \\ * & * & * & \gamma I & \end{bmatrix} > 0 \quad (12.22)$$

$\forall(\theta, \Delta\theta) \in \Theta \times \mathcal{V}$, then the system S_{cl} is exponentially stable and $\|T_{zw}(\theta)\|_2 < \gamma$. The symbol $*$ means inferred by symmetry.

The parameter-varying BRL just shown can be also applied to the case where $w(k)$ is not an energy signal ($\|w(k)\|_2$ not finite) but has a nonzero root mean-square (RMS) value

$$w_{\text{RMS}} := \left[\lim_{h \rightarrow \infty} \frac{1}{h} \sum_{k=0}^{h-1} w(k)^T w(k) \right]^{1/2} \neq 0.$$

In this context, \mathcal{L}_2 -norm of a system is given in terms of the RMS values of the signals of interest, instead of $\|\cdot\|_2$. Such a situation is more appropriate to interpret control performance of a wind turbine, since the turbulent wind is a stochastic disturbance that persists for long periods of time, thus $\|w(k)\|_2$ is not a good measure of the signal.

When an LPV controller with performance level γ is not given but should be found (synthesized), the inequality (12.22) is no longer an LMI in the unknown variables due to the product between the variables $K(\theta)$ and $\mathcal{P}(\theta)$. Thus, convex

optimization algorithms cannot be applied to the condition *as it is*. Reformulations into sufficient (possibly conservative) LMI constraints are readily available for particular controller structures and type of parameter dependencies [9, 10].

We propose to design the controllers via an iterative algorithm, instead of attempting to reduce the problem to LMIs. The iterative algorithm relies on the following equivalent non-LMI parametrization that is suitable for iterative design [2]. If there exist $K(\theta)$, $\mathcal{P}(\theta) = \mathcal{P}(\theta)^T$, and $\mathcal{G}(\theta)$ satisfying:

$$\begin{bmatrix} \mathcal{P}(\theta + \Delta\theta) & \mathcal{A}(\theta, K(\theta)) & \mathcal{B}(\theta, K(\theta)) & 0 \\ * & -\mathcal{G}(\theta)^T \mathcal{P}(\theta) \mathcal{G}(\theta) + \mathcal{G}(\theta)^T + \mathcal{G}(\theta) & 0 & \mathcal{C}(\theta, K(\theta))^T \\ * & * & \gamma I & \mathcal{D}(\theta, K(\theta))^T \\ * & * & * & \gamma I \end{bmatrix} > 0, \quad (12.23)$$

$\forall (\theta, \Delta\theta) \in \Theta \times \mathcal{V}$, then the system S_{cl} is exponentially stable and $\|T_{zw}(\theta)\|_2 < \gamma$.

The affine dependence of the reformulated condition on $K(\theta)$ allows the controller matrices to be variables, irrespective of the chosen controller structure. The inequality remains nonconvex due to the product between $\mathcal{P}(\theta)$ and the introduced slack variable $\mathcal{G}(\theta)$. Furthermore, it involves the satisfaction of infinitely many inequalities, since (12.23) should hold for all $(\theta, \Delta\theta) \in \Theta \times \mathcal{V}$.

In order to make the problem computationally tractable, the iterative algorithm solves LMI optimization problems with the slack matrix $\mathcal{G}(\theta)$ constant during an iteration. An *iteration* should be understood to be an LMI-constrained optimization. The use of $\mathcal{G}(\theta)$ as a parameter-dependent slack variable is facilitated by updating its value at each iteration according to some predefined rule. In particular, the update rule is

$$\mathcal{G}(\theta)^{\{j+1\}} = \left(\mathcal{P}(\theta)^{\{j\}} \right)^{-1}, \quad (12.24)$$

where $\{\cdot\}$ is the iteration index and j is the current iteration number.

The iterative algorithm for the design of a structured LPV controller with minimum performance level γ is formulated next.

Algorithm 0: Set $j = 0$, a convergence tolerance ε , an initial $\mathcal{G}(\theta)^{\{0\}}$ and start to iterate:

(A.1) For fixed $\mathcal{G}(\theta)^{\{j\}}$, find $\mathcal{P}(\theta)^{\{j\}}$, $\mathcal{P}(\theta + \Delta\theta)^{\{j\}}$, $K(\theta)^{\{j\}}$, and $\gamma^{\{j\}}$ satisfying the LMI-constrained problem

Minimize γ subject to (12.23).

(A.2) If $|\gamma^{\{j\}} - \gamma^{\{j-1\}}| \leq \varepsilon$, stop. Otherwise, $\mathcal{G}(\theta)^{\{j+1\}} = \left(\mathcal{P}(\theta)^{\{j\}} \right)^{-1}$, set $j = j + 1$ and go to step 1.

12.3.1 Initial Slack Matrix $\mathcal{G}(\theta)^{\{0\}}$

The initial value of $\mathcal{G}(\theta)^{\{0\}}$ required to initialize Algorithm 0 can be obtained in different ways. If a given initial controller $K(\theta)$ satisfies the following optimization problem:

$$\text{Minimize } \gamma \text{ subject to (12.22), } \forall(\theta, \Delta\theta) \in \Theta \times \mathcal{V},$$

then the resulting $\mathcal{P}(\theta)$ can be utilized to derive $\mathcal{G}(\theta)^{\{0\}} = \mathcal{P}(\theta)^{-1}$. The example section shows the usage of this approach.

Alternatively, an iterative feasibility algorithm can be created by relaxing the inequality (12.23). Instead of requiring the inequality to be positive definite (> 0), a variable term is included to the right hand side ($> \text{diag}(\tau I, \tau G^T G, \tau I, \tau I)$), where τ is a scalar variable. The algorithm maximizes τ until the value reaches a certain chosen $\nu > 0$.

Algorithm 1: Set $j = 0$, a convergence tolerance ε , a $\nu > 0$, an initial $\mathcal{G}(\theta)^{\{0\}} = I$ and start to iterate:

(A.1) For fixed $\mathcal{G}(\theta)^{\{j\}}$, find $\mathcal{P}(\theta)^{\{j\}}$, $\mathcal{P}(\theta + \Delta\theta)^{\{j\}}$, $K(\theta)^{\{j\}}$, $\gamma^{\{j\}}$, and scalar τ satisfying the LMI-constrained problem

$$\text{Maximize } \tau \text{ subject to (12.23) with the right hand side changed from } > 0 \text{ to } > \text{diag}(\tau I, \tau G^T G, \tau I, \tau I), \text{ and } \tau < \nu.$$

(A.2) If $|\tau^{\{j\}} - \tau^{\{j-1\}}| \leq \varepsilon$, stop. Otherwise, $\mathcal{G}(\theta)^{\{j+1\}} = (\mathcal{P}(\theta)^{\{j\}})^{-1}$, set $j = j + 1$ and go to step 1.

The resulting $\mathcal{G}(\theta)^{\{0\}}$ can subsequently be used to initialize Algorithm 0.

12.3.2 From Infinite to Finite Dimensional

The LMI problems of Algorithm 0 involve infinitely many LMIs, as θ and $\Delta\theta$ are defined in a continuous space. When LMIs depend affinely on θ and $\Delta\theta$, the synthesis problem at each iteration is reduced to an optimization problem with a finite number of LMIs checked at $(\theta, \Delta\theta) \in \text{Vert } \Theta \times \text{Vert } \mathcal{V}$. Note that $\text{Vert } \Theta$ is the set of all vertices of Θ . For LMIs polynomially θ -dependent, relaxations based on multiconvexity arguments also reduce the problem to check LMIs at the vertices of the parameter space [1, 2]. This procedure, based on sufficient conditions, may lead to extra conservatism. In the general case, where no restrictions on the parameter dependence are imposed, one has to resort to ad-hoc gridding methods [4]. The gridding procedure consists of defining a gridded parameter subset denoted $\Theta_g \subset \Theta$, designing a controller that satisfies the LMIs $\forall \theta \in \Theta_g$, and checking the LMI-constraints in a denser grid. If the last step fails, the process is repeated with a finer grid.

Due to the assumption of general parameter dependence of the open-loop plant on the scheduling variables (12.17), the gridding approach is used in the controller design. The Lyapunov and the LPV controller matrices are affine in the basis functions

$$\mathcal{P}(\theta) = P_0 + \sum_{i=1}^{n_p} \rho_i(\theta_k) P_i + \sum_{i=1}^{n_{\theta_f}} \theta_{f,i} P_{n_p+i}, \quad (12.25a)$$

$$K(\theta) = K_0 + \sum_{i=1}^{n_p} \rho_i(\theta) K_i + \sum_{i=1}^{n_{\theta_f}} \theta_{f,i} K_{n_p+i}. \quad (12.25b)$$

Due to the bounded parameter rate set \mathcal{V} assumed known, the Lyapunov function at sample $k+1$ can be described as

$$\mathcal{P}(\theta + \Delta\theta) = P_0 + \sum_{i=1}^{n_p} \rho_i(\theta + \Delta\theta) P_i + \sum_{i=1}^{n_{\theta_f}} (\theta_{f,i} + \Delta\theta_{f,i}) P_{n_p+i}. \quad (12.26)$$

Note the general parameter dependence of (12.26) on $\Delta\theta$ occasioned by $\rho_i(\theta + \Delta\theta)$. Conveniently, the basis functions at sample $k+1$ are represented as a linear function of $\rho(\theta)$ and $\Delta\theta$

$$\rho_i(\theta + \Delta\theta) := \rho_i(\theta) + \frac{\partial \rho_i(\theta)}{\partial \theta} \Delta\theta, \quad (12.27)$$

thereby turning inequality (12.23) affine dependent on the rate of variation $\Delta\theta$. Thus, it is sufficient to verify (12.23) with (12.26) and (12.27) only at Vert \mathcal{V} .

The iterative algorithm for a chosen grid $\Theta_g \subset \Theta$ is presented in the sequel.

Algorithm 2: Set $j = 0$, a convergence tolerance ε , initialize $\mathcal{G}(\theta)^{\{0\}} \forall \theta \in \Theta_g$, and start to iterate:

(A.1) For fixed $\mathcal{G}(\theta)^{\{j\}}$, and $i = 0, 1, \dots, n_p + n_{\theta_f}$, find $P_i^{\{j\}} > 0$, $K_i^{\{j\}}$, and $\gamma^{\{j\}}$ satisfying the LMI-constrained problem

$$\text{Minimize } \gamma \text{ subject to (12.23), } \forall (\theta, \Delta\theta) \in \Theta_g \times \text{Vert } \mathcal{V}.$$

(A.2) If $|\gamma^{\{j\}} - \gamma^{\{j-1\}}| \leq \varepsilon$, stop. Otherwise, $\mathcal{G}(\theta)^{\{j+1\}} = \mathcal{P}(\theta)^{\{j\}-1}$, $\forall \theta \in \Theta_g$. Set $j = j+1$ and go to step 1.

The Lyapunov variable $\mathcal{P}(\theta)^{\{j\}} > 0$ may be close to singular at each iteration, making the inversion required to compute $\mathcal{G}(\theta)$ possibly ill conditioned. To alleviate this issue, an additional LMI constraint

$$\mathcal{P}(\theta)^{\{j\}} > \mu I,$$

improves numerical condition of the inversion by imposing a lower bound on the eigenvalues of $\mathcal{P}(\theta)^{\{j\}}$, where $\mu > 0$ is a chosen scalar. There exists a tradeoff between the value of μ and the attained value of γ . Higher values of μ may lead to more conservative controllers, although from our experience, the small value of μ required to better condition the inversion does not influence significantly on the performance level γ .

The gridding procedure for controller synthesis can be summarized by the following steps:

- (A.1) Define a grid Θ_g for the compact set Θ .
- (A.2) Find initials $\mathcal{G}(\theta)^{\{0\}}$, $\forall \theta \in \Theta_g$.
- (A.3) Solve Algorithm 2.
- (A.4) Define a denser grid.
- (A.5) Verify the feasibility of the LMI (12.22) with the computed controller $K(\theta)$, in each point of the new grid. If it is infeasible, choose a denser grid and go to step 2.

12.3.3 Controller Implementation

The iterative LMI optimization algorithm provides the controller matrices $A_{c,i}$, $B_{c,i}$, $C_{c,i}$, $D_{c,i}$, for $i = 0, 1, \dots, n_p + n_{\theta_f}$. These matrices, the basis functions, and the value of the scheduling variables are the only required information to determine the control signal u . At each sample time k , the scheduling variable θ is measured (or estimated) and a control signal is obtained as follows:

- (A.1) Compute the value of the basis functions $\rho_i(\theta)$, for $i = 0, 1, \dots, n_p$. The basis functions may be stored in a lookup table that takes θ as an input and outputs an interpolated value of $\rho(\theta)$.
- (A.2) With the value of the basis functions in hand, determine the controller matrices $A_c(\theta)$, $B_c(\theta)$, $C_c(\theta)$, $D_c(\theta)$ according to

$$\begin{aligned}
 A_c(\theta) &= A_{c,0} + \sum_{i=1}^{n_p} \rho_i(\theta) A_{c,i} + \sum_{i=1}^{n_{\theta_f}} \theta_{f,i} A_{c,n_p+i}, \\
 B_c(\theta) &= B_{c,0} + \sum_{i=1}^{n_p} \rho_i(\theta) B_{c,i} + \sum_{i=1}^{n_{\theta_f}} \theta_{f,i} B_{c,n_p+i}, \\
 C_c(\theta) &= C_{c,0} + \sum_{i=1}^{n_p} \rho_i(\theta) C_{c,i} + \sum_{i=1}^{n_{\theta_f}} \theta_{f,i} C_{c,n_p+i}, \\
 D_c(\theta) &= D_{c,0} + \sum_{i=1}^{n_p} \rho_i(\theta) D_{c,i} + \sum_{i=1}^{n_{\theta_f}} \theta_{f,i} A_{c,n_p+i}.
 \end{aligned}$$

- (A.3) Once the controller matrices have been found, the control signal $u(k)$ can be obtained by the dynamic equation (12.19) of the LPV controller, which only involves multiplications and additions.

12.4 Example: LPV PI Controller Tolerant to Pitch Actuator Faults

The proportional and integral (PI) is the most utilized controller by the wind energy industry. At low wind speeds, the PI speed control using generator torque as controlled input can be quite slow, thus tuning is not significantly challenging. However, at high wind speeds, the PI speed control using pitch angle as controlled input strongly couples with the tower dynamics, denoting a multivariable problem, and should be properly designed. Inappropriate gain selection can make rotational speed regulation “loose” around the set point or make the system unstable, as well as excite poorly damped structural modes [7].

The concepts seen throughout this chapter are here applied to the state-of-the-art controller structure of the wind turbine industry [8]. The present example intends to show that theoretical rigorosity on the design of gain-scheduled controllers may bring advantages in terms of performance and reliability of wind turbines in a closed loop.

12.4.1 Controller Design

For a clear and didactic exposure, the adopted control structure depicted in Fig. 12.10 is simpler than an industry-standard Region III controller [8], but includes the most common control loops.

The generator speed is regulated by a PI controller of the form

$$G_{\text{PI}} := k_p(\theta) + k_i(\theta) \frac{(s + z_I)}{s},$$

where s denotes the Laplace operator. Instead of a pure integrator, the PI controller is composed by an integrator filter

$$G_I(s) := \frac{s + z_I}{s},$$

for reasons to be explained later, where the filter zero z_I is a design parameter.

It is possible to provide an extra signal by using an accelerometer mounted in the nacelle, allowing the controller to better recognize between the effect of wind speed disturbances and tower motion on the measured power or generator speed. With

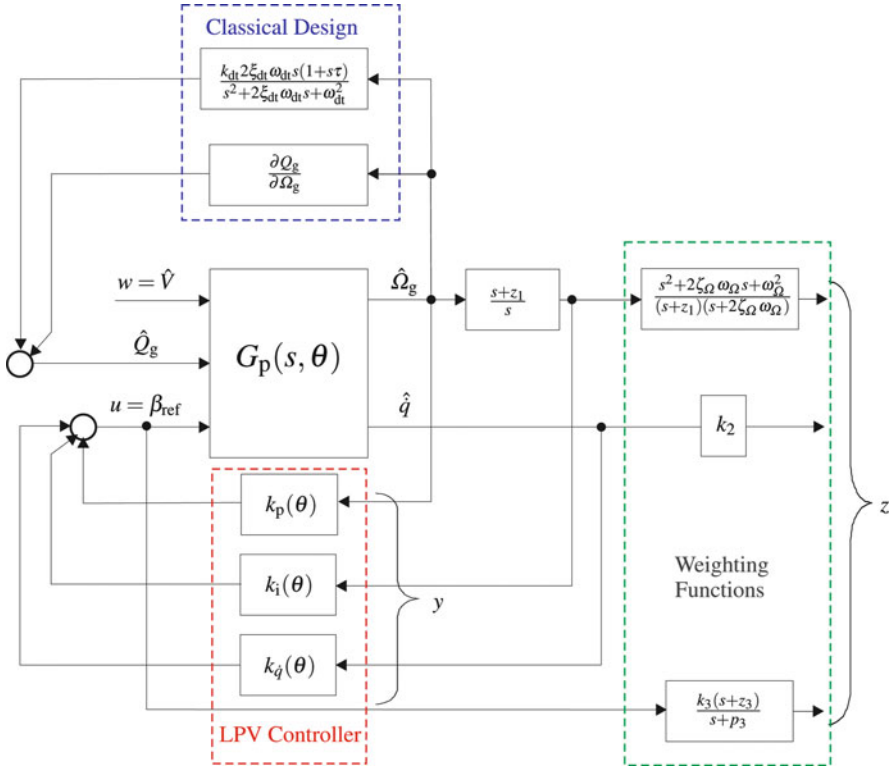


Fig. 12.10 Schematic block diagram of a controlled wind turbine in Region III

this extra feedback signal, tower bending moments loads can be reduced without significantly affecting speed or power regulation [7]. Therefore, it is assumed that tower velocity \dot{q} is available for measurement, by integrating tower acceleration \ddot{q} , and is multiplied by a parameter-dependent constant $k_{\dot{q}}(\theta)$ for feedback.

Additionally, active drive train damping is deployed by adding a signal to the generator torque to compensate for the oscillations in the drive train. This signal should have a frequency, ω_{dt} , equal to the eigenfrequency of the drive train, which is obtained by filtering the measurement of the generator speed using a bandpass filter of the form

$$G_{dt} := K_{dt} \frac{2\zeta_{dt}\omega_{dt}s(1 + \tau_{dt}s)}{s^2 + 2\zeta_{dt}\omega_{dt}s + \omega_{dt}^2}.$$

The time constant, τ_{dt} , introduces a zero in the filter, and can be used to compensate for time lags in the converter system. The filter gain k_{dt} and the damping ratio ζ_{dt} are selected based on classical design techniques.

A power controller for reducing fast power variations is treated simplistically as a proportional feedback from generator speed to generator torque. Considering a constant power control scheme, the generator torque can be represented as a function of the generator speed. The proportional feedback is nothing but the partial derivative of generator torque with respect to generator speed

$$\frac{\partial Q_g(\Omega_g)}{\partial \Omega_g} = -\frac{P_N}{N_g \Omega_{g,N}^2}.$$

In real implementations, a slow integral component is added to the loop to include asymptotic power tracking.

Instead of the classical control techniques, the design of PI speed and tower feedback loops are revisited under the LPV framework. For a didactic and clear exposure, the interconnection of the drive train with the damper is now considered as a first order low pass filter from aerodynamic torque to generator speed, and the rotor speed proportional to the generator speed. The LPV controller can now be designed to trade off the tracking of generator speed and tower oscillations with control effort (wear on pitch actuator). The dynamic model of the variable-speed wind turbine can then be expressed as an LPV model of the form

$$G: \begin{cases} \dot{x} = A(\theta)x + B_w(\theta)\hat{u} + B_u(\theta)\beta_{\text{ref}} \\ y = C_y x \end{cases},$$

where states, controllable input and measurements are

$$x = [\Omega_r \dot{q} q \dot{\beta} \beta x_{\Omega,i}]^T, \quad u = \beta_{\text{ref}}, \quad y = [\Omega_g y_{\Omega,i} \dot{q}]^T.$$

with open-loop system matrices

$$A(\theta) = \begin{bmatrix} \rho_1(\theta) - \frac{1}{J_r + J_g N_g^2} \frac{\partial Q_g}{\partial \Omega} & -\rho_2(\theta) & 0 & 0 & \rho_3(\theta) & 0 \\ \rho_4(\theta) & -\frac{1}{M_t} B_t - \rho_5(\theta) - \frac{K_t}{M_t} & 0 & \rho_6(\theta) & 0 & 0 \\ 0 & 1 & 0 & 0 & 0 & 0 \\ 0 & 0 & 0 & a_{44}(\theta_f) & -a_{12}(\theta_f) & 0 \\ 0 & 0 & 0 & 1 & 0 & 0 \\ N_g & 0 & 0 & 0 & 0 & 0 \end{bmatrix},$$

$$B_u = [\rho_2(\theta) \ \rho_5(\theta) \ 0 \ 0 \ 0 \ 0]^T, \quad B_w = [0 \ 0 \ 0 \ b_{4,1}(\theta_f) \ 0 \ 0]^T, \quad C_y = \begin{bmatrix} N_g & 0 & 0 & 0 & 0 \\ z_1 & 0 & 0 & 0 & 1 \\ 0 & 1 & 0 & 0 & 0 \end{bmatrix},$$

$$a_{12}(\theta_f) = b_{41}(\theta_f) = (1 - \theta_f(t))\omega_{n,0}^2 + \theta_f(t)\omega_{n,lp}^2,$$

$$a_{44}(\theta_f) = -2(1 - \theta_f(t))\zeta_0 \omega_{n,0} - 2\theta_f(t)\zeta_{lp} \omega_{n,lp}.$$

The basis functions $\rho_1(\theta), \dots, \rho_6(\theta)$ related to the parameter-varying aerodynamic gains are selected as

$$\begin{aligned} \rho_1 &:= \frac{1}{J_r + J_g N_g^2} \left. \frac{\partial Q}{\partial \Omega} \right|_{\hat{v}}, & \rho_2 &:= \frac{1}{J_r + J_g N_g^2} \left. \frac{\partial Q}{\partial V} \right|_{\hat{v}}, & \rho_3 &:= \frac{1}{J_r + J_g N_g^2} \left. \frac{\partial Q}{\partial \beta} \right|_{\hat{v}}, \\ \rho_4 &:= \frac{1}{M_t} \left. \frac{\partial T}{\partial \Omega} \right|_{\hat{v}}, & \rho_5 &:= \frac{1}{M_t} \left. \frac{\partial T}{\partial V} \right|_{\hat{v}}, & \rho_6 &:= \frac{1}{M_t} \left. \frac{\partial T}{\partial \beta} \right|_{\hat{v}}. \end{aligned}$$

Notice the PI controller integrator filter G_I conveniently augmented into the state-space of G , represented by the state $x_{\Omega,i}$ and the output $y_{\Omega,i}$. The plant G_p is defined as the wind turbine model solely (plant G without the augmentation of G_I).

Considering G as the plant for synthesis purposes, the LPV controller structure reduces to a parameter-dependent SOF of the form

$$\begin{aligned} K(\theta) &= D_{c,0} + \sum_{i=1}^6 \rho_i(\theta) D_{c,i} + \theta_f D_{c,7}, \quad D_{c,n} := [D_{p,n} \ D_{i,n} \ D_{\dot{q},n}], \\ n &= 0, 1, \dots, 7. \end{aligned}$$

Controller tuning follows a procedure similar to the \mathcal{H}_∞ design. Notice that, for fixed values of the varying parameter θ , and initially neglecting the tower velocity feedback, the controller design becomes a mixed sensitivities optimization problem intended to minimize the norm

$$\left\| \begin{array}{c} W_{z1} G_I S G_v \\ W_u G_{PI} S G_v \end{array} \right\|_\infty,$$

where S is the sensitivity defined as $S := (I + G_p G_{PI})^{-1}$, G_v is the transfer function from \hat{V} to $\hat{\Omega}_g$, W_{z1} and W_u are weighting functions. The weight W_{z1} applied to the generator speed deviations can be used to shape the closed-loop response of rotational speed in face of wind disturbances, given by $\hat{\Omega}(t) = S G_v \hat{V}(t)$. The desired sensitivity in closed loop is

$$S_\Omega(s) := \frac{s^2 + 2\xi_\Omega \omega_\Omega s}{s^2 + 2\xi_\Omega \omega_\Omega s + \omega_\Omega^2},$$

where the natural frequency ω_Ω and damping ratio ξ_Ω are design parameters that select the desired second-order closed-loop behavior. The desired sensitivity S_Ω can be applied as a loop-shaping weight by defining W_{z1} as

$$W_{z1}(s) := \frac{1}{G_I(s) S_\Omega(s)} = \frac{s^2 + 2\xi_\Omega \omega_\Omega s + \omega_\Omega^2}{(s + z_1)(s + 2\xi_\Omega \omega_\Omega)}.$$

W_u is a first order high-pass filter that penalizes high-frequency content on the pitch angle

$$W_u(s) := k_3 \frac{s + z_3}{s + p_3}.$$

W_{z_1} and W_u governs the tradeoff between rotational speed regulation and pitch wear. Due to the resonance characteristics of the transfer function from \hat{V} to \dot{q} , the weighting function W_{z_2} is chosen as a scalar k_2 that tradeoffs the desired tower damping.

Two LPV controllers are designed, one fault intolerant and another tolerant to pitch actuator faults. The only difference on their synthesis is the inclusion of the fault-dependent terms $P_7\theta_f$ and $D_{c,7}\theta_f$ of the Lyapunov and controller matrices, respectively. The parameters for the loop-shaping weight W_{z_1} are selected as $\omega_\Omega = 0.6283$ rad/s (0.1 Hz) and $\xi_\Omega = 0.7$, with the zero of the integrator filter located at $z_1 = 1.0$ rad/s. A special attention must be devoted to the choice of W_u . Due to the fact that the pitch system has slower dynamics in the presence of low oil pressure, the bandwidth of this filter must be made large enough to allow rotational speed and tower damping control in the occurrence of faults. Defining Ω_{3P} as three times the nominal rotational speed $\Omega_{r,N}$, in the present example, $k_3 = 1$, $p_3 = 1.5\Omega_{3P}$ and $z_3 = 15\Omega_{3P}$.

Remember that the iterative LMI algorithm is a synthesis procedure in discrete time. Therefore, the augmented LPV plant in continuous time is discretized using a bilinear (Tustin) approximation [3] with sampling time $T_s = 0.02$ s, at each point $\Theta_g \times \text{Vert } \mathcal{V}$. The rate of variation of the scheduling variables in continuous time must as well be converted to discrete-time by the relation $\Delta\theta(k) = T_s\Delta\theta(t)$.

The initial slack matrices $G(\theta, \Delta\theta)^{\{0\}}$, $\forall(\theta, \Delta\theta) \in \Theta_g \times \text{Vert } \mathcal{V}$ required to initialize the LMI-based algorithm are determined from the solution of the following LMI optimization problem:

$$\text{Minimize } \gamma \text{ subject to (12.22), (12.26), (12.27), } \forall(\theta, \Delta\theta) \in \Theta_g \times \text{Vert } \mathcal{V}$$

with a given initial controller $K(\theta)$. The resulting Lyapunov matrix determines $G(\theta, \Delta\theta)^{\{0\}} = \mathcal{P}(\theta, \Delta\theta)^{-1}$. The proportional and integral gains of the given initial controller can be computed by placement of the poles of the transfer function from \hat{V} to $\hat{\Omega}_g$. Neglecting pitch actuator dynamics, and considering a pure integrator, the k_p and k_i gains can be described analytically as [16]

$$k_p(\theta) = \frac{2\xi_\Omega \omega_\Omega (J_r + N_g^2 J_g) - N_g \frac{\partial Q_g}{\partial \Omega_g} + \rho_1(\theta)}{-N_g \rho_3(\theta)}, \quad k_i(\theta) = \frac{\omega_\Omega^2 (1 + \xi_\Omega^2) (J_r + N_g^2 J_g)}{-N_g \rho_3(\theta)}.$$

The tower feedback gain of the initial controller is $k_{\dot{q}}(\theta) = 0$, meaning no active tower damping.

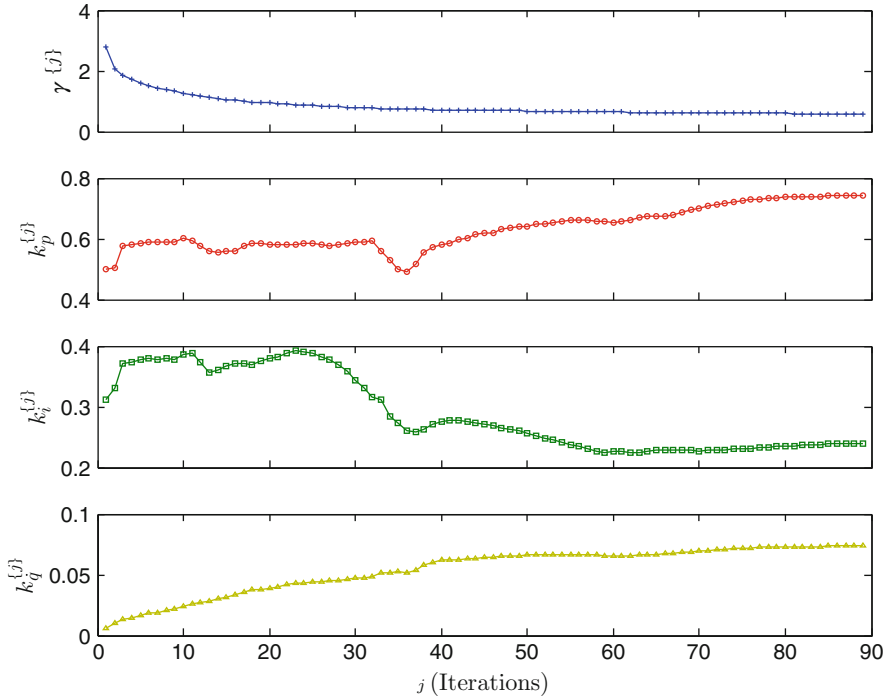


Fig. 12.11 Evolution of performance level γ and controller gains k_p , k_i , k_q during the iterative LMI synthesis. Controller gains computed at $\theta_{op} = 15$ m/s, $\theta_f = 0$

Convergence tolerance of the iterative algorithm is set to $\varepsilon = 10^{-3}$. After 89 iterations, convergence is achieved to a performance level $\gamma = 0.586$. The evolution of $\gamma^{(j)}$ versus the iteration number is depicted in Fig. 12.11, where the monotonically decreasing property of the sequence is noticeable. The proportional and integral gains depicted on the figures are multiplied by the gearbox ratio N_g for better illustration. The controller gains $K(\theta) = [k_p(\theta), k_i(\theta), k_q(\theta)]$ computed at $\theta_{op} = 15$ m/s, $\theta_f = 0$, during the course of the iterative LMI algorithm, are also shown. The synthesis procedure converge to controller gains different than the gains of the initial controller. The tower feedback gain k_q , null in the initial controller, has converged to a nonzero value, meaning active tower damping.

The proportional, integral, and tower feedback gains as three-dimensional surfaces of the scheduling parameters \bar{V} and θ_f are illustrated in Fig. 12.12a–c. The controller gains capture the dependence of the LPV system on the wind speed given by the basis functions. Compare the shape of the surfaces with the aerodynamic gains (Fig. 12.8). Also notice the slight changes in k_p and k_q and the changes in k_i scheduled by θ_f .

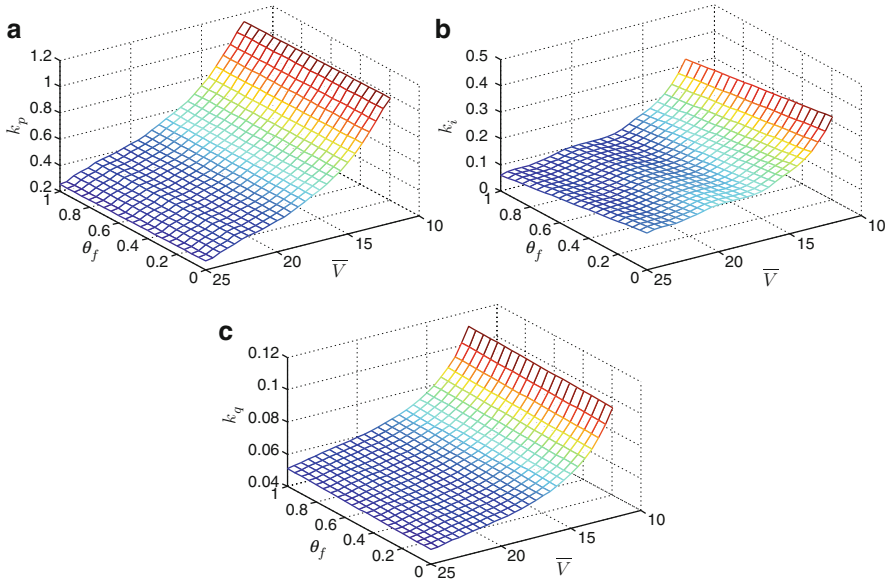


Fig. 12.12 Proportional, integral and tower feedback gains as functions of the operating point and fault scheduling variables

12.4.2 Simulation Results

The performance of the LPV controllers are accessed in a nonlinear wind turbine simulation environment [12]. The effective wind speed is estimated by an unknown input observer that uses measurements of generator speed, generator torque, and pitch angle [20]. Figures 12.13a–12.14d depict time series of the variables of interest resulting from a 600 s simulation. A mean speed of 17 m/s with 12% turbulence intensity and shear exponent of 0.1 characterizes the wind field (Fig. 12.13a). At time $t = 200$ s, the pitch system experiences a fault with θ_f increasing from 0 to 1 (Fig. 12.13b). At $t = 430$ s, the pitch system comes to normality with θ_f decreasing from 1 to 0. Both variations on the fault scheduling variable are made with maximum rate of variation.

Results of LPV controllers intolerant and tolerant to pitch actuator faults are compared to support a discussion of the consequences of the fault on the closed-loop system as well as fault accommodation. When the wind turbine is controlled by the fault intolerant LPV PI controller, the rotational speed (Fig. 12.13c) experiences poor and oscillatory regulation during the occurrence of faults, more pronouncedly while θ_f is varying. The threshold for a shutdown procedure due to overspeed is usually between 10% and 15% over the nominal speed [23]; in this particular case, the overspeed would not cause the wind turbine to shut down. The FT-LPV PI controller successfully accommodates the fault, maintaining rotor speed

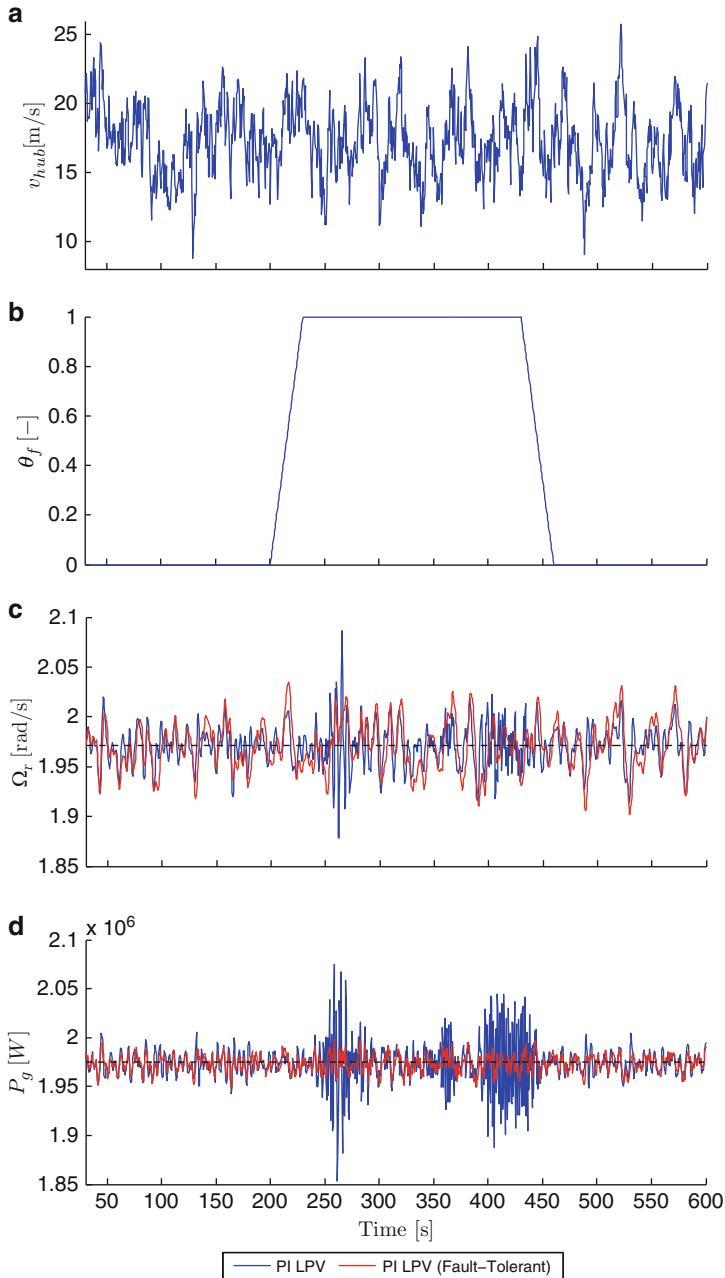


Fig. 12.13 Time series of (a) hub height wind speed (b) fault scheduling variable (c) rotor speed and (d) electrical power. Simulation results of a 2 MW wind turbine controlled by a fault-intolerant and a fault-tolerant LPV PI controller

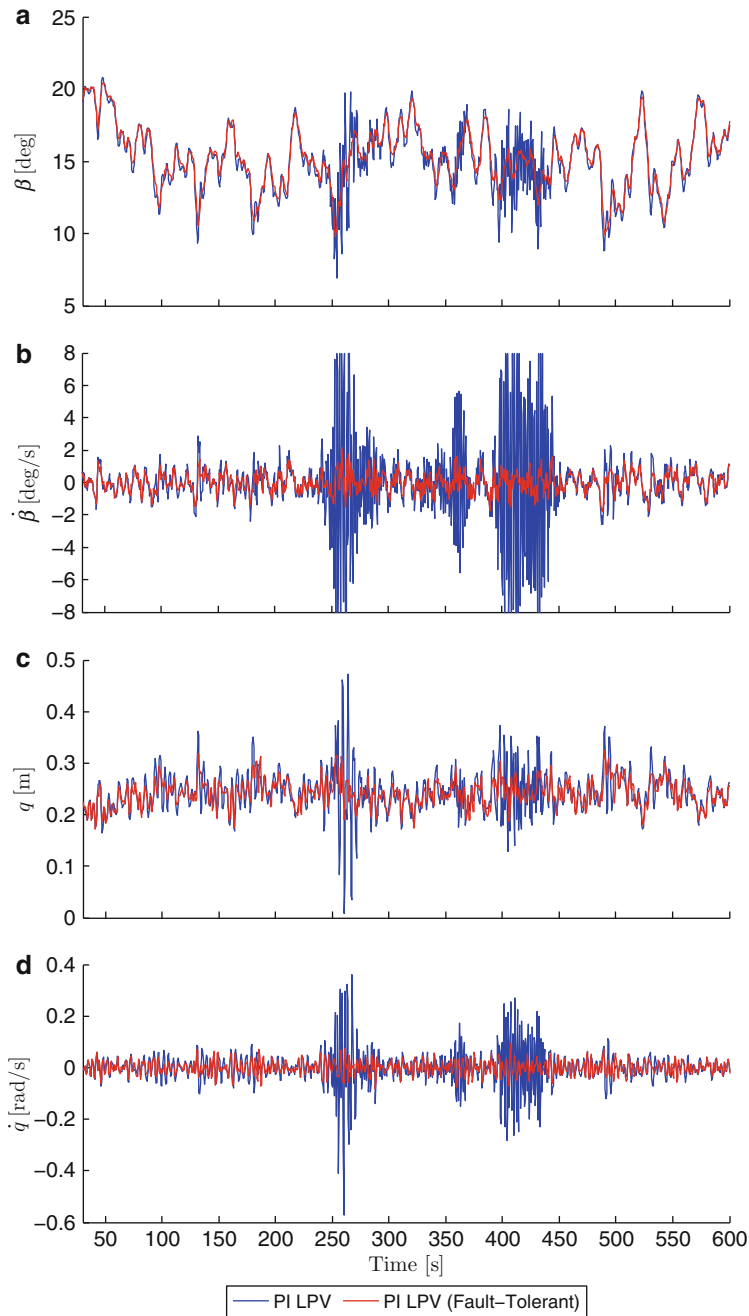


Fig. 12.14 Time series of (a) pitch angle (b) pitch velocity (c) fore-aft tower position and (d) fore-aft tower velocity. Simulation results of a 2 MW wind turbine controlled by a fault-intolerant and a fault-tolerant LPV PI controller

properly regulated. Oscillatory power overshoots of up to 6% of the nominal power (Fig. 12.13d) degrades power quality; the same does not happen to the FT-LPV controlled system.

More serious than the effects on rotational speed and power are the consequences of faults on the pitch system and tower. Excessive pitch angle excursions during faults (Fig. 12.14a) with the limits on velocity of ± 8 deg/s being reached (Fig. 12.14b) may cause severe wear on pitch bearings. The FT-LPV controller maintain pitch excursions and velocities within normal limits. The tower experiences displacements (Fig. 12.14c) of up to 0.48 m, an increase of approximately 60% when compared to the FT-LPV. The displacements comes along with very high tower velocities of almost 0.4 m/s, 260% higher than the fault accommodated case.

In such a situation, the supervisory controller would shut down the wind turbine due to excessive vibrational levels measured by the nacelle accelerometer. The same would not be necessary if the wind turbine is controlled by the FT-LPV. Therefore, fault-tolerance leads to higher energy generation and availability. It also collaborates to a better management of condition-based maintenance; higher priority of maintenance can be given to wind turbines with faults that cannot be accommodated by the control system. These are examples of the benefits that the LPV control design framework presented in this chapter can bring to wind turbines in closed loop with industry-standard as well as more elaborate controllers.

12.5 Conclusions

This chapter initially presents the modeling of a wind turbine model as an LPV system, considering faults on actuators and sensors. Later, an iterative LMI-based algorithm for the design of structured LPV controllers is described. This constitutes a unified LMI-based design framework to address gain-scheduling, fault-tolerance, and robustness on the design of wind turbine controllers.

The method is based on parameter-dependent Lyapunov functions, which reduces conservativeness of control for systems with rate bounds, which is the case in this work. The iterative algorithm may be computationally expensive depending on the number of plant states and scheduling variables, but brings desired flexibility in terms of the controller structure: decentralized of any order, dynamic (reduced-order) output feedback, SOF, and state feedback are among the possible ones. Moreover, the resulting controller can also be easily implemented in practice due to low data storage and simple math operations. In fact, the required data to be stored on the controller memory is only the controller matrices, and scalar functions of the scheduling variables representing plant nonlinearities. The mathematical operations needed to compute the controller at each sampling time are look-up tables with interpolation, products between a scalar and a matrix, and sums of matrices.

A design example of a fault-tolerant controller for the Region III, with a structure similar to the state-of-the-art industrial controllers, intends to show that theoretical rigorosity on the design of gain-scheduled controllers may bring advantages in

terms of performance and reliability of wind turbines in closed loop. The presented framework is not limited to the specific example shown. Due to its flexibility, the framework can be applied to other known wind turbine controller structures or even to explore different control philosophies.

Simulations indeed confirm that the fault-tolerant LPV controllers have superior performance in the occurrence of faults. The LPV controller designed for the nominal system start oscillating when the fault is introduced. In a real situation, the supervisory controller would shut down the wind turbine due to excessive vibrational levels measured by the nacelle accelerometer. The same would not be necessary if the wind turbine is controlled by the FT-LPV. Therefore, higher energy generation and availability is achieved. It also contributes to a better management of condition-based maintenance; priority on maintenance can be given to wind turbines with faults that cannot be accommodated by the control system.

Acknowledgments The third author acknowledges the Danish Ministry of Science, Technology and Innovation for the financial support.

References

1. Adegas F, Stoustrup J (2011) Robust structured control design via LMI optimization. In: Proceedings of the 18th IFAC world congress, Milano, Italy, pp 7933–7938
2. Adegas F, Stoustrup J (2011) Structured control of affine linear parameter varying systems. In: Proceedings of the American control conference, San Francisco, CA, USA, pp 739–744
3. Apkarian P (1997) On the discretization of LMI-synthesized linear parameter-varying controllers. *Automatica* 33(4):655–661. DOI 10.1016/S0005-1098(96)00211-7
4. Apkarian P, Adams R (1998) Advanced gain-scheduling techniques for uncertain systems. *IEEE Trans Contr Syst Technol* 6(1):21–32. DOI 10.1109/87.654874
5. Bianchi FD, Battista HD, Mantz RJ (2007) Wind turbine control systems: Principles, modelling and gain scheduling design. Springer, London
6. Bianchi D, Mantz RJ, Christiansen CF (2005) Gain scheduling control of variable-speed wind energy conversion systems using quasi-LPV models. *Contr Eng Pract* 13(2):247–255. DOI 10.1016/j.conengprac.2004.03.006
7. Bossanyi EA (2000) The design of closed loop controllers for wind turbines. *Wind Energy* 3(3):149–163. DOI 10.1002/we.34
8. Bossanyi E, Witcher D (2011) “controller for 5 MW reference turbine”, deliverable 5.1.1, project upwind. Tech. rep., Garrad Hassan & Partners
9. Caigny JD, Camino JF, Oliveira RCLF, Peres PLD, Swevers J (2010) Gain-scheduled H_2 and H_∞ control of discrete-time polytopic time-varying systems. *IET Contr Theor Appl* 4(3):362–380. DOI 10.1049/iet-cta.2008.0364
10. Caigny JD, Camino JF, Oliveira RCLF, Peres PLD, Swevers J (2011) Gain-scheduled dynamic output feedback control for discrete-time LPV systems. *Int J Robust Nonlinear Contr* DOI 10.1002/rnc.1711
11. Dolan DSL, Lehn PW (2006) Simulation model of wind turbine 3p torque oscillations due to wind shear and tower shadow. *IEEE Trans Energ Convers* 21(3):717–724. DOI 10.1109/TEC.2006.874211
12. Esbensen T, Sloth C (2009) Fault diagnosis and fault-tolerant control of wind turbines. Master’s thesis, Aalborg University

13. Florin I (2004) Anca Daniela Hansen, Poul Srensen, Frede Blaabjerg, Wind Turbine Blockset in Matlab/Simulink
14. GWEC (2010) Annual market update 2010. Tech. rep., Global Wind Energy Council
15. Hansen MOL (2008) Aerodynamics of wind turbines. Earthscan, London
16. Hansen MH, Bye S (2011) Effect of dynamic inflow on tuning of a PI pitch controller
17. Niss MOK, Esbensen T, Sloth C, Stoustrup J, Odgaard PF (2009) A youla-kucera approach to gain-scheduling with application to wind turbine control. In: Proceedings of the 3rd IEEE multi-conference on systems and control, Saint Petersburg, Russia, pp 1489–1494. DOI 10.1109/CCA.2009.5281172
18. Odgaard PF, Stoustrup J, Kinnaert M (2009) Fault tolerant control of wind turbines – a benchmark model. In: Proceedings of the 7th IFAC symposium on fault detection, supervision and safety of technical processes, Barcelona, Spain, pp 155–160. DOI 10.3182/20090630-4-ES-2003.00026
19. Østergaard KZ (2008) Robust, gain-scheduled control of wind turbines. PhD thesis, Aalborg University
20. Østergaard K, Brath P, Stoustrup J (2007) Estimation of effective wind speed. J Phys Conf Ser 75(1):1–9. DOI 10.1088/1742-6596/75/1/012082
21. Østergaard K, Brath P, Stoustrup J (2009) Linear parameter varying control of wind turbines covering both partial load and full load conditions. Int J Robust Nonlinear Contr 19(1):92–116. DOI 10.1002/rnc.1340
22. Rugh W, Shamma J (2000) Research on gain scheduling. Automatica 36(10):1401–1425. DOI 10.1016/S0005-1098(00)00058-3
23. Savini B, Lupto R (2011) Supervisory controller and load calculation with individual pitch controller for 5 MW reference turbine. Tech. rep., GL Garrad Hassan
24. Skelton RE, Iwasaki T, Grigoriadis K (1998) A unified algebraic approach to linear control design. Taylor & Francis, London
25. Sloth C, Esbensen T, Niss MOK, Stoustrup J, Odgaard PF (2009) Robust LMI-based control of wind turbines with parametric uncertainties. In: Proceedings of the 3rd IEEE multi-conference on systems and control, Saint Petersburg, Russia, pp 776–781. DOI 10.1109/CCA.2009.5281171
26. Sloth C, Esbensen T, Stoustrup J (2011) Robust and fault-tolerant linear parameter-varying control of wind turbines. Mechatronics 21(4):645–659. DOI 10.1016/j.mechatronics.2011.02.001
27. de Souza CE, Barbosa KA, Neto AT (2006) Robust H_∞ filtering for discrete-time linear systems with uncertain time-varying parameters. IEEE Trans Signal Process 54(6):2110–2118. DOI 10.1109/TSP.2006.874349

Chapter 13

Attitude Regulation for Spacecraft with Magnetic Actuators: An LPV Approach

Andrea Corti and Marco Lovera

Abstract Magnetic torquers are an effective and reliable technology for the attitude control of small satellites in low Earth orbit. Such actuators operate by generating a magnetic dipole which interacts with the magnetic field of the Earth. The main difficulty in the design of attitude control laws based on magnetic torquers is that the torques they generate are instantaneously constrained to lie in the plane orthogonal to the local direction of the geomagnetic field vector, which varies according to the current orbital position of the spacecraft. This implies that the attitude regulation problem is formulated over a time-varying model. In recent years, this control problem has been studied extensively, either using methods based on averaged models or via approaches which exploit the quasi-periodic variability of the geomagnetic field. With the exception of other approaches based on Model Predictive Control, none of the above actually exploits at the design stage the fact that the geomagnetic field can be reliably measured on board and, therefore, the above mentioned time-variability of the attitude dynamics can be represented in LPV form. Therefore, in this chapter an LPV approach to the problem of magnetic attitude control law design is proposed. To this purpose, an LPV model of the attitude dynamics is first derived, LPV control laws suitable for on board implementation are synthesized and eventually tested in simulation.

13.1 Introduction

Electromagnetic actuators are a particularly effective and reliable technology for the attitude control of small satellites. Such actuators operate on the basis of the interaction between the magnetic field generated by a set of three orthogonal,

A. Corti • M. Lovera (✉)

Dipartimento di Elettronica e Informazione, Politecnico di Milano, Milano, Italy
e-mail: corti@elet.polimi.it; lovera@elet.polimi.it

current-driven coils and the magnetic field of the Earth and provide a simple solution to the problem of generating torques on board of a satellite, both for attitude control in momentum biased or gravity gradient architectures and as secondary actuators for momentum management tasks in zero momentum reaction wheel based configurations (see [25]).

The main difficulty in the design of magnetic attitude control laws is related to the fact that magnetic torques are instantaneously constrained to lie in the plane orthogonal to the local direction of the geomagnetic field vector. Controllability of the attitude dynamics is ensured for a wide range of orbit altitudes and inclinations in spite of this constraint, thanks to the variability of the geomagnetic field. However, this implies that the attitude control engineer has to deal with a time-varying model in the control design process.

In recent years, considerable effort has been devoted to the analysis of this control problem. In particular, as far as the linear attitude regulation problem is concerned, two main lines of work can be identified in the literature:

- Methods based on averaged models. The idea is to replace the time-varying dynamics of the magnetically actuated spacecraft with an approximate time-invariant model obtained using *averaging* techniques. The advantage of this approach is that the control problem becomes time-invariant. The main drawbacks are that: the designer has to verify a posteriori that the designed controller actually stabilizes the original time-varying dynamics with a satisfactory performance level; averaging implies limitations in closed-loop performance. This approach, originally proposed in [27], was further developed in [9] to deal with the (relatively simple) stabilization problem for the coupled roll/yaw dynamics of a momentum biased spacecraft using a magnetic torquer aligned with the pitch axis.
- Methods based on periodic models. As the variability of the geomagnetic field is *almost* time-periodic, most of the recent work on the linear magnetic attitude control problem has focused on the use of optimal and robust periodic control theory for the design of state and output feedback regulators [13, 14, 19, 20, 26, 30, 34, 35, 37]. While periodic control design methods have the advantage of guaranteeing closed-loop stability a priori, they lead to the synthesis of time-periodic regulators, which are difficult to implement and operate in practice. Therefore, more recent contributions aim at designing constant gain periodically optimal controllers (see [21, 31, 38]).

With the exception of other approaches based on Model Predictive Control, none of the above actually exploits at the design stage the fact that the geomagnetic field can be reliably measured on board and, therefore, the above-mentioned time-variability of the attitude dynamics can be represented in linear parameter-varying (LPV) form. Therefore, in this chapter, an LPV approach to the problem of magnetic attitude control law design is proposed. To this purpose, an LPV model of the attitude dynamics is first derived, LPV control laws suitable for on board implementation are synthesized and eventually tested on a realistic spacecraft simulator. LPV analysis and synthesis methods have been an active area of research

for almost two decades. Provided that a reliable LPV model for the plant to be controlled is available (see, e.g., [15] for an overview of the state-of-the-art in LPV modelling and identification), a number of methods are now available to obtain both state and output-feedback LPV controllers, see, e.g., [1, 2, 4, 17, 23, 24, 36]. As the corresponding tools reach maturity and allow to deal with problems of increasing size and complexity, the possibility of achieving a prescribed level of performance for a parameter-dependent system using a single, parametrically varying controller can be pursued in practice for a wide range of applications. In addition, implementation issues, which have proved critical in many cases, are increasingly well understood (see, e.g., [29] and the references therein) as well as the effect of noise on the measured scheduling parameters (see [22]).

The chapter is organized as follows. Section 13.2 provides a description of the spacecraft considered in the study as well as the derivation of a linearized model for its attitude dynamics. An overview of existing modelling approaches for magnetic attitude control system design is provided in Sect. 13.3, while Sect. 13.4 is devoted to the presentation of the proposed LPV technique. Finally, the results obtained in the simulation of the designed control laws are presented and discussed in Sect. 13.5.

13.2 Mathematical Model and Problem Statement

In order to represent the attitude motion of an Earth-pointing spacecraft on a circular orbit, the following reference systems are adopted:

- Earth centered inertial reference axes (ECI). The Earth's center is the origin of these axes. The positive X -axis points in the vernal equinox direction. The Z -axis points in the direction of the North Pole. The Y -axis completes the right-handed orthogonal triad.
- Orbital Axes (X_0, Y_0, Z_0). The origin of these axes is at the satellite center of mass. The X -axis points to the Earth's center; the Y -axis points in the direction of the orbital velocity vector. The Z -axis is normal to the satellite orbit plane.
- Satellite Body Axes. The origin of these axes is at the satellite center of mass; in nominal Earth-pointing conditions, the X_b (yaw), Y_b (roll) and Z_b (pitch) axes are aligned with the corresponding orbital axes.

A spacecraft with inertia matrix $I = \text{diag} [I_{xx} \ I_{yy} \ I_{zz}]$ is considered, equipped with a single-momentum wheel aligned with the body z -axis, with moment of inertia J and angular velocity Ω relative to the body frame. The aim of the attitude control scheme is to maintain the satellite body axes aligned with the orbital axes, while exploiting the gyroscopic effect due to the momentum wheel. Note that the choice of this spacecraft configuration is not particularly restrictive, since by assuming that $\Omega = 0$ and $I_{xx} \ll I_{yy}$, $I_{xx} \ll I_{zz}$ a gravity-gradient configuration can be obtained as a particular case. Similarly, the assumptions of a circular orbit and of a diagonal inertia matrix are made only for ease of presentation, but they are by no means necessary for the applicability of the proposed design approach.

Indeed, unlike existing design methods based on averaging (see, e.g., [9]), inertial coupling between roll/yaw and pitch dynamics can be handled in the design problem. The angular kinematics and dynamics of the spacecraft are modelled using as state variables the quaternion $q = [q_1 \ q_R^T]^T = [q_1 \ q_2 \ q_3 \ q_4]^T$ describing the attitude of the body axes with respect to the orbital axes and the inertial angular velocity vector $\omega = [\omega_x \ \omega_y \ \omega_z]^T$ with respect to the body axes.

In the following, we will present a linearized dynamic model for the formulation of this control problem. With respect to the selected state variables, the nominal, Earth-pointing, equilibrium corresponds to the attitude quaternion $\bar{q} = [1 \ 0 \ 0 \ 0]^T$ and to the angular rate $\bar{\omega} = [0 \ 0 \ -\Omega_0]^T$, where Ω_0 is the orbital angular rate.

Define the state vector $x = [\delta q_R^T \ \delta \omega^T]^T$ formed with small displacements of the vector part q_R of the attitude quaternion q from the nominal values $\bar{q}_R = [0 \ 0 \ 0]^T$ and small deviations of the body rates from the nominal values $\bar{\omega}_x = \bar{\omega}_y = 0, \bar{\omega}_z = -\Omega_0$.

Then the attitude dynamics can be linearized and the local linear dynamics for the attitude can be defined as [14]

$$\dot{x}(t) = Ax(t) + B_T [T_m(t) + T_d(t)], \tag{13.1}$$

where T_m is the magnetic control torque vector, T_d is the disturbance torque vector and

$$A = \left[\begin{array}{cc|ccc} A_{11} & A_{12} & & & & \\ A_{21} & A_{22} & & & & \end{array} \right] = \left[\begin{array}{ccc|ccc} 0 & -\Omega_0 & 0 & 0.5 & 0 & 0 \\ \Omega_0 & 0 & 0 & 0 & 0.5 & 0 \\ 0 & 0 & 0 & 0 & 0 & 0.5 \\ \hline 0 & 0 & 0 & 0 & W_x & 0 \\ 0 & -6k_y\Omega_0^2 & 0 & W_y & 0 & 0 \\ 0 & 0 & +6k_z\Omega_0^2 & 0 & 0 & 0 \end{array} \right], \tag{13.2}$$

$$B_T = \begin{bmatrix} 0 & 0 & 0 \\ 0 & 0 & 0 \\ 0 & 0 & 0 \\ I_{xx}^{-1} & 0 & 0 \\ 0 & I_{yy}^{-1} & 0 \\ 0 & 0 & I_{zz}^{-1} \end{bmatrix}, \tag{13.3}$$

and $k_x = \frac{I_{yy} - I_{zz}}{I_{xx}}, k_y = \frac{I_{zz} - I_{xx}}{I_{yy}}, k_z = \frac{I_{xx} - I_{yy}}{I_{zz}}, W_x = -k_x\Omega_0 + k_{wx}\bar{\Omega}, W_y = -k_y\Omega_0 - k_{wy}\bar{\Omega}, k_{wx} = \frac{J}{I_{xx}}, k_{wy} = \frac{J}{I_{yy}}$. Here, $\bar{\Omega}$ is the nominal wheel speed.

Taking into account that T_m can be written as

$$T_m(t) = m(t) \times b(t) = S(b(t))m(t) = -b(t) \times m(t), \quad (13.4)$$

where $b = [b_x \ b_y \ b_z]^T$ is the geomagnetic field vector (in body frame), m is the dipole vector of the magnetic torquers and

$$S(b) = \begin{bmatrix} 0 & b_z & -b_y \\ -b_z & 0 & b_x \\ b_y & -b_x & 0 \end{bmatrix},$$

(13.1) can be equivalently written as

$$\dot{x}(t) = Ax(t) + B_m(t)m(t) + B_T T_d(t), \quad (13.5)$$

where $B_m(t) = B_T S(b(t))$. Note that, while A is constant, the control matrix $B_m(t)$ corresponding to the control input m turns out to be time-varying because of the dependence on the geomagnetic field vector $b(t)$. Such time variability turns out to be approximately time-periodic with period equal to the orbital period $T = 2\pi/\Omega_0$. Deviations from exact periodicity are due to Earth rotation and to orbit perturbations.

As can be seen from (13.2) (and well known in the literature, see, e.g., [10, 25]), the A matrix shows that the pitch dynamics is decoupled from the roll/yaw dynamics. Therefore, in the case of a spacecraft equipped with three independent torque actuators, it would be possible to design separate controllers for the two subsystems. Unfortunately, as can be seen from the expression of matrix $B_m(t)$ in (13.3), the use of magnetic actuators introduces a coupling between the roll/yaw and the pitch subsystems. Similarly, coupling terms appear if the spacecraft inertia matrix I is not diagonal—a situation which occurs frequently in practice.

A very common structure for magnetic attitude control laws, which goes back to classical papers such as [16], consists of control laws of the kind

$$m(t) = \frac{1}{\|b(t)\|^2} S^T(b(t)) T_{id}(t), \quad (13.6)$$

where $b(t)$ is the measurement, at time t , of the geomagnetic field b and $T_{id}(t)$ is an “ideal” control torque to be determined on the basis of a suitable feedback of state or output variables, according to the specific attitude control architecture of the considered spacecraft. The above control law can be readily given a simple geometric interpretation. Indeed, recalling (13.4) we can express the torque generated by the magnetic coils as

$$T_m(t) = \frac{1}{\|b(t)\|^2} S(b(t)) S^T(b(t)) T_{id}(t) = \Gamma(b(t)) T_{id}(t), \quad (13.7)$$

where matrix $\Gamma(b(t))$ is structurally symmetric and positive semidefinite for all values of $b(t)$. Equation (13.7) can be easily interpreted as the projection of vector T_{id} onto the plane orthogonal to the direction of the magnetic field vector b (hence the name of “projection-based” controllers). Letting now

$$B(t) = B_T \Gamma(b(t)) \quad (13.8)$$

and choosing as control variable $u(t) = T_{id}(t)$, one gets to the final design model

$$\dot{x}(t) = Ax(t) + B(t)u(t) + B_T T_{id}(t). \quad (13.9)$$

Different control strategies can be adopted using the fixed structure projection approach; in this chapter we will focus on state-feedback control, with either constant or parameter-dependent gain.

Remark 13.1. In view of the digital implementation of the controller, the above-described geometric view of magnetic control holds only in an approximate sense, but still represents a good interpretation of the operation of the controller since the sampling interval for the implementation of this type of controller is normally short (from 0.1 s to 1 s at most) with respect to the period of the geomagnetic field along a low Earth orbit (the orbital period of a LEO orbit is typically about 6,000 s).

Note that the advantage of the considered controller structure is that only constant parameters (i.e., the ones defining T_{id} as a function of the state vector) have to be designed, while the time-dependence of the control law is carried by the (measurable) value of the components of the geomagnetic field b entering (13.6). In the following section, an overview of possible approaches to the optimal tuning of this class of attitude controllers will be proposed.

In view of the above, the goal of the design problem considered in this chapter is to derive state-feedback controllers for the system in (13.9) satisfying (as many as possible of) the following requirements:

- (A.1) Nominal closed-loop stability: as shown above, the local dynamics of a magnetically controlled spacecraft is time varying, therefore, the stabilization problem cannot be faced by means of conventional LTI design tools.
- (A.2) Nominal closed-loop performance: the spacecraft is subject to external disturbances, which can be decomposed in a secular (i.e., constant) and a cyclic (i.e., periodic, with period equal to the orbit period $T = \frac{2\pi}{\Omega}$); the controller must try and attenuate the effect of such disturbances on the attitude.
- (A.3) Stability and performance robustness: the dynamics of the spacecraft is subject to a number of sources of uncertainty, the most important of which are the moments of inertia of the spacecraft and the actual behavior of the magnetic field (as opposed to the mathematical model used in the design).

- (A.4) Implementation issues: time-varying gains are not easily implemented on board, as they give rise to a sensitive synchronization problem. Therefore, we seek either constant-gain controllers or gain-scheduled controllers which can exploit on board measurements of the magnetic field vector.

13.3 Approaches to Modelling for Magnetic Attitude Control Design

In Sects. 13.3.1 and 13.3.2, a short overview of modelling approaches based, respectively, on averaging and on periodic models is presented, while the LPV approach to the problem is introduced in Sect. 13.3.3 and further developed in Sect. 13.4.

13.3.1 Averaging-Based Modelling of Magnetically Controlled Spacecraft

The simplest approach to the design of a magnetic attitude control law in the setting established in the previous section is based on the idea of *averaging* to derive an approximate LTI model from (13.9). From a practical point of view, one can simply replace $\Gamma(b(t))$ in (13.9) with the constant matrix $\bar{\Gamma}$ defined as

$$\bar{\Gamma} = \frac{1}{T} \int_0^T \Gamma(b(t)) dt \quad (13.10)$$

to get

$$\dot{x}(t) = Ax(t) + \bar{B}u(t) + B_T T_d(t), \quad (13.11)$$

where $\bar{B} = B_T \bar{\Gamma}$. One can then resort to the methods and tools for state-feedback design for LTI systems to compute the sought after control law.

Although averaging has been used somewhat heuristically in the attitude control literature (see [9] and the references therein), the theoretical foundation for this approach is the following result (reported from [11]), which provides conditions under which it is possible to approximate a linear time-periodic system with an averaged one.

Theorem 13.1. *Consider the linear time-periodic system*

$$\dot{x}(t) = \varepsilon A(t)x(t), \quad (13.12)$$

with $A(t+T) = A(t)$ and $\varepsilon > 0$ and define the averaged system associated to (13.12) as

$$\dot{x}(t) = \varepsilon \bar{A}x(t), \quad (13.13)$$

where

$$\bar{A} = \frac{1}{T} \int_0^T A(\tau) d\tau. \quad (13.14)$$

Then if \bar{A} is Hurwitz there exists $\varepsilon^* > 0$ such that for all $0 < \varepsilon < \varepsilon^*$ $x = 0$ is an exponentially stable equilibrium for (13.12).

It is apparent from the above theorem that using an averaging approach only low-bandwidth controllers can be obtained, as stability of the feedback system is preserved only provided that the closed-loop dynamics turn out to be sufficiently slow.

13.3.2 Periodic Modelling of Magnetically Controlled Spacecraft

A less restrictive design approach consists in adopting as an approximation of $\Gamma(b(t))$ in (13.9) a periodic matrix obtained by either using a simplified periodic model for $b(t)$ (such as the tilted dipole model, see, e.g., [32]) or by replacing $b(t)$ with a time-periodic approximation obtained by least-squares fitting either flight data or simulated data obtained from a high-fidelity geomagnetic field model. As an example, in Fig. 13.1, the geomagnetic field along an 87° inclination, 450 km altitude orbit computed using the IGRF model is compared to its time-periodic approximation. $\Gamma(b(t))$ in (13.9) is then replaced with a time-periodic approximation $\Gamma_P(t)$, to get the linear time-periodic model

$$\dot{x}(t) = Ax(t) + B_P(t)u(t) + B_T T_d(t), \quad (13.15)$$

where $B_P(t) = B_T \Gamma_P(t)$. The controller design problem can then be faced using the methods and tools for state-feedback design for linear time-periodic systems. Unfortunately, the classical theory for optimal and robust control of linear time-periodic systems (see e.g., [5, 14, 33]) leads to the design of time-periodic controllers, which turn out to be impractical from the point of view of implementation. In view of this, a number of recent results (see [21, 38]) aim at the design of constant gain, periodically optimal controllers, which represent a trade-off between accuracy and complexity. Simulation results reported in [21] demonstrate that this approach can lead to significant improvements with respect to the averaging-based one, both in terms of stability (faster closed-loop dynamics) and performance (smaller steady-state pointing errors).

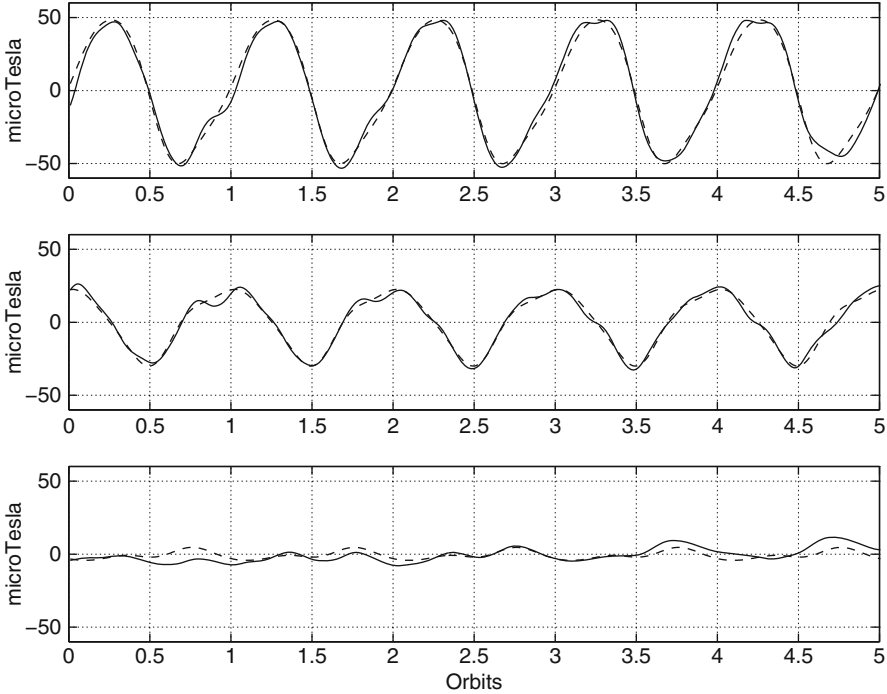


Fig. 13.1 Periodic approximation of the geomagnetic field in Pitch–Roll–Yaw coordinates, 87° inclination orbit, 450 km altitude

13.3.3 *Parameter-Dependent Modelling of Magnetically Controlled Spacecraft*

An alternative parameter-dependent approach is proposed in this section. At each time instant, the matrix $\Gamma(b(t))$ can be expressed as the sum of its average defined in (13.10) with the set of perturbed elements

$$\Gamma(b(t)) = \bar{\Gamma} + \Delta\Gamma(b(t)). \tag{13.16}$$

The elements of the matrix $\Delta\Gamma(b(t)) \in \mathbb{R}^{3 \times 3}$ can be interpreted as model parameters ρ and this leads to the LPV formulation

$$\dot{x}(t) = Ax(t) + B_T(\bar{\Gamma} + \Delta\Gamma(\rho))u(t) + B_T T_d(t). \tag{13.17}$$

The geomagnetic field $b(t)$ is measured online and $\bar{\Gamma}$ is computed offline, so the model parameters can be computed online and used for gain-scheduling. Moreover, the matrix $\Gamma(b(t))$ is symmetric, $\bar{\Gamma}$ is diagonal, so $\Delta\Gamma(b(t))$ is symmetric and is completely defined by six parameters only.

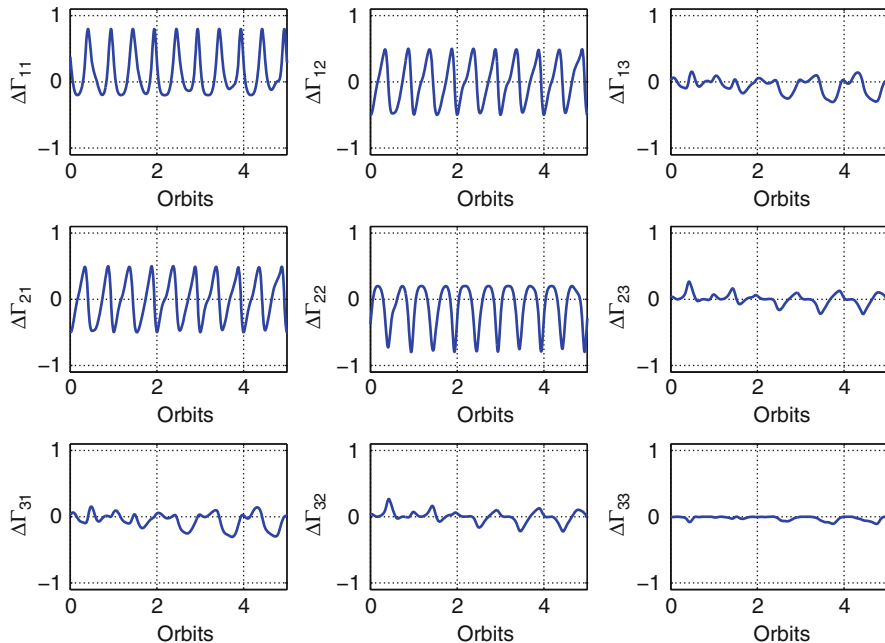


Fig. 13.2 Elements of the matrix $\Delta\Gamma(b(t))$, 87° inclination orbit, 450 km altitude, simulated for five orbits

Most LPV synthesis techniques require prior knowledge of the parameters variation range. These values are obtained using the IGRF geomagnetic field model and simulating for 24 h the motion of a spacecraft along the chosen orbit. As an example, in Fig. 13.2 the components of $\Delta\Gamma(b(t))$ are depicted for an 87° inclination, 450 km altitude orbit.

It can be noticed how $\Delta\Gamma_{33}$ has small variations, so it can be neglected. Furthermore, at each time instant for polar orbits the diagonal elements of $\Delta\Gamma(b(t))$ are related by (13.18)

$$\Delta\Gamma_{11}(b(t)) + \Delta\Gamma_{22}(b(t)) + \Delta\Gamma_{33}(b(t)) \approx 0. \tag{13.18}$$

Under the above assumptions, the number of parameters required can be reduced to four and the simplified matrix $\Delta\Gamma(\rho)$ is given by

$$\Delta\Gamma(\rho(b)) = \begin{bmatrix} \Delta\Gamma_{11}(b) & \Delta\Gamma_{12}(b) & \Delta\Gamma_{13}(b) \\ \Delta\Gamma_{12}(b) & \Delta\Gamma_{22}(b) & \Delta\Gamma_{23}(b) \\ \Delta\Gamma_{13}(b) & \Delta\Gamma_{23}(b) & \Delta\Gamma_{33}(b) \end{bmatrix} = \begin{bmatrix} \rho_1(b) & \rho_2(b) & \rho_3(b) \\ \rho_2(b) & -\rho_1(b) & \rho_4(b) \\ \rho_3(b) & \rho_4(b) & 0 \end{bmatrix}. \tag{13.19}$$

13.4 LPV Design of Magnetic Attitude Control Laws

13.4.1 Parameter-Dependent State-Feedback Problem for LPV Systems

Given a compact set $\mathcal{P} \subset \mathbb{R}^s$, consider the LPV system

$$\begin{bmatrix} \dot{x}(t) \\ z_1(t) \\ z_2(t) \end{bmatrix} = \begin{bmatrix} A(\rho(t)) & B_w(\rho(t)) & B_u(\rho(t)) \\ C_{1x}(\rho(t)) & 0 & 0 \\ C_{2x}(\rho(t)) & 0 & I_{n_{z_2}} \end{bmatrix} \begin{bmatrix} x(t) \\ w(t) \\ u(t) \end{bmatrix}, \quad (13.20)$$

where $x \in \mathbb{R}^n$ is the state vector, $w \in \mathbb{R}^{m_w}$ is the exogenous disturbance vector, $u \in \mathbb{R}^{m_u}$ is the control signal vector, and $z_1 \in \mathbb{R}^{n_{z_1}}$ and $z_2 \in \mathbb{R}^{n_{z_2}}$ are performance variable vectors. As the system is a linear-parametrically varying one, the matrices in (13.20) depend on the parameter vector $\rho \in \mathcal{P}$. The problem under study is to determine a parameter-dependent state-feedback control law that stabilizes the closed-loop system and makes the induced \mathcal{L}_2 norm from exogenous disturbances to some performance variables less than a specified performance level γ . The parameter-dependent state-feedback problem for LPV systems has been studied extensively in the last few years and a number of publications in the literature address this problem. In the following, the approach of [36] will be summarized (see, e.g., [3, 6, 8, 18] for recent applications of this synthesis method), as far as state feedback is concerned.

The necessary and sufficient conditions for the existence of a parameter-dependent state-feedback controller have been expressed in the form of LMIs in [36]. The main result is the following.

Theorem 13.2 ([36]). *Given a compact set $\mathcal{P} \in \mathbb{R}^s$, the performance level $\gamma > 0$, and the LPV system (13.20), the parameter-dependent state-feedback problem is solvable if and only if there exists a function $X \in C^1(\mathbb{R}^s, \mathcal{S}^{n \times n})$ such that for all $\rho \in \mathcal{P}$ such that $|\dot{\rho}_i| < v_i$, $i = 1, \dots, s$, the conditions*

$$\begin{bmatrix} X(\rho) > 0 \\ X(\rho)\hat{A}^T(\rho) + \hat{A}(\rho)X(\rho) - \sum_{i=1}^s \pm \left(v_i \frac{\partial X}{\partial \rho_i} \right) - B_u(\rho)B_u^T(\rho) & X(\rho)C_{1x}^T(\rho) & \gamma^{-1}B_w(\rho) \\ C_{1x}(\rho)X(\rho) & -I_{n_{z_1}} & 0 \\ \gamma^{-1}B_w^T(\rho) & 0 & -I_{m_w} \end{bmatrix} < 0 \quad (13.21)$$

hold, where

$$\hat{A}(\rho) := A(\rho) - B_u(\rho)C_{2x}(\rho). \quad (13.22)$$

If the LMIs (13.21) are feasible, the state-feedback control law

$$u = F(\rho)x = - [B_u^T(\rho)X^{-1}(\rho) + C_{2x}(\rho)]x$$

guarantees that the closed-loop system is exponentially stable and that the induced \mathcal{L}_2 norm from the disturbances w to the performance variables z_1 and z_2 is less than γ .

The considered LMI problem is in general an infinite-dimensional one; however, the problem can be turned into a finite-dimensional one using a finite number of basis functions for the Lyapunov variable $X(\rho)$. Moreover, if the open-loop system can be expressed in an affine form, the feasibility of the LMIs (13.21) has to be checked only at the vertices of the polytope; thus, only $2^{s+1} + s$ LMIs have to be solved simultaneously. However, such parametrization leads to a sufficient condition for the parameter-dependent γ -performance problem and it leads to conservatism as the feasibility of the LMIs (13.21) depends on the selected basis functions.

Finally, Theorem 13.2 holds for a given performance index $\gamma > 0$. In order to minimize the induced \mathcal{L}_2 norm, the following convex optimization problem can be implemented:

$$\begin{aligned} \min_{X(\rho)} \quad & -\alpha \\ \text{s.t.} \quad & (13.21), \end{aligned} \tag{13.23}$$

where $\alpha = 1/\gamma$.

13.4.2 LPV Design of Magnetic Attitude Controllers

Given the satellite attitude dynamics expressed as an LPV system (13.17) and assuming the value of the geomagnetic field b and of the state vector x are available, we can design an LPV state-feedback controller.

Since the model is obtained by linearization and many effects, such as, e.g., magnetic residual dipoles (see [7]), are not taken into account, the controller should be able to attenuate the effect of any torque disturbance acting on the attitude variables q . For this aim, we have chosen $w(t) = T_d(t)$, $z_1(t), z_2(t) \in \mathbb{R}^3$ and defined the matrices $C_{1x} = C_{2x} = [I_3 \ 0]$.

Moreover, the structure of the basis functions must be fixed a priori to get a finite dimensional convex design problem. As recommended in [3], the parameter-dependent Lyapunov function structure has been chosen in accordance to the parameter dependence of the plant: $X(\rho) = X_0 + \rho_1 X_1 + \rho_2 X_2$. Only two parameters (ρ_1 and ρ_2) have been used for gain-scheduling, so as to limit the number of LMIs. The other two parameters ρ_3 and ρ_4 have lower variability and they have been considered uncertain. The parameter ranges used for the controller design are summarized in Table 13.1.

Note that the control input matrix $B(\rho)$ (13.17) depends on the scheduling parameter vector ρ . Since this type of LPV system does not satisfy the condition

Table 13.1 Parameter ranges and variation rates, 87° inclination orbit, 450 km altitude

# ρ	ρ_{\min}	ρ_{\max}	$ \dot{\rho} $
ρ_1	-0.2	0.8	2×10^{-3}
ρ_2	-0.5	0.5	1×10^{-3}
ρ_3	-0.25	0.25	1×10^{-3}
ρ_4	-0.25	0.25	1×10^{-3}

that the control input matrix is parameter independent, it cannot be solved with a finite number of LMIs [2]. However, this problem can be circumvented by inserting a first-order input pre-filter. Define a new control input vector $\tilde{u} \in \mathbb{R}^3$ by

$$\begin{aligned}\dot{x}_f(t) &= A_f x_f(t) + B_f \tilde{u}(t), \\ u(t) &= C_f x_f(t),\end{aligned}\tag{13.24}$$

where coefficients matrices $A_f \in \mathbb{R}^{3 \times 3}$, $B_f \in \mathbb{R}^{3 \times 3}$, $C_f \in \mathbb{R}^{3 \times 3}$ are design parameters. A first-order filter with A_f , B_f , C_f diagonal matrices has been chosen, so it can be characterized with a single parameter: the cutoff frequency.

From (13.24), defining a new state vector $x_e = [x^T \ x_f^T]^T$ the augmented system is given by

$$\dot{x}_e(t) = A(\rho)x_e(t) + B_u u(t) + B_w w(t),\tag{13.25}$$

where

$$A(\rho) = \begin{bmatrix} A & B_T(\bar{\Gamma} + \Delta\Gamma(\rho))C_f \\ 0 & A_f \end{bmatrix}, \quad B_u = \begin{bmatrix} 0 \\ B_f \end{bmatrix}, \quad B_w = \begin{bmatrix} B_T \\ 0 \end{bmatrix}.\tag{13.26}$$

As the system is affine in the parameter, the feasibility of the above finite-dimensional problem has to be checked only at the vertices of the polytopes via Yalmip [12] and SDPT3 [28].

13.5 Simulation Study

In this section, the performance of the considered control law will be illustrated in a simulation study. The considered spacecraft is of the type described in Sect. 13.2; the numerical values for the parameters of the linearized model, corresponding to a typical small satellite platform for a LEO mission, are

- Satellite inertia (kg m^2): $I = \text{diag}[35 \ 17 \ 25]$
- Momentum wheel inertia (kg m^2): $J = 0.01$
- Nominal wheel speed (rad/s): $\bar{\Omega} = -200$

A saturation limit of $\pm 20 \text{ A m}^2$ for the dipoles of the magnetic coils has been assumed. The considered configuration corresponds to a satellite characterized by

coupled roll/yaw dynamics—marginally stable thanks to the wheel momentum—and unstable pitch dynamics, due to the unfavourable gravity gradient effect ($k_z > 0$ in (13.2)). Note, however, that the open-loop instability of the pitch dynamics is compensated by the fact that the pitch axis is easier to control using magnetic torquers than the roll and yaw axes, as for the considered (polar) orbit the geomagnetic field lies essentially in the orbital plane, so that the pitch dynamics is controllable throughout the entire orbit. The spacecraft operates in a near polar orbit (87° inclination) with an altitude of 450 km and a corresponding orbital period of 5,614.8 s. Matrix $\Gamma(b(t))$ for this orbit has been characterized in Sect. 13.4.

13.5.1 Simulation Results

In order to illustrate the time-domain behaviour of the LPV controllers, some simulation examples are presented, showing the transient following an initial perturbation of the attitude dynamics with respect to the nominal Earth-pointing equilibrium. In particular, the following initial perturbations have been applied to the angular rate vector: $\delta\omega(0) = [1 \times 10^{-3} \ 2 \times 10^{-3} \ 0]^T$ rad/s. While this may appear to be an extremely small initial condition, it actually represents a significant perturbation as far as nominal regulation of attitude dynamics is concerned.

The input filter acts as a weight on the control action. Time histories of the norm of the orientation error $\sqrt{\delta q_r^T \delta q_r}$, as well as norm on the magnetic control dipole $\sqrt{m^T m}$ are depicted during the first orbit, i.e., $t \in [0, T]$ and during the following four orbits, $t \in [T, 5T]$ in Figs. 13.3 and 13.4, respectively. Figure 13.3 shows how the transient related to a non-zero initial condition is slower and less damped, when decreasing the cutoff frequency of the input filter. On the other hand, increasing the cutoff frequency increases the required control effort, as well. As for the effects of external disturbances, see Fig. 13.4, using a faster input filter provides a better rejection of the disturbance torque but does not require an additional effort in the control signal. These results are similar to the ones obtained in [38] using a robust periodic state-feedback approach.

As can be seen from the figure, both controllers damp out the effect of the initial angular rate perturbation in less than one orbit (an adequate performance for a magnetic attitude control scheme) and bring the system to its steady-state response under the effect of the cyclic external disturbance torques.

13.6 Conclusions

The problem of designing attitude controllers for magnetically actuated spacecraft has been considered. An approach to the tuning of LPV “projection based” controllers has been proposed, relying on state-feedback control techniques. The

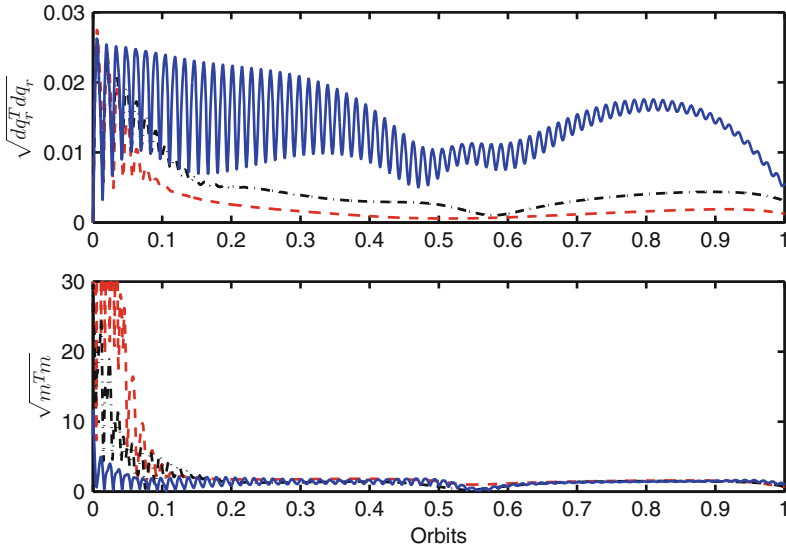


Fig. 13.3 Norm of the orientation error δq_r and of the magnetic dipole m for different cutoff frequencies of the input filter. *Solid line:* 0.001 rad/s; *dashed-dotted line:* 0.01 rad/s; *dashed line:* 0.1 rad/s

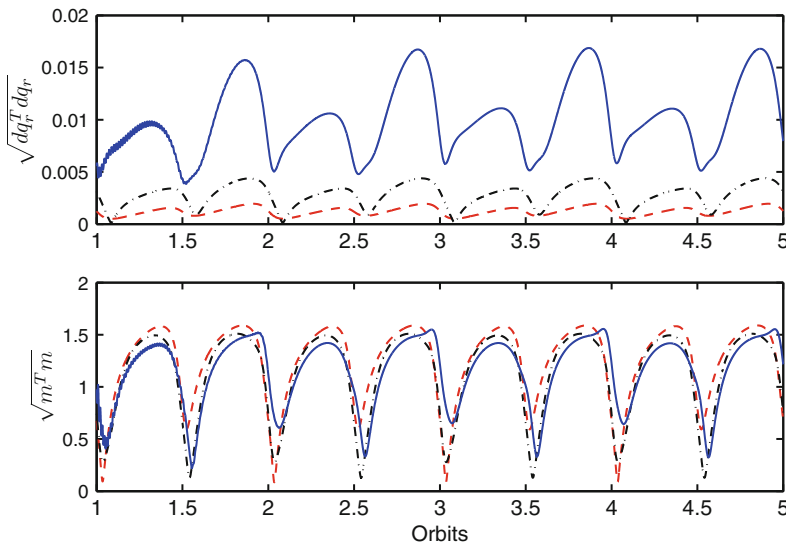


Fig. 13.4 Norm of the orientation error δq_r and of the magnetic dipole m for different cutoff frequencies of the input filter. *Solid line:* 0.001 rad/s; *dashed-dotted line:* 0.01 rad/s; *dashed line:* 0.1 rad/s

performance of the proposed control algorithms has been discussed and illustrated in a detailed simulation study. The considered control design has provided highly satisfactory performance, and proved the capability to overcome some of the restrictions posed by existing control design approaches for this problem.

References

1. Apkarian P, Gahinet P (1995) A convex characterization of gain-scheduled H_∞ controllers. *IEEE Trans Automat Contr* 40(5):853–864
2. Apkarian P, Gahinet P, Becker G (1995) Self-scheduled H_∞ control of linear parameter varying systems: a design example. *Automatica* 31(9):1251–1261
3. Balas G (2002) Linear, parameter-varying control and its application to a turbofan engine. *Int J Robust Nonlinear Contr* 12(9):763–796
4. Biannic JM, Apkarian P (1995) Self-scheduled H_∞ control of missile via linear matrix inequalities. *J Guid Contr Dyn* 18(3):532–538
5. Bittanti S, Colaneri P (2008) *Periodic systems: Filtering and control*. Springer, London
6. Chen J, Gu W, Postlethwhite I, Natesan K (2008) Robust LPV control of UAV with parameter dependent performance. In: *Proceedings of the 17th IFAC world congress*, Seoul, South Korea, pp 1838–1843
7. Corno M, Lovera M (2009) Spacecraft attitude dynamics and control in the presence of large magnetic residuals. *Control Eng Pract* 17(4):456–468
8. Corno M, Savaresi S, Balas G (2009) On linear parameter varying (LPV) slip-controller design for two-wheeled vehicles. *Int J Robust Nonlinear Contr* 19(12):1313–1336
9. Hablani H (1995) Comparative stability analysis and performance of magnetic controllers for bias momentum satellites. *J Guid Contr Dyn* 18(6):1313–1320
10. Hughes P (1986) *Spacecraft attitude dynamics*. Wiley, New York
11. Khalil H (1992) *Nonlinear systems*. Macmillan, New York
12. Lofberg J (2004) Yalmip: A toolbox for modeling and optimization in matlab. In: *2004 IEEE international symposium on computer aided control systems design*, pp 284–289
13. Lovera M (2001) Optimal magnetic momentum control for inertially pointing spacecraft. *Eur J Contr* 7(1):30–39
14. Lovera M, De Marchi E, Bittanti S (2002) Periodic attitude control techniques for small satellites with magnetic actuators. *IEEE Trans Contr Syst Technol* 10(1):90–95
15. Lovera M, Novara C, Dos Santos PL, Rivera D (2011) Guest editorial special issue on applied LPV modeling and identification. *IEEE Trans Contr Syst Technol* 19(1):1–4
16. Martel F, Pal P, Psiaki M (1988) Active magnetic control system for gravity gradient stabilised spacecraft. In: *2nd annual AIAA/USU conference on small satellites*, Logan (Utah), USA, 1988
17. Packard A (1994) Gain scheduling via linear fractional transformations. *Syst Contr Lett* 22:79–92
18. Pfifer H, Hecker S (2010) LPV controller synthesis for a generic missile model. In: *Proceedings of the 4th IEEE multi-conference on systems and control*, Yokohama, Japan, pp 1838–1843
19. Pittelkau M (1993) Optimal periodic control for spacecraft pointing and attitude determination. *J Guid Contr Dyn* 16(6):1078–1084
20. Psiaki M (2001) Magnetic torquer attitude control via asymptotic periodic linear quadratic regulation. *J Guid Contr Dyn* 24(2):386–394
21. Pulecchi T, Lovera M, Varga A (2010) Optimal discrete-time design of three-axis magnetic attitude control laws. *IEEE Trans Contr Syst Technol* 18(3):714–722

22. Sato M, Ebihara Y, Peaucelle D (2010) Gain-scheduled state-feedback controllers using inexactly measured scheduling parameters: H_2 and H_∞ problems. In: Proceedings of the 2010 American control conference, Baltimore, USA
23. Scherer C (1996) Mixed h_2/h_∞ control for time-varying and linear parametrically-varying systems. *Int J Robust Nonlinear Contr* 6(9–10):929–952
24. Scherer C (2001) LPV control and full block multipliers. *Automatica* 37(3):361–375
25. Sidi M (1997) Spacecraft dynamics and control. Cambridge University Press, Cambridge
26. Silani E, Lovera M (2005) Magnetic spacecraft attitude control: a survey and some new results. *Contr Eng Pract* 13(3):357–371
27. Stickler A, Alfriend K (1976) An elementary magnetic attitude control system. *J Spacecr Rockets* 13(5):282–287
28. Toh K, Todd M, Tutuncu R (1999) Sdpt3-a matlab software package for semidefinite programming. *Optim Methods Softw* 11(12):545–581
29. Toth R, Lovera M, Heuberger P, van den Hof P (2009) Discretization of linear fractional representations of LPV systems. In: Proceedings of the 48th IEEE conference on decision and control, Shanghai, China
30. Varga A, Pieters S (1998) Gradient-based approach to solve optimal periodic output feedback control problems. *Automatica* 34(4):477–481
31. Vigano L, Bergamasco M, Lovera M, Varga A (2010) Optimal periodic output feedback control: a continuous-time approach and a case study. *Int J Contr* 83(5):897–914
32. Wertz J (1978) Spacecraft attitude determination and control. D. Reidel Publishing Company, Dordrecht
33. Wisniewski R (2000) Linear time-varying approach to satellite attitude control using only electromagnetic actuation. *J Guid Contr Dyn* 23(4):640–646
34. Wisniewski R, Markley L (1999) Optimal magnetic attitude control. In: 14th IFAC world congress, Beijing, China
35. Wood M, Chen WH, Fertin D (2006) Model predictive control of low earth orbiting spacecraft with magneto-torquers. In: IEEE international conference on control applications, Munich, Germany
36. Wu F (1995) Control of linear parameter varying systems. PhD thesis, University of California, Berkeley, USA
37. Yan H, Ross IM, Alfriend KT (2007) Pseudospectral feedback control for three-axis magnetic attitude stabilization in elliptic orbits. *J Guid Contr Dyn* 30(4):1107–1115
38. Zanchettin A, Lovera M (2011) H_∞ attitude control of magnetically actuated satellites. In: IFAC world congress, Milano, Italy

Chapter 13

Attitude Regulation for Spacecraft with Magnetic Actuators: An LPV Approach

Andrea Corti and Marco Lovera

Abstract Magnetic torquers are an effective and reliable technology for the attitude control of small satellites in low Earth orbit. Such actuators operate by generating a magnetic dipole which interacts with the magnetic field of the Earth. The main difficulty in the design of attitude control laws based on magnetic torquers is that the torques they generate are instantaneously constrained to lie in the plane orthogonal to the local direction of the geomagnetic field vector, which varies according to the current orbital position of the spacecraft. This implies that the attitude regulation problem is formulated over a time-varying model. In recent years, this control problem has been studied extensively, either using methods based on averaged models or via approaches which exploit the quasi-periodic variability of the geomagnetic field. With the exception of other approaches based on Model Predictive Control, none of the above actually exploits at the design stage the fact that the geomagnetic field can be reliably measured on board and, therefore, the above mentioned time-variability of the attitude dynamics can be represented in LPV form. Therefore, in this chapter an LPV approach to the problem of magnetic attitude control law design is proposed. To this purpose, an LPV model of the attitude dynamics is first derived, LPV control laws suitable for on board implementation are synthesized and eventually tested in simulation.

13.1 Introduction

Electromagnetic actuators are a particularly effective and reliable technology for the attitude control of small satellites. Such actuators operate on the basis of the interaction between the magnetic field generated by a set of three orthogonal,

A. Corti • M. Lovera (✉)

Dipartimento di Elettronica e Informazione, Politecnico di Milano, Milano, Italy
e-mail: corti@elet.polimi.it; lovera@elet.polimi.it

current-driven coils and the magnetic field of the Earth and provide a simple solution to the problem of generating torques on board of a satellite, both for attitude control in momentum biased or gravity gradient architectures and as secondary actuators for momentum management tasks in zero momentum reaction wheel based configurations (see [25]).

The main difficulty in the design of magnetic attitude control laws is related to the fact that magnetic torques are instantaneously constrained to lie in the plane orthogonal to the local direction of the geomagnetic field vector. Controllability of the attitude dynamics is ensured for a wide range of orbit altitudes and inclinations in spite of this constraint, thanks to the variability of the geomagnetic field. However, this implies that the attitude control engineer has to deal with a time-varying model in the control design process.

In recent years, considerable effort has been devoted to the analysis of this control problem. In particular, as far as the linear attitude regulation problem is concerned, two main lines of work can be identified in the literature:

- Methods based on averaged models. The idea is to replace the time-varying dynamics of the magnetically actuated spacecraft with an approximate time-invariant model obtained using *averaging* techniques. The advantage of this approach is that the control problem becomes time-invariant. The main drawbacks are that: the designer has to verify a posteriori that the designed controller actually stabilizes the original time-varying dynamics with a satisfactory performance level; averaging implies limitations in closed-loop performance. This approach, originally proposed in [27], was further developed in [9] to deal with the (relatively simple) stabilization problem for the coupled roll/yaw dynamics of a momentum biased spacecraft using a magnetic torquer aligned with the pitch axis.
- Methods based on periodic models. As the variability of the geomagnetic field is *almost* time-periodic, most of the recent work on the linear magnetic attitude control problem has focused on the use of optimal and robust periodic control theory for the design of state and output feedback regulators [13, 14, 19, 20, 26, 30, 34, 35, 37]. While periodic control design methods have the advantage of guaranteeing closed-loop stability a priori, they lead to the synthesis of time-periodic regulators, which are difficult to implement and operate in practice. Therefore, more recent contributions aim at designing constant gain periodically optimal controllers (see [21, 31, 38]).

With the exception of other approaches based on Model Predictive Control, none of the above actually exploits at the design stage the fact that the geomagnetic field can be reliably measured on board and, therefore, the above-mentioned time-variability of the attitude dynamics can be represented in linear parameter-varying (LPV) form. Therefore, in this chapter, an LPV approach to the problem of magnetic attitude control law design is proposed. To this purpose, an LPV model of the attitude dynamics is first derived, LPV control laws suitable for on board implementation are synthesized and eventually tested on a realistic spacecraft simulator. LPV analysis and synthesis methods have been an active area of research

for almost two decades. Provided that a reliable LPV model for the plant to be controlled is available (see, e.g., [15] for an overview of the state-of-the-art in LPV modelling and identification), a number of methods are now available to obtain both state and output-feedback LPV controllers, see, e.g., [1, 2, 4, 17, 23, 24, 36]. As the corresponding tools reach maturity and allow to deal with problems of increasing size and complexity, the possibility of achieving a prescribed level of performance for a parameter-dependent system using a single, parametrically varying controller can be pursued in practice for a wide range of applications. In addition, implementation issues, which have proved critical in many cases, are increasingly well understood (see, e.g., [29] and the references therein) as well as the effect of noise on the measured scheduling parameters (see [22]).

The chapter is organized as follows. Section 13.2 provides a description of the spacecraft considered in the study as well as the derivation of a linearized model for its attitude dynamics. An overview of existing modelling approaches for magnetic attitude control system design is provided in Sect. 13.3, while Sect. 13.4 is devoted to the presentation of the proposed LPV technique. Finally, the results obtained in the simulation of the designed control laws are presented and discussed in Sect. 13.5.

13.2 Mathematical Model and Problem Statement

In order to represent the attitude motion of an Earth-pointing spacecraft on a circular orbit, the following reference systems are adopted:

- Earth centered inertial reference axes (ECI). The Earth's center is the origin of these axes. The positive X -axis points in the vernal equinox direction. The Z -axis points in the direction of the North Pole. The Y -axis completes the right-handed orthogonal triad.
- Orbital Axes (X_0, Y_0, Z_0). The origin of these axes is at the satellite center of mass. The X -axis points to the Earth's center; the Y -axis points in the direction of the orbital velocity vector. The Z -axis is normal to the satellite orbit plane.
- Satellite Body Axes. The origin of these axes is at the satellite center of mass; in nominal Earth-pointing conditions, the X_b (yaw), Y_b (roll) and Z_b (pitch) axes are aligned with the corresponding orbital axes.

A spacecraft with inertia matrix $I = \text{diag} [I_{xx} \ I_{yy} \ I_{zz}]$ is considered, equipped with a single-momentum wheel aligned with the body z -axis, with moment of inertia J and angular velocity Ω relative to the body frame. The aim of the attitude control scheme is to maintain the satellite body axes aligned with the orbital axes, while exploiting the gyroscopic effect due to the momentum wheel. Note that the choice of this spacecraft configuration is not particularly restrictive, since by assuming that $\Omega = 0$ and $I_{xx} \ll I_{yy}$, $I_{xx} \ll I_{zz}$ a gravity-gradient configuration can be obtained as a particular case. Similarly, the assumptions of a circular orbit and of a diagonal inertia matrix are made only for ease of presentation, but they are by no means necessary for the applicability of the proposed design approach.

Indeed, unlike existing design methods based on averaging (see, e.g., [9]), inertial coupling between roll/yaw and pitch dynamics can be handled in the design problem. The angular kinematics and dynamics of the spacecraft are modelled using as state variables the quaternion $q = [q_1 \ q_R^T]^T = [q_1 \ q_2 \ q_3 \ q_4]^T$ describing the attitude of the body axes with respect to the orbital axes and the inertial angular velocity vector $\omega = [\omega_x \ \omega_y \ \omega_z]^T$ with respect to the body axes.

In the following, we will present a linearized dynamic model for the formulation of this control problem. With respect to the selected state variables, the nominal, Earth-pointing, equilibrium corresponds to the attitude quaternion $\bar{q} = [1 \ 0 \ 0 \ 0]^T$ and to the angular rate $\bar{\omega} = [0 \ 0 \ -\Omega_0]^T$, where Ω_0 is the orbital angular rate.

Define the state vector $x = [\delta q_R^T \ \delta \omega^T]^T$ formed with small displacements of the vector part q_R of the attitude quaternion q from the nominal values $\bar{q}_R = [0 \ 0 \ 0]^T$ and small deviations of the body rates from the nominal values $\bar{\omega}_x = \bar{\omega}_y = 0, \bar{\omega}_z = -\Omega_0$.

Then the attitude dynamics can be linearized and the local linear dynamics for the attitude can be defined as [14]

$$\dot{x}(t) = Ax(t) + B_T [T_m(t) + T_d(t)], \tag{13.1}$$

where T_m is the magnetic control torque vector, T_d is the disturbance torque vector and

$$A = \left[\begin{array}{cc|ccc} A_{11} & A_{12} & & & & \\ A_{21} & A_{22} & & & & \end{array} \right] = \left[\begin{array}{ccc|ccc} 0 & -\Omega_0 & 0 & 0.5 & 0 & 0 \\ \Omega_0 & 0 & 0 & 0 & 0.5 & 0 \\ 0 & 0 & 0 & 0 & 0 & 0.5 \\ \hline 0 & 0 & 0 & 0 & W_x & 0 \\ 0 & -6k_y\Omega_0^2 & 0 & W_y & 0 & 0 \\ 0 & 0 & +6k_z\Omega_0^2 & 0 & 0 & 0 \end{array} \right], \tag{13.2}$$

$$B_T = \begin{bmatrix} 0 & 0 & 0 \\ 0 & 0 & 0 \\ 0 & 0 & 0 \\ I_{xx}^{-1} & 0 & 0 \\ 0 & I_{yy}^{-1} & 0 \\ 0 & 0 & I_{zz}^{-1} \end{bmatrix}, \tag{13.3}$$

and $k_x = \frac{I_{yy} - I_{zz}}{I_{xx}}, k_y = \frac{I_{zz} - I_{xx}}{I_{yy}}, k_z = \frac{I_{xx} - I_{yy}}{I_{zz}}, W_x = -k_x\Omega_0 + k_{wx}\bar{\Omega}, W_y = -k_y\Omega_0 - k_{wy}\bar{\Omega}, k_{wx} = \frac{J}{I_{xx}}, k_{wy} = \frac{J}{I_{yy}}$. Here, $\bar{\Omega}$ is the nominal wheel speed.

Taking into account that T_m can be written as

$$T_m(t) = m(t) \times b(t) = S(b(t))m(t) = -b(t) \times m(t), \quad (13.4)$$

where $b = [b_x \ b_y \ b_z]^T$ is the geomagnetic field vector (in body frame), m is the dipole vector of the magnetic torquers and

$$S(b) = \begin{bmatrix} 0 & b_z & -b_y \\ -b_z & 0 & b_x \\ b_y & -b_x & 0 \end{bmatrix},$$

(13.1) can be equivalently written as

$$\dot{x}(t) = Ax(t) + B_m(t)m(t) + B_T T_d(t), \quad (13.5)$$

where $B_m(t) = B_T S(b(t))$. Note that, while A is constant, the control matrix $B_m(t)$ corresponding to the control input m turns out to be time-varying because of the dependence on the geomagnetic field vector $b(t)$. Such time variability turns out to be approximately time-periodic with period equal to the orbital period $T = 2\pi/\Omega_0$. Deviations from exact periodicity are due to Earth rotation and to orbit perturbations.

As can be seen from (13.2) (and well known in the literature, see, e.g., [10, 25]), the A matrix shows that the pitch dynamics is decoupled from the roll/yaw dynamics. Therefore, in the case of a spacecraft equipped with three independent torque actuators, it would be possible to design separate controllers for the two subsystems. Unfortunately, as can be seen from the expression of matrix $B_m(t)$ in (13.3), the use of magnetic actuators introduces a coupling between the roll/yaw and the pitch subsystems. Similarly, coupling terms appear if the spacecraft inertia matrix I is not diagonal—a situation which occurs frequently in practice.

A very common structure for magnetic attitude control laws, which goes back to classical papers such as [16], consists of control laws of the kind

$$m(t) = \frac{1}{\|b(t)\|^2} S^T(b(t)) T_{id}(t), \quad (13.6)$$

where $b(t)$ is the measurement, at time t , of the geomagnetic field b and $T_{id}(t)$ is an “ideal” control torque to be determined on the basis of a suitable feedback of state or output variables, according to the specific attitude control architecture of the considered spacecraft. The above control law can be readily given a simple geometric interpretation. Indeed, recalling (13.4) we can express the torque generated by the magnetic coils as

$$T_m(t) = \frac{1}{\|b(t)\|^2} S(b(t)) S^T(b(t)) T_{id}(t) = \Gamma(b(t)) T_{id}(t), \quad (13.7)$$

where matrix $\Gamma(b(t))$ is structurally symmetric and positive semidefinite for all values of $b(t)$. Equation (13.7) can be easily interpreted as the projection of vector T_{id} onto the plane orthogonal to the direction of the magnetic field vector b (hence the name of “projection-based” controllers). Letting now

$$B(t) = B_T \Gamma(b(t)) \quad (13.8)$$

and choosing as control variable $u(t) = T_{id}(t)$, one gets to the final design model

$$\dot{x}(t) = Ax(t) + B(t)u(t) + B_T T_{id}(t). \quad (13.9)$$

Different control strategies can be adopted using the fixed structure projection approach; in this chapter we will focus on state-feedback control, with either constant or parameter-dependent gain.

Remark 13.1. In view of the digital implementation of the controller, the above-described geometric view of magnetic control holds only in an approximate sense, but still represents a good interpretation of the operation of the controller since the sampling interval for the implementation of this type of controller is normally short (from 0.1 s to 1 s at most) with respect to the period of the geomagnetic field along a low Earth orbit (the orbital period of a LEO orbit is typically about 6,000 s).

Note that the advantage of the considered controller structure is that only constant parameters (i.e., the ones defining T_{id} as a function of the state vector) have to be designed, while the time-dependence of the control law is carried by the (measurable) value of the components of the geomagnetic field b entering (13.6). In the following section, an overview of possible approaches to the optimal tuning of this class of attitude controllers will be proposed.

In view of the above, the goal of the design problem considered in this chapter is to derive state-feedback controllers for the system in (13.9) satisfying (as many as possible of) the following requirements:

- (A.1) Nominal closed-loop stability: as shown above, the local dynamics of a magnetically controlled spacecraft is time varying, therefore, the stabilization problem cannot be faced by means of conventional LTI design tools.
- (A.2) Nominal closed-loop performance: the spacecraft is subject to external disturbances, which can be decomposed in a secular (i.e., constant) and a cyclic (i.e., periodic, with period equal to the orbit period $T = \frac{2\pi}{\Omega}$); the controller must try and attenuate the effect of such disturbances on the attitude.
- (A.3) Stability and performance robustness: the dynamics of the spacecraft is subject to a number of sources of uncertainty, the most important of which are the moments of inertia of the spacecraft and the actual behavior of the magnetic field (as opposed to the mathematical model used in the design).

- (A.4) Implementation issues: time-varying gains are not easily implemented on board, as they give rise to a sensitive synchronization problem. Therefore, we seek either constant-gain controllers or gain-scheduled controllers which can exploit on board measurements of the magnetic field vector.

13.3 Approaches to Modelling for Magnetic Attitude Control Design

In Sects. 13.3.1 and 13.3.2, a short overview of modelling approaches based, respectively, on averaging and on periodic models is presented, while the LPV approach to the problem is introduced in Sect. 13.3.3 and further developed in Sect. 13.4.

13.3.1 Averaging-Based Modelling of Magnetically Controlled Spacecraft

The simplest approach to the design of a magnetic attitude control law in the setting established in the previous section is based on the idea of *averaging* to derive an approximate LTI model from (13.9). From a practical point of view, one can simply replace $\Gamma(b(t))$ in (13.9) with the constant matrix $\bar{\Gamma}$ defined as

$$\bar{\Gamma} = \frac{1}{T} \int_0^T \Gamma(b(t)) dt \quad (13.10)$$

to get

$$\dot{x}(t) = Ax(t) + \bar{B}u(t) + B_T T_d(t), \quad (13.11)$$

where $\bar{B} = B_T \bar{\Gamma}$. One can then resort to the methods and tools for state-feedback design for LTI systems to compute the sought after control law.

Although averaging has been used somewhat heuristically in the attitude control literature (see [9] and the references therein), the theoretical foundation for this approach is the following result (reported from [11]), which provides conditions under which it is possible to approximate a linear time-periodic system with an averaged one.

Theorem 13.1. *Consider the linear time-periodic system*

$$\dot{x}(t) = \varepsilon A(t)x(t), \quad (13.12)$$

with $A(t+T) = A(t)$ and $\varepsilon > 0$ and define the averaged system associated to (13.12) as

$$\dot{x}(t) = \varepsilon \bar{A}x(t), \quad (13.13)$$

where

$$\bar{A} = \frac{1}{T} \int_0^T A(\tau) d\tau. \quad (13.14)$$

Then if \bar{A} is Hurwitz there exists $\varepsilon^* > 0$ such that for all $0 < \varepsilon < \varepsilon^*$ $x = 0$ is an exponentially stable equilibrium for (13.12).

It is apparent from the above theorem that using an averaging approach only low-bandwidth controllers can be obtained, as stability of the feedback system is preserved only provided that the closed-loop dynamics turn out to be sufficiently slow.

13.3.2 Periodic Modelling of Magnetically Controlled Spacecraft

A less restrictive design approach consists in adopting as an approximation of $\Gamma(b(t))$ in (13.9) a periodic matrix obtained by either using a simplified periodic model for $b(t)$ (such as the tilted dipole model, see, e.g., [32]) or by replacing $b(t)$ with a time-periodic approximation obtained by least-squares fitting either flight data or simulated data obtained from a high-fidelity geomagnetic field model. As an example, in Fig. 13.1, the geomagnetic field along an 87° inclination, 450 km altitude orbit computed using the IGRF model is compared to its time-periodic approximation. $\Gamma(b(t))$ in (13.9) is then replaced with a time-periodic approximation $\Gamma_P(t)$, to get the linear time-periodic model

$$\dot{x}(t) = Ax(t) + B_P(t)u(t) + B_T T_d(t), \quad (13.15)$$

where $B_P(t) = B_T \Gamma_P(t)$. The controller design problem can then be faced using the methods and tools for state-feedback design for linear time-periodic systems. Unfortunately, the classical theory for optimal and robust control of linear time-periodic systems (see e.g., [5, 14, 33]) leads to the design of time-periodic controllers, which turn out to be impractical from the point of view of implementation. In view of this, a number of recent results (see [21, 38]) aim at the design of constant gain, periodically optimal controllers, which represent a trade-off between accuracy and complexity. Simulation results reported in [21] demonstrate that this approach can lead to significant improvements with respect to the averaging-based one, both in terms of stability (faster closed-loop dynamics) and performance (smaller steady-state pointing errors).

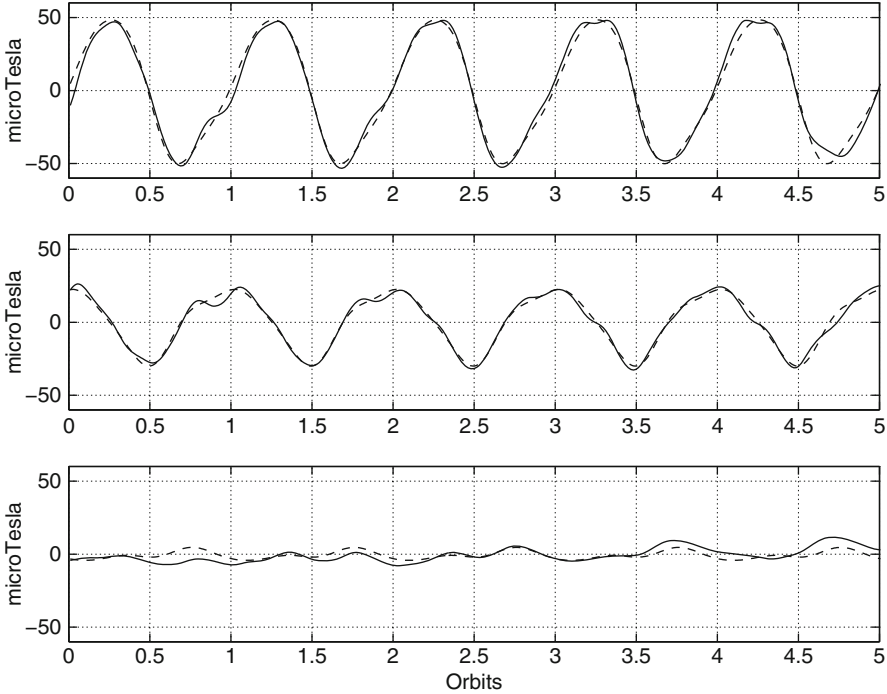


Fig. 13.1 Periodic approximation of the geomagnetic field in Pitch–Roll–Yaw coordinates, 87° inclination orbit, 450 km altitude

13.3.3 *Parameter-Dependent Modelling of Magnetically Controlled Spacecraft*

An alternative parameter-dependent approach is proposed in this section. At each time instant, the matrix $\Gamma(b(t))$ can be expressed as the sum of its average defined in (13.10) with the set of perturbed elements

$$\Gamma(b(t)) = \bar{\Gamma} + \Delta\Gamma(b(t)). \tag{13.16}$$

The elements of the matrix $\Delta\Gamma(b(t)) \in \mathbb{R}^{3 \times 3}$ can be interpreted as model parameters ρ and this leads to the LPV formulation

$$\dot{x}(t) = Ax(t) + B_T(\bar{\Gamma} + \Delta\Gamma(\rho))u(t) + B_T T_d(t). \tag{13.17}$$

The geomagnetic field $b(t)$ is measured online and $\bar{\Gamma}$ is computed offline, so the model parameters can be computed online and used for gain-scheduling. Moreover, the matrix $\Gamma(b(t))$ is symmetric, $\bar{\Gamma}$ is diagonal, so $\Delta\Gamma(b(t))$ is symmetric and is completely defined by six parameters only.

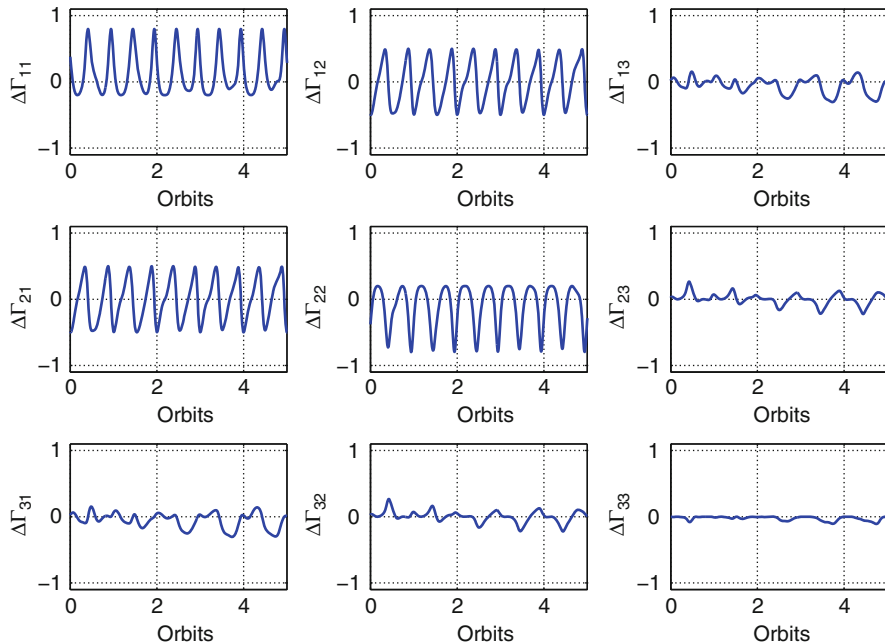


Fig. 13.2 Elements of the matrix $\Delta\Gamma(b(t))$, 87° inclination orbit, 450 km altitude, simulated for five orbits

Most LPV synthesis techniques require prior knowledge of the parameters variation range. These values are obtained using the IGRF geomagnetic field model and simulating for 24 h the motion of a spacecraft along the chosen orbit. As an example, in Fig. 13.2 the components of $\Delta\Gamma(b(t))$ are depicted for an 87° inclination, 450 km altitude orbit.

It can be noticed how $\Delta\Gamma_{33}$ has small variations, so it can be neglected. Furthermore, at each time instant for polar orbits the diagonal elements of $\Delta\Gamma(b(t))$ are related by (13.18)

$$\Delta\Gamma_{11}(b(t)) + \Delta\Gamma_{22}(b(t)) + \Delta\Gamma_{33}(b(t)) \approx 0. \tag{13.18}$$

Under the above assumptions, the number of parameters required can be reduced to four and the simplified matrix $\Delta\Gamma(\rho)$ is given by

$$\Delta\Gamma(\rho(b)) = \begin{bmatrix} \Delta\Gamma_{11}(b) & \Delta\Gamma_{12}(b) & \Delta\Gamma_{13}(b) \\ \Delta\Gamma_{12}(b) & \Delta\Gamma_{22}(b) & \Delta\Gamma_{23}(b) \\ \Delta\Gamma_{13}(b) & \Delta\Gamma_{23}(b) & \Delta\Gamma_{33}(b) \end{bmatrix} = \begin{bmatrix} \rho_1(b) & \rho_2(b) & \rho_3(b) \\ \rho_2(b) & -\rho_1(b) & \rho_4(b) \\ \rho_3(b) & \rho_4(b) & 0 \end{bmatrix}. \tag{13.19}$$

13.4 LPV Design of Magnetic Attitude Control Laws

13.4.1 Parameter-Dependent State-Feedback Problem for LPV Systems

Given a compact set $\mathcal{P} \subset \mathbb{R}^s$, consider the LPV system

$$\begin{bmatrix} \dot{x}(t) \\ z_1(t) \\ z_2(t) \end{bmatrix} = \begin{bmatrix} A(\rho(t)) & B_w(\rho(t)) & B_u(\rho(t)) \\ C_{1x}(\rho(t)) & 0 & 0 \\ C_{2x}(\rho(t)) & 0 & I_{n_{z_2}} \end{bmatrix} \begin{bmatrix} x(t) \\ w(t) \\ u(t) \end{bmatrix}, \quad (13.20)$$

where $x \in \mathbb{R}^n$ is the state vector, $w \in \mathbb{R}^{m_w}$ is the exogenous disturbance vector, $u \in \mathbb{R}^{m_u}$ is the control signal vector, and $z_1 \in \mathbb{R}^{n_{z_1}}$ and $z_2 \in \mathbb{R}^{n_{z_2}}$ are performance variable vectors. As the system is a linear-parametrically varying one, the matrices in (13.20) depend on the parameter vector $\rho \in \mathcal{P}$. The problem under study is to determine a parameter-dependent state-feedback control law that stabilizes the closed-loop system and makes the induced \mathcal{L}_2 norm from exogenous disturbances to some performance variables less than a specified performance level γ . The parameter-dependent state-feedback problem for LPV systems has been studied extensively in the last few years and a number of publications in the literature address this problem. In the following, the approach of [36] will be summarized (see, e.g., [3, 6, 8, 18] for recent applications of this synthesis method), as far as state feedback is concerned.

The necessary and sufficient conditions for the existence of a parameter-dependent state-feedback controller have been expressed in the form of LMIs in [36]. The main result is the following.

Theorem 13.2 ([36]). *Given a compact set $\mathcal{P} \in \mathbb{R}^s$, the performance level $\gamma > 0$, and the LPV system (13.20), the parameter-dependent state-feedback problem is solvable if and only if there exists a function $X \in C^1(\mathbb{R}^s, \mathcal{S}^{n \times n})$ such that for all $\rho \in \mathcal{P}$ such that $|\dot{\rho}_i| < v_i$, $i = 1, \dots, s$, the conditions*

$$\begin{bmatrix} X(\rho) > 0 \\ X(\rho)\hat{A}^T(\rho) + \hat{A}(\rho)X(\rho) - \sum_{i=1}^s \pm \left(v_i \frac{\partial X}{\partial \rho_i} \right) - B_u(\rho)B_u^T(\rho) & X(\rho)C_{1x}^T(\rho) & \gamma^{-1}B_w(\rho) \\ C_{1x}(\rho)X(\rho) & -I_{n_{z_1}} & 0 \\ \gamma^{-1}B_w^T(\rho) & 0 & -I_{m_w} \end{bmatrix} < 0 \quad (13.21)$$

hold, where

$$\hat{A}(\rho) := A(\rho) - B_u(\rho)C_{2x}(\rho). \quad (13.22)$$

If the LMIs (13.21) are feasible, the state-feedback control law

$$u = F(\rho)x = - [B_u^T(\rho)X^{-1}(\rho) + C_{2x}(\rho)]x$$

guarantees that the closed-loop system is exponentially stable and that the induced \mathcal{L}_2 norm from the disturbances w to the performance variables z_1 and z_2 is less than γ .

The considered LMI problem is in general an infinite-dimensional one; however, the problem can be turned into a finite-dimensional one using a finite number of basis functions for the Lyapunov variable $X(\rho)$. Moreover, if the open-loop system can be expressed in an affine form, the feasibility of the LMIs (13.21) has to be checked only at the vertices of the polytope; thus, only $2^{s+1} + s$ LMIs have to be solved simultaneously. However, such parametrization leads to a sufficient condition for the parameter-dependent γ -performance problem and it leads to conservatism as the feasibility of the LMIs (13.21) depends on the selected basis functions.

Finally, Theorem 13.2 holds for a given performance index $\gamma > 0$. In order to minimize the induced \mathcal{L}_2 norm, the following convex optimization problem can be implemented:

$$\begin{aligned} \min_{X(\rho)} \quad & -\alpha \\ \text{s.t.} \quad & (13.21), \end{aligned} \tag{13.23}$$

where $\alpha = 1/\gamma$.

13.4.2 LPV Design of Magnetic Attitude Controllers

Given the satellite attitude dynamics expressed as an LPV system (13.17) and assuming the value of the geomagnetic field b and of the state vector x are available, we can design an LPV state-feedback controller.

Since the model is obtained by linearization and many effects, such as, e.g., magnetic residual dipoles (see [7]), are not taken into account, the controller should be able to attenuate the effect of any torque disturbance acting on the attitude variables q . For this aim, we have chosen $w(t) = T_d(t)$, $z_1(t), z_2(t) \in \mathbb{R}^3$ and defined the matrices $C_{1x} = C_{2x} = [I_3 \ 0]$.

Moreover, the structure of the basis functions must be fixed a priori to get a finite dimensional convex design problem. As recommended in [3], the parameter-dependent Lyapunov function structure has been chosen in accordance to the parameter dependence of the plant: $X(\rho) = X_0 + \rho_1 X_1 + \rho_2 X_2$. Only two parameters (ρ_1 and ρ_2) have been used for gain-scheduling, so as to limit the number of LMIs. The other two parameters ρ_3 and ρ_4 have lower variability and they have been considered uncertain. The parameter ranges used for the controller design are summarized in Table 13.1.

Note that the control input matrix $B(\rho)$ (13.17) depends on the scheduling parameter vector ρ . Since this type of LPV system does not satisfy the condition

Table 13.1 Parameter ranges and variation rates, 87° inclination orbit, 450 km altitude

# ρ	ρ_{\min}	ρ_{\max}	$ \dot{\rho} $
ρ_1	-0.2	0.8	2×10^{-3}
ρ_2	-0.5	0.5	1×10^{-3}
ρ_3	-0.25	0.25	1×10^{-3}
ρ_4	-0.25	0.25	1×10^{-3}

that the control input matrix is parameter independent, it cannot be solved with a finite number of LMIs [2]. However, this problem can be circumvented by inserting a first-order input pre-filter. Define a new control input vector $\tilde{u} \in \mathbb{R}^3$ by

$$\begin{aligned}\dot{x}_f(t) &= A_f x_f(t) + B_f \tilde{u}(t), \\ u(t) &= C_f x_f(t),\end{aligned}\tag{13.24}$$

where coefficients matrices $A_f \in \mathbb{R}^{3 \times 3}$, $B_f \in \mathbb{R}^{3 \times 3}$, $C_f \in \mathbb{R}^{3 \times 3}$ are design parameters. A first-order filter with A_f , B_f , C_f diagonal matrices has been chosen, so it can be characterized with a single parameter: the cutoff frequency.

From (13.24), defining a new state vector $x_e = [x^T \ x_f^T]^T$ the augmented system is given by

$$\dot{x}_e(t) = A(\rho)x_e(t) + B_u u(t) + B_w w(t),\tag{13.25}$$

where

$$A(\rho) = \begin{bmatrix} A & B_T(\bar{\Gamma} + \Delta\Gamma(\rho))C_f \\ 0 & A_f \end{bmatrix}, \quad B_u = \begin{bmatrix} 0 \\ B_f \end{bmatrix}, \quad B_w = \begin{bmatrix} B_T \\ 0 \end{bmatrix}.\tag{13.26}$$

As the system is affine in the parameter, the feasibility of the above finite-dimensional problem has to be checked only at the vertices of the polytopes via Yalmip [12] and SDPT3 [28].

13.5 Simulation Study

In this section, the performance of the considered control law will be illustrated in a simulation study. The considered spacecraft is of the type described in Sect. 13.2; the numerical values for the parameters of the linearized model, corresponding to a typical small satellite platform for a LEO mission, are

- Satellite inertia (kg m^2): $I = \text{diag}[35 \ 17 \ 25]$
- Momentum wheel inertia (kg m^2): $J = 0.01$
- Nominal wheel speed (rad/s): $\bar{\Omega} = -200$

A saturation limit of $\pm 20 \text{ A m}^2$ for the dipoles of the magnetic coils has been assumed. The considered configuration corresponds to a satellite characterized by

coupled roll/yaw dynamics—marginally stable thanks to the wheel momentum—and unstable pitch dynamics, due to the unfavourable gravity gradient effect ($k_z > 0$ in (13.2)). Note, however, that the open-loop instability of the pitch dynamics is compensated by the fact that the pitch axis is easier to control using magnetic torquers than the roll and yaw axes, as for the considered (polar) orbit the geomagnetic field lies essentially in the orbital plane, so that the pitch dynamics is controllable throughout the entire orbit. The spacecraft operates in a near polar orbit (87° inclination) with an altitude of 450 km and a corresponding orbital period of 5,614.8 s. Matrix $\Gamma(b(t))$ for this orbit has been characterized in Sect. 13.4.

13.5.1 Simulation Results

In order to illustrate the time-domain behaviour of the LPV controllers, some simulation examples are presented, showing the transient following an initial perturbation of the attitude dynamics with respect to the nominal Earth-pointing equilibrium. In particular, the following initial perturbations have been applied to the angular rate vector: $\delta\omega(0) = [1 \times 10^{-3} \ 2 \times 10^{-3} \ 0]^T$ rad/s. While this may appear to be an extremely small initial condition, it actually represents a significant perturbation as far as nominal regulation of attitude dynamics is concerned.

The input filter acts as a weight on the control action. Time histories of the norm of the orientation error $\sqrt{\delta q_r^T \delta q_r}$, as well as norm on the magnetic control dipole $\sqrt{m^T m}$ are depicted during the first orbit, i.e., $t \in [0, T]$ and during the following four orbits, $t \in [T, 5T]$ in Figs. 13.3 and 13.4, respectively. Figure 13.3 shows how the transient related to a non-zero initial condition is slower and less damped, when decreasing the cutoff frequency of the input filter. On the other hand, increasing the cutoff frequency increases the required control effort, as well. As for the effects of external disturbances, see Fig. 13.4, using a faster input filter provides a better rejection of the disturbance torque but does not require an additional effort in the control signal. These results are similar to the ones obtained in [38] using a robust periodic state-feedback approach.

As can be seen from the figure, both controllers damp out the effect of the initial angular rate perturbation in less than one orbit (an adequate performance for a magnetic attitude control scheme) and bring the system to its steady-state response under the effect of the cyclic external disturbance torques.

13.6 Conclusions

The problem of designing attitude controllers for magnetically actuated spacecraft has been considered. An approach to the tuning of LPV “projection based” controllers has been proposed, relying on state-feedback control techniques. The

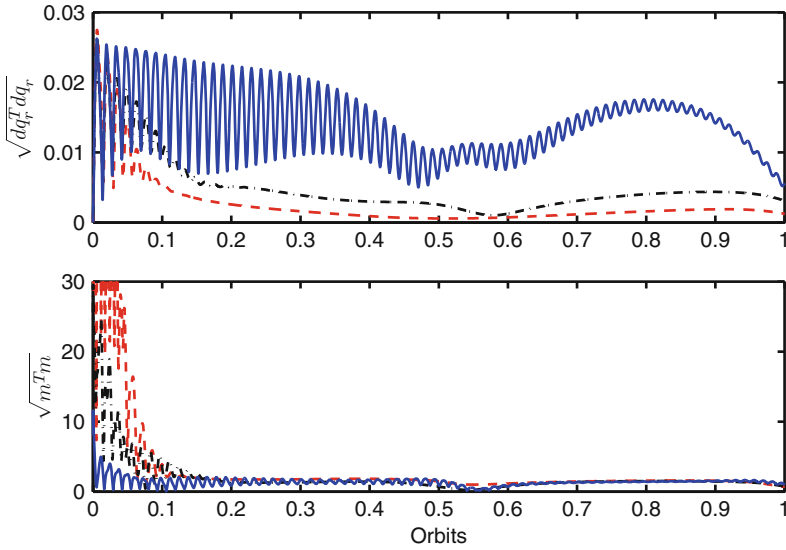


Fig. 13.3 Norm of the orientation error δq_r and of the magnetic dipole m for different cutoff frequencies of the input filter. *Solid line:* 0.001 rad/s; *dashed-dotted line:* 0.01 rad/s; *dashed line:* 0.1 rad/s

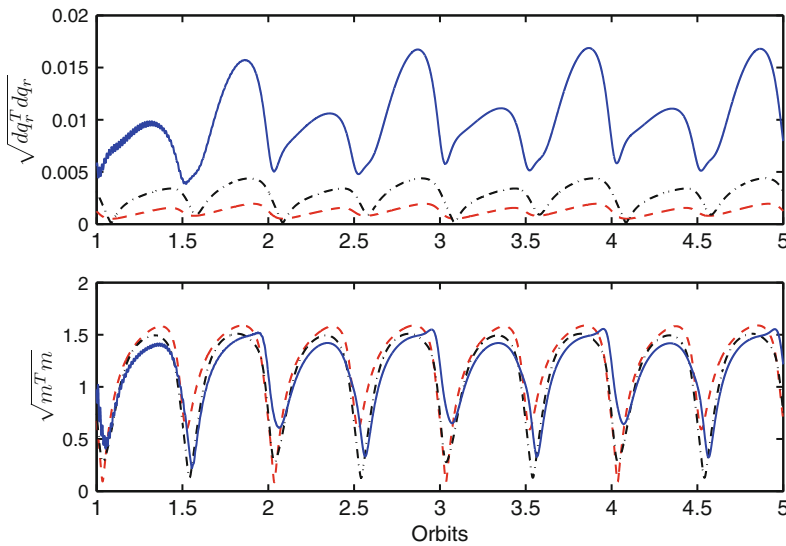


Fig. 13.4 Norm of the orientation error δq_r and of the magnetic dipole m for different cutoff frequencies of the input filter. *Solid line:* 0.001 rad/s; *dashed-dotted line:* 0.01 rad/s; *dashed line:* 0.1 rad/s

performance of the proposed control algorithms has been discussed and illustrated in a detailed simulation study. The considered control design has provided highly satisfactory performance, and proved the capability to overcome some of the restrictions posed by existing control design approaches for this problem.

References

1. Apkarian P, Gahinet P (1995) A convex characterization of gain-scheduled H_∞ controllers. *IEEE Trans Automat Contr* 40(5):853–864
2. Apkarian P, Gahinet P, Becker G (1995) Self-scheduled H_∞ control of linear parameter varying systems: a design example. *Automatica* 31(9):1251–1261
3. Balas G (2002) Linear, parameter-varying control and its application to a turbofan engine. *Int J Robust Nonlinear Contr* 12(9):763–796
4. Biannic JM, Apkarian P (1995) Self-scheduled H_∞ control of missile via linear matrix inequalities. *J Guid Contr Dyn* 18(3):532–538
5. Bittanti S, Colaneri P (2008) *Periodic systems: Filtering and control*. Springer, London
6. Chen J, Gu W, Postlethwhite I, Natesan K (2008) Robust LPV control of UAV with parameter dependent performance. In: *Proceedings of the 17th IFAC world congress*, Seoul, South Korea, pp 1838–1843
7. Corno M, Lovera M (2009) Spacecraft attitude dynamics and control in the presence of large magnetic residuals. *Control Eng Pract* 17(4):456–468
8. Corno M, Savaresi S, Balas G (2009) On linear parameter varying (LPV) slip-controller design for two-wheeled vehicles. *Int J Robust Nonlinear Contr* 19(12):1313–1336
9. Hablani H (1995) Comparative stability analysis and performance of magnetic controllers for bias momentum satellites. *J Guid Contr Dyn* 18(6):1313–1320
10. Hughes P (1986) *Spacecraft attitude dynamics*. Wiley, New York
11. Khalil H (1992) *Nonlinear systems*. Macmillan, New York
12. Lofberg J (2004) Yalmip: A toolbox for modeling and optimization in matlab. In: *2004 IEEE international symposium on computer aided control systems design*, pp 284–289
13. Lovera M (2001) Optimal magnetic momentum control for inertially pointing spacecraft. *Eur J Contr* 7(1):30–39
14. Lovera M, De Marchi E, Bittanti S (2002) Periodic attitude control techniques for small satellites with magnetic actuators. *IEEE Trans Contr Syst Technol* 10(1):90–95
15. Lovera M, Novara C, Dos Santos PL, Rivera D (2011) Guest editorial special issue on applied LPV modeling and identification. *IEEE Trans Contr Syst Technol* 19(1):1–4
16. Martel F, Pal P, Psiaki M (1988) Active magnetic control system for gravity gradient stabilised spacecraft. In: *2nd annual AIAA/USU conference on small satellites*, Logan (Utah), USA, 1988
17. Packard A (1994) Gain scheduling via linear fractional transformations. *Syst Contr Lett* 22:79–92
18. Pfifer H, Hecker S (2010) LPV controller synthesis for a generic missile model. In: *Proceedings of the 4th IEEE multi-conference on systems and control*, Yokohama, Japan, pp 1838–1843
19. Pittelkau M (1993) Optimal periodic control for spacecraft pointing and attitude determination. *J Guid Contr Dyn* 16(6):1078–1084
20. Psiaki M (2001) Magnetic torquer attitude control via asymptotic periodic linear quadratic regulation. *J Guid Contr Dyn* 24(2):386–394
21. Pulecchi T, Lovera M, Varga A (2010) Optimal discrete-time design of three-axis magnetic attitude control laws. *IEEE Trans Contr Syst Technol* 18(3):714–722

22. Sato M, Ebihara Y, Peaucelle D (2010) Gain-scheduled state-feedback controllers using inexactly measured scheduling parameters: H_2 and H_∞ problems. In: Proceedings of the 2010 American control conference, Baltimore, USA
23. Scherer C (1996) Mixed h_2/h_∞ control for time-varying and linear parametrically-varying systems. *Int J Robust Nonlinear Contr* 6(9–10):929–952
24. Scherer C (2001) LPV control and full block multipliers. *Automatica* 37(3):361–375
25. Sidi M (1997) Spacecraft dynamics and control. Cambridge University Press, Cambridge
26. Silani E, Lovera M (2005) Magnetic spacecraft attitude control: a survey and some new results. *Contr Eng Pract* 13(3):357–371
27. Stickler A, Alfriend K (1976) An elementary magnetic attitude control system. *J Spacecr Rockets* 13(5):282–287
28. Toh K, Todd M, Tutuncu R (1999) Sdpt3-a matlab software package for semidefinite programming. *Optim Methods Softw* 11(12):545–581
29. Toth R, Lovera M, Heuberger P, van den Hof P (2009) Discretization of linear fractional representations of LPV systems. In: Proceedings of the 48th IEEE conference on decision and control, Shanghai, China
30. Varga A, Pieters S (1998) Gradient-based approach to solve optimal periodic output feedback control problems. *Automatica* 34(4):477–481
31. Vigano L, Bergamasco M, Lovera M, Varga A (2010) Optimal periodic output feedback control: a continuous-time approach and a case study. *Int J Contr* 83(5):897–914
32. Wertz J (1978) Spacecraft attitude determination and control. D. Reidel Publishing Company, Dordrecht
33. Wisniewski R (2000) Linear time-varying approach to satellite attitude control using only electromagnetic actuation. *J Guid Contr Dyn* 23(4):640–646
34. Wisniewski R, Markley L (1999) Optimal magnetic attitude control. In: 14th IFAC world congress, Beijing, China
35. Wood M, Chen WH, Fertin D (2006) Model predictive control of low earth orbiting spacecraft with magneto-torquers. In: IEEE international conference on control applications, Munich, Germany
36. Wu F (1995) Control of linear parameter varying systems. PhD thesis, University of California, Berkeley, USA
37. Yan H, Ross IM, Alfriend KT (2007) Pseudospectral feedback control for three-axis magnetic attitude stabilization in elliptic orbits. *J Guid Contr Dyn* 30(4):1107–1115
38. Zanchettin A, Lovera M (2011) H_∞ attitude control of magnetically actuated satellites. In: IFAC world congress, Milano, Italy

Chapter 14

Modeling and Control of LPV Systems: A Vibroacoustic Application

Jan De Caigny, Juan F. Camino, Ricardo C.L.F. Oliveira, Pedro L.D. Peres,
and Jan Swevers

Abstract This chapter presents recent advances in both modeling and control of linear parameter-varying (LPV) systems. The proposed modeling technique follows the state-space model interpolation of local estimates (SMILE) approach which is based on the interpolation of a set of linear time invariant (LTI) models that are estimated for different fixed operating conditions and yields a state-space LPV model with a polytopic dependency on the scheduling parameter. The proposed control design technique considers a priori known bounds on the rate of parameter variation and can be used to compute stabilizing gain-scheduled state feedback as well as dynamic output feedback controllers for discrete-time LPV systems through linear matrix inequalities (LMIs). As extensions, H_∞ , \mathcal{H}_2 , and suboptimal multiobjective control design problems can be conveniently solved. The presented techniques are applied to a vibroacoustic setup whose dynamics is highly sensitive to variations of the temperature. The numerical results show the advantages and versatility of the proposed approaches on a realistic engineering problem.

J. De Caigny • J. Swevers
Department of Mechanical Engineering, Katholieke Universiteit Leuven,
Celestijnenlaan 300B, Heverlee B-3001, Belgium
e-mail: jan.decaigny@mech.kuleuven.be; jan.swevers@mech.kuleuven.be

J.F. Camino
School of Mechanical Engineering, University of Campinas – UNICAMP,
Campinas, SP 13083-860, Brazil
e-mail: camino@fem.unicamp.br

R.C.L.F. Oliveira • P.L.D. Peres (✉)
School of Electrical and Computer Engineering, University of Campinas – UNICAMP,
Campinas, SP 13083-852, Brazil
e-mail: ricfow@dt.fee.unicamp.br; peres@dt.fee.unicamp.br

14.1 Introduction

For many practical systems (such as wafer steppers, compressors, etc.), the assumption that the dynamics is linear and time invariant does not hold true. Indeed, many systems exhibit dynamic behavior that depends on one or more time-varying scheduling parameters. To increase the performance of these systems, it is necessary to take the parameter-dependency of the dynamics into account in the control design. In this context, the linear parameter-varying (LPV) modeling and control framework has been one of the most fruitful strategies of the last decades.

This chapter presents some recent advances in both modeling and control of LPV systems and applies them to a temperature-dependent vibroacoustic system. The chapter is divided into three main parts. Section 14.2 introduces the state-space model interpolation of local estimates (SMILE), an LPV modeling technique that can be used to compute a polytopic LPV state-space model based on a set of local linear time-invariant (LTI) state-space models that were estimated for fixed operating conditions. Section 14.3 presents synthesis conditions for stabilizing gain-scheduled state feedback and dynamic output feedback controllers for polytopic LPV systems. These design techniques can consider a priori known bounds on the rate of the parameter variation to reduce the conservatism associated with traditional control techniques (based on quadratic stability) that allow only arbitrarily fast parameter variation. Afterwards, in Sect. 14.4, the proposed modeling and control techniques are applied to a vibroacoustic system whose dynamics depends strongly on the ambient temperature. It is interesting to note that Sects. 14.2 and 14.3 are stand-alone parts in the sense that they can be read independently from each other. This is also reflected in the application section which has a distinct subsection for modeling (Sect. 14.4.1) and one for control (Sect. 14.4.2). Section 14.5 concludes the chapter with some final thoughts.

14.1.1 Notation and Terminology

The set of real numbers is denoted by \mathbb{R} and the set of natural (nonnegative integer) numbers by \mathbb{N} . A prime $'$ is used to indicate the transpose. The space of square-summable sequences on \mathbb{N} is given by $\ell_2^n \triangleq \{f : \mathbb{N} \rightarrow \mathbb{R}^n \mid \sum_{k=0}^{\infty} f(k)' f(k) < \infty\}$ and the corresponding 2-norm is defined as $\|x(k)\|_2^2 = \sum_{k=0}^{\infty} x(k)' x(k)$. The trace operator is denoted by $\text{Tr}\{\cdot\}$. The floor function is indicated as $\lfloor \cdot \rfloor$ and maps a real number to the largest previous integer. Identity matrices (resp. zero matrices) are denoted as I (resp. 0) in case the size is clear from the context. The convex hull of a set X is denoted by $\text{co}\{X\}$. The unit-simplex Λ_N of dimension $N \in \mathbb{N}$, with $N \geq 2$, is given by $\Lambda_N = \{\xi = (\xi_1, \xi_2, \dots, \xi_N) \in \mathbb{R}^N \mid \sum_{j=1}^N \xi_j = 1, \xi_j \geq 0, j = 1, \dots, N\}$. The symbol \star represents a symmetric block in a linear matrix inequality (LMI).

To simplify the exposition of Sect. 14.2, the following short notation is used for state-space models

$$H = \left[\begin{array}{c|c} A & B \\ \hline C & D \end{array} \right] = \begin{cases} \delta[x] = Ax + Bu \\ y = Cx + Du \end{cases},$$

where the operator $\delta[\cdot]$ denotes the time derivative for a continuous-time model and the forward time shift for a discrete-time model. For SISO state-space models, the operation \prod should be interpreted as the state-space series connection, obtained using the output of the first model as the input of the second model, such that

$$\prod_{i=1}^2 \left[\begin{array}{c|c} A_i & B_i \\ \hline C_i & D_i \end{array} \right] = \left[\begin{array}{cc|c} A_1 & 0 & B_1 \\ \hline B_2 C_1 & A_2 & B_2 D_1 \\ \hline D_2 C_1 & C_2 & D_2 D_1 \end{array} \right].$$

To distinguish between LPV models and LTI models, the following notation is used: LPV models, their system matrices, and elements are denoted using standard font, e.g., A_k , whereas LTI models, their system matrices, and elements are denoted using San Serif font, e.g., A_ℓ . The subscript ℓ indicates the index of the local LTI model.

14.2 Interpolation-Based Modeling of LPV Systems

This section presents the proposed SMILE modeling technique to obtain state-space LPV models for multiple-input multiple-output (MIMO) systems. The technique is based on the interpolation of LTI models that are estimated for fixed operating conditions of the system, that is, for constant values of the scheduling parameters. As the local LTI models can be either continuous- or discrete-time, both continuous- and discrete-time LPV models can be obtained. The interpolation technique is formulated as a linear least-squares problem that can be efficiently solved. The obtained LPV models are numerically well conditioned and, therefore, suitable for Lyapunov-based state-space LPV control synthesis.

14.2.1 Problem Statement

The following polytopic state-space representation is chosen for the interpolating LPV model

$$H(\alpha) = \left[\begin{array}{c|c} A(\alpha) & B(\alpha) \\ \hline C(\alpha) & D(\alpha) \end{array} \right] = \sum_{i=1}^N \alpha_i \left[\begin{array}{c|c} A_i & B_i \\ \hline C_i & D_i \end{array} \right] \in \left[\begin{array}{c|c} \mathbb{R}^{n_x \times n_x} & \mathbb{R}^{n_x \times n_u} \\ \hline \mathbb{R}^{n_y \times n_x} & \mathbb{R}^{n_y \times n_u} \end{array} \right], \quad (14.1)$$

where the time-varying scheduling parameter α takes values in the unit-simplex Λ_N of dimension $N \in \mathbb{N}$. Using (14.1), the aim is to interpolate the m local minimal LTI models

$$\tilde{H}_\ell = \left[\begin{array}{c|c} \tilde{A}_\ell & \tilde{B}_\ell \\ \hline \tilde{C}_\ell & \tilde{D}_\ell \end{array} \right] \in \left[\begin{array}{c|c} \mathbb{R}^{n_x \times n_x} & \mathbb{R}^{n_x \times n_u} \\ \hline \mathbb{R}^{n_y \times n_x} & \mathbb{R}^{n_y \times n_u} \end{array} \right], \quad \text{for } \ell = 1, \dots, m, \quad (14.2)$$

identified at distinct operating conditions of the scheduling parameter α . Thus, during the identification of the local LTI model \tilde{H}_ℓ , the scheduling parameter α is fixed at a constant value, denoted by $\tilde{\alpha}_\ell$.

As the state-space representation is not unique, the local models (14.2) cannot be readily interpolated since it is not guaranteed that they are represented with respect to a consistent state-space basis. Therefore, a similarity transformation matrix T_ℓ needs to be calculated for each local model \tilde{H}_ℓ such that the transformed models

$$H_\ell = \left[\begin{array}{c|c} A_\ell & B_\ell \\ \hline C_\ell & D_\ell \end{array} \right] = \left[\begin{array}{c|c} T_\ell^{-1} \tilde{A}_\ell T_\ell & T_\ell^{-1} \tilde{B}_\ell \\ \hline \tilde{C}_\ell T_\ell & \tilde{D}_\ell \end{array} \right] \quad \ell = 1, \dots, m \quad (14.3)$$

are represented in a consistent state-space form. Once the consistent local models (14.3) have been calculated, an optimization problem can be formulated and solved to find the optimal interpolating LPV model (14.1). The following section explains the modeling approach in more detail.

14.2.2 State-Space Model Interpolation of Local Estimates

First, four steps need to be followed to ensure that all local LTI models are represented in a consistent state-space form. Afterwards, in a final step, an optimization problem is solved to obtain the interpolating LPV model. These five steps are now briefly presented (see [2, 4] for more details).

Step 1: Choice of one IO combination: The first step consists of choosing one Input–Output (IO) combination (i, j) to select the m local SISO LTI models

$$\tilde{H}_{\ell, (i,j)} = \left[\begin{array}{c|c} \tilde{A}_\ell & \tilde{B}_{\ell, (:,j)} \\ \hline \tilde{C}_{\ell, (i,:)} & \tilde{D}_{\ell, (i,j)} \end{array} \right], \quad \text{for } \ell = 1, \dots, m. \quad (14.4)$$

The choice of the IO combination is restricted due to the fact that all selected SISO models $\tilde{H}_{\ell, (i,j)}$ need to have the same number of zeros (denoted as $z_{\ell, (i,j)}$), which is necessary for the correct sorting of the zeros in Step 2. A useful heuristic in choosing the IO combination is to calculate the zeros $z_{\ell, (i,j)}$ for all IO combinations and to select the combination whose zeros are the easiest to sort in Step 2.

Step 2: Calculating and sorting poles and zeros: In Step 2, the poles p_ℓ and zeros $z_{\ell, (i,j)}$ of the m local SISO models $\tilde{H}_{\ell, (i,j)}$ are calculated and sorted. The sorting is

necessary to assure that for all original SISO models $\tilde{H}_{\ell,(i,j)}$, the poles p_ℓ and the zeros $z_{\ell,(i,j)}$ are arranged in the same order. This consistent order will be used to transform the original SISO models $\tilde{H}_{\ell,(i,j)}$ to the consistent SISO models $H_{\ell,(i,j)}$.

Step 3: Constructing consistent SISO models: In Step 3, the original local SISO models $\tilde{H}_{\ell,(i,j)}$ are transformed to a new consistent state-space form by representing them as a gain $K_{\ell,(i,j)}$ multiplied with the state-space series connection of τ_1 first-order and τ_2 second-order state-space submodels. This new representation is denoted by

$$H_{\ell,(i,j)} = K_{\ell,(i,j)} \prod_{\tau=1}^{\tau_1+\tau_2} H_{\ell,(i,j)}^\tau, \quad \text{with} \quad H_{\ell,(i,j)}^\tau = \left[\begin{array}{c|c} A_\ell^\tau & B_\ell^\tau \\ \hline C_\ell^\tau & D_\ell^\tau \end{array} \right], \quad (14.5)$$

where the subscript τ indicates the index of the submodel for $\tau = 1, \dots, \tau_1 + \tau_2$ and where $\tau_1 \in \mathbb{N}$ is the number of first-order submodels associated with a single real pole and $\tau_2 \in \mathbb{N}$ is the number of second-order submodels associated with a pair of complex conjugate poles or with two real poles. All local SISO models are chosen to have the same number τ_1 and the same number τ_2 , determined as follows: $\tau_2 = \lfloor n_x/2 \rfloor$ and $\tau_1 = n_x - 2\tau_2$. Since the poles p_ℓ and zeros $z_{\ell,(i,j)}$ of all local SISO models have been sorted in Step 2, they can be assigned to the $\tau_1 + \tau_2$ local submodels $H_{\ell,(i,j)}^\tau$ in a consistent way. The pole (or a zero) assigned to submodel τ of the local SISO model ℓ is denoted by p_ℓ^τ (or by $z_{\ell,(i,j)}^\tau$). To assure that the local submodels $H_{\ell,(i,j)}^\tau$ are consistent, they are represented in the observable form. For example, a submodel with two poles $p_{\ell,1}^\tau, p_{\ell,2}^\tau$ and two zeros $z_{\ell,(i,j),1}^\tau, z_{\ell,(i,j),2}^\tau$ is represented by

$$H_{\ell,(i,j)}^\tau = \left[\begin{array}{c|c} 0 & a_{\ell,1}^\tau & b_{\ell,1}^\tau \\ 1 & a_{\ell,2}^\tau & b_{\ell,2}^\tau \\ \hline 0 & 1 & 1 \end{array} \right] \quad \text{where} \quad \begin{cases} a_{\ell,1}^\tau = -p_{\ell,1}^\tau p_{\ell,2}^\tau, \\ b_{\ell,1}^\tau = z_{\ell,(i,j),1}^\tau z_{\ell,(i,j),2}^\tau - p_{\ell,1}^\tau p_{\ell,2}^\tau, \\ a_{\ell,2}^\tau = p_{\ell,1}^\tau + p_{\ell,2}^\tau, \\ b_{\ell,2}^\tau = -(z_{\ell,(i,j),1}^\tau + z_{\ell,(i,j),2}^\tau) + (p_{\ell,1}^\tau + p_{\ell,2}^\tau). \end{cases}$$

Once the local SISO models, $\tilde{H}_{\ell,(i,j)}$ are split into local submodels, the consistent SISO models $H_{\ell,(i,j)}$ can be obtained by explicitly calculating the state-space series connection described in (14.5).

Step 4: Calculating the similarity transformations: After the first three steps have been performed, two sets of SISO models are available: the original SISO models $\tilde{H}_{\ell,(i,j)}$, selected in Step 1, and the consistent SISO models $H_{\ell,(i,j)}$, calculated in Step 3. In Step 4, the unique similarity transformation matrix T_ℓ that transforms the original SISO model $\tilde{H}_{\ell,(i,j)}$ in the consistent SISO model $H_{\ell,(i,j)}$ is computed for each ℓ . These matrices T_ℓ are found by solving

$$A_\ell = T_\ell^{-1} \tilde{A}_\ell T_\ell, \quad B_{\ell,(i,j)} = T_\ell^{-1} \tilde{B}_{\ell,(i,j)} \quad \text{and} \quad C_{\ell,(i,j)} = \tilde{C}_{\ell,(i,j)} T_\ell, \quad \text{for } \ell = 1, \dots, m. \quad (14.6)$$

The conditions for the existence of a unique solution for (14.6) can be found in [5]. Once the matrices T_ℓ are computed, they are applied to the original local MIMO models \tilde{H}_ℓ to obtain the consistent local MIMO models H_ℓ , given by (14.3).

Step 5: Interpolation and optimization: In the final step, the consistent local MIMO models are interpolated by solving an optimization problem to find the unknown parameters A_i , B_i , C_i , and D_i , for $i = 1, \dots, N$, of the interpolating LPV model (14.1). The following cost function is chosen:

$$\mathbb{E} = \sum_{\ell=1}^m \left\| \sum_{i=1}^N \tilde{\alpha}_{\ell,i} \begin{bmatrix} A_i & B_i \\ C_i & D_i \end{bmatrix} - \begin{bmatrix} A_\ell & B_\ell \\ C_\ell & D_\ell \end{bmatrix} \right\|_F^2, \quad (14.7)$$

where $\|\cdot\|_F$ represents the Frobenius norm. This cost function can be rewritten as a standard unconstrained linear least-squares optimization problem that can be efficiently solved.

In Sect. 14.4.1, the potential of the SMILE technique is demonstrated through a numerical example based on experimental data obtained from a vibroacoustic setup whose dynamics show a strong dependency on the ambient temperature.

Remark: In this section, a polytopic parametrization was chosen for the interpolating LPV model (14.1). However, by selecting a set of N base functions $f_i(\alpha)$, for $i = 1, \dots, N$, a more general parametrization is obtained

$$H(\alpha) = \sum_{i=1}^N f_i(\alpha) \begin{bmatrix} A_i & B_i \\ C_i & D_i \end{bmatrix},$$

while the cost function (14.7) still gives rise to a linear least-squares problem. One interesting choice for the base functions $f_i(\alpha)$ is to use homogeneous polynomials (as proposed in [5]). Homogeneous polynomial models offer more flexibility for the interpolation of the local LTI models, while they retain some of the useful properties of polytopic models for LPV control design techniques based on LMIs (see [4, 10]).

14.3 Gain-Scheduled Feedback Control

This section provides stabilizing gain-scheduled control design techniques for the following discrete-time polytopic LPV system:

$$H = \begin{cases} x(k+1) = A(\alpha(k))x(k) + B_w(\alpha(k))w(k) + B_u(\alpha(k))u(k), \\ z(k) = C_z(\alpha(k))x(k) + D_{zw}(\alpha(k))w(k) + D_{zu}(\alpha(k))u(k), \\ y(k) = C_y(\alpha(k))x(k) + D_{yw}(\alpha(k))w(k), \end{cases} \quad (14.8)$$

where $x(k) \in \mathbb{R}^{n_x}$ is the state, $w(k) \in \mathbb{R}^{n_w}$ the exogenous disturbance input, $z(k) \in \mathbb{R}^{n_z}$ the performance output, $y(k) \in \mathbb{R}^{n_y}$ the measured output, and $u(k) \in \mathbb{R}^{n_u}$ the control input. The system matrices have appropriate dimensions and admit a polytopic parameter-dependency on the scheduling parameter $\alpha(k) \in \Lambda_N$ that is a priori unknown, but can be measured in real time.

Finite sets of LMI conditions for the design of both state feedback controllers (Sect. 14.3.2) and full-order dynamic-output feedback controllers (Sect. 14.3.3) are presented. While only the LMI conditions for stabilizing control design are presented, the proposed technique is generic and can be used to design \mathcal{H}_2 , \mathcal{H}_∞ , and multi-objective controllers. Section 14.3.4 briefly introduces these possible extensions. First, however, Sect. 14.3.1 presents a technique to model the uncertainty domain where the scheduling parameter and its rate of variation can assume values. This modeling will allow bounds on the rate of variation to be considered in the control designs.

14.3.1 Modeling the Uncertainty Domain

In this section, a modeling technique is presented for the uncertainty domain where the vector¹ $(\alpha, \Delta\alpha) \in \mathbb{R}^{2N}$, consisting of the scheduling parameter and its rate of variation, assumes values. This modeling was previously introduced in [11] and [3].

14.3.1.1 Rate of Parameter Variation and the Bound b

The rate of variation of the parameter α_i , for $i = 1, \dots, N$, is defined as the change of α_i in one discrete time instant:

$$\Delta\alpha_i(k) = \alpha_i(k+1) - \alpha_i(k). \quad (14.9)$$

Due to this definition and the fact that $\alpha_i(k) \in \Lambda_N$, it is clear that

$$\sum_{i=1}^N \Delta\alpha_i(k) = \sum_{i=1}^N \alpha_i(k+1) - \sum_{i=1}^N \alpha_i(k) = 1 - 1 = 0. \quad (14.10)$$

It is assumed that the rate of variation of each parameter α_i is limited by an a priori known bound $b \in \mathbb{R}$ such that

$$-b \leq \Delta\alpha_i(k) \leq b, \quad \text{for } k \geq 0 \quad (14.11)$$

¹In the modeling of the uncertainty domain, $\alpha \in \mathbb{R}^N$ and $\Delta\alpha \in \mathbb{R}^N$ represent *column* vectors, that is, $\alpha \in \mathbb{R}^{N \times 1}$ and $\Delta\alpha \in \mathbb{R}^{N \times 1}$. Likewise, $(\alpha, \Delta\alpha)$ is a column vector $(\alpha, \Delta\alpha) \in \mathbb{R}^{2N \times 1}$. For reasons of compactness, this is not explicitly mentioned throughout the remainder of the text.

with $b \in [0, 1]$. Three distinct situations can be considered for the bound b . In case $b = 0$, the parameter α is *time invariant*. If $b = 1$, α can change in one time instant from any given value inside the unit-simplex to any other value and consequently, α is an *arbitrarily fast time-varying* parameter. Finally, if $0 < b < 1$, the variation of α_i is limited such that α *cannot* change from any given value to any other value. Hence, α is a *bounded time-varying* parameter.

14.3.1.2 Modeling of the Uncertainty Domain

Given the bound $b \in \mathbb{R}$ on the rate of variation $\Delta\alpha$, the uncertainty domain where the vector $(\alpha, \Delta\alpha) \in \mathbb{R}^{2N}$ assumes values can be modeled by the compact set

$$\Gamma_{b,N} = \left\{ \varphi \in \mathbb{R}^{2N} : \varphi \in \text{co} \{v^1, \dots, v^M\}, v^j = \begin{bmatrix} f^j \\ h^j \end{bmatrix}, f^j \in \mathbb{R}^N, h^j \in \mathbb{R}^N, \right. \\ \left. \sum_{i=1}^N f_i^j = 1 \text{ with } f_i^j \geq 0, i = 1, \dots, N, \sum_{i=1}^N h_i^j = 0, j = 1, \dots, M \right\}, \quad (14.12)$$

defined as the convex combination of the $M \in \mathbb{N}$ vectors v^j , for $j = 1, \dots, M$, which can be constructed using the bound b . Since $(\alpha, \Delta\alpha) \in \Gamma_{b,N}$, it is clear that using $\gamma \in \Lambda_M$, the vector $(\alpha, \Delta\alpha)$ can be represented as the following convex combination:

$$(\alpha, \Delta\alpha) = \sum_{j=1}^M v^j \gamma_j, \text{ that is, } \alpha = \sum_{j=1}^M f^j \gamma_j, \text{ and } \Delta\alpha = \sum_{j=1}^M h^j \gamma_j. \quad (14.13)$$

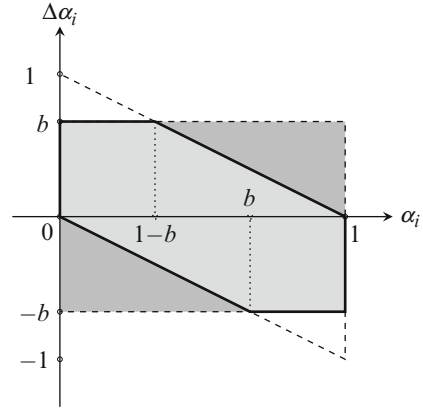
Note that the definition of $\Gamma_{b,N}$ ensures that $\alpha \in \Lambda_N$ and that (14.10) is satisfied. The vectors $v^j \in \Gamma_{b,N}$, for $j = 1, \dots, M$, can be constructed in a systematic way for a given b by searching for all possible solutions of the equalities

$$\sum_{i=1}^N \alpha_i = 1 \quad \text{and} \quad \sum_{i=1}^N \Delta\alpha_i = 0 \quad (14.14)$$

using the extreme points of the constraints given in (14.11), for $i = 1, \dots, N$. However, taking into account just (14.11) introduces conservatism since the bounds on $\Delta\alpha_i$ are considered independent of α_i while in fact, they are highly dependent on the value of α_i , as illustrated in Fig. 14.1. In this figure, the light gray region indicates the region in the $(\alpha_i, \Delta\alpha_i)$ -space where $\Delta\alpha_i$ assumes values as a function of α_i , given the bound b . Obviously, this region is a polytope with six vertices given by

$$\mathcal{V} = \{(0, 0), (0, b), (1 - b, b), (1, 0), (1, -b), (b, -b)\}. \quad (14.15)$$

Fig. 14.1 Region in the $(\alpha_i, \Delta\alpha_i)$ -space where $\Delta\alpha_i$ assumes values as a function of α_i (indicated in light gray). The dark gray region is unreachable since $\alpha \in \Lambda_N$



In case only (14.11) is considered, the dark gray regions are taken into account as well, thus producing conservative results. Therefore, to find the vectors v^j , the solutions of the equalities (14.14) need to be sought using the vertices (14.15) of the feasible region in the $(\alpha_i, \Delta\alpha_i)$ -space, for $i = 1, \dots, N$.

In [3], it is shown how the M vectors v^j , for $j = 1, \dots, M$, of the uncertainty set $\Gamma_{b,N}$ can be generated automatically. As an example, consider $\alpha \in \Lambda_2$. In this case, $M = 6$ and the vectors v^j , for $j = 1, \dots, 6$, can be found to be

$$[v^1 \ v^2 \ \dots \ v^6] = \begin{bmatrix} 1 & 1 & 0 & 0 & b & 1-b \\ 0 & 0 & 1 & 1 & 1-b & b \\ 0 & -b & 0 & b & -b & b \\ 0 & b & 0 & -b & b & -b \end{bmatrix}.$$

In this case, $(\alpha, \Delta\alpha) = (\alpha_1, \alpha_2, \Delta\alpha_1, \Delta\alpha_2) \in \mathbb{R}^4$ and due to (14.10), $\Delta\alpha_1 = -\Delta\alpha_2$. Thus, for illustration purposes, the uncertainty region can be represented in the three-dimensional $(\alpha_1, \alpha_2, \Delta\alpha)$ -space, where $\Delta\alpha = \Delta\alpha_1 = -\Delta\alpha_2$ (see Fig. 14.2). The dark gray region, bounded by the thick black lines, indicates the modeled uncertainty region, which has six vertices (black bullets). The projection of this region on the $(\alpha_1, \Delta\alpha)$ -plane and on the $(\alpha_2, \Delta\alpha)$ -plane yields the two light gray regions indicated with dashed lines. Clearly, these regions coincide with the light gray uncertainty region shown in Fig. 14.1.

This characterization of α and $\Delta\alpha$ can be exploited in the derivation of a finite-dimensional set of LMI conditions for control design, as shown in the following sections.

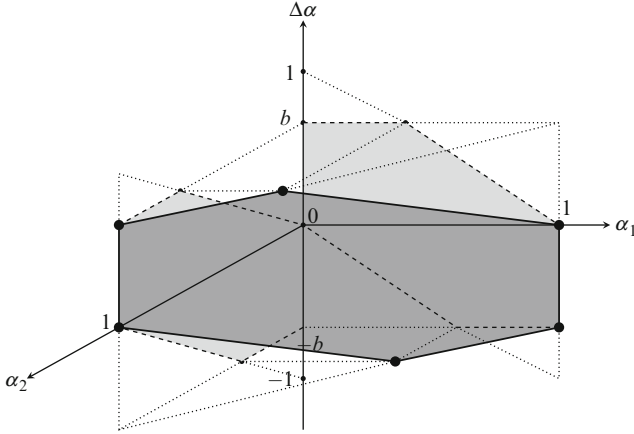


Fig. 14.2 Uncertainty region in the $(\alpha_1, \alpha_2, \Delta\alpha)$ -space for $\alpha \in \Lambda_2$ and $0 < b < 1$

14.3.2 Gain-Scheduled State Feedback

This section presents LMI conditions for the design of a gain-scheduled stabilizing state feedback controller for system (14.8). For full-state feedback, it is assumed that $y(k) = x(k)$ and the goal is to provide a parameter-dependent control law

$$u(k) = K(\alpha(k))y(k), \quad \text{with } K(\alpha(k)) \in \mathbb{R}^{n_u \times n_x},$$

such that the closed-loop system

$$H_{cl} = \begin{cases} x(k+1) = A_{cl}(\alpha(k))x(k) + B_w(\alpha(k))w(k), \\ z(k) = C_{cl}(\alpha(k))x(k) + D_w(\alpha(k))w(k) \end{cases} \quad (14.16)$$

with

$$\begin{aligned} A_{cl}(\alpha(k)) &= A(\alpha(k)) + B_u(\alpha(k))K(\alpha(k)), \\ C_{cl}(\alpha(k)) &= C_z(\alpha(k)) + D_u(\alpha(k))K(\alpha(k)) \end{aligned} \quad (14.17)$$

is exponentially stable for all possible variations of the parameter $\alpha(k) \in \Lambda_N$. It is well known that the closed-loop system (14.16) is stable (see, for example, [1]) if

$$\begin{bmatrix} P(\alpha(k+1)) & A_{cl}(\alpha(k))G(\alpha(k)) \\ \star & G(\alpha(k)) + G(\alpha(k))' - P(\alpha(k)) \end{bmatrix} > 0, \quad \forall k \geq 0, \quad (14.18)$$

which, using (14.17) and defining

$$K(\alpha) = Z(\alpha)G(\alpha)^{-1}, \quad (14.19)$$

yields

$$\begin{bmatrix} P(\alpha(k+1)) & A(\alpha(k))G(\alpha(k)) + B_u(\alpha(k))Z(\alpha(k)) \\ \star & G(\alpha(k)) + G(\alpha(k))' - P(\alpha(k)) \end{bmatrix} > 0, \quad \forall k \geq 0. \quad (14.20)$$

Verifying this condition for all $k \geq 0$ yields an infinite-dimensional problem. However, a finite-dimensional set of sufficient LMI conditions can be obtained by imposing a particular structure on the Lyapunov matrix $P(\alpha)$ and on the variables $G(\alpha)$ and $Z(\alpha)$. Choosing $P(\alpha)$, $G(\alpha)$, and $Z(\alpha)$ to have the following affine structure $P(\alpha) = \sum_{i=1}^N \alpha_i P_i$ with $\alpha \in \Lambda_N$, it can be shown, using (14.13), that

$$\begin{aligned} P(\alpha) &= \sum_{i=1}^N \alpha_i P_i = \sum_{i=1}^N \left(\sum_{j=1}^M f_i^j \gamma_j \right) P_i = \sum_{j=1}^M \gamma_j \left(\sum_{i=1}^N f_i^j P_i \right) \\ &= \sum_{j=1}^M \gamma_j \hat{P}_j = \hat{P}(\gamma) \end{aligned} \quad (14.21)$$

with $\hat{P}_j = \sum_{i=1}^N f_i^j P_i$. Similarly, $G(\alpha)$, $Z(\alpha)$, and all system matrices in (14.8) can be converted to a new representation in terms of $\gamma \in \Lambda_M$. Moreover, combining (14.13) and the fact that $\alpha(k+1) = \alpha(k) + \Delta\alpha(k)$, it follows that

$$\begin{aligned} P(\alpha(k+1)) &= \sum_{i=1}^N (\alpha_i(k) + \Delta\alpha_i(k)) P_i = \sum_{i=1}^N \left(\sum_{j=1}^M (f_i^j + h_i^j) \gamma_j(k) \right) P_i \\ &= \sum_{j=1}^M \gamma_j(k) \left(\sum_{i=1}^N (f_i^j + h_i^j) P_i \right) = \sum_{j=1}^M \gamma_j(k) \tilde{P}_j = \tilde{P}(\gamma(k)) \end{aligned} \quad (14.22)$$

with $\tilde{P}_j = \sum_{i=1}^N (f_i^j + h_i^j) P_i$. As a result of this new representation, the LMI (14.20) can be rewritten with a dependency on $\gamma(k)$, resulting in

$$\begin{bmatrix} \tilde{P}(\gamma(k)) & \hat{A}(\gamma(k))\hat{G}(\gamma(k)) + \hat{B}_u(\gamma(k))\hat{Z}(\gamma(k)) \\ \star & \hat{G}(\gamma(k)) + \hat{G}(\gamma(k))' - \tilde{P}(\gamma(k)) \end{bmatrix} > 0, \quad \forall k \geq 0.$$

Note that this LMI shows a dependency on the present time instant k only, whereas (14.20) showed a dependency on both k and $k+1$. Now, for this LMI to hold for all time instants k , it suffices that the following LMI holds:

$$\begin{bmatrix} \tilde{P}(\gamma) & \hat{A}(\gamma)\hat{G}(\gamma) + \hat{B}_u(\gamma)\hat{Z}(\gamma) \\ \star & \hat{G}(\gamma) + \hat{G}(\gamma)' - \tilde{P}(\gamma) \end{bmatrix} > 0, \quad \forall \gamma \in \Lambda_M. \quad (14.23)$$

This LMI is a second-order polynomial in γ . A finite set of sufficient LMIs guaranteeing (14.23) is provided by the next theorem, obtained following the lines of [13].

Theorem 14.1 (Gain-scheduled state feedback control). Assume that the vectors f^j and h^j of $\Gamma_{b,N}$ are given. If there exist, for $i = 1, \dots, N$, matrices $G_i \in \mathbb{R}^{n_x \times n_x}$, $Z_i \in \mathbb{R}^{n_u \times n_x}$ and symmetric positive-definite matrices $P_i \in \mathbb{R}^{n_x \times n_x}$ such that $\Theta_j > 0$, for $j = 1, \dots, M$, and $\Theta_{j\ell} > 0$, for $j = 1, \dots, M-1$ and $\ell = j+1, \dots, M$, with

$$\Theta_j = \begin{bmatrix} \tilde{P}_j & \hat{A}_j \hat{G}_j + \hat{B}_{u,j} \hat{Z}_j \\ \star & \hat{G}_j + \hat{G}'_j - \hat{P}_j \end{bmatrix},$$

$$\Theta_{j\ell} = \begin{bmatrix} \tilde{P}_j + \tilde{P}_\ell & \hat{A}_j \hat{G}_\ell + \hat{A}_\ell \hat{G}_j + \hat{B}_{u,j} \hat{Z}_\ell + \hat{B}_{u,\ell} \hat{Z}_j \\ \star & \hat{G}_j + \hat{G}'_j + \hat{G}_\ell + \hat{G}'_\ell - \hat{P}_j - \hat{P}_\ell \end{bmatrix},$$

where $\hat{P}_j = \sum_{i=1}^N f_i^j P_i$, $\tilde{P}_j = \sum_{i=1}^N (f_i^j + h_i^j) P_i$, $\hat{G}_j = \sum_{i=1}^N f_i^j G_i$, and $\hat{Z}_j = \sum_{i=1}^N f_i^j Z_i$, then the parameter-dependent state feedback gain (14.19) with $Z(\alpha) = \sum_{i=1}^N \alpha_i Z_i$ and $G(\alpha) = \sum_{i=1}^N \alpha_i G_i$ stabilizes system H .

Proof. If $\Theta_j > 0$, for $j = 1, \dots, M$, and $\Theta_{j\ell} > 0$, for $j = 1, \dots, M-1$ and $\ell = j+1, \dots, M$, it is clear for any $\gamma \in \Lambda_M$ that

$$\hat{\Theta} = \sum_{j=1}^M \gamma_j^2 \Theta_j + \sum_{j=1}^{M-1} \sum_{\ell=j+1}^M \gamma_j \gamma_\ell \Theta_{j\ell}$$

$$= \begin{bmatrix} \left(\sum_{j=1}^M \gamma_j \right) \tilde{P}(\gamma) & \hat{A}(\gamma) \hat{G}(\gamma) + \hat{B}_u(\gamma) \hat{Z}(\gamma) \\ \star & \left(\sum_{j=1}^M \gamma_j \right) \left(\hat{G}(\gamma) + \hat{G}'(\gamma) - \hat{P}(\gamma) \right) \end{bmatrix} > 0,$$

which implies that (14.23) holds. Therefore, under the chosen affine parametrizations for $P(\alpha)$, $G(\alpha)$, and $Z(\alpha)$, in combination with the modeling of the uncertainty domain (14.13), feasibility of the LMIs $\Theta_j > 0$ and $\Theta_{j\ell} > 0$ ensures (14.18). \square

14.3.3 Gain-Scheduled Dynamic Output Feedback

In this section, the aim is to provide for system (14.8) a finite-dimensional set of sufficient LMI conditions for the synthesis of a gain-scheduled stabilizing strictly proper full-order dynamic output feedback controller

$$K = \begin{cases} x_c(k+1) = A_c(\alpha(k))x_c(k) + B_c(\alpha(k))y(k) \\ u(k) = C_c(\alpha(k))x_c(k) \end{cases} \quad (14.24)$$

with state $x_c(k) \in \mathbb{R}^{n_x}$ and system matrices $A_c(\alpha(k)) \in \mathbb{R}^{n_x \times n_x}$, $B_c(\alpha(k)) \in \mathbb{R}^{n_x \times n_y}$, and $C_c(\alpha(k)) \in \mathbb{R}^{n_u \times n_x}$, such that the closed-loop system

$$H_{cl} = \begin{cases} x_{cl}(k+1) = A_{cl}(\alpha(k))x_{cl}(k) + B_{cl}(\alpha(k))w(k) \\ z(k) = C_{cl}(\alpha(k))x_{cl}(k) + D_{cl}(\alpha(k))w(k) \end{cases} \quad (14.25)$$

with state $x_{\text{cl}}(k) = [x(k)' \ x_c(k)']' \in \mathbb{R}^{2n_x}$ and system matrices

$$\begin{aligned} A_{\text{cl}}(\alpha) &= \begin{bmatrix} A(\alpha) & B_u(\alpha)C_c(\alpha) \\ B_c(\alpha)C_y(\alpha) & A_c(\alpha) \end{bmatrix}, & B_{\text{cl}}(\alpha) &= \begin{bmatrix} B_w(\alpha) \\ B_c(\alpha)D_{yw}(\alpha) \end{bmatrix}, \\ C_{\text{cl}}(\alpha) &= [C_z(\alpha) \ D_{zu}(\alpha)C_c(\alpha)], & D_{\text{cl}}(\alpha) &= [D_{zw}(\alpha)] \end{aligned} \quad (14.26)$$

is exponentially stable. The proposed synthesis procedure has been presented for the design of \mathcal{H}_2 and \mathcal{H}_∞ controllers in [4] and is an extension to the LPV case of the technique presented for LTI systems in [6], which can be seen as the discrete-time counter part of the previous results [9, 15] for continuous-time systems.

Following (14.18), the closed-loop system (14.25) is stable if there exists a symmetric positive definite matrix $\mathbb{P}(\alpha) \in \mathbb{R}^{2n_x \times 2n_x}$ and a matrix $\mathbb{G}(\alpha) \in \mathbb{R}^{2n_x \times 2n_x}$ such that

$$\begin{bmatrix} \mathbb{P}(\alpha(k+1)) & A_{\text{cl}}(\alpha(k))\mathbb{G}(\alpha(k)) \\ * & \mathbb{G}(\alpha(k)) + \mathbb{G}(\alpha(k))' - \mathbb{P}(\alpha(k)) \end{bmatrix} > 0, \quad \forall k \geq 0. \quad (14.27)$$

Substituting for the closed-loop matrices (14.26) in (14.27) yields a nonlinear matrix inequality due to the product of the controller matrices (14.24) and $\mathbb{G}(\alpha)$. Consequently, a change of variables is necessary to transform this nonlinear matrix inequality into an equivalent LMI. In the following, $\mathbb{G}(\alpha)$ is chosen to be independent of α , that is, $\mathbb{G}(\alpha) = \mathbb{G}$. In [4], it is explained that a parameter-dependent $\mathbb{G}(\alpha)$ would lead to a controller that depends on the present as well as the *future* value of the scheduling parameter which, for most applications, cannot be implemented in practice.

In [4], it is shown that (14.27) can be transformed into an equivalent LMI in the matrices $J(\alpha)$, $L(\alpha)$, $Q(\alpha)$, $R(\alpha)$, S , X , Y , and the symmetric positive definite matrices $E(\alpha)$ and $P(\alpha)$, given by

$$\begin{bmatrix} P(\alpha(k+1)) & J(\alpha(k+1)) & \Psi_{13}(\alpha(k)) & A(\alpha(k)) \\ * & E(\alpha(k+1)) & Q(\alpha(k)) & \Psi_{24}(\alpha(k)) \\ * & * & X + X' - P(\alpha(k)) & I + S' - J(\alpha(k)) \\ * & * & * & Y + Y' - E(\alpha(k)) \end{bmatrix} > 0, \quad \forall k \geq 0, \quad (14.28)$$

where

$$\begin{aligned} \Psi_{13}(\alpha(k)) &= A(\alpha(k))X + B_u(\alpha(k))L(\alpha(k)), \\ \Psi_{24}(\alpha(k)) &= YA(\alpha(k)) + R(\alpha(k))C_y(\alpha(k)). \end{aligned}$$

If the LMI (14.28) is satisfied, the system matrices of the gain-scheduled stabilizing controller can be recovered through the nonlinear transformation

$$\begin{aligned}
A_c(\alpha) &= V^{-1} \left(Q(\alpha) - YA(\alpha)X - YB_u(\alpha)L(\alpha) - R(\alpha)C_y(\alpha)X \right) U^{-1}, \\
B_c(\alpha) &= V^{-1}R(\alpha), \\
C_c(\alpha) &= L(\alpha)U^{-1},
\end{aligned} \tag{14.29}$$

where the matrices U and V are found as the solution of $VU = S - YX$. In [6], it is shown that nonsingular matrices U and V , satisfying this constraint, always exist.

Using similar steps as for the state feedback case, a finite-dimensional set of sufficient LMI conditions can be derived for the infinite-dimensional LMI problem (14.28). This is the context of the next theorem.

Theorem 14.2 (Gain-scheduled dynamic output feedback). *Assume that the vectors f^j and h^j of $\Gamma_{b,N}$ are given. Then, the gain-scheduled dynamic output feedback controller (14.24) with controller matrices (14.29) stabilizes H if there exist matrices $J_i \in \mathbb{R}^{n_x \times n_x}$, $L_i \in \mathbb{R}^{n_u \times n_x}$, $Q_i \in \mathbb{R}^{n_x \times n_x}$ and $R_i \in \mathbb{R}^{n_x \times n_y}$ and symmetric positive definite matrices $E_i \in \mathbb{R}^{n_x \times n_x}$ and $P_i \in \mathbb{R}^{n_x \times n_x}$, for $i = 1, \dots, N$, and if there exist matrices $S \in \mathbb{R}^{n_x \times n_x}$, $X \in \mathbb{R}^{n_x \times n_x}$ and $Y \in \mathbb{R}^{n_x \times n_x}$ such that $\Psi_j > 0$, for $j = 1, \dots, M$, and $\Psi_{j\ell} > 0$, for $j = 1, \dots, M-1$ and $\ell = j+1, \dots, M$, with*

$$\begin{aligned}
\Psi_j &= \begin{bmatrix} \tilde{P}_j & \tilde{J}_j & \hat{A}_j X + \hat{B}_{u,j} \hat{L}_j & \hat{A}_j \\ * & \tilde{E}_j & \hat{Q}_j & Y \hat{A}_j + \hat{R}_j \hat{C}_{y,j} \\ * & * & X + X' - \hat{P}_j & I + S' - \hat{J}_j \\ * & * & * & Y + Y' - \hat{E}_j \end{bmatrix}, \\
\Psi_{j\ell} &= \begin{bmatrix} \tilde{P}_j + \tilde{P}_\ell & \tilde{J}_j + \tilde{J}_\ell & \hat{A}_j X + \hat{A}_\ell X + \hat{B}_{u,j} \hat{L}_\ell + \hat{B}_{u,\ell} \hat{L}_j & \hat{A}_j + \hat{A}_\ell \\ * & \tilde{E}_j + \tilde{E}_\ell & \hat{Q}_j + \hat{Q}_\ell & Y \hat{A}_j + Y \hat{A}_\ell + \hat{R}_j \hat{C}_{y,\ell} + \hat{R}_\ell \hat{C}_{y,j} \\ * & * & 2X + 2X' - \hat{P}_j - \hat{P}_\ell & 2I + 2S' - \hat{J}_j - \hat{J}_\ell \\ * & * & * & 2Y + 2Y' - \hat{E}_j - \hat{E}_\ell \end{bmatrix}.
\end{aligned}$$

The matrix coefficients associated with the system matrices \hat{A}_j , $\hat{B}_{u,j}$, and $\hat{C}_{y,j}$ and with the decision variables \tilde{P}_j , \hat{P}_j , \tilde{E}_j , \hat{E}_j , \tilde{J}_j , \hat{J}_j , \hat{L}_j , \hat{Q}_j , and \hat{R}_j can be constructed, for $j = 1, \dots, M$, using a similar derivation as (14.21) and (14.22).

The proof can be constructed following steps similar to the proof of Theorem 14.1.

14.3.4 Extensions

This section presents several extensions to the synthesis problems introduced in the previous sections. First, only the design of stabilizing gain-scheduled controllers has been discussed. However, in practice, it is usually desirable to minimize over some well-defined objective function to achieve the best possible closed-loop performance. Second, as the LMI conditions in Theorems 14.1 and 14.2 are only

sufficient and not necessary, it is interesting to point out some ways to decrease their conservatism. Third, for systems with multiple scheduling parameters that have different bounds on their rate of variation, it is necessary to consider a more general class of systems than the standard polytopic description.

14.3.4.1 Multi-objective Control Design with Guaranteed \mathcal{H}_∞ and \mathcal{H}_2 Performance

This section provides an LMI characterization to compute guaranteed upper bounds on the \mathcal{H}_∞ and \mathcal{H}_2 performance for discrete-time LPV systems. For system H , given by (14.8), a bound on the \mathcal{H}_∞ performance can be computed using the following LMI characterization (see, for instance, [16]).

Theorem 14.3 (Extended \mathcal{H}_∞ performance). *If there exist a bounded matrix $G(\alpha) \in \mathbb{R}^{n_x \times n_x}$ and a bounded symmetric positive-definite matrix $P(\alpha) \in \mathbb{R}^{n_x \times n_x}$ such that for all $k \geq 0$*

$$\begin{bmatrix} P(\alpha(k+1)) & A(\alpha(k))G(\alpha(k)) & B_w(\alpha(k)) & 0 \\ * & G(\alpha(k)) + G(\alpha(k))' - P(\alpha(k)) & 0 & G(\alpha(k))'C_z(\alpha(k))' \\ * & * & \eta I & D_{zw}(\alpha(k))' \\ * & * & * & \eta I \end{bmatrix} > 0,$$

then, system H is exponentially stable and $\|H\|_\infty \leq \inf_{P(\alpha), G(\alpha), \eta} \eta$.

A bound on the \mathcal{H}_2 performance can be computed using the following LMI characterization (see [3]).

Theorem 14.4 (Extended \mathcal{H}_2 performance). *If there exist a bounded matrix $G(\alpha) \in \mathbb{R}^{n_x \times n_x}$ and bounded symmetric positive definite matrices $P(\alpha) \in \mathbb{R}^{n_x \times n_x}$ and $W(\alpha) \in \mathbb{R}^{n_z \times n_z}$ such that for all $k \geq 0$*

$$\begin{bmatrix} P(\alpha(k+1)) & A(\alpha(k))G(\alpha(k)) & B_w(\alpha(k)) \\ * & G(\alpha(k)) + G(\alpha(k))' - P(\alpha(k)) & 0 \\ * & * & I \end{bmatrix} > 0,$$

$$\begin{bmatrix} W(\alpha(k)) - D_{zw}(\alpha(k))D_{zw}(\alpha(k))' & C_z(\alpha(k))G(\alpha(k)) \\ * & G(\alpha(k)) + G(\alpha(k))' - P(\alpha(k)) \end{bmatrix} > 0,$$

then, system H is exponentially stable and $\|H\|_2 \leq \inf_{P(\alpha), G(\alpha), W(\alpha)} \sqrt{\text{Tr}\{W(\alpha)\}}$.

Similar to the stabilizing control designs from the previous sections, sufficient LMI conditions for the design of \mathcal{H}_∞ or \mathcal{H}_2 performance guaranteeing gain-scheduled state feedback and dynamic output feedback controllers can be derived based on Theorems 14.3 and 14.4. These synthesis conditions and the respective suboptimal multiobjective control designs are presented in [3, 4].

14.3.4.2 LMI Relaxations

The LMI conditions given by Theorems 14.1 and 14.2 are only sufficient and not necessary for the existence of stabilizing gain-scheduled controllers. Therefore, it is interesting to point out some techniques to alleviate their conservatism. First, instead of the affine parametrizations used in the previous section for the Lyapunov matrices and the slack variables, it is possible to consider more general polynomial parametrizations for discrete-time LPV systems (see, amongst others, [4, 11]). A second technique to reduce the conservatism is based on an extension of Pólya's Theorem for matrix-valued coefficients, as presented in [14]. This type of relaxations has been applied, amongst others, in [11].

14.3.4.3 Homogeneous Polynomially Parameter-Dependent System with Scheduling Parameters Varying in the Multisimplex

This class of systems (discussed in [10]) forms a very general and powerful system description. The multisimplex Λ is defined as the Cartesian product of L unit-simplices $\Lambda = \Lambda_{N_1} \times \dots \times \Lambda_{N_L}$ of size $N_\ell \in \mathbb{N}$, for $\ell = 1, \dots, L$. One advantage of the modeling of the uncertainty domain of Sect. 14.3.1 is that a different bound b_ℓ can be considered for each different unit-simplex. This means that, in the same design, LMI conditions can be derived to handle time-invariant, arbitrarily time-varying and bounded time-varying parameters defined in their own appropriate uncertainty domain. Moreover, it can be shown that polytopic, affine, multiaffine, polynomial, and multivariable polynomial parametrizations can be recovered as special cases of the homogeneous polynomial parametrization with parameters in the multisimplex.

14.4 Vibroacoustic Application

The vibroacoustic setup (displayed in Fig. 14.3) consists of a lexan plate clamped on a rigid baffle in a semianechoic room. For details see [18]. The vibration of the plate is caused by a point force (exogenous disturbance w) driven by a shaker. A piezoelectric patch is attached to the plate providing a flexural moment (control input u) that can counteract the vibrations caused by the shaker to attenuate, inside the semianechoic room, the sound pressure measured by a microphone (measured output y) located near the plate. The dynamics of this system is highly sensitive to variations of the ambient temperature.

14.4.1 Modeling

For this system, local LTI identification experiments are performed for four temperatures $\theta = \{22.9, 23.4, 24.4, 25.4\}^\circ\text{C}$ by measuring frequency response

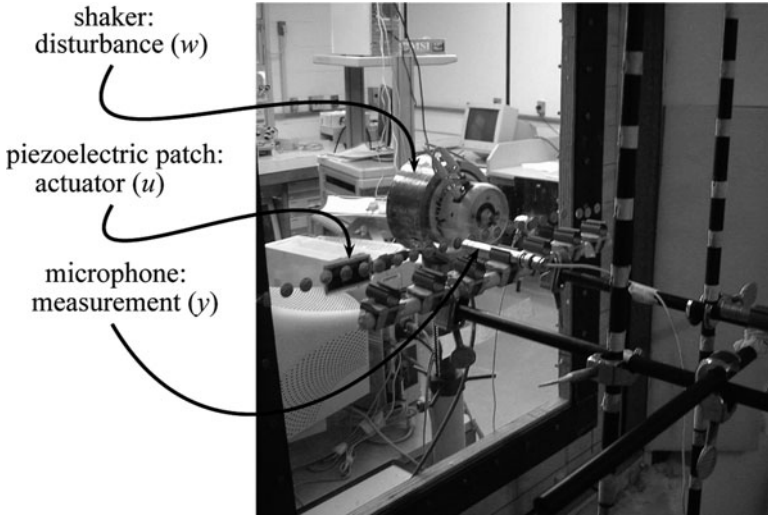


Fig. 14.3 Vibroacoustic setup

functions (FRFs) in the frequency range 120–260 Hz from the disturbance w and the control input u to the output y (using a sample frequency of 2,048 Hz). For each operating condition, a tenth-order discrete-time state-space model is estimated using standard identification tools in the frequency-domain [7, 12]. Figure 14.4 presents the amplitude and phase of the experimental FRFs (black, solid) and of the estimated models (gray, dashed). The arrows indicate increasing temperature θ . The estimated LTI models clearly fit the experimental FRFs well. Now, the SMILE technique can be applied to these four local LTI models.

First, it is necessary to choose the parametrization of the LPV model. As the vibroacoustic setup depends on one bounded scheduling parameter θ , it is possible to have a polytopic representation by defining $\alpha = (\alpha_1, \alpha_2)$, with

$$\alpha_1 = \frac{\theta - \underline{\theta}}{\bar{\theta} - \underline{\theta}} \text{ and } \alpha_2 = \frac{\bar{\theta} - \theta}{\bar{\theta} - \underline{\theta}}, \text{ with } \bar{\theta} = 25.4^\circ \text{ and } \underline{\theta} = 22.9^\circ.$$

Step 1: Choice of one IO combination: The LTI models have two inputs and one output. Here, the IO combination (1, 2) is chosen, which provides, for $\ell = 1, \dots, 4$, the SISO LTI models $\hat{H}_{\ell, (1,2)}$ from the control input u to the microphone y .

Step 2: Calculating and sorting poles and zeros: Figure 14.5a shows the real and imaginary part of the poles of the four SISO models as a function of the scheduling parameter α_1 . All models have five complex conjugate pole pairs, indicating five resonances. As shown in Fig. 14.5b, all SISO models have one unstable real zero and four complex conjugate zero pairs, indicating four antiresonances. Based on Fig. 14.5, the poles and zeros can be easily sorted. The lines connecting the poles and zeros indicate this consistent sort.

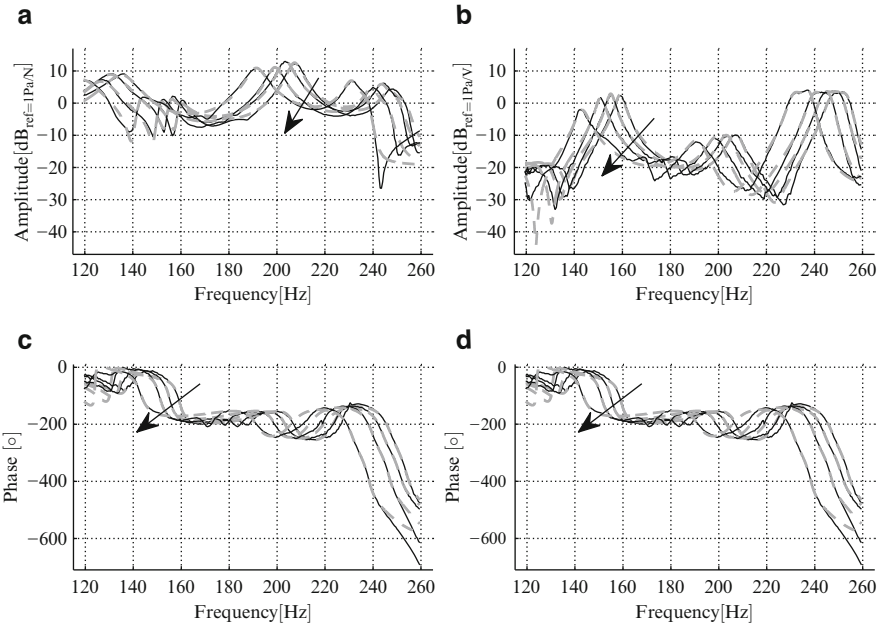


Fig. 14.4 Measured FRFs (black, solid) and estimated local LTI models (gray, dashed), for four different temperatures (arrows indicate increasing temperature) (a) $w \rightarrow y$: Amplitude (b) $u \rightarrow y$: Amplitude (c) $w \rightarrow y$: Phase (d) $u \rightarrow y$: Phase

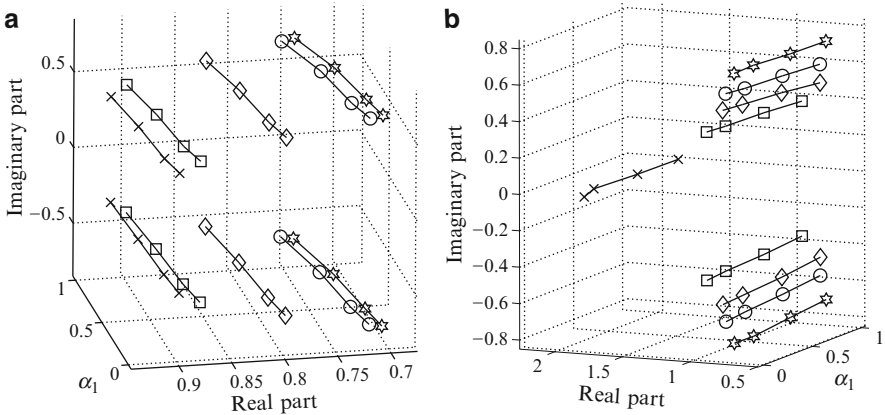


Fig. 14.5 Real and imaginary part of the poles p_ℓ and the zeros $z_{\ell,(1,2)}$ of the local LTI models $\tilde{H}_{\ell,(1,2)}$ as a function of the scheduling parameter α_1 (a) Poles p_ℓ (b) Zeros $z_{\ell,(1,2)}$

Step 3: Constructing consistent SISO models: Since all original SISO LTI models are tenth-order, they can be represented by a gain multiplied with the series connection of $\tau_2 = 5$ second-order submodels. In Fig. 14.5, this division is emphasized by assigning the poles and zeros five different markers: poles and zeros with the same

marker are assigned to the same SISO submodel. After the submodels have been defined, the consistent SISO state-space models $H_{\ell,(1,2)}$ can be computed.

Step 4: Calculating the similarity transformations: From the original SISO models $\tilde{H}_{\ell,(1,2)}$ and the consistent SISO models $H_{\ell,(1,2)}$, a similarity transformation matrix T_ℓ is calculated by solving (14.6), for $\ell = 1, \dots, 4$. The obtained T_ℓ is used to transform the original MIMO models \tilde{H}_ℓ into a consistent form, denoted by H_ℓ .

Step 5: Interpolation and optimization: The optimization problem (14.7) is solved to obtain the interpolating LPV model, given by

$$\begin{cases} x(k+1) = A(\alpha(k))x(k) + B_w(\alpha(k))w(k) + B_u(\alpha(k))u(k) \\ y(k) = C_z(\alpha(k))x(k). \end{cases}$$

14.4.1.1 Validation

Figure 14.6 compares the four original local LTI models (gray, solid) with the interpolating LPV model (black, solid with dots), evaluated at 11 equidistant values of $\alpha_1 \in [0, 1]$. The LPV model clearly shows a smooth interpolation of the local LTI models.

14.4.2 Control

In this section, \mathcal{H}_∞ , \mathcal{H}_2 , and multiobjective gain-scheduled state feedback and dynamic output feedback controllers are designed for the vibroacoustic system using the extensions of Theorems 14.1 and 14.2 for \mathcal{H}_∞ and \mathcal{H}_2 design mentioned in Sect. 14.3.4. For both the state feedback as well as the dynamic output feedback, the microphone output signal $y(k)$ is used as performance measure, that is $z(k) = y(k)$. In the dynamic output control design, the microphone signal $y(k)$ is also the input for the controller, while in the state feedback design, all ten states are assumed available for feedback.

Since for this system, the rate of variation of the scheduling parameter (the ambient temperature) is obviously bounded and usually slow, the application of synthesis procedures that consider bounds on the rate of variation is particularly interesting.

14.4.2.1 \mathcal{H}_∞ and \mathcal{H}_2 Control Design

Gain-scheduled state feedback and dynamic output feedback controllers that guarantee an upper bound on the closed-loop \mathcal{H}_∞ and \mathcal{H}_2 performance from the disturbance w to the performance output y of the vibroacoustic setup (indicated as $\|T_{yw}\|_\infty$ and $\|T_{yw}\|_2$) are computed. To assess the impact of the bound b on the rate of parameter variation, controllers are designed for 101 equidistant values of b in the

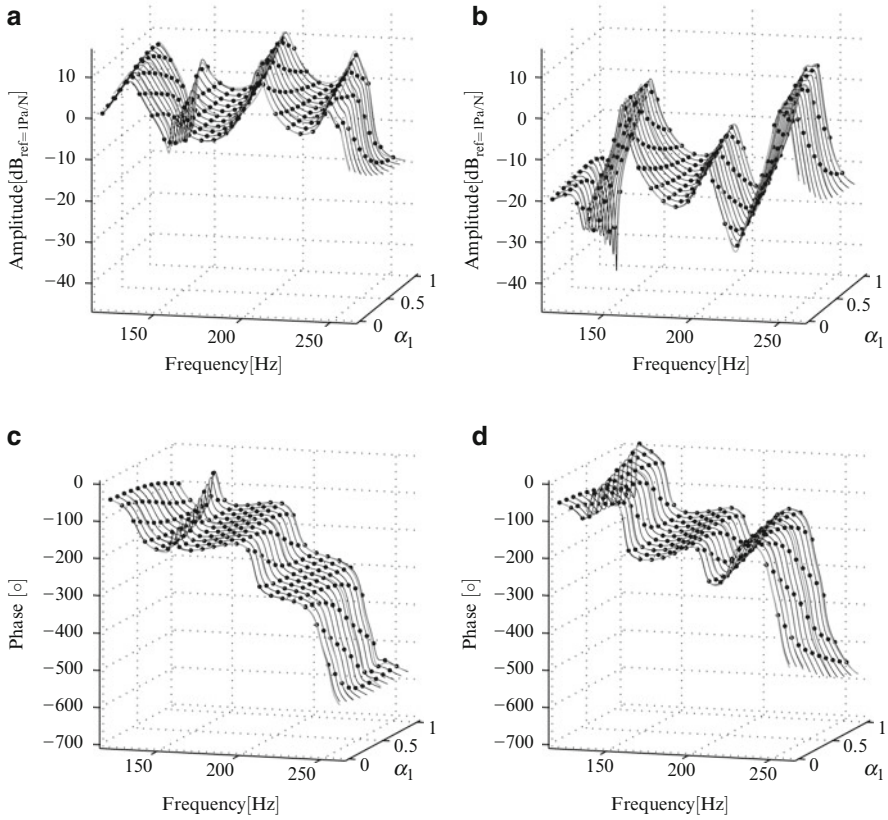


Fig. 14.6 Local LTI models (*gray, solid*) and interpolating LPV model (*black, solid with dots*), evaluated for 11 values of α_1 (a) $w \rightarrow y$: Amplitude (b) $u \rightarrow y$: Amplitude (c) $w \rightarrow y$: Phase (d) $u \rightarrow y$: Phase

interval $[0, 1]$. All problems are modeled in `Yalmip` [8] and solved using `SeDuMi` [17] within the `Matlab` environment.

The results of the \mathcal{H}_∞ and \mathcal{H}_2 control designs are presented in Fig. 14.7 which shows the obtained bounds η on $\|T_{yw}\|_\infty$ (Fig. 14.7a) and $\sqrt{\text{Tr}\{\bar{W}\}}$ on $\|T_{yw}\|_2$ (Fig. 14.7b) as a function of the bound b on the rate of the parameter variation. The bound on the open-loop performance (computed using the LMI conditions of [3]) is indicated with thick dash-dotted lines, the guaranteed closed-loop performance using gain-scheduled state feedback with thick dashed lines and the guaranteed closed-loop performance using gain-scheduled dynamic output feedback with thin solid lines. It is clear that both the state feedback and dynamic output feedback dramatically outperform the open-loop system. Furthermore, it can be concluded for both the \mathcal{H}_∞ and \mathcal{H}_2 control design that the state feedback controllers achieve better performance than the dynamic output feedback controllers. This is expected, since the dynamic controllers are based on the measurement of the single scalar output y

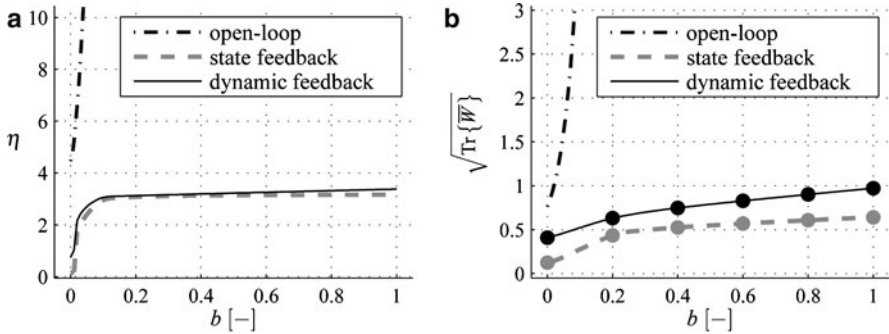


Fig. 14.7 Comparison between the upper bound on the open-loop performance (*dash-dotted*) and the guaranteed upper bound on the closed-loop performance obtained with state feedback (*dashed*) and dynamic output feedback (*solid*) (a) \mathcal{H}_∞ design (b) \mathcal{H}_2 design

only, whereas the state feedback controllers have access to all ten states. However, for the \mathcal{H}_∞ control designs (see Fig. 14.7a), the difference is small, as can be seen from the fact that the thick dashed and thin solid line almost coincide. This suggests that a dynamic controller, based on the measurement of one single microphone, can be used without significantly decreasing the closed-loop performance. This is a crucial point for the practical implementation in acoustic systems since, in general, it is not possible to measure all the state variables.

14.4.2.2 Multi-objective Design

In this design, the aim is to minimize a bound $\sqrt{\text{Tr}\{\overline{W}\}}$ on $\|T_{yw}\|_2$, while a bound η is imposed on the closed-loop \mathcal{H}_∞ performance from the disturbance w to the control signal u (indicated as $\|T_{uw}\|_\infty$) to obtain controllers that do not have excessive control signals. Six bounds on the rate of variation are considered: $b \in \{0.0, 0.2, 0.4, 0.6, 0.8, 1.0\}$ and the bound η takes 101 equidistant values in the interval $[0.01, 200]$.

Figure 14.8 shows the obtained trade-off between the prescribed \mathcal{H}_∞ bound η and the obtained \mathcal{H}_2 bound $\sqrt{\text{Tr}\{\overline{W}\}}$. Thick lines indicate state feedback control designs, whereas thin lines indicate dynamic output feedback control designs. The six cases for the bound b are indicated as follows: $b = 0.0$, gray solid; $b = 0.2$, black dashed; $b = 0.4$, gray dash-dotted; $b = 0.6$, black solid; $b = 0.8$, gray dashed; and $b = 1$, black dash-dotted. It is clear that, similarly to the results presented in Fig. 14.7, higher values of b result in a decrease in guaranteed \mathcal{H}_2 closed-loop performance (manifested as an increase in $\sqrt{\text{Tr}\{\overline{W}\}}$). Second, tighter bounds on $\|T_{uw}\|_\infty$, yield a decrease in guaranteed closed-loop \mathcal{H}_2 performance as well. Third, like in Fig. 14.7, it is clear that the state feedback controllers outperform the dynamic output feedback controllers. Fourth, it seems that for high values of η , all curves

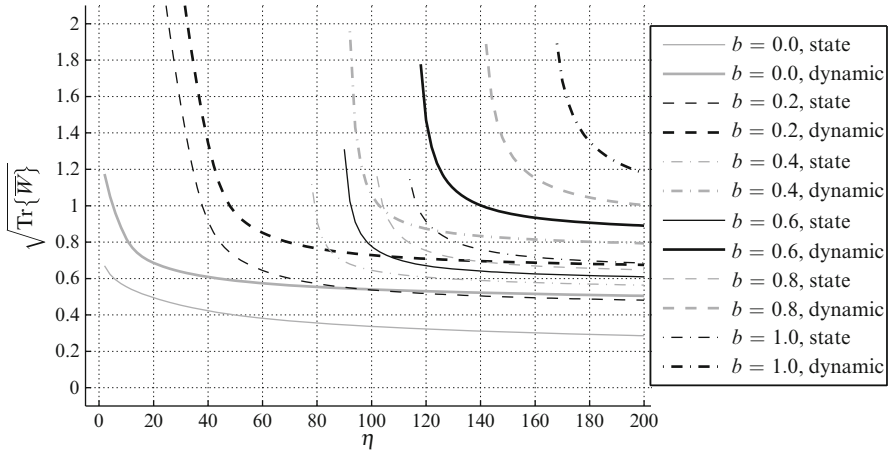


Fig. 14.8 Trade-off between the imposed upper bound η on $\|T_{uw}\|_\infty$ and the guaranteed upper bound $\sqrt{\text{Tr}\{\bar{W}\}}$ on $\|T_{yw}\|_2$. Comparison between gain-scheduled state feedback (*thick*) and dynamic output feedback (*thin*)

tend to a constant value. For each value of b , this value can be found in Fig. 14.7b (indicated with circles), which shows the best guaranteed \mathcal{H}_2 performance that can be achieved since no bound on $\|T_{uw}\|_\infty$ is imposed.

14.5 Conclusion

This chapter has presented a practical local LPV modeling technique that yields polytopic LPV models based on a set of LTI models estimated for fixed operating conditions and synthesis conditions for the design of gain-scheduled state feedback and dynamic output feedback controllers. The merit of these recent advances is that they offer practical, state-of-the-art methods for LPV modeling and control design. As demonstrated on the vibroacoustic application, the techniques can be successfully applied on realistic engineering problems.

However, there is still room for improvement in both areas. With respect to the modeling, the SMILE technique needs to be further automated by avoiding heuristic steps like the choice of the IO combination and the pole and zero sort. For the LPV control, it is interesting to investigate reduced-order LPV control design techniques and ways to include robustness against parametric and dynamic uncertainty in the LPV model as well as uncertainty on the measurement of the scheduling parameters. Moreover, less conservative path-dependent controllers can be designed that, in addition to the current value $\alpha(k)$ of the scheduling parameter, also depend on previous values $\alpha(k-1)$, $\alpha(k-2)$, etc. These are topics of current research.

Acknowledgment The authors J.F. Camino, R.C.L.F. Oliveira and P.L.D. Peres are partially supported by the Brazilian agencies CAPES, CNPq and FAPESP. The authors J. De Caigny and

J. Swevers are supported by the following funding: project G.0002.11 of the Research Foundation-Flanders (FWO-Vlaanderen), K.U.Leuven-BOF PFV/10/002 Center-of-Excellence Optimization in Engineering (OPTEC) and the Belgian Programme on Interuniversity Attraction Poles, initiated by the Belgian Federal Science Policy Office. The scientific responsibility rests with its author(s).

References

1. Daafouz J, Bernussou J (2001) Parameter dependent Lyapunov functions for discrete time systems with time varying parametric uncertainties. *Syst Control Lett* 43(5):355–359
2. De Caigny J, Camino JF, Swevers J (2009) Interpolating model identification for SISO linear parameter-varying systems. *Mech Syst Signal Process* 23(8):2395–2417
3. De Caigny J, Camino JF, Oliveira RCLF, Peres PLD, Swevers J (2010) Gain-scheduled \mathcal{H}_2 and \mathcal{H}_∞ -control of discrete-time polytopic time-varying systems. *IET Control Theory Appl* 4(3):362–380
4. De Caigny J, Camino JF, Oliveira RCLF, Peres PLD, Swevers J (2011a) Gain-scheduled dynamic output feedback for discrete-time LPV systems. *Int J Robust Nonlinear Control*. doi: 10.1002/rnc.1711
5. De Caigny J, Camino JF, Swevers J (2011b) Interpolation-based modelling of MIMO LPV systems. *IEEE Trans Control Syst Technol* 19(1):46–63
6. de Oliveira MC, Geromel JC, Bernussou J (2002) Extended \mathcal{H}_2 and \mathcal{H}_∞ norm characterizations and controller parameterizations for discrete-time systems. *Int J Control* 75(9):666–679
7. Ljung L (1999) *System identification: Theory for the user*. Prentice-Hall, Upper Saddle River, NJ, USA
8. Löfberg J (2004) Yalmip: a toolbox for modeling and optimization in matlab. In: Proceedings of the 2004 IEEE international symposium on computer aided control systems design, Taipei, Taiwan. URL <http://control.ee.ethz.ch/~joloef/yalmip.php>
9. Masubuchi I, Ohara A, Suda N (1998) LMI-based controller synthesis: a unified formulation and solution. *Int J Robust Nonlinear Contr* 8(8):669–686
10. Oliveira RCLF, Bliman PA, Peres PLD (2008) Robust LMIs with parameters in multi-simplex: Existence of solutions and applications. In: Proceedings of the 47th IEEE conference on decision and control, Cancun, Mexico, pp 2226–2231
11. Oliveira RCLF, Peres PLD (2009) Time-varying discrete-time linear systems with bounded rates of variation: Stability analysis and control design. *Automatica* 45(11):2620–2626
12. Pintelon R, Schoukens J (2001) *System identification: A frequency domain approach*. Institute of Electrical and Electronics Engineers, Inc., New York
13. Ramos DCW, Peres PLD (2001) A less conservative LMI condition for the robust stability of discrete-time uncertain systems. *Syst Control Lett* 43(5):371–378
14. Scherer CW (2005) Relaxations for robust linear matrix inequality problems with verifications for exactness. *SIAM J Matrix Anal Appl* 27(2):365–395
15. Scherer CW, Gahinet P, Chilali M (1997) Multiobjective output-feedback control via LMI optimization. *IEEE Trans Automat Contr* 42(7):896–911
16. de Souza CE, Barbosa KA, Trofino A (2006) Robust \mathcal{H}_∞ filtering for discrete-time linear systems with uncertain time-varying parameters. *IEEE Trans Signal Process* 54(6):2110–2118
17. Sturm JF (1999) Using sedumi 1.02, A matlab toolbox for optimization over symmetric cones. *Optim Methods Softw* 11(1):625–653
18. Donadon LV, Siviero DA, Camino JF, Arruda JRF (2006) Comparing a filtered-X LMS and an \mathcal{H}_2 controller for the attenuation of the sound radiated by a panel. *Proc. Int. Conf. Noise Vibr. Engin.*, pp 199–210

Chapter 15

LPV Modeling and Control of Semi-active Dampers in Automotive Systems

Anh-Lam Do, Olivier Sename, and Luc Dugard

Abstract The aim of this chapter is to emphasize the interest of the LPV methodology for suspension modeling and control. Indeed, the main features of a semi-active automotive suspensions are:

- The damper can only dissipate energy.
- The damper has a nonlinear behavior which is important to account for in the control design step.

New methodologies have been recently designed to separately cope with these constraints (Do AL et al., An LPV control approach for semi-active suspension control with actuator constraints, 2010; Poussot-Vassal et al., *Contr Eng Pract* 16(12):1519–1534, 2008; Savaresi et al., Semi-active suspension control for vehicles, 2010). In this study, recent developments are presented to:

- First, develop an LPV model for an automotive suspension system starting from a nonlinear semi-active damper model.
- Second, using an original LPV representation of the dissipativity of the semi-active damper, develop an ad hoc H_∞ /LPV controller.

The whole LPV model is used to design a polytopic H_∞ controller for an automotive suspension system equipped with a Magneto-Rheological semi-active damper. This controller aims at improving ride comfort and/or road holding, depending on the required specifications. Some simulation results are given on realistic vehicle and damper models (whose validation on real data has been performed), allowing to show the efficiency of the approach.

A.-L. Do • O. Sename (✉) • L. Dugard
GIPSA-Lab, Control Systems Department, CNRS-Grenoble INP, ENSE3, BP 46,
F-38402 St Martin d'Hères cedex, France
e-mail: anh-lam.do@gipsa-lab.grenoble-inp.fr; olivier.sename@gipsa-lab.grenoble-inp.fr;
luc.dugard@gipsa-lab.grenoble-inp.fr

15.1 Introduction

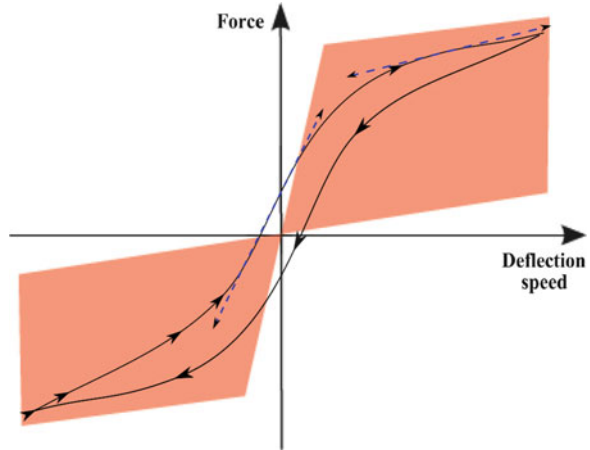
When a vehicle travels, it is excited by a broad spectrum of vibrations. The vibration sources may come from the driveline, engine, tire/wheel assemblies, and the road roughness. Among these vibration sources, the road roughness influences dramatically the vehicle dynamics: the vertical acceleration, the wheel–road contact, the rollover, the cornering and braking behavior, etc. It is well known that, for vibration isolation, vehicles are equipped with suspension systems which usually consist of an elastic element and a damping element connected in parallel. Indeed, suspension design has about 100 years of development, from the appearance of very simple passive dampers in Roll Royce (in 1913) to sophisticated controllable MR dampers in the most recent cars such as Audi TT, Audi R8, Ferrari 599 GTB, etc. Today, it plays an important role in the automotive industry because, besides the vibration isolation capacity (through energy dissipativity), suspension systems can further improve the safety and the handling (by minimizing the tire load variation). In general, suspensions are classified into three types according to their controllability (see, e.g., [23] for a detailed classification):

- *Passive suspensions*, found in low-cost vehicles, consist of a spring connected in parallel with a passive damper. They can only dissipate the energy and their property is time-invariant.
- *Semi-active suspensions*, found in mid-range and expensive vehicles, consist of a spring and a semi-active damper. Like passive suspensions, they can only dissipate the energy but their property (the damping coefficient) can be changed by external control signals.
- *Active suspensions*, found in small number in mid-range and expensive vehicles, use a spring and an active damper. For such types of suspensions, external actuators are required to supply energy to the systems. Hence, they can both dissipate and generate the energy.

The main objectives in suspension design are related to ride comfort and road holding. Ride comfort concerns the pleasure of passenger and driver, road holding influences the drive safety. While passive suspensions achieve only a compromise between ride comfort and road holding, the semi-active and active suspensions can enhance both performance objectives. This is the reason why the latter suspensions have been studied more intensively in recent years. However, only the semi-active suspensions are used widely in automotive industry because, compared with fully active suspensions, the semi-active ones provide a better compromise between the cost and the performances. Semi-active suspensions can potentially achieve the majority of the performance criteria (see [24, 33]) while they are smaller in weight and volume, cheaper in price, more reliable in work (the robustness due to their dissipative property), and less energy consuming (see also [14, 15, 21, 27, 39, 40]).

In this chapter, the semi-active suspensions are studied. The control design problem for such suspensions has been tackled with many approaches during the last three decades. One of the first comfort-oriented control methods, successfully

Fig. 15.1 Realistic MR damper force with bi-viscosity (pre-yield and post-yield viscous damping) and hysteresis



applied in commercial vehicles, is the Skyhook control proposed by Karnopp et al. [26]. In this control design, the damping coefficient is adjusted continuously or switched between a maximum and a minimum value. Contrary to the Skyhook, the Groundhook controller [43] was designed to improve road holding. Then numerous approaches have also been developed such as optimal control [39], clipped optimal control [6, 16], or H_∞ control [35, 36], LPV control [34]. Recently, the mixed Skyhook and ADD (SH-ADD) algorithm proposed by [40] has been known to be one of the most efficient comfort-oriented controllers. An overview of some recent methodologies in terms of performances was done in [38].

In the studies presented previously, the nonlinear characteristics (the bi-viscous and the hysteretic behaviors of semi-active dampers, see Fig. 15.1) are not taken into account in the controller design. This may result in bad performance when these controllers are implemented and applied to real suspension systems. The main contribution of this chapter is to propose a new control design method for nonlinear semi-active suspensions using the LPV approach. The methodology is based on a nonlinear static model of the semi-active damper where the bi-viscous and hysteretic behaviors of the damper are taken into consideration. The nonlinear system associated with the quarter vehicle model is reformulated in the LPV framework. The dissipativity problem is brought into the input saturation one, using a simple change of variable. To improve ride comfort and road holding, the H_∞ controller for LPV system (see [2, 41]) is used. Finally, a weighting-function optimization for multiobjective H_∞ design using Genetic Algorithms is proposed. The results in [11, 12] show that this procedure is quite efficient for the particular problem of semi-active suspension control and it is general enough for other multi-objective optimization designs for LPV systems.

15.2 Semi-Active Suspension Modeling

Many models have been proposed for semi-active suspension modeling. For example, the Bingham model is a phenomenological model that describes the behavior of an Electro-Rheological (ER) damper [42]. The model consists of a viscous damper in parallel with a Coulomb friction element. Another well-known method is the semi-phenomenological Bouc–Wen model. It was first introduced by Bouc [4] and then modified by Wen [44]. This model has been used widely to describe hysteretic systems.

Recently, the Magneto-Rheological (MR) dampers have been analyzed in many studies. They use MR fluids whose characteristics can be changed through the application of a magnetic field. Compared with other kinds of semi-active dampers, they have great advantages like fast time response as well as stable hysteretic behavior over a broad range of temperature, low battery voltages consumption, etc. They represent a new generation of semi-active dampers and are applied in many applications like shock absorbers and damping devices, clutches breaks, actuators or artificial joints, operational earthquake dampers to reduce motion in buildings and of course in automotive systems... For the modeling of these dampers, in [25] Spencer proposed a modified Bouc–Wen model or in [37], Savaresi et al. presented a black box model. In 2006, Shuqi Guo et al. proposed a semi-phenomenological model [20]. Besides accuracy, this model has an interesting structure which can be extended for LPV control synthesis.

15.2.1 Shuqi Guo Model for MR Damper

The behavior of the semi-active damper is represented using the following nonlinear equation, as in [20]:

$$F_{\text{shuqi-guo}} = a_2 \left(\dot{x}_{\text{mr}} + \frac{v_0}{x_0} x_{\text{mr}} \right) + a_1 \tanh \left(a_3 \left(\dot{x}_{\text{mr}} + \frac{v_0}{x_0} x_{\text{mr}} \right) \right), \quad (15.1)$$

where $F_{\text{shuqi-guo}}$ is the damper force, x_{mr} is the suspension deflection, a_1 is the dynamic yield force of the MR fluid, a_2 and a_3 are related to the post-yield and pre-yield viscous damping coefficients, v_0 and x_0 denote the absolute value of hysteretic critical velocity \dot{x}_0 and hysteretic critical deflection x_0 where \dot{x}_0 and x_0 are defined as the velocity and deflection when the MR damper force is zero.

The model is of semi-phenomenological type and based on a tangent hyperbolic function to model the hysteresis and bi-viscous characteristic of a damper. This model has a simple and elegant formulation, but the control input signal (current, for MR dampers) is not present. Obviously, it cannot be used for the controller synthesis.

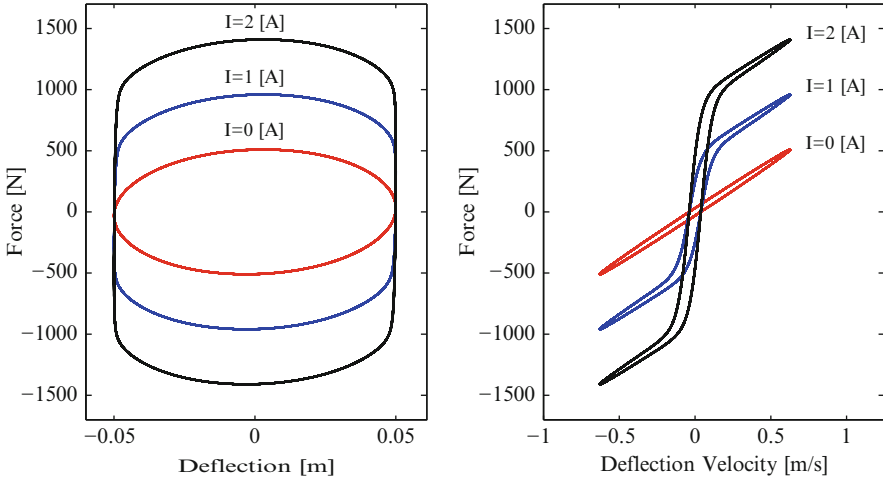


Fig. 15.2 MR damper characteristics with different current values I : force vs. deflection (*Left*) and force vs. velocity (*Right*)

15.2.2 Control-Oriented MR Damper Model

In [31], the authors have shown that if each coefficient in (15.1) is defined as a polynomial function of electric current, the obtained model will approach the real data better. However, for control purpose, a simpler control-oriented model where only one parameter depends on the input signal was proposed and first studied in [9, 13]. According to the authors, a control-oriented model for semi-active damper can be given by

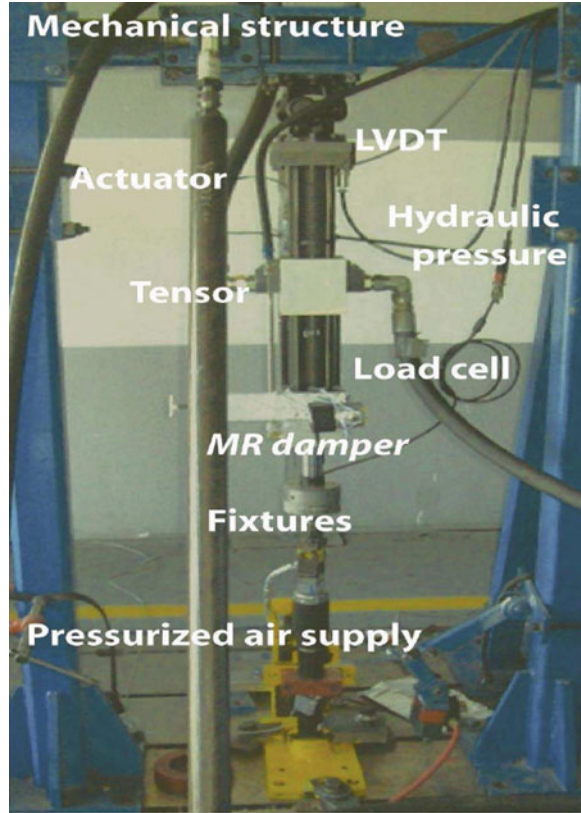
$$F_{\text{mr}} = c_0 \dot{x}_{\text{mr}} + k_0 x_{\text{mr}} + f_I \tanh(c_1 \dot{x}_{\text{mr}} + k_1 x_{\text{mr}}), \quad (15.2)$$

where F_{mr} is the damper force, c_0 , c_1 , k_0 , and k_1 are constant parameters and f_I is the controllable force coefficient which is varying according to the electrical current I in coil ($0 \leq f_{I\text{min}} < f_I \leq f_{I\text{max}}$).

Compared with the model (15.1) whose characteristics are static and uncontrollable, the model (15.2) reflects the realistic behavior of an MR damper. This model allows fulfilling the dissipativity constraint of the semi-active damper and introduces a control input f_I . The limitation of the model is in the assumption that the MR dampers' hysteresis is invariant with respect to the current I . Figure 15.2 presents the dependency of damper force to the input current. Changing the current in the coil of an MR damper changes its characteristics. Here, the bi-viscous and the hysteresis can be clearly observed.

The model's parameters used in Fig. 15.2 are the following: $c_0 = 810.78$ (Ns/m), $k_0 = 620.79$ (N/m), $c_1 = 13.76$ (s/m), $k_1 = 10.54$ (1/m). These experimental

Fig. 15.3 Experimental test-rig for MR damper parameter identification



parameters are identified by our colleague Jorge de Jesus Lozoya-Santos (see [29,30]) on the test-rig at *Metalsa*¹ (see Fig. 15.3).

The experimental system consists of three key blocks: an actuator *FlexTest GT MTS*TM, an electric current controller, and an acquisition system. The man-machine interface interacts with the control systems and the acquisition system. The specifications of the actuator are from 25 to 3,000 psi and a stroke of 150 mm. A sensor is used for measuring the displacement. Electrical current is measured by a resistor connected in series with the coil of the MR damper. An InstronTM load cell measures the generated forces.

For model identification, a sinusoidal displacement (about 4 Hz) is randomly modulated in amplitude, and a random signal of electric current is used. Figure 15.4 presents the experimental data in the interval 30–33 s. As seen in Fig. 15.5, the model tracks well the real data. The average ESR (Error-to-Signal-Ratio) is around 7%, and the maximum ESR is about 20% (in high frequencies where the MR force changes rapidly). It is recommended to find more details on the experimental results in [29,30].

¹www.metalsa.com.mx.

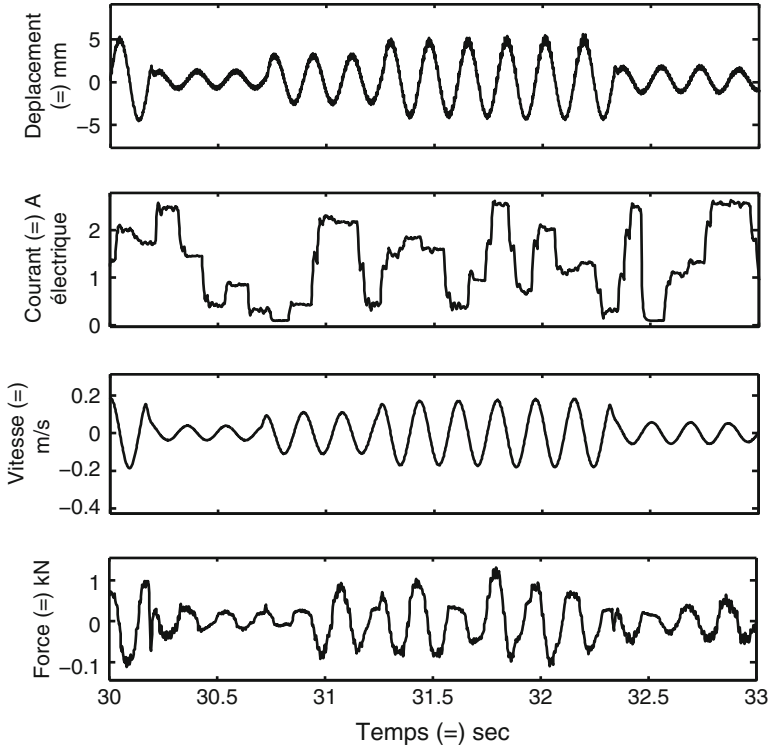


Fig. 15.4 Experimental data

Let us return to the model 15.2, which has an interesting characteristic that can be exploited for LPV design. Note that the function $\tanh(c_1\dot{x}_{mr} + k_1x_{mr})$ is bounded in $[-1;1]$ for any value of \dot{x}_{mr} and x_{mr} . Moreover, the function value is known because the damper deflection x_{mr} and velocity \dot{x}_{mr} can be measured using a unique displacement sensor. It is hence naturally a scheduling parameter in LPV design.

15.3 The Quarter Vehicle Model and Suspension Performance Objectives

15.3.1 Quarter Vehicle Model

To study the vertical dynamics of a vehicle equipped with suspension systems, it is well known that a 2-DOF quarter vehicle model (see Fig. 15.6) is used. The model is simple and suitable for a preliminary design. It represents a single corner of a vehicle. In this model, the quarter vehicle body is represented by the sprung mass

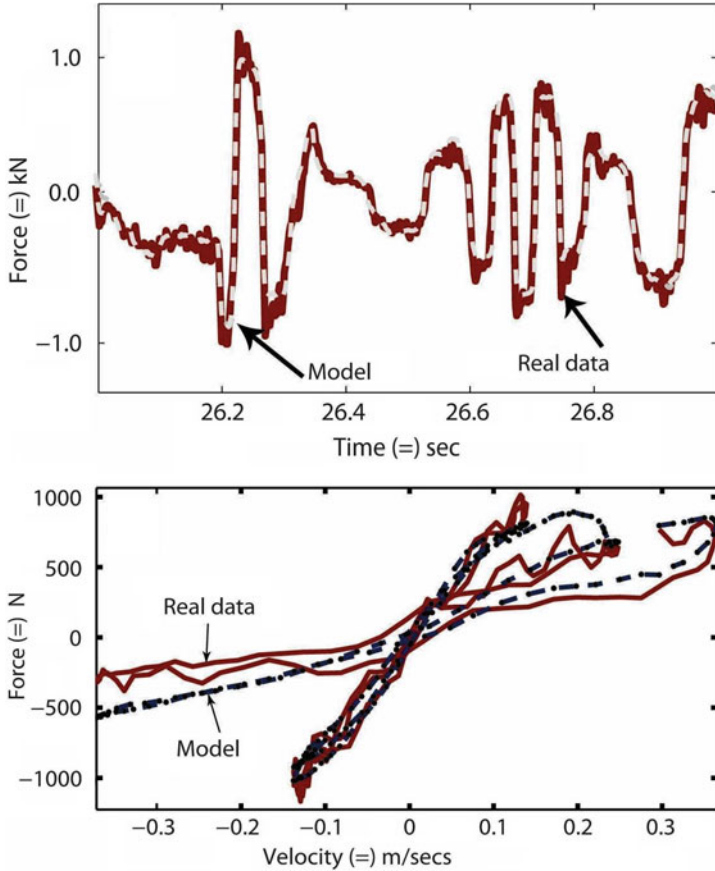


Fig. 15.5 Model’s force vs. real data

(m_s) and the wheel and tire are represented by the unsprung mass (m_{us}). They are connected by a spring with the stiffness coefficient k_s and a semi-active damper. The tire is modeled by a spring with the stiffness coefficient k_t . As seen in the figure, z_s (respectively, z_{us}) is the vertical displacement around the equilibrium point of m_s (respectively, m_{us}) and z_r is the road profile. It is assumed that the wheel–road contact is ensured. By applying the second law of Newton, the dynamical equations of a quarter vehicle are given by

$$\begin{cases} m_s \ddot{z}_s = -F_{spring} - F_{mr} \\ m_{us} \ddot{z}_{us} = F_{spring} + F_{mr} - k_t (z_{us} - z_r) \end{cases} \quad (15.3)$$

where $F_{spring} = k_s (z_s - z_{us})$ is the spring force. The damper force F_{mr} is given as in (15.2) and satisfies the dissipativity constraint:

$$0 < f_{lmin} < f_l \leq f_{lmax} \quad (15.4)$$

Fig. 15.6 Model of quarter vehicle with a semi-active damper

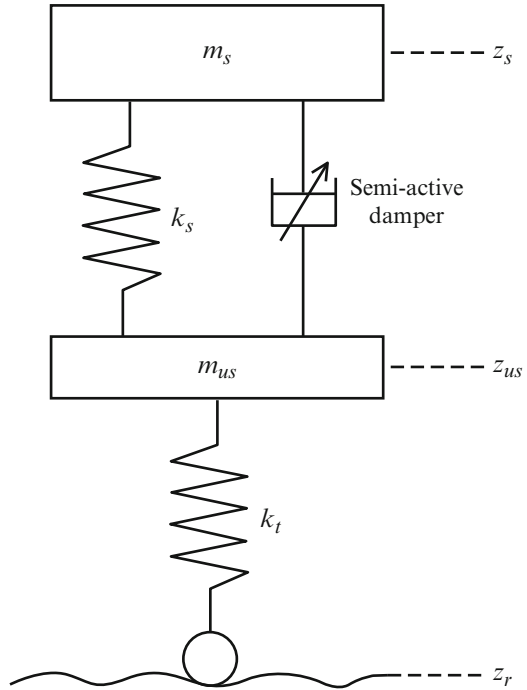


Table 15.1 Parameter values of the quarter car model equipped with an MR damper

1/4 RMC	Value	Unit	MR damper	Value	Unit
m_s	315	(kg)	c_0	810.78	(Ns/m)
m_{us}	37.5	(kg)	k_0	620.79	(N/m)
k_t	210,000	(N/m)	f_{min}	0	(N)
–	–	–	f_{max}	800	(N)
–	–	–	c_1	13.76	(s/m)
–	–	–	k_1	10.54	(1/m)

The dynamical equations are rewritten as follows:

$$\begin{cases} m_s \ddot{z}_s = -k_s(z_s - z_{us}) - c_0(\dot{z}_s - \dot{z}_{us}) - k_0(z_s - z_{us}) \\ \quad - f_I \tanh(c_1(\dot{z}_s - \dot{z}_{us}) + k_1(z_s - z_{us})) \\ m_{us} \ddot{z}_{us} = k_s(z_s - z_{us}) + c_0(\dot{z}_s - \dot{z}_{us}) + k_0(z_s - z_{us}) \\ \quad + f_I \tanh(c_1(\dot{z}_s - \dot{z}_{us}) + k_1(z_s - z_{us})) - k_t(z_{us} - z_r). \end{cases} \quad (15.5)$$

It is worth noting that (15.5) is a nonlinear differential equation system. In this chapter, the 1/4 Renault Mégane Coupé (1/4 RMC) equipped with an MR damper presented in Sect. 15.2 is studied. The model parameters are given in Table 15.1.

15.3.2 Performance Objective Quantification for Suspension Control

As mentioned previously, in semi-active suspension control, the two main objectives are ride comfort and road holding. While road holding can be directly quantified by the analysis of the dynamic tire force, ride comfort is, however, more difficult to quantify because it is a subjective matter. The human sensitivity to vibration is frequency dependent. Furthermore, at the same frequencies, the different parts of the human body feel the vibration in different ways. To answer to the question on which is the good measure to evaluate ride comfort, let us recall some criteria existing in the literature (see [19]).

Denote X the maximum allowed displacement amplitude, ω the angular frequency, f the frequency, and t the time. Janeway's comfort criterion (1965) relates the comfort to vertical vehicle body displacement. At low frequencies, the criterion states that

$$X\omega^3 = 12.6 \quad (15.6)$$

and at high frequencies, in the range 6–20 Hz, the vehicle body acceleration peak value should not exceed 0.33 m/s^2 , whilst between 20 and 60 Hz the maximum velocity should stay below 2.7 mm/s .

Steffens (1966) proposed to evaluate the comfort using the following criterion:

$$X[\text{cm}^2] = 7.62 \times 10^{-3} \left(1 + \frac{125}{f^2} \right). \quad (15.7)$$

Another criterion is the vibration dose (VD) value proposed by Griffin (1984) which provides an indication based on the integral of the fourth power of the frequency weighted acceleration a

$$VD = \int_0^t a^4 dt. \quad (15.8)$$

The most general criterion is the standard ISO 2631 (1978). It is a general standard applicable not only to vehicles but also to all vibrating environments. It defines the exposure limits for body vibration in the range 1–80 Hz, defining limits for reduced comfort, for decreased proficiency and for preservation of health. According to this criterion, human being is more sensible to the vertical acceleration in the range of 4–8 Hz. The ISO 2631 filter applied on the sprung mass acceleration is approximated by the following transfer function (see [48]):

$$W_{\text{ISO-2631}} = \frac{81.89s^3 + 796.6s^2 + 1937s + 0.1446}{s^4 + 80.00s^3 + 2264s^2 + 7172s + 21196}. \quad (15.9)$$

15.3.2.1 Criteria for Suspension Performance Evaluation

In the following, the criteria to evaluate the performance of the semi-active suspension systems are given. By abuse of language, let us denote \ddot{z}_s/z_r (respectively, $(z_{us} - z_r)/z_r$) the “frequency response” from the road disturbance z_r to the vehicle body acceleration \ddot{z}_s (respectively, the dynamic tire deflection $z_{us} - z_r$).

In general, the vehicle body acceleration between 0 and 20 Hz should be filtered to guarantee a good ride comfort, although it is worth noting again that human is the most sensible to vertical acceleration around 4–8 Hz (ISO 2631). On the other side, to maintain the road–wheel contact, it is necessary that the dynamic tire force is smaller than $g(m_s + m_{us})$ (where g is the gravity). Hence, for the road holding improvement, the dynamic tire force $k_t(z_{us} - z_r)$, in other words the dynamic tire deflection $z_{us} - z_r$, should be small in the frequency range 0–30 Hz. Also noting that, road holding is improved by limiting the up and down bouncing of the wheel z_{us} around its resonant 10–15 Hz.

In summary, with the remarks above, the performance objectives in the frequency domain are described explicitly as follows:

- Comfort

$$J_{CF} = \int_0^{20} \ddot{z}_s/z_r(f) df. \quad (15.10)$$

- Road holding

$$J_{RH} = \int_0^{30} (z_{us} - z_r)/z_r(f) df. \quad (15.11)$$

The performance objectives above for ride comfort and road holding are consistent with the ones given in [36, 38].

15.4 LPV Model for Semi-Active Suspension Control

With the defined system and performance objectives in the previous section, in the following, an LPV model for controller synthesis is formulated. Denote:

- $c_p = c_0$
- $k_p = k_s + k_0$
- $z_{\text{def}} = z_s - z_{us}$
- $\dot{z}_{\text{def}} = \dot{z}_s - \dot{z}_{us}$
- $\hat{p} = \tanh(c_0(\dot{z}_s - \dot{z}_{us}) + k_0(z_s - z_{us}))$

From (15.5), the state-space representation of the quarter vehicle model can be deduced as follows:

$$\begin{cases} \dot{x}_s = A_s x_s + B_s \hat{p} f_I + B_{sw} w \\ z = C_{sz} x_s + D_{sz} \hat{p} f_I \\ y = C_s x_s \end{cases}, \quad (15.12)$$

where $x_s = (z_s, \dot{z}_s, z_{us}, \dot{z}_{us})^T$, $w = z_r$, $y = (z_s - z_{us}, \dot{z}_s - \dot{z}_{us})^T$, $z = (\ddot{z}_s, z_{us})^T$.

$$A_s = \begin{pmatrix} 0 & 1 & 0 & 0 \\ -\frac{k_p}{m_s} & -\frac{c_p}{m_s} & \frac{k_p}{m_s} & \frac{c_p}{m_s} \\ 0 & 0 & 0 & 1 \\ \frac{k_p}{m_{us}} & \frac{c_p}{m_{us}} & -\frac{k_p+k_t}{m_{us}} & -\frac{c_p}{m_{us}} \end{pmatrix}, B_s = \begin{pmatrix} 0 \\ -\frac{1}{m_s} \\ 0 \\ \frac{1}{m_{us}} \end{pmatrix}, B_{sw} = \begin{pmatrix} 0 \\ 0 \\ 0 \\ \frac{k_t}{m_{us}} \end{pmatrix},$$

$$C_s = \begin{pmatrix} 1 & 0 & -1 & 0 \\ 0 & 1 & 0 & -1 \end{pmatrix}^T, C_{sz} = \begin{pmatrix} -\frac{k_p}{m_s} & -\frac{c_p}{m_s} & \frac{k_p}{m_s} & \frac{c_p}{m_s} \\ 0 & 0 & 1 & 0 \end{pmatrix}, D_{sz} = \begin{pmatrix} -\frac{1}{m_s} \\ 0 \end{pmatrix}.$$

Remark 15.1. The considered measurement outputs are the suspension deflection and suspension deflection velocity, which allows to state that $\hat{\rho}$ can be known in real time.

Remark 15.2. As mentioned in the previous section, the performance objectives are ride comfort and road holding. Ride comfort is clearly related to the vehicle body acceleration \ddot{z}_s . Road holding, beside being quantified by the dynamic tire deflection $z_{us} - z_r$, is related to the bouncing of the wheel z_{us} . Consequently, the controlled output vector may be as $z = (\ddot{z}_s, z_{us})^T$.

As explained above, to guarantee the dissipativity of an MR damper, the control signal f_I must satisfy the constraint (15.4). By defining $u_I = f_I - f_0$, where $f_0 = (f_{Imin} + f_{Imax})/2$, the dissipativity constraint on f_I is recast as a saturation constraint on u_I , i.e.,

$$-\bar{u} \leq u_I \leq \bar{u}, \tag{15.13}$$

where $\bar{u} = \frac{f_{Imax} - f_{Imin}}{2}$.

With this modification, the state-space representation of the quarter vehicle is given as follows:

$$P : \begin{cases} \dot{x}_s = (A_s + B_{s1} \frac{\hat{\rho}}{C_{s1}x_s} C_{s1})x_s + B_s \hat{\rho} u_I + B_{sw} w \\ z = (C_{sz} + D_{s1} \frac{\hat{\rho}}{C_{s1}x_s} C_{s1})x_s + D_{sz} \hat{\rho} u_I \\ y = C_s x_s \end{cases}, \tag{15.14}$$

where $B_{s1} = \begin{pmatrix} 0 & -\frac{f_0}{m_s} & 0 & \frac{f_0}{m_{us}} \end{pmatrix}^T$, $C_{s1} = (k_1 \ c_1 \ -k_1 \ -c_1)$, $D_{s1} = \begin{pmatrix} -\frac{f_0}{m_s} & 0 \end{pmatrix}$.

In this study, the LPV model (15.14) can be used to design an LPV controller. However, such a controller may not ensure the closed-loop stability and performances since the saturation constraint (i.e., the dissipativity constraint) is not accounted for in the design. Some solutions for this problem have been proposed. For example, in [34], a scheduling parameter is indeed defined as the difference between the real controlled damper force and the required one given by the controller. However, the dissipativity constraint is not theoretically fulfilled. Another possible method is to add, in the closed-loop system, an AWBT (Anti Wind-up Bumpless Transfer) compensation to minimize the adverse effects of the control

input saturation on the closed-loop performance [17, 18, 28, 32]. In the next section, a simple method is presented to solve the problem by considering the input saturation as a scheduling parameter. This approach is indeed related to [45].

Define the saturation function $sat(\cdot)$ as follows:

$$sat(u_I) = \begin{cases} \bar{u} & \text{if } u_I > \bar{u} \\ u_I & \text{if } -\bar{u} \leq u_I \leq \bar{u} \\ -\bar{u} & \text{if } u_I < -\bar{u} \end{cases} . \quad (15.15)$$

The state-space representation of the system (15.14) subject to the input saturation constraint (15.13) is rewritten as

$$P : \begin{cases} \dot{x}_s = (A_s + B_{s1} \frac{\hat{\rho}}{C_{s1} x_s} C_{s1}) x_s + B_s \hat{\rho} \frac{sat(u_I)}{u_I} u_I + B_{sw} w \\ z = (C_{sz} + D_{s1} \frac{\hat{\rho}}{C_{s1} x_s} C_{s1}) x_s + D_{sz} \hat{\rho} \frac{sat(u_I)}{u_I} u_I \\ y = C_s x_s \end{cases} . \quad (15.16)$$

Denote $\rho_1 = \hat{\rho} \frac{sat(u_I)}{u_I}$ and $\rho_2 = \frac{\hat{\rho}}{C_{s1} x_s}$. From (15.16), the following LPV system is now obtained

$$P : \begin{cases} \dot{x}_s = (A_s + B_{s1} C_{s1} \rho_2) x_s + B_s \rho_1 u_I + B_{sw} w \\ z = (C_{sz} + D_{s1} C_{s1} \rho_2) x_s + D_{sz} \rho_1 u_I \\ y = C_s x_s \end{cases} . \quad (15.17)$$

In (15.17) the control input matrix $B_s \rho_1$ is parameter dependent, which is not consistent with the solution of the H_∞ design problem for polytopic systems [2]. This problem can be overcome by adding the following filter into (15.17) to make the controlled input matrix independent from the scheduling parameter:

$$W_f : \begin{pmatrix} \dot{x}_f \\ u_I \end{pmatrix} = \begin{pmatrix} A_f & B_f \\ C_f & 0 \end{pmatrix} \begin{pmatrix} x_f \\ u \end{pmatrix} \quad (15.18)$$

with

$$\|W_f\|_\infty \leq 1, \quad (15.19)$$

where A_f, B_f, C_f are constant matrices.

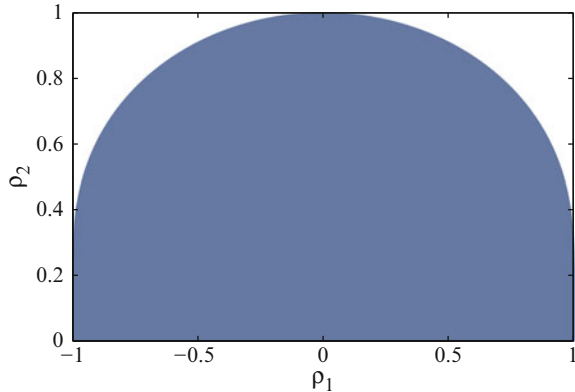
Remark 15.3. The condition (15.19) ensures that the saturation constraint on u_I is kept for the new control input u . It means that the following implies (15.13):

$$-\bar{u} \leq u \leq \bar{u}. \quad (15.20)$$

From (15.17) and (15.18), the control oriented model is now represented by an LPV system with two scheduling parameters ρ_1 and ρ_2 :

$$\begin{cases} \dot{x} = A(\rho_1, \rho_2) x + Bu + B_1 w \\ z = C_z(\rho_1, \rho_2) x \\ y = Cx \end{cases} , \quad (15.21)$$

Fig. 15.7 Set of scheduling parameters (ρ_1, ρ_2) (shaded area)



where

$$x = \begin{pmatrix} x_s^T & x_f^T \end{pmatrix}^T,$$

$$A(\rho_1, \rho_2) = \begin{pmatrix} A_s + \rho_2 B_{s1} C_{s1} & \rho_1 B_s C_f \\ 0 & A_f \end{pmatrix}, B = \begin{pmatrix} 0 \\ B_f \end{pmatrix}, B_1 = \begin{pmatrix} B_{s1} \\ 0 \end{pmatrix},$$

$$C = \begin{pmatrix} C_s \\ 0 \end{pmatrix}^T, C_z(\rho_1, \rho_2) = \begin{pmatrix} C_{sz} + \rho_2 D_{s1} C_{s1} & \rho_1 D_{sz} C_f \end{pmatrix},$$

$$\rho_1 = \tanh(C_{s1} x_s) \frac{\text{sat}(c_f x_f)}{c_f x_f}, \rho_2 = \frac{\tanh(C_{s1} x_s)}{C_{s1} x_s}.$$

Notice also that ρ_1 and ρ_2 are not independent. As seen in Fig. 15.7, the set of (ρ_1, ρ_2) is represented by the shaded area and this set is not a polytope. In the following section, a polytopic approach will be applied for LPV system (15.21) by considering a polytope that includes all possible scheduling parameter trajectories of (ρ_1, ρ_2) .

Indeed, we aim at finding an LPV controller that guarantees the stability and the H_∞ performance for the system (15.21). It is well known that the quality of this controller depends on the choice of some weighting functions. In the next section, a general procedure for the optimization of the weighting functions selection will be proposed and then applied to the semi-active suspension control.

15.5 Optimizing H_∞ /LPV Controller for Semi-Active Suspensions

The H_∞ control design approach is an efficient tool to improve the performances of a closed-loop system in pre-defined frequency ranges. The key step of the H_∞ control design relies on the selection of the weighting functions which depend on the engineer skill and experience. In many real applications, it is more difficult in choosing the weighting functions because the performance specifications are not accurately defined, i.e., it is simply to achieve the best possible performances

(optimal design) or to achieve an optimally joint improvement of more than one objective (multi-objective design). Therefore, it appears interesting to optimize the selection of the weighting functions to get the desired closed-loop performances. As studied in [3, 22], it has been proposed to consider a system, no matter how complex it is, as a combination of subsystems of the first and second order, for which it is easy to find the good weighting functions to be used in the H_∞ control methodology. However, there is no explicit method to find these functions in the general case. The usual way is to proceed by trial and error. Recently, as in [1], the use of nonlinear optimization tools, such as the Genetic Algorithms, has been proved to be interesting since the parameter design is here related to nonlinear cost functions. Below, the problem formulation of the H_∞ /LPV control design for polytopic systems is presented according to the considered application.

Indeed, in the particular case of semi-active suspension control, ride comfort and road holding are two essential but conflicting control objectives. It is shown that, for example, it is impossible to improve ride comfort without degrading road holding and vice versa around the wheel resonance 10–15 Hz. In this section, the aim is to use Genetic Algorithms (GAs) to obtain the best controllers (for ride comfort and/or road holding) through optimizing the selection of the weighting functions for the H_∞ /LPV control of semi-active suspensions.

15.5.1 Control Scheme

The control configuration for semi-active suspensions is given in Fig. 15.8. The controlled outputs are the vehicle body acceleration \ddot{z}_s (for the ride comfort improvement) and the wheel displacement z_{us} (for the road holding improvement, see Sect. 15.3.2). The measurement outputs are the suspension deflection z_{def} and suspension deflection velocity \dot{z}_{def} (needed for computing the scheduling parameters as well). To obtain the closed-loop performances (see Sect. 15.3.2), the weighting functions on controlled outputs $\{W_{z_s}, W_{z_{us}}\}$ and disturbance input W_{z_r} are used.

Notice that, due to the self-dependence between ρ_1 and ρ_2 , the set of all $\bar{\rho} = (\rho_1, \rho_2)$ is not a polytope, as seen in Fig. 15.7. In this study, a polytopic approach is developed for the LPV control design (which leads to some conservatism). As a consequence, ρ_1 and ρ_2 are considered as independent parameters and $\bar{\rho}$ belongs to a polytope Θ whose vertices are $\bar{\rho}_1 = (1, 1)$, $\bar{\rho}_2 = (-1, 1)$, $\bar{\rho}_3 = (-1, 0)$, $\bar{\rho}_4 = (1, 0)$.

Consider the augmented system (corresponding to Fig. 15.8) made of the plant (15.21) and the weighting functions, represented by

$$\begin{aligned}\dot{\xi} &= \mathcal{A}^V(\bar{\rho})\xi + \mathcal{B}_1^V(\bar{\rho})\bar{w} + \mathcal{B}_2^V u, \\ \bar{z} &= \mathcal{C}_1^V(\bar{\rho})\xi + \mathcal{D}_{11}^V(\bar{\rho})\bar{w} + \mathcal{D}_{12}^V u, \\ y &= \mathcal{C}_2\xi + \mathcal{D}_{21}\bar{w},\end{aligned}\tag{15.22}$$

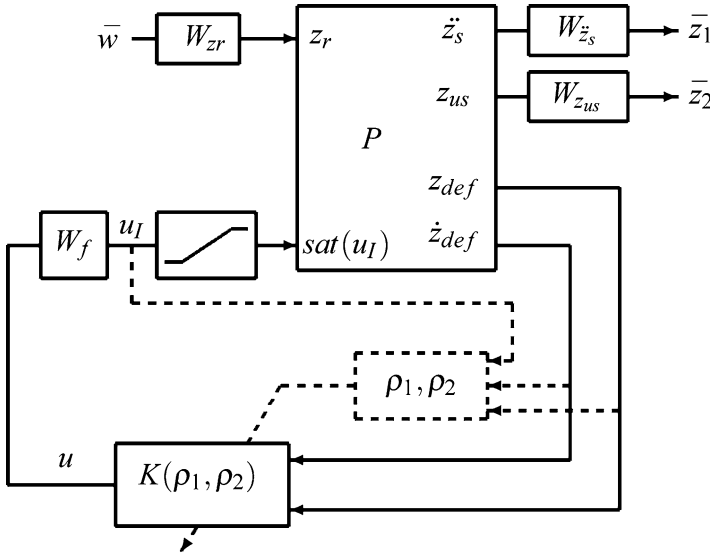


Fig. 15.8 Block diagram for semi-active suspension control

where $\xi = (x^T x_w^T)^T$, x_w being the state vector of the weighting functions, $\bar{\rho} = (\rho_1, \rho_2)$ the vector of scheduling parameters. Note that v represents the vector of all weighting function parameters. The LPV controller is defined as follows:

$$K(\bar{\rho}) : \begin{pmatrix} \dot{x}_c \\ u \end{pmatrix} = \begin{pmatrix} A_c^v(\bar{\rho}) & B_c^v(\bar{\rho}) \\ C_c^v(\bar{\rho}) & D_c^v(\bar{\rho}) \end{pmatrix} \begin{pmatrix} x_c \\ y \end{pmatrix}, \tag{15.23}$$

where x_c , y , and u are, respectively, the state, the input, and the output of the controller associated with the system (15.22). All matrices have appropriate dimensions.

Remark 15.4. Since v represents the vector of the weighting function parameters, it is used as an exponent in the notation of (15.22) and (15.23) to emphasize the dependence of the generalized plant, and then of the controller, on the parameters of the weighting functions.

H_∞/LPV problem—The objective of the synthesis is to find an LPV controller $K(\rho)$ of the form (15.23) such that the closed-loop system is quadratically stable and that, for a given positive real γ , the L_2 -induced norm of the operator mapping \bar{w} into \bar{z} is bounded by γ , i.e.,

$$\forall \bar{\rho} \in \Theta, \frac{\|\bar{z}_w\|_2}{\|w\|_2} \leq \gamma. \tag{15.24}$$

Here the polytopic approach with a quadratic Lyapunov function is employed. It is stated that for known weighting functions and a suitable predefined real positive scalar γ , the sufficient condition that solves the H_∞ /LPV problem is given by (15.25) and (15.26) where the decision variables are X , Y , \hat{A} , \hat{B} , \hat{C} , and \hat{D} (see the detail of the solution in [41]). It is worth noting that the weighting function parameter set v is present in the LMIs problem to cope with optimization purpose of the controller (which is presented in Sect. 15.5.2).

$$\begin{bmatrix} M_{11}^v(\bar{\rho}_i) & * & * & * \\ M_{21}^v(\bar{\rho}_i) & M_{22}^v(\bar{\rho}_i) & * & * \\ M_{31}^v(\bar{\rho}_i) & M_{32}^v(\bar{\rho}_i) & -\gamma I_m & * \\ M_{41}^v(\bar{\rho}_i) & M_{42}^v(\bar{\rho}_i) & M_{43}^v(\bar{\rho}_i) & -\gamma I_p \end{bmatrix} \prec 0, \quad (15.25)$$

$$\begin{bmatrix} X & I \\ I & Y \end{bmatrix} \succ 0 \quad (15.26)$$

for $i = 1 : 4$,

where

$$\begin{aligned} M_{11}^v(\bar{\rho}_i) &= \mathcal{A}^v(\bar{\rho}_i)X + X\mathcal{A}^v(\bar{\rho}_i)^T + \mathcal{B}_2\hat{C}(\bar{\rho}_i) + \hat{C}(\bar{\rho}_i)^T\mathcal{B}_2^T, \\ M_{21}^v(\bar{\rho}_i) &= \hat{A}(\bar{\rho}_i) + \mathcal{A}^v(\bar{\rho}_i)^T + \mathcal{C}_2^T\hat{D}(\bar{\rho}_i)^T\mathcal{B}_2^T, \\ M_{22}^v(\bar{\rho}_i) &= Y\mathcal{A}^v(\bar{\rho}_i) + \mathcal{A}^v(\bar{\rho}_i)^TY + \hat{B}(\bar{\rho}_i)\mathcal{C}_2 + \mathcal{C}_2^T\hat{B}(\bar{\rho}_i)^T, \\ M_{31}^v(\bar{\rho}_i) &= \mathcal{B}_1^v(\bar{\rho}_i)^T + \mathcal{D}_2^T\hat{D}(\bar{\rho}_i)^T\mathcal{B}_2^T, \\ M_{32}^v(\bar{\rho}_i) &= \mathcal{B}_1^v(\bar{\rho}_i)^TY + \mathcal{D}_2^T\hat{B}(\bar{\rho}_i)^T, \\ M_{41}^v(\bar{\rho}_i) &= \mathcal{C}_1^v(\bar{\rho}_i)X + \mathcal{D}_1\hat{C}(\bar{\rho}_i), \\ M_{42}^v(\bar{\rho}_i) &= \mathcal{C}_1^v(\bar{\rho}_i) + \mathcal{D}_1\hat{D}(\bar{\rho}_i)C_2, \\ M_{43}^v(\bar{\rho}_i) &= \mathcal{D}_1^v(\bar{\rho}_i) + \mathcal{D}_1\hat{D}(\bar{\rho}_i)\mathcal{D}_{21}. \end{aligned}$$

The controller K_{c_i} at vertex i is then reconstructed as

$$\begin{aligned} D_c^v(\bar{\rho}_i) &= \hat{D}(\bar{\rho}_i), \\ C_c^v(\bar{\rho}_i) &= (\hat{C}(\bar{\rho}_i) - D_c^v(\bar{\rho}_i)C_2X)M^{-T}, \\ B_c^v(\bar{\rho}_i) &= N^{-1}(\hat{B}(\bar{\rho}_i) - YB_2D_c^v(\bar{\rho}_i)), \\ A_c^v(\bar{\rho}_i) &= N^{-1}(\hat{A}(\bar{\rho}_i) - YA(\bar{\rho}_i)X - YB_2D_c^v(\bar{\rho}_i)C_2X)M^{-T} \\ &\quad - B_c^v(\bar{\rho}_i)C_2XM^{-T} - N^{-1}YB_2C_c^v(\bar{\rho}_i), \end{aligned} \quad (15.27)$$

where M , N are defined such that $MN^T = I_n - XY$ which can be solved through a singular value decomposition and a Cholesky factorization. The global H_∞ /LPV controller is then the convex combination of these local controllers.

15.5.2 Controller Optimization Using Genetic Algorithms

According to the prescribed objectives in Sect. 15.3.2, the following weighting functions are used for the H_∞/LPV synthesis:

$$W_{z_r} = 3 \times 10^{-2}, \quad (15.28)$$

$$W_f = \frac{\Omega_f}{s + \Omega_f}, \quad (15.29)$$

$$W_{z_s} = k_{z_s} \frac{s^2 + 2\xi_{11}\Omega_{11}s + \Omega_{11}^2}{s^2 + 2\xi_{12}\Omega_{12}s + \Omega_{12}^2}, \quad (15.30)$$

$$W_{z_{us}} = k_{z_{us}} \frac{s^2 + 2\xi_{21}\Omega_{21}s + \Omega_{21}^2}{s^2 + 2\xi_{22}\Omega_{22}s + \Omega_{22}^2}. \quad (15.31)$$

Define the set of parameters

$$v = [\Omega_f \ \Omega_{11} \ \Omega_{12} \ \xi_{11} \ \xi_{12} \ k_{z_s} \ \Omega_{21} \ \Omega_{22} \ \xi_{21} \ \xi_{22} \ k_{z_{us}}]^T \quad (15.32)$$

that, in the context of GAs, is a part of the decision vector. By experience, we have chosen to let γ as a decision parameter in order to add more degrees of freedom, and then to solve a suboptimal H_∞ control problem.

In a usual H_∞/LPV problem, the attenuation level γ is to be minimized to satisfy the H_∞ performance objectives. Thanks to the Genetic Algorithms optimization, the provided methodology will rather allow here to minimize a cost function representing the true performance objectives. Therefore, the optimization problem of interest relies on the minimization of this cost function and not on the minimization of γ .

Let us define the optimization problem for semi-active suspension control

$$\min_{\{v, \gamma\} \in \mathbb{R}_+^{12}} J^D(v, \gamma) = \left[\begin{array}{c} J_{\text{Comfort}}^D(v, \gamma) \\ J_{\text{RoadHolding}}^D(v, \gamma) \end{array} \right]. \quad (15.33)$$

Remark 15.5. The dimension of the searching space is 12×1 because there are 11 parameters for the weighting functions v and 1 attenuation level scalar γ . This space can be made smaller than \mathbb{R}_+^{12} . Effectively, we can define the bounds of each parameter, basing on the frequency range of interest at which the weighting functions act. This is also an explanation for the question of why we use weighting function parameter optimization instead of controller parameter optimization, specially when the controller order is high.

Based on the remarks on the comfort and road holding performances in Sect. 15.3.2, the two objectives are defined so that the vehicle body acceleration at low and middle frequencies and the wheel displacement at high frequencies will be minimized for each vertex of the considered polytope. Hence, in the optimization problem 15.33, the following frequency-based objective functions are considered:

$$J_{\text{Comfort}}^D = \sum_{i=1}^4 \int_0^{12} \ddot{z}_s / z_r(f)_i df, \quad (15.34)$$

$$J_{\text{RoadHolding}}^D = \sum_{i=1}^4 \int_{10}^{20} (z_{us} / z_r(f))_i df. \quad (15.35)$$

Note that, in the equations above, “D” is used to differentiate these design objective functions with the ones in Sect. 15.3.2 and the index “ i ” stands for the i th vertex of the polytope Θ (see Fig. 15.7). The number of elements in each sum is four; however, in this particular case, the polytope is symmetric in ρ_1 , only computations at two vertices $\{1, 4\}$ or $\{2, 3\}$ are needed.

Remark 15.6. The feasibility of the LMIs (15.25) and (15.26) may be violated by the “bad” decision vectors generated by GAs. The problem can be overcome by repeating the crossover or mutation until the feasible solution is obtained. However, a simpler way is to assign a large objective value (for instant $J^D = \infty$) to these infeasible solutions and then, they will be eliminated by the selection procedure after some generations.

Remark 15.7. In many cases, to preserve the performance of the closed-loop system with input saturation, a stable stabilizing controller is required. Other advantages for the use of stable controllers concern the practical aspects. The stable controllers are easier to be implemented than the unstable ones and the closed-loop system (provided that the open-loop system is already stable, e.g., open-loop semi-active suspension systems) remains stable even when the feedback sensors fail. For LTI systems, this problem (usually called *strong stabilization* problem) has been studied by some authors such as [5, 7], etc Similarly, for the H_∞ /LPV control of LPV systems, to obtain a stable LPV controller, it suffices to ensure that all local controllers at each vertex of the polytope are stable. In this study, the theoretical solution for the existence of a stable LPV controller is not given. However, a stable LPV controller can be obtained by eliminating the “unstable solutions” corresponding to at least one unstable local controller during the synthesis. It can be accomplished with GAs by simply choosing $J^D = \infty$ for “unstable solutions.” Due to the “survival of the fittest” property, these “unstable solutions” will disappear after some generations.

To sum up, the objective function using in GAs is chosen as follows.

Algorithm 3: Objective value assignment

if (15.25) and (15.26) are feasible **and** all K_{c_i} in (15.27) are stable **then**
 Calculate J^D using (15.34) and (15.35)
else
 $J^D = \infty$
end.

Proposed Weighting Function Optimization Procedure for H_∞ /LPV Synthesis

- *Step 1:* Initiate with random positive weighting functions $v = v^0$ and random positive real $\gamma_{ga} = \gamma_{ga}^0$.
- *Step 2:* Solve the minimization problem of γ subject to the LMIs (15.25) and (15.26) to compute the minimal real scalar γ_{min} . Solve again the LMIs (15.25) and (15.26) with the couple (v, γ) where $\gamma = \gamma_{min} + \gamma_{ga}$. At the end of this step, compute the objective function $J^D(v, \gamma)$ using *Algorithm 3*.
- *Step 3:* Select the individuals.
- *Step 4:* Apply crossover and mutation to generate new generation: $v = v^{new}$ and $\gamma_{ga} = \gamma_{ga}^{new}$.
- *Step 5:* Evaluate the new generation: If the criteria of interest (for example, reaching the limit number of generation) are not satisfied, go to Step 2 with $v = v^{new}$ and $\gamma_{ga} = \gamma_{ga}^{new}$; else, stop and save the best individual $v^{opt} = v^{new}$ and $\gamma^{opt} = \gamma_{ga}^{new}$.

The genetic operations presented in Steps 3 and 4 can be done using efficient multi-objective optimization algorithm like SPEA2 [47], NSGA-II [8].

Remark 15.8. In Step 2, to avoid the infeasibility of the LMIs (15.25) and (15.26) resulting from the bad (i.e., too small) value of γ generated by GAs, γ will be decomposed into two positive real elements γ_{min} and γ_{ga} , where γ_{min} is the minimal γ satisfying the LMIs (15.25) and (15.26), and γ_{ga} is tuned by GAs. Due to the convexity of the LMIs problem, the existence of γ_{min} will ensure the feasibility of LMIs (15.25) and (15.26) with $\gamma = \gamma_{min} + \gamma_{ga}$ for all positive real γ_{ga} . The minimal value γ_{min} can be found by using LMIs toolbox like Yalmip and Sedumi.

15.6 Numerical Analysis and Results

For simulation analysis, we use the quarter car Renault Mégane Coupé (RMC) model (see [46]) with the parameters presented in Table 15.1. It is worth noting that the spring used in this simulation has a nonlinear characteristic (see Fig. 15.9).

With the proposed method, the solution of the multi-objective problem (15.33) is given by a Pareto set as in Fig. 15.10. Now the conflicting relation between comfort and road holding criteria can be observed clearly from the figure.

Among the solutions in the Pareto set, two LPV controllers are chosen. One is comfort oriented (belonging to Set 1) and the other is road holding oriented (belonging to Set 2, because the solutions in Set 3 improve road holding only in high frequencies). The parameters for the synthesis of these two controllers are found in Table 15.2.

In the following, two different closed-loop control strategies as well as passive open-loop ones for MR dampers are presented and considered as referenced methods to evaluate the efficiency of the proposed LPV controllers.

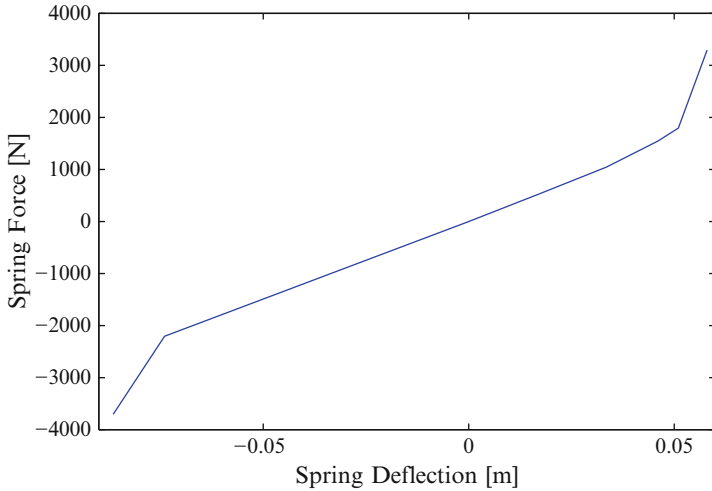


Fig. 15.9 Nonlinear RMC spring

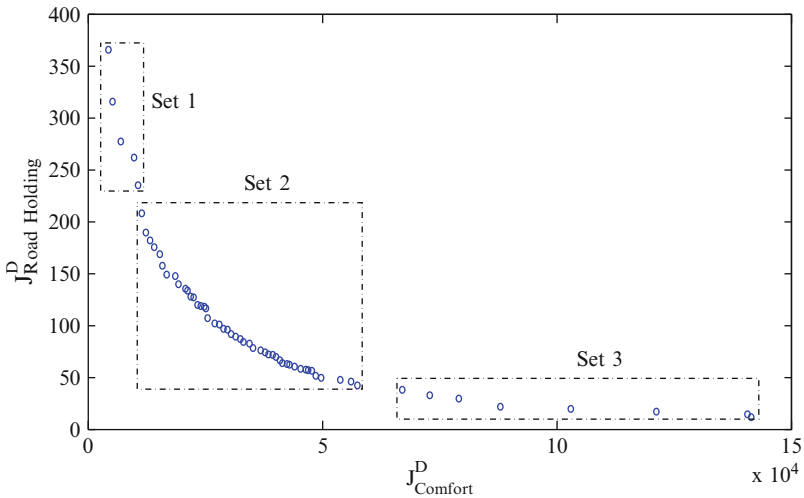


Fig. 15.10 Pareto set obtained by proposed method

15.6.1 The Based-Lines

The well-known Skyhook [26] has been first proposed by Karnopp in 1974 and up to now it is still widely used in many real applications. Recently, the Mixed Skyhook-ADD [40] (see also [38] and references therein) has been proved to be almost optimal for ride comfort. These two control strategies have been, however, originally designed for linear dampers where the nonlinear characteristics (i.e., the

Table 15.2 Parameters for H_∞ /LPV semi-active suspension design (obtained by genetic optimization)

Controllers	Scalar $\gamma_{\min} - \gamma_{\text{ga}} (\times 10^5)$	Filter Ω_f	W_{z_s}					$W_{z_{us}}$				
			Ω_{11}	Ω_{12}	ξ_{11}	ξ_{12}	k_{z_s}	Ω_{21}	Ω_{22}	ξ_{21}	ξ_{22}	$k_{z_{us}}$
LPV-Comfort	0.2 – 1.66	90	48.2	7.1	99	8.48	159	99.9	1.3	5.4	99	90.6
LPV-Road Holding	3.7 – 3.16	1.4	60.8	12.9	99.7	29.7	436	83.6	0.29	96	89	145

bi-viscous and the hysteretic behaviors) have not been taken into account. In [10], the extended versions of the Skyhook and Mixed Skyhook-ADD were proposed for MR dampers. We recall here these control methods.

15.6.1.1 Extended Skyhook for MR Dampers

The main idea of the Skyhook for linear suspension system is that the damper exerts a force that reduces the velocity of the body mass \dot{z}_s . By using the same principle, the modified Skyhook for MR damper will be as follows:

$$f_I = \begin{cases} f_{\max} & \text{if } \dot{z}_s \hat{\rho} > 0 \\ f_{\min} & \text{if } \dot{z}_s \hat{\rho} \leq 0 \end{cases}, \tag{15.36}$$

where $\hat{\rho} = \tanh(c_1 \dot{z}_{\text{def}} + k_1 z_{\text{def}})$.

15.6.1.2 Extended Mixed Skyhook-ADD (SH-ADD) for MR Dampers

It is well known that the Skyhook provides the best ride comfort at low frequency while the ADD improves considerably ride comfort at high frequency. The Extended Mixed SH-ADD algorithm guarantees the best behavior of both Skyhook and ADD and is given as follows:

$$f_I = \begin{cases} f_{\max} & \text{if } (\ddot{z}_s^2 - \alpha \dot{z}_s^2 \leq 0 \wedge \dot{z}_s \hat{\rho} > 0) \vee \\ & (\ddot{z}_s^2 - \alpha \dot{z}_s^2 > 0 \wedge \dot{z}_s \hat{\rho} > 0) \\ f_{\min} & \text{if } (\ddot{z}_s^2 - \alpha \dot{z}_s^2 \leq 0 \wedge \dot{z}_s \hat{\rho} \leq 0) \vee \\ & (\ddot{z}_s^2 - \alpha \dot{z}_s^2 > 0 \wedge \dot{z}_s \hat{\rho} \leq 0) \end{cases}, \tag{15.37}$$

where $\hat{\rho} = \tanh(c_1 \dot{z}_{\text{def}} + k_1 z_{\text{def}})$.

The amount $(\ddot{z}_s^2 - \alpha \dot{z}_s^2)$ is the frequency-range selector and the SH-ADD crossover frequency $\alpha = 2\pi f_{\text{SHADD}}$ rad/s, where $f_{\text{SHADD}} = 2$ Hz (see [40]).

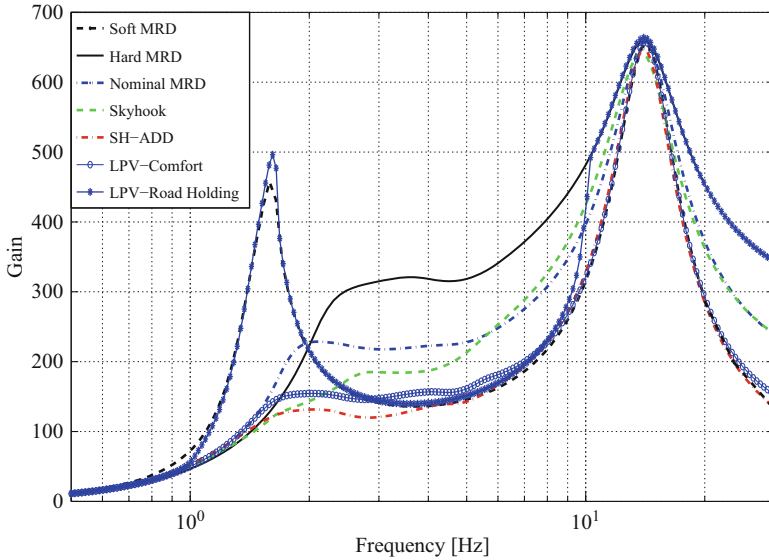


Fig. 15.11 Frequency responses \ddot{z}_s/\ddot{z}_r

15.6.1.3 Passive MR Dampers

Beside the three controlled methods presented above, the three following passive open-loop cases are also useful for the analysis:

- Soft MR damper where the controllable input $f_I = f_{\min}$
- Hard MR damper where the controllable input $f_I = f_{\max}$
- Nominal MR damper where the controllable input $f_I = (f_{\min} + f_{\max})/2$ (i.e., when control input $u = 0$)

15.6.2 Frequency Domain Analysis

In this section, the evaluation in the frequency domain of referenced and proposed methods is performed via the nonlinear frequency responses which are computed by the “Variance Gain” algorithm [37]. This algorithm is simple and provides a good approximation to frequency response.

Some general remarks can be done from Figs. 15.11 and 15.12:

- Between 0 and 2 Hz, the Hard MRD is the best strategy for both ride comfort and road holding.

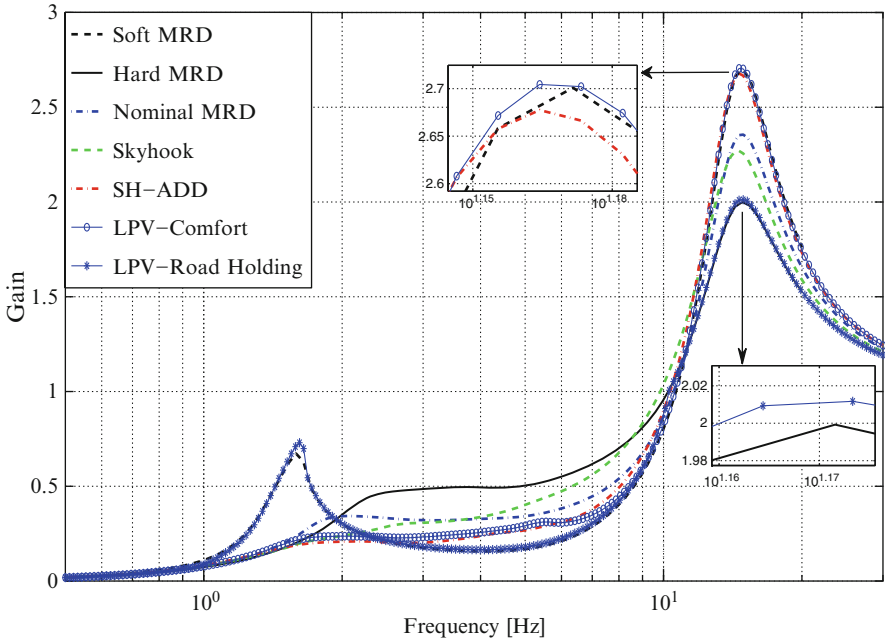


Fig. 15.12 Frequency responses $(z_{us} - z_r)/z_r$

Table 15.3 Optimal controllers

Controllers	0–2 Hz	2–12 Hz	12–30 Hz
Comfort-oriented	$f_l = f_{lmax}$	$f_l = f_{lmin}$	$f_l = f_{lmin}$
Road holding-oriented	$f_l = f_{lmax}$	$f_l = f_{lmin}$	$f_l = f_{lmax}$

- Between 2 and 12 Hz, the Soft MRD is the best strategy for both ride comfort and road holding.
- Between 12 and 30 Hz, the trade-off between ride comfort and road holding is unavoidable. The best for ride comfort is the Soft MRD, the best for road holding is the Hard MRD.

With the remarks above, the optimal solutions for ride comfort and road holding can be roughly defined and once again, the conflict between two objectives, at high frequency (12–30 Hz), can be seen from Table 15.3.

Some remarks can be made for the five strategies, in the frequency range of interest 0–30 Hz.

The *Nominal MRD* and the *Extended Skyhook* provide medium performances for both ride comfort and road holding.

The *Extended Mixed SH-ADD* is the best one for ride comfort. It approaches the optimal solution of the comfort-oriented controller. As a consequence, this controller does not guarantee a good road holding around the wheel resonance which is more important than in other frequency ranges.

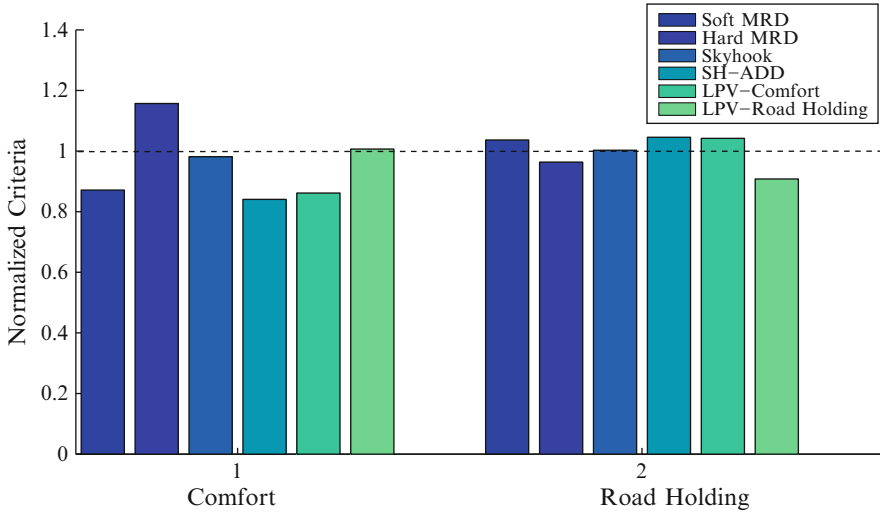


Fig. 15.13 Performances comparison (in frequency domain)

The *LPV-Road Holding* is the best one for road holding.

The *LPV-Comfort* approaches very well the Extended Mixed SH-ADD from 3 to 30 Hz. At low frequencies 1–4 Hz, it is not so good but this is not so important because, as mentioned before in Sect. 15.3.2, the human being is most sensible to vehicle acceleration in the frequencies around 4–8 Hz.

The remarks above are summarized by Fig. 15.13. The performance criteria (15.10) and (15.11) in Sect. 15.3.2 are calculated for each strategy and then are normalized by performance values of the nominal MR damper and compared with the soft and hard MRDs.

15.6.3 Time Domain Analysis

The road profile could be viewed as a random signal, because it is not predicted by the vehicle. However, in practice, its bandwidth is limited. In this test, a road profile is represented by an integrated white noise, band-limited within the frequency range 0–30 Hz (see Fig. 15.14).

To evaluate the performances of the strategies, the spectrum of vehicle acceleration and dynamic tire deflection are depicted in Figs. 15.15 and 15.16. The results obtained are coherent with the frequency domain analysis: the Extended Mixed SH-ADD and LPV-Comfort are the best strategies for ride comfort, the LPV-Road Holding and Hard MRD are the most suitable for the road holding improvement.

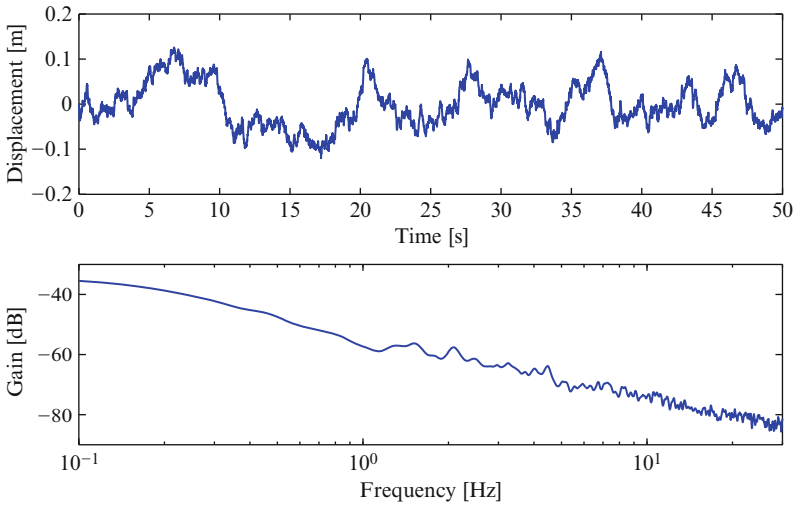


Fig. 15.14 Road profile z_r

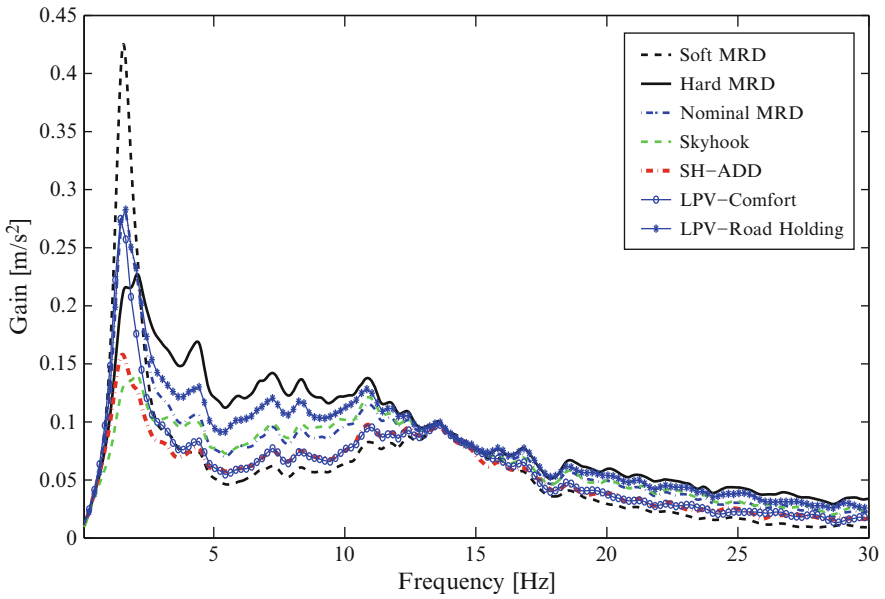


Fig. 15.15 Spectrum of \ddot{z}_s

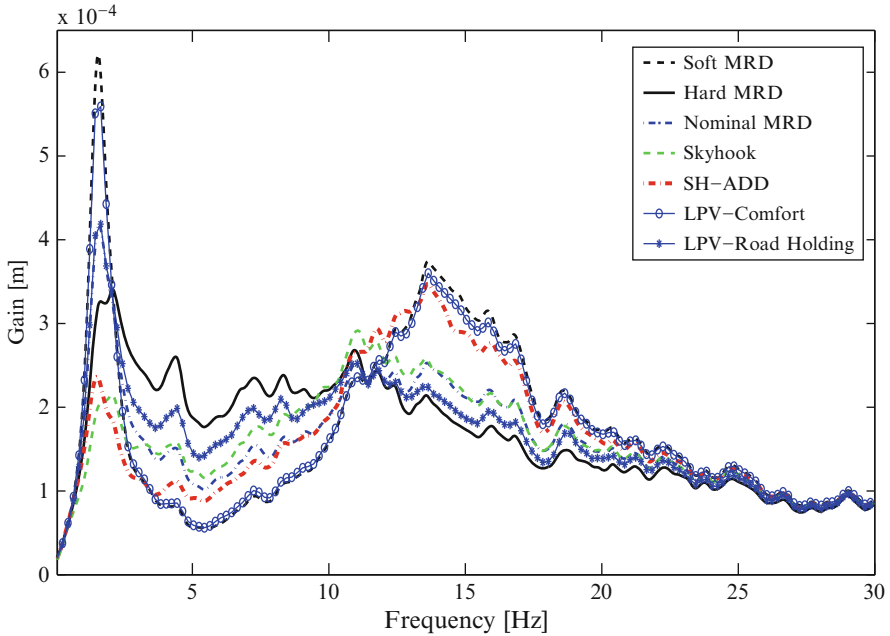


Fig. 15.16 Spectrum of $z_{us} - z_r$

Furthermore, the comfort in time domain can be evaluated, using the following criterion:

$$RMS_{\text{Comfort}} = \sqrt{\frac{\int_0^T \ddot{z}_s^2(t) dt}{T}}, \tag{15.38}$$

where $\ddot{z}_s(t)$ is the filtered vehicle body acceleration (by the approximated ISO 2631 filter (15.9)) (m/s^2) and T is the simulation time (s). In Fig. 15.17, the RMS_{Comfort} values of different strategies, normalized by that value for the nominal damper, are depicted. The results mentioned previously have been proved again. The LPV-Comfort approaches the Extended Mixed SH-ADD.

15.7 Conclusion

In this chapter, an application of LPV control to semi-active suspensions has been presented. The contribution of the chapter may be summarized as follows:

- An LPV control-oriented model of MR dampers is proposed where the bi-viscous and hysteresis characteristics are taken into account. This model was validated by experimental tests. It can be seen that the model provides a good approximation of a real MR damper.

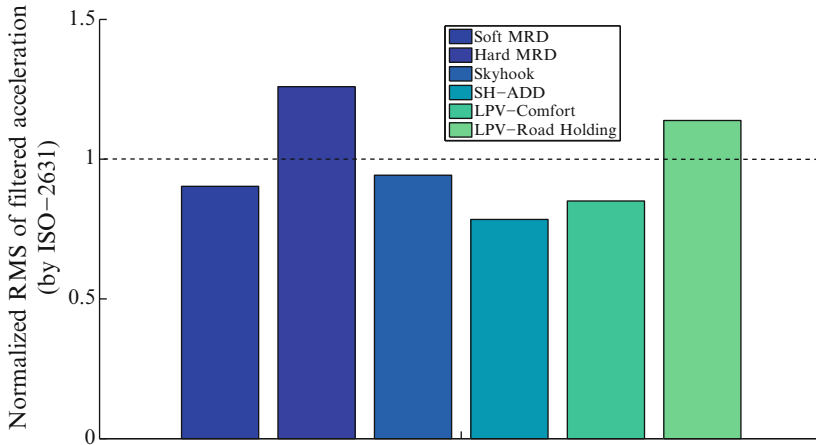


Fig. 15.17 Normalized RMS value of filtered \ddot{z}_s (by ISO-2631)

- The quarter vehicle model equipped with the proposed MR damper model is written in an LPV framework which can be used for LPV design (H_∞ , H_2 or mixed H_∞/H_2 , etc.).
- A multi-objective optimization procedure using genetic algorithms that achieves the desired suspension performances is also introduced. It leads to a generic methodology to find a controller satisfying the required performance whatever the criteria are.
- From the practical implementation point of view, as seen in Fig. 15.8, the proposed control method is simple and easy to implement: a single relative displacement sensor to measure the suspension deflection (the deflection velocity can be deduced numerically from the deflection) is needed and the LPV controller is stable.

The simulations on the nonlinear quarter vehicle model equipped with a validated MR damper (in the frequency and time domains) have been analyzed. The results have shown the interest of the proposed method: the obtained comfort-oriented and road holding-oriented LPV controller can be then used with a switching rule which can be adapted to different road conditions (in cities and suburbs).

Acknowledgments The authors would like to thank the co-authors of the referenced papers, specially Jorge de Jesus Lozoya-Santos, Ricardo Ambrocio Ramirez-Mendoza, Ruben Morales-Menendez (TEC Monterrey, Mexico), who have worked with us on the modeling and control of MR dampers; Sergio Savaresi, Cristiano Spelta, and Diego Delvecchio (Politecnico di Milano, Italy) for the discussions on the Mixed SH-ADD control.

References

1. Alfaro-Cid E, McGoogin EW, Murray-Smith DJ (2008) Optimisation of the weighting functions of an \mathcal{H}_∞ controller using genetic algorithms and structured genetic algorithms. *Int J Syst Sci* 39(4):335–347
2. Apkarian P, Gahinet P (1995) A convex characterization of gain scheduled \mathcal{H}_∞ controllers. *IEEE Trans Automat Contr* 40(5):853–864
3. Beaven RW, Wright MT, Seaward DR (1996) Weighting function selection in the \mathcal{H}_∞ design process. *Contr Eng Pract* 4(5):625–633
4. Bouc R (1967) Forced vibration of mechanical systems with hysteresis. In: *Proceedings of the Fourth Conference on Nonlinear Oscillation, Prague, Czechoslovakia*, p 315
5. Campos-Delgado DU, Zhou K (2001) \mathcal{H}_∞ strong stabilization. *IEEE Trans Automat Contr* 46(12):1968–1972
6. Canale M, Milanese M, Novara C (2006) Semi-active suspension control using fast model-predictive techniques. *IEEE Trans Contr Syst Tech* 14(6):1034–1046
7. Cao YY, Lam J (2000) On simultaneous \mathcal{H}_∞ control and strong \mathcal{H}_∞ stabilization. *Automatica* 36(6):859–865
8. Deb K, Pratap A, Agarwal S, Meyarivan T (2002) A fast elitist multi-objective genetic algorithm: NSGA-II. *IEEE Trans Evol Comput* 6(2):182–197
9. Do AL, Sename O, Dugard L (2010) An LPV control approach for semi-active suspension control with actuator constraints. In: *Proceedings of the IEEE American control conference (ACC), Baltimore, Maryland, USA*
10. Do AL, Sename O, Dugard L, Savaresi S, Spelta C, Delvecchio D (2010) An extension of mixed sky-hook and add to magneto-rheological dampers. In: *Proceedings of the 4th IFAC symposium on system, structure and control (SSSC), Ancona, Italy*
11. Do AL, Sename O, Dugard L (2011) Optimisation par algorithme génétique d'une commande LPV de suspension semi-active. In: *Journée Doctorale MACS, Marseille, France*
12. Do AL, Sename O, Dugard L, Soualmi B (2011) Multi-objective optimization by genetic algorithms in \mathcal{H}_∞ /LPV control of semi-active suspension. In: *Proceedings of the 18th IFAC world congress (WC), Milan, Italy*
13. Do AL, Spelta C, Savaresi S, Sename O, Dugard L, Delvecchio D (2010) An LPV control approach for comfort and suspension travel improvements of semi-active suspension systems. In: *Proceedings of the 49th IEEE conference on decision and control (CDC), Atlanta, GA*, pp 5660–5665
14. Fialho I, Balas G (2002) Road adaptive active suspension design using linear parameter varying gain scheduling. *IEEE Trans Contr Syst Tech* 10(1):43–54
15. Gillespie TD (1992) *Fundamentals of vehicle dynamics*. Society of Automotive Engineers Inc, Warrendale, PA
16. Giorgetti N, Bemporad A, Tseng H, Hrovat D (2006) Hybrid model predictive control application toward optimal semi-active suspension. *Int J Robust Nonlinear Contr* 79(5):521–533
17. Gomes da Silva Jr JM, Limon D, Alamo T, Camacho EF (2008) Dynamic output feedback for discrete-time systems under amplitude and rate actuator constraints. *IEEE Trans Automat Contr* 53(10):2367–2372
18. Grimm G, Hatfield J, Postlethwaite I, Teel A, Turner M, Zaccarian L (2003) Antiwindup for stable linear systems with input saturation: An LMI-based synthesis. *IEEE Trans Automat Contr* 48(9):1509–1525
19. Guglielmino E, Sireteanu T, Stammers C, Ghita G, Giuclea M (2008) *Semi-active suspension control*. Springer, Berlin
20. Guo S, Yang S, Pan C (2006) Dynamic modeling of magnetorheological damper behaviors. *J Intell Mater Syst Struct* 17:3–14
21. Hrovat D (1997) Survey of advanced suspension developments and related optimal control application. *Automatica* 33(10):1781–1817
22. Hu J, Bohn C, Wu HR (2000) Systematic \mathcal{H}_∞ weighting function selection and its application to the real-time control of a vertical take-off aircraft. *Contr Eng Pract* 8:241–252

23. Isermann R (2003) *Mechatronic systems: fundamentals*. Springer, UK
24. Ivers DE, Miller LR (1989) Experimental comparison of passive, semi-active on-off, and semi-active continuous suspensions. SAE Technical Paper 892484
25. Jr BS, Dyke S, Sain M, Carlson J (1997) Phenomenological model of an MR damper. *J Engng Mech* 123(3):230–238
26. Karnopp D, Crosby M, Harwood R (1974) Vibration control using semi-active force generators. *J Eng Ind* 96:619–626
27. Kiencke U, Nielsen L (2000) *Automotive control systems for engine, driveline, and vehicle*. Springer, Berlin
28. Kothare MV, Campo PJ, Morari M, Nett CN (1994) A unified framework for the study of anti-windup designs. *Automatica* 30:1869–1883
29. Lozoya-Santos JJ, Aubouet S, Morales-Menendez R, Sename O, Ramirez-Mendoza RA, Dugard L (2010) Simulation performance of a quarter of vehicle including an MR damper model with hysteresis. In: 7th Eurosim congress on modelling and identification, Prague, Czech Republic
30. Lozoya-Santos JJ, Morales-Menendez R, Ramirez-Mendoza RA, Nino-Juarez E (2009) Frequency and current effects in an MR damper. *Int J Veh Autonom Syst* 7(3/4):121–140
31. Lozoya-Santos JJ, Ruiz-Cabrera JA, Morales-Menéndez R, Ramírez-Mendoza R, Diaz-Salas V (2009) Building training patterns for modelling MR dampers. In: ICINCO-SPSMC, pp 156–161
32. Mulder EF, Tiwari PY, Kothare MV (2009) Simultaneous linear and anti-windup controller synthesis using multiobjective convex optimization. *Automatica* 45:805–811
33. Patten WN, He Q, Kuo CC, Liu L, Sack RL (1994) Suppression of vehicle induced bridge vibration via hydraulic semi-active vibration dampers. In: *Proceeding of the 1st world conference on structural control*, vol 3, pp 30–38
34. Poussot-Vassal C, Sename O, Dugard L, Gáspár P, Szabó Z, Bokor J (2008) New semi-active suspension control strategy through LPV technique. *Contr Eng Pract* 16(12):1519–1534
35. Rossi C, Lucente G (2004) \mathcal{H}_∞ control of automotive semi-active suspensions. In: *Proceedings of the 1st IFAC symposium on advances in automotive control (AAC)*, Salerno, Italy
36. Sammier D, Sename O, Dugard L (2003) Skyhook and \mathcal{H}_∞ control of active vehicle suspensions: some practical aspects. *Vehicle Syst Dyn* 39(4):279–308
37. Savaresi S, Bittanti S, Montiglio M (2005) Identification of semi-physical and black-box models: the case of MR-dampers for vehicles control. *Automatica* 41:113–117
38. Savaresi S, Poussot-Vassal C, Spelta C, Sename O, Dugard L (2010) *Semi-active suspension control for vehicles*. Elsevier, UK
39. Savaresi S, Silani E, Bittanti S (2005) Acceleration driven damper (ADD): an optimal control algorithm for comfort oriented semi-active suspensions. *ASME Trans J Dyn Syst Meas Contr* 127(2):218–229
40. Savaresi S, Spelta C (2007) Mixed sky-hook and ADD: Approaching the filtering limits of a semi-active suspension. *ASME Transactions: J Dyn Syst Meas Contr* 129(4):382–392
41. Scherer C, Gahinet P, Chilali M (1997) Multiobjective output-feedback control via LMI optimization. *IEEE Trans Automat Contr* 42(7):896–911
42. Stanway R, Sproston J, Stevens N (1987) Non-linear modelling of an electro-rheological vibration damper. *J Electrostat* 20(2):167–184
43. Valasek M, Novak M, Sika Z, Vaculin O (1997) Extended groundhook – new concept of semi-active control of trucks suspension. *Veh Syst Dyn* 29:289–303
44. Wen T (1976) Method for random vibration of hysteretic systems. *J Eng Mech ASCE* 102(EM2):249–263
45. Wu F, Grigoriadis KM, Packard A (2000) Anti-windup controller design using linear parameter-varying control methods. *Int J Contr* 73(12):1104–1114
46. Zin A, Sename O, Basset M, Dugard L, Gissinger G (2004) A nonlinear vehicle bicycle model for suspension and handling control studies. In: *Proceedings of the IFAC conference on advances in vehicle control and safety (AVCS)*, Genova, Italy, pp 638–643

47. Zitzler E, Laumanns M, Thiele L (2001) SPEA2: improving the strength pareto evolutionary algorithm. Tech. rep.
48. Zuo L, Nayfeh SA (2007) \mathcal{H}_2 optimal control of disturbance-delayed systems with application to vehicle suspensions. Veh Syst Dyn 45:3:233–247

Chapter 17

Identification of Low-Complexity LPV Input–Output Models for Control of a Turbocharged Combustion Engine

Andreas Kominek, Herbert Werner, Maiko Garwon,
and Matthias Schultalbers

Abstract Complexity issues related to experimentally identified LPV models are addressed, in particular the trade-off between model accuracy and number of scheduling parameters. For this purpose, an existing identification algorithm for LPV input–output models is combined with a parameter reduction technique based on principal component analysis. The approach is illustrated with experimental results on control of a turbocharged combustion engine. A low-complexity LPV input–output model is identified and validated. After transforming this model into state-space form—taking dynamic dependence on scheduling parameters into account—an LPV gain-scheduling controller is designed and assessed in closed-loop simulation with a validated nonlinear model.

17.1 LPV Models for Control of Combustion Engines

LPV models are often derived from accurate physical models [12], which can, however, be hard to obtain. Even when an LPV model can be constructed, the number of scheduling parameters and the order may be high. Using ad hoc measures or model-order reduction will reduce model accuracy. For this reason, black-box identification of LPV models from measured input–output data is receiving increasing attention. In this chapter, this problem is addressed, and ways of solving it are illustrated in a case study. The control problem considered in this case study is air charge control of a turbocharged gasoline engine. Its highly nonlinear nature makes the use of

A. Kominek • H. Werner (✉)

Hamburg University of Technology, Hamburg, Germany
e-mail: andreas.kominek@tu-harburg.de; h.werner@tu-harburg.de

M. Garwon • M. Schultalbers

IAV GmbH Ingenieurgesellschaft Auto und Verkehr, Berlin, Germany
e-mail: maiko.garwon@iav.de; Matthias.Schultalbers@iav.de

nonlinear control necessary and the combustion engine a suitable application for LPV modeling and control.

A suitable model class for the identification of LPV systems in discrete time is Input–Output (IO) models [6, 7, 9]. Using this class, identification methods for linear time-invariant (LTI) systems can easily be extended to LPV system identification. Controller synthesis, however, often requires an LPV model in State-Space (SS) representation. For this reason, in this contribution an LPV-IO model is identified, which can readily be transformed into LPV-SS representation. Subspace identification of LPV-SS models could also be considered for this purpose. In standard form, the latter used to suffer from the curse of dimensionality as reported in [19]. Modified versions of subspace algorithms have been reported in [8, 20] to overcome the curse of dimensionality. A comparison of IO and subspace methods would be interesting but is not addressed in this chapter.

In [17], an LPV-IO black-box identification scheme was used to identify a valid discrete-time description of a gasoline engine. This LPV-IO scheme is based on the method presented in [6]. A similar LPV-IO gray-box identification was employed in [21] for the identification of the air path of a turbocharged diesel engine based on measurement data. By dividing the engine system into subsystems using a priori knowledge of the system, each block was provided with its specific scheduling signals. Using physical insight about the system structure can help to improve system identification, but such gray-box identification schemes are in general not transferable to other systems.

In this contribution, an LPV-IO black-box identification scheme is presented, which relies only to a small degree on a priori knowledge about the system structure. One problem addressed in this contribution is that LPV-IO black-box identification can result in models with a high number of scheduling parameters.

The computational burden of controller synthesis techniques based on polytopic LPV models depends exponentially on the number of scheduling parameters and on the model order. This motivates the development of algorithms to construct LPV models of low order and with low number of scheduling parameters for a given nonlinear plant.

A principal component analysis based parameter reduction scheme, referred to as *parameter set mapping* (PSM) [13], has been used in a number of studies for parameter reduction, e.g., [1, 11]. A similar method for complexity reduction of polytopic LPV models employing higher order singular value decomposition was presented in [16]. In this contribution, a parametrization which is similar to the one obtained by PSM is applied to approximate the scheduling functions with a reduced number of parameters. This results in a nonlinear parametrization, which is initialized by applying PSM and estimated by employing an iterative algorithm. This algorithm is described in Sect. 17.6.

In the next section, the engine system used for the case study is introduced. This is followed by some preliminaries about LPV-IO and LPV-SS model classes in Sect. 17.3. An LPV-IO model structure is applied to identify an LPV-IO model of the turbocharged combustion engine in Sect. 17.4. The obtained model has five

scheduling parameters—too many for control based on a polytopic model. This motivates the parameter reduction in Sect. 17.5. A strategy for parameter reduction is applied to the case study in Sect. 17.6 leading to polytopic LPV models, suitable for controller synthesis. Finally, a controller is synthesized based on the obtained model in Sect. 17.7, which is tested in closed loop and compared to the industrial standard controller. This chapter ends with a summary and conclusion in Sect. 17.8.

17.2 Charge Control of a Turbocharged Combustion Engine

The problem considered in this case study is charge control of a turbocharged gasoline engine, which is highly nonlinear. It is an engine setting in a test car for which experimental data and a validated nonlinear simulation model were supplied by IAV GmbH.

A schematic diagram of the air path of the engine is shown in Fig. 17.1. The air enters through the filter and is compressed by a compressor. The air flow into the cylinders is regulated by a throttle. After the throttle, the air temperature is

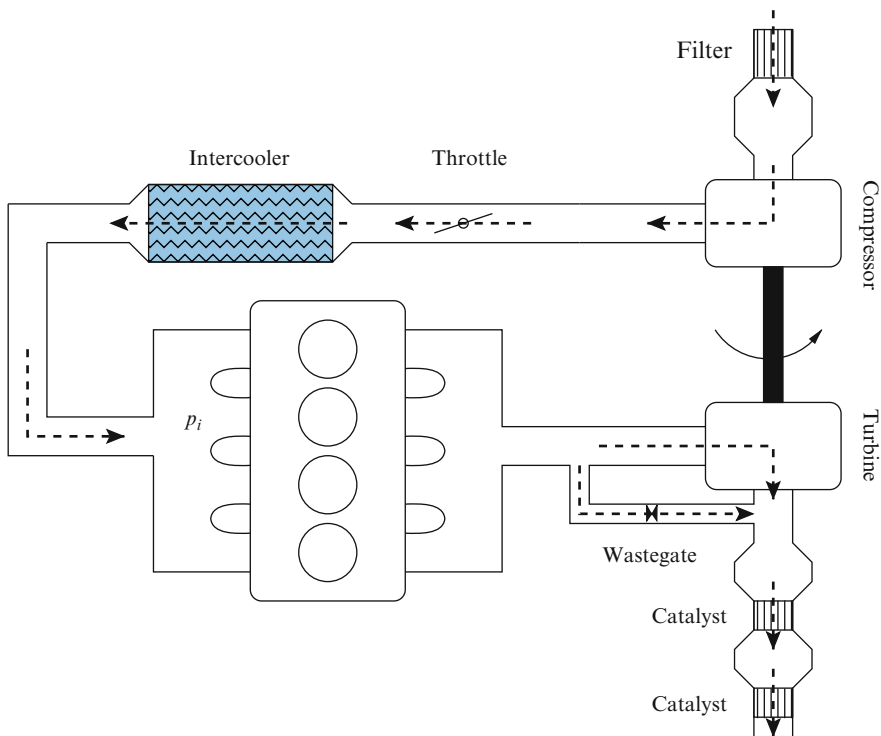
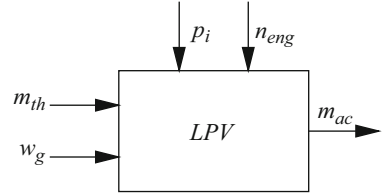


Fig. 17.1 Schematic of the air path of the considered turbocharged combustion engine

Fig. 17.2 Structure of the plant model to be identified as LPV model for controller synthesis



cooled down by an intercooler before it enters the cylinders. The mass flow over the throttle m_{th} is considered as actuator variable for this system. The exhaust coming from the cylinders drives a turbine, which in turn drives the compressor. A bypass from the turbine is given by a wastegate, which leads part of the exhaust flow directly to the catalyts. This bypass is regulated by a valve w_g , which is a second actuator for this system. The controlled variable is the air charge m_{ac} of the cylinders.

The scheduling signals which are chosen to describe the nonlinear behavior of the system are the pressure after the throttle (referred to as intake manifold pressure p_i) and the rotational speed of the engine n_{eng} . The plant model to be identified is depicted in Fig. 17.2.

$$u = \begin{bmatrix} m_{th} \\ w_g \end{bmatrix}, \quad y = m_{ac}, \quad \rho = \begin{bmatrix} p_i \\ n_{eng} \end{bmatrix}. \quad (17.1)$$

For the identification and validation of the LPV models, experimental test data were obtained. The data consist of measurements of the inputs u , the output y , and the scheduling signals ρ , which are explained in (17.1). It was taken in a test car in closed-loop operation with an industrial standard controller in the engine control unit (ECU). The car was started and used with disengaged clutch. The driver used the gas pedal to excite the engine system in as many maneuvers as possible to cover the whole parameter and frequency range. The maneuvers were done twice to obtain two data sets, one for identification and one for validation. Some measurements are shown in Figs. 17.3 and 17.4.

Model classes which are suitable for identifying LPV models of nonlinear systems and for controller synthesis are described in the following section.

17.3 Polytopic LPV State-Space and Input–Output Models

An LPV-SS model is given by

$$x(k+1) = A^r(\rho(k))x(k) + B^r(\rho(k))u(k), \quad (17.2)$$

$$y(k) = C^r(\rho(k))x(k) + D^r(\rho(k))u(k), \quad (17.3)$$

where $A^r(\rho(k)) : \mathbb{R}^{n_p} \rightarrow \mathbb{R}^{n \times n}$, $B^r(\rho(k)) : \mathbb{R}^{n_p} \rightarrow \mathbb{R}^{n \times n_u}$, $C^r(\rho(k)) : \mathbb{R}^{n_p} \rightarrow \mathbb{R}^{n_y \times n}$, $D^r(\rho(k)) : \mathbb{R}^{n_p} \rightarrow \mathbb{R}^{n_y \times n_u}$. θ is a time-dependent parameter vector given as

$$\theta(k) = [\theta_1(k) \ \theta_2(k) \ \dots \ \theta_{n_\theta}(k)]^T \in \mathbb{R}^{n_\theta}, \quad (17.4)$$

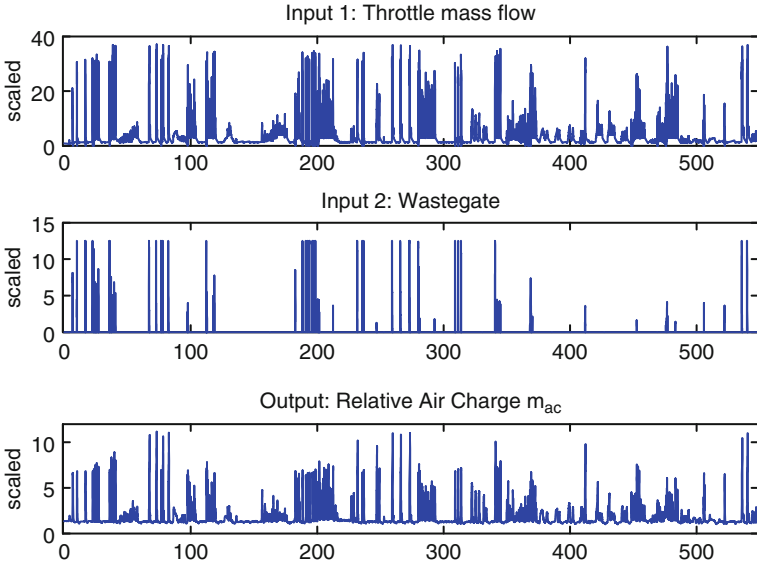


Fig. 17.3 Measured inputs and outputs

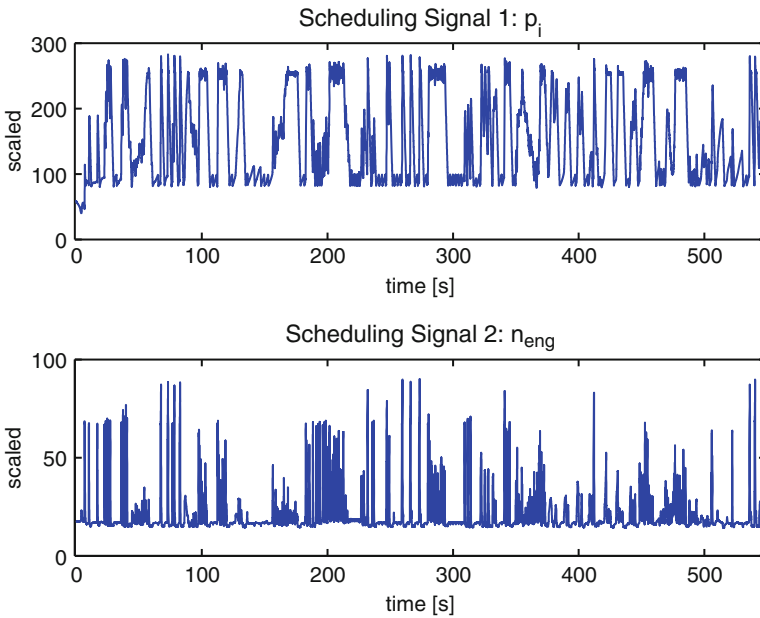


Fig. 17.4 Measured scheduling signals

which is assumed to be a function $\theta(k) = p(\rho(k))$ of the scheduling signal vector ρ , where the parameter function $p: \mathbb{R}^{n_\rho} \mapsto \mathbb{R}^{n_\theta}$ is an analytic mapping. We refer to θ as scheduling parameter and to p as scheduling function. For controller design, a widely used synthesis tool requires a polytopic LPV representation, see e.g. [5]. One advantage of this form is that it is less conservative compared to controller synthesis based on LFR models, see [3]. For this approach, the model must be affine in the parameters, so that it can be represented as

$$\begin{bmatrix} A^s(\theta(k)) & B^s(\theta(k)) \\ C^s(\theta(k)) & D^s(\theta(k)) \end{bmatrix} := \begin{bmatrix} A_0^s & B_0^s \\ C_0^s & D_0^s \end{bmatrix} + \sum_{i=1}^{n_\theta} \theta_i \begin{bmatrix} A_i^s & B_i^s \\ C_i^s & D_i^s \end{bmatrix}. \quad (17.5)$$

An affine LPV-SS model where θ ranges over a fixed polytope \mathcal{P} is called a polytopic LPV system. If $\underline{\theta}_i \leq \theta_i \leq \bar{\theta}_i$, then the polytope can be represented in terms of its $n_\nu = 2^{n_\theta}$ vertices $\theta_{v_1}, \theta_{v_2}, \dots, \theta_{v_{n_\nu}}$. Then for any parameter $\theta(k_a)$ that can be represented as

$$\theta(k_a) = \sum_{i=1}^{n_\nu} \alpha_i \theta_{v_i} \quad \text{with} \quad \sum_{i=1}^{n_\nu} \alpha_i = 1, \quad \alpha_i \geq 0. \quad (17.6)$$

the corresponding state-space model at $\theta(k_a)$ can be represented as a convex combination of the state-space models evaluated at the vertices as

$$\begin{bmatrix} A^s(\theta(k_a)) & B^s(\theta(k_a)) \\ C^s(\theta(k_a)) & D^s(\theta(k_a)) \end{bmatrix} = \sum_{i=1}^{n_\nu} \alpha_i \begin{bmatrix} A^s(\theta_{v_i}) & B^s(\theta_{v_i}) \\ C^s(\theta_{v_i}) & D^s(\theta_{v_i}) \end{bmatrix}. \quad (17.7)$$

In [18] it was shown that a straightforward conversion of the IO model class suggested in [6] to a polytopic LPV-SS model leads to an SS model where—in contrast to (17.5)—the system matrices at time k do not depend only on $\theta(k)$, but also on past values of theta. In [17], different SISO IO model classes are proposed, which are readily convertible to LPV-SS models that depend statically on the scheduling parameters. The so-called *Shifted Form* is provided here for MIMO systems, which requires the following model class for the identification of the IO model:

$$A(\rho(\cdot), q)y(k) = B(\rho(\cdot), q)u(k) + e(k), \quad (17.8)$$

$$A(\rho(\cdot), q) = I + \sum_{i=1}^{n_a} A_i(\rho(k-i))q^{-i}, \quad (17.9)$$

$$B(\rho(\cdot), q) = \sum_{j=0}^{n_b} B_j(\rho(k-j))q^{-j}, \quad (17.10)$$

where $A(\rho(\cdot), q)$ means that A can be a function not only of $\rho(k)$ but also of $\rho(k-1), \rho(k-2), \dots$, with $A_i(\cdot)$ and $B_j(\cdot)$ defined as

$$A_i(\rho(k-i)) = A_{i,0} + \sum_{l=1}^{n_f} A_{i,l} f_l(\rho(k-i)), \quad i = 1, \dots, n_a, \quad (17.11)$$

$$B_j(\rho(k-j)) = B_{j,0} + \sum_{l=1}^{n_f} B_{j,l} f_l(\rho(k-j)), j = 1, \dots, n_b. \quad (17.12)$$

The $n_a + n_b + 1$ parametric functions $A_i(\rho) : \mathbb{R}^{n_\rho} \rightarrow \mathbb{R}^{n_y \times n_y}$ and $B_j(\rho) : \mathbb{R}^{n_\rho} \rightarrow \mathbb{R}^{n_y \times n_u}$ to be identified are assumed to depend affinely on a known set of fixed basis functions $\{f_1, \dots, f_{n_f}\}$. This is done to achieve a model structure, where parameter estimation is a linear optimization problem and to allow for a conversion to a polytopic model. One possible choice of basis functions is the set of all multivariable monomials up to a given total order in the scheduling signals ρ . If the scheduling function is chosen to be the functional basis as

$$\theta(k) = p(\rho(k)) = f(\rho(k)), \quad (17.13)$$

the above can be written as

$$A_i(\theta(k-i)) = A_{i,0} + \sum_{l=1}^{n_\theta} A_{i,l} \theta_l(k-i), \quad i = 1, \dots, n_a, \quad (17.14)$$

$$B_j(\theta(k-i)) = B_{j,0} + \sum_{l=1}^{n_\theta} B_{j,l} \theta_l(k-j), \quad j = 1, \dots, n_b \quad (17.15)$$

with $\theta(k) = [\theta_1(k) \ \theta_2(k) \ \dots \ \theta_{n_\theta}(k)]^T$ and $n_\theta = n_p = n_f$.

The obtained MIMO LPV-IO model can be converted to a MIMO LPV-SS model of the form in (17.5). A strictly proper system is assumed, so $D^s = 0$. For $n_a = n_b = n$ the state-space matrices of the identified model can be expressed as

$$A^s(\theta(k)) = \begin{bmatrix} -A_1(\theta(k)) & I & [0] & \cdots & [0] \\ \vdots & [0] & \ddots & \ddots & \vdots \\ \vdots & \vdots & \ddots & \ddots & [0] \\ -A_{n-1}(\theta(k)) & [0] & \cdots & [0] & I \\ -A_n(\theta(k)) & [0] & \cdots & \cdots & [0] \end{bmatrix}, \quad B^s(\theta(k)) = \begin{bmatrix} B_1(\theta(k)) \\ \vdots \\ \vdots \\ B_{n-1}(\theta(k)) \\ B_n(\theta(k)) \end{bmatrix}, \quad C^s(\theta(k)) = \begin{bmatrix} I \\ [0] \\ \vdots \\ \vdots \\ [0] \end{bmatrix}. \quad (17.16)$$

If the model requires $n_a \neq n_b$, the state-space matrices can be expressed analogously with the corresponding block matrices set to zero in $A^s(\theta)$ and $B^s(\theta)$, respectively.

The class of LPV-IO models in shifted form is not a subclass of the class of standard LPV-IO models proposed in [6]. Instead, they are both subclasses of the class of output affine models. The identification of LPV-IO models in shifted form is employed without loss of generality compared to standard LPV-IO models.

17.4 Identification Results

For the identification of an LPV-IO model of the turbocharged engine system, a sufficiently rich set of measurements of the inputs u , the scheduling signals ρ , and the output y is required. The experiments employed to obtain them were described in Sect. 17.2. For the model order, satisfactory results were obtained with $n_a = n_b = 2$.

An additional feature, which needs to be selected for the identification, is the basis $\{f_i\}$ in (17.13), which will be employed to describe the nonlinear behavior of the system. For this purpose, a polynomial basis is used here, which consists of all monomials in the scheduling signals up to a fixed total order. Such a polynomial basis can be interpreted as the polynomial terms, which would appear in a multivariate Taylor approximation of the unknown scheduling function. By Taylor's Theorem any at a point P k -times continuously differentiable function can be approximated around P by a multivariate Taylor series expansion of degree k . An approximation to any accuracy can be obtained, when k can be chosen arbitrarily high. Such a polynomial basis can be described by the Veronese map defined in [10]: the Veronese map $v_i : \mathbb{R}^{n_\rho} \mapsto \mathbb{R}^{M_i(n_\rho)}$ of degree i is the polynomial function of order i defined as $v_i : [\rho_1, \dots, \rho_{n_\rho}] \mapsto [\dots, \rho^l, \dots]$, where ρ^l ranges over all monomials of total degree i in $\rho_1, \dots, \rho_{n_\rho}$. The dimension $M_i(n_\rho)$ of the range space is given as: $M_i(n_\rho) = \binom{n_\rho - 1 + i}{i}$.

A functional basis for the identification of LPV-IO models is given by all monomials of maximum total degree d in the variables $\rho_1, \dots, \rho_{n_\rho}$:

$$f_i(\rho) = \begin{cases} v_1(\rho)_l, l = 1, \dots, M_1(n_\rho) \\ v_2(\rho)_l, l = M_1(n_\rho) + 1, \dots, M_1(n_\rho) + M_2(n_\rho) \\ \vdots \\ v_d(\rho)_l, l = 1 + \sum_{k=1}^{d-1} M_k(n_\rho), \dots, \sum_{k=1}^d M_k(n_\rho), \end{cases}, \quad (17.17)$$

where $v_i(\rho)_l$ is the l th element of the vector $v_i(\rho)$. The total number of basis functions is then $n_f = \sum_{k=1}^d M_k(n_\rho)$.

When this is applied to the case study with the two scheduling signals $\rho_1 = n_{\text{eng}}$, $\rho_2 = p_i$ and $d = 2$, we have:

$$f(\rho) = [v_1(\rho), v_2(\rho)]^T = [\rho_1, \rho_2, \rho_1^2, \rho_1\rho_2, \rho_2^2]^T.$$

Now all the input to the identification algorithm is available. The validation accuracy can be evaluated for single-output systems by the best fit rate (BFR) according to [14]:

$$\text{BFR} = 100\% \cdot \max \left(1 - \frac{\|Y - \hat{Y}\|}{\|Y - Y_m\|}, 0 \right), \quad (17.18)$$

where Y is a column vector containing the measurements reserved for validation, Y_m is a column vector containing the mean of Y and \hat{Y} is the approximation of

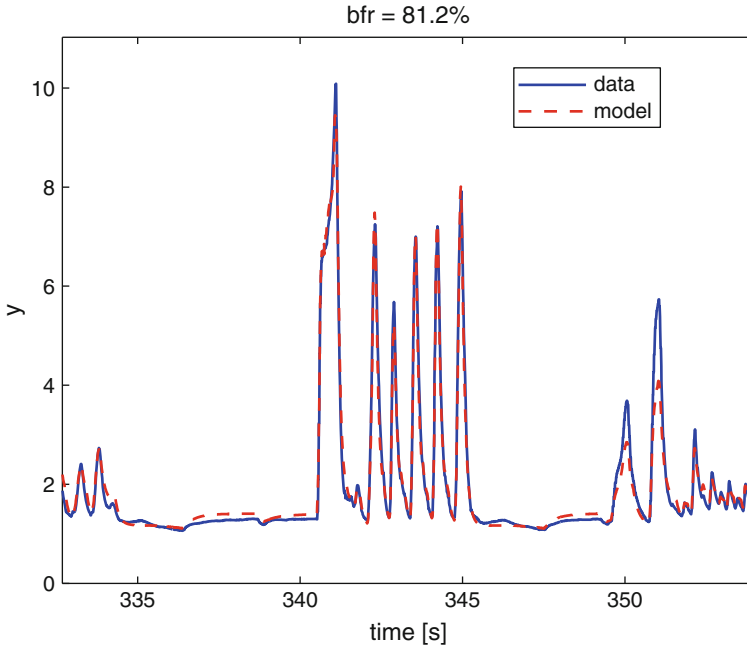


Fig. 17.5 Cross validation of the identification result with five scheduling parameters

Y obtained by open-loop simulation with the identified model. The identification result is depicted in Fig. 17.5. The zoom into the trajectory shows that the identified model follows the dynamics very well and the BFR of 81.2% shows a good fit. The model is considered accurate enough for controller synthesis, however the complexity of the resulting polytopic model is with five parameters too high for a practical implementation.

17.5 Parameter Reduction

A first attempt to complexity reduction could be PSM. The result of a parameter reduction by employing the method proposed in [13] to the above model is shown in Fig. 17.6. It is shown that the number of parameters of the LPV model can be reduced to two parameters at the cost of a lower BFR of 67.8%. PSM has previously been applied to LPV models, which were obtained by either physical modeling or gray-box modeling. In these models, the specific scheduling parameters were obtained by the physical relationships. In the context of black-box identification, the scheduling parameters are obtained by applying the basis functions $\{f_i\}$ to the scheduling signals ρ . The PSM method approximates the trajectories of a high

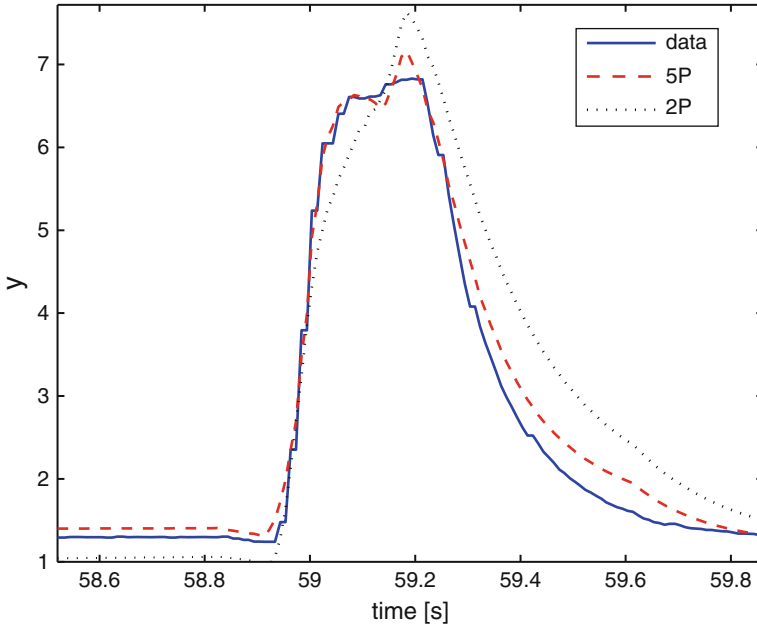


Fig. 17.6 Cross validation of the identification result with two scheduling parameters

number of scheduling parameters n_θ by a lower number of scheduling parameters n_ϕ . This method is based on the information contained in the variation of the individual parameters; it does, however, not consider their relative significance for the plant dynamics.

In (17.8)–(17.15), the complexity, given by the number of scheduling parameters, results from the definition of the scheduling parameter vector as $\theta(k) = p(\rho(k)) = f(\rho(k))$. To take a closer look, (17.11) and (17.12) are repeated:

$$A_i(\rho(k-i)) = A_{i,0} + \sum_{l=1}^{n_f} A_{i,l} \underbrace{f_l(\rho(k-i))}_{\theta_l(k-i)}, i = 1, \dots, n_a, \quad (17.19)$$

$$B_j(\rho(k-j)) = B_{j,0} + \sum_{l=1}^{n_f} B_{j,l} \underbrace{f_l(\rho(k-j))}_{\theta_l(k-j)}, j = 1, \dots, n_b. \quad (17.20)$$

In this case, the number of scheduling parameters is given by $n_\theta = n_f$. If the number of basis functions n_f is very high, one might consider selecting a different scheduling parameter vector.

A definition of a low-complexity scheduling parameter vector ϕ is

$$A_i(\rho(k-i)) = A_{i,0} + \sum_{l=1}^{n_\phi} A_{i,l} \underbrace{\tilde{p}_l(\rho(k-i))}_{\phi_l(k-i)}, i = 1, \dots, n_a, \quad (17.21)$$

$$B_j(\rho(k-j)) = B_{j,0} + \sum_{l=1}^{n_\phi} B_{j,l} \underbrace{\tilde{p}_l(\rho(k-j))}_{\phi_l(k-j)}, j = 1, \dots, n_b \quad (17.22)$$

with

$$\phi_l(k) := \tilde{p}_l(\rho(k)) := U_c f(\rho(k)) + 1 \quad (17.23)$$

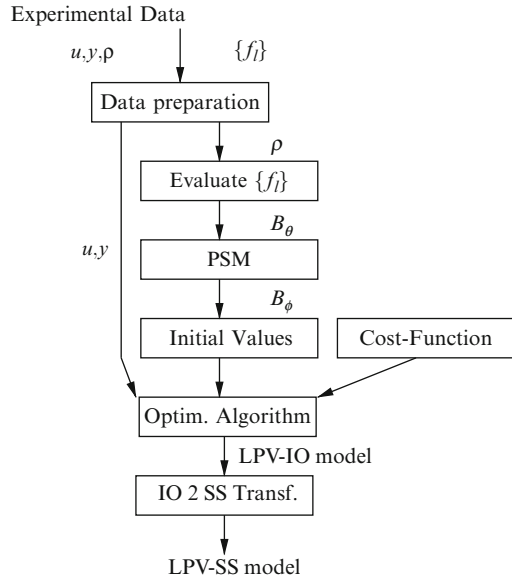
with a coefficient matrix $U_c \in \mathbb{R}^{n_\phi \times n_f}$, the vector of basis functions $f(\rho) \in \mathbb{R}^{n_f}$ and 1 being a vector of ones with appropriate dimensions. This model class is still the class of shifted LPV-IO models, because (17.21) and (17.22) are equivalent to (17.19) and (17.20). This can easily be shown by renaming the basis functions. Nevertheless, the form of low-complexity LPV IO models in (17.21)–(17.23) illustrates an approach to identification of low-complexity LPV-IO models. In the standard approach, the LPV-IO model is identified with the basis functions $f_l, l = 1, \dots, n_f$, which are employed to describe the nonlinear relationship between the scheduling signals ρ and the systems input u and output y . Consequently, the number of scheduling parameters indicating model complexity is $n_\theta = n_f$. The low-complexity approach aims at identifying a smaller set of basis functions $\tilde{p}_l, l = 1, \dots, n_\phi$ as a weighted sum of the original basis functions $f_l, l = 1, \dots, n_f$. When such a basis is found with $n_\phi < n_f$, the complexity can be reduced by identifying a model with the basis $\tilde{p}_l, l = 1, \dots, n_\phi$. Such a parametrization can be computed by employing PSM, which was applied to the case study in the previous section. As reasoned there, the reduced parameters obtained by employing PSM can be further optimized by an iterative nonlinear optimization, which is further described in the next section.

17.6 Identification of Low-Complexity Input–Output LPV Models

A flow diagram of the algorithm is given in Fig. 17.7. The individual steps are described in the following.

Inputs to the algorithm are measured trajectories of the input u , the output y , and the scheduling signals ρ , as well as a functional basis $\{f_l\}$. After the data preparation step, the functional basis is evaluated, resulting in the scheduling parameter vector θ . Then PSM is applied to θ to obtain a mapping \tilde{p}_l on reduced parameters ϕ . This mapping is used as an initialization and further improved using

Fig. 17.7 Flow diagram of identification procedure initialized by PSM



a nonlinear optimization method like the simplex method. This optimization is applied iteratively. The decision variables for nonlinear optimization are given by the elements of $U_c \in \mathbb{R}^{n_\phi \times n_f}$ from (17.23). The minimization problem, which is solved by a downhill simplex method, is given by

$$\min_{U_c} \text{BFR}. \tag{17.24}$$

To compute the cost function, a linear regression is performed, which for a fixed mapping \tilde{p}_l determines the set of coefficients given in (17.21) and (17.22). The resulting LPV-IO model is simulated in open-loop and the BFR is computed to evaluate the cost function for the nonlinear optimization.

The results of the identification are shown in Fig. 17.8. A BFR of 81.0% is considered satisfactory for controller synthesis. The plot of the zoom into the trajectory for comparison to the other two methods shows a significant improvement compared to the model obtained by PSM.

The optimized set of parameters for the coefficient matrix U_c is

$$U_{\text{opt}} = \begin{bmatrix} -0.8338 & -0.1925 & 0.5109 & -0.3281 & -0.3224 \\ -0.1210 & -0.0589 & -0.0694 & -0.1891 & -0.1308 \end{bmatrix}. \tag{17.25}$$

This shows that all basis functions are contributing to the scheduling functions, but it can be concluded, that the second basis function, which is ρ_2 , is less significant than the first being ρ_1 .

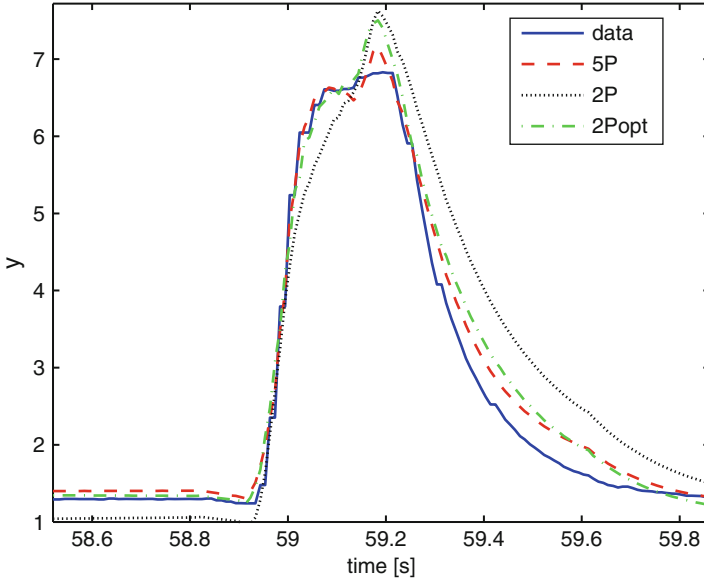


Fig. 17.8 Identification results resulting from the proposed algorithm

17.7 Controller Synthesis and Closed-Loop Results

The identified IO model has two scheduling parameters $n_\theta = 2$. It is converted to a polytopic LPVSS model of the form (17.5) using (17.16). Polytopic LPV controller synthesis methods demand a further transformation of the model into a vertex model given in (17.7). Resulting from $n_\theta = 2$, four vertices are obtained. These vertices are substituted in the polytopic model (17.5) to obtain the vertex models (17.7). The obtained model has a parameter varying system matrix $A(\phi)$, a parameter varying input matrix $B(\phi)$, and constant output matrices C and D , resulting from (17.16). The controller synthesis method employed in the following requires the input matrix $B(\phi)$ of the LPV model to be constant. Input weighting filters are used as suggested in [4] to obtain an LPV model of the plant with a constant input matrix $B(\phi) = B$.

The vertex model (17.7) is a convex combination of LTI systems. In norm-optimal controller synthesis based on polytopic models for each of these vertices a generalized plant is constructed.

LPV controller synthesis, using a fixed Lyapunov function as in [5], turned out to be too restrictive for mixed-sensitivity design for the considered engine model. Therefore, a method of dilated LMIs, a controller synthesis allowing for parameter varying Lyapunov functions, was employed. An efficient method of using a parameter varying Lyapunov function for controller synthesis is explained in [15]. In this paper, a robust controller for an uncertain system is designed using LMI techniques. This method was applied to LPV systems in [2].

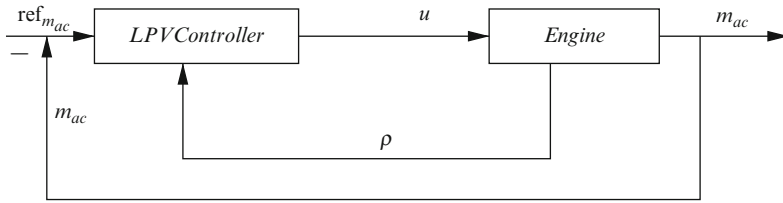


Fig. 17.9 Closed-loop system configuration

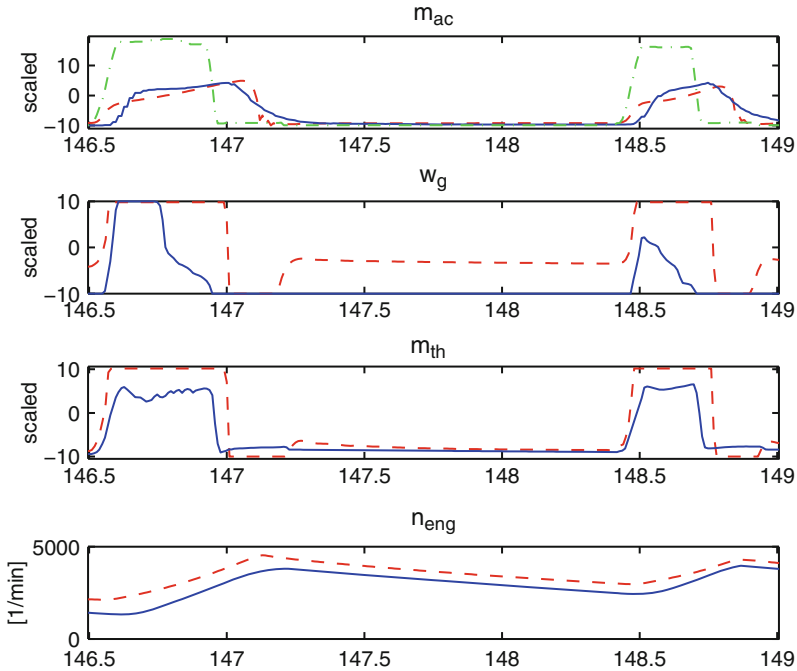


Fig. 17.10 Closed-loop simulation results: *dash-dotted*: reference, *dashed*: simulation, *solid*: measurements

For the case study considered in this chapter, the controller was tuned by evaluating the sensitivities and the closed-loop step responses of the LPV-SS model evaluated at the vertices and adapted in closed-loop simulations with the nonlinear model. The performance of the controller is finally evaluated through simulations with the validated nonlinear model. The closed-loop system is depicted in Fig. 17.9, showing the LPV controller, which is gain scheduled by the scheduling signals and the engine model to simulate the plant. The closed-loop simulation results are shown in Fig. 17.10. The dash-dotted line shows the reference given by the ECU. In the two peaks, the reference cannot be followed very tightly due to physical limitations as can be seen, when comparing the reference to the measured output obtained by

the industrial standard controller of the ECU (solid line). The simulation results obtained by the new controller are shown by the dashed line. By comparing it to the measurement, a very similar performance can be observed. For reference with n_{eng} , one of the scheduling signals is shown.

17.8 Conclusion and Future Work

An LPV identification scheme has been proposed, which provides an easily applicable tool for low-complexity black-box LPV-IO model identification. Identification results based on experimental data show that the combination of PSM with LPV-IO identification is very promising, if extended by an additional nonlinear optimization. Closed-loop simulation results suggest that based on the obtained models, gain-scheduled controllers can be designed. Tests of the controller in experiment are currently being prepared.

Acknowledgment The authors would like to thank all colleagues and students who contributed to this study. We are grateful to Santiago Remolina Cano for his work on the nonlinear validation model and for taking the measurements.

References

1. Abbas H, Werner H (2011) Frequency-weighted discrete-time lpv model reduction using structurally balanced truncation. *IEEE Trans Contr Syst Tech* 19(1):140–147
2. Ali M, Werner H (2011) Discrete-time LPV controller synthesis using dilated LMIs with application to an arm-driven inverted pendulum. In: 18th IFAC World Congress, Milano, Italy, pp 7708–7712
3. Apkarian P, Becker G, Gahinet P, Kajiwaru H (1996) LMI techniques in control engineering from theory to practice. In: Workshop notes CDC, IEEE, Kobe, Japan
4. Apkarian P, Gahinet P (1995) A convex characterization of gain scheduled \mathcal{H}_∞ controllers. *IEEE Trans Automat Contr* 40:853–864
5. Apkarian P, Gahinet P, Becker G (1995) Self-scheduled H_∞ control of linear parameter-varying systems: a design example. *Automatica* 31(9):1251–1261
6. Bamieh B, Giarré L (2002) Identification of linear parameter varying models. *Int J Robust Nonlinear Contr* 12(9):841–853
7. Boonto S, Werner H (2010) Closed-loop identification of LPV models using cubic splines with application to an arm-driven inverted pendulum. In: Proceedings of the American control conference, Baltimore, USA, pp 3100–3105
8. Felici F, Wingerden J, Verhaegen M (2007) Dedicated periodic scheduling sequences for LPV system identification. In: Proceedings of the 8th European control conference, pp 4896–4902
9. Giarré L, Bauso D, Falugi P, Bamieh B (2006) LPV model identification for gain scheduling control: an application to rotating stall and surge control problem. *Contr Eng Pract* 14:351–361
10. Harris J (1992) Algebraic geometry: a first course. Springer, New York
11. Hashemi SM, Abbas H, Werner H (2009) LPV modelling and control of a 2-DOF robotic manipulator using PCA-based parameter set mapping. In: Proceedings of the 48th IEEE conference on decision and control, Shanghai, China, pp 7418–7423. URL <http://dx.doi.org/10.1109/CDC.2009.5400621>

12. Kwiatkowski A, Blath J, Werner H, Schultalbers M (2006) Application of LPV gain scheduling to charge control of a SI engine. In: Proceedings of the IEEE international symposium on computer-aided control systems design, Munich, Germany. URL [dx.doi.org/10.1109/CACSD-CCA-ISIC.2006.4777003](https://doi.org/10.1109/CACSD-CCA-ISIC.2006.4777003)
13. Kwiatkowski A, Werner H (2008) PCA-based parameter set mappings for LPV models with fewer parameters and less overbounding. *IEEE Trans Contr Syst Tech* 16(4):781–788
14. Ljung L (1999) *System identification, theory for the user*, 2nd edn. Prentice-Hall Inc., USA
15. d Oliveira MC, Geromel JC, Bernussou J (2002) Extended H_2 and H_∞ norm characterizations and controller parameterizations for discrete-time systems. *Int J Contr* 75(9):666–679
16. Rövid A, Várlaki P, Szeidl L (2011) Hosvd based data representation and lpv model complexity reduction. In: Proceedings of the 2011 American conference on applied mathematics and the 5th WSEAS international conference on Computer engineering and applications, World Scientific and Engineering Academy and Society (WSEAS), Stevens Point, Wisconsin, USA, pp 164–169
17. Toth R, Abbas HS, Werner H (2012) On the State Space Realization of LPV Input-Output Models: Practical Approaches. *IEEE Trans Contr Syst Tech* 20(1):139–153
18. Toth R, Felici F, Heuberger P, van den Hof P (2007) Discrete time lpv i/o and state space representations, differences of behavior and pitfalls of interpolation. In: Proceedings of the European control conference 2007, VDM Verlag Dr. Müller, Saarbrücken, D, pp 5418–5425
19. Verdult V, Verhaegen M (2001) Identification of multivariable lpv state space systems by local gradient search. In: Proceedings of the European control conference, Porto, Portugal, pp 3675–3680
20. Verdult V, Verhaegen M (2005) Kernel methods for subspace identification of multivariable LPV and bilinear systems. *Automatica* 41(9):1557–1565
21. Wei X, d Re L (2007) Gain scheduled H_∞ control for air path systems of diesel engines using LPV techniques. *IEEE Trans Contr Syst Tech* 15(3):406–415

Chapter 16

LPV H_∞ Control for Flexible Hypersonic Vehicle

Hunter D. Hughes and Fen Wu

Abstract This chapter demonstrates the method to synthesize and simulate an H_∞ linear parameter-varying (LPV) controller for a flexible air-breathing hypersonic vehicle (HSV) model. The output feedback design used velocity tracking for both the flexible and rigid body hypersonic vehicle models. A parametric study was conducted to determine the number of gridding points in the parameter space and the parameter variation rate limits in the system. The study reveals a 7×7 grid ranging from Mach 7 to Mach 9 in velocity and from 70,000 ft to 90,000 ft in altitude, and a parameter variation rate limit of $[.1 \ 200]^T$ is preferable. The resulting H_∞ robust performances were $\gamma = 113.2146$ for the flexible body case and $\gamma = 83.6931$ for the rigid body case. The H_∞ LPV controllers were applied to the flexible nonlinear plant model. The results show that the controller is robust to disturbance, parametric uncertainty, and modeling errors for the tracking and regulation states.

16.1 Introduction to Hypersonic Vehicle Controls

Research into air-breathing hypersonic vehicles started in the 1960s and continued through the 1990s with the National Aerospace Plane [5, 6]. Hypersonic vehicles provide several possibilities that current technology cannot achieve. They are being considered as a favorable means of reaching both low Earth orbit, and affordable, reliable outer space access [5, 6, 14, 20, 36]. Hypersonic vehicles have also been proposed as a means of providing a quick response to global threats [20, 36].

H.D. Hughes

Georgia Tech Research Institute, 7220 Richardson Road, Smyrna, GA 30080, USA

e-mail: hunter.hughes@gtri.gatech.edu

F. Wu (✉)

North Carolina State University, Mechanical and Aerospace Engineering, Box 7910,

Raleigh, NC 27695, USA

e-mail: fwu@eos.ncsu.edu

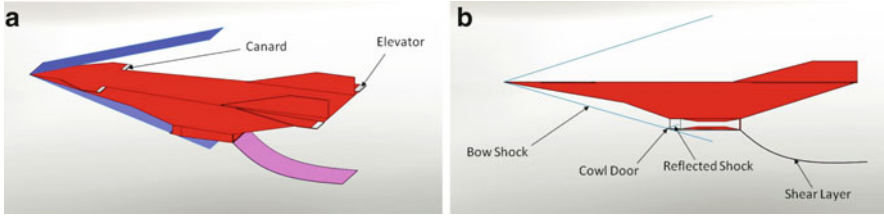


Fig. 16.1 Hypersonic vehicle schematic drawing (a) Isometric view (b) Side view

It has even been suggested that hypersonic vehicles could be used in commercial and military applications to reduce flight times since hypersonic vehicles have the ability to carry larger payloads (due to the requirement of fuel and oxygen for rockets as opposed to just fuel for the hypersonic vehicle) than the equivalent rocket powered systems [15, 28]. More recently, NASA has successfully designed and flown a hypersonic aircraft X-43A. The X-43A is 12 ft long and incorporates an integrated scramjet engine. The top recorded speed of X-43A test flight was Mach 9.6, which was achieved in November, 2004 over the Pacific ocean west of California [19, 20, 34].

Hypersonic vehicle design requires a highly integrated approach which causes many significant design challenges for control engineers. For hypersonic flight, an airframe with a highly integrated scramjet is required for optimum performance [6, 36]. Moreover, deriving models and control systems for hypersonic vehicle can be very difficult. Attempts to provide more integrated approaches to modeling and controlling flexible aircraft have been under way for some time [24]. Figure 16.1a provides a schematic drawing on the basic design and layout of a hypersonic vehicle. Notice the scramjet on the bottom of the vehicle. This particular configuration shows a canard on the front of the vehicle. Figure 16.1b shows how the scramjet and integrated airframe work together. The bow shock off the nose of the hypersonic vehicle acts as a compression stage to the scramjet. This is essential to generate the proper pressure and flow rate needed in maintaining the combustion to produce the thrust for hypersonic flight. The offset of the scramjet causes a strong coupling between the thrust, lift, drag, and pitching moment of the vehicle [19, 36]. Moreover, the vehicle flexibility must also be considered since it is long and slender with a relatively light weight [20]. This flexibility will change the bow shock position which in turn affects the propulsion of the hypersonic vehicle. Additionally, the overall drag and lift for the vehicle will be affected. Therefore, the flexible nature of the hypersonic vehicle must be included in the construction of the HSV model [20, 28, 36].

The modeling of hypersonic vehicles has been an ongoing research topic. One of the earlier studies in this area was performed by Shaughnessy et al. [30]. After the work by Shaughnessy et al., Schmidt and his coworkers have contributed to the advancement of hypersonic vehicle dynamic modeling [29]. Their study recognizes the strong couplings between the airframe, the scramjet engine, and the elastic

modes of the vehicle. It is suggested that the use of a control effector to change the diffuser area ratio of the hypersonic vehicle may be necessary to maintain stable combustion. They also discovered that the actuation of the diffuser area ratio must be of the same bandwidth or more than the fuel flow rate in the combustion chamber. The functionality of scramjet is most directly affected by the pitch control inputs to the airframe.

More recently, Chavez and Schmidt have made an effort to model the air-breathing hypersonic vehicle [10]. This work provides the foundation of the HSV model used in this chapter. The conclusion of their study is that hypersonic vehicles are dependent upon both aerodynamic and propulsive effects. Since the hypersonic vehicle is elastic, the deformation of the vehicle's forebody and its pitch response will affect the inlet conditions of the propulsion system. This will cause disturbances in the engine if this is not properly modeled. They simplified the hypersonic modeling problem by using two-dimensional Newtonian impact theory to characterize the aerodynamic pressure distribution. Nevertheless, the studies by Bolender and Doman [5, 6] have shown that the impact theory does not accurately capture the location of the shock wave for all flight conditions.

Bilimoria and Schmidt have also worked on the flexible hypersonic vehicle model [3]. In their study, they attempt to describe the hypersonic vehicle dynamics using the Lagrangian approach. This modeling effort was an attempt at developing a complete usable set of kinematic equations for the hypersonic vehicle. Rigid body motion, elastic deformation, fluid flow, rotating machinery, wind, and the curvature of the Earth were all considered in their study.

Similarly, Mirmirani et al. have managed to incorporate many of the coupled dynamics and physics of the hypersonic vehicle using a computational fluid dynamics (CFD) approach [25]. Their approach uses a high fidelity CFD based model in conjunction with multi-physics software to model the dynamics of the hypersonic vehicle. It gives a lot of insight into the different coupled parameters of the hypersonic vehicle, but does not provide a closed form set of equations for control synthesis.

There are currently many different control techniques that have been proposed for the hypersonic vehicle. NASA researchers suggested using classical controls and simple gain scheduling for the control of their hypersonic vehicle [12]. Moreover, an optimal controller for the hypersonic vehicle was developed by Parker et al. [28]. This control design incorporates the high fidelity plant model introduced by Bolender and Doman [5], and applies an inner loop feedback linearization with an outer loop LQR controller with integral augmentation. Groves et al. proposed a control technique for the hypersonic vehicle that uses a linear approximation for the HSV around a trim condition and an LQR controller [20]. These controllers are only applied to a single linearized equilibrium position, and therefore have a limited operating range and limited robust capabilities. Also, it is desirable to use output feedback control algorithm for the HSV.

The work done by Xu et al. attempted to use an adaptive sliding mode controller with an observer for output feedback [38]. This method is robust, but requires very large control forces. It is also assumed that the hypersonic vehicle dynamics are

rigid body. The work done by Mooij also used a rigid body controller [26] and incorporated a model reference adaptive control (MRAC) algorithm. The designed controller does not guarantee stability of the HSV, and requires tuning of weight functions. These control algorithms suffer from the lack of a realistic representation of the true hypersonic vehicle dynamics. The work by Gibson et al. looked into the use of adaptive control for a hypersonic vehicle in the presence of modeling uncertainty [17]. Their study examined the effects of uncertainty but used a limited range of operation for the vehicle. Fidan et al. have done work on the longitudinal motion control of a hypersonic vehicle based on linear time-varying models with adaptive and nonlinear control systems; however, it is purely a mathematical study [13]. There are no simulated data to show the results of this study.

The work done by Buschek and Calise, as well as Gregory et al., investigated the application of H_∞ and μ -synthesis control algorithms to the hypersonic vehicle [8, 9, 18]. The study by Gregory et al. considered two controllers: the standard H_∞ controller and a μ -synthesis controller with a structured uncertainty block. Their study showed that the μ -synthesis controller had a better performance than the H_∞ controller when actuator uncertainty was incorporated into the control design [18]. Similar studies by Buschek and Carlise also confirmed that μ -synthesis has good robust performance properties [8, 9].

The work done by Sigthorsson et al. investigates nonlinear tracking control for an overactuated hypersonic vehicle with steady-state constraints [31]. Their study uses state feedback LQR control for stabilization and optimization of steady-state control in both constrained and unconstrained cases. Though there is the potential for some robust capabilities with this method, it does not demonstrate that the system will be robust. Robust nonlinear control of a hypersonic aircraft was developed by Wilcox et al. in the presence of aerothermal effects by using temperature-dependent parameter-varying state-space models [35]. This controller is supposed to be robust to sensor noise, exogenous perturbations, parametric uncertainty, and plant nonlinearities, but there is no simulation results available to back up the theory.

The work done by Jankovsky et al. involves applying output feedback control to the hypersonic vehicle model as well as investigating the need for proper sensor placement [22]. They proposed two controllers: the first is an output feedback controller that relies on an observer to reconstruct the full-state information of the HSV, and the second is a controller using robust output feedback to ensure stabilization without an observer. Their study has suggested that gain scheduling or adaptive control may be able to yield an improved performance for the HSV output feedback problem.

Linear parameter-varying (LPV) control techniques have been applied to the flexible hypersonic vehicle thermocontrol problem in the past [23]. This technique involved using a multiloop controller where the inner loop controller was an LPV controller to augment active structural damping in the aeroelastic modes while the outer loop was a traditional rigid body aircraft controller. This multi-loop control technique is successful in using LPV to control the hypersonic vehicle thermodynamics, but the research does not go further to investigate attitude and velocity control of HSV.

This chapter will design and implement an LPV H_∞ controller for the longitudinal dynamics of the flexible air-breathing hypersonic vehicle as modeled by Bolender and Doman [4, 6]. The output feedback LPV controller will be developed in this regard. Additionally, this chapter will investigate the feasibility of treating aircraft flexibility as a disturbance to the system by synthesizing a controller using the rigid body HSV model and simulating the results on the flexible body HSV dynamics. The effect of disturbance and parametric uncertainty will also be investigated to show the robustness of the proposed control technique. It should be noted that more extensive study might be needed before the implementation of such a controller on an actual hypersonic vehicle.

The notations used throughout the chapter are fairly standard. \mathbf{R} presents the set of real numbers; \mathbf{R}^n stands the n -dimensional real vector set; $\mathbf{R}^{m \times n}$ is the set of real $m \times n$ matrices. $\mathbf{S}^{n \times n}$ will be used to denote real, symmetric $n \times n$ matrices, and $\mathbf{S}_+^{n \times n}$ for positive definite matrices. For two integers $k_1, k_2, k_1 < k_2$, it will be denoted that $\mathbf{I}[k_1, k_2] = \{k_1, k_1 + 1, \dots, k_2\}$. Given $\mathcal{P} \subset \mathbf{R}^s$ as a compact set, we define the parameter v -variation set as

$$\mathcal{F}_{\mathcal{P}}^v := \{ \rho \in C^1(\mathbf{R}_+, \mathbf{R}^s) : \rho(t) \in \mathcal{P}, v_k \leq \dot{\rho}_k \leq \bar{v}_k, k = 1, 2, \dots, s, \forall t \in \mathbf{R}_+ \}$$

For $x \in \mathbf{R}^n$, its Euclidean norm is $\|x\| := (x^T x)^{1/2}$. L_2 is the space of square-integrable signals such that for any $x \in L_2$, $\|x\|_2 := (\int_0^\infty x^T(t)x(t)dt)^{1/2} < \infty$. The H_∞ norm (more precisely, L_2 gain) of a stable LPV system G_ρ with input d and output e is defined as

$$\|G_\rho\|_\infty = \sup_{u \in \mathcal{L}_2, \|u\|_2 \neq 0} \sup_{\rho(\cdot) \in \mathcal{F}_{\mathcal{P}}^v} \frac{\|e\|_2}{\|d\|_2}$$

16.2 Review of LPV Control Techniques

In this section, some background knowledge of LPV control theory will be provided. More details can also be founded in [1, 2, 37].

The LPV system P_ρ is a class of linear systems with its state-space matrices depending continuously on a time-varying vector $\rho(t)$

$$\dot{x}(t) = A(\rho(t))x(t) + B_1(\rho(t))d(t) + B_2(\rho(t))u(t), \quad (16.1)$$

$$e(t) = C_1(\rho(t))x(t) + D_{11}(\rho(t))d(t) + D_{12}(\rho(t))u(t), \quad (16.2)$$

$$y(t) = C_2(\rho(t))x(t) + D_{21}(\rho(t))d(t) + D_{22}(\rho(t))u(t) \quad (16.3)$$

where the state $x \in \mathbf{R}^n$. u is control input and y is measured output. d is disturbance and e is controlled output. It is assumed that the scheduling parameter ρ evolves continuously over time and its range is limited to a compact set $\rho \in \mathcal{P} \subset \mathbf{R}^s$.

In addition, its time derivative is bounded and satisfies the constraint $\underline{v}_k \leq \dot{\rho}_k \leq \bar{v}_k$, $k = 1, 2, \dots, s$. Moreover, it is assumed that

(A1) The matrix triple $(A(\rho), B_2(\rho), C_2(\rho))$ is parameter-dependent stabilizable and detectable

(A2) The matrices $D_{21}(\rho)$ and $D_{12}^T(\rho)$ have full-row rank for all $\rho \in \mathcal{P}$

(A3) $D_{22}(\rho) = 0$

For LPV plant, the parameter ρ is measurable in real time. Therefore, it is possible to construct the LPV controller whose dynamics adjust according to the variation in the plant. To this end, consider the LPV output feedback controller K_ρ in the form of

$$\dot{x}_k(t) = A_k(\rho(t), \dot{\rho}(t))x_k(t) + B_k(\rho(t))y(t), \quad (16.4)$$

$$u(t) = C_k(\rho(t))x_k(t) + D_k(\rho(t))y(t) \quad (16.5)$$

where $x_k \in \mathbf{R}^{n_k}$. The state dimension n_k is yet to be determined. Note that the controller gain will be scheduled by parameter ρ and its derivative $\dot{\rho}$ in general.

Using a parameter-dependent quadratic Lyapunov function $V(x) = x_{cl}^T P(\rho) x_{cl}$, the solution of the H_∞ LPV output feedback synthesis problem [2, 37] is to find a pair of continuously differentiable matrix functions $R(\rho), S(\rho) \in \mathbf{S}_+^{n \times n}$ which satisfy

$$\begin{aligned} & \begin{bmatrix} N_R(\rho) & 0 \\ 0 & I \end{bmatrix}^T \begin{bmatrix} \left\{ \begin{array}{l} A(\rho)R(\rho) + R(\rho)A^T(\rho) \\ -\sum_{i=1}^s \{ \underline{v}_i, \bar{v}_i \} \frac{\partial R}{\partial \rho_i} \end{array} \right\} R(\rho)C_1^T(\rho) & B_1(\rho) \\ C_1(\rho)R(\rho) & -\gamma I & D_{11}(\rho) \\ B_1^T(\rho) & D_{11}^T(\rho) & -\gamma I \end{bmatrix} \\ & \times \begin{bmatrix} N_R(\rho) & 0 \\ 0 & I \end{bmatrix} < 0 \end{aligned} \quad (16.6)$$

$$\begin{aligned} & \begin{bmatrix} N_S(\rho) & 0 \\ 0 & I \end{bmatrix}^T \begin{bmatrix} \left\{ \begin{array}{l} A^T(\rho)S(\rho) + S(\rho)A(\rho) \\ +\sum_{i=1}^s \{ \underline{v}_i, \bar{v}_i \} \frac{\partial S}{\partial \rho_i} \end{array} \right\} S(\rho)B_1(\rho) & C_1^T(\rho) \\ B_1^T(\rho)S(\rho) & -\gamma I & D_{11}^T(\rho) \\ C_1(\rho) & D_{11}(\rho) & -\gamma I \end{bmatrix} \\ & \times \begin{bmatrix} N_S(\rho) & 0 \\ 0 & I \end{bmatrix} < 0 \end{aligned} \quad (16.7)$$

$$\begin{bmatrix} R(\rho) & I \\ I & S(\rho) \end{bmatrix} \geq 0 \quad (16.8)$$

for all $\rho \in \mathcal{P}$. $N_R(\rho) = \ker [B_2^T(\rho) D_{12}^T(\rho)]$, $N_S(\rho) = \ker [C_2(\rho) D_{21}(\rho)]$. After solving the synthesis condition, one n th-order LPV controller can be constructed as

$$\begin{aligned}
A_k(\rho, \dot{\rho}) = & -N^{-1}(\rho) \left\{ \hat{A}^T(\rho) + S(\rho) [\hat{A}(\rho) + \hat{B}_2(\rho)F(\rho) + L(\rho)\hat{C}_2(\rho)] R(\rho) \right. \\
& + \sum_{i=1}^s \left(\dot{\rho}_i \frac{\partial S}{\partial \rho_i} \right) R(\rho) + \frac{1}{\gamma} S(\rho) [\hat{B}_1(\rho) + L(\rho)\hat{D}_{21}(\rho)] D_i(\rho) \hat{B}_1^T(\rho) \\
& \left. + \frac{1}{\gamma} \hat{C}_1^T(\rho) D_h(\rho) [\hat{C}_1(\rho) + \hat{D}_{12}(\rho)F(\rho)] R(\rho) \right\} M^{-T}(\rho), \quad (16.9)
\end{aligned}$$

$$B_k(\rho) = N^{-1}(\rho) S(\rho) L(\rho), \quad (16.10)$$

$$C_k(\rho) = F(\rho) R(\rho) M^{-T}(\rho), \quad (16.11)$$

$$D_k(\rho) = \Pi(\rho), \quad (16.12)$$

where $M(\rho)N^T(\rho) = I - R(\rho)S(\rho)$. $F(\rho)$, $L(\rho)$ and $\Pi(\rho)$ are defined as

$$F(\rho) = - [D_{12}^T(\rho) D_h(\rho) D_{12}(\rho)]^{-1} [D_{12}^T(\rho) D_h^T(\rho) \hat{C}_1(\rho) + \gamma \hat{B}_2^T(\rho) R^{-1}(\rho)],$$

$$L(\rho) = - [\hat{B}_1(\rho) D_i^T(\rho) D_{21}^T(\rho) + \gamma S^{-1}(\rho) \hat{C}_2^T(\rho)] [D_{21}(\rho) D_i(\rho) D_{21}^T(\rho)]^{-1}$$

$$\begin{aligned}
\Pi(\rho) = & -\hat{D}_{12}(\rho) \left\{ \left[I - \frac{1}{\gamma^2} D_{11}(\rho) (I - \hat{D}_{21}(\rho) D_{21}(\rho)) D_{11}^T(\rho) \right. \right. \\
& \left. \left. \times (I - D_{12}(\rho) \hat{D}_{12}(\rho)) \right]^{-1} D_{11}(\rho) \right\} \hat{D}_{21}(\rho)
\end{aligned}$$

with

$$D_i(\rho) = \left[I - \frac{1}{\gamma^2} \hat{D}_{11}^T(\rho) \hat{D}_{11}(\rho) \right]^{-1},$$

$$D_h(\rho) = \left[I - \frac{1}{\gamma^2} \hat{D}_{11}(\rho) \hat{D}_{11}^T(\rho) \right]^{-1},$$

$$\hat{A}(\rho) = A(\rho) + B_2(\rho) \Pi(\rho) C_2(\rho) + \frac{1}{\gamma^2} \hat{B}_1(\rho) \hat{D}_{11}^T(\rho) D_h(\rho) \hat{C}_1(\rho),$$

$$\hat{B}_1(\rho) = B_1(\rho) + B_2(\rho) \Pi(\rho) D_{21}(\rho),$$

$$\hat{B}_2(\rho) = B_2(\rho) + \frac{1}{\gamma^2} \hat{B}_1(\rho) \hat{D}_{11}^T(\rho) D_h(\rho) D_{12}(\rho),$$

$$\hat{C}_1(\rho) = C_1(\rho) + D_{12}(\rho) \Pi(\rho) C_2(\rho),$$

$$\hat{C}_2(\rho) = C_2(\rho) + \frac{1}{\gamma^2} D_{21}(\rho) \hat{D}_{11}^T(\rho) D_h(\rho) \hat{C}_1(\rho),$$

$$\hat{D}_{11}(\rho) = D_{11}(\rho) + D_{12}(\rho)\Pi(\rho)D_{21}(\rho),$$

$$\hat{D}_{12}(\rho) = [D_{12}^T(\rho)D_{12}(\rho)]^{-1}D_{12}^T(\rho),$$

$$\hat{D}_{21}(\rho) = D_{21}^T(\rho)[D_{21}(\rho)D_{21}^T(\rho)]^{-1}$$

The LPV synthesis condition is given by the set of infinite-dimensional linear matrix inequalities (LMIs) as a convex problem. The optimal H_∞ performance of closed-loop P_ρ with K_ρ can be obtained by minimizing the performance level γ using efficient interior point optimization techniques. Nevertheless, the optimization variables are matrix functions $R(\rho)$ and $S(\rho)$. They must be parameterized using a finite number of basis functions [37] as

$$R(\rho) = \sum_{i=1}^{N_f} f_i(\rho)R_i \quad S(\rho) = \sum_{j=1}^{N_g} g_j(\rho)S_j$$

where $f_i(\rho), i = 1, 2, \dots, N_f$ and $g_j(\rho), j = 1, 2, \dots, N_g$ are user specified basis functions. For the special cases when $R(\rho)$ or $S(\rho)$ is constant, the controller gains will not depend on $\dot{\rho}$, but on ρ only. Furthermore, it is noted that the synthesis condition is specified over the entire parameter set \mathcal{P} . This means that the LMIs involve an infinite number constraints. To resolve this problem, the parameter space will be gridded such that a finite number of points for each parameter in the system will be chosen to represent the system as a whole. It is important to realize that each of these discretized parameter points will represent a linear model of the system. Therefore, these gridding points will be chosen in a way such that the discrete points are close enough that the range for which each linearized region is valid overlaps with another gridding point. Once the parametrization and gridding have taken place, the LPV synthesis problem can be solved.

16.3 Hypersonic Vehicle Modelling

This section will present the nonlinear equations of motion for the hypersonic vehicle as originally derived by Blender and Doman [6]. Based on this set of nonlinear equations of motion, an LPV model will be derived.

16.3.1 Nonlinear Equations of Motion

By assuming the structure of vehicle body as a free-free beam, it decouples the rigid body dynamics from the elastic modes and the equation of motion consists of a set of equations for the traditional rigid body motion and a set for the flexible mode vibrations [5]. As a result, the longitudinal equation of motion of the flexible hypersonic vehicle is given by

$$\dot{V}_t = \frac{T \cos \alpha - D}{m} - g \sin(\theta - \alpha), \quad (16.13)$$

$$\dot{\alpha} = \frac{-L - T \sin \alpha}{mV_t} + \frac{g}{V_t} \cos(\theta - \alpha) + Q, \quad (16.14)$$

$$\dot{Q} = \frac{M_p}{I_{yy}}, \quad (16.15)$$

$$\dot{h} = V_t \sin(\theta - \alpha), \quad (16.16)$$

$$\dot{\theta} = Q, \quad (16.17)$$

$$\dot{\eta}_i = -2\zeta_i \omega_{n_i} \dot{\eta}_i - \omega_{n_i}^2 \eta_i + N_i, \quad i = 1, 2, \dots, n, \quad (16.18)$$

where $V_t, \alpha, Q, h, \theta$ are true airspeed, angle-of-attack, pitch rate, altitude, and pitch attitude of the vehicle. T, D, L are thrust, drag, and lift forces. M_p is the pitching moment and I_{yy} is the moment of inertia. The elasticity of the vehicle is described by the flexible modes in (16.18), where $\eta_i, \omega_i, \zeta_i$, and N_i are generalized flexible coordinate, natural frequencies, and damping coefficients of the i th elastic mode and its associated modal force.

The vibrational mode of fuselage is derived using assumed mode method [36], which determines the evolution of natural frequencies and their associated mode shapes. This technique chooses the mode shapes of a simple structure (e.g., a free-free beam) as a set of basis functions to generate approximated mode shapes for the actual structure and accounts for the actual mass and stiffness distribution of the true structure. Typically, as the number of basis functions increases, the first few approximated natural frequencies and mode shapes will converge to their true values quickly. It is necessary to use a model with less elastic modes as additional flexible states will make the controller synthesis more complicated. Bolender and Doman used only three vibrational modes in their study. Williams et al. have shown that there is a good convergence of the first natural frequency with only three elastic modes [6, 36]. Simulation and open-loop analysis also verify that three modes will accurately capture the flexible effects of the hypersonic vehicle [21].

As a result, the state variables of HSV longitudinal dynamics include five rigid body states $V_t, \alpha, Q, h, \theta$ and six flexible states $\eta_1, \dot{\eta}_1, \eta_2, \dot{\eta}_2, \eta_3, \dot{\eta}_3$ describing its first three elastic modes. In the latest HSV configuration, a canard was added as a redundant pitch control effector at the forebody of vehicle to enlarge the angle and velocity control bandwidth [5]. Thus the control inputs are $\delta_e, \delta_c, \phi, A_d$, which are elevator angle, canard angle, throttle ratio, and diffuser area ratio. These control inputs do not appear directly in the equations of motion (16.13)–(16.18), but enter them through the forces and moment T, L, D, N_i , and M_p . Equations (16.13)–(16.18) represent the total nonlinear equations of motion for the flexible hypersonic vehicle.

Since the modeling of HSVs is not the main focus of this research, the derivation of aerodynamics, propulsion system, and flexible modes governing the equations of motion will be omitted here. Interested readers may refer to [4–6, 36] for more details.

Table 16.1 Actuator saturation limits

Actuator	Lower limit	Upper limit
δ_e	$-\frac{\pi}{12}$	$\frac{\pi}{6}$
δ_c	$-\frac{\pi}{9}$	$\frac{\pi}{9}$
ϕ	0.1	0.77
A_d	0.01	1

16.3.2 Actuator Dynamics

Though it is not a part of the equations of motion as shown in the previous subsection, it is important to include the actuator dynamics of the HSV. Specifically, there are bandwidth limitations as well as saturation limits imposed by the actuators in the system. If the control command is outside of the operating range of the actuators or if the desired actuator response is faster than the actuator can perform, then the hypersonic vehicle will lose its control capability. This motivates the need to include actuator dynamics in the control design and simulation study.

Attempts have been made to model the actuator dynamics using simple second-order differential equations [17, 28]. The second-order model does potentially describe the actuator dynamics, but for the purposes of this chapter it was decided that a simpler model would be preferable. As suggested by Groves et al. and Sigthorsson et al., the actuators can be modeled as low pass filters [20, 31]. This will incorporate a bandwidth limitation on the actuator response without concerns about their internal mechanism. Therefore, the actuator dynamics are

$$\dot{x}_d = A_d x_d + B_d u_d \quad (16.19)$$

where

$$A_d = \begin{bmatrix} -20 & 0 & 0 & 0 \\ 0 & -20 & 0 & 0 \\ 0 & 0 & -10 & 0 \\ 0 & 0 & 0 & -10 \end{bmatrix}, \quad B_d = \begin{bmatrix} 20 & 0 & 0 & 0 \\ 0 & 20 & 0 & 0 \\ 0 & 0 & 10 & 0 \\ 0 & 0 & 0 & 10 \end{bmatrix}$$

In the actuator dynamics, the cutoff frequency for δ_e and δ_c is roughly 20 Hz, while the cutoff frequency for ϕ and A_d is chosen as 10 Hz. This will render the actuator response of the control command within a realistic range.

It will also be necessary to apply saturation limits to the actuators themselves, but this will be taken care of in the nonlinear simulation only. Table 16.1 shows the saturation limits imposed upon the actuators.

16.3.3 Model Linearization

When designing an H_∞ LPV controller, the nonlinear HSV dynamics will be turned into a finite number of linearized models for a set of given parameters to the system.

Table 16.2 State and control input bounds in solving trim points

States	Control inputs
$\alpha \in [0, \pi/60]$ rad	$\delta_c \in [\pi/30, \pi/12]$ rad
$Q = 0$ rad/s	$\delta_c \in [-\pi/9, \pi/9]$ rad
$\theta \in [0, \pi/60]$ rad	$\phi \in [0.15, 0.5]$
$\eta_i \in [0, 1]$	$A_d \in [0.75, 0.95]$
$\dot{\eta}_i = 0$	

Linear controllers are then synthesized at each of these linearized points through LPV control techniques.

To derive LPV models of HSV, the velocity and altitude were chosen as the scheduling parameters, i.e., $\rho = [V_t \ h]^T$ and a flight envelop with Mach number $M \in [7, 9]$ and altitude $h \in [70,000, 90,000]$ ft was specified. For better controlled performance, it is important to have LPV models as close to the nonlinear HSV dynamics as possible. Basically, the more gridding that is chosen, the better the approximation the LPV plant will be. Nevertheless, the computational cost of solving LPV controller synthesis conditions will increase exponentially for more gridding points.

Based on the nonlinear HSV model (16.13)–(16.18), the trim conditions (equilibrium points) can be calculated through a constrained optimization approach. At each trim point, V_t and h will be fixed at their gridding value. Pitch rate Q and all elastic mode derivatives $\dot{\eta}_i$ are also set to 0. Moreover, all other states and inputs are constrained within desired states and actuator ranges as listed in Table 16.2.

Subsequently, the linearized LPV model can be obtained by linearizing the nonlinear HSV dynamics at specified trim points by Jacobian linearization. The resulting state vectors for the linearized plant will be

$$x_{p,f} = [V_t \ \alpha \ Q \ h \ \theta \ \eta_1 \ \dot{\eta}_1 \ \eta_2 \ \dot{\eta}_2 \ \eta_3 \ \dot{\eta}_3]^T, \quad (16.20)$$

$$x_{p,r} = [V_t \ \alpha \ Q \ h \ \theta]^T \quad (16.21)$$

where the subscripts f and r in the linearized states $x_{p,*}$ denote the flexible and rigid bodies, respectively. Note that there are 11 states in the flexible model while there are only 5 of them in the rigid body model.

For this particular study, total of 49 linearized models will be derived based upon the variation of the velocity and altitude of the vehicle. These linearized models will be obtained by gridding the parameter space $M \times h$ with seven points evenly in each dimension. Then the LPV system describing the linearized dynamics at the trim conditions will be

$$\dot{x}_{p,*} = A_{p,*}(\rho)x_{p,*} + B_{p,*}(\rho)u, \quad (16.22)$$

$$y_{p,*} = C_{p,*}(\rho)x_{p,*} \quad (16.23)$$

By checking all linearized models, it was found that all LPV models are unstable. Moreover, $\{A(\rho), B_2(\rho)\}$ pair is controllable, and $\{A(\rho), C_2(\rho)\}$ pair is observable. These linearized models of HSV will be used to construct the open-loop interconnected plant.

16.4 LPV Control Synthesis

This section will discuss output feedback control design for the HSV velocity tracking problem. It may not always be feasible to measure all the states of the HSV system because of physical or fiscal limitations. Therefore, output feedback control is more realistic for the hypersonic vehicle. Because of the importance of elastic modes to HSV, this study will also examine the differences between the synthesis using a rigid body model versus a flexible body one. It is important to look at the effects of elastic modes on the system. By making the comparison between the rigid body controller and the flexible body controller, it will be determined whether it is necessary to include the flexible body dynamics into the control synthesis.

16.4.1 *Open-Loop Interconnection*

To synthesize an output feedback controller, it will be necessary to construct the open-loop interconnected plant at each trim condition. It is assumed that the only five rigid body states that are not directly associated with the flexibility of the hypersonic vehicle are measurable. The remaining six states that represent elastic modes of the vehicle will be estimated within the control algorithm. These assumptions were made on the basis that it would be difficult to actually measure the flexible body states which are dependent upon the displacement of the vehicle body itself with respect to the rigid body states. In principle, there would be some noise present in the sensors. Therefore the rigid body control case is still considered to be output feedback because all five measured rigid body states will have sensor noise added into them.

To improve steady-state tracking performance, the integral of the error between the reference velocity and the actual velocity of the vehicle will be added as a state to the open-loop system. Augmenting the linearized plant model (16.22) and (16.23) with the actuator dynamics (16.19) along with the integral state will give the open-loop interconnected plant, as shown in Fig. 16.2. It can be seen from Fig. 16.2a that the linearized plant P has five rigid body states as output from the block. The flexible body model, P , has eleven states, but there will only be five states in P for the rigid-body case. Additionally, W_{act} represents the actuator dynamics from (16.19).

Figure 16.2b shows the augmented plant P_{act} has six measured outputs and six controlled outputs. The measured outputs are the five rigid body states, and the integral of the tracking error. The controlled outputs include altitude, the integral state, and four actuator outputs. This setup will render an integral and a proportional feedback action for the control design. The integral feedback provides zero steady-state error tracking of the velocity, while the proportional control will regulate the altitude of the HSV. This means that the altitude will never actually converge to a

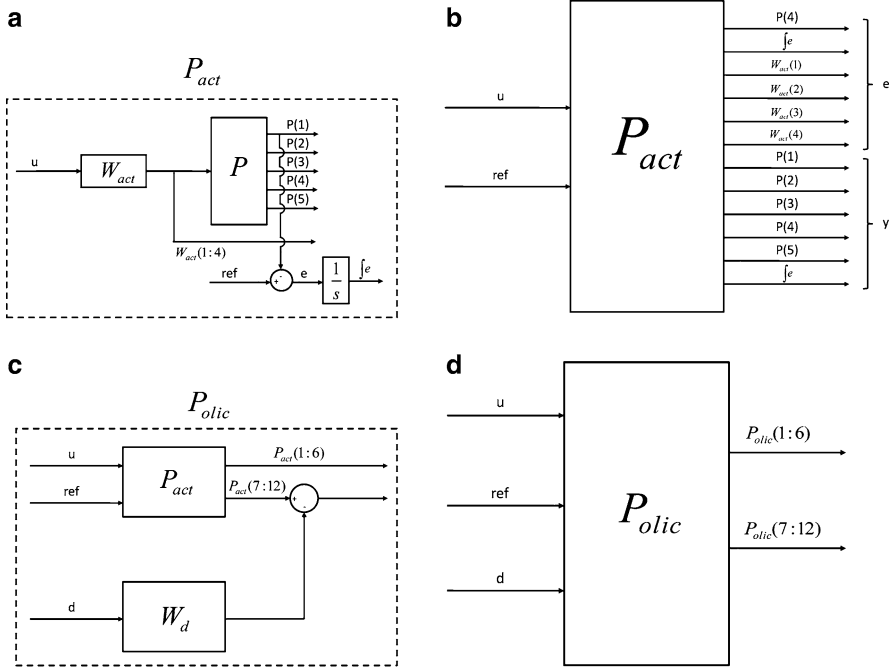


Fig. 16.2 Open-loop interconnection for the output feedback velocity tracking problem (a) Plant with actuator and integral augmentation (b) P_{act} (c) Plant with weighted disturbance (d) Open-loop interconnected plant

value, but the change in the altitude will be minimized. To this end, a weighting function W is introduced to penalize the controlled output as

$$W = \begin{bmatrix} 1 & 0 & 0 & 0 & 0 & 0 \\ 0 & .5 & 0 & 0 & 0 & 0 \\ 0 & 0 & 1,000 & 0 & 0 & 0 \\ 0 & 0 & 0 & 1,000 & 0 & 0 \\ 0 & 0 & 0 & 0 & 316.2778 & 0 \\ 0 & 0 & 0 & 0 & 0 & 1,000 \end{bmatrix}$$

Note that a frequency-dependent weighting function could yield an even better result than the constant weight function used here. In this weighting function, the first two terms are applied to the error states in the system, and the last four terms are applied to the actuator efforts. By selecting this weighting function, the controller will penalize the control efforts heavily. It is beneficial to choose high weightings on the outputs associated with the actuator efforts in the system to keep the actuators from saturation. On the other hand, the weights on the error states are chosen much

smaller. Consequently, the augmented plant P_{act} will be

$$P_{\text{act}} \stackrel{ss}{=} \left[\begin{array}{c|cc} A_{\text{act}}(\rho) & B_{1\text{act}}(\rho) & B_{2\text{act}}(\rho) \\ \hline WC_{1\text{act}}(\rho) & WD_{11\text{act}}(\rho) & WD_{12\text{act}}(\rho) \\ C_{2\text{act}}(\rho) & D_{21\text{act}}(\rho) & D_{22\text{act}}(\rho) \end{array} \right].$$

The augmented plant P_{act} is then combined with disturbance vector $d \in \mathbf{R}^6$, as shown in Fig. 16.2c. W_d is a weighting function capturing the disturbance characteristics and is defined as

$$W_d = \begin{bmatrix} .01 & 0 & 0 & 0 & 0 & 0 \\ 0 & .01 & 0 & 0 & 0 & 0 \\ 0 & 0 & .01 & 0 & 0 & 0 \\ 0 & 0 & 0 & .01 & 0 & 0 \\ 0 & 0 & 0 & 0 & .01 & 0 \\ 0 & 0 & 0 & 0 & 0 & .01 \end{bmatrix}$$

These disturbances are added to the measured states as well as the integral state. They are intended to represent measurement noise and the disturbance to the integration of the error state representing numerical error during the integration process.

Finally, the open-loop interconnected plant P_{olic} can be seen in Fig. 16.2d. The state vector of P_{olic} is $x = [x_{p,*} \ \delta_e \ \delta_c \ \phi \ A_d \ \int(\text{ref} - v)dt]^T$. As a result, the number of states for flexible and rigid body cases are 16 and 10, respectively. The measured output from P_{olic} is $y = [V_t \ \alpha \ Q \ h \ \theta \ \int(\text{ref} - v)dt]^T$, while controlled output $e = [h \ \int(\text{ref} - v)dt \ \delta_e \ \delta_c \ \phi \ A_d]^T$. The system has the control input $u = [\delta_e \ \delta_c \ \phi \ A_d]^T$, the reference velocity, and the disturbance as inputs. Therefore, there are total of 12 outputs and 11 inputs for the interconnected plant.

This concludes the setup of the open-loop interconnection at a single trim condition for both the flexible and rigid body cases. By extension, this method can be applied to all of the chosen trim conditions for the hypersonic vehicle.

16.4.2 LPV H_∞ Control Design

After a set of open-loop interconnected plants has been generated, it is possible to synthesize a set of LPV H_∞ controllers for the hypersonic vehicle. The LPV output-feedback synthesis condition consists of three LMIs as seen in (16.6)–(16.8). Before these LMIs can be solved, matrix functions $R(\rho)$ and $S(\rho)$ must be parameterized. In this study, the basis function vectors $f(\rho)$ and $g(\rho)$ take the form of

Table 16.3 γ performance for different parameter variation rates

Parameter variation bound ν	Flexible body γ	Rigid body γ
[.01 200]	112.7380	83.2507
[.05 200]	112.9252	83.4346
[.1 200]	113.2146	83.6931
[.2 200]	113.6599	84.1999
[.3 200]	114.2606	84.7131
[.4 200]	115.2945	85.1583
[.5 200]	116.9904	85.6793
[.1 50]	113.1878	84.1295
[.1 100]	113.1951	84.1639
[.1 300]	113.2558	84.2772
[.1 400]	113.4078	84.4805
[.1 500]	114.3578	84.9415
[.5 500]	117.9836	86.6760

$$f(\rho) = [1 \ \rho_1 \ \rho_2]^T \quad g(\rho) = [1].$$

Therefore, $R(\rho)$ and $S(\rho)$ are parameterized as $R(\rho) = R_0 + \rho_1 R_1 + \rho_2 R_2$ and $S(\rho) = S_0$. Since $S(\rho)$ is constant, the controller gains will depend only on ρ but not $\dot{\rho}$. It is also necessary to define a set of bounds for the parameter variation rate ν such that $|\dot{\rho}| \leq \nu$. The first term of ν will represent the limitation on how quickly the Mach number of the hypersonic vehicle can change. The second term describes how fast the altitude can change.

Based on a 7×7 gridding point, the synthesis conditions (16.6)–(16.8) have been solved using efficient LMI techniques [7, 16]. After obtaining $R(\rho)$, $S(\rho)$, and the performance level γ , the LPV output feedback controller gains can be calculated using (16.9)–(16.12). It has been verified that these controllers stabilize their corresponding linearized models as expected.

After the LPV controller for the hypersonic vehicle is established, it would be interesting to examine the effects that differing parameter variation bounds and differing numbers of gridding points have on the control synthesis results. This parametric study will be used to guide the design and selection of the LPV controller, and then analyze the response of the resulting closed-loop system.

The selection of the parameter variation bounds could affect the trade-off between the robust capabilities and the performance associated with the H_∞ LPV control problem. Therefore, it is beneficial to investigate the effect of the parameter variation bounds ν on the H_∞ performance level, γ . Table 16.3 shows that the smaller parameter variation rate limits yield lower γ values, which translates to improved robust performance for the system. However, there are limitations on the rate of change in Mach number and altitude imposed by the hypersonic vehicle operation requirement. For this study, it was decided that the case where $\nu = [.1 \ 200]^T$ would provide the best balance between performance and operating capability of the HSV.

Table 16.4 γ performance for different number of gridding points

Grid dimension	Flexible body			Rigid body		
	γ	LMIs	OVs	γ	LMIs	OVs
4×4	93.4078	96	545	61.1913	96	221
5×5	110.4690	150	545	69.3434	150	221
6×6	110.7171	216	545	77.5342	216	221
7×7	113.2146	294	545	84.1999	294	221

For fixed parameter variation bounds, the effect of additional gridding points on the system's robust capabilities will also be evaluated. Typically in H_∞ LPV control problems, having a denser grid in the parameter space will increase the H_∞ γ performance value since additional LMI constraints will be included in the optimization. For the purposes of this study, however, the change of spacing of the grid points could result in different trim conditions and a different set of linearized plants. To avoid this, the gridding density will be handled by choosing a large set of trim conditions, or removing some of trim conditions from the parameter space. Table 16.4 shows the result of the gridding point study. It is observed that the H_∞ γ performance decreases with less points. Though the smaller gridding sizes may yield a better performance value, it is preferable to use a denser grid to ensure that the entire parameter space is adequately covered by the controllable region of synthesized LPV controllers. For this reason, the 7×7 grid was chosen which results in a total of 49 different linear controllers over the entire parameter space.

Note that there is a difference in the H_∞ performance level between the flexible and rigid body cases. It is observed from Tables 16.3 and 16.4 that the rigid body cases have smaller γ values than the flexible body cases. It makes sense that the rigid body cases would have lower γ values because they are simpler than the flexible body cases. Each flexible body case has 545 optimization variables (OVs) to be solved for, while the rigid body case has 221 optimization variables. As a result, the optimization problem is easier to solve. In addition, less gridding points would lead to less number of LMIs. Therefore, it is conceivable that the rigid body cases would achieve better solutions.

The control synthesis was calculated using Matlab 200d8a on a Dell Precision T5400 with an Intel Xeon processor operating at 2.33 GHz per core and 16 gigabytes of RAM. The operating system was Windows XP 64-bit edition. The synthesis task typically took between four and six hours to complete.

From the design considerations mentioned above, the final output feedback velocity tracking controller for the simulation will have parameter variation bounds of $[-1 \ 200]^T$, a 7×7 grid over the parameter range of $[7, 9] \times [70,000, 90,000]$ ft. The controlled performances are provided in Tables 16.3 and 16.4. Since all of the flexible effects on the rigid body model will be treated as disturbance, this set of controllers will be subject to more disturbance than the flexible cases will. Consequently, the simulation performance will not necessarily be better than that of the flexible body case.

16.5 LPV Control Implementation

There are a total of 49 linear controllers that have been designed for the hypersonic vehicle model at discrete locations of the parameter space. Therefore, there is a need to schedule different controllers as the vehicle moves over the flight envelop. Several different ways of handling this switching exist in the current literature, such as, interpolation, blending, and digital switching, etc.

The design process for the H_∞ LPV controller assumes that the output of each controller is based on the change from its trim conditions for a given linear controller. Denoting the trim values for the plant states and control forces by \bar{x} and \bar{u} , it yields

$$x = \bar{x} + \Delta x, \quad u = \bar{u} + \Delta u, \quad y = \bar{y} + \Delta y.$$

Since the trim conditions are known for the system from the control synthesis and the plant states, x , are known for the system from the nonlinear plant model, it will be possible to calculate the control effort, u , needed. Consequently, the control input for nonlinear HSV will be calculated using the the following equations:

$$\dot{x}_k = A_k x_k + B_k \left[\begin{array}{c} \Delta y \\ \int edt \end{array} \right], \quad (16.24)$$

$$u = \bar{u} + \left(C_k x_k + D_k \left[\begin{array}{c} \Delta y \\ \int edt \end{array} \right] \right) \quad (16.25)$$

where x_k represents the internal states of the output feedback controller. Note that even though the five measured states from the system are with respect to a set of trim conditions, the reference signal does not change with respect to a set of trim conditions. Therefore, it will be beneficial to use a switching algorithm so that the least amount of trim condition changes will be imposed upon the system. There is a potential problem with interpolation type methods. When interpolating the controllers, it is also necessary to interpolate the set of trim conditions \bar{x} and \bar{u} as well. This can pose some stability issues since the interpolated set of trim conditions may not exist, or at least may not be accurately represented by a linear interpolation. It is also difficult to ensure that the resulting controller gains are stabilizing. For this reason, a digital switching algorithm will be implemented due to its simplicity as well as its computational benefits.

With two parameters involved in the H_∞ LPV control, the parameter set can be described by a two-dimensional space. The best possible time to trigger the switch from one controller to the next was if the system reached the next trim condition along a given parameter. Such a switching condition has been shown in Fig. 16.3. It illustrates the switching mechanism once the threshold of the next trim condition has been reached. The idea behind this implementation is that the hypersonic vehicle states will be as close to the trim conditions as possible so that any disturbance

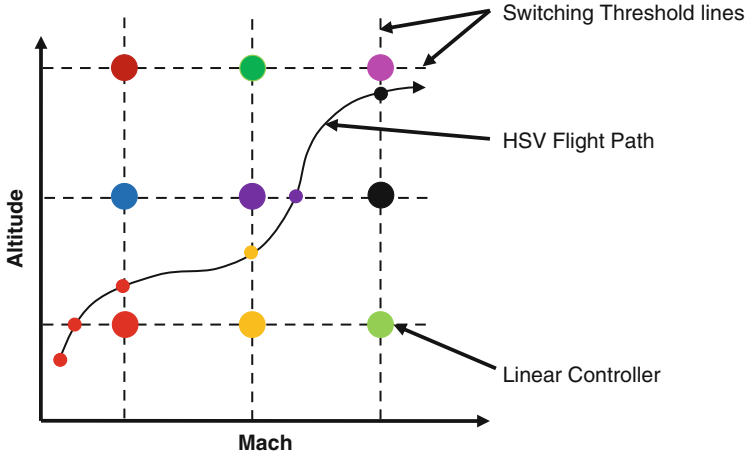


Fig. 16.3 Switching threshold for linear controllers in 2D parameter space along the Mach number axis

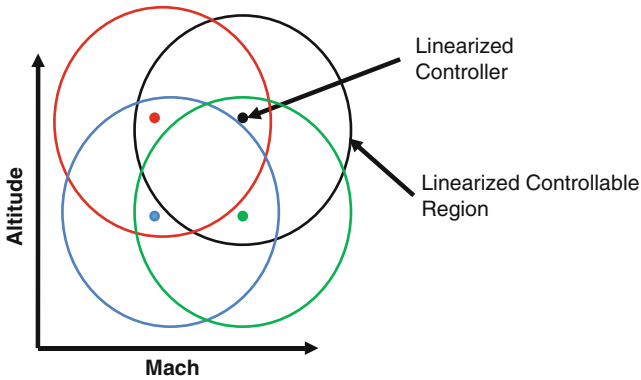


Fig. 16.4 Controllable region for linear controller in 2D parameter space

caused by the controller switch will have minimal effect on the system. This usually results in the controller being switched due to either Mach or altitude, but not both simultaneously.

Moreover, Fig. 16.4 shows that the system is designed such that the controllable region of one trim point overlaps the subsequent trim conditions closest to it in all directions. This requirement can be validated for a given reference command through the nonlinear simulation.

Moreover, it is important to have a method for resetting the integral of error when switching from one controller to the next. Otherwise, there is a risk of running into integral windup which can lead to saturation in the control efforts, or even cause

the system to leave the range of operability. This situation is not quite the same as the problem discussed in the work by Groves et al. [19], which is a situation where the control effort is saturated by the linear controller. In this study, the problem of controller windup is a consequence of building up of the integral state to large values at new trim conditions. This could also lead to the saturation of the control efforts. To counteract this effect, it is proposed to simply reset the integral state such that the change in the control effort was minimized at the switching instant [21]. Since the integral state represents artificial quantities in the system, it is acceptable to change this value during control implementation. In fact, this has often been done in the past with simple PID systems [33]. For the LPV output feedback control, there are also controller states that do not physically represent physical system quantities. They can be reset to gain additional control over the integral windup problem as well. To this end, a suitable switching algorithm was designed to alleviate controller windup.

To minimize the change in the control effort u , a new set of values for the controller state x_k and the integral state $\int e dt$ can be solved through the LMI conditions

$$\begin{aligned}
 & \min \delta \\
 \text{subj. to} & \quad \begin{bmatrix} \delta & u_+^T \\ u_+ & \gamma I \end{bmatrix} > 0 \\
 & \quad V_{\text{cl}}([x_p^- \ x_k^-]) - V_{\text{cl}}([x_p^+ \ x_k^+]) \geq 0 \\
 & \quad u_{\text{lb}} \leq u \leq u_{\text{ub}},
 \end{aligned} \tag{16.26}$$

where $V_{\text{cl}} = x_{\text{cl}}^T P x_{\text{cl}}$ is the closed-loop Lyapunov function. u_{lb} and u_{ub} are the lower and upper limits of the actuators' inputs. By solving this optimization problem at switching instant, it will give the new vector \tilde{x}_k that minimizes the control effort after switching while keeping the Lyapunov function monotonically decreasing the minimal change in the control effort keeps the actuators from saturating and helps to maintain the HSV stability.

16.6 Nonlinear Simulation Study

This section will outline the procedure used to simulate the response of the nonlinear hypersonic vehicle using the previously synthesized controllers. It also examines the results from the nonlinear simulation. Both the rigid and flexible body cases will be discussed. Moreover, it is interesting to study the system responses for both the perturbed and nominal system parameters.

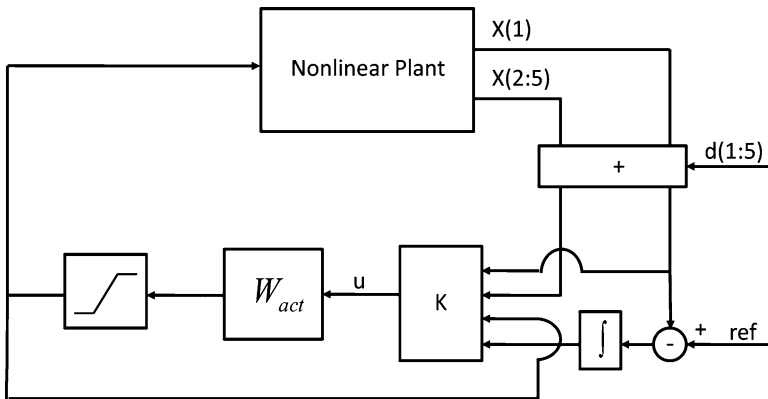


Fig. 16.5 Block diagram of closed loop system for the velocity tracking case

16.6.1 Setup

The block diagram for the HSV velocity tracking problem can be seen in Fig. 16.5. Due to the fact that the measured states are the rigid body states, there is no difference in the block diagram for the flexible and rigid body cases. There are also saturation functions that apply to the actuators, where the saturation levels can be seen in Table 16.1.

For the purpose of simulation, the full nonlinear plant model will be used for both the flexible and rigid body cases. The nonlinear plant used in the simulation is the same model as provided in Sect. 16.3 [5,6]. The flexible effects will help to evaluate the differences between the flexible and rigid body controllers and draw conclusions as to whether the rigid body controller is a valid option to the hypersonic vehicle.

During the nonlinear simulation, a ramp reference signal was chosen for investigating each controller designed. The ramp command represents a gradual change of operating conditions of the HSV. The input starts at the middle of the range for both Mach number and altitude and ends near the end of the range of operation.

The H_∞ LPV controller is intended to control the hypersonic vehicle over a large flight envelop while exhibiting robust capabilities. Robust capabilities are the system's ability to handle uncertainties and perturbations to the system. Uncertainties are considered to be things that may exist in the physical system that are not properly modeled. Perturbations are external disturbance that inject into the system. In this study, some aspects of uncertainty and perturbation in the hypersonic vehicle operation will be investigated.

Some of uncertainty sources of the HSV include thermal effects, fuel consumption (a change in mass), and fluctuations in the atmospheric air data [11, 32, 36]. These all have an impact on the hypersonic vehicle and should be properly modeled for a HSV mission. It is assumed that the thermal effects of the system change

Table 16.5 Sensor noise variance and seed values

State	Seed	Variance
V	23	.01 ft/s
α	1	.00035 rad
Q	314159265	.001 rad/s
h	1.23×10^6	1 ft
θ	61	.001 rad

the vehicle's moment of inertia as well as the length of the vehicle. Additionally, the mass of the vehicle is changed due to fuel consumption and the inaccurate air density, pressure, and temperature from the lookup table [27]. The purpose of adding perturbations to the system is not necessarily to model the effects of uncertainties in the system, but rather to see the effects that modeling error has on the performance of the LPV controllers. Therefore, the emphasis will be to look at the results of changing these parameters as opposed to developing accurate perturbation models. To this end, each of the previously mentioned parameters (air density, air pressure, air temperature, vehicle length, and vehicle moment of inertia) was increased by 5% from their nominal values. This is to capture any changes in the model due to heating and inaccurate air property tables. On the other hand, the value of the vehicle mass was decreased by 5% from its nominal value to capture the fuel consumption during the hypersonic flight. Simulations will be run for perturbed and nominal cases.

There are many external inputs that could affect the hypersonic vehicle. In this study, however, only the sensor noise will be considered for simplicity. Since the HSV is a high-performance vehicle, and given its relatively large price tag, it is suitable to assume that very high quality sensors would be used with relatively small measurement noise. Table 16.5 provides the noise levels, which are modeled as random number blocks in the nonlinear simulation. Though the disturbance for the integration of the error was included in the control synthesis, this will not be added into the simulation as this value would be very small.

16.6.2 Nonlinear Simulation Results

For both flexible and rigid body controllers, a ramp input command signal will be considered. The tracking signal used for this study starts at a velocity of 7,819.6 ft/s and has a slope of 20 ft/s² for a duration of 60 s. After the 60 s interval, the slope of the ramp is reduced 0 ft/s² for a total simulation time of 100 s. The simulation results for both the flexible and rigid body cases can be seen in Figs. 16.6–16.11.

Figure 16.6 shows the velocity, angle of attack, and the pitch rate for both cases. From this figure, the perturbed and nominal cases for both the flexible and rigid body controllers are included. It can be seen that for both the flexible and rigid body cases, the velocity tracking is achieved at essentially the same rate. It should also be noted that the perturbed and nominal cases have the same velocity curve. This

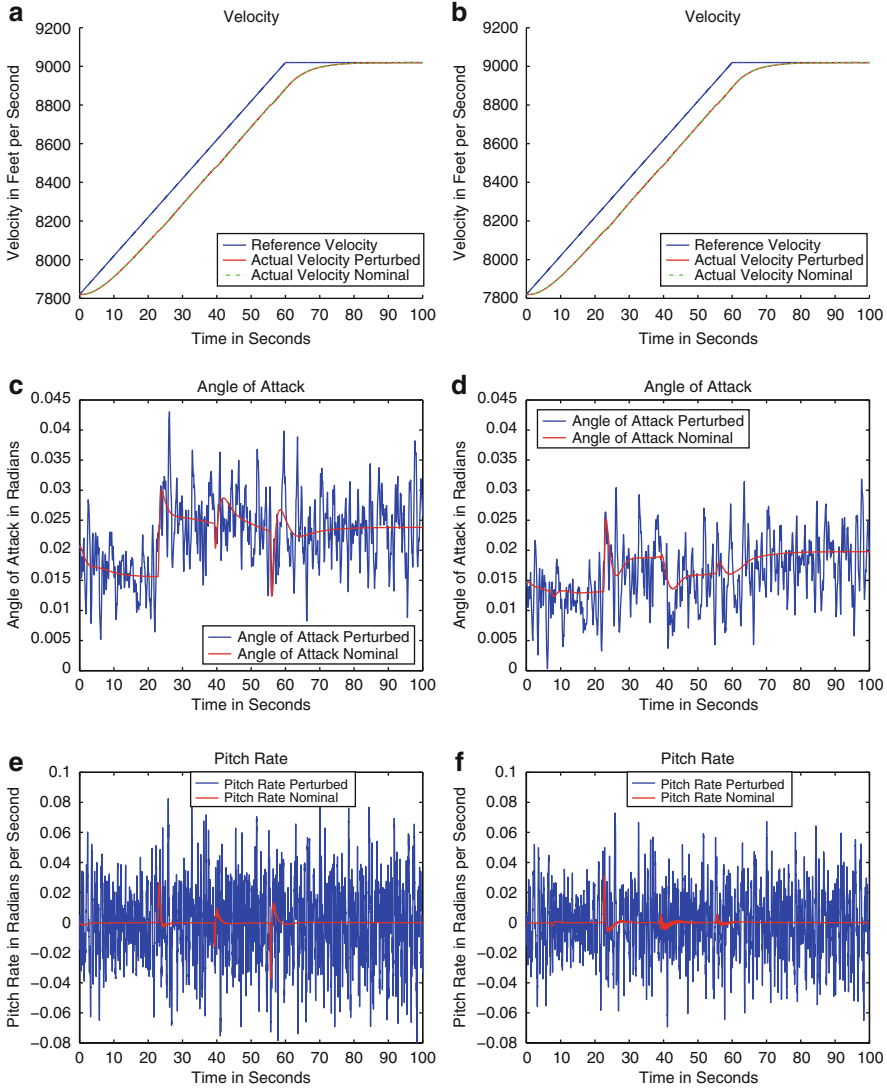


Fig. 16.6 Ramp velocity tracking: Rigid body states (a) Velocity (flexible case) (b) Velocity (rigid case) (c) Angle of attack (flexible case) (d) Angle of attack (rigid case) (e) Pitch rate (flexible case) (f) Pitch rate (rigid case)

shows that the velocity tracking is successful for each case both with and without perturbations in the system. This suggests that a rigid body controller could be used for the velocity tracking case.

Figure 16.6c,d show the angle of attack for the flexible and rigid body cases respectively. These figures show that the maximum angle of attack for the flexible body case is roughly 2.6° , while the maximum angle of attack for the rigid body

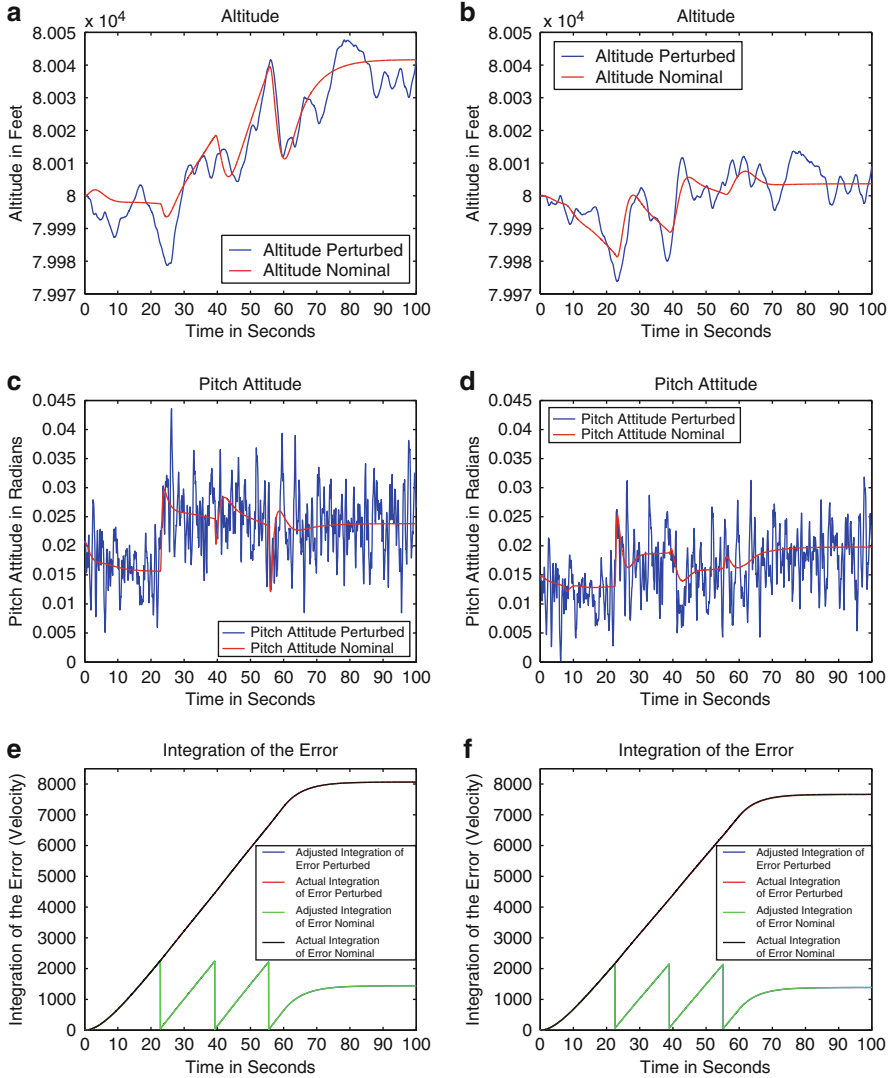


Fig. 16.7 Ramp velocity tracking: Rigid body states and integration error (a) Altitude (flexible case) (b) Altitude (rigid case) (c) Pitch attitude (flexible case) (d) Pitch attitude (rigid case) (e) Integral of tracking error (flexible case) (f) Integral of tracking error (rigid case)

case is roughly 2.0° . There are some minor differences between the responses seen between the angle of attack for the two systems, but what should be noted is the difference seen between the perturbed and nominal cases. It appears as though the hypersonic vehicle angle of attack is very sensitive to perturbation in the system. The propagation of noise is very evident from these figures.

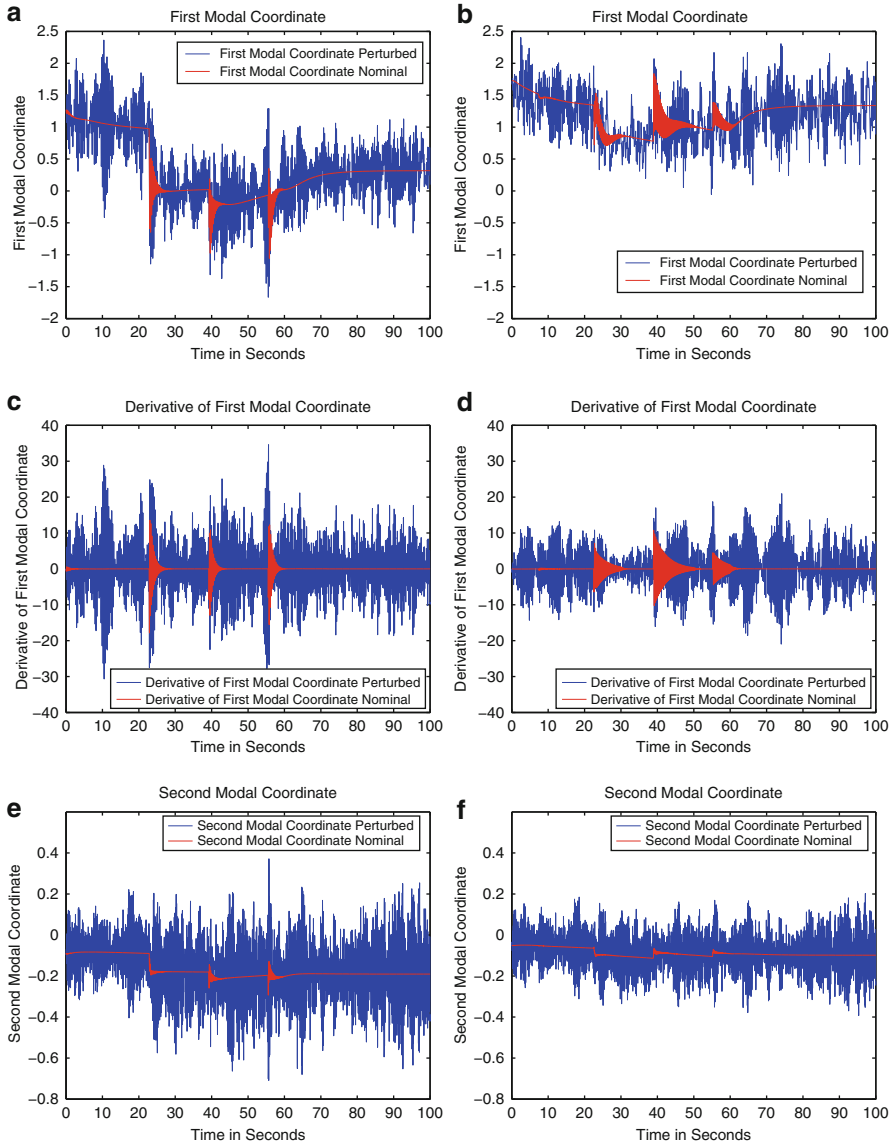


Fig. 16.8 Ramp velocity tracking: Flexible body states I (a) η_1 (flexible case) (b) η_1 (rigid case) (c) $\dot{\eta}_1$ (flexible case) (d) $\dot{\eta}_1$ (rigid case) (e) η_2 (flexible case) (f) η_2 (rigid case)

Figure 16.6e,f show the pitch rate for the two cases, respectively. As seen with the angle of attack, the pitch rate of the vehicle is similar for the flexible and rigid body cases, but this state is also sensitive to perturbation in the system. The maximum pitch rate for the flexible body case is approximately 4.6° , while the maximum pitch rate for the rigid body case is roughly 3.4° . Again it is not desirable to have such an

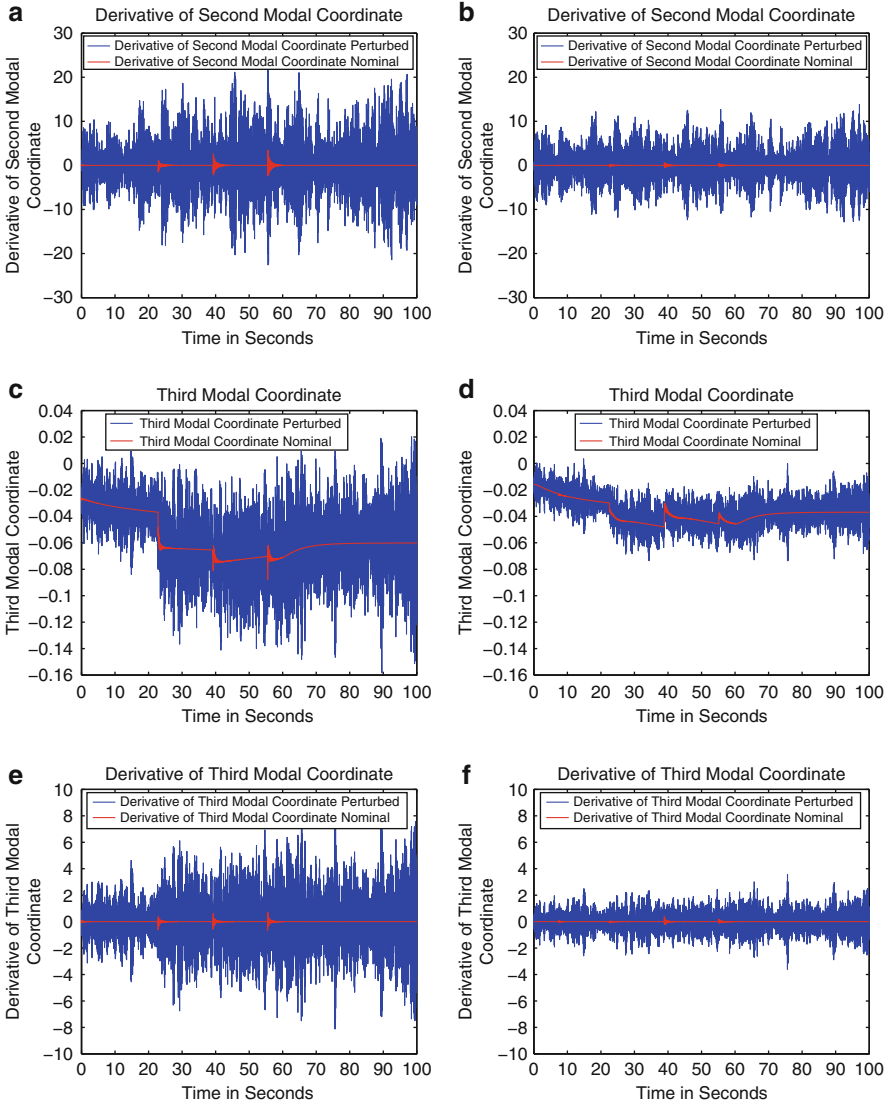


Fig. 16.9 Ramp velocity tracking: Flexible body states II (a) $\dot{\eta}_2$ (flexible case) (b) $\dot{\eta}_2$ (rigid case) (c) $\dot{\eta}_3$ (flexible case) (d) $\dot{\eta}_3$ (rigid case) (e) $\dot{\eta}_3$ (flexible case) (f) $\dot{\eta}_3$ (rigid case)

influence from the perturbation of the system, but the highly coupled nature of the hypersonic vehicle makes this a difficult thing to achieve. The velocity tracking is not effected by the noise in these other states, however, so this simulation is considered a success.

Figure 16.7 shows the altitude, pitch attitude, and the integration of the error for both cases. From this figure, the perturbed and nominal cases for both the flexible and rigid body controllers are included. It is shown that for both cases, the altitude

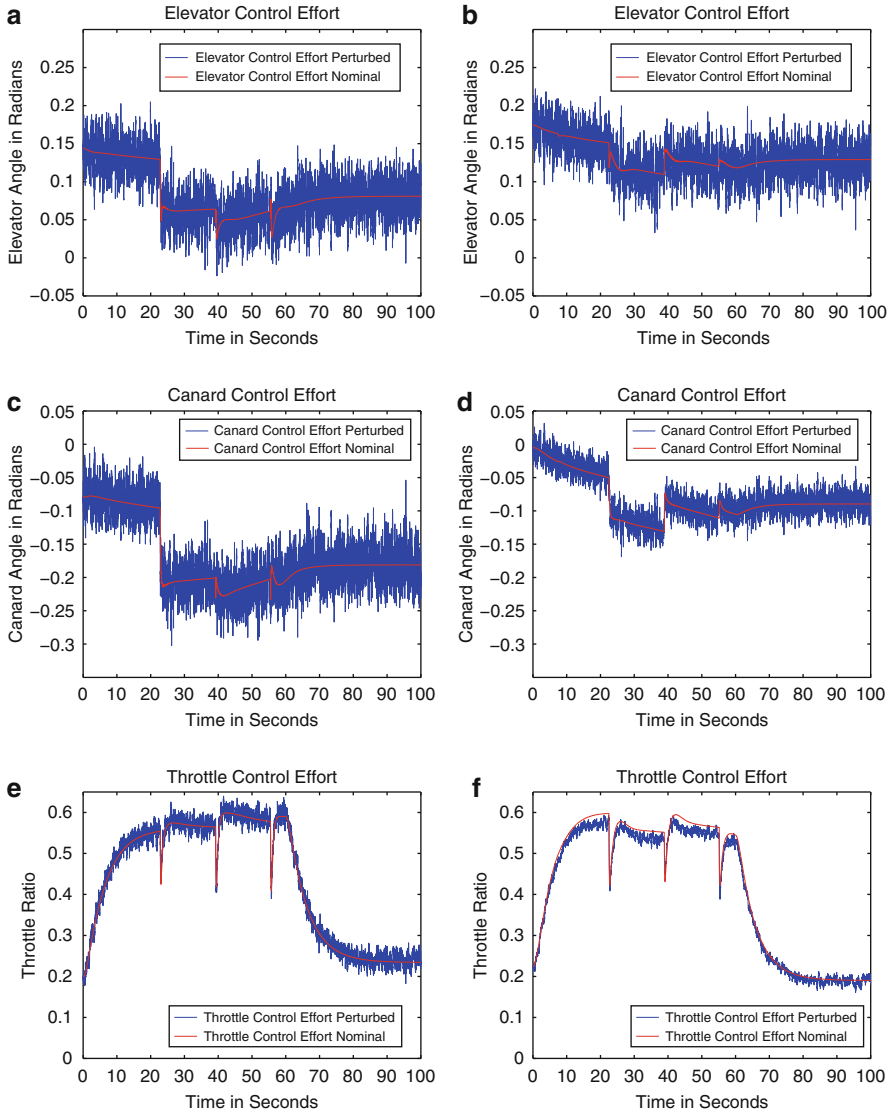


Fig. 16.10 Ramp velocity tracking: Actuator input (a) Elevator (flexible case) (b) Elevator (rigid case) (c) Canard (flexible case) (d) Canard (rigid case) (e) Fuel equivalence ratio (flexible case) (f) Fuel equivalence ratio (rigid case)

of the hypersonic vehicle is close. In fact, the steady-state conditions for the two simulations run have a difference of about 35 ft. It is also shown that the effects of perturbation in the system have only a small effect on the altitude of the vehicle. This is partially due to the fact that there is a unity gain regulating the altitude tracking.

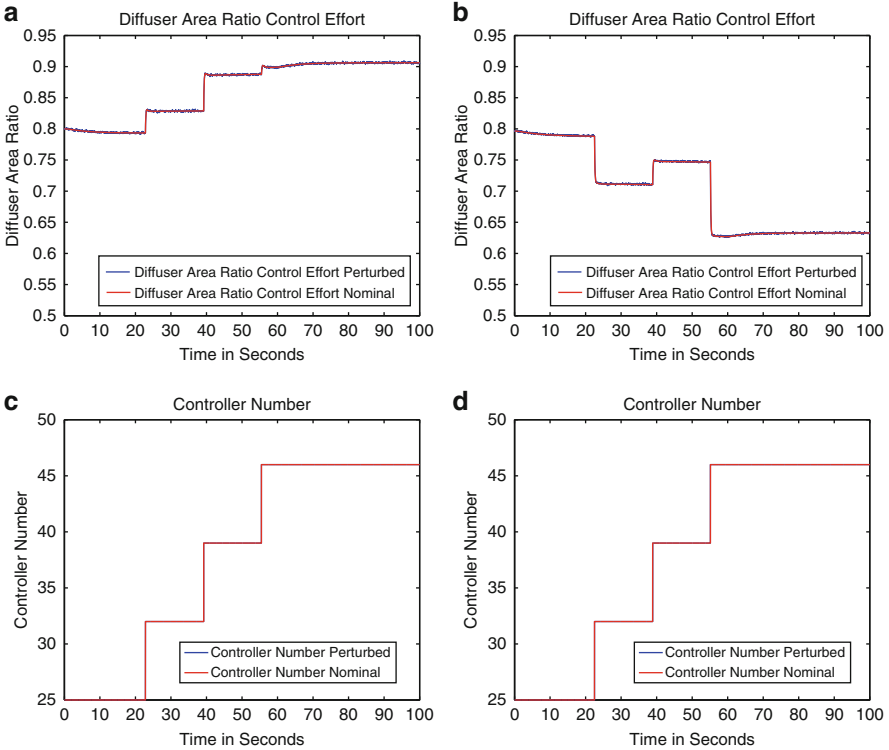


Fig. 16.11 Ramp velocity tracking: controller ID (a) Diffuser area ratio (flexible case) (b) Diffuser area ratio (rigid case) (c) Controller reference number (flexible case) (d) Controller reference number (rigid case)

Since this state is now included as a regulation state in the control synthesis, it is more robust to perturbation in the system.

Figure 16.7c,d show the pitch attitude for the two cases, respectively. From these plots, it can be seen that the perturbation in the system has a large effect on the pitch attitude of the hypersonic vehicle for both the flexible and rigid body cases. The flexible body case has a slightly larger pitch attitude than the rigid body case does. The maximum value of the pitch attitude for the flexible body case is approximately 2.6° while the maximum value for the rigid body case is approximately 2.0° .

Figure 16.7e,f show the integration of the error for the two cases, respectively. From these two figures, it can be seen that the flexible body case accumulates a slightly larger amount of error, but that the adjusted integration of the error is approximately the same for the two cases. Also, it should be noted that the integration of the error is reset when switching takes place in the controller. Both the flexible and rigid body cases are switching at roughly the same times. This would indicate that rigid body assumptions would be valid for controlling the vehicle during velocity tracking.

Figures 16.8 and 16.9 show the flexible modes of the hypersonic vehicle for both cases. It can be seen that the perturbation in the system has a very large effect on the flexibility of the hypersonic vehicle for both the flexible and rigid body cases. From these figures, it can also be seen that the first mode of vibration has a response that is similar in magnitude for the flexible and rigid body cases. The derivative of the first mode of vibration, however, shows that the flexible body case has a higher value. For the higher order modes of vibration and their respective derivatives, the flexible body case has higher values than those seen in the rigid body case. This would signify that the flexible body case does have a slightly larger deflections due to vibration, but since the first mode is the dominant mode, the differences are not significant. This would support the idea that the rigid body controller is suitable for the flexible body case.

Figure 16.10 shows the elevator deflection angle, the canard deflection angle, and the fuel equivalence ratio for the two cases. From this plot, it can be seen that the perturbed case has larger frequencies and magnitudes on their responses than the nominal cases for both the flexible and rigid body controllers. Even though there is a high frequency for the perturbed case, they still fall within the defined bandwidth limitations discussed in Sect. 16.3. Note how the perturbed case oscillates around the nominal case. It appears as though the mean of the perturbed case is the nominal case.

Figure 16.10a,b show the response of the elevator control effort. This plot shows that the flexible body case has a slightly larger range of motion. The rigid body case operates between 2.3° and 12.6° , where the flexible body case operates between -1.7° and 12.0° . Also note that there is a different initial trim value for the flexible and rigid body cases.

Figure 16.10c,d show the response of the canard control effort. As seen with the elevator, the canard plots show that the flexible body case has a slightly larger range of motion. The rigid body case operates between 2.3° and -9.2° , where the flexible body case operates between 0° and -18.3° . Also note that there is a different initial trim value for the flexible and rigid body cases.

Figure 16.10e,f show the response of the fuel equivalence ratio for the two cases, respectively. These two cases have responses that are similar in value. This would make sense seeing as how the velocity and altitude of the vehicle were roughly the same as well. The fuel equivalence ratio is the control effort that is most directly linked to the thrust of the vehicle, so this relationship falls in line with the previous results. Also note how the perturbation has less of an effect on the fuel equivalence ratio as compared to the elevator and canard control efforts.

Figure 16.11a,b show the response of the diffuser area ratio for the two cases, respectively. These two figures show that the perturbation present in the system has very little effect on the diffuser area ratio. It should be noted, however, that the response seen in the flexible body case is completely different from the one seen in the rigid body case.

Figure 16.11c,d show the controller reference numbers for the flexible and rigid body cases, respectively. It should be noted in Figs. 16.6–16.11 that there are spikes or small discontinuities that take place at about 20 s, 40 s, and 60 s into the simulation. These spikes are the results of controller switching. It can be seen from Fig. 16.11c,d that the different cases all switch at approximately the same time, and that they all use the same controllers.

16.7 Conclusions

This chapter has presented the design and simulation of flexible and rigid body output feedback H_∞ LPV controllers for the flexible hypersonic vehicle model. A velocity tracking problem for the HSV is studied and the difference between perturbed and nominal cases is examined. This section will seek to draw some deeper understanding from the control synthesis and nonlinear simulation results of the HSV.

The control synthesis study showed the effects of changing the parameter variation rates as well as the operational range of the vehicle. From the study, it can be concluded that choosing the appropriate parameter variation bounds and operational range on the hypersonic vehicle is critical to the controlled performance and the robust capabilities of the closed-loop HSV system. It is important to trade-off between the computational cost and achievable performance. For this study, it was concluded that an evenly spaced grid containing 49 controllers for the flight envelop from Mach 7 to Mach 9 and an altitude from 70,000 ft to 90,000 ft would be the best option. In addition, the parameter variation bounds were established as $v = [.1 \ 200]^T$ to provide adequate response speeds for the HSV. This is due to its relatively large operational range and its robust capabilities with currently available computational power. After all, it will be important for a designer to make the appropriate decisions when designing an LPV controller for the air-breathing hypersonic vehicle.

From the control synthesis stage, it can be seen that the rigid body controllers have a better H_∞ performance than the flexible body case do. Though this may be the case from the LPV synthesis perspective, it is not supported by the nonlinear simulation study. This is due to the fact that the rigid body controller was synthesized using a rigid body hypersonic vehicle model, but then it was applied to the nonlinear flexible body HSV dynamics. Therefore, there is an additional amount of perturbation in the rigid body model due to the flexible body dynamics.

This study considered the output feedback control strategy for a nonlinear flexible HSV. Even though this may be more realistic than the full-state feedback, some critical assumptions have been made to facilitate the study. It was assumed for this study that all of the rigid body states were measurable. Moreover, the sensor noise was chosen to be relatively small. This choice was made based upon the assumption that an expensive and high performance vehicle like this would require high quality sensors. Though some assumptions that may not accurately represent

the actual system, the nonlinear simulation results have shown the characteristics of an H_∞ LPV controller on flexible HSV. It can be seen that the amount of perturbation added to the system for this study is within a reasonable range, and that it does not have a significant effect on the tracking or regulation states. The introduced perturbation may have a large effect on the other system variables, especially flexible body states and the control efforts, but they remain within a reasonable range for hypersonic flight.

This study has also shown the effects that controller switching has on the hypersonic vehicle. From the nonlinear simulation results, it can be seen that there are sharp changes and transients in the system states as a result of switching from one controller to another. This effect seems to be one of the largest limiting factors to this controller. The HSV is very sensitive to the switching that takes place in the controller, so effort must be made to reduce the amount of controller switching that takes place. This is not always feasible, and thus limits the capabilities of the controller.

The simulation in this study showed that there is a strong correlation between the angle of attack and the flexible states of the vehicle. As the angle of attack increases, the motions for the flexible mode increase. It is important to understand the relationship because both of these values play into the efficiency of the scramjet engine. There is also a strong coupling between the angle of attack, the pitch attitude, and the pitch rate of the hypersonic vehicle. They affect how much air flows into the scramjet engine and as a result, they will decide how much thrust is produced by the scramjet engine. It is desirable to keep the angle of attack relatively small so that the scramjet stays within its operational range. This could be achieved by penalizing the angle of attack in the control synthesis stage to minimize the amount of fluctuation seen.

Acknowledgements The authors would like to thank Dr. Machael Bolender from the Air Force Research Laboratory, Wright-Peterson AFB, for providing them a hypersonic model and its MATLAB code.

References

1. Apkarian P, Adams R (1998) Advanced gain-scheduling techniques for uncertain systems. *IEEE Trans Contr Syst Tech* 6(1):21–32
2. Becker G, Packard A (1994) Robust performance of linear parametrically varying systems using parametrically-dependent linear feedback. *Syst Contr Lett* 23:205–215
3. Bilimoria K, Schmidt D (1995) Integrated development of the equations of motion for elastic hypersonic flight vehicles. *J Guid Contr Dyn* 18(1):73–81
4. Bolender M (2009) An overview on dynamics and controls modeling of hypersonic vehicles. In: 2009 American control conference, pages 2507–2512. AACC
5. Bolender M, Doman D (2007) Nonlinear longitudinal dynamical model of an air-breathing hypersonic vehicle. *J Spacecraft Rockets* 44(2):374–387
6. Bolender M, Doman D (2010) A non-linear model for the longitudinal dynamics of a hypersonic air-breathing vehicle. In: AIAA guidance, navigation, and control conference and exhibit, AIAA 2005-6255

7. Boyd SP, El Ghaoui L, Feron E, Balakrishnan V (1994) Linear matrix inequalities in systems and control theory. SIAM, Philadelphia, PA
8. Buschek H, Calise A (1993) Robust control of hypersonic vehicles considering propulsive and aeroelastic effects. In: In Proceedings of the 1993 AIAA guidance, navigation and control conference, pp 93–3762
9. Buschek H, Calise A (1994) Fixed order robust control design for hypersonic vehicles. In: AIAA guidance, navigation and control conference, pp 94–3662
10. Chavez F, Schmidt D (1994) Analytical aeropulsive/aeroelastic hypersonic-vehicle model with dynamic analysis. *J Guid Contr Dyn* 17(6):1308–1319
11. Culler A, Williams T, Bolender M (2007) Aerothermal modeling and dynamic analysis of a hypersonic vehicle. In: AIAA atmospheric flight mechanics conference and exhibit, pp 375–395. AIAA
12. Davidson J, Lallman F, McMinn J, Martin J, Pahle J, Stephenson M, Selmon J (1999) Flight control laws for NASA's hyper-x research vehicle. NASA Technical Memorandum AIAA-99-4124
13. Fidan B, Kuipers M, Ioannou P, Mirmirani M (2006) Longitudinal motion control of air-breathing hypersonic vehicles based on time-varying models. In: 14th AIAA/AHI space planes and hypersonic systems and technologies conference, pp 1705–1717. AIAA
14. Fiorentini L, Serrani A, Bolender M, Doman D (2008) Nonlinear control of a hypersonic vehicle with structural flexibility. In: Proceedings of the 47th IEEE conference on decision and control, pp 578–583
15. Fiorentini L, Serrani A, Bolender M, Doman D (2008) Robust nonlinear sequential loop closure design for an air-breathing hypersonic vehicle model. In: American control conference, pp 3458–3463
16. Gahinet P, Nemirovski A, Laub AJ, Chilali M (1995) LMI control toolbox. Mathworks, Natick, MA
17. Gibson T, Crespo L, Annaswamy A (2009) Adaptive control of hypersonic vehicles in the presence of modeling uncertainties. In: 2009 American control conference, pp 3178–3183. AACC
18. Gregory I, Chowdhry R, McMinn J, Shaughnessy J (1992) Hypersonic vehicle control laws development using H_∞ and μ -synthesis. NASA Technical Memorandum 107689
19. Groves K, Serrani A, Yurkovich S, Bolender M, Doman D (2006) Anti-windup control for an air-breathing hypersonic vehicle model. In: AIAA guidance, navigation, and control conference and exhibit, AIAA 2006–6557
20. Groves K, Sighthorsson D, Serrani A, Yurkovich S, Bolender M, Doman D (2005) Reference command tracking for a linearized model of an air-breathing hypersonic vehicle. In: AIAA guidance, navigation, and control conference and exhibit, AIAA 2005–6144
21. Hughes H (2010) LPV H_∞ Control for the Longitudinal Dynamics of A Flexible Hypersonic Vehicle. PhD thesis, North Carolina State University, Raleigh, NC
22. Jankovsky P, Sighthorsson D, Serrani A, Yurkovich S, Bolender M, Doman D (2007) Output feedback control and sensor placement for a hypersonic vehicle model. In: AIAA guidance, navigation, and control conference and exhibit, pp 247–268. AIAA
23. Lind R (2002) Linear parameter-varying modeling and control of structural dynamics with aeroelastic effects. *J Guid Contr Dyn* 25(4):733–739
24. Meirovitch L, Tuzcu I (2003) Integrated approach to the dynamics and control of maneuvering flexible aircraft. NASA/CR-2003-211748
25. Mirmirani M, Wu C, Clark A, Choi S, Colgran R (2005) Modeling for control of a generic airbreathing hypersonic vehicle. In: AIAA guidance, navigation, and control conference and exhibit, pp 3959–3977. AIAA
26. Mooij E (2001) Numerical investigation of model reference adaptive control for hypersonic aircraft. *J Guid Contr Dyn* 24(2):315–323
27. NOAA, NASA, and USAF (1976) U.S. Standard Atmosphere 1976. U.S. Government Printing Office, Washington D.C.
28. Parker J, Serrani A, Yurkovich S, Bolender M, Doman D (2007) Control-oriented modeling of an air-breathing hypersonic vehicle. *J Guid Contr Dyn* 30(3):856–869

29. Schmidt D (1992) Dynamics and control of hypersonic aeropropulsive/aeroelastic vehicles. AIAA Paper, (AIAA-92-4326-CP)
30. Shaughnessy J, Pinckney S, McMinn J, Cruz C, Kelley M (1990) Hypersonic vehicle simulation model: Winged-cone configuration. NASA Technical Memorandum 102610
31. Sighthorsson D, Serrani A, Yurkovich S, Bolender M, Doman D (2006) Tracking control for an over-actuated hypersonic air-breathing vehicle with steady state constraints. In: AIAA guidance, navigation, and control conference and exhibit, Keystone, Colorado, pp 3663–3679. AIAA
32. Soloway D, Rodriguez A, Dickeson J, Cifdaloz O, Benavides J, Sridharan S, Kelkar A, Vogel J (2009) Constraint enforcement for scramjet-powered hypersonic vehicles with significant aeroelastic-propulsion interactions. In: 2009 American control conference, pp 3154–3159. AACC
33. The Institution of Electrical Engineers (1997) Control engineering solutions: a practical approach. The Institution of Electrical Engineers, London, United Kingdom, pp 63–71
34. Thompson E, Henry K, Williams L (2005) Faster than a speeding bullet: Guinness recognizes NASA scramjet. http://www.nasa.gov/home/hqnews/2005/jun/HQ_05_156_X43A_Guinness.html
35. Wilcox Z, MacKunis W, Bhat S, Lind R, Dixon W (2009) Robust nonlinear control of a hypersonic aircraft in the presence of aerothermal effects. In: 2009 American control conference, pp 2533–2538. AACC
36. Williams T, Bolender M, Doman D, Morataya O (2006) An aerothermal flexible mode analysis of a hypersonic vehicle. In: AIAA atmospheric flight mechanics conference and exhibit
37. Wu F, Yang X, Packard A, Becker G (1996) Induced l_2 -norm control for lpv systems with bounded parameter variation rates. *Int J Robust Nonlinear Contr* 6:983–998
38. Xu H, Mirmirani M, Ioannou P (2004) Adaptive sliding mode control design for a hypersonic flight vehicle. *J Guid Contr Dyn* 27(5):829–838

Chapter 18

Constrained Freeway Traffic Control via Linear Parameter Varying Paradigms

T. Luspay, T. Péni, and B. Kulcsár

Abstract A novel freeway traffic control design framework is proposed in the chapter. The derivation is based on the parameter-dependent reformulation of the second-order macroscopic freeway model. Hard physical constraints are handled implicitly, by introducing additional scheduling parameter for controller saturation measure. The ramp metering problem is then formulated as an induced \mathcal{L}_2 norm minimization, where the effects of undesired traffic phenomena are attenuated on the network throughput. The solution of the resulting problem involves convex optimization methods subjected to Linear Matrix Inequalities. A numerical example is given to validate the parameter-dependent controller and evaluate its effectiveness under various traffic situations.

18.1 Introduction

Ramp metering has been identified as one of the most effective traffic control measures by controlling the merging flow using traffic signals [15]. Excessive research has been performed since the 1970s to evaluate its impact and to design appropriate algorithms accordingly. The most important property of ramp metering is that it can prevent traffic breakdown and off-ramp blockage by controlling the entering vehicle volume.

T. Luspay • T. Péni

Systems and Control Laboratory, Computer and Automation Research Institute,
Hungarian Academy of Sciences, 1111 Kende u. 14-17. Budapest, Hungary
e-mail: tluspay@sztaki.hu; pt@scl.sztaki.hu

B. Kulcsár (✉)

Department of Signals and Systems, Chalmers University of Technology,
SE-412 96, Gothenburg, Sweden
e-mail: kulcsar@chalmers.se

Ramp metering strategies can be categorized according to their behavior as static (fixed time) or as dynamic (traffic responsive) ones [8, 15]. The design of static algorithms is carried out off-line, based on historical traffic data. By assuming constant traffic trend in the future, a fix metering rate is determined off-line through optimization techniques [21]. These methods are favorable because of their inexpensive computation needs and effortless implementation in real applications. Their disadvantage is obvious. Whenever the actual traffic situation diverges from the presumed one, the control performance is diminished.

A more sophisticated approach is proposed by introducing traffic responsive or dynamic ramp metering algorithms, when the controller is driven by real-time traffic measurements [8]. The measurement data are then used for determining the actual metering rate in a feed-forward [13] or feedback structure [8, 15]. According to the involved traffic measurements, one can distinguish between local (isolated) and coordinated ramp metering strategies. While local algorithms use limited measurements from their vicinity of their location of installation only, coordinated methods utilize increased amount of data from detectors and other controllers. To design efficient responsive ramp metering algorithms, a dynamical model is required for the prediction of traffic evolution.

In case of traffic prediction for control purposes it is beneficial to neglect the motion of individual vehicles and use aggregated spatiotemporal traffic variables, such as traffic density ($\rho(t, x)$), space-mean speed ($v(t, x)$), and traffic flow ($q(t, x)$). According to their level of detail, these models are referred to as macroscopic (or continuum) models [10, 14]. Dynamical equations of such models can be derived by exploiting the hydrodynamical analogy between traffic flow and streaming fluids. These models can be then further categorized according to the number of variables involved. First-order models predict the time evolution of density (conservation of mass) [10], while second-order ones incorporate the dynamics of space-mean speed (conservation of momentum) in addition [18]. The resulting partial differential equations (PDE) are then temporally and spatially discretized for practical implementation and use [14].

In order to reproduce the complex behavior of freeway traffic, most macroscopic models are nonlinear and physically constrained in their variables. From control point of view it is important that the on-ramp volume is physically limited. The maximal throughput (capacity) of the on-ramp forms an upper bound on the allowable inflow, while for practical reasons a lower bound is introduced by requesting a minimal metering flow to avoid queue spill-over due to on-ramp blockage [15]. Accordingly, successful model-based traffic control should reflect the nonlinear nature of the process and handle hard physical constraints eventually. Even though the literature of ramp-metering is large and diverse, only a few techniques can face both of these challenges.

The use of linear or linearized models for ramp metering appears in many applications [7, 16]. The advantage is clearly the applicability of well-established linear constrained control techniques. At the same time, the drawback of these techniques is the loss of information due to the use of simplified prediction models. Incorporating advanced traffic models implies nonlinear numerical optimization techniques subject to dynamical and hard physical constraints [5, 6, 9].

Identifying these trade-offs has gained more and more attention in systems and control theory, leading to the theory of linear parameter varying (LPV) systems (see, e.g., [1, 19, 20, 23] and the references therein). LPV systems are considered as an alternative representation of nonlinear systems, where the nonlinearities are hidden by introducing the so-called scheduling parameters. This concept offers the systematic and numerically efficient extension of well-established linear methods for nonlinear systems. Consequently, LPV paradigms carry great potential for traffic control.

The chapter proposes a novel control design method for freeway ramp metering, which (1) exploits the complex nonlinear description of traffic phenomena and (2) handles physical constraints of the on-ramp control input. The recently established LPV reformulation of the non-linear macroscopic freeway model serves as a basis of the design [11, 12]. Accordingly, the chapter is organized as follows. After the Introduction, the fundamental concept of model-based traffic control is discussed in Sect. 18.2. The resulting nonlinear optimization problem is then reformulated by using LPV paradigms. The constrained ramp metering problem is stated as an induced \mathcal{L}_2 norm minimization in Sect. 18.3. The solution of the obtained control formulation is given in Sect. 18.4, where the design of the parameter-dependent dynamical controller is carried out by using linear matrix inequalities (LMIs). Section 18.5 provides a benchmark simulation problem, where the effectiveness of the control structure is investigated. Concluding remarks and further research directions close the chapter in Sect. 18.6.

18.2 Problem Statement: Model-Based Traffic Control

Microscopic traffic models trace the motion of each participating vehicle and their interactions, and offer high-detailed dynamical descriptions of traffic processes at the expense of superior computational demand. Therefore, macroscopic models are preferred to predict traffic behavior for traffic flow control applications, since the numerical complexity is decreased through introducing cumulated variables. By relating the number of vehicles on a stretch to the length of the road, one gets the so-called traffic density (denoted by: ρ in $[\frac{\text{veh}}{\text{km lane}}]$), while the average speed of vehicles in question is represented by the space-mean speed (v in $[\frac{\text{km}}{\text{h}}]$). The dynamical evolution of macroscopic variables in space (x) and in time (t) can be formulated as a set of PDEs based on hydrodynamical analogies. The PDEs are then discretized in both space (with variable space step Δ_i , $x = \Delta_i \cdot i$ where $i \in \mathcal{Z}$) and in time (with sampling time T , $t = T \cdot k$ where $k \in \mathcal{Z}$) for implementation purposes. The discretized version of a so-called extended Payne–Whitham type macroscopic model is considered through the chapter [18, 22]. It has been proven that the second-order model in question is able to reproduce various traffic phenomena, such as free and congested flow, wide moving jams and capacity drop, as well as stop-and-go traffic more accurately than first-order models [14].

The dynamical representation of an n -lane stretch with length Δ_i (called segment) can be formulated by:

$$\rho_i(k+1) = \rho_i(k) + \frac{T}{\Delta_i n} [q_{i-1}(k) - q_i(k) + r_i(k) - s_i(k)], \quad (18.1)$$

$$s_i(k) = \beta_i \cdot q_{i-1}(k), \quad (18.2)$$

$$v_i(k+1) = v_i(k) + \frac{T}{\tau} [V(\rho_i(k)) - v_i(k)] + \frac{T}{\Delta_i} v_i(k) [v_{i-1}(k) - v_i(k)] - \frac{\nu T}{\tau \Delta_i} \frac{\rho_{i+1}(k) - \rho_i(k)}{\rho_i(k) + \kappa} - \frac{\delta T}{\Delta_i n} \frac{r_i(k) v_i(k)}{\rho_i(k) + \kappa}, \quad (18.3)$$

$$V(\rho_i(k)) = v_f \exp \left[-\frac{1}{a} \left(\frac{\rho_i(k)}{\rho_{cr}} \right)^a \right], \quad (18.4)$$

$$q_i(k) = \rho_i(k) \cdot v_i(k) \cdot n, \quad (18.5)$$

$$l_i(k+1) = l_i(k) + T (d_{o,i}(k) - r_i(k)). \quad (18.6)$$

The following notations are used in (18.1)–(18.6):

- Discretized traffic density $\rho_i(k)$ is the number of vehicles in segment i at time step kT , divided by the segment length Δ_i and lane number n , $\left[\frac{\text{veh}}{\text{km lane}} \right]$.
- Discretized space-mean speed $v_i(k)$ is the average speed of vehicles in segment i at time step kT , $\left[\frac{\text{km}}{\text{h}} \right]$.
- Discretized traffic flow $q_i(k)$ is the number of vehicles leaving segment i during the time period $[(k-1)T, kT]$, divided by T , $\left[\frac{\text{veh}}{\text{h}} \right]$.
- The discrete variables $r_i(k)$, $s_i(k)$ are the on- and off-ramp volumes, respectively, to segment i during the time period $[(k-1)T, kT]$ in $\left[\frac{\text{veh}}{\text{h}} \right]$.
- $l_i(k)$ denotes the queue length at ramp i at time step kT , [veh], while $d_{o,i}(k)$ denotes the demand entering the i th ramp during the time period $[(k-1)T, kT]$.

Moreover, β_i , τ , ν , κ , δ , v_f , ρ_{cr} , and a are supposed to be constant model parameters. Equation (18.4) expresses the average speed decrease according to density increments, characterized by the constant parameters v_f , ρ_{cr} , and a . Substituting $v_i(k)$ with (18.4) in the flow equation (18.6), one can obtain the maximal throughput (i.e., capacity) at ρ_{cr} . This distinct density value is referred to as critical density [10, 18].

The model uses three dynamical equations expressing mass conservation ((18.1) for the main lanes and (18.6) for merging on-ramp) and space-mean speed evolution (18.3) over one specific segment. Longer sections can be built by interconnecting individual segment dynamics through the boundary variables $q_{i-1}(k)$, $v_{i-1}(k)$ and $\rho_{i+1}(k)$. Variables involved in an arbitrary interconnected chain of S segments can be then sorted according to their physical nature. Variables with dynamical equations are considered as the state variables of the system, i.e.:

$$x(k) = [\rho_1(k), v_1(k), l_1(k), \dots, \rho_i(k), v_i(k), l_i(k), \dots, \rho_S(k), v_S(k), l_S(k)]^T. \quad (18.7)$$

On-ramps are assumed to be controlled by traffic signals, therefore, the flow entering the freeway through on-ramps is considered as the control input:

$$u(k) = [r_1(k), \dots, r_i(k), \dots, r_S(k)]^T. \quad (18.8)$$

The control input $u(k)$ is subject to an element-wise constraint in the following form:

$$r_{i,\min} \leq r_i(k) \leq r_{i,\max}, \quad \forall i, \forall k. \quad (18.9)$$

Variables that cannot be effected by traffic control measures are collected into the generalized disturbance vector $d(k)$:

$$d(k) = [q_0(k), v_0(k), d_{o,1}(k), \dots, d_{o,i}(k), \dots, d_{o,S}(k), \rho_{S+1}(k)]^T.$$

The vector $d(k)$ consists of boundary variables representing upstream ($q_0(k)$ and $v_0(k)$) and downstream ($\rho_{S+1}(k)$) traffic conditions and uncontrolled on-ramp demands $d_{o,i}(k)$, $i = 1, 2, \dots, S$.

By using these notations, the second-order freeway dynamics, of S interconnected segments, can be generally expressed as:

$$x(k+1) = f(x(k), d(k), u(k)). \quad (18.10)$$

The general goal of traffic control is to achieve a network-wide optimum which is beneficial for all participants in an average sense.¹ Therefore, macroscopic indicators are favorable to characterize the network-wide performance level. The total time spent (TTS) measure is a widely used quantity to describe network efficiency by summing the time that vehicles spend in a traffic network [15]. TTS can be defined over an arbitrary time period K as follows:

$$J_{\text{TTS}}(K) = \sum_{k=1}^K TN(k), \quad (18.11)$$

where $N(k)$ is the number of vehicles in the network at time step k . Obviously, lower values of TTS refer to better network efficiency, hence the minimization of (18.11) is a network-wide control objective for traffic control. The vehicle number $N(k)$ can be expressed by using the introduced macroscopic variables and by distinguishing vehicles in the main flow and on-ramps:

$$N(k) = \underbrace{\sum_{i=1}^S \rho_i(k) \Delta_i n}_{\text{vehicles in main lanes}} + \underbrace{\sum_{i=1}^S l_i(k)}_{\text{vehicles at on-ramps}}. \quad (18.12)$$

¹In contrast to individual user based optimum.

Furthermore, a generic mass-conservation dynamics can be formulated for the underlying traffic network as

$$N(k+1) = N(k) + T(d(k) - s(k)), \quad (18.13)$$

where $s(k)$ represents the sum of all exiting flow through off-ramps and main lanes, $s(k) = \sum_{i=1}^S s_i(k) + q_S(k)$, while $d(k)$ is the total number of vehicles entering the network in the time period $[(k-1)T, kT]$, i.e.: $d(k) = \sum_{i=1}^S d_{o,i}(k) + q_0(k)$. Consequently, the TTS objective is written as

$$\begin{aligned} J_{\text{TTS}}(K) &= T \sum_{k=1}^K (N(k) + T(d(k-1) - s(k-1))) = \\ &= T \sum_{k=1}^K \left(N(0) + T \sum_{\kappa=0}^{k-1} (d(\kappa) - s(\kappa)) \right). \end{aligned} \quad (18.14)$$

Vehicles waiting at on-ramps are incorporated into the traffic control objective in order to avoid ramp closure. Since neither the initial number of vehicles $N(0)$ nor the generalized disturbance $d(k)$ can be directly controlled, it can be seen from (18.14) that the minimization of $J_{\text{TTS}}(K)$ is equivalent with the maximization of time-weighted exit flow $Q(x, u, d, K) = T^2 \sum_{k=1}^K \sum_{\kappa=0}^{k-1} s(\kappa)$. A further, strong relation between the network-wide outflow and TTS has been reported in [15], stating that even a slight improvement in the outflow can significantly improve the TTS measure.

Accordingly, the freeway traffic control problem can be formulated as a constrained nonlinear optimization problem by

$$\begin{aligned} &\max_{u(k)} Q(x, u, d, K) \\ \text{s. t.: } &x(k+1) = f(x(k), d(k), u(k)) \\ &u_{i,\min} \leq u_i(k) \leq u_{i,\max}. \end{aligned} \quad (18.15)$$

The nonlinear optimization problem above subjected to dynamical and hard physical constraints implies complex numerical needs. In order to avoid real-time numerical optimization, parameter-varying concepts are adopted in the following section.

18.3 Parameter Varying Problem Formulation

18.3.1 Basic Notions

In the quasi-linear parameter varying (qLPV) framework, a scheduling parameter is introduced and used for capturing nonlinearities and imitating linearity in the variables. The system is then continuously scheduled with these functions; therefore, the entire operation domain is covered with an infinite number of linear

systems (in contrast to the classical gain-scheduling). The model can then be formulated under the following generic form in discrete time:

$$x(k+1) = A(p(k))x(k) + E(p(k))d(k) + B(p(k))u(k), \quad (18.16a)$$

$$y(k) = C_2(p(k))x(k) + D_{21}(p(k))d(k) + D_{22}(p(k))u(k). \quad (18.16b)$$

qLPV systems are read whenever the scheduling vector $p(k)$ depends on the state of the system, otherwise (18.16a) and (18.16b) represent a generic LPV model class. The continuous dependency of the system's matrix functions on the scheduling vector is expressed as: $A \in \mathcal{C}^0(\mathcal{R}^{n_p}, \mathcal{R}^{n_x \times n_x})$, $B \in \mathcal{C}^0(\mathcal{R}^{n_p}, \mathcal{R}^{n_x \times n_u})$, $E \in \mathcal{C}^0(\mathcal{R}^{n_p}, \mathcal{R}^{n_x \times n_d})$, $C_2 \in \mathcal{C}^0(\mathcal{R}^{n_p}, \mathcal{R}^{n_y \times n_x})$, $D_{21} \in \mathcal{C}^0(\mathcal{R}^{n_p}, \mathcal{R}^{n_y \times n_d})$, $D_{22} \in \mathcal{C}^0(\mathcal{R}^{n_p}, \mathcal{R}^{n_y \times n_u})$. The state-dependency of the scheduling parameter vector $p(k)$ might be neglected in the analysis, estimation, or control design, and can be assumed as an exogenous signal that takes its value from the compact set $\mathcal{P} \subset \mathcal{R}^{n_p}$ [23]. Considering $p(k)$ as an independent variable may lead to conservative solutions, since some of the known information is not exploited. The main reason why LPV models are still appealing is that systematic analysis and design methods developed for linear systems can be extended, since the structural similarity [1, 2]. Furthermore, during the implementation, controllers (or observers) are usually scheduled with the same $p(k)$; therefore, acceptable performance can be achieved through the natural adaptivity offered by scheduling [4]. Consequently, the parameter $p(k)$ should be available during operation for scheduling purposes, hence its value is assumed to be measured or estimated. Additionally, the conservativeness of the parameter-dependent design methods can be decreased by incorporating complementary information on the scheduling parameter (e.g., bounds or rate of change).

Alternatively, many control problems can be formulated with relaxed computational needs by using polytopic modeling framework. A discrete-time polytopic system is a linear time varying (LTV) model in the following form:

$$x(k+1) = A(k)x(k) + E(k)d(k) + B(k)u(k), \quad (18.17a)$$

$$y(k) = C_2(k)x(k) + D_{21}(k)d(k) + D_{22}(k)u(k). \quad (18.17b)$$

Restricting the system matrices to belong to the prespecified set Ω :

$$[A(k) \ B(k) \ E(k) \ C_2(k) \ D_{21}(k) \ D_{22}(k)] \in \Omega. \quad (18.18)$$

In addition, Ω is assumed to be a polytope of matrices:

$$\Omega = \text{Co} \{ [A^1 \ B^1 \ E^1 \ C_2^1 \ D_{21}^1 \ D_{22}^1], \dots, [A^{n_\lambda} \ B^{n_\lambda} \ E^{n_\lambda} \ C_2^{n_\lambda} \ D_{21}^{n_\lambda} \ D_{22}^{n_\lambda}] \}, \quad (18.19)$$

where Co refers to the convex hull. Note that the vertices of Ω , i.e., the matrices A^j , B^j , E^j , C_2^j , D_{21}^j , D_{22}^j with $j = 1, \dots, n_\lambda$, form n_λ number of LTI systems. According

to (18.18), the time-varying system can be expressed as the convex combination of the vertex systems:

$$\begin{aligned} A(k) &= \sum_{j=1}^{n_\lambda} A^j \lambda^j(k), & B(k) &= \sum_{j=1}^{n_\lambda} B^j \lambda^j(k), \\ E(k) &= \sum_{j=1}^{n_\lambda} E^j \lambda^j(k), & C_2(k) &= \sum_{j=1}^{n_\lambda} C_2^j \lambda^j(k), \\ D_{21}(k) &= \sum_{j=1}^{n_\lambda} D_{21}^j \lambda^j(k), & D_{22}(k) &= \sum_{j=1}^{n_\lambda} D_{22}^j \lambda^j(k), \end{aligned} \quad (18.20)$$

where the convex combinations are given with weighting functions $\lambda^1, \lambda^2, \dots, \lambda^{n_\lambda}$ satisfying:

$$\sum_{i=1}^{n_\lambda} \lambda^i = 1, \quad 0 \leq \lambda^j \leq 1 \quad \forall j. \quad (18.21)$$

Polytopic systems can be used for approximating nonlinear ones by the convex combination of LTI systems with state-dependent weighting functions $\lambda^j(x(k))$.

18.3.2 LPV Reformulation of the Extended Payne–Whitham Model

The following method is proposed to transform the nonlinear freeway model into an LPV form [11, 12]:

(A.1) Determine steady-state solutions of the nonlinear difference (18.1)–(18.6), satisfying $x(k+1) = x(k) = x^*$. The resulting algebraic equations in the generic form $0 = f(x^*, u^*, d^*)$ are underdetermined, therefore additional design freedoms are given which can be capitalized according to the nature of the problem in question. For the case of traffic control, the following selections can be done:

- According to the fundamental theory of freeway traffic, sections reach their capacity when they operate at the critical density. Therefore, one could be interested in a steady-state solution where the densities of segments with outflow capabilities (through off-ramps or main-lanes) equal the critical value ρ_{cr} .
- Furthermore, the corresponding on-ramp volumes can be fixed as the mean of the hard physical constraints: $r_i^* = \frac{r_{i,\text{min}} + r_{i,\text{max}}}{2}$.

(A.2) Introduce shifted variables as: $\tilde{x}(k) = x(k) - x^*$, $\tilde{u}(k) = u(k) - u^*$, $\tilde{d}(k) = d(k) - d^*$ and rewrite system dynamics in the new coordinate frame. According to the steady-state specification, the origin of the system in the

centered coordinates reflects maximal throughput. Furthermore, symmetric input constraints are obtained in the shifted coordinate frame because of the imposed steady-state selection on the control input.

- (A.3) Rewrite the system dynamics in terms of centered variables and steady-state values. Time-varying variables can be then factorized from the resulting nonlinearities (denoted by $e(\tilde{x}(k))$) by using the following transformation:

$$e(\tilde{x}(k)) = E(\tilde{x}(k))\tilde{x}(k), \quad E(\tilde{x}(k)) = \int_0^1 \frac{\partial e(\varphi\tilde{x}(k))}{\partial \varphi} d\varphi, \quad (18.22)$$

with the use of the auxiliary variable φ . Such relationship is valid for functions that satisfy $e(0) = 0$. This condition is guaranteed in the underlying traffic model due to the shift of the coordinate frame to the steady-state operation point.

- (A.4) Rearrange the factorized terms according to their nature (state, input, or disturbance) to obtain quasi-LPV structure in the form

$$\tilde{x}(k+1) = A(p(k))\tilde{x}(k) + E(p(k))\tilde{d}(k) + B(p(k))\tilde{u}(k), \quad (18.23)$$

where the scheduling parameter vector $p(k)$ is used for capturing nonlinearities, therefore depends on $\tilde{x}(k)$.

Since no approximation is introduced through the derivation, the obtained parameter-dependent structure in (18.23) is numerically equivalent with the nonlinear representation of the process (18.1)–(18.6).

18.3.3 Constraint Handling

As it has been highlighted before, the above selection of r_i^* implies a 0-symmetric constraint representation of the physical limitations in the shifted coordinate frame. A possible way to model these types of constraints is the consideration of the saturation limit in the following form [24]:

$$\sigma(\tilde{u}(k)) = \begin{cases} \tilde{u}(k) & |\tilde{u}(k)| \leq \bar{u} \\ \text{sign}(\tilde{u}(k))\bar{u} & |\tilde{u}(k)| \geq \bar{u} \end{cases}, \quad (18.24)$$

where the unified bound \bar{u} on the centered on-ramp volume equals $\frac{r_{\max} - r_{\min}}{2}$ in the underlying problem. LPV concepts can be then applied for input saturated systems by introducing the following saturation parameter [24]:

$$\theta(\tilde{u}(k)) = \frac{\sigma(\tilde{u}(k))}{\tilde{u}(k)}, \quad (18.25)$$

and defining $\theta(0) = 1$ in addition. Consequently, the domain of the saturation parameter is $(0, 1]$. Expressing the saturated input with $\theta(\tilde{u}(k))$ as $\sigma(\tilde{u}(k)) = \theta(k)\tilde{u}(k)$ the system equation (18.23) can be rewritten in the form

$$\tilde{x}(k+1) = A(p(k))\tilde{x}(k) + E(p(k))\tilde{d}(k) + B(p(k))\theta(\tilde{u}(k))\tilde{u}(k). \quad (18.26)$$

LPV paradigms can be applied in a straightforward way to address the problem, namely by considering the saturation parameter $\theta(\tilde{u}(k))$ as an additional scheduling parameter of the system. Note that since the bounds of the parameter are known, and its value can be computed online, it is suitable for scheduling the controller.

Remark 18.1. Increasing the number of scheduling parameters results in a parameter-varying controller that also depends on $\theta(\tilde{u}(k))$, consequently the controller is continuously informed of the actual level of saturation. This implicit information has to be distinguished from the explicit solution proposed in Wu et al. [24]. In the latter solution, the measurement equation is extended with $\tilde{u}(k) - \sigma(\tilde{u}(k))$. That is when the saturated input is directly fed back to the controller as it is usual in anti-windup setups. Applying explicit solution requires the controller to be strictly proper in order to ensure causality [24]. In this chapter only $\theta(\tilde{u}(k))$ is involved, hence the controller may have a direct feed-through term from $\tilde{y}(k)$ to $\tilde{u}(k)$, and still it remains causal.

Remark 18.2. It also should be emphasized that the proposed method for constraint handling does not automatically prevent constraint violations. Since the domain of $\theta(\tilde{u}(k))$ is $(0, 1]$ there always exists a practical lower bound $\theta_{\min} \neq 0$ on the saturation parameter, which is used through the design. Although the resulting control input $\tilde{u}(k)$ is unbounded, one should take care that its value does not exceed $\theta_{\min}^{-1}\bar{u}$. Furthermore, the value of θ_{\min} means a trade-off in the controller design, since as its value is decreased so is the effect of the control input lowered.

18.3.4 Polytopic Representation

Polytopic systems can cover nonlinear or LPV systems by allowing the weighting functions to depend on state variables. Polytopic models are widely used for various engineering problems because of their numerically favorable properties.

In order to transform the obtained generic LPV representation of the freeway model, a Tensor-Product (TP) model transformation is applied [3]. Generally speaking, the TP model transformation is a numerical tool with proved numerical reconstruction capabilities, to reformulate quasi-LPV models into a polytopic form (18.17a), with state-dependent convex combination of LTI vertex systems.

The first step of the TP model transformation is the evaluation of the investigated quasi-LPV system (18.26) over an arbitrary selected domain Ψ , representing the parameter variation set of the scheduling parameters (or of the state variables they

depend on). In order to evaluate the qLPV dynamics over Ψ , an n_p dimensional grid should be defined. The qLPV system matrices are then sampled over the predefined grid, resulting in a hyper-dimensional data matrix. Higher-order singular value decomposition (HOSVD) is then applied for the decomposition of the data matrix. The number of local LTI systems used for approximating the nonlinear dynamics can be determined according to the singular values and their condition number. Then the discretized weighting functions of the polytopic model ensuring convexity are constructed by executing the HOSVD decomposition of the LPV data matrix.

Remark 18.3. According to the proposed constraint handling technique, the scheduling parameter has been extended with the saturation parameter. Consequently, the weighting functions of the polytopic description depend on the saturation level, i.e., the system polytope contains both saturated and unsaturated dynamics.

18.3.5 Parameter-Dependent Control Formulation

The generic nonlinear freeway model (18.1)–(18.6) is transformed into the following polytopic form, by executing steps described in Sects. 18.3.2–18.3.4:

$$x(k+1) = A(k)x(k) + E(k)d(k) + B(k)u(k), \quad (18.27)$$

where the state vector $x(k)$ contains the centered density and space-mean speed variables,² $u(k)$ represents the unbounded on-ramp volumes, while centered upstream, respectively, downstream variables are compressed in the disturbance vector $d(k)$. Moreover $d(k)$ can be partitioned according to its unmeasured ($w(k)$) and measured ($\bar{w}(k)$) components. Consequently, the knowledge of states and the disturbances are written in the output equation as follows:

$$y(k) = C_2x(k) + D_{21}d(k), \quad (18.28)$$

where only measured disturbance signals influence the system's output through the term $D_{21}d(k)$. The ramp metering problem can then be formulated by defining the performance output of the system. According to the fundamental theory of traffic flow, network capacity is maximized if the density reaches its critical value. This coincides with the origin of the centered coordinate frame due to the selection $\rho_i^* = \rho_{cr}$. Furthermore, large input deviations can also be penalized in the performance output. In order to enhance the performance specifications

²For ease notations.

(dynamical, possibly parameter-dependent), weighting functions can be added at the plant output or input [19, 25], i.e., one can write the following formula for the performance of the freeway traffic problem:

$$z(k) = C_1(k)x(k) + D_{12}(k)u(k), \quad (18.29)$$

i.e., the disturbance does not effect directly the performance output.

As it has been showed in previous studies, disturbances such as shock waves lead to the degradation of throughput, therefore they are undesirable. Consequently, the effects of disturbance should be minimized on the capacity output which lead us to the following formal control problem.

Consider thus the polytopic representation of the process described by (18.27)–(18.29), where the system matrices belong to the polytope Ω . The aim is to guarantee certain performance specifications from the unmeasured disturbances $w(k) = E_w d(k)$ ³ to the performance output $z(k) \in \mathcal{R}^{n_z}$. A possible candidate of this performance specification can be given by defining the induced \mathcal{L}_2 gain from the disturbance $w(k)$ to $z(k)$:

$$\sup_{0 < \|w(k)\| < \infty} \frac{\|z(k)\|}{\|w(k)\|} < \gamma. \quad (18.30)$$

In order to achieve the control objectives, a finite dimensional ($x_c \in \mathcal{R}^{n_{x_c}}$) polytopic controller is proposed in the following form [19]:

$$x_c(k+1) = A_c(k)x_c(k) + B_c(k)y(k), \quad (18.31a)$$

$$u(k) = C_c x_c(k) + D_c y(k). \quad (18.31b)$$

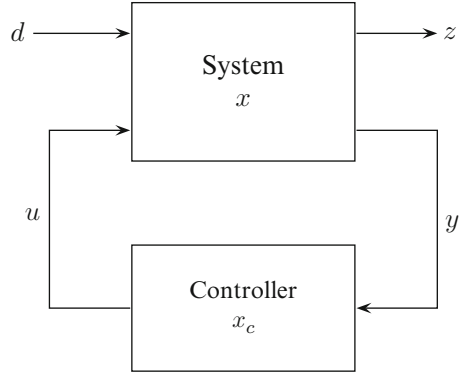
with time-varying system matrices $[A_c(k) B_c(k)] \in \Omega$, and constant C_c, D_c . The latter assumption on C_c and D_c ensures the convexity of the controller design as discussed in the following section.

18.4 Controller Setup

Hereunder we give the general derivation of the controller design applied for the ramp metering problem. We follow the derivation of [19] developed for continuous-time LTI systems.

³ E_w selects the unmeasured part of the generalized disturbance $d(k)$.

Fig. 18.1 Closed-loop interconnection of the system and controller



The closed-loop interconnection of the system (18.27)–(18.29) with the controller (18.31a) and (18.31b) is given in Fig. 18.1 with the following dynamics:

$$\begin{bmatrix} x(k+1) \\ x_c(k+1) \\ z(k) \end{bmatrix} = \begin{bmatrix} A(k) + B(k)D_c C_2 & B(k)C_c & E(k) + B(k)D_c D_{21} \\ B_c(k)C_2 & A_c(k) & B_c(k)D_{21} \\ C_1(k) + D_{12}(k)D_c C_1 & D_{12}(k)C_c & D_{12}(k)D_c D_{21} \end{bmatrix} \begin{bmatrix} x(k) \\ x_c(k) \\ d(k) \end{bmatrix}. \quad (18.32)$$

Introducing shorthand notations for the closed-loop state vector ($\xi(k) \in \mathcal{R}^{n_\xi}$, $n_\xi = n_x + n_{x_c}$) and for closed-loop system matrices, the following compact form is used:

$$\begin{bmatrix} \xi(k+1) \\ z(k) \end{bmatrix} = \begin{bmatrix} \mathcal{A}(k) & \mathcal{B}(k) \\ \mathcal{C}(k) & \mathcal{D}(k) \end{bmatrix} \begin{bmatrix} \xi(k) \\ d(k) \end{bmatrix}, \quad (18.33)$$

where $\mathcal{A}(k) \in \mathcal{R}^{n_\xi \times n_\xi}$, $\mathcal{B}(k) \in \mathcal{R}^{n_\xi \times n_d}$, $\mathcal{C}(k) \in \mathcal{R}^{n_z \times n_\xi}$, and $\mathcal{D}(k) \in \mathcal{R}^{n_z \times n_d}$. The closed-loop system is said to be dissipative with supply function $s(w(k), z(k))$ if there exists a storage function $V : \mathcal{R}^{n_\xi} \rightarrow \mathcal{R}$ such that [19]:

$$V(\xi(k+1)) - V(\xi(k)) \leq s(w(k), z(k)), \quad (18.34)$$

where a widely used candidate for V is the quadratic form

$$V(\xi(k)) = \xi^T(k) \mathcal{X} \xi(k) \quad (18.35)$$

with $\mathcal{X} \in \mathcal{R}^{n_\xi \times n_\xi}$, $\mathcal{X} = \mathcal{X}^T \succeq 0$. Furthermore, if (18.34) is satisfied with the supply function in the form

$$s(w(k), z(k)) = \gamma^2 \|w(k)\|^2 - \|z(k)\|^2, \quad (18.36)$$

then:

$$\sup_{0 < \|w(k)\| < \infty} \frac{\|z(k)\|}{\|w(k)\|} < \gamma. \quad (18.37)$$

i.e., the induced \mathcal{L}_2 norm from the unmeasured disturbance to the performance output is bounded by $\gamma > 0$ [1, 19]. The closed-loop dissipativity with the quadratic storage function (18.35) and supply function (18.36) reads as follows:

$$\xi(k+1)^T \mathcal{X} \xi(k+1) - \xi(k)^T \mathcal{X} \xi(k) \leq \begin{bmatrix} w(k) \\ z(k) \end{bmatrix}^T \begin{bmatrix} \gamma^2 I_{n_w} & 0 \\ 0 & -I_{n_z} \end{bmatrix} \begin{bmatrix} w(k) \\ z(k) \end{bmatrix}. \quad (18.38)$$

After substituting closed-loop dynamics (18.33) and rearranging terms:

$$\begin{bmatrix} \xi(k) \\ d(k) \end{bmatrix}^T \begin{bmatrix} \mathcal{A}(k)^T \mathcal{X} \mathcal{A}(k) - \mathcal{X} \mathcal{A}(k)^T \mathcal{X} \mathcal{B}(k) & \\ \mathcal{B}(k)^T \mathcal{X} \mathcal{A}(k) & \mathcal{B}(k)^T \mathcal{X} \mathcal{B}(k) \end{bmatrix} \begin{bmatrix} \xi(k) \\ d(k) \end{bmatrix} \quad (18.39)$$

$$\leq \begin{bmatrix} \xi(k) \\ d(k) \end{bmatrix}^T \begin{bmatrix} 0 & E_w \\ \mathcal{C}(k) & \mathcal{D}(k) \end{bmatrix}^T \begin{bmatrix} \gamma^2 I_{n_w} & 0 \\ 0 & -I_{n_z} \end{bmatrix} \begin{bmatrix} 0 & E_w \\ \mathcal{C}(k) & \mathcal{D}(k) \end{bmatrix} \begin{bmatrix} \xi(k) \\ d(k) \end{bmatrix}. \quad (18.40)$$

Dissipativity is a system's property, regardless of $\xi(k)$ and $d(k)$, therefore the quadratic expression above should be satisfied for all $[\xi^T(k) \ d^T(k)]^T$. Consequently, a matrix definiteness problem obtained, which takes the following form after rearrangement:

$$\begin{bmatrix} \mathcal{X} & 0 \\ 0 & \gamma^2 E_w^T E_w \end{bmatrix} - \begin{bmatrix} \mathcal{A}(k)^T \mathcal{X} \mathcal{C}(k)^T \\ \mathcal{B}(k)^T \mathcal{X} \mathcal{D}(k)^T \end{bmatrix} \begin{bmatrix} \mathcal{X}^{-1} & 0 \\ 0 & I_{n_z} \end{bmatrix} \begin{bmatrix} \mathcal{X} \mathcal{A}(k) & \mathcal{X} \mathcal{B}(k) \\ \mathcal{C}(k) & \mathcal{D}(k) \end{bmatrix} \succeq 0. \quad (18.41)$$

Then, by using Schur-complement one gets the following expression of the system's dissipativity:

$$\begin{bmatrix} \mathcal{X} & 0 & \mathcal{A}(k)^T \mathcal{X} \mathcal{C}(k)^T \\ 0 & \gamma^2 E_w^T E_w & \mathcal{B}(k)^T \mathcal{X} \mathcal{D}(k)^T \\ \mathcal{X} \mathcal{A}(k) & \mathcal{X} \mathcal{B}(k) & \mathcal{X} & 0 \\ \mathcal{C}(k) & \mathcal{D}(k) & 0 & I_{n_z} \end{bmatrix} \succeq 0. \quad (18.42)$$

Note that (18.42) is nonlinear in the unknown variables, since the product of \mathcal{X} and closed-loop system matrices $\mathcal{A}(k)$ and $\mathcal{B}(k)$, containing the controller matrices. A standard method to handle such nonlinearities is the use of an appropriate congruent transformation [1, 19]. For this purpose, we introduce the following partition of the Lyapunov matrix \mathcal{X} and its inverse:

$$\mathcal{X} = \begin{bmatrix} X & U \\ U^T & \star \end{bmatrix}, \quad \mathcal{X}^{-1} = \begin{bmatrix} Y & V \\ V^T & \star \end{bmatrix}, \quad (18.43)$$

where \star denotes an arbitrary matrix partition. By definition, the following connection holds for the new variables X, Y, U, V :

$$\mathcal{X} \mathcal{X}^{-1} = \begin{bmatrix} XY + UV^T & XV + U\star \\ U^T Y + \star V^T & U^T V + \star\star \end{bmatrix} = \begin{bmatrix} I_{n_x} & 0 \\ 0 & I_{n_x} \end{bmatrix}. \quad (18.44)$$

Furthermore, we define the following variable

$$\mathcal{Y} = \begin{bmatrix} Y & I_{n_x} \\ V^T & 0 \end{bmatrix}. \quad (18.45)$$

These variables are used to construct and perform the congruent transformation, i.e., we multiply inequality (18.42) with $\text{diag}(\mathcal{Y}, I_{n_d}, \mathcal{Y}, I_{n_z})$ from the right and with its transpose from the left. The congruent of \mathcal{X} reads as follows:

$$\mathcal{Y}^T \mathcal{X} \mathcal{Y} = \begin{bmatrix} Y & I_{n_x} \\ I_{n_x} & X \end{bmatrix} = \mathbf{X}(v), \quad (18.46)$$

where the transformed variable \mathbf{X} has been introduced and depends on the new variables $v = (X, Y)$.

Furthermore:

$$\begin{bmatrix} \mathcal{Y} & 0 \\ 0 & I_{n_x} \end{bmatrix}^T \begin{bmatrix} \mathcal{X} \mathcal{A}(k) & \mathcal{X} \mathcal{B}(k) \\ \mathcal{C}(k) & \mathcal{D}(k) \end{bmatrix} \begin{bmatrix} \mathcal{Y} & 0 \\ 0 & I_{n_x} \end{bmatrix} = \begin{bmatrix} \mathbf{A}(k, v) & \mathbf{B}(k, v) \\ \mathbf{C}(k, v) & \mathbf{D}(k, v) \end{bmatrix}, \quad (18.47)$$

where the new matrices are obtained as follows. Firstly,

$$\mathbf{A}(k, v) = \mathcal{Y}^T \mathcal{X} \mathcal{A}(k) \mathcal{Y} = \begin{bmatrix} A(k)Y + B(k)M & A(k) + B(k)NC_2 \\ K(k) & XA(k) + L(k)C_2 \end{bmatrix} \quad (18.48)$$

with the new variables defined as

- $K(k) = XA(k)Y + XB(k)D_c C_2 Y + UB_c(k)C_2 Y + XB(k)C_c V^T + UA_c(k)V^T$
- $L(k) = XB(k)D_c + UB_c(k)$
- $M = D_c C_2 Y + C_c V^T$
- $N = D_c$

Secondly,

$$\mathbf{B}(k, v) = \mathcal{Y}^T \mathcal{X} \mathcal{B}(k) = \begin{bmatrix} E(k) + B(k)ND_{21} \\ XE(k) + L(k)D_{21} \end{bmatrix}, \quad (18.49)$$

thirdly,

$$\mathbf{C}(k, v) = \mathcal{C}(k) \mathcal{Y} = [C_1(k)Y + D_{11}(k)M \quad C_1(k) + D_{12}(k)NC_2]. \quad (18.50)$$

And finally, $\mathbf{D}(k, v) = D_{12}(k)ND_{21}$. Note that $\mathbf{A}(k, v)$, $\mathbf{B}(k, v)$, $\mathbf{C}(k, v)$, $\mathbf{D}(k, v)$ are linear in the new variables:

$$v = \left(X, Y, \begin{pmatrix} K(k) & L(k) \\ M & N \end{pmatrix} \right). \quad (18.51)$$

Consequently, the congruent transformation of (18.42) results in:

$$\begin{bmatrix} \mathbf{X}(v) & 0 & \mathbf{A}^T(k, v) & \mathbf{C}^T(k, v) \\ 0 & \gamma^2 I_{n_w} & \mathbf{B}^T(k, v) & \mathbf{D}^T(k, v) \\ \mathbf{A}(k, v) & \mathbf{B}(k, v) & \mathbf{X}(v) & 0 \\ \mathbf{C}(k, v) & \mathbf{D}(k, v) & 0 & I_{n_z} \end{bmatrix} \succeq 0, \quad (18.52)$$

which is linear in the new variables v , i.e., (18.52) is a LMI.

The controller design is then formulated as an optimization problem.

$$\begin{aligned} & \min_{X, Y, \begin{pmatrix} K(k) & L(k) \\ M & N \end{pmatrix}} \gamma^2, \\ & \text{subject to (18.52)}. \end{aligned} \quad (18.53)$$

Note that due to the polytopic structure of the system and the controller, it is sufficient to add a finite number of LMI constraints to the optimization problem, according to the number of vertices of Ω .

18.5 Numerical Example

In order to investigate the numerical properties of the proposed method, the following benchmark problem is proposed. An isolated ramp metering section has been selected, with $n = 2$ number of lanes and $\Delta = 0.5$ km length. The nonlinear state vector of the configuration consists of segment's density and space-mean speed: $x(k) = [\rho(k) v(k)]^T$. A one-lane ramp is connected to the segment with the maximal capacity inflow $r_{\max} = 2,000 \frac{\text{veh}}{\text{h}}$, while the required minimum volume is set $r_{\min} = 360 \frac{\text{veh}}{\text{h}}$. Accordingly, the control input in the nonlinear coordinate frame is: $u(k) = r(k)$. It is assumed that only the segment-wide traffic variables are gathered through detector measurements with a $T = 10$ s sampling time. That is to say, upstream and downstream variables are collected into the generalized disturbance vector $d(k) = [q_-(k) v_-(k) \rho_+(k)]$.

Such configuration allows us to directly compare the proposed method with the most well-known ramp metering algorithm, called ALINEA [16, 17]. The control equation of the ALINEA method reads as follows:

$$r(k) = r(k-1) + K(\hat{\rho} - \rho_{\text{out}}(k)), \quad (18.54)$$

Table 18.1 Nonlinear model parameters

a	v_{free}	ρ_{cr}	κ	τ	v	δ
1.4	110 km/h	25 veh/km/lane	10 veh/km/lane	0.01 h	20 km ² /h	1.7

Table 18.2 Steady-state values

ρ^*	v^*	ρ_+^*	r^*	v_-^*	q_-^*
25 veh/km/lane	53.8496 km/h	25 veh/km/lane	1180 veh/h	82.5067 km/h	3024 veh/h

where K is the regulator gain and $\hat{\rho}$ is the desired downstream density, i.e., ALINEA is a linear integral control law for freeway ramp metering.⁴ Several field test experiences have been reported from Paris, Amsterdam, and Glasgow [17], where ALINEA has been successfully applied, offering acceptable control performance. Hard physical constraints (i.e., minimal and maximal ramp metering rates) are taken into consideration indirectly through a saturation applied at the implementation.

The model parameters of the second-order macroscopic model are summarized in Table 18.1.

According to our previous discussion, the steady-state conditions have been determined and the results summarized in Table 18.2.

Initially, a minimal saturation parameter $\theta_{\min} = 0.4$ has been assumed, which represents approx. doubled allowable domain according to $\theta_{\min}^{-1}\bar{u}$. Accordingly, the parameter-dependent model structure has been established and evaluated over the following domain in the centered density, space-mean speed, and saturation parameter space Ψ :

$$\Psi = \begin{bmatrix} -18 & 80 \\ -60 & 50 \\ 0.4 & 1 \end{bmatrix}. \quad (18.55)$$

Consequently, 12 number of LTI vertex systems have been obtained by the proposed TP transformation of the qLPV model. Furthermore, the assumed detector setup implies the following output mappings: $C_2 = I_2$ and $D_{21} = 0^{2 \times 3}$.

In the numerical example, only the centered density variable is used as a performance output. In order to ensure advanced disturbance attenuation, at this performance output a time invariant dynamical performance weighting function is introduced. Note that the generic derivation of the controller design allows more flexible polytopic mappings $C_1(k)$ and $D_{12}(k)$. The involvement of the dynamical weight indirectly enhances the reachable closed-loop performance by improving tracking performance in low-frequency regions, including steady-state behavior [25]. For the underlying problem, the following performance weight has been selected in the z -domain:

$$W_p(z) = \frac{1.493z - 0.4975}{z - 0.99} \quad (18.56)$$

⁴That is where the acronym ALINEA originates from.

with a sampling time $T = 10$ s. Consequently, the obtained polytopic system is extended with the dynamic and parameter-independent performance weight $W_p(z)$, and the dimension of the augmented plant is increased with the states of the proposed weighting function.

A full-order $n_{x_c} = n_x$ dynamical controller is designed for the augmented plant by solving the proposed optimization problem subject to the LMI constraints. According to the vertices of the system polytope, 12 number of LMI constraints are formulated. The optimization problem was solved by using the SeDuMi optimization tool. The retrieved controllers $A_c(k), B_c(k), C_c, D_c$ were found to be stable at all vertices.

In order to evaluate and compare the impact of the proposed design under various conditions, a simulated traffic scenario has been selected as follows. A stable traffic flow is used for representing the normal operation. After half an hour, a sharp discontinuity is introduced in the downstream traffic conditions to mimic a shock wave (or wide moving jam). Once the shock wave is dissolved autonomously after an other half an hour, the upstream conditions start to change, imitating peak hour conditions. More precisely, a slowly increasing density is simulated in the upstream direction. According to a typical rush hour scenario, upstream demand starts to decrease after 1 h in the simulation setup.

Three control setups have been investigated under the same demand scenario:

- The uncontrolled case, when no control action is applied at the on-ramp volume, and a constant number of 1,300 vehicles enter the freeway per hour.
- The newly proposed parameter-dependent controller (constrained LPV).
- The well-known ALINEA control case.

Comparative simulation results are given in Figs. 18.2–18.4.

Figure 18.2 shows the evolution of density for the three setups. One can see the effect of ramp metering in contrast to the uncontrolled case, by observing in Fig. 18.2. Both the shock wave and the rush hour traffic conditions lead to congestion when no control action is applied. Secondly, under smooth traffic conditions the different on-ramp control algorithms provide similar results. At the same time, the newly proposed polytopic controller over-performs ALINEA under changing traffic conditions. ALINEA reacts to the variation with a large overshoot, while the polytopic controller suppresses the effect according to its disturbance rejection property. Note that the density reaches the congested region for a limited period when the ALINEA method is applied, which may propagate backward in a more realistic traffic simulation (since it effects the upstream condition in contrast with the scenario in question).

Similar effects can be observed at the space-mean speed evolution (see Fig. 18.3). The average speed of vehicles drops according to the congested traffic conditions. One can also note the similar response of the two controlled densities and speeds during the shock wave excitation period. The reason of the similarity lies in the saturated on-ramp volumes as illustrated on Fig. 18.4. One can observe the more sensitive and faster response of the polytopic controller compared to the integrator-based control law.

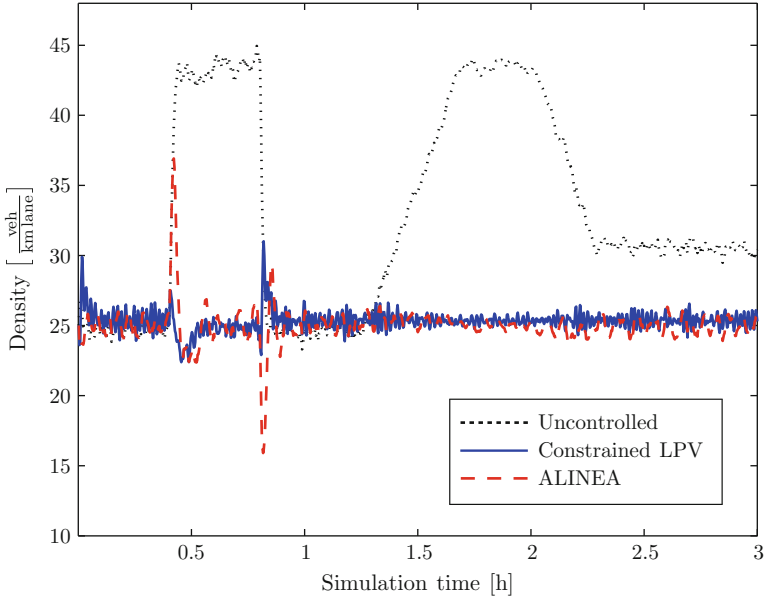


Fig. 18.2 Comparison of the density evolution for the uncontrolled, polytopic controlled, and the ALINEA controlled cases

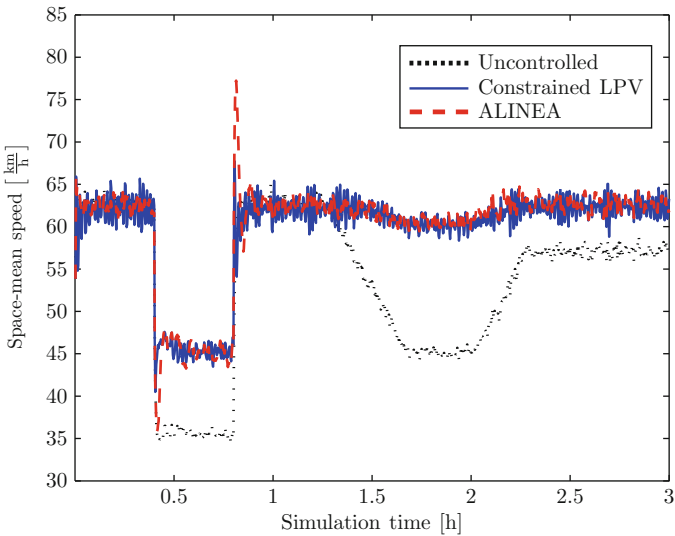


Fig. 18.3 Comparison of the space-mean speed evolution for the uncontrolled, polytopic controlled and the ALINEA controlled cases

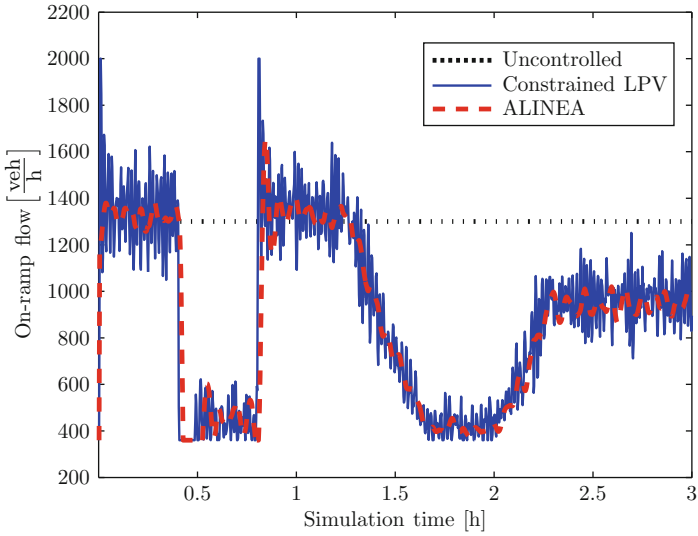


Fig. 18.4 Comparison of the on-ramp volume for the polytopic controlled, and the ALINEA controlled cases

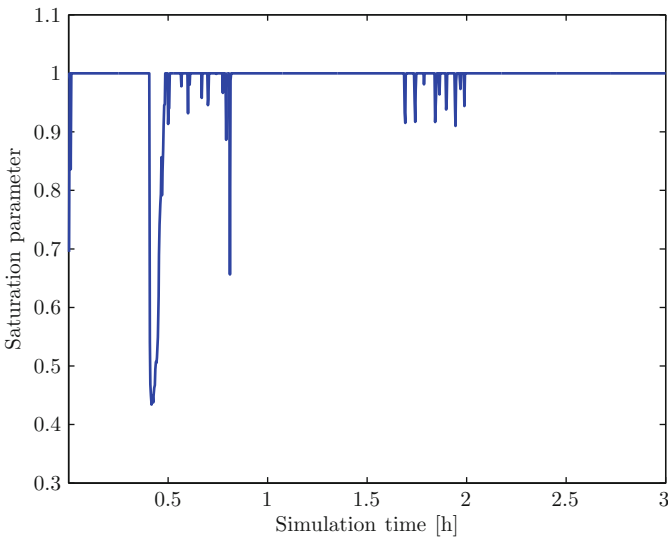


Fig. 18.5 The variation of the saturation parameter $\theta(u(k))$

Finally, the time evolution of the controller saturation level is depicted in Fig. 18.5, where one can ensure that the initial assumption on the minimal saturation parameter value $\theta_{\min} = 0.4$ has not been violated in the simulation scenario.

The advantage of the polytopic model-based controller design is the increased performance under changing disturbance conditions. Moreover, the systematic design methodology, offered by parameter-dependent paradigms, can be exploited. One can easily extend the model with an additional queue dynamics and incorporate the waiting queue in the performance output. The performance output of the system can also be extended, because of the second-order description, with space-mean speed. Since the centered variable characterizes the difference from the equilibrium speed, the extended performance output would be equal with the flow maximizing control objective. Furthermore, the possibility of additional measurements can be incorporated through the design, since the generality of the derived control synthesis. The disadvantage of the constrained LPV design method is the need of complex computational algorithms compared to ALINEA.

18.6 Conclusions and Further Research

Parameter-dependent methods have been adopted in the chapter for constrained freeway traffic control problem. For this purpose, the nonlinear second-order macroscopic model was transformed into a parameter-dependent polytopic form. Hard physical constraints were modeled as saturation limit and handled by using LPV methods. A dynamic controller was then proposed for the solution of the underlying control problem, where the effects of unmeasured signals were suppressed to avoid network throughput degradation. Solution was obtained as a standard optimization problem subject to convex constraints formulated by LMIs. A numerical example was given for the evaluation of the proposed method. Comparative simulation scenarios showed the improved disturbance rejection property of the constrained polytopic controller.

Further research will focus on evaluating the constrained LPV controller in more complex traffic scenarios and topology. Furthermore, the relaxation of computational needs arising in large-scale freeway networks will be addressed by adopting decentralized or distributed control schemes.

Acknowledgments This work is connected to the scientific program of the “Development of quality-oriented and harmonized R+D+I strategy and functional model at BME” project. The authors gratefully acknowledge to the support by the New Széchenyi Plan (Project ID: TÁMOP-4.2.1/B-09/1/KMR-2010-0002) and by the Hungarian scientific research fund (OTKA) through grant No. CNK 78168. This work has been partially supported by Chalmers’ new initiatives in Transportation, therefore B. Kulcsár acknowledges the support of the Area of Advance in Transportation and Aeje.

The authors would like to address special thanks to the head of Systems and Control Research Group, Professor József Bokor for his unique support of this research.

References

1. Apkarian P, Gahinet P (1995) A convex characterization of gain-scheduled \mathcal{H}_∞ controllers. *IEEE Trans Automat Contr* 40(5):853–864
2. Apkarian P, Gahinet P, Becker G (1995) Self-scheduled \mathcal{H}_∞ control of linear parameter-varying systems: a design example. *Automatica* 31(9):1251–1261
3. Baranyi P (2004) TP model transformation as a way to LMI based controller design. *IEEE Trans Ind Electron* 51(2):387–400
4. Becker G, Packard A (1994) Robust performance of linear parametrically varying systems using parametrically dependent linear feedback. *Syst Contr Lett* 23(3): 205–215
5. Bellemans T, De Schutter B, De Moor B (2003) Anticipative model predictive control for ramp metering in freeway networks. *Proc Am Contr Conf Denver Colorado*, 4070–4082
6. Hegyi A, De Schutter B, Hellendoorn H (2005) Model predictive control for optimal coordination of ramp metering and variable speed limits. *Transport Res C* 13(3):185–209
7. Jacquet D, Jaglin J, Koenig D, De Wit CC (2006) Non-local feedback ramp metering controller design. In: *Proceedings of the 11th IFAC Symposium on Control in Transportation Systems*, CTS
8. Kachroo P, Özbay K (2004) *Feedback ramp metering in intelligent transportation systems*. Kluwer Academic, New York
9. Kotsialos A, Papageorgiou M (2004) Nonlinear optimal control applied to coordinated ramp metering. *IEEE Trans Contr Syst Tech* 12(6):920–933
10. Lighthill MJ, Whitham GB (1955) On kinematic waves II. A theory of traffic flow on long crowded roads. *Proc Roy Soc Lond Ser A Math Phys Sci* 229:317–345
11. Luspay T, Kulcsár B, Varga I, Bokor J (2010) Parameter-dependent modeling of freeway traffic flow. *Transport Res C* 18(4):471–488
12. Luspay T, Kulcsár B, van Wingerden J-W, Verhaegen M, Bokor J (2011) Linear parameter varying identification of freeway traffic models. *IEEE Trans Contr Syst Tech* 19(1):31–45
13. Masher DP, Ross DW, Wong PJ, Tuan PL, Zeidler PL, Peracek S (1975) *Guidelines for design and operating of ramp control systems*. SRI, Menid Park, CA, Stanford Res. Inst. Rep. NCHRP 3-22, SRI Project 3340
14. Papageorgiou M (1998) Some remarks on macroscopic traffic flow modeling. *Transport Res A* 32(5):323–329
15. Papageorgiou M (2002) Freeway ramp metering: an overview. *IEEE Trans Intell Transport Syst* 3(4):271–281
16. Papageorgiou M, Blosseville JM, Hadj-Salem H (1990) Modelling and real-time control of traffic flow on the southern part of Boulevard Phiprique in Paris: Part I: Modelling, Part II. Coordinated on-ramp metering. *Transport Res A* 24(5):345–370
17. Papageorgiou M, Hadj-Salem H, Middelham F (1998) ALINEA local ramp metering - summary of field result. *Transport Res Rec* 1603:90–98
18. Payne HJ (1971) Models of freeway traffic and control. *Simulat Counc Proc Ser Math Model Publ Syst* 1(1):51–61
19. Scherer C, Weiland S (2005) *Linear matrix inequalities in control*. Lecture notes DISC
20. Shamma J, Athans M (1991) Guaranteed properties of gain scheduled control of linear parameter-varying plants. *Automatica* 27(3):559–564
21. Wattleworth JA (1965) Peak-period analysis and control of freeway system. *Highway Res Rec* 157:1–21
22. Whitham GB (1974) *Linear and nonlinear waves*. John Wiley, NY
23. Wu F (1995) *Control of linear parameter varying systems*. PhD dissertation, University of California at Berkeley
24. Wu F, Grigoriadis KM, Packard A (2000) Anti-windup controller design using linear parameter-varying control methods. *Int J Contr* 73(12):1104–1114
25. Zhou K, Doyle JC, Glover K (1996) *Robust and optimal control*, Prentice Hall, Englewood Cliffs, New Jersey

Chapter 19

Linear Parameter-Varying Control for the X-53 Active Aeroelastic Wing

Peter Seiler, Gary J. Balas, and Andrew Packard

Abstract Fuel efficiency, endurance, and noise requirements are pushing modern aircraft to lighter, more flexible designs. This causes the structural modes to occur at lower frequencies increasing the coupling with the rigid body dynamics. The traditional approach to handle aeroservoelastic interaction is to design gain-scheduled flight control laws based on the rigid body dynamics and then use filters to avoid exciting the structural modes. This decoupled approach may not be possible in future, more flexible aircraft without reducing the flight control law bandwidth. Linear parameter-varying (LPV) techniques provide a framework for modeling, analysis, and design of the control laws across the flight envelope. This chapter applies LPV techniques to the roll control of NASA Dryden's X-53 Active Aeroelastic Wing testbed. LPV techniques are first used to analyze a gain-scheduled classical controller. Gain-scheduling is still the dominant design method in industrial flight control laws and LPV analysis tools can play an important role in certifying the performance of these systems. Next, an LPV controller is designed and its performance is compared against the gain-scheduled classical controller. All results are obtained with a set of LPV tools which makes use of object-oriented programming to enable easy construction and manipulation of LPV models.

19.1 Introduction

Increased fuel efficiency and operational range are significant design drivers for modern commercial aircraft, e.g., the Boeing 787. Similar design objectives are also critical for future military aircraft, e.g., the SensorCraft concept aircraft [14, 18, 31].

P. Seiler (✉) • G.J. Balas
MUSYN, Inc., Minneapolis, MN, USA
e-mail: peter.j.seiler@gmail.com; balas@musyn.com

A. Packard
MUSYN, Inc., Berkeley, CA, USA
e-mail: andrew.packard60@gmail.com

In both cases, lighter aircraft are required to meet these objectives. The reduction in weight is typically achieved by reducing the structure in the wings and fuselage of the aircraft. This makes the aircraft more flexible and causes the structural modes occur at lower frequencies. The main consequence is that lighter, more flexible aircraft have tight coupling between the rigid body and elastic structural modes. This increases the likelihood of adverse aeroservoelastic phenomena including flutter and control surface reversal.

The traditional approach to handle aeroservoelastic interaction is to design the flight control laws based on the rigid body dynamics and then use filters to avoid exciting the structural modes. The control laws are typically designed at various points in the flight envelope and then gain-scheduled by interpolating these point designs. This gain-scheduled approach may not be possible on future, more flexible aircraft for which the structural modes occur at lower frequencies. The design will need to consider coupling between the rigid body dynamics, structural modes, and the time-varying gain-scheduled controller. Flexible aircraft would significantly benefit from an integrated aeroservoelastic and rigid body control system.

Several issues must be addressed to enable integrated active control to become a reality. First, the aeroelastic effects involve unsteady flows [15–17]. In addition, there can be nonlinear effects, e.g., nonlinear coupling between the structural modes and the aerodynamics [5, 15]. Advanced tools are needed to model these effects across the entire flight envelope. A second issue is that an integrated control design must account for the tight coupling between the rigid body and structural modes. This will likely require novel sensors that can measure, in real time, the aerodynamic flow around the aircraft structures. Such sensors are currently being developed [15–17] and new control architectures may be required to take advantage of these novel measurements. A third issue is that analysis tools are required to certify that the designed feedback system meets structural load requirements and is free from aeroservoelastic instabilities. Existing approaches based on robust flutter margins [6, 8, 13] form a starting point but may need to be extended to handle the complexities introduced by the integrated design approach. To summarize, advanced tools are required for modeling, integrated controller synthesis, and analysis of flexible aircraft.

This chapter investigates the use of linear parameter-varying (LPV) analysis and control techniques for flexible aircraft control. There are two main objectives of this chapter. The first is to introduce new software tools for LPV modeling, analysis, and control synthesis. These tools implement existing analysis and synthesis conditions drawn from the large body of literature on LPV systems including [1, 4, 19, 20, 24, 25, 27, 28, 32–34]. Implementation of the LPV algorithms makes use of object-oriented programming to enable easy construction and manipulation of LPV models. The second objective is to apply LPV techniques to NASA Dryden's X-53 active aeroelastic wing (AAW) testbed [21–23]. The AAW is an experimental flight test capability for aeroservoelastic control research. This chapter will focus on roll rate control of the AAW in the supersonic regime.

The remainder of the chapter has the following outline. First, a brief review of the AAW program is given in Sect. 19.2. The LPV software data structures and their

functionality are described in Sect. 19.3. Next, the AAW rigid body and aeroelastic dynamics are described in Sect. 19.4. A gain-scheduled classical control law is designed and analyzed in Sect. 19.5. Gain-scheduled classical control is the standard in industry for flight control design. LPV analysis tools can play an important role in certifying the performance of these systems and identifying potential issues due to fast variations in the gain-scheduling parameters. The LPV analysis tools provide a useful complement to existing approaches, e.g., margin requirements at each flight condition or robust flutter margins [6, 8, 13]. Section 19.6 describes an LPV controller for the AAW and compares this design against the gain-scheduled classical design. Finally, conclusions are given in Sect. 19.7. Early versions of these results appear in [26].

19.2 Active Aeroelastic Wing

NASA Dryden's X-53 AAW [21–23] was an experimental flight test capability for aeroservoelastic control research. NASA and the USAF developed this test bed to investigate the use of aeroelastic flexibility for improved performance of high aspect ratio wings. The effectiveness of the conventional aircraft surfaces, e.g., ailerons and trailing edge flaps, is reduced at higher dynamic pressures due to the flexibility of the wing. This can lead to control reversal at sufficiently high dynamic pressures. The standard solution is to reduce wing flexibility by adding structure, and hence additional weight, to the wings.

The main objective of the AAW Flight Research program was to test an alternative concept that uses wing flexibility to improve control effectiveness. The AAW has inner and outer flaps on the leading edge of the wings. Small movements of these surfaces cause the wing to twist in the direction that increases the local angle of attack and induces a rolling moment on the aircraft. These flaps do not undergo a control reversal and, in fact, their effectiveness increases at higher dynamic pressures. Thus the wing flexibility and twist act in a direction beneficial for control.

To test this concept, the AAW wings were modified from the standard F/A-18 wings to reduce the torsional stiffness [22]. This increases the wing flexibility and reduces the frequency of the flexible modes. Advanced tools are required to model the aeroelastic effects because they involve unsteady flows [15–17] and there can be nonlinearities [5, 15]. For control design, linear models of the rigid body and aeroelastic dynamics are obtained at each flight condition via linearization. This naturally falls within the class of LPV models that are scheduled as a function of the flight condition.

The flight-tested AAW control architecture is a modified version of the production F/A-18 control laws [11]. The basic architecture uses roll rate feedback to track roll rate commands from the pilot lateral stick inputs. The lateral controller commands the aileron, trailing edge flaps, inner leading edge flaps, and outer leading edge flaps (OLEFs). Each surface command is the sum of a proportional roll rate feedback term and a proportional roll rate tracking error term. The control gains

were tuned to maximize roll rate performance while satisfying structural load and handling quality requirements [11]. The gains were tuned using the multiobjective optimization tool CONDUIT [30]. This tool performs nonlinear optimization incorporating results from a high-fidelity simulation model.

The AAW control laws were designed and flight tested at separate design points in the flight envelope [10]. These control laws were tested during 34 Phase II test flights conducted from December 2004 through March 2005 [22]. The tests spanned the transonic and supersonic flight conditions and included 360° rolling maneuvers, 5g wind up turns, and 4g rolling pullouts. The flight test program validated the AAW concept and was deemed a success. Additional details on the existing AAW flight control laws and flight tests can be found in [10, 11, 22].

19.3 Tools for LPV Analysis and Design

LPV models are time-varying, state-space models of the form

$$\begin{bmatrix} \dot{x}(t) \\ y(t) \end{bmatrix} = \begin{bmatrix} A(\rho(t)) & B(\rho(t)) \\ C(\rho(t)) & D(\rho(t)) \end{bmatrix} \begin{bmatrix} x(t) \\ u(t) \end{bmatrix}, \quad (19.1)$$

where $A(\rho(t))$ is the state matrix, $B(\rho(t))$ is the input matrix, $C(\rho(t))$ is the output state matrix, $D(\rho(t))$ is the input transformation matrix, $\rho \in \mathbb{R}^{n_\rho}$ is a vector of measurable parameters, $x \in \mathbb{R}^{n_x}$ is the state, $y \in \mathbb{R}^{n_y}$ is the measurement, and $u \in \mathbb{R}^{n_u}$ is the control input. The dimensions of (A, B, C, D) are compatible with the signal dimensions.

LPV models arise in many contexts. In industrial settings, a finite collection of linear models is often used to describe the behavior of a system throughout an operating envelope. The linearized models describe the small signal behavior of the system at a specific operating point. The collection is parameterized by one or more physical variables whose values represent the operating point. For example, the LPV design model used in this chapter for the AAW roll rate dynamics is based on a parameterized family of linearizations. The models are scheduled across the aircraft (Altitude, Mach) flight envelope. Alternatively, LPV models can be constructed by considering state transformations on a class of nonlinear “quasi-LPV” systems [27]. This method essentially ignores some nonlinear relationships in the system dynamics and hence introduces conservatism in the control design.

LPV software tools have been developed to enable the modeling, analysis, controller synthesis, and simulation for LPV systems. One issue is that several different methods have arisen for representing the parameter dependence in LPV models (19.1). These include linear fractional transformations (LFTs) [1, 19, 20, 24, 25], linearizations on a gridded domain [4, 33, 34], and polytopic (affine) dependence of the state matrices on the parameters [2, 3, 9, 29]. Each of these different representations has benefits and drawbacks in terms of the modeling effort

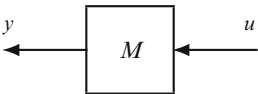
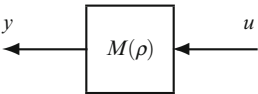
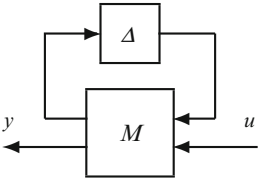
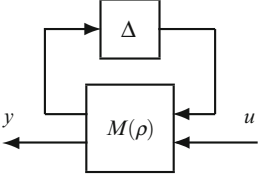
and model structure that can be exploited in developing computational algorithms. It would be useful for the controls community to have a single LPV toolbox that easily supports the different representations. Ideally this would include tools to transform an LPV model in one representation to another representation. This would enable easy comparison between the various LPV methods and with classical gain-scheduling approaches.

As a starting point, the initial implementation of the LPV algorithms focuses on models defined on gridded domains. This is motivated by aircraft aeroelastic control problems for which models are typically constructed as linearizations around various flight operating points. A key component of the software tools is the core LPV data structure object, referred to as a `pss` (denoting parameter-varying state-space model). The LPV systems in (19.1) are conceptually represented by a state-space system S that depends on a parameter vector ρ in some domain of \mathbb{R}^{n_ρ} . For general LPV systems, this conceptual representation requires storing the state-space system at an infinite number of points in the domain of ρ . The data structure object `pss` approximates this conceptual representation by storing the LPV system as a state-space array defined on a finite, gridded domain. As a simple example, consider an LPV system $S(\rho)$ that depends on a single parameter ρ in the domain $\rho \in [a, b]$. The infrastructure requires the user to specify the domain with a finite grid, e.g. N points in the interval $[a, b]$. The software tools include an `rgrid` data object to facilitate the creation and manipulation of the multivariable parameter domains. The user must also specify the values of the state-space system S at each point ρ in this gridded domain. The `pss` object stores the state-space array data using the standard MATLAB Control System Toolbox `ss` object. Thus the `pss` can be viewed as the parameter-varying extension of the standard `ss` object. To summarize, the LPV system $S(\rho)$ is represented by a `pss` data object which stores the gridded domain and the array that defines the state-space data at each point in the domain.

The notions of parameter-varying matrices and parameter-varying frequency responses arise naturally to complement the `pss` objects. LPV systems are time-varying and hence frequency responses cannot be used to represent the system behavior as parameters vary. However, frequency responses are useful to gain intuition about the system performance at fixed locations in the operating domain. The parameter-varying matrices and frequency responses are represented by `pmat` and `pfrd` data objects, respectively. These two data objects are both stored as a data array defined on a gridded domain. Table 19.1 shows the relation between the LPV data objects (`pmat`, `pss`, `pfrd`) and existing MATLAB objects. The first row of the Table (“Nominal”) shows the basic MATLAB objects: matrices are `double` objects, state-space systems are `ss` objects, and frequency responses are `frd` objects. `double` objects are in the standard MATLAB release while the `ss` and `frd` objects are part of the Control System Toolbox. The second row of Table 19.1 (“Parameter Varying”) shows the core LPV objects. The LPV objects (`pmat`, `pss`, `pfrd`) can be viewed as parameter-varying extensions of the standard MATLAB and Control Toolbox objects (`double`, `ss`, `frd`).

The third row of the table (“Uncertain”) shows the equivalent objects used to represent uncertainty: uncertain matrices, state-space systems, and frequency responses

Table 19.1 Relation between MATLAB objects

Object Type	Block	Matrix	System	Frequency Response
Nominal		double	ss	frd
Parameter Varying		pmat	pss	pfrd
Uncertain		umat	uss	ufrd
Uncertain Parameter Varying		upmat	upss	upfrd

are represented by `umat`, `uss`, and `ufrd` objects, respectively. These objects are part of the MATLAB Robust Control Toolbox. The Robust Control Toolbox models the uncertainty as a perturbation Δ wrapped in feedback around a nominal part M , i.e., uncertainty is represented using a linear fractional transformation. Real parametric, complex parametric, and unmodeled dynamic uncertainties can be modeled. The last row of Table 19.1 (“Uncertain Parameter Varying”) shows the corresponding parameter-varying objects with uncertainty: uncertain parameter-varying matrices, state-space systems, and frequency responses are represented by `upmat`, `upss`, and `upfrd` objects, respectively. The parameter-varying uncertain objects are not yet implemented but they are essential to developing robustness analysis and design tools for LPV systems. There is also a natural overlap with the linear fractional representation for LPV systems.

The LPV objects are being developed within MATLAB’s object-oriented programming framework. A benefit of object-oriented programming is that key operations can be overloaded to provide seamless, consistent functionality across a variety of objects. For example, if A and B are `double` objects then the syntax $A*B$ simply multiplies the matrices. If A and B are `pmat` objects then the syntax $A*B$ multiplies the parameter-varying matrices at each point in the parameter domain.

The manipulation of parameter-varying objects is facilitated by this extension of the $*$ operation to a meaningful, intuitive operation for `pmat` objects. In addition, standard MATLAB syntaxes, e.g., `M(i, j)` to index into the (i, j) element of an array, have been overloaded and extended for parameter-varying objects. Object-oriented programming enables this overloading of key functions and this enables meaningful, intuitive extensions for parameter-varying objects.

To summarize, development of object-oriented LPV software tools will help expand the functionality and tools for LTI systems, as developed in the MATLAB Control and Robust Control Toolboxes, to linear parameter-varying systems. SIMULINK blocks have also been developed to simulate LPV systems. There are several challenges and open issues going forward. These include the numerical stability and scalability of the algorithms, incorporation of uncertainty analysis, and development of the data infrastructure and tools to encompass the various LPV representations. The remainder of the chapter will demonstrate the application of LPV analysis and control design techniques to the AAW control design example.

19.4 AAW Roll Rate Model

The AAW rigid body roll rate dynamics are given by

$$\dot{p} = L_p(h, M)p + L_\delta(h, M)\delta \quad (19.2)$$

where p is roll rate (deg/s) and δ is the OLEF position (deg). The OLEF is effective across the supersonic flight envelope of interest. Thus only this surface is used for roll rate control design in this chapter. The rigid body LPV model from OLEF to roll rate (19.2) is denoted G_{rig} .

L_p and L_δ are defined on a grid of altitude h (ft) and Mach M (unitless) with values provided in Tables 19.2 and 19.3. These data were constructed from nondimensional aerodynamic coefficients obtained from NASA Dryden [7]. The nondimensional L_δ data were rescaled to obtain a mean gain of 2 over the flight envelope. Hence the variations of the L_δ data in Table 19.3 across the flight envelope accurately represent the AAW OLEF gain but the absolute magnitude contains a scaling factor. This scaling will be discussed in the following paragraphs.

The AAW wings were modified for increased flexibility leading to flexible modes occurring at lower frequencies. Models of the AAW aeroelastic dynamics were obtained from NASA Dryden [7] on a grid of altitude, Mach, and remaining

Table 19.2 AAW rigid body data, L_p

	M = 1.1	M = 1.2	M = 1.3
h = 10k	-0.5652	-0.4614	-0.4009
h = 15k	-0.5415	-0.4363	-0.3737
h = 20k	-0.5165	-0.4128	-0.3606
h = 25k	-0.5034	-0.3982	-0.3531

Table 19.3 AAW rigid body data, L_{δ}

	M = 1.1	M = 1.2	M = 1.3
h = 10k	1.2916	1.3756	1.2425
h = 15k	0.9305	1.0524	1.1958
h = 20k	0.6032	0.7009	0.8326
h = 25k	0.3056	0.4110	0.5258

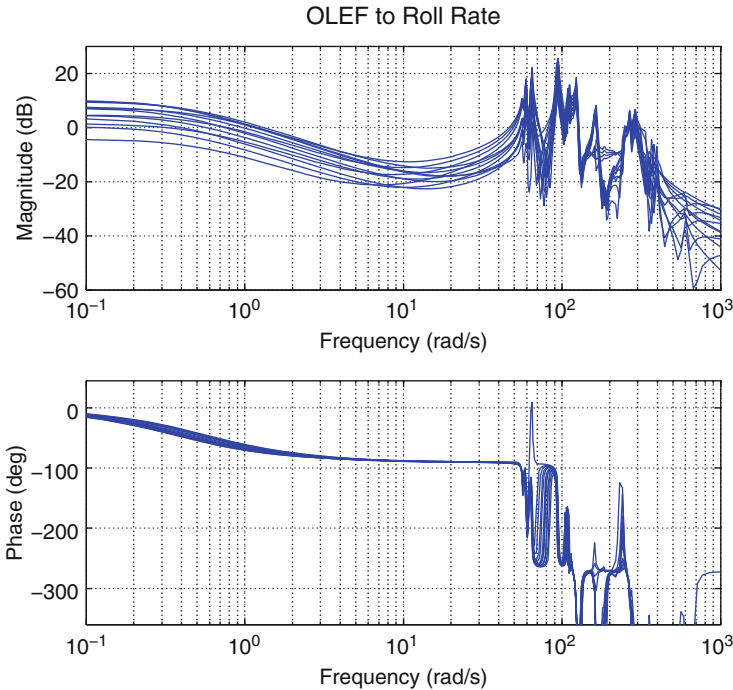


Fig. 19.1 Open-loop Bode plots from OLEF to roll rate

fuel. The dependence on remaining fuel is neglected and the models at 60% fuel are used for the design and analysis. The aeroelastic dynamics are defined on the same (h, M) grid used to define the rigid body dynamics, i.e., the aeroelastic dynamics are defined on the grid $h = \{10,000, 15,000, 20,000, 25,000\}$ ft and $M = \{1.1, 1.2, 1.3\}$. At each flight condition, the aeroelastic dynamics are modeled as a state-space system with 164 states. This model includes 64 states for the first 32 flexible modes and another 100 states for aerodynamic lags. The aerodynamic lag states can be truncated at each point in flight envelope with minimal impact on the OLEF to roll rate dynamics. The resulting aeroelastic model, denoted G_{flex} , has 64 states at each (h, M) flight condition.

The aeroelastic dynamics are added in parallel to the rigid body dynamics to obtain the full 65 state model, $G_{full} = G_{rig} + G_{flex}$. Figure 19.1 shows the open-loop

Bode plots of G_{full} from OLEF to roll rate at each point in the (h, M) domain. As noted above, the L_{δ} data were rescaled to give a mean gain of 2 across the flight envelope. This effectively increases the significance of the flexible modes relative to the rigid body dynamics. In particular, several of the flexible modes have magnitude exceeding 15 dB at points in the flight envelope. The first cluster of flexible modes occur around 55–65 rad/s. The OLEF actuator has a bandwidth of 75 rad/s. This bandwidth is not fast enough to actively suppress these flexible modes. The original intent was to use LPV techniques to actively control the AAW flexible modes. The AAW aircraft does not require active attenuation of the flexible modes nor is the OLEF actuator sufficiently fast to suppress these modes. Thus any control law must roll-off to avoid exciting these modes. Since the OLEF actuator dynamics are substantially faster than the AAW roll subsidence mode (L_p) these dynamics will be neglected in most of the design and analysis in the subsequent sections.

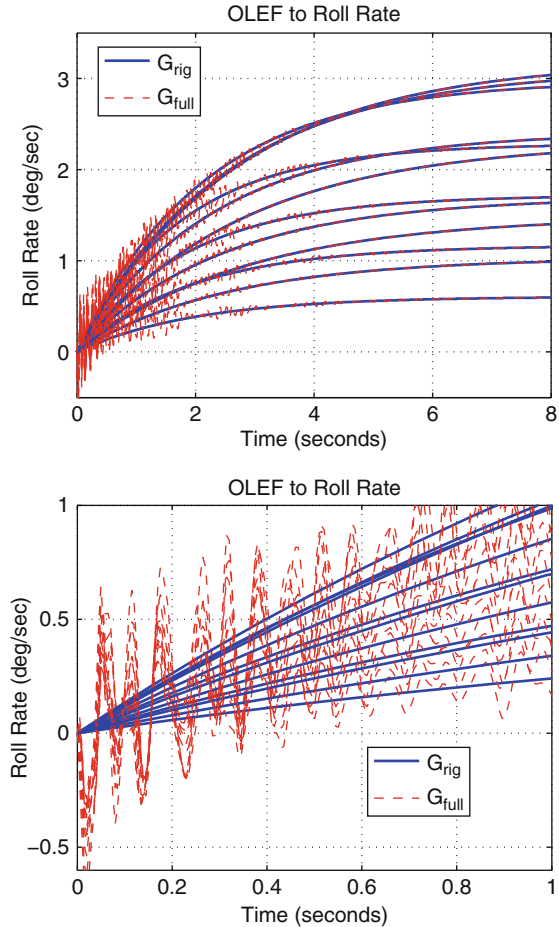
Figure 19.2 shows the open-loop roll rate responses due to an OLEF step of magnitude $\delta = 1^\circ$. The top plot shows the response over an 8 s time scale and the bottom plot zooms in on the transient response over the first second. In both plots the solid curves are the rigid body responses at each point in the (h, M) domain while the dashed curves are the responses of the full model with the flexible modes. The rigid body responses in the top plot show the variation in DC gain and time constant across the flight envelope. Based on the data in Table 19.2, the time constant varies from a minimum of 1.77 s to a maximum of 2.83 s. The responses of G_{full} show the transient effects of the flexible modes which are excited by the step input. The bottom plot more clearly shows this transient response. The flexible modes create a roll rate oscillation with an amplitude of approximately 0.6 deg/s in the first 0.5 to 1.0 s of the step responses. These lightly damped oscillations decay to a negligible amplitude after 2–3 s.

As described in Sect. 19.3, the core infrastructure for LPV modeling was developed using MATLAB object-oriented class programming. The overloading of key functions enables easy manipulation and analysis of these gridded models.

19.5 Gain-Scheduled Classical Control

Gain-scheduling via interpolation of point designs is still the predominant method used in industry to develop a full-envelope flight control law. LPV analysis can play an important role in certifying the performance of these control laws. Moreover, LPV analysis tools can uncover potential stability and performance degradations caused by rapid variations in the operating condition. This is especially important for systems with significant aeroelastic effects because flexible modes may be excited during aircraft maneuvers. This section analyzes the performance of a gain-scheduled classical roll rate control design using LPV techniques.

Fig. 19.2 Open-loop step responses from OLEF to roll rate (*Top*: Long time scale, *Bottom*: Zoom on transient response)



19.5.1 Control Design

The primary flight control objective is to design a feedback law to track roll rate commands. The variation in the speed of response and gain of the AAW rigid body dynamics across the (h, M) flight envelope (Tables 19.2 and 19.3) poses one issue for the control design. The roll subsidence mode varies from -0.56 rad/s to -0.35 rad/s and the input gain varies from 0.31 to 1.29. A gain-scheduled controller is designed to achieve a consistent bandwidth of 1.25 rad/s and zero steady-state error due to step roll rate commands across the envelope. Another design issue is that the controller must be robust to the flexible modes. The gain-scheduled controller is designed so that, in closed loop, the flexible modes have magnitude less than -20 dB at each point in the flight envelope. This is to ensure the flexible wing modes are not excited by the flight control system. In addition, the gain-scheduled

controller should achieve 6 dB of gain margin and 45° of phase margin at each point in the envelope. These are standard margin requirements for military aircraft. The margin specifications at each point in the envelope essentially assume a quasi-steady approximation for (h, M) . LPV analysis tools will be used to determine the impact of variations in (h, M) on the closed-loop performance.

A classical gain-scheduled controller is designed to achieve these objectives. The basic idea is to invert the rigid body dynamics and replace them with a desired loop shape. In other words, the controller is given by $K_{cl} = G_{inv}G_{ls}$ where G_{inv} inverts the plant dynamics and G_{ls} is the desired loop shape. At each flight condition, the AAW rigid body roll rate dynamics are given by $\frac{L_\delta}{s+L_p}$. The rigid body dynamics are, in general, time-varying due to the dependence on (h, M) and hence the transfer function representation is not correct. However, this representation will be used to provide the basic insight into the control design. The controller inverts the rigid body dynamics up to a bandwidth ω_{ro} to prevent exciting the flexible modes, $G_{inv} = \frac{s+L_p}{L_\delta} \frac{\omega_{ro}}{s+\omega_{ro}}$. The roll-off is chosen to be $\omega_{ro} = 12.5$ rad/s. This is fast enough to have minimal impact on the roll rate response but slow enough to avoid excessive excitation of the flex modes at 55–65 rad/s. The desired loop shape is $G_{ls} = \frac{\omega_d^2}{s^2+2\zeta\omega_d}$. The values used in the control design are $\zeta = 0.8$ and $\omega_d = 1.25$ rad/s. This desired loop shape provides a second-order step response with small overshoot, zero steady-state error, and a rise time of approximately 2.2 s.

As noted above, the plant and controller are both, in general, time-varying systems and transfer function representations are not meaningful. State-space representations should be used instead. The gain-scheduled classical controller $K_{cl} = G_{inv}G_{ls}$ is given by the state-space representations:

$$\left[\begin{array}{c|c} A_{ls} & B_{ls} \\ \hline C_{ls} & D_{ls} \end{array} \right] := \left[\begin{array}{cc|c} -2\zeta\omega_d & 1 & 0 \\ 0 & 0 & \omega_d \\ \hline \omega_d & 0 & 0 \end{array} \right], \quad (19.3)$$

$$\left[\begin{array}{c|c} A_{inv} & B_{inv} \\ \hline C_{inv} & D_{inv} \end{array} \right] := \left[\begin{array}{c|c} -\omega_{ro} & \omega_{ro} \\ \hline -\frac{L_p(h, M) + \omega_{ro}}{L_\delta(h, M)} & \frac{\omega_{ro}}{L_\delta(h, M)} \end{array} \right]. \quad (19.4)$$

The dependence on (h, M) has been made explicit for clarity. The controller state matrices are defined on the 4×3 (h, M) grid for which plant data are available (see Tables 19.2 and 19.3). The classical controller is gain-scheduled by linearly interpolating the state matrices for G_{ls} and G_{inv} .

A simple, but important observation is that time-varying systems, in general, do not commute. Thus the closed-loop performance will be impacted by reordering the controller as $G_{ls}G_{inv}$ or using an alternative state-space realization for G_{inv} . The realization of G_{inv} in (19.4) isolates all time-variations in the output and feedthrough matrices. This realization enables the controller to instantly cancel variations in the plant dynamics. A drawback is that this realization of the controller will be sensitive to errors in the AAW gain-scheduled model.

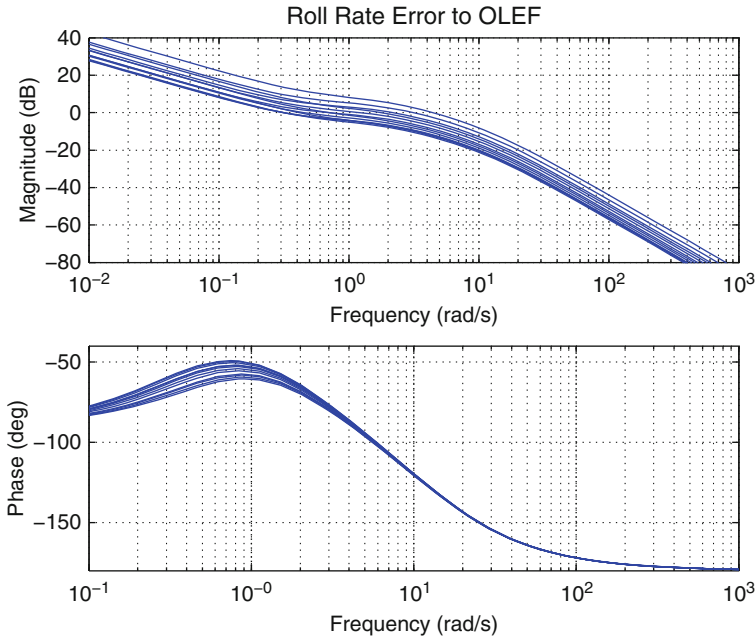


Fig. 19.3 Bode plots of classical controller

19.5.2 LTI Point Analysis

Insight into the control design and feedback system can be obtained by studying the LTI performance at each point in the flight envelope. Figure 19.3 shows the Bode plots for the classical controller K_{cl} at each point in the flight envelope. The controller has proportional–integral action at low frequencies with a second-order roll-off beyond ω_{ro} to avoid exciting the flexible modes. These Bode plots show an intuitive classical design at each point in the flight domain.

Figure 19.4 shows the Bode plots for the (open)-loop function $G_{full}K_{cl}$ at each point in the flight envelope. The loop function again shows integral action at low frequencies. In addition, the loop transfer function $G_{full}K_{cl}$ shows significant attenuation of the flexible modes in comparison with the open-loop Bode G_{full} (Fig. 19.1). The loop $G_{full}K_{cl}$ has all modes below -19 dB at all points in the flight envelope. In closed-loop the flexible modes are still well attenuated. The closed-loop response from roll rate command to roll rate has the flexible modes below -18.5 dB at all points in the domain. The loop function $G_{full}K_{cl}$ has gain and phase margins exceeding 21.3 dB and 65.9° at each point in the flight domain. Thus the classical controller has good gain and phase margins at each point in the flight envelope.

Figure 19.5 shows the closed-loop unit step responses to a 1° roll rate command at all points in the flight envelope. The full model with flexible modes G_{full} and gain-scheduled classical controller K_{cl} is used to generate these closed-loop responses.

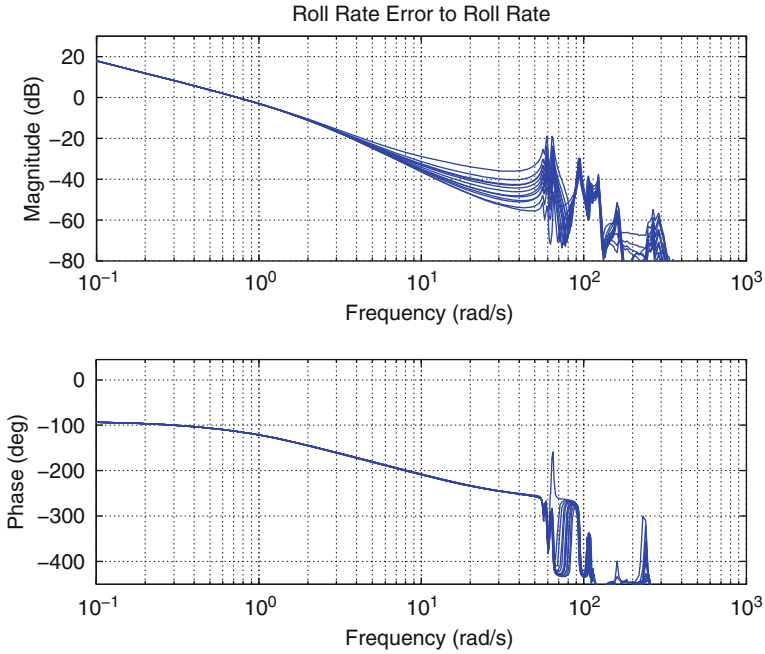
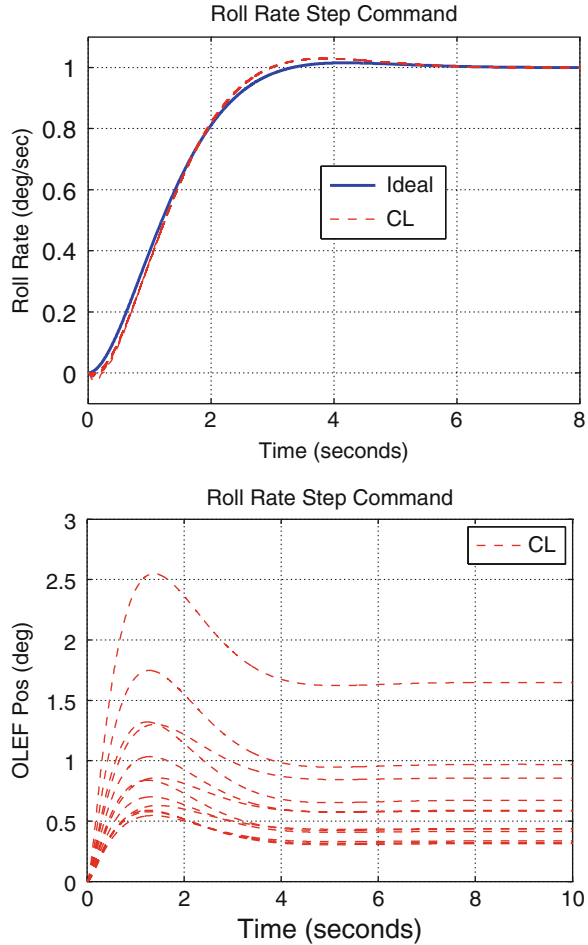


Fig. 19.4 Bode plots of loop function $G_{full}K_{cl}$

The top plot shows the roll rate response and the bottom plot shows the OLEF position. The blue solid curve in the top plot shows the ideal closed-loop response given by the open-loop specification G_{ls} . The red dashed curves in both plots show the closed-loop responses at each point in the (h, M) domain. The classical controller achieves consistent dynamic performance across the flight envelope with zero steady-state error (top plot). The bottom plot shows the variation in the control actuation required to achieve this uniform tracking performance. In addition, the closed-loop step responses (top plot of Fig. 19.5) indicate only small oscillations in the initial transient due to the flexible modes. This is due to the high-frequency roll-off of K_{cl} which attenuates the flexible modes. Finally, the closed-loop responses (top plot) have a small deviation from the ideal response. This is due to the high-frequency roll-off in G_{inv} to avoid exciting the flexible modes.

The closed-loop performance can be evaluated using the induced L_2 norm of various closed-loop sensitivity functions in the feedback loop. Table 19.4a shows results computed for the feedback system consisting of the rigid body dynamics G_{rig} and the gain-scheduled classical controller K_{cl} . The rows labelled S_i , T_i , S_o , and T_o provide induced L_2 norm bounds for the input sensitivity, input complementary sensitivity, output sensitivity, and output complementary sensitivity. The second column, labelled Point H_∞ , is the maximum H_∞ norm over all points in the flight envelope. For the row labelled S_i , this result was obtained by computing the H_∞ norm of the input sensitivity function at each point in the flight envelope and then

Fig. 19.5 Closed-loop responses to step roll rate command with K_{cl}



maximizing over the flight envelope. The results in the other rows were obtained similarly. Each data point in this column took, on average, 0.21 s to compute on a laptop with a dual-core 2.16 GHz Intel processor. At a fixed point in the flight envelope, the H_∞ norm for each sensitivity function is equal to its induced L_2 norm. This is a lower bound on the actual induced L_2 norm for the gain-scheduled system since it does not account for parameter variations. The results for the input and output functions are equal because the feedback loop is SISO and the pointwise H_∞ norm assumes time-invariant dynamics at each point in the domain. The remaining columns in Table 19.4a are discussed in the following section.

The pointwise H_∞ analysis can also be used to investigate the impact of the flexible modes at each point in the domain. The full-model G_{full} with rigid body and aeroelastic dynamics has 65 states. For this analysis, a reduced order model, G_{red} , that captures the first three flexible modes was constructed by residualizing

Table 19.4 L_2 induced norms for closed-loop sensitivity functions with gain-scheduled classical controller

(a) Closed loop with $(G_{\text{rig}}, K_{\text{cl}})$				
	Point H_∞	LPV1	LPV2	LPV3
S_i	1.292	3.786	2.222	1.590
T_i	1.000	3.685	2.116	1.431
S_o	1.292	1.295	1.296	1.298
T_o	1.000	1.000	1.000	1.001
(b) Closed loop with $(G_{\text{red}}, K_{\text{cl}})$				
S_i	1.314	Inf	2.202	1.548
T_i	1.000	Inf	2.143	1.418
S_o	1.314	Inf	2.406	1.347
T_o	1.000	Inf	2.096	1.009

the higher frequency flexible modes at all points in the flight envelope. G_{red} has a total of seven states: one state for the rigid body dynamics and six states for the first three flexible modes. The closed-loop sensitivity functions are then formed with G_{red} and K_{cl} . Table 19.4b shows the various norms computed for the closed-loop sensitivity functions with G_{red} and K_{cl} . The rows and columns of this table can be compared with the previous analysis for the closed-loop with the rigid body dynamics (Table 19.4a). The maximum H_∞ norm over the flight envelope (column: Point H_∞) shows only minor differences with the results for the rigid body dynamics. Thus the H_∞ norms computed at each point in the flight domain indicate that the aeroelastic dynamics will have minimal impact on the gain-scheduled performance.

19.5.3 LPV Analysis

The analysis of the gain-scheduled classical controller has, up to this point, focused on the performance at each point in the (h, M) flight envelope. This analysis neglects the impact of time variations in altitude and Mach. The induced L_2 norm for an LPV system is the maximum input/output gain over all inputs and a class of allowable parameter trajectories. A generalization of the Bounded Real Lemma leads to linear matrix inequality (LMI) conditions for computing bounds on the induced L_2 norm. A brief review is provided in Appendix.

Upper bounds on the induced L_2 norm of the various closed-loop sensitivity functions were computed to gain insight into the effect of variations in (h, M) . The results for the closed-loop with G_{rig} and K_{cl} are given in the columns LPV1, LPV2, and LPV3 of Table 19.4a. The results in these columns involve LPV-induced L_2 norm upper bounds of various complexity. The column labelled LPV1 used constant Lyapunov matrices in the induced L_2 norm LMI conditions. This is equivalent to an analysis that assumes no knowledge of the parameter rates. The results in columns LPV2 and LPV3 both assume the rate bounds $|\dot{M}| \leq 0.02$ 1/s and $|\dot{h}| \leq 1,000$ ft/s. LPV2 uses a parameter-dependent Lyapunov function of the form $X(\rho) = X_0 + MX_1 + hX_2$ while LPV3 also includes quadratic basis functions,

$X(\rho) = X_0 + MX_1 + hX_2 + M^2X_3 + MhX_4 + h^2X_5$. In theory, the upper bounds on the induced L_2 norm should progressively decrease from analysis LPV1 to LPV2 to LPV3. The results for S_o and T_o in Table 19.4a do not demonstrate this theoretical trend but the results are within the stopping tolerances of the optimization solver.

There are several interesting aspects to the LPV analysis results in Table 19.4a. First, the output sensitivity functions, S_o and T_o , have an induced norm almost exactly equal to the pointwise H_∞ lower bound. This is because the classical controller perfectly cancels the rigid body dynamics for reference commands that enter at the plant output. However, the cancellation is not perfect for disturbances that enter at the plant input. Thus there is a gap between the upper bounds for S_i and T_i and the pointwise H_∞ lower bounds. The gap is reduced by including additional basis functions in the LPV analysis. The price paid for this improved upper bound is an increased computational complexity. Each LPV1, LPV2, and LPV3 analysis took 0.75, 10.1, and 37.6 s, on average. These results indicate that the variations in (h, M) are unlikely to affect the reference tracking but it may have some effect on disturbance rejection at the plant input.

It should also be re-emphasized that the performance depends on the state realization for G_{inv} . An alternative realization for G_{inv} is given by $B_{inv} = \frac{\omega_{ro}}{L_\delta(h, M)}$ and $C_{inv} = -(L_p(h, M) + \omega_{ro})$ with the same A_{inv} and D_{inv} given in (19.4). The alternative realization is identical to the original realization for fixed flight conditions and hence it yields the same pointwise H_∞ norms as in Table 19.4a. However, the LPV3 analysis results yield norms of 3.433, 3.416, 1.365, and 1.107 for S_i , T_i , S_o , and T_o , respectively. These are significantly larger than the LPV3 results in Table 19.4a for the original state-space realization of G_{inv} in (19.4). It should be noted that the alternative state-space realization for G_{inv} has parameter dependence in the input matrix. This parameter dependence must pass through the G_{inv} dynamics before it is able to cancel the variations in the plant dynamics. Thus one might have anticipated that this alternative realization leads to degraded performance when compared to the original realization in (19.4). This analysis demonstrates that the LPV-induced norm bounds can be used to aid the design engineer in selecting the best realization for gain-scheduling.

The LPV analysis can also be used to investigate the impact of the flexible modes. As described in the previous section, a reduced order, 7-state aeroelastic model was obtained by retaining the first three flexible modes in the full model. This model reduction was mainly motivated by the computational complexity of the LPV analysis condition with respect to the plant state dimension. The 65-state model G_{full} is too large to be handled by current optimization solvers but the 7-state reduced order model can be analyzed in a reasonable amount of time. Columns LPV1, LPV2, and LPV3 in Table 19.4b shows the LPV upper bounds computed for the closed-loop sensitivity functions with G_{red} and K_{cl} . The rows and columns of this table can be compared with the previous analysis for the closed loop with the rigid body dynamics (Table 19.4a). The LPV upper bounds computed with using linear and quadratic basis functions (column LPV3 in Table 19.4b) are roughly the same as the results obtained with the rigid body dynamics (column LPV3 in Table 19.4a).

This indicates that the aeroelastic dynamics will have a minor impact on the gain-scheduled closed-loop performance. This agrees with the results obtained using pointwise H_∞ norms. The results labelled *Inf* in column LPV1 indicate that no provable upper bound on the induced L_2 norm can be obtained using constant, quadratic Lyapunov functions.

The LPV analysis (Table 19.4a, b) has gaps between the pointwise H_∞ lower bounds and the LPV3 analysis upper bound. The user could continue adding basis functions and see if the LPV3 analysis bound can be reduced. However, there is a computational penalty to be paid for adding basis functions. Each point H_∞ , LPV1, LPV2, and LPV3 analysis in Table 19.4b took 0.08, 0.58, 91.6, and 360.6 s, on average. An alternative is to compute improved lower bounds via simulation. This is discussed in the next section.

19.5.4 Worst-Case Simulation

A SIMULINK block has been developed to enable easy simulation of LPV systems. This block is similar to the SIMULINK state-space block but with an additional input to specify the parameter trajectory. The function `wcsim` has been developed to perform a worst-case LPV analysis directly on a SIMULINK model. “Worst-case” refers to maximizing or minimizing a user-specified cost over a set of parameter trajectories subject to user-specified constraint functions.

`wcsim` works directly on a SIMULINK model that contains feedback interconnections of LTI and/or LPV systems. The user specifies ρ to be a linear combination of piecewise continuous functions, i.e., $\rho_c(t) \in \mathcal{P} := \{\rho(t) = \sum_{i=1}^{n_b} c_i \rho_i(t)\}$ where $\{\rho_i\}$ are the user-specified basis functions. Let $y_c : [0, t_f] \rightarrow \mathbb{R}^{n_y}$ denote the vector of output signals from the SIMULINK diagram for a given choice of the parameter vector coefficients, $c \in \mathbb{R}^{n_b}$. The worst-case simulation problem is

$$\begin{aligned} & \max_{c \in \mathbb{R}^{n_b}} G(y_c) \\ & \text{subject to: } \underline{C} \leq C(y_c) \leq \bar{C}. \end{aligned} \quad (19.5)$$

$G : L_2^{n_y}[0, t_f] \rightarrow \mathbb{R}$ denotes the objective functional that quantifies the performance of the output by $G(y_c)$. $C : L_2^{n_y}[0, t_f] \rightarrow \mathbb{R}^m$ denotes a constraint function that defines a set of m constraints on the output. \underline{C} and $\bar{C} \in \mathbb{R}^m$ specify the lower and upper bounds on the constraint function. Maximization is without loss of generality. The objective and constraint functions for a worst-case simulation are specified with specialized SIMULINK Objective Function and Constraint Function blocks. These blocks are similar to a standard To Workspace block except their dialog boxes contain additional fields to specify the objective and constraint functions.

The `wcsim` function optimizes the objective function over the set of allowable parameter trajectories subject to the specified constraints. The basic syntax is `wcrho = wcsim('mdl')`. The input specifies the SIMULINK diagram with LPV blocks, Objective Function, and (optionally) Constraint Function blocks. `wcsim` returns the worst-case parameter trajectory. No assumptions are made about the objective function G or constraint function C . As a result, the optimization is, in general, not convex and it may have many local optima that are not global optima. `wcsim` simply uses gradient-based optimization to find a parameter trajectory that achieves a local maxima. While this does not necessarily find the global optima, it does provide a means to improve upon “bad” parameter trajectories found with other heuristic methods.

The gradient-based optimization is performed by `fmincon` and thus requires the MATLAB Optimization toolbox. At each iteration, `fmincon` requires multiple evaluations of the objective and constraint functions in order to compute numerical gradients. An evaluation of all objective and constraint functions specified in a SIMULINK diagram requires one simulation of the model. At each iteration `fmincon` evaluates the objective function at the current value $c \in \mathbb{R}^{n_b}$ of the parameter trajectory coefficients well as at small perturbations along each coefficient direction. If the parameter trajectory contains n_b coefficients, `fmincon` will perform approximately $n_b + 1$ simulations at each iteration. Simulating the system is typically responsible for the bulk of the computation time to perform a worst-case simulation. Thus the total time for `wcsim` with no constraint blocks will be roughly $(n_c + 1)N_i\tau$ where τ is the computation time for one simulation and N_i is the number of iterations. If the model contains constraint blocks, then `fmincon` will typically perform additional function evaluations, and hence additional simulations, per iteration.

Figure 19.6 shows the SIMULINK diagram used to investigate the AAW closed-loop roll rate tracking performance. The diagram contains the controller K_{cl} in the LPV block labelled “Gain-Scheduled Controller.” The LPV block labelled “LPV AAW” contains the full AAW model, G_{full} . In addition, the OLEF actuator dynamics have been included in the feedback loop. The diagram contains inputs for roll rate command and plant step input disturbance. The LPV analysis in the previous section indicated that the input sensitivity functions were more likely to be affected by parameter variations. This section focuses on the OLEF actuator position response due to the step input disturbance. The roll rate command is set to zero.

The model was simulated at each point in the flight domain to investigate the closed-loop performance. The L_2 norm of the OLEF actuator position response to the input step disturbance varied from 2.720 to 2.723 across the flight domain. This indicates uniform disturbance rejection performance at each point in the flight envelope. The OLEF response due to the input step disturbance is shown as the solid line (“Nominal”) in the top subplot of Fig. 19.7. This simulation was performed at the center of the flight envelope, i.e., $(h, M) = (17, 500 \text{ ft}, 1.2)$. The response is well damped and shows no oscillations due to the flexible modes. In addition, the OLEF position cancels the disturbance in steady state. The average time to complete one simulation is 25.3 s.

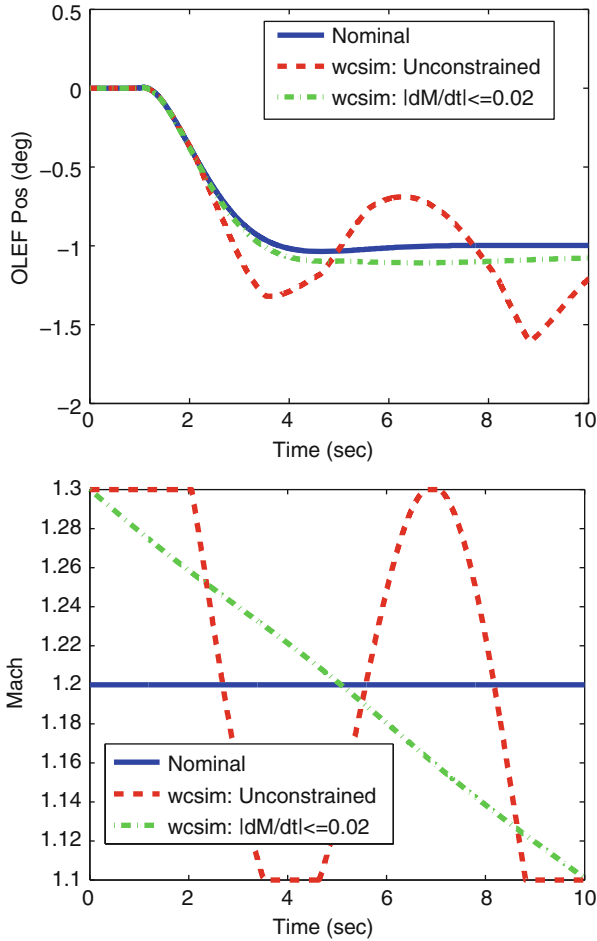


Fig. 19.7 Simulation results due to step input disturbance

Next `wcsim` is used to perform a search for time-varying trajectories that degrade the disturbance rejection performance. For this example, `wcsim` maximizes the L_2 norm of the OLEF position by searching over parameter trajectories of the form $c_0 + c_1t + c_2 \cos(t) + c_3 \sin(t)$ where c_i are constants to be optimized. Both the Mach and Altitude parameter trajectories are restricted to have this form and thus there are a total of eight coefficients to be optimized. The objective function is specified using the block labeled “Objective” in Fig. 19.7. For this example, the `wcsim` objective is to maximize the L_2 norm of the OLEF position response due to the input step disturbance.

Initially, no constraints are placed on the parameter trajectory and parameter rates. The trajectories are projected to lie within the bounds of the (h, M) parameter

domain at all times using a saturation block. After $N_i = 4$ gradient steps, `wcsim` finds a parameter trajectory that achieves an OLEF position L_2 norm of 3.096. The worst-case OLEF position response due to the step input disturbance is shown as the dashed curve in the top subplot of Fig. 19.7. The worst-case Mach trajectory computed by `wcsim` is shown as the dashed curve in the bottom subplot of Fig. 19.7. The worst-case altitude trajectory is not shown since it is a constant 17,500 ft to within 0.25 ft. These results indicate that variations in altitude have a small impact on the closed-loop disturbance rejection. The expected computation for this `wcsim` is $(n_c + 1)N_i\tau \approx 910$ s based on $n_c = 8$ coefficients, $N_i = 4$ iterations, and $\tau = 25.3$ seconds per simulation. The actual `wcsim` optimization ran 60 simulations and took 1,735 s to complete. The worst-case Mach trajectory (bottom subplot of Fig. 19.7) shows fast variations with a peak rate of $|\dot{M}| \approx 0.156$ 1/s. These are unrealistic Mach rates for the actual AAW aircraft.

Another `wcsim` optimization is run with the constraint $|\dot{M}| \leq 0.02$ 1/s. This constraint is enforced in the “Parameter Rate Constraint” subsystem in Fig. 19.6 using an approximate derivative and a `wcsim Constraint Function` block. The altitude was held constant at 17,500 ft for this optimization since altitude variations appear to have minor impact on the OLEF position response. Thus `wcsim` only optimizes over the four coefficients in the Mach trajectory. After $N_i = 6$ gradient steps, `wcsim` finds a parameter trajectory that achieves an OLEF position L_2 norm of 2.948. The worst-case OLEF position response due to the step input disturbance is shown as the dash-dotted curve in the top subplot of Fig. 19.7. The worst-case Mach trajectory computed by `wcsim` is shown as the dash-dotted curve in the bottom subplot of Fig. 19.7. The worst-case trajectory returned by `wcsim` satisfies $|\dot{M}| \leq 0.0202$ 1/s. This slight violation of the enforced constraint is due to the restriction of $N_i = 6$. The Mach trajectory computed by `wcsim` simply slows the AAW down from its upper Mach limit to its lower limit over the ten-second simulation. The expected computation for this `wcsim` is $(n_c + 1)N_i\tau \approx 759$ s based on $n_c = 4$ coefficients, $N_i = 6$ iterations, and $\tau = 25.3$ s per simulation. The actual `wcsim` optimization ran 38 simulations and took 1,154 s to complete.

19.6 LPV Control Design

This section describes an LPV control design that provides guaranteed performance with respect to time variations in the (h, M) parameters. The design approach is based on signal-weighted induced L_2 norms. Figure 19.8 shows the design interconnection used for the control synthesis. The performance objective is to minimize the induced L_2 norm from the design interconnection inputs to the outputs. The various I/O signals are weighted to obtain the desired trade-offs between reference tracking, disturbance/noise rejection, and actuation usage.

The rigid body AAW dynamic models G_{rig} are used in the design. The design interconnection formulates a model-matching problem. The key performance objective is for the closed-loop response from p_{cmd} to p to match the ideal

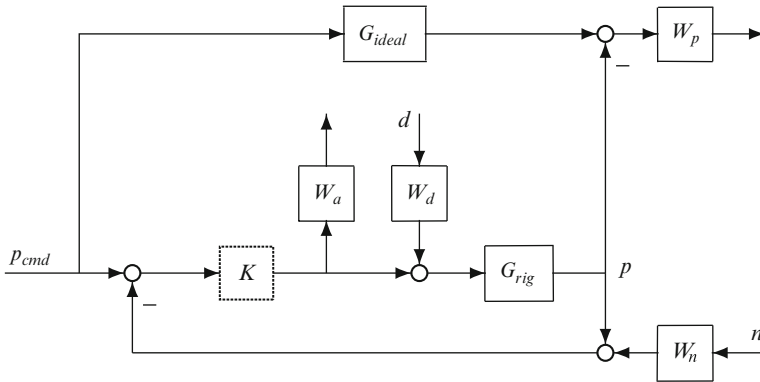


Fig. 19.8 Design interconnection AAW roll rate control

response given by $G_{ideal} = \frac{\omega_d^2}{s^2 + 2\zeta\omega_d s + \omega_d^2}$. The ideal response natural frequency and damping are given by $\zeta = 0.8$ and $\omega_d = 1.25$ rad/s. This is the same ideal response given by the loop shape G_{ls} in the gain-scheduled classical design. The actuation and performance penalties are given by $W_a = \frac{100s+25}{s+2500}$ and $W_p = \frac{0.01s+12.5}{s+0.125}$. This emphasizes tracking of the ideal response up to ≈ 11.25 rad/s and penalizes control usage at higher frequencies. The input disturbance and noise weights are chosen as $W_d = 0.1$ and $W_n = 0.01$. The small values are chosen to emphasize the actuation / performance trade-off. The ideal model and all weights are independent of the flight condition. Thus the performance objective aims to achieve similar performance across the flight envelope. The standard Robust Control Toolbox command `sysic` has been overloaded to allow interconnections of `pss` objects and standard MATLAB system objects. This overloaded `sysic` command was used to generate the LPV design interconnection shown in Fig. 19.8.

To understand the limits of performance, the H_∞ optimal control problem specified by this design interconnection was solved at each point in the flight envelope. The optimal performance varied from a minimum of $\gamma = 1.008$ at $(h, M) = (25,000 \text{ ft}, 1.1)$ to a maximum of $\gamma = 3.726$ at $(h, M) = (15,000 \text{ ft}, 1.3)$. The optimal performance of any LPV design must be greater than or equal to the optimal H_∞ performance achieved at any point in the domain. Hence $\gamma = 3.726$ is a lower bound on the achievable performance by the optimal LPV controller. For comparison, the gain-scheduled classical controller, K_{cl} , achieves a minimum gain of $\gamma = 1.000$ at $(h, M) = (25,000 \text{ ft}, 1.1)$ and a maximum gain of $\gamma = 3.857$ at $(h, M) = (15,000 \text{ ft}, 1.3)$.

Next, an LPV controller was synthesized without using knowledge about the rate variations of altitude and Mach. This control synthesis is performed a set of parameterized LMIs using a constant (nonparameter varying) Lyapunov function. The parameterized LMI conditions are based on results in [33]. The nonrate bounded design achieves an optimal gain of $\gamma_{pv,nr} = 3.844$. This is very close to the

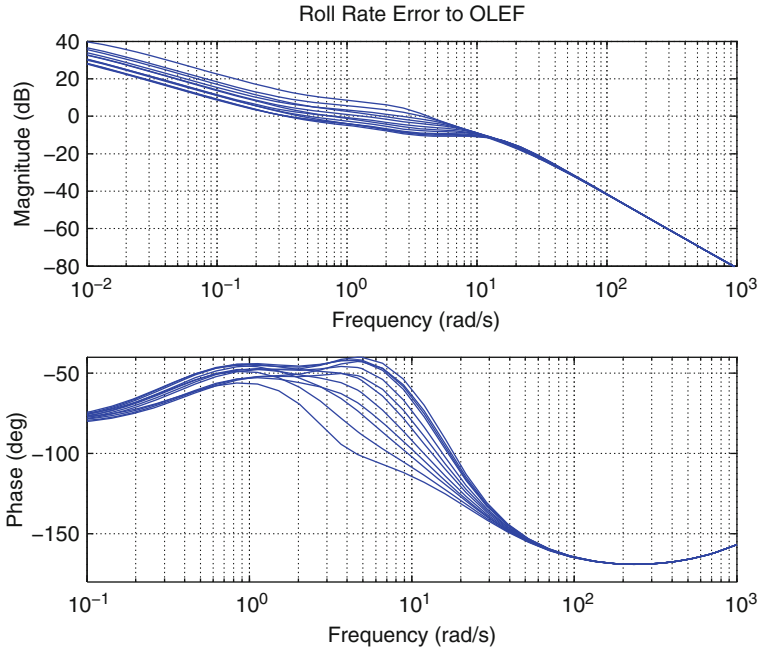


Fig. 19.9 Bode magnitude plots of LPV controller

performance lower bound computed based on the pointwise H_∞ designs. The design interconnection has a total of five states: one for the rigid body AAW dynamics, two for the ideal response model, and one each for the actuation and performance weights. The nonrate bounded controller K_{lpv} has the same number of states as the design interconnection, i.e., K_{lpv} has five states. A rate-bounded LPV controller was also synthesized assuming $|\dot{M}| \leq 0.02$ and $|\dot{h}| \leq 1,000$ ft/s and using basis functions $\{1, M, h\}$. The rate bounded design achieved a gain of $\gamma_{pv,rb} = 3.797$. This is a small improvement over the nonrate bounded design. Hence the bound on the rate of the parameter variation does not play a significant role in the AAW design. The remainder of the section will focus on the nonrate bounded control design.

Figure 19.9 shows the Bode plots for nonrate bounded LPV controller K_{lpv} at each point in the flight envelope. The controller has proportional–integral action at low frequencies and a second-order roll-off beyond ω_{r0} to avoid exciting the flexible modes. Both these characteristics are similar to gain-scheduled classical design shown in Fig. 19.3. One difference is that K_{lpv} has additional phase lead between 1 and 10 rad/s. In addition, K_{lpv} has the same high-frequency gain at all points in the flight envelope while the high-frequency gain of the classical design K_{cl} varies with the flight condition. The point-wise Bode plots of K_{lpv} show an intuitive classical design at each point in the flight domain and this provides confidence in the LPV design tools. One benefit of the LPV design tools, even for single-input

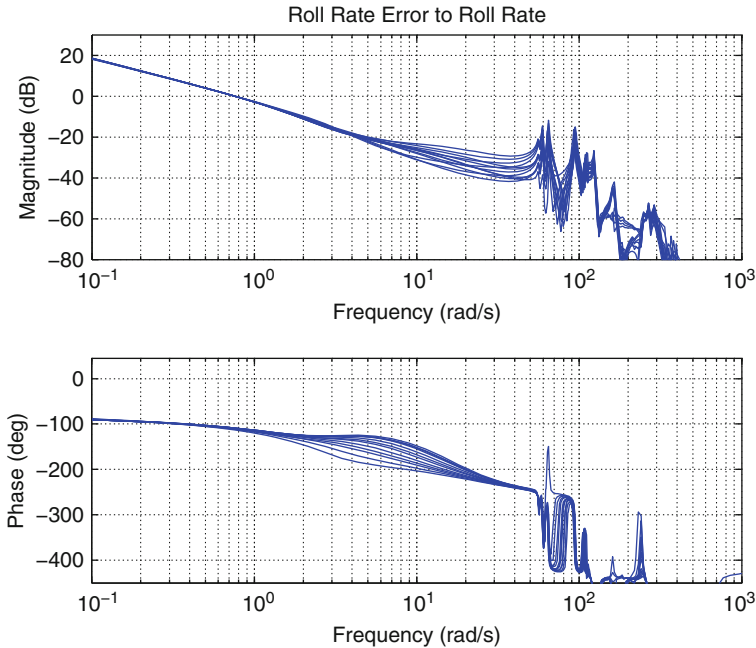


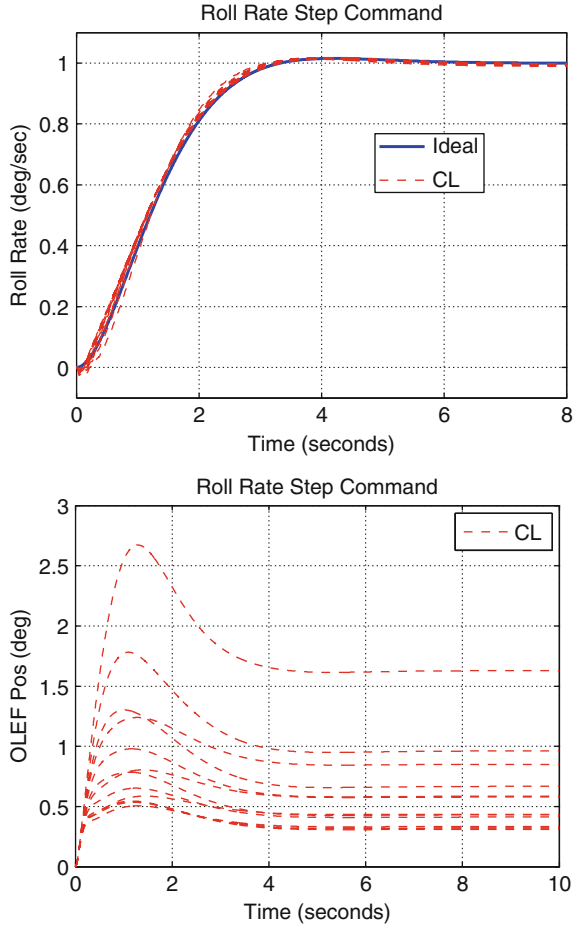
Fig. 19.10 Bode plots of loop function $G_{\text{full}}K_{\text{nr}}$

single-output gain-scheduling, is that the designer does not have to worry about the impact of the differing state-space realizations. The impact of the state realization on the gain-scheduled performance is built into the design.

Figure 19.10 shows the Bode plots for the (open)-loop function $G_{\text{full}}K_{\text{nr}}$ at each point in the flight envelope. The loop function again shows integral action at low frequencies. The loop $G_{\text{full}}K_{\text{nr}}$ has all modes below -12.0 dB at all points in the flight envelope. In closed loop, the response from roll rate command to roll rate has the flexible modes below -12.4 dB at all points in the domain. This is slightly less attenuation than achieved by the gain-scheduled classical controller. The additional phase lead in K_{nr} is evident from 1 to 10 rad/s in the Bode plot of $G_{\text{full}}K_{\text{nr}}$. The loop function $G_{\text{full}}K_{\text{cl}}$ has gain and phase margins exceeding 18.8 dB and 66.7° at each point in the flight domain. This is a slightly smaller gain margin than K_{cl} but the phase margins of K_{cl} and K_{nr} are essentially the same.

Figure 19.11 shows the closed-loop unit step responses to a 1° roll rate command at all points in the flight envelope. The full model with flexible modes G_{full} and LPV controller K_{nr} are used to generate these closed-loop responses. The top plot shows the roll rate response and the bottom plot shows the OLEF position. The blue solid curve in the top plot shows the ideal closed-loop response specified by the ideal model G_{ideal} . The red dashed curves in both plots show the closed-loop responses at each point in the (h, M) domain. The LPV controller achieves consistent dynamic

Fig. 19.11 Closed-loop responses to step roll rate command with K_{nr}



performance across the flight envelope with good attenuation of the flexible modes. The LPV controller provides slightly better tracking of the ideal response when compared to the classical design (Fig. 19.5). Both K_{nr} and K_{cl} have similar actuator usage for the step roll rate command.

Table 19.5a, b show the bounds on the LPV-induced L_2 norms of the various closed-loop sensitivity functions. Table 19.5a was computed using G_{rig} and K_{lpv} while the results in Table 19.5b were computed with the reduced aeroelastic model G_{red} and K_{lpv} . These results can be compared with the gain-scheduled classical controller performance K_{cl} in Table 19.4a, b. The LPV controller has achieved slightly better performance based on the rate-bounded upper bounds computed using the linear and quadratic basis functions (column LPV3).

Table 19.5 L_2 induced norms for closed-loop sensitivity functions with LPV controller

(a) Closed loop with $(G_{\text{rig}}, K_{\text{lpv}})$				
	Point H_∞	LPV1	LPV2	LPV3
S_i	1.302	3.682	2.063	1.434
T_i	0.995	3.586	2.004	1.358
S_o	1.302	1.315	1.309	1.306
T_o	0.995	1.002	0.998	0.998
(b) Closed loop with $(G_{\text{red}}, K_{\text{lpv}})$				
S_i	1.328	Inf	2.087	1.450
T_i	0.995	Inf	2.036	1.360
S_o	1.328	Inf	1.356	1.357
T_o	0.995	Inf	1.007	0.999

19.7 Conclusions

This chapter investigated the use of LPV techniques for the roll control of NASA Dryden's X-53 AAW testbed. LPV analysis of a gain-scheduled classical controller indicated that variations in scheduling parameter would have minimal impact on reference tracking but may have some impact on disturbance rejection at the plant input. An LPV controller was also synthesized using a model matching design. The LPV controller has an intuitive classical control characteristics and its performance was similar to the gain-scheduled classical design. All results were obtained using new LPV modeling, analysis, and design software tools. Future work will consider the scalability of the numerical algorithms, incorporation of uncertainty analysis, and development of the data infrastructure and tools to encompass the various LPV representations.

Acknowledgments This research was supported under the NASA Dryden SBIR NNX11CD58P entitled "Adaptive Linear Parameter-Varying Control for Aeroelastic Suppression". The technical contract monitor is Dr. Martin J. Brenner.

Appendix: Induced L_2 Analysis for LPV Systems

This appendix briefly defines the L_2 norm for LPV systems and provides a set of conditions for computing a bound on this norm. The presentation essentially follows that given in [33].

Consider an LPV system of the form

$$\begin{bmatrix} \dot{x}(t) \\ y(t) \end{bmatrix} = \begin{bmatrix} A(\rho(t)) & B(\rho(t)) \\ C(\rho(t)) & D(\rho(t)) \end{bmatrix} \begin{bmatrix} x(t) \\ u(t) \end{bmatrix}, \quad (19.6)$$

where (A, B, C, D) are continuous functions of ρ defined on a compact set $\mathcal{P} \subset \mathbb{R}^{n_\rho}$. The signal dimensions are $\rho \in \mathbb{R}^{n_\rho}$, $y \in \mathbb{R}^{n_y}$, $u \in \mathbb{R}^{n_u}$, and $x \in \mathbb{R}^{n_x}$. The dimensions of the state matrices are compatible with these signal dimensions.

ρ is a piecewise continuous function from \mathbb{R} to \mathbb{R}^{n_ρ} . It is assumed that $\rho(t) \in \mathcal{P} \forall t$. In addition, it is assumed that there exist $\{v_i\}_{i=1}^{n_\rho} \in \mathbb{R}$ such that $|\dot{\rho}_i| \leq v_i \forall t$. In other words, the $\{v_i\}_{i=1}^{n_\rho}$ are known rate bounds on the parameter trajectories. Let $\mathcal{F}_{\mathcal{P}, v}$ denote the set of piecewise continuous parameter trajectories that are restricted to \mathcal{P} and whose rates satisfy the bounds specified by $\{v_i\}_{i=1}^{n_\rho}$.

Let G denote the LPV system along with the set of allowable parameter trajectories $\mathcal{F}_{\mathcal{P}, v}$. The induced L_2 norm of G is defined as

$$\|G\|_{i,2} := \sup_{\rho \in \mathcal{F}_{\mathcal{P}, v}} \sup_{\substack{u \in L_2 \\ \|u\|_2 \neq 0}} \frac{\|y\|_2}{\|u\|_2}, \quad (19.7)$$

where $\|\cdot\|_2$ denotes the L_2 norm. In calculating this induced norm, it is assumed that $x(0) = 0$. This norm is the maximum input/output gain over all inputs and all allowable parameter trajectories.

The following theorem, taken from [33], gives a condition for an upper bound on the induced L_2 norm.

Theorem 19.1. *If there exists a piecewise continuous function $X : \mathbb{R}^{n_\rho} \rightarrow \mathcal{S}^{n_x \times n_x}$ such that $X(\rho) > 0$ and*

$$\begin{bmatrix} A^T(\rho)W(\rho) + W(\rho)A(\rho) + \sum_{i=1}^{n_\rho} \beta_i \frac{\partial W}{\partial \rho_i} & W(\rho)B(\rho) & \gamma^{-1}C^T(\rho) \\ B^T(\rho)W(\rho) & -I_{n_u} & \gamma^{-1}D^T(\rho) \\ \gamma^{-1}C(\rho) & \gamma^{-1}D(\rho) & -I_{n_y} \end{bmatrix} < 0 \quad (19.8)$$

$\forall \rho \in \mathcal{P}$ and $|\beta_i| \leq v_i$ ($i = 1, \dots, n_\rho$) then:

(A.1) *The system G is parametrically dependent stable over \mathcal{P} .*

(A.2) *$\exists k$ with $0 \leq k < \gamma$ such that $\|G\|_{i,2} \leq k$.*

Functions to compute an upper bound on the induced L_2 norm for an LPV system based on this result have been developed. There are two implementations of the induced LPV norm. The first computes an upper bound Γ on the induced L_2 norm of the pss G using a constant (parameter independent) Lyapunov matrix $X(\rho) = X$. The use of a constant X is equivalent to computing the induced norm with no parameter rate bounds, i.e., a parameter-independent Lyapunov function can be used for rate unbounded analysis.

The second implementation computes a tighter (less conservative) bound on the induced L_2 norm by using a parameter-dependent matrix Lyapunov $X(\rho)$ and bounds on the parameter rates of variation. $X(\rho)$ is assumed to be a linear combination of basis functions specified by

$$X(\rho) = \sum_{j=1}^{n_b} f_j(\rho)X_j. \quad (19.9)$$

The functions $f_j : \mathbb{R}^{n_\rho} \rightarrow \mathbb{R}$ are piecewise continuous functions. The toolbox searches for $\{X_j\}_{j=1}^{n_b}$ such that $X(\rho)$ satisfies the conditions in the theorem. The norm bound computed by this second syntax is less conservative at the expense of higher computational complexity.

The conditions in Theorem 19.1 are a parameterized set of LMIs that must be verified for all $\rho \in \mathcal{P}$ and all $|\beta_i| \leq v_i$. We approximately solve these conditions by enforcing the LMIs on a set of gridded points of \mathcal{P} . The terms involving parameter rates are handled by exploiting the fact that the β_i enter affinely in (19.8). Specifically, if the LMIs hold for all combinations of $\beta_i = \pm v_i$ (a total of 2^{n_ρ} combinations) then they hold for all $|\beta_i| \leq v_i$.

The computational growth of these conditions is an issue. Let n_g denote the total number of grid points used to approximate \mathcal{P} . A rate bounded analysis must enforce the LMI conditions at all n_g grid points and for all 2^{n_ρ} combinations of $\beta_i = \pm v_i$. Thus there are a total of $n_g 2^{n_\rho}$ constraints for each of dimension $(n_x + n_u + n_y)$. If there are n_b basis functions, then the Lyapunov matrix has n_b symmetric matrix decision variables $\{X_j\}_{j=1}^{n_b}$ for each of dimension $n_x \times n_x$. This gives a total of $n_b \frac{n_x(n_x+1)}{2}$ individual decision variables in the rate bounded analysis. LMI optimization solvers have an asymptotic complexity that depends on both the number of decision variables and the number/dimension of LMI constraints. For example, LMILab has a floating point operation growth of $O(n_r n_v^3)$, where n_r is the total row dimension of the LMI conditions and n_v is the total number of decision variables [12]. This complexity assumes the default Cholesky factorization of the Hessian matrix is used to solve the least squares problem that arises in each iteration. Thus the complexity of solving the LPV analysis condition is roughly $O\left(n_g 2^{n_\rho} (n_x + n_u + n_y) (n_b n_x^2)^3\right)$. This growth limits the analysis to a modest number of parameters, grid points, and basis functions.

References

1. Apkarian P, Gahinet P (1995) A convex characterization of gain-scheduled H_∞ controllers. *IEEE Trans Automat Contr* 40(5):853–864
2. Balas G, Bokor J, Szabo Z (2003) Invariant subspaces for LPV systems and their applications. *IEEE Trans Automat Contr* 48(11):2065–2069
3. Baranyi P, Yam Y, Varlaki P (2011) Tensor product model transformation in polytopic model-based control. Taylor & Francis, Boca Raton FL
4. Becker G (1993) Quadratic stability and performance of linear parameter dependent systems. PhD thesis, University of California, Berkeley
5. Boehm B, Flick P, Sanders B, Pettit C, Reichenbach E, Zillmer S (2001) Static aeroelastic response predictions of the active aeroelastic wing (AAW) flight research vehicle. In: AIAA/ASME/ASCE/AHS/ASC structures, structural dynamics & materials conference, AIAA 2001-1372
6. Brenner M (2002) Aeroservoelastic model uncertainty bound estimation from flight data. *AIAA J Guid Contr Dyn* 25(4):748–754
7. Brenner M (2011) Personal Communication

8. Brenner M, Lind R (1998) Wavelet-processed flight data for robust aeroservoelastic stability margins. *AIAA J Guid Cont Dyn* 21(6):823–829
9. Bruzelius F, Breitholtz C (2001) Gain scheduling via affine linear parameter-varying systems and h_∞ synthesis. In: *IEEE conference on decision and control*, pp 713–718
10. Clarke R, Allen M, Dibley R, Gera J, Hodgkinson J (2005) Flight test of the F/A-18 active aeroelastic wing airplane. Tech. Rep. TM-2005-213664, NASA
11. Dibley R, Allen M, Clarke R, Gera J, Hodgkinson J (2005) Development and testing of control laws for the active aeroelastic wing program. Tech. Rep. TM-2005-213666, NASA
12. Gahinet P, Nemirovski A, Laub A, Chilali M (1995) LMI control toolbox user's guide. Tech. rep., The Mathworks
13. Lind R, Brenner M (1998) Analyzing aeroservoelastic stability margins using the μ method. In: *AIAA structures, structural dynamics, and materials conference*, AIAA 98-1895, pp 1672–1681
14. Lucia D (2005) The sensorcraft configurations: A non-linear aeroservoelastic challenge for aviation. In: *AIAA/ASME/ASCE/AHS/ASC structures, structural dynamics and materials conference and exhibit*, AIAA-2005-1943
15. Mangalam S, Flick P, Brenner M (2007) Higher level aerodynamics input for aeroservoelastic control of flexible aircraft. In: *AIAA atmospheric flight mechanics conference*, AIAA 2007-6380
16. Mangalam A, Mangalam S, Flick P (2008) Unsteady aerodynamic observable for gust load alleviation and flutter suppression. In: *AIAA atmospheric flight mechanics conference*, AIAA 2008-7187
17. Mangalam A, Moes T (2004) Real-time unsteady loads measurements using hot-film sensors. In: *AIAA applied aerodynamics conference*, AIAA 2004–5371
18. Martinez J, Flick P, Perdsock J, Dale G, Davis M (2008) An overview of sensorcraft capabilities and key enabling technologies. In: *AIAA applied aerodynamics conference*, AIAA-2008-7185
19. Packard A (1994) Gain scheduling via linear fractional transformations. *Syst Contr Lett* 22(2):79–92
20. Packard A, Kantner M (1996) Gain scheduling the LPV way. In: *IEEE conference on decision and control*, pp 3938–3941
21. Pendleton E, Bessette D, Field P, Miller G, Griffin K (2000) Active aeroelastic wing flight research program: Technical program and model analytical development. *J Aircraft* 37(4):554–561
22. Pendleton E, Flick P, Voracek D, Reichenbach E, Griffin K, Paul D (2007) The X-53: A summary of the active aeroelastic wing flight research program. In: *AIAA structures, structural dynamics, and materials conference*, paper 2007–1855
23. Pendleton E, Griffin K, Kehoe M, Perry B (1996) A flight research program for active aeroelastic wing technology. In: *AIAA/ASME/ASCE/AHS/ASC structures, structural dynamics and materials conference and exhibit*, paper 96-1574-CP
24. Scherer C (2001) LPV control and full block multipliers. *Automatica* 37(3):361–375
25. Scherer C, Weiland S (2000) Linear matrix inequalities in control. *DISC Lecture notes*
26. Seiler P, Balas G, Packard A (2011) Linear parameter varying control for the X-53 active aeroelastic wing. In: *AIAA guidance, navigation, and control conference*
27. Shamma J, Athans M (1991) Gain scheduling: potential hazards and possible remedies. In: *American control conference*, pp 516–521
28. Sharuz S, Behtash S (1990) Design of controllers for linear parameter-varying systems by the gain-scheduling technique. In: *IEEE conference on decision and control*, pp 2490–2491
29. Sun X, Postlethwaite I (1998) Affine LPV modeling and its use in gain-scheduled helicopter control. In: *UKACC international conference on control*, pp 1504–1509
30. Tischler M, Colbourne J, Morel M, Biezad D, Levine W, Moldoveanu V (1997) CONDUIT: A new multidisciplinary integration environment for flight control development. In: *AIAA guidance, navigation, and control conference*, AIAA-1997-3773

31. Vartio E, Shimko A, Tilman C, Flick P (2005) Structural mode control and gust alleviation for a sensorcraft concept. In: AIAA/ASME/ASCE/AHS/ASC structures, structural dynamics and materials conference and exhibit, AIAA-2005-1840
32. Veenman J, Scherer C (2010) On robust LPV controller synthesis: A dynamic integral quadratic constraint based approach. In: IEEE conference on decision and control, pp 591–596
33. Wu F (1993) Control of linear parameter varying systems. PhD thesis, University of California, Berkeley
34. Wu F, Yang X, Packard A, Becker G (1996) Induced l_2 norm control for LPV systems with bounded parameter variation rates. *Int J Nonlinear Robust Contr* 6:983–998

Chapter 20

Design of Integrated Vehicle Chassis Control Based on LPV Methods

Zoltán Szabó, Péter Gáspár, and József Bokor

Abstract The aim of this chapter is to present a multilayer supervisory architecture for the design and development of reconfigurable and integrated control systems in road vehicles. The individual performance specifications are guaranteed by the local controllers, while the coordination of these components is provided by the supervisor in order to meet global performance specifications and avoid the interference and conflict between components. Monitoring components provide the supervisor with information needed to make decisions about the necessary interventions into the vehicle motion and guarantee the robust operation of the vehicle. In the proposed architecture, these decisions are propagated between the supervisor and the local components through a well-defined interface encoded as suitable monitoring signals. This interface uses the monitoring signals as additional scheduling variables of the individual linear parameter varying (LPV) controllers introduced to distinguish the performances that correspond to different operational modes. The advantage of this architecture is that local LPV controllers are designed independently provided that the monitoring signals are taken into consideration in the formalization of their performance specifications. Moreover, the operation of a local controller can be extended to reconfigurable and fault-tolerant functions. The operation of the control systems is demonstrated through various simulation vehicle maneuvers.

Z. Szabó • P. Gáspár (✉) • J. Bokor
Systems and Control Laboratory, Computer and Automation Research Institute,
Hungarian Academy of Sciences, Budapest, Hungary
e-mail: szaboz@sztaki.hu; gaspar@sztaki.hu; bokor@sztaki.hu

20.1 Introduction and Motivation

Recently, there has been a growing demand for vehicles with ever better driving characteristics in which efficiency, safety, and performance are ensured. In line with the requirements of the vehicle industry, several performance specifications are in the focus of research, e.g., improving road holding, passenger comfort, roll and pitch stability, guaranteeing the reliability of vehicle components, reducing fuel consumption and proposing fault-tolerant solutions, see [7]. In order to meet these requirements, an increasing number of active components with high versatility are applied.

The control components used in a vehicle system are often in interaction or even in conflict with each other in terms of the full vehicle. An integrated control system is designed in such a way that the effects of a control system on other vehicle functions are taken into consideration in the design process by selecting the various performance specifications. Redundancy on sensor and actuator levels makes it possible to realize the same functionality using different sensor and actuator configurations, i.e., control reconfigurations. Thus integrated design is also motivated by the needs of reconfigurable and reliable control, see, e.g., [17, 18]. Recently, several important papers have been presented in this topic, see, e.g., [13, 19, 23].

A possible solution to an integrated control could be to set the design problem for the whole vehicle and include all the performance demands in a single specification. Besides the complexity of the resulting problem, the formulation of a suitable performance specification is the main obstacle for this direct global approach. In the framework of available design techniques, the formulation and successful solution of complex multi-objective control tasks are highly nontrivial, see, e.g., [2, 8].

Another solution to the integrated control is a quasi-decentralized control structure where the components are designed independently, see, e.g., [4, 22]. In the chapter, the quasi-decentralized control system is augmented with a supervisor as illustrated in Fig. 20.1. The role of the supervisor is to meet performance specifications and prevent the interference and conflict between components. The supervisor has information about the current operational mode of the vehicle, i.e., the various vehicle maneuvers or the different fault operations gathered from monitoring components and fault-detection and identification (FDI) filters. The supervisor is able to make decisions about the necessary interventions into the vehicle components and guarantee the reconfigurable and fault-tolerant operation of the vehicle. These decisions are propagated to the lower layers through predefined interfaces encoded as suitable scheduling signals.

In the proposed solution, the design of local control components is based on linear parameter varying (LPV) methods. LPV methods are well elaborated and successfully applied to various industrial problems. The LPV approaches allow us to take into consideration the highly nonlinear effects in the state-space description [1, 12]. Moreover, in the LPV method, both performance specifications and model uncertainties are taken into consideration. The main point of the proposed approach

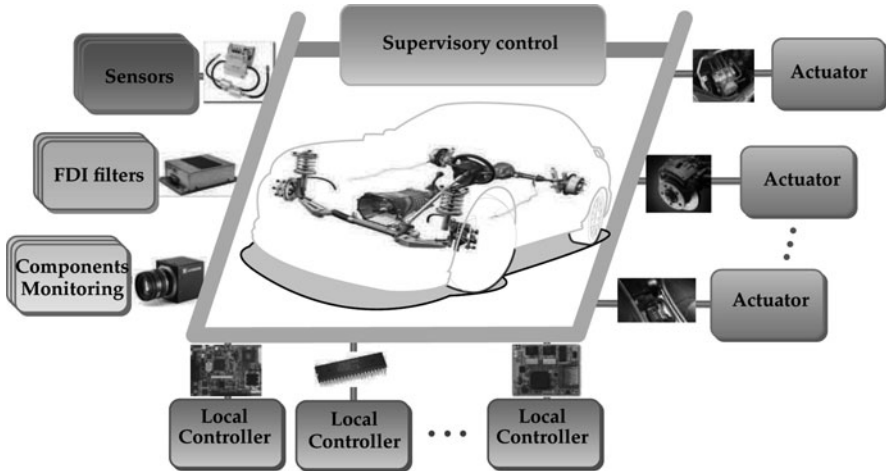


Fig. 20.1 The supervisory decentralized architecture of integrated control

is that in the control design of the local components scheduling variables received from the supervisor are used as a key of the integration. In this way, the operation of a local controller can be extended to reconfigurable and fault-tolerant functions.

The structure of the chapter is as follows. In Sect. 20.2, the architecture of the supervisory integrated control is presented. In Sect. 20.3, as an illustration, the control-oriented LPV modeling is described. In this section, the weighting strategy in the closed-loop interconnection structure is also illustrated. In Sect. 20.4, the selection of the sensors and monitored components is presented. In Sect. 20.5, the integration of the actuators based on the operation modes is shown. In Sect. 20.6, the global performances based on the supervisory activity are analyzed. In Sect. 20.7, the integrated control mechanism is presented through simulation examples. Finally, Sect. 20.8 contains concluding remarks.

20.2 Architecture of the Integrated Control

The term configuration refers to a well-defined sensor and actuator set that is associated with a given functionality. Control reconfiguration is motivated by the following requirements: the achieved control performance in certain scenarios must be improved and an increased reliability in the presence of sensor or actuator faults must be achieved. The term event is related to the occurrence of such a scenario. A finite set of events \mathcal{E} are always assumed. On a higher level, an event is handled based on a given functionality thus one can associate a certain event $e \in \mathcal{E}$ with a set of configurations \mathcal{C}_e . Reconfigurable control strategies define a policy $\mathcal{J} : \mathcal{E} \times \mathcal{C} \rightarrow \mathcal{C}_e$ to select a possibly new configuration $K = \mathcal{J}(e)$ when an event e

occurs in a specific, usually baseline, configuration. In a normal situation, a baseline configuration is formed by a single local component, e.g., steering, otherwise it is composed of several local components that can fulfill the same functional behavior, e.g., steering and brake for generating yaw moment.

The event set \mathcal{E} , the corresponding class of the configuration sets \mathcal{C}_e , and the policy \mathcal{S} are determined in the preliminary step of the design. The specification of the configuration sets and that of the corresponding reconfiguration policy is a cornerstone of the proposed method and it may be a highly nontrivial task requiring a lot of engineering knowledge. However, the analysis of the configurations, events, and possible reconfigurations is necessary for any reconfiguring control strategy.

20.2.1 Supervisory Control

The role of the supervisor is to coordinate the local components and handle the interactions between them. Since the performance specifications of local controllers are often in conflict, the supervisor must also guarantee a balance or trade-off between them. This trade-off is formulated on the level of local controllers as a result of an engineering knowledge. However, when an event occurs the preferences, i.e., the trade-off levels, are subject to change. This fact is reflected in the structure of the policy \mathcal{S} .

As an example, the effect of actuator saturation may prevent a specific performance requirement to be fulfilled. The encountered performance degradation might be treated as an event, if there is a configuration that potentially can improve the performance, which in practical situations is closely related to a safety requirement. Recovering to the normal parameters creates another event that makes the supervisor to select the baseline configuration.

In order to implement a transition defined by the policy \mathcal{S} , a safety feature, the operation of a local controller, must be modified by a supervisory command. This is realized through appropriately set scheduling variables that are transmitted to the local controllers. At a local level, the behavior of the controller is affected by these scheduling variables through the performance weighting functions. The difficulty in the supervisory control is that global stability and performance are difficult to guarantee. The information provided by the supervisor is composed of messages and signals sent by the monitoring components and fault-detection and isolation (FDI) filters. Based on this information, the supervisor is able to make decisions about the necessary vehicle maneuvers and guarantee reconfigurable and fault-tolerant operation of the vehicle and send messages to the local controllers.

The design of the supervisor does not involve dynamical systems explicitly. However, due to the time variation of the signals, the policy \mathcal{S} defines time varying conditions and relations, i.e., the designer should check the validity of relations based on a temporal logic. The difficult part of the design is to ensure the correctness of the specification, see [11, 14]. It must be stressed at this point that the baseline configurations handle only one actuator, which is associated with a given task

(functionality). The hierarchy of the configurations and corresponding scheduling variables ensure that the additional actuator(s) considered improve the stability properties of the given functionality. These two design principles facilitate the verification of the specification considerably.

In contrast to the controller switching strategy, the proposed approach uses a performance weighting strategy. On the supervisor level, the required configurations are defined uniquely by the specific values of a set of marker signals. These marker signals are used as scheduling variables on the level of local controllers. The task of the supervisor design is to specify these marker signals in such a way that the different combinations of their values define the specific event (functionality) in a unique way. The different combinations of the marker signals encode the designers specification (option) in dealing with multiobjective or conflicting scenarios.

As an illustration, consider the tracking problem which is handled by using active steering. When the vehicle is performing a maneuver, e.g., a double lane change or a cornering, the lateral loads might generate overturning moments. The role of the brake mechanism is to reduce the lateral tire forces by generating a yaw moment and decelerate the vehicle. However, using the brake, the real path significantly deviates from the desired trajectory. This deviation must be compensated for by the active steering system. Performing road tracking and increasing roll stability at the same time pose a difficult problem since these tasks are in contradiction.

20.2.2 Local Components

A local component is a well-defined ensemble of a controller, an actuator, and a set of related physical or virtual sensors, e.g., units for monitoring components and FDI filters. The virtual sensors might be provided by the vendors of the specific sensors or actuators, or they might be designed and implemented on a global vehicle level. These elements are able to detect emergency vehicle operations, various fault operations or performance degradations in controllers. They send messages to the supervisor in order to guarantee the safe operation of the vehicle.

Each of the local components is governed by a local controller. A local controller must meet the predefined performance specifications. The signals of monitoring components and those of FDI filters are built in the performance specifications of the controller by using a parameter-dependent form. The performance specifications are formalized in a parameter-dependent way in which the corresponding scheduling variable is given by the supervisor. Thus the controller is able to modify or reconfigure its normal operations in order to focus on other performances instead of the actual performances. It sends messages about the changes to the supervisor and it receives messages from the supervisor about the special requirements.

For example, if there is a lock failure in the operation of the active anti-roll bars, i.e., the piston of the hydraulic actuator remains locked in a particular position, then the hydraulic actuator will not be able to operate after the fault has occurred. Different control components are able to substitute for the faulty active anti-roll

bars and the selection of the appropriate controller is determined by the supervisor. However, this substitution is based on at least two requirements: the reconfigurable controller must handle the fault operation of active anti-roll bars and the signal from the supervisor about the performance degradation or the fatal failure is received.

The aims of active suspension systems are to improve passenger comfort and road holding and minimize the effects of harmful road irregularities. The operations of the suspension system can be extended to roll and pitch stability. This is based on the fact that the system is able to generate a stabilizing moment to balance the overturning moment during maneuvers and generate a moment to balance the pitching moment during abrupt and hard braking. In case of an emergency, e.g., in an imminent rollover, the controller must focus only on enhancing the critical performances, e.g., road holding or drivability, and guaranteeing comfort performances is no longer a priority.

20.3 Modeling and Control of Vehicle Systems

20.3.1 LPV Modeling of Vehicle Systems

The proposed design strategy is illustrated through an application example. The objective of the control design is to track a predefined path, guarantee road holding, and increase pitch and roll stability. Five control components are applied in the system: the active brake, steering, anti-roll bars, the suspension system, and the driveline system, see Fig. 20.2. The longitudinal force is generated by the driveline and the brake systems. The tracking of the predefined road geometry is performed by the active steering. During maneuvers active anti-roll bars are used to improve roll stability. Road holding and passenger comfort are guaranteed by applying an active suspension system. This system also improves both the roll and the pitch stability. The brake system might also be activated to provide the lateral stability of the vehicle. Since the driver inputs considered are the braking and steering, two force types are considered, i.e., the longitudinal forces together with brake forces and lateral forces from all four tires. The longitudinal and lateral forces generated by each tire, F_{lx}, F_{ly} , are the result of the normal forces acting on each wheel and the tire slip angles. The vehicle is steered by the front tires and the steering angle δ_f . The forces generated by the active suspension and the active anti-roll bars on the left-hand and right-hand side at the front and the rear are denoted by F_{zij} .

The chassis vertical (z_s), longitudinal (x), lateral (y), roll (θ), pitch (ϕ), and yaw (ψ) dynamics are given by the following equations. Here v_x and v_y are the velocities of the chassis in x -directions and y -directions, z_s and z_u are the displacement of the sprung mass and the unsprung masses in z -direction.

$$m\dot{v}_x = -F_{lxf} \cos \delta_f - F_{lxf} - F_{lyf} \sin \delta_f - m\dot{\psi}v_y, \quad (20.1)$$

$$m\dot{v}_y = -F_{lyf} \sin \delta_f + F_{lyf} + F_{lxf} \cos \delta_f + m\dot{\psi}v_x, \quad (20.2)$$

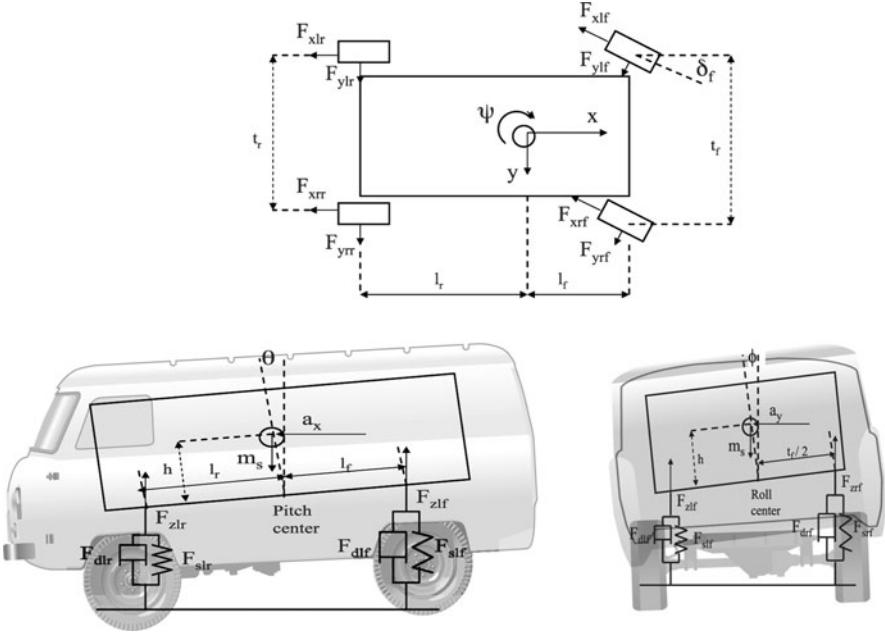


Fig. 20.2 Vehicle body for yaw, roll, and pitch motions

$$m_s \ddot{z}_s = -F_{zf} - F_{zr} - F_{dz}, \tag{20.3}$$

$$m_{usij} \ddot{z}_{usij} = F_{zij} - F_{tizj}, \tag{20.4}$$

$$I_x \ddot{\theta} = t_r (F_{zrl} - F_{zrr}) + t_f (F_{zfl} - F_{zfr}) + mh \dot{v}_y, \tag{20.5}$$

$$I_y \ddot{\phi} = l_f F_{zf} - l_r F_{zr} - mh \dot{v}_x, \tag{20.6}$$

$$I_z \ddot{\psi} = (l_f (-F_{txf} \sin \delta_f + F_{tyf} \cos \delta_f) - l_r (F_{tyr} + t_f (F_{txfr} - F_{txfl}) \cos \delta_f - t_r (F_{txrr} - F_{txrl})) + M_{dz}. \tag{20.7}$$

The relationship between the yaw dynamics $\dot{\psi}$ and the dynamics of the side slip angle of the center of gravity $\dot{\beta}$ is $\dot{\beta} = \dot{\psi} + (F_{tyf} + F_{tyr})/m/v_x$. Using small steering angle, the following approximations are applied: $\sin \delta = \delta$ and $\cos \delta = 1$.

The local controllers are designed based on vehicle models with different complexity. Their design is based on state-space representation form

$$\dot{x} = A(\rho)x + B_1(\rho)w + B_2(\rho)u, \tag{20.8}$$

where x , w , and u are the state, disturbance, and input, respectively. Vector ρ includes the scheduling variables. In the first step, the state equation is defined and then the performances and measured output are selected considering the control tasks.

The primary role of the brake is to reduce the forward velocity of the vehicle or stop it. It is also able to generate unilateral brake forces at the front and the rear wheels at either of the two sides $u_b = \Delta F_b$. In the control system, the brake is able to modify the yaw angle of the vehicle during a cornering and reduce the effect of lateral acceleration. Thus, the brake is able to substitute for different vehicle components if they are affected by a fault or degradation in terms of performances. The steering is used to follow the desired course. The control input is the steering angle: $u_d = \delta_f$. Considering the practice in these tasks, the measured signals are the lateral acceleration and the yaw rate.

Active suspensions are used to provide good handling characteristics and improve ride comfort while harmful vibrations caused by road irregularities act upon the vehicle. The suspension system is also able to improve pitch and roll stability by generating pitch moment during abrupt braking and roll moments during emergency maneuver. The control inputs are generated by the suspension actuators: $u_s = [f_{fl}, f_{fr}, f_{rl}, f_{rr}]^T$. The measured signals are the relative displacements between the sprung and unsprung masses over the wheels. For more details, see [5, 6].

The role of the active anti-roll bars is to keep roll stability even during vehicle maneuvers such as a sharp cornering, double lane changing, or overtaking. The active anti-roll bars operate continuously during traveling and generate stabilizing roll moments between the sprung and unsprung masses to improve roll stability. The control inputs are the roll moments at the front and the rear between the sprung and unsprung masses generated by active anti-roll bars: $u_r = [u_{rf}, u_{rr}]^T$. The measured signals are the lateral acceleration and the roll rate.

The nonlinear effects of the forward velocity, the adhesion coefficient of the vehicle in the lateral direction, or the nonlinear characteristics in the suspension spring and damper components are taken into consideration $\rho = [v, \mu, \rho_{bij}, \rho_{kij}]^T$, where ρ_{kij} and ρ_{bij} are the relative displacement and its velocity. It is assumed that with suitably selected scheduling variables ρ , these nonlinear components can be transformed into affine parameter-dependent forms. Then the nonlinear models are transformed into LPV models in which nonlinear terms are hidden with suitably selected scheduling variables. This transformation requires that the components of vector ρ be measured, see [3, 16].

The design of a local controller is based on the control-oriented LPV model and weighting strategy. The closed-loop system applied in the design of integrated control includes the feedback structure of the model $G(\rho)$, the compensator, and elements associated with the uncertainty models and performance objectives:

$$z = C(\rho)x + D_1(\rho)w + D_2(\rho)u, \quad (20.9)$$

where $w = [d \ n]^T$ includes both the external disturbances and the sensor noise.

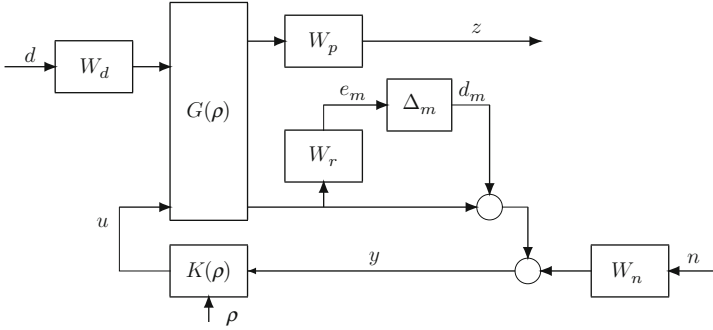


Fig. 20.3 The closed-loop interconnection structure

20.3.2 LPV Control of Vehicle Systems

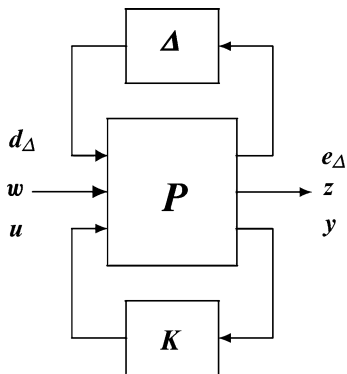
A typical interconnection structure is shown in Fig. 20.3. In this framework performance requirements z are imposed by a suitable choice of the weighting functions W_p . Usually the purpose of weighting functions W_p is to define penalty functions, i.e., weights should be large where small signals are desired and small where large performance outputs can be tolerated. The proposed approach realizes the reconfiguration of the performance objectives by an appropriate scheduling of these weighting functions. Δ_m block contains the uncertainties of the system, such as unmodeled dynamics and parameter uncertainty. In this augmented plant unmodeled dynamics is represented by a weighting function W_r and a block Δ_m . The purpose of the weighting functions W_w and W_n is to reflect the disturbance and sensor noises.

Finally, the control problem can be formulated in the general $P - K - \Delta$ structure (Fig. 20.4), where P is the generalized plant and Δ contains both the uncertainties and the scheduling variables. In the design of local controllers, the quadratic LPV performance problem is to choose the parameter-varying controller in such a way that the resulting closed-loop system is quadratically stable and the induced L_2 norm from the disturbance and the performances is less than the value γ . The minimization task is the following:

$$\inf_K \sup_{\Delta} \sup_{\|w\|_2 \neq 0, w \in L_2} \frac{\|z\|_2}{\|w\|_2}. \tag{20.10}$$

The existence of a controller that solves the quadratic LPV γ -performance problem can be expressed as the feasibility of a set of linear matrix inequalities (LMIs), which can be solved numerically. Stability and performance are guaranteed by the design procedure, for details see [12, 15, 20]. For the sake of simplicity, in this chapter the parameter gridding method of [21] combined by a weighted small gain approach for the uncertainties was used.

Fig. 20.4 The $P - K - \Delta$ structure



20.4 Sensors and Monitored Components in the Distributed Control System

The local components also include units for monitoring vehicle operations and FDI filters. These components are able to detect emergency vehicle operations, various fault operations, or performance degradations in controllers. They also send messages to the supervisor. In the reconfigurable and fault-tolerant control of the local controller, several signals must be monitored and scheduling variables are added to the scheduling vector in order to improve the safety of the vehicle, e.g., variables are needed to encode the rollover risk, represent the harmful effects of abrupt braking, and take a detected failure of an active component into consideration.

The efficient operation of the supervisor and the local controllers require reliable and highly accurate signals from the system. To meet this requirement redundant sensors, diverse calculations and fault-detection filters are needed. To achieve the efficient and optimal intervention, the detections of faulty sensors are important since they must be substituted for in operations based on these sensors. Low-cost solutions are preferred in the vehicle industry, thus simple sensors and software-based redundancy must be applied.

In the following several examples for monitored components related to specific control goals are presented:

20.4.1 Yaw Stability

Yaw stability is achieved by limiting the effects of the lateral load transfers. The purpose of the control design is to minimize the lateral acceleration, which is monitored by a performance signal: $z_a = a_y$. Unilateral braking is one of the solutions, in which brake forces are generated in order to achieve a stabilizing yaw moment. In the second solution, additional steering angle is generated in order to reduce the effect of the lateral loads. These solutions, however, require active driver intervention into the motion of the vehicle to keep the vehicle on the road.

20.4.2 Road Tracking

Another control task is to follow the road geometry. The purpose of the control is to minimize the difference between the yaw rate and the reference yaw rate to be minimized: $z_e = |\psi_{\text{act}} - \psi_{\text{ref}}|$. In practice, the calculation of this difference is based on signals of a video camera.

20.4.3 Roll Stability

Roll stability is achieved by limiting the lateral load transfers on both axles to below the levels for wheel lift-off during various vehicle maneuvers. The lateral load transfer is $\Delta F_{zi} = k_i \phi_{ti}$, where ϕ_{ti} is the monitored roll angle of the unsprung mass at the front and the rear. The normalized lateral load transfer is introduced: $\rho_R = \Delta F_{zy}/(mg)$. The aim of the control design is to reduce the maximum value of the normalized lateral load transfer if it exceeds a predefined critical value.

20.4.4 Pitch Stability

The pitch angle of the sprung mass may increase significantly during a sudden and hard braking. Pitch stability is achieved by limiting the longitudinal load transfers to below a predefined level. The normalized longitudinal load transfer is the normalized value of the pitch angle: $\rho_P = \theta/\theta_{\text{max}}$, where θ is the monitored pitch angle and θ_{max} is the maximal value of the pitch angle. The aim of the control design during braking is to reduce the pitching dynamics if the normalized longitudinal load transfer exceeds a critical value. Besides the basic control problems, these monitoring components require additional sensors. The tracking task requires one or two cameras for reasons of redundancy, the pitch and roll stability require the pitch and roll angle of the sprung mass. In the vehicle industry, roll and pitch rates are measured and then the angles are calculated by a numerical procedure. Different methods are also used to filter out the offset error from the angles, e.g., Kalman filter.

20.4.5 Actuator Selection

In the control design, the distribution of the wheel forces must also be taken into consideration. In a front-wheel-driven vehicle, the traction force is distributed between the front wheels by using the differential gear. The steering angle is limited by construction (δ_{crit}), therefore when the maximal steering angle is reached the desired lateral dynamics of the vehicle must be achieved by the brake moment.

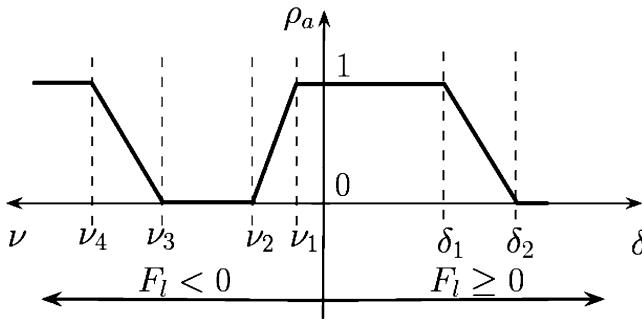


Fig. 20.5 Relationship between the parameter ρ_a and the actuator selection

During braking, the load of wheels is modified due to the pitch dynamics of the vehicle. The braking of the front wheels must be stronger while the braking of the rear wheels must be reduced. The wheel forces must be monitored in view of the momentary friction margin of the tire. It requires the estimation of friction coefficient μ , which is also necessary for the determination of maximal cornering velocity. An estimation method for the adhesion coefficient is proposed by Gustafsson [9].

The maximal longitudinal force of the wheels ($F_{i,max}$) is calculated and compared to the momentary longitudinal wheel forces (F_i). Note that the maximal longitudinal force depends on the maximal adhesion coefficient and the static and dynamic components of the vertical force at the wheel, i.e., the lateral and pitch dynamics. The variable $\nu = \max\{F_i/F_{i,max}\}$ is the maximal value between the force ratios considering all the wheels and ν_{crit} is a design parameter.

A weighting factor ρ_{act} , which depends on the vehicle operation, i.e., the traction and the brake, will be used in the weighting strategy of the control design, see Fig. 20.5. This factor might depend on other parameters less such as forward velocity, lateral loads, maneuvers.

20.4.6 Fault Monitoring

The fault-tolerant control requires fault information in order to guarantee performances and modify its operation. Thus, FDI filters are also designed for the operation of the actuators. As an example, the fault information provided by a fault-detection filter is given by $\rho_D = f_{act}/f_{max}$, where f_{act} is an estimation of the failure (output of the FDI filter) and f_{max} is an estimation of the maximum value of the potential failure (fatal error). The estimated value f_{act} means the rate of the performance degradation of an active component. The value of a possible fault signal is normalized into the interval $\rho_D = [0, 1]$ and it is used as a scheduling variable that directly affects the performance specification (performance weight) of the corresponding component.

The actuator reconfiguration is based on the fact that two actuators are able to influence the same vehicle dynamics. Thus, the fault-free actuator is able to substitute for the operation of another actuator which has been affected by a failure or its performance has degraded. The control design is based on two factors: the failure or performance degradation has already been detected and the fault information ρ_D and the necessary intervention possibilities are built into its control design. Instead of a switching type controller reconfiguration, the control structure changes due to a reconfiguration of the performance goal achieved by a scheduling of the performance weights.

The detection of a sensor failure as accurately as possible is crucial since the controller may generate fault actuator intervention as a result of fault sensor information. In practice, the probability of a sensor failure can be reduced by using redundant sensors. In this case, the faulty sensor is substituted for by another fault-free sensor which provides the same or similar signal. Sensor failures may also prevent certain actuators from being used; then handling the sensor failure leads to an actuator reconfiguration problem. Thus complex vehicle systems require various FDI filters both for actuator and sensor failures.

20.5 Actuators and Operation Modes in the Distributed Control System

This section gives a short overview about the main control systems and their operation modes in the vehicle. At each subsystem, the most common performance specifications and the corresponding weighting strategies are formulated.

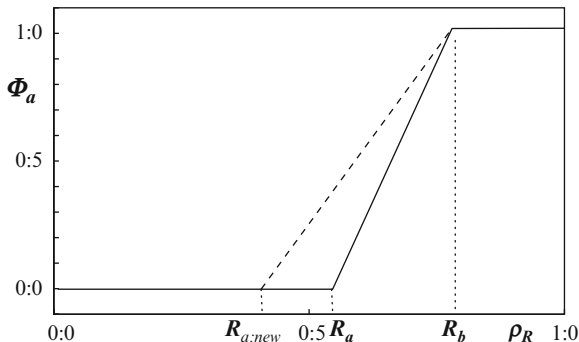
20.5.1 Steering System

In order to solve the yaw rate tracking problem in the design of the steering system, the command signal must be fed forward to the controller (y_{ref}). The command signal is a predefined reference displacement and the performance signal is the tracking error: z_e . The weighting function of the tracking error is selected as

$$W_{pe} = \kappa_e(T_{d1}s + 1)/(T_{d2}s + 1), \quad (20.11)$$

where T_{di} are time constants. Here, it is required that the steady-state value of the tracking error should be below $1/\kappa_e$ in steady state.

Fig. 20.6 Parameter-dependent gain Φ_a



20.5.2 Brake System

In the design of the brake system, the command signal is the difference in brake forces while the performance signal is the lateral acceleration: $z_b = [a_y, u_r]^T$. The weighting function of the lateral acceleration is selected as

$$W_{pa} = \phi_a (T_{b1}s + 1) / (T_{b2}s + 1), \tag{20.12}$$

where T_{bi} are time constants and

$$\phi_a = \begin{cases} 1 & \text{if } |\rho_R| > R_b, \\ \frac{|\rho_R| - R_a}{R_b - R_a} & \text{if } R_a \leq |\rho_R| \leq R_b, \\ 0 & \text{if } |\rho_R| < R_a. \end{cases} \tag{20.13}$$

Here ϕ_a is a gain, which reflects the relative importance of the lateral acceleration and it is chosen to be parameter dependent, i.e., the function of ρ_R . When ρ_R is small ($|\rho_R| < R_b$), i.e., when the vehicle is not in an emergency, ϕ_a is small, indicating that the LPV control should not focus on minimizing acceleration. On the other hand, when ρ_R approaches the critical value, i.e., when $|\rho_R| \geq R_b$, ϕ_a is large, it indicates that the control should focus on preventing the rollover. Here R_b defines the critical status when the vehicle is close to the rollover situation, i.e., all wheels are on the ground but the lateral tire force of the inner wheels tends to zero. Parameter R_a shows how fast the control should focus on minimizing the lateral acceleration. These parameters guarantee the smooth transient of the signals (Fig. 20.6).

If a fault is detected in the operation of the anti-roll bars, the brake system will be activated at a smaller critical value than in a fault-free case, i.e., when $|\rho_{Da}| > 0$. Consequently, the brake is activated in a modified way and the brake moment is able to assume the role of the anti-roll bars or the suspension actuator in which the fault has occurred. The modified critical value is

$$R_{a,new} = R_a - \alpha \cdot \rho_{Da}, \tag{20.14}$$

where α is a predefined constant factor.

If a fault is detected in the steering system ($|\rho_{Ds}| > 0$), the brake must focus on yaw dynamics in order to reduce the tracking error. Thus, in the control design of the brake, the performance specification concerning the steering system is also built in

$$W_{pe} = \phi_e(T_{b3}s + 1)/(T_{b4}s + 1), \quad (20.15)$$

where ϕ_e is

$$\phi_e = \begin{cases} 1 & \text{if } |\rho_{Ds}| > \rho_{\text{crit}}, \\ \frac{|\rho_{\text{R}}| - \rho_{\text{tol}}}{\rho_{\text{crit}} - \rho_{\text{tol}}} & \text{if } \rho_{\text{tol}} \leq |\rho_{Ds}| \leq \rho_{\text{crit}}, \\ 0 & \text{if } |\rho_{Ds}| < \rho_{\text{tol}}. \end{cases} \quad (20.16)$$

In this weighting the critical value of the brake intervention is used together with a tolerance value.

20.5.3 Anti-roll Bars

The performance signals in the control design of active anti-roll bars are the lateral load transfers and control inputs: $z_f = [\Delta F_{zf} \ \Delta F_{zf} \ u]^T$. Considering the vehicle masses at the front and rear weighting functions

$$W_{p_f} = \kappa_f(T_{f1}s + 1)/(T_{f2}s + 1) \quad (20.17)$$

are applied to the lateral load transfers, where the gain κ_f and time constants T_{fi} are tuning parameters of the specification.

20.5.4 Suspension System

The performance signals in the suspension design are: $z_s = [a_z \ s_d \ t_d \ u_s]^T$. The goals are to keep the heave accelerations $a_z = \ddot{q}$, suspension deflections $s_d = x_{1ij} - x_{2ij}$, wheel travels $t_d = x_{2ij} - w_{ij}$, and control inputs small over the desired operation range. The performance weighting functions for heave acceleration, suspension deflections, and tire deflections are selected as

$$W_{p,az} = \phi_{az}(T_{s1} + 1)/(T_{s2} + 1), \quad (20.18)$$

$$W_{p,sd} = \phi_{sd}(T_{s3} + 1)/(T_{s4} + 1), \quad (20.19)$$

$$W_{p,t_d} = \kappa_{td}(T_{s5} + 1)/(T_{s6} + 1), \quad (20.20)$$

where T_{si} and κ_{td} are time constants and the parameter-dependent gains are

$$\phi_{az} = \begin{cases} 1 & \text{if } |\rho_{kij}| < \rho_1, \\ \frac{|\rho_{kij}| - \rho_2}{\rho_1 - \rho_2} & \text{if } \rho_1 \leq |\rho_{kij}| \leq \rho_2, \\ 0 & \text{if } R \geq R_s \text{ or } |\rho_{kij}| > \rho_2, \end{cases} \quad (20.21)$$

$$\phi_{sd} = \begin{cases} 0 & \text{if } |\rho_{kij}| < \rho_1, \\ \frac{|\rho_{kij}| - \rho_1}{\rho_2 - \rho_1} & \text{if } \rho_1 \leq |\rho_{kij}| \leq \rho_2, \\ 1 & \text{if } R \geq R_s \text{ or } |\rho_{kij}| > \rho_2. \end{cases} \quad (20.22)$$

In normal cruising, the suspension system focuses on the conventional performances based on the parameter-dependent gain, which is a function of the suspension deflection ρ_{kij} . A large gain ϕ_{az} and a small gain ϕ_{sd} correspond to a design that emphasizes passenger comfort while choosing ϕ_{az} small and ϕ_{sd} large corresponds to a design that focuses on suspension deflection. The idea of the reconfigurable suspension system is based on the fact that active suspension systems are used not only to eliminate the effects of road irregularities but also to generate roll moments to improve roll stability or generate pitch moment to improve pitch stability.

$$W_{p,\theta} = \phi_P(T_{s7} + 1)/(T_{s8} + 1), \quad (20.23)$$

$$W_{p,\phi} = \phi_R(T_{s7} + 1)/(T_{s8} + 1). \quad (20.24)$$

For a reconfigurable suspension system, the parameter-dependent gains are selected as functions of the normalized lateral load transfer ρ_R and the normalized value of the pitch angle ρ_P . If ρ_P exceeds a predefined critical value, i.e., when $|\rho_P| \geq R_P$, the controller must focus on pitch stability. In an emergency, however, i.e., when $|\rho_R| \geq R_s$, the suspension system must reduce the rollover risk and guaranteeing passenger comfort (and pitch angle) is no longer a priority.

20.6 Global Performances Based on the Supervisor Activity

In order to provide a formal verification of the achieved control performance on a global level, the problem must be formulated globally. Only on this extended level are the performance variables which are relevant for the whole vehicle available. Once the local controllers have been designed, however, it is possible to perform an analysis step in the same robust control framework on a global level, for details see [10]. This might be a highly computation intensive procedure. Moreover, the presence of competing multiobjective criteria denies the applicability of this global approach. For example, in emergency events certain performance components gain absolute priority over others, thus requiring a given performance level for the ignored performance components is not justified. On the other hand, the local design

guarantees the prescribed performance level for the critical components. Therefore, in practice the formal global verification is often omitted and the quality of the overall control scheme is assessed through simulation experiments.

The relationship between the supervisor and the local controllers guarantee that the system meets the specified performances. Applying parameter-dependent weighting a balance between different controllers is achieved. In different critical cases related to extreme maneuvers or performance degradations/faults in sensors or actuators, the controllers reconfigure their operations.

However, maneuvers in which different critical performances must be achieved simultaneously may occur. For example, in a high-speed cornering maneuver the risk of a rollover increases significantly. The performances are in contradiction: deviating from the lane might cause the vehicle to run off the road while increasing roll dynamics might lead to rollover. This maneuver requires an intensive cooperation between the steering and the brake. The supervisor sends critical signals to these controllers and consequently these control systems are activated. However, reducing the rollover risk, the yaw dynamics is modified and the deviation from the predefined path may increase. In contrast, reducing the difference from the path might improve the rollover risk. Since both interventions are critical, the supervisor is not able to resolve the problem, thus the performances are handled by the actuators with performance degradation. In similar emergency cases, the supervisor is able to handle only a trade-off between critical performances.

20.7 Simulation Examples

As an illustration, an integrated control is proposed for tracking the path of the vehicle, guaranteeing road holding and improving pitch and roll stability. The control design is performed by using the Matlab/Simulink while the verification of the designed controller is performed by using the CarSim simulation software. In cruising mode, the steering minimizes the tracking error while the active anti-roll bars and the suspension system are operating. When the monitoring signals have reached their critical values, the brake is also activated in order to improve roll and pitch stability.

The operation of the integrated control in a heavy vehicle is illustrated in a double-lane-changing maneuver, which is defined by the signal yaw rate. The maneuver has a 4 m path deviation over 100 m. The velocity of the vehicle is 120 km/h. The operation of three control systems is shown in Fig. 20.7. The integrated control performs the maneuver in a fault-free operation (solid), operation in which there is a float failure in the active anti-roll bar at the rear (dashed dotted), and operation in which there is a float failure in the active anti-roll bar both at the front and the rear (dashed). During the faulty operation the anti-roll bars cannot generate enough stabilizing moment to balance the overturning moment. When there is a fault in the front anti-roll bar the brake is activated earlier than in the fault-free case. Moreover,

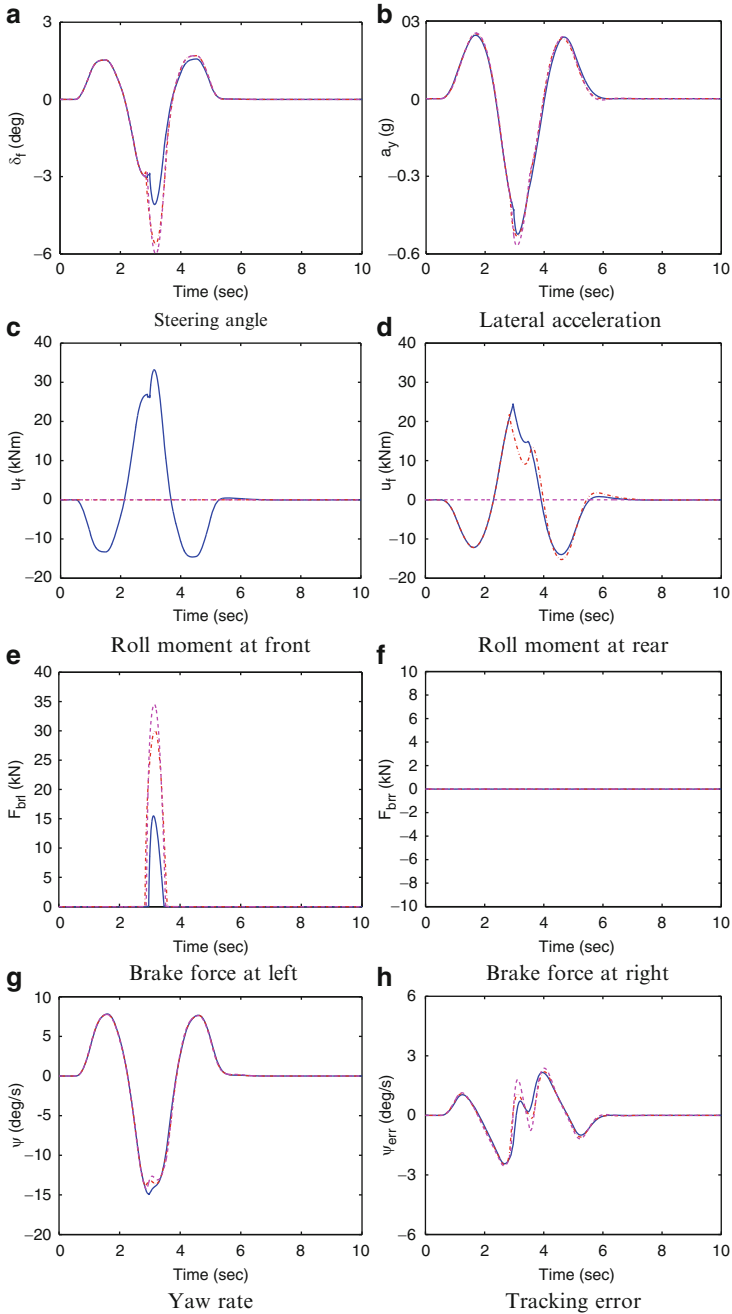


Fig. 20.7 Time responses of the tracking control based on a supervisory control (*solid*: fault-free, *dashed-dotted*: fault in the roll moment at front; *dashed*: fault in the roll moments) (a) Steering angle (b) Lateral acceleration (c) Roll moment at front (d) Roll moment at rear (e) Brake force at left (f) Brake force at right (g) Yaw rate (h) Tracking error

the braking lasts longer and the brake forces are greater than in the normal situation. The reason for this is that in the fault case the critical value of R_a is smaller than in the fault-free case.

The supervisor uses three signals, i.e., the normalized lateral load ρ_R from a component, which monitors the roll dynamics of the vehicle, the normalized longitudinal load ρ_P from a component, which monitors the pitch dynamics, and the fault information ρ_D from an FDI filter, which monitors the operation of the active anti-roll bars. The supervisor sends ρ_R and ρ_D signals to the active brake, which focuses on the roll stability. The integration is carried out through the parameter-dependent weighting function used in the design of the brake. The brake activates and generates a yaw moment in order to reduce the influence of the lateral loads. The supervisor also sends ρ_R , ρ_P , and ρ_D signals to the active suspension system, which provides road holding and passenger comfort. The control design is based on the LPV method since it is able to handle parameter dependence in the weighting strategy and guarantee that the designed controller meets the performance specifications.

In the second example, the supervisory controller is compared to the conventional distributed controller. In order to compare these cases, weighting functions are used in the design of the conventional controller. Figure 20.8 shows the time responses of the controlled systems when there is a float failure in the active anti-roll bar at the front. The results show the benefit of the proposed solution, which uses a supervisor over the completely decentralized approach, i.e., the required control inputs and the control energy are considerably smaller.

20.8 Conclusions

In this chapter, a multilayer supervisory architecture for the design and development of integrated vehicle control systems has been proposed. The local controllers are designed independently by taking into consideration the monitoring and fault signals received from the supervisor. In this architecture, the supervisor is able to make decisions about the necessary interventions and guarantee the reconfigurable and fault-tolerant operation of the vehicle. The design of local vehicle controllers has been carried out by using LPV methods. In the control-oriented modeling, the monitoring variables and the signals from the FDI filters play an important role. The supervisor sends these signals to the local controllers and handles the interactions and trade-off between these components. It is shown that the performance specifications are formalized in parameter-dependent weighting and the LPV method guarantees that the supervisory integrated control meets the defined performance specifications.

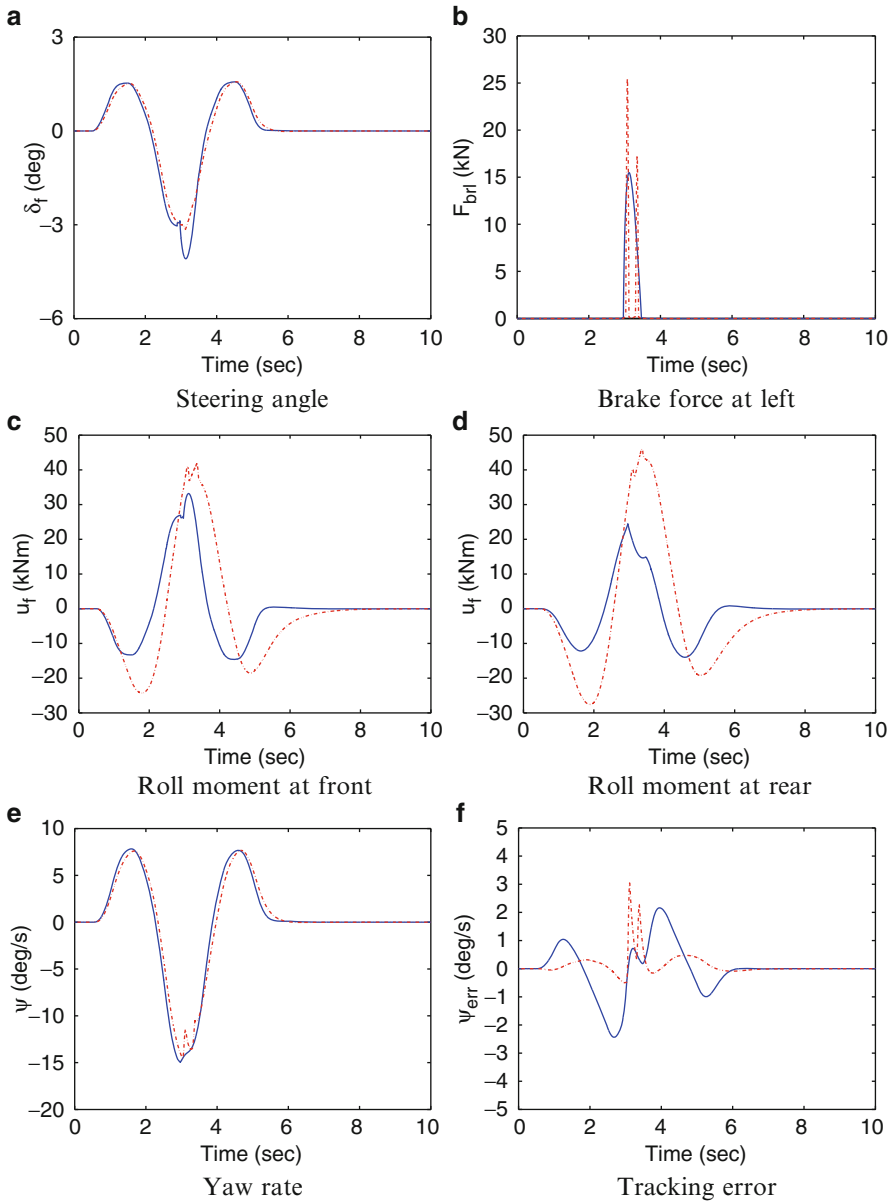


Fig. 20.8 Time responses of the tracking control based on a supervisory (*solid*) and the conventional distributed (*dashed*) control (a) Steering angle (b) Brake force at left (c) Roll moment at front (d) Roll moment at rear (e) Yaw rate (f) Tracking error

Acknowledgments The research was supported by the Hungarian National Office for Research and Technology through the project “Innovation of distributed driver assistance systems for a commercial vehicles platform” (TECH_08_2/2-2008-0088) which is gratefully acknowledged. This research work has been supported by Control Engineering Research Group, Hungarian Academy of Sciences at the Budapest University of Technology and Economics.

References

1. Bokor J, Balas G (2005) Linear parameter varying systems: a geometric theory and applications. In: 16th IFAC World Congress, Prague
2. Burgio G, Zegelaar P (2006) Integrated vehicle control using steering and brakes. *Int J Contr* 79:534–541
3. Gáspár P, Szabó Z, Bokor J (2007) Estimation of the friction coefficient for road vehicles. American Control Conference, New York
4. Gáspár P, Szabó Z, Bokor J (2008) An integrated vehicle control with actuator reconfiguration. IFAC World Congress, Seoul, Korea
5. Gáspár P, Szászi I, Bokor J (2003) Active suspension design using the mixed μ synthesis. *Vehicle Syst Dyn* 40(4):193–228
6. Gáspár P, Szászi I, Bokor J (2003) The design of a combined control structure to prevent the rollover of heavy vehicles. *Eur J Contr* 10(2):1–15
7. Gillespie T (1992) Fundamentals of vehicle dynamics. Society of Automotive Engineers Inc., Warrendale
8. Gordon T, Howell M, Brandao F (2003) Integrated control methodologies for road vehicles. *Vehicle Syst Dyn* 40:157–190
9. Gustafsson F (1997) Slip-based tire-road friction estimation. *Automatica* 33:1087–1099
10. Langbort C, Chandra RS, D’Andrea R (2004) Distributed control design for systems interconnected over an arbitrary graph. *IEEE Trans Automat Contr* 49(9):1502–1519
11. Niinomi T, Krogh B, Cury J (1995) Synthesis of supervisory controllers for hybrid systems based on approximating automata. In: Proceedings of the 34th IEEE Conference on Decision and Control, pp 1461–1466
12. Packard A, Balas G (1997) Theory and application of linear parameter varying control techniques. In: Proceedings of the American Control Conference, Albuquerque, New Mexico
13. Palkovics L, Fries A (2001) Intelligent electronic systems in commercial vehicles for enhanced traffic safety. *Vehicle Syst Dyn* 35:227–289
14. Platzer A (2008) Differential dynamic logic for verifying parametric hybrid systems. *J Autom Reasoning* 41:143–189
15. Scherer CW (2001) LPV control and full block multipliers. *Automatica* 27(3):325–485
16. Song C, Uchanski M, Hedrick J (2002) Vehicle speed estimation using accelerometer and wheel speed measurements. In: Proceedings of the SAE Automotive Transportation Technology, Paris
17. Staroswiecki M (2006) Robust fault tolerant linear quadratic control based on admissible model matching. In: 45th IEEE Conference on Decision and Control, pp 3506–3511
18. Stoustrup J (2009) Plug and play control: control technology towards new challenges. *Eur J Contr* 15(3):311–330
19. Trachtler A (2004) Integrated vehicle dynamics control using active brake, steering and suspension systems. *Int J Vehicle Des* 36:1–12
20. Wu F (2001) A generalized LPV system analysis and control synthesis framework. *Int J Contr* 74(7):745–759
21. Wu F, Yang X, Packard A, Becker G (1996) Induced L_2 norm controller for LPV systems with bounded parameter variation rates. *Int J Robust Nonlinear Contr* 6:983–988

22. Xiao H, Chen W, Zhou H, Zu J (2011) Integrated control of active suspension system and electronic stability programme using hierarchical control strategy: theory and experiment. *Vehicle Syst Dyn* 49:381–397
23. Yu F, Li D, Crolla D (2008) Integrated vehicle dynamics control: State-of-the art review. *IEEE Vehicle Power and Propulsion Conference*, Harbin, China

Index

A

Active aeroelastic wing (AAW), 485–486. *See also* X-53 active aeroelastic wing

Active fault-tolerant controller (AFTC), 305

Actuator

dynamics, for flexible hypersonic vehicle, 422

input, ramp velocity tracking, 438, 440

and operation modes, in distributed control system, 525–528

selection, distributed control system, 523–524

ALINEA method, 476, 477, 479, 480

Alumina refineries, process control in

bauxite ore, dilution, 235–236

Bayer process

alumina/caustic ratio vs. temperature, equilibrium curve of, 237

departments of, 235–236

counter-current washing circuit

APRC-based decentralised MPC, 242, 243

multiplier matrices, 242

parallel redundant subsystem, in hydro-metallurgical processes, 239, 240

state space realisation matrices, of linearised models, 241

mud washing department in, 238

plant-wide process control for, 237, 239

predesilication process, 242

decentralised MPC, with quadratic programming, 246–248

large-scale process, 244

multiplier matrices, 246, 249

parallel subsystems, 244, 245

predictive horizons of, 246

state space realisation matrices, 244, 246

yield, 236

Anti-roll bars, 527

Anti wind-up bumpless transfer (AWBT), 392–393

Arbitrary time variations

Lyapunov structure, 12–13

quadratic vs. non-quadratic stability, 11

stability, 10–11

ARX. *See* Autoregressive with exogenous input (ARX)

Asymptotically positive realness constraint (APRC), decentralised MPC, 235

constrained optimisation problem for, 233

definition, 228

local controllers, 234, 235

one-time-step control constraint, 234

quadratic supply rate, 228

Asymptotic output regulation, 127

Autoregressive with exogenous input (ARX) and ARMAX structures, 40–41

identifiability, 44–45

informative data set, 45

PE identification, 46

FIR and OBF models, estimation of, 49–50

instrumental variable approach, 48–49

linear regression, 46–47

B

Bauxite ore, 235–236

Bayer process, alumina refineries

departments of, 235–236

equilibrium curve of, 237

Bode plots, X-53 active aeroelastic wing, 490, 491, 494, 495, 505, 506
 Bounded real lemma (BRL), 94, 95, 321, 497
 Box–Jenkins (BJ) structures, 43
 Brake system, 526–527

C

Causal dynamic dependence, 33
 Cholesky's decomposition, 69, 76
 Classical model structures, LPV-PE
 identification
 LPV-ARX and ARMAX, 40–41
 LPV-BJ and OE, 43
 LPV-FIR and series expansion, 41–43
 noise model, 39–40
 process model, 38–39
 Closed-loop system, 64, 106, 109–111, 167
 dynamics, 132, 144, 145
 gain properties, 209
 stability analysis
 norm-bounded approach, 94–96
 polytopic approach, 93–94
 Combustion engines control, LPV models for, 445–447. *See also* Turbocharged combustion engine control, low-complexity LPV input-output models
 Consistency, LPV prediction-error framework, 37
 Constrained freeway traffic control, LPV paradigms
 controller setup
 closed-loop interconnection, 473
 congruent transformation, 475, 476
 dissipativity, Schur-complement, 474
 LMI, controller design, 476
 Lyapunov matrix, 474, 475
 optimization problem, 476
 dynamical model, 462
 induced L_2 norm, 472, 474
 model-based control, problem statement
 control input, 465
 dynamical representation, of n -lane stretch, 463–464
 generalized disturbance vector, 465
 macroscopic models, 463
 nonlinear optimization problem, 466
 on-ramps, 465
 total time spent (TTS), 465, 466
 vehicle number, 465, 466
 numerical properties of, 481
 ALINEA method, 476, 477, 479, 480
 density evolution comparison, 478, 479

isolated ramp metering, 476
 nonlinear model parameters, 477
 on-ramp volume comparison, 478, 480
 saturation parameter, variation of, 480
 space-mean speed evolution
 comparison, 478, 479
 steady-state values, 477
 z-domain, performance weight selection
 in, 477, 478
 parameter varying problem formulation
 capacity maximization, 471
 convex combination, of vertex systems, 468
 discrete time, 467
 extended Payne–Whitham model, 468–469
 implicit constraint handling, 470
 input saturation parameter, 469
 linear time varying (LTV) model,
 polytopic system, 467
 parameter-dependent, 471–472
 polytopic representation, 470–471
 quasi-linear parameter varying (qLPV)
 framework, 466, 467
 saturation parameter, 469–470
 scheduling vector, 467
 Tensor-Product (TP) model
 transformation, 470
 performance output of, 471, 472, 474, 477, 481
 ramp metering, 461, 462
 second-order macroscopic model, 477, 481
 Conventional design methods, recovery of, 196–199
 Convergence, LPV prediction-error framework, 37
 Convex optimization, 253–277
 Cost of electricity (COE), 304

D

Data-generating system, 31–33
 Dead-beat LPV control problem, 78–79
 Decentralised model predictive control (MPC),
 of time-varying splitting parallel systems
 alumina refineries, process control in
 bauxite ore, dilution, 235–236
 Bayer process, departments of, 235–236
 Bayer process, equilibrium curve of, 237
 counter-current washing circuit, 239–243
 mud washing department in, 238

- plant-wide process control for, 237, 239
 - predesilication process, 242, 244–249
 - yield, 236
 - asymptotically positive realness constraint, 228–229, 233–235
 - dissipativity matrices of, 230
 - dynamically coupled subsystems, 220, 233
 - industrial plant-wide process control and APRC, 221
 - continuous control strategy, 219, 220
 - departmentalisation and mixed operational mode, 218–219
 - parallel connection of, 219
 - mixed connection configuration, 220, 227, 239
 - model development and problem statement
 - block diagram, of large-scale system, 225–226
 - bounded control constraint, 225
 - control and system model, 223–227
 - discrete-time state space model, 223
 - inter-subsystem communication, 227
 - parallel connections, within one unit, 224–227
 - problem description and rationale, 227
 - serial connections, 223–224
 - subsystems, units and large-scale system, denotations for, 223
 - parallel configuration, 219
 - quadratically dissipative, 221, 229, 231
 - serial configuration, 218, 219
 - stability and feasibility conditions, 229–233
 - state jumps, 219, 227
- Delay-independent stabilization, 280
- Delay-system, LMIs application, 101
- Discrete-time systems, 11, 19, 73–77. *See also* Switched LPV systems, in discrete time
- Distributed control system
 - actuators and operation modes in
 - anti-roll bars, 527
 - brake system, 526–527
 - steering system, 525
 - suspension system, 527–528
 - sensors and monitored components in
 - actuator selection, 523–524
 - fault monitoring, 524–525
 - pitch stability, 523
 - road tracking, 523
 - roll stability, 523
 - yaw stability, 522
- Disturbance attenuation, 153, 154, 157–178
- Disturbance rejection, 20–21
- Duality, 62, 75
- Dynamic dependence, 31
- Dynamic output feedback, 288, 320
- E**
- Earth centered inertial (ECI) reference axes, 341
- Engine control, 445–448
- Error-to-signal-ratio (ESR), 386
- Eventually periodic systems, 110
- Explicit controller parametrizations, using LMIs
 - closed loop stability analysis, 93
 - norm-bounded approach, 94–96
 - polytopic approach, 93–94
 - control design, LMIs, 96–98
 - delay-system, application to, 101
 - inverse of matrix, 102
 - mixed objective synthesis, 100
 - nonsingular matrix, 102, 103
 - vs. norm-bounded results, 100
 - vs. polytopic results, 99–100
 - polytopic vs. norm-bounded approaches, 98–99
 - problem formulation, 91–92
 - robust control, 102
 - Schur complement formula, 103
 - symmetric matrix, 102
- Exponential stability, 172
- Extended mixed Skyhook-ADD (SH-ADD), 402, 404, 405
- F**
- Factorized denominator, transfer functions with, 69–71
- Fault-detection and identification (FDI) filters, 517, 522, 524, 531
- Finite impulse response (FIR), 41, 42, 49, 55, 78
 - and OBF, 42, 49–50
 - and series expansion structures, 41–43
- Fixed pole assignment, 77–78
- Flexible hypersonic vehicle, LPV H_∞ control
 - angle of attack in, 442
 - continuously differentiable matrix functions, 418
 - control design
 - basis function vectors, 426–427
 - gridding points, γ performance for, 428
 - parameter variation rates, γ performance for, 427
 - robust parametric study, 427
 - control implementation

- Flexible hypersonic vehicle, LPV H_∞ control
(*cont.*)
 control effort, 431
 2D parameter space, controllable region
 in, 430
 2D parameter space, switching
 threshold for, 429, 430
 nonlinear HSV, control input for, 429
 trim values for, 429
 finite number, of basis functions, 420
 gain-scheduled control, 415, 416
 modelling
 actuator dynamics, 422
 linearization, 422–423
 motion, nonlinear equations of,
 420–421
 rigid body dynamics, 420
 state and control input bounds, in
 solving trim points, 423
 nonlinear simulation study
 actuator input, ramp velocity tracking,
 438, 440
 block diagram, of closed loop system,
 432
 controller ID, ramp velocity tracking,
 439–441
 flexible body states, ramp velocity
 tracking, 436–437, 440
 integration error, ramp velocity
 tracking, 435, 437, 439
 results, 433–441
 rigid body states, ramp velocity
 tracking, 433–435
 sensor noise variance and seed values,
 433
 setup, 432–433
 velocity tracking and regulation, 439
 n th-order LPV controller, 418–420
 open-loop interconnection
 augmented plant, 426
 output feedback velocity tracking
 problem, 424, 425
 weighting function, 425
 output feedback control design, 424
 time-varying vector, 417
 Flight control, 6, 484–486
 Frequency domain inequality (FDI), 260
 Frequency response functions (FRFs), 372–374
- G**
 Gain-scheduled (GS) controllers, 181
 Gain-scheduled feedback control
 discrete-time polytopic LPV system, 362
 dynamic output feedback, 368–370
 extensions
 H_2 and H_∞ performance, 371
 homogeneous polynomially parameter-
 dependent system, 372
 LMI relaxations, 372
 state feedback, 366–368
 uncertainty domain
 modeling of, 364–366
 rate of parameter variation, 363–364
 Gain-scheduled output-feedback (GSOFF)
 controllers, 181
 basic lemmas, 187–190
 conventional design methods, recovery of,
 196–199
 design methods, classification, 182
 methods
 H_∞ control-type problem, 191–192
 H_2 control-type problem, 192–193
 PDBMIs, algorithm for solving, 194
 unmeasurable parameters, LPV systems
 with, 194–195
 numerical examples, 201–210
 Bode plots, 209
 gain properties, closed-loop systems,
 209
 parameter-dependent decision matrices,
 202
 polynomially parameter-dependent,
 199–201
 state-space matrices, 202, 206, 212
 problem definitions, 187
 system definitions, 184–186
 Gain-scheduling, 3, 4, 6, 7, 61–87, 253–277
 Generalized asymptotic regulation (GAR),
 127
 classical theory, 127
 course control designs, 153
 design ingredients, 137, 138
 design variables, 136, 137
 under H_2 -type constraint, 147–151
 illustrative example, 151–154
 under L_2 gain constraint, 142–147
 online-measurable parameters, 128, 139
 problem setup
 closed-loop dynamics, 132–133
 detectability, 131
 exo-system dynamics, 130
 infinite-energy disturbance, 129
 neutrally stable exo-system, 131
 positive-definite function, 132
 stabilizability, 131
 uncertain parameters, 129
 robust GAR

- parameter derivative dependence in
 - controller, 139
 - problem, 133–134
 - solution, 135–139
 - sufficient condition, 134–135
 - transient behavior, shaping, 141–142
 - unmeasurable parameters, absence of, 139–141
 - robust GAR constraint
 - closed-loop system, 147–149
 - LTI systems performance, 150
 - transient shaping, 150–151
 - velocity-dependent system parameters, 152
 - General noise models, PE identification, 50
 - instrumental variable approach, 53–55
 - nonlinear optimization, 53
 - pseudolinear regression, 50–53
 - Genetic algorithms, 398–400
 - multi-objective optimization, 408
 - stable controllers, 399
 - strong stabilization, 399
 - Global identification approach, 50
 - GS controllers. *See* Gain-scheduled (GS) controllers
 - GSOE. *See* Gain-scheduled output-feedback (GSOE) controllers
 - GS state-feedback (GSSF) controllers, 182, 206, 207, 213
- H**
- H_∞ control-type problem, 191–192
 - H_2 control-type problem, 192–193
 - H_2 performance, robust GAR with, 148–149
 - H_2 -type constraint
 - robust GAR problem with, 147–148
 - shaping transient behavior with, 150–151
 - Hurwitz denominator, 63, 68, 69
 - Hurwitz region, LPV stability within, 82–85
 - Hybrid systems, 106
 - dynamical, 5
 - Hydro-metallurgical processes, parallel
 - redundant subsystem, 239, 240
 - Hypersonic vehicle (HSV) controls. *See also* Flexible hypersonic vehicle, LPV
 - H_∞ control
 - control techniques, 415–416
 - isometric and side view of, 414
 - modeling of, 414–415
 - parameter v -variation set, 417
- I**
- Implementability, 181–213
 - Impulse response coefficients, 30, 31
 - Impulse response representation (IRR), 30, 31, 33, 35, 38–41, 55
 - Induced L_2 analysis, for LPV systems, 497–499, 508–510
 - Induced non-minimum phasedness, 8
 - Industrial plant-wide process control and time-varying splitting systems, 222
 - APRC, 221
 - continuous control strategy, 219, 220
 - decentralised control strategy, 220
 - departmentalisation and mixed operational mode
 - interconnected system, 218
 - issues, 218–219
 - parallel connection of, 219
 - Input-output (IO) models
 - representations, 28
 - robust stability, of LPV systems, 14, 15
 - state-space model interpolation of local estimates, 360
 - turbocharged combustion engine control (*see* Turbocharged combustion engine control, low-complexity LPV input-output models)
 - vibroacoustic application, 373
 - Instrumental variable approach, 53–55
 - ARX case, PE identification, 48–49
 - general noise models, PE identification, 53–55
 - Integral quadratic constraint (IQC)
 - analysis, 259–261
 - parameterizing dynamic
 - dynamic D/G-scalings, 262
 - static full-block multipliers, 263
 - time-varying parametric uncertainties with bounds, 262–263
 - squaring, 265
 - Integrated vehicle chassis control, design of
 - architecture of
 - configuration, 515
 - event set, 515, 516
 - local components, 517–518
 - supervisory control, 516–517
 - decentralized control system, 514
 - distributed control system, actuators and operation modes in
 - anti-roll bars, 527
 - brake system, 526–527
 - parameter-dependent gain, 526, 528
 - steering system, 525
 - suspension system, 527–528
 - distributed control system, sensors and monitored components in

- Integrated vehicle chassis control, design of
(cont.)
 actuator selection, 523–524
 fault monitoring, 524–525
 pitch stability, 523
 road tracking, 523
 roll stability, 523
 yaw stability, 522
 fault-detection and identification (FDI)
 filters, 517, 522, 524, 531
 global performances, supervisor activity,
 528–529
 LPV control, of vehicle systems, 521, 522
 LPV modeling, of vehicle systems,
 518–520
 parameter-dependent weighting, 529, 531
 performance weighting functions, 516, 527
 reconfigurable and fault-tolerant operation,
 514, 516, 522, 531
 road holding, 514, 518, 529, 531
 robust control, 528
 simulation in
 conventional distributed control, 531,
 532
 supervisory control, 530–532
 tracking control, time responses of, 529,
 530, 532
 supervisory decentralized architecture of,
 514, 515
- Interpolation-based modeling
 polytopic state-space representation,
 359–360
 state-space model interpolation of local
 estimates
 input–output combination, 360
 interpolation and optimization, 362
 poles and zeros, 360–361
 polytopic parametrization, 362
 similarity transformation matrix,
 361–362
 SISO models, 361
 time varying scheduling parameter, 360
- IQC. *See* Integral quadratic constraint (IQC)
- IRR. *See* Impulse response representation
 (IRR)
- J**
- Jump linear systems, 5–6
- K**
- Kalman–Yakubovich–Popov (KVP) lemma,
 111, 158, 172, 255, 260
- L**
- Least squares (LS) criterion, 36
 ARX case, PE identification, 46
 FIR and OBF models, estimation of,
 49–50
 instrumental variable approach, 48–49
 linear regression, 46–47
 general noise models, PE identification, 50
 instrumental variable approach, 53–55
 nonlinear optimization, 53
 pseudolinear regression, 50–53
- LFR. *See* Linear-fractional representations
 (LFR)
- LFT framework. *See* Linear fractional
 transformation (LFT) framework
- L_2 gain constraint
 robust GAR problem, 142
 shaping transient behavior with, 147
- L_2 gain performance, robust GAR with,
 143–146
- L_2 -induced norm, 106
- Linear differential inclusions, 61
- Linear-fractional representations (LFR), 28,
 42, 450
- Linear fractional transformation (LFT)
 framework, 106, 257
- Linear-in-the-coefficients property, 42, 45, 50
- Linear matrix inequalities (LMIs), 16–18, 106,
 230
 analysis, reformulation of
 gluing, 266–267
 IQC squaring, 265
 explicit controller parametrizations
 closed loop stability analysis, 93–96
 control design, 96–98
 delay-system, application to, 101
 inverse of matrix, 102
 mixed objective synthesis, 100
 nonsingular matrix, 102, 103
 vs. norm-bounded results, 100
 vs. polytopic results, 99–100
 polytopic vs. norm-bounded
 approaches, 98–99
 problem formulation, 91–92
 robust control, 102
 Schur complement formula, 103
 symmetric matrix, 102
 slack variables, 286–288
- Linear parameter varying (LPV) systems
 applications, 6
 assessing properties, 5
 control design
 linear matrix inequality (LMI) method,
 16–18

- set-invariance method, 19–22
 - stable realization, 18–19
 - feedback gain, 5
 - gain-scheduling, 3
 - hybrid dynamical systems, 5
 - induced non-minimum phasedness, time variation, 8
 - jump linear systems, 5–6
 - vs. LTI systems, 4
 - vs. LTV systems, 4–5
 - origins, 3–4
 - stability
 - arbitrary time variations, 10–13
 - instability and time variation, 7–8
 - robust, 14–16
 - slow time variations, 8–10
 - stable realization, 63–64, 67–71 (*see also* Parametric gain-scheduling control, LPV-stable realization)
 - Linear parametrization, 38
 - Linear regression, 46–47
 - Linear time-invariant (LTI) system, 4, 256, 257
 - frequency response functions and, 374
 - and interpolating LPV model, 376
 - IO combination, 360, 373
 - plants, online parameter tuning for, 79–82
 - point analysis, X-53 active aeroelastic wing, 494–497
 - poles and zeros, 374
 - robust GAR
 - with H_∞ performance, 146–147
 - with H_2 performance, 150
 - Linear time varying (LTV) systems, 4–5
 - LMIs. *See* Linear matrix inequalities (LMIs)
 - Local identification approach, 36, 37, 45
 - LPV systems. *See* Linear parameter varying (LPV) systems
 - LS criterion. *See* Least squares (LS) criterion
 - LTV systems. *See* Linear time varying (LTV) systems
 - Lyapunov function
 - parameter-dependent, 106–107
 - parameter-independent, 106–107
 - Lyapunov inequalities, 158
 - Lyapunov–Krasovskii functionals, 281–284
 - Lyapunov matrix, 474, 475
 - Lyapunov structure, 12–13
- M**
- Magnetic attitude control
 - LPV design
 - control input matrix, 350, 351
 - convex optimization, 350
 - induced L_2 norm, 349, 350
 - parameter-dependent state-feedback problem, 349–350
 - parameter ranges and variation rates, 350, 351
 - Yalmip, 351
 - magnetically controlled spacecraft
 - averaging-based modelling, 345–346
 - parameter-dependent modelling, 347–348
 - periodic modelling, 346–347
 - Magneto-rheological (MR) dampers
 - bi-viscosity and hysteresis, 383
 - control-oriented model, 385–388
 - extended mixed Skyhook-ADD, 402
 - extended Skyhook, 402
 - passive, 403
 - Shuqi Guo model, 384
 - test-rig, 386
 - MATLAB objects, X-53 active aeroelastic wing, 487, 488
 - Milling process, 292
 - Mixed objective synthesis, 100
 - Model predictive control (MPC), of time-varying splitting parallel systems. *See* Decentralised model predictive control (MPC), of time-varying splitting parallel systems
 - Moore–Penrose pseudoinverse approach, 46
 - Multiconvexity relaxation technique, 119–120
 - Multiple-input multiple-output (MIMO) systems, 359, 362, 375
- N**
- NASA Dryden’s X-53 AAW, 485
 - Noise model, 39–40
 - Nonlinear optimization, 53
 - Non-negative garrote (NNG), 39
 - Nonquadratic cost minimization, 21–22
 - Non stationary LPV (NSLPV), 105–107
 - definition, 108
 - matrix-valued function, 108–109
 - plant and controller, 108–109
 - switched systems, control of SLPV system, 115
 - state-space subregions, 116
 - Norm-bounded approach
 - closed loop system, 94–96
 - vs. polytopic approach, 98–99
 - NSLPV. *See* Nonstationary LPV (NSLPV)

O

- Observer-based controller, 67, 68
- One-step-ahead predictor, 29, 31, 33, 34, 36, 42, 43, 50
- Open-loop interconnection, flexible hypersonic vehicle
 - augmented plant, 426
 - output feedback velocity tracking problem, 424, 425
 - weighting function, 425
- Optimal disturbance attenuation, 175, 176
- Orbits, 105, 110
- Orthonormal basis functions (OBFs), 42
 - and FIR, 49–50
- Outer leading edge flaps (OLEFs), X-53 active aeroelastic wing, 490–492
- Output-error (OE) structure, 42, 43

P

- Parameter-dependent bilinear matrix inequalities (PDBMIs), 183, 193, 194
- Parameter-dependent decision matrices, 202
- Parameter-dependent LMIs (PDLMIs), 183–185, 193, 194, 200, 201, 208, 212
- Parameter-dependent Lyapunov approach, NSLPV systems control, 105
 - analysis and synthesis, 110–114
 - controller construction, 120–124
 - algorithm, 121
 - matrix-valued continuous function, 120, 121
 - polynomial functions, 123
 - solutions, 120
 - control problem solving, 106
 - parameterized LMI relaxation
 - multiconvexity relaxation technique, 119–120
 - sum of squares (SOS) method, 116–118
 - plant and controller, 108–110
 - switched systems, 114–116
 - uses, 106, 107
- Parameter-dependent Lyapunov functions (PDLFs), 182, 183, 193, 196, 197, 199
- Parameterized linear matrix inequalities (PLMIs), 107, 114, 116, 120, 123, 124
 - multiconvexity relaxation technique, 119–120
 - sum of squares (SOS) method, 116–118

- Parameter set mapping (PSM), 455, 456
- Parametric gain-scheduling control, LPV-stable realization
 - applications
 - dead-beat LPV control problem, 78–79
 - fixed pole assignment, 77–78
 - Hurwitz region, LPV stability within, 82–85
 - online tuning for LTI plants, 79–82
 - pointwise optimality and LPV stability, 85–86
 - discrete-time case, 73–77
 - factorized denominator, transfer functions with, 69–71
 - preliminary results, 65–68
 - problem statement
 - closed-loop control system, 64
 - LPV stabilizing controller realization, 64
 - LPV-stable realization, 63–64
 - LPV synthesis, 64–65
 - state-space representation, 63
 - stabilizing compensator realizations, 72–73
- Parametric transfer function, LPV-stable realization of, 68–71
- Parameterized model, LPV systems, 35–36
- Payne–Whitham model, constrained freeway traffic control, 468–469
- PDBMIs. *See* Parameter-dependent bilinear matrix inequalities (PDBMIs)
- PDLFs. *See* Parameter-dependent Lyapunov functions (PDLFs)
- PDLMIs. *See* Parameter-dependent LMIs (PDLMIs)
- Peaking vs. stability, 8–9
- Periodic systems, 110, 113
- PLMIs. *See* Parameterized linear matrix inequalities (PLMIs)
- Pointwise optimality and LPV stability, 85–86
- Polynomial parameter-dependence, 106, 112
 - GSOFC controllers, 199–201
- Polytopes, 108, 164, 165
- Polytopic approach
 - closed loop system, 93–94
 - vs. norm-bounded approach, 98–99
- Prediction-error identification, 27
 - ARX case, LS criterion
 - FIR and OBF models, 49–50
 - instrumental variable approach, 48–49
 - linear regression, 46–47
 - classical model structures
 - LPV-ARX and ARMAX, 40–41
 - LPV-BJ and OE, 43
 - LPV-FIR and series expansion, 41–43

- noise model, 39–40
- process model, 38–39
- framework
 - consistency, 37
 - convergence, 37
 - data-generating system, 31–33
 - identifiability, 36–37
 - informativity, 37
 - noisy p , v_o prediction with, 34
 - parameterized models and estimation, 35–36
 - v_o prediction, 33–34
- general noise models, LS criterion, 50
- instrumental variable approach, 53–55
- nonlinear optimization, 53
- pseudo-linear regression, 50–53
- informativity and identifiability, 43–45
- LPV series-expansion representation, 29–31
- LS criterion, 45
- y , prediction of, 34–35
- Process model, 38–39
- Proportional and integral (PI) controller
 - controller design
 - aerodynamic gains, 329
 - bandpass filter, 327
 - drive train, 327, 328
 - integrator filter, 326, 329
 - LMI optimization problem, 330
 - loop-shaping weight, 329, 330
 - Lyapunov matrix, 330
 - mixed sensitivities optimization problem, 329
 - open-loop system matrices, 328
 - performance level and controller gains, 331
 - proportional, integral and tower feedback gains, 331, 332
 - schematic block diagram, 327
 - static output feedback, 329
 - variable-speed wind turbine, 328
 - simulation results
 - fault-tolerance, 335
 - time series, 332–334
- Pseudolinear regression, 50–53
- Q**
- Quadratic vs. non-quadratic stability, 11
- Quarter vehicle model, 387–389
- R**
- Ramp metering, 461, 462
- Ramp velocity tracking
 - actuator input, 438, 440
 - controller ID, 439–441
 - flexible body states, 436–437, 440
 - integration error, 435, 437, 439
 - rigid body states, 433–435
- Reference tracking, 498, 503, 508
- Refined instrumental variable (RIV) approach, 43, 54
- Renault Mégane Coupé (RMC), 389, 400, 401
- Road tracking, in distributed control system, 523
- Robust controller, designing, 102
- Robust estimation, with partial gain-scheduling
 - convex optimization
 - dualization and elimination, 272–277
 - gain-scheduled estimation problem, 256–257
 - KYP lemma, 255, 260
 - linear fractional transformation (LFT), 254, 257
 - LMI, 255
 - LTI system, minimal realization of, 256, 257
 - numerical
 - estimation error, 270, 271
 - estimator, 269–270
 - singular value plots of, 271, 272
 - uncertain LPV system, 269
 - result, 267–269
 - scheduling operator, 257
 - stability and performance analysis
 - from analysis to synthesis, 263–264
 - with IQCs, 259–261
 - LMIs analysis, reformulation of, 264–267
 - nominal stability, characterization of, 264
 - parameterizing dynamic IQCs, 261–263
 - realization of, 258
 - standard configuration for, 257, 258
 - star-convex set, 256
 - uncertain dynamical system, 254
 - uncertain parameters, 254
 - well-posed, 257–261, 264
- Robust finite-path-dependent state feedback, 173, 174, 176, 178
- Robust generalized asymptotic regulation (GAR)
 - with H_2 performance, 148–149
 - H_2 -type constraint
 - problem with, 147–148
 - shaping transient behavior with, 150–151
 - L_2 gain constraint

- Robust generalized asymptotic regulation (GAR) (*cont.*)
 - robust GAR with, 142
 - shaping transient behavior with, 147
- with L_2 gain performance, 143–146
- LTI systems
 - H_∞ performance for, 146–147
 - H_2 performance for, 150
- parameter derivative dependence in controller, 139
- problem, 133–134
- solution, 135–139
- sufficient condition, 134–135
- transient behavior, shaping, 141–142
- unmeasurable parameters, absence of, 139–141
- Robustness, 181–213
- Robust stability, 14
 - slowly varying operators, 14–15
 - small-gain condition, 15–16
- Root mean-square (RMS) value, 321, 408
- Routh–Hurwitz table, 82
- S**
- Schur complement formula, 103, 121, 123, 146, 162, 167, 171
- Semi-active suspensions
 - frequency domain analysis
 - extended mixed SH-ADD, 404
 - frequency responses, 403, 404
 - nominal MRD and extended Skyhook, 404
 - optimal controllers, 404
 - performances comparison, 405
- H_∞ /LPV controller
 - control scheme, 395–397
 - genetic algorithms, 398–400
 - stable controllers, 399
 - strong stabilization, 399
- LPV model
 - deflection velocity, 392
 - input saturation constraint, 393
 - ride comfort and road holding, 392
 - saturation function, 393
 - scheduling parameters, 393, 394
 - state-space representation, 391–392
- magneto-rheological dampers
 - bi-viscosity and hysteresis, 383
 - control-oriented model, 385–388
 - extended mixed Skyhook-ADD, 402
 - extended Skyhook, 402
 - passive, 403
 - Shuqi Guo model, 384
 - test-rig, 386
 - nonlinear RMC spring, 400, 401
 - Pareto set, 400, 401
 - performance objective quantification
 - road holding improvement, 391
 - vehicle body acceleration, 391
 - vibration dose value, 390
 - quarter vehicle model, 387–389
 - time domain analysis, 405–408
- Set-invariance method, 19
 - disturbance rejection, 20–21
 - nonquadratic cost minimization, 21–22
- Shuqi Guo model, 384
- SIMULINK model, X-53 active aeroelastic wing, 499–501
- Single-input single-output (SISO) model, 29, 78, 359–361, 373–375, 393, 450, 496
 - state-space model interpolation of local estimates, 360–362
 - vibroacoustic application, 373–375
- Sinusoidal disturbance attenuation, 128, 152, 153
- Slack variable (SV), LMI relaxation, 286–288
- Slow time variations
 - characterization, 10
 - stability vs. peaking, 8–9
- SLPV systems. *See* Stationary LPV (SLPV) systems
- Small-gain theorem, 15–16
- SOS method. *See* Sum of squares (SOS) method
- Spacecraft, magnetic actuators
 - averaged models, 340
 - magnetic attitude control design
 - averaging-based modelling, 345–346
 - parameter-dependent modelling, 347–348
 - periodic modelling, 346–347
 - time-periodic system, 345–346
- mathematical model
 - angular kinematics and dynamics, 342
 - earth centered inertial reference axes, 341
 - geomagnetic field vector, 343
 - LEO orbit, 344
 - local linear dynamics, 342
 - magnetic coils, 343
 - magnetic torquers, 343
 - orbital axes, 341
 - satellite body axes, 341
- periodic models, 340
- simulation study
 - orientation error, 352, 353
 - small satellite platform, 351

- state-feedback controllers
 - implementation issues, 345
 - nominal closed-loop performance, 344
 - nominal closed-loop stability, 344
 - stability and performance robustness, 344
 - SRP transfer function. *See* Stable regular parametric (SRP) transfer function
 - Stability, 62
 - arbitrary time variations
 - Lyapunov structure, 12–13
 - quadratic vs. non-quadratic stability, 11
 - stability, 10–11
 - of discrete time switched LPV systems, 159–164
 - within Hurwitz region, 82–85
 - instability and time variation
 - induced instability, 7–8
 - induced non-minimum phasedness, 8
 - vs. peaking, 8–9
 - and pointwise optimality, 85–86
 - robust, 14
 - slowly varying operators, 14–15
 - small-gain condition, 15–16
 - slow time variations
 - characterization, 9–10
 - stability vs. peaking, 8–9
 - Stable regular parametric (SRP) transfer function, 68–69, 76–77
 - State-feedback controller, 165
 - State-space equation, 108
 - State-space matrices, 202, 206, 212
 - State-space model interpolation of local estimates (SMILE)
 - input–output combination, 360
 - interpolation and optimization, 362
 - poles and zeros, 360–361
 - polytopic parametrization, 362
 - similarity transformation matrix, 361–362
 - SISO models, 361
 - State-space (SS) representation, 3, 28, 63, 72, 282, 293, 359, 360, 391–393, 493, 519
 - State-space trajectory, 70, 71
 - Static dependence, 28, 30, 31
 - Static output feedback (SOF), 319, 320, 329
 - Static state feedback (SSF), 320
 - Stationary LPV (SLPV) systems, 107, 115
 - Steering system, 525
 - Sub predictors, 36, 50, 52
 - Sum of squares (SOS) method, 116–118
 - Switched LPV systems, in discrete time, 174–178
 - Kalman–Yakubovich–Popov inequalities, 158
 - Lyapunov inequalities, 158
 - notation, 159
 - optimal control, 176
 - performance optimization, 172–174
 - problem evaluation
 - error output sequence, 168
 - Kalman–Yakubovich–Popov (KVP) inequality, 172
 - Schur complement formula, 170, 171
 - state-space description, 169
 - robust finite-path-dependent state feedback, 173, 174, 176, 178
 - stability, 159–164
 - stabilization
 - closed-loop system, 167
 - feedback gain matrices, 168
 - polytopes, 164, 165
 - state-feedback controller, 165
 - Switching systems, 67
- T**
- Time-delay systems
 - blade rotating speed, 294, 295
 - control effort, 295
 - displacements of mass, 295, 296
 - gain-scheduled controllers, 280
 - gridding parameter space, 295
 - Jensen’s lemma, 283
 - L_2 gain performance analysis, 280, 281, 297
 - Lyapunov–Krasovskii functionals, 281, 283, 284
 - milling process, 292
 - output feedback control design
 - closed loop system, 288–290
 - inequality, 291
 - slack variable matrix, 290
 - state-space matrices, 291
 - parameter-varying systems, 280
 - performance analysis
 - asymptotic stability, 284–286
 - LMI relaxation, slack variables, 286–288
 - Schur complement lemma, 286
 - projection lemma, 283
 - stabilization, 280
 - state-space representation, 282, 293
 - transport delay, 280
- Time-varying splitting parallel systems. *See* Decentralised model predictive control (MPC), of time-varying splitting parallel systems

Traffic control. *See* Constrained freeway traffic control, LPV paradigms

Trajectory tracking, 92, 106, 110–112, 116

Transfer functions
 with factorized denominator, 69–71
 Hurwitz denominator, 69
 SRP transfer function, 68–69
 state-space trajectory, 70, 71

Transient behavior, shaping
 with L_2 -gain constraint, 147
 robust GAR, 141–142

Turbocharged combustion engine control,
 low-complexity LPV input-output models

basis functions, 451–456
 black-box identification, 445, 446, 453
 charge control of
 air path, 447
 measured inputs and outputs, 449
 measured scheduling signals, 449
 plant model, structure of, 448
 controller synthesis and closed-loop results
 dilated LMIs, 457
 Lyapunov function, 457
 parameter varying matrix, 457
 simulation results, 458
 system configuration, 458
 vertex model, 457

identification of
 coefficient matrix, 456
 downhill simplex method, 456
 flow diagram, of algorithm, 456
 parameter set mapping (PSM), 455, 456

identification results, 456, 457
 best fit rate (BFR), 452
 cross validation, with scheduling parameters, 453
 functional basis for, 452
 polynomial basis, 452

parameter reduction
 cross validation, of identification result, 453, 454
 scheduling parameter vector., 454, 455

polytopic state-space and, 448, 450–451
 principal component analysis, 446
 scheduling function, 446, 450–452, 456
 shifted form, 450, 451

U

Unmeasurable parameters, LPV systems with, 194–195

V

Vehicle dynamics, 382

Vehicle systems. *See also* Integrated vehicle chassis control, design of

LPV control
 closed-loop interconnection structure, 521
 minimization task, 521
 P–K–D structure, 521, 522

LPV modeling
 brake and anti-roll bars, 520
 dynamics, 518–519
 state-space representation form, 519
 suspension system, 520
 yaw, roll, and pitch motions, 518, 519

Viability theory, 20

Vibroacoustic application
 control design, 375–377
 modeling
 frequency response functions, 372–374
 input–output combination, 373
 interpolation and optimization, 375
 poles and zeros, 373
 similarity transformation matrix, 375
 SISO models, 374–375
 validation, 375
 multi-objective design, 377–378

W

Wind turbines

aerodynamics
 Taylor series, 313
 tower dynamics, 315
 typical control strategy, 312–313
 typical 2 MW wind turbine, 314

automatic control, 304

controller structure, 306

cost of electricity, 304

fault diagnosis and fault-tolerant control, 305

faults
 biased pitch sensor, 315
 high air content, 317
 hydraulic leakage, 317
 hydraulic pitch model, 317
 pitch systems, 316, 317
 power converter, 316
 pump wear, 317
 ranges and rate limits, 316
 gain-scheduling approach, 304
 low data storage, 306

LPV controller design method
 bounded real lemma, 321

- closed-loop matrices, 320
 - controller implementation, 325–326
 - controller matrices, 320
 - decentralized controllers, 319
 - general parameter dependence, 324
 - gridding procedure, 325
 - induced L_2 -norm, 319, 321
 - infinite to finite dimensional, 323–325
 - initial slack matrix, 323
 - input–output operator, 321
 - iterative algorithm, 322
 - Lyapunov function, 324
 - nonconvex, 319, 322
 - parameter-dependent Lyapunov function, 319
 - parameter-dependent slack variable, 322
 - root mean-square value, 321
 - static output feedback, 319, 320
 - static state feedback, 320
 - LPV PI controller
 - aerodynamic gains, 329
 - bandpass filter, 327
 - drive train, 327, 328
 - integrator filter, 326, 329
 - LMI optimization problem, 330
 - loop-shaping weight, 329, 330
 - Lyapunov matrix, 330
 - mixed sensitivities optimization problem, 329
 - open-loop system matrices, 328
 - performance level and controller gains, 331
 - proportional, integral and tower feedback gains, 331, 332
 - schematic block diagram, 327
 - simulation results, 332–335
 - static output feedback, 329
 - variable-speed wind turbine, 328
 - mathematical operations, 306
 - nonlinear model
 - aerodynamic torque and thrust, 309–311
 - blade element, 308
 - converter dynamics, 311
 - drive train, 310
 - hydraulic pitch systems, 311
 - mass-spring-damper system, 311
 - power coefficient, 310
 - thrust coefficient, 310
 - system description, 318–319
 - variable-speed variable-pitch, 307
 - wind model, 307–308
- X**
- X-53 active aeroelastic wing
 - aeroservoelastic interaction, 484
 - flexible aircraft, 484
 - gain-scheduled classical control
 - Bode plots of, 494, 495
 - closed-loop responses, 495, 496
 - control design, 492–493
 - L_2 induced norms for, 497–499
 - LPV analysis, 497–499
 - LTI point analysis, 494–497
 - parameter trajectory, 503
 - SIMULINK model, 499–501
 - state-space representations, 493
 - step input disturbance, 502
 - worst-case simulation, 499–503
 - integrated active control, issues, 484
 - LPV analysis and design, tools for
 - gridded domains, 487
 - MATLAB objects, 487, 488
 - object-oriented programming, 488, 489
 - parameter-varying matrices and frequency, 487
 - pfrd, 487
 - pmat, 487–489
 - pss, 487
 - state-space models of, 486
 - LPV control design
 - Bode magnitude plots of, 505
 - Bode plots of loop function, 506
 - closed-loop responses, to step roll rate, 506, 507
 - design interconnection roll rate control, 503, 504
 - L_2 induced norms, for closed-loop sensitivity functions, 507, 508
 - LPV simulation, 486, 499
 - parameter dependent Lyapunov function, 497
 - roll rate model
 - altitude, Mach, 489
 - dynamics, 489, 490
 - open-loop Bode plots, from OLEF, 490, 491
 - open-loop step responses, from OLEF, 491, 492
 - rigid body data, 489, 490
- Y**
- Yaw stability, distributed control system, 522
 - Youla–Kucera parameter, 62, 72, 73, 76–78, 84